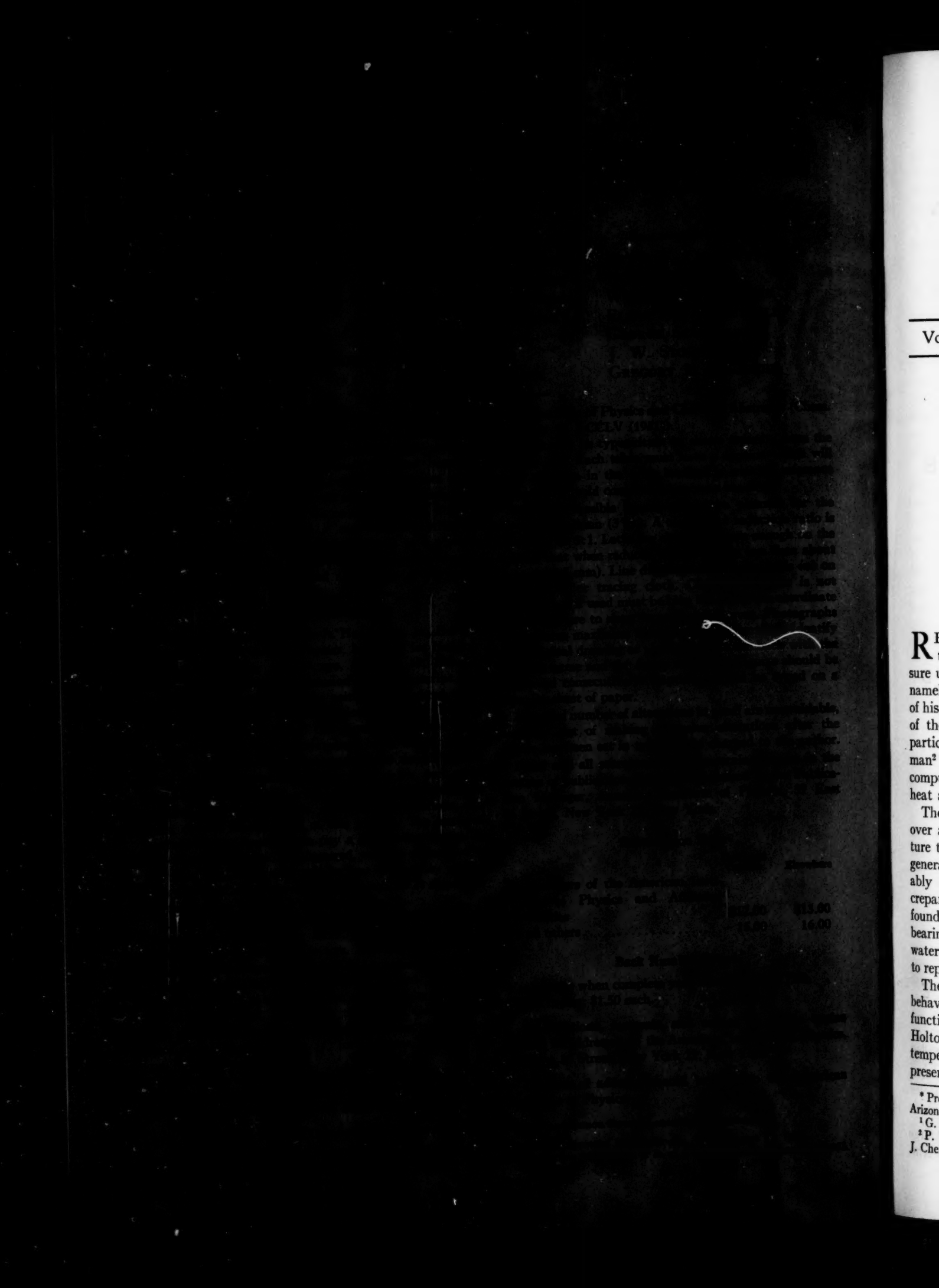

THE JOURNAL
OF
CHEMICAL PHYSICS

VOLUME 22, NUMBER 3 MARCH, 1954

The Velocity of Sound in Water as a Function of Temperature and Pressure

A. H. SMITH* AND A. W. LAWSON
Institute for the Study of Metals, The University of Chicago, Chicago, Illinois
(Received September 10, 1953)

The velocity of sound in water has been measured by an ultrasonic echo technique in the temperature range from −12°C to 129°C under hydrostatic pressures varying up to 9600 kg/cm². Even at the highest pressures the temperature dependence of the velocity of sound is found to be abnormal. In contradiction to certain previous results, the temperature at which the velocity of sound is a maximum is found to increase with increasing pressure. The behavior of the sound velocity is discussed in the light of recent theories concerning the structure of water. The internal consistency of the data with existing pressure standards is also analyzed.

INTRODUCTION

RECENTLY Holton[1] has reported measurements on the velocity of sound in water as a function of pressure up to 6000 kg/cm² at two differentte mperatures, namely, 30°C and 50°C. Holton pointed out the utility of his data in improving the accuracy of our knowledge of the thermodynamical properties of water and, in particular, by correlating his data with that of Bridgman[2] on the isothermal compressibility of water, he computed improved values for the ratio of the specific heat at constant pressure to that at constant volume.

The purpose of the present paper is to report data over a more extended range of pressure and temperature than that investigated by Holton. Although, in a general way, the results reported below agree reasonably well with those obtained by Holton, small discrepancies between the two sets of measurements are found. These discrepancies may have a significant bearing on the various theories about the structure of water. Consequently, it has been deemed desirable to report them in some detail.

The principal discrepancy under review involves the behavior of the maximum in the velocity of sound as a function of temperature as the pressure is increased. Holton concludes from his measurements that this temperature decreases with increasing pressure; the present authors conclude exactly the reverse. Our measurements indicate that the abnormal temperature dependence of the velocity of sound persists even to 10 000 atmospheres. If this be so, Eucken's[3] use of *PVT* data obtained in this pressure range for computing the behavior of "normal" water may be less justifiable than had hitherto been supposed.

APPARATUS

The velocity of sound is measured by a pulse-echo technique, similar to that employed by other investigators[4–7] for sound velocity determinations as well as the absorption of sound in water. This method is particularly adapted for measurements at high pressures because the experimental chamber is sufficiently small to be readily mounted in a high-pressure vessel of limited capacity. A schematic diagram of the apparatus in Fig. 1 shows the arrangement of the high-pressure components together with the control and measuring units.

The pressure system has been described previously[8] in the literature. It will not be described in detail here because the mode of pressure generation is immaterial to this investigation. On the other hand, measurement of the pressure is of the essence. Pressures were de-

* Present address: Motorola Research Laboratories, Phoenix, Arizona.

[1] G. Holton, J. Appl. Phys. 22,1407 (1951).

[2] P. W. Bridgman, Proc. Am. Acad. Arts Sci. 48, 309 (1912); J. Chem. Phys. 3, 597 (1935).

[3] A. Eucken, Nachr. Ges. Wiss. Göttingen 1, 36 (1946); Z. Electrochem. 52, 255 (1943); Z. Electrochem. 53, 102 (1949).

[4] R. Pelham and J. Gault, J. Chem. Phys. 14, 608 (1946).

[5] A. Weissler and V. del Grosso, J. Acoust. Soc. Am. 23, 221 (1951).

[6] J. M. M. Pinkerton, Nature 160, 128 (1947).

[7] P. Rosenberg, Radiation Laboratory, Massachusetts Institute of Technology, Report No. 56, 1946.

[8] D. Lazarus, Phys. Rev. 76, 545 (1949).

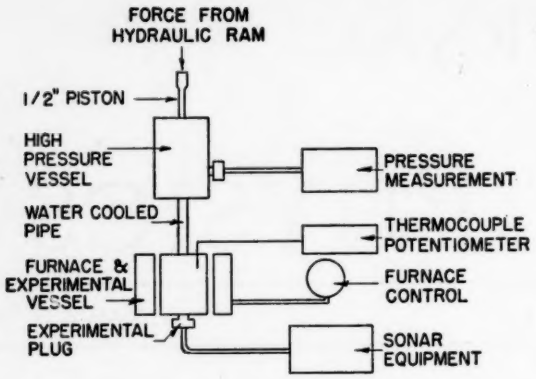

FIG. 1. Schematic diagram showing arrangement of high-pressure equipment, controls, and apparatus for measuring the velocity of sound.

termined by means of a manganin resistance gauge. This gauge was calibrated by determining the resistance of the gauge at two pressures established by others as accepted standards by the careful use of free piston techniques. The standard pressures used were the freezing point of mercury as determined by Bridgman[9] (7640 kg/cm² at 0°C) and the freezing point of CO_2 as determined by a blocked capillary method by Michels[10] (3439 kg/cm² at 0°C). The pressure coefficient of resistance of the gauge was the same at both pressures, indicating a linear dependence of resistance on pressure for this particular gauge. The pressure coefficient of resistance $1/R\ dR/dP$ was found to be $2.43_8 \times 10^{-6}$ cm²/kg. Because our determination of the CO_2 melting point was also by a blocked capillary technique, it is presumed that a comparison of our determination with that of Michels is to be preferred to a comparison with that of Bridgman, who used a technique involving a change in volume on freezing. Since the latter method gave a freezing point for CO_2 at 0°C about 1 percent lower than that found by Michels, it is by no means clear whether the most appropriate procedure has been followed. We shall re-address ourselves to this problem below when we consider the internal consistency of the sound velocity data with the pressure calibration.

Depending on the temperature range, the temperature was varied either by a furnace or by a bath surrounding the pressure vessel. The temperature was controlled by a proportioning controller. In view of the large heat capacity of the system, it is believed that the tem-

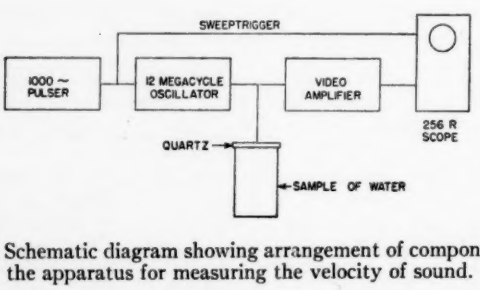

FIG. 2. Schematic diagram showing arrangement of components in the apparatus for measuring the velocity of sound.

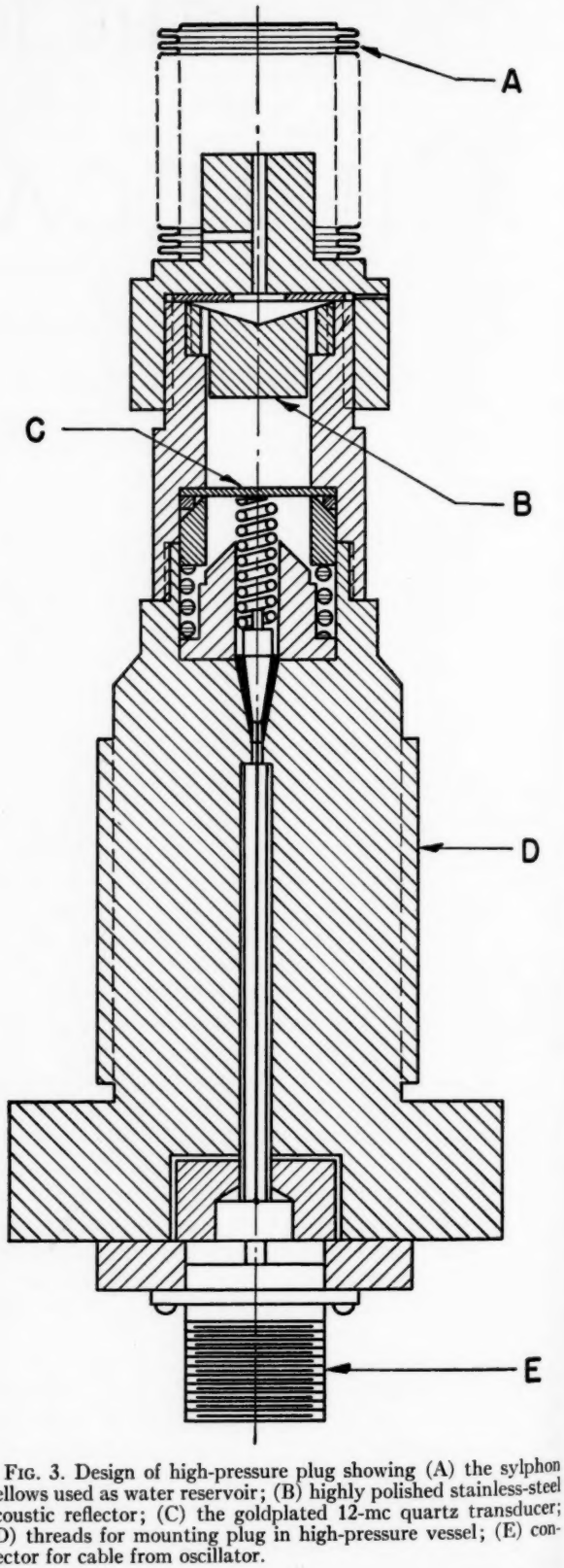

FIG. 3. Design of high-pressure plug showing (A) the sylphon bellows used as water reservoir; (B) highly polished stainless-steel acoustic reflector; (C) the goldplated 12-mc quartz transducer; (D) threads for mounting plug in high-pressure vessel; (E) connector for cable from oscillator.

[9] P. W. Bridgman, *Physics of High Pressures* (G. Bell and Sons, London, 1931).
[10] A. Michels, Physica **9**, 565 (1942).

peratures are known to 0.2°C, the limit being set by the technique employed, now to be described. The temperature was measured in the wall of the high-pressure vessel at a point about 1 inch from the interior. A correction was then applied for the temperature gradient between this point and the water under study. This gradient was determined by a separate experiment. All temperatures were measured with a chromel-alumel thermocouple by means of a type *K*-2 Leeds and Northrup potentiometer.

The ultrasonic pulse was introduced to the water by an X-cut quartz transducer having a natural frequency of 12 megacycles. The oscillator, pulser, receiver, and detector are the same as those previously described by Lazarus,[8] and are indicated in the block diagram Fig. 2. The repetition frequency used was 1000 cps, the pulse length varied from 1 to 10μsec, and the peak voltage of the pulse was about 30 v.

The echo chamber used is shown in Fig. 3. A necessary feature in the design of this chamber is the separation of the water under study from the pressure transmitting fluid, which was silicone oil or hexane, depending on the temperature. This separation is accomplished at one end of the echo chamber by sealing the edge of the quartz transducer *C* with a Neoprene washer. This arrangement not only affords a better acoustical match between the quartz and the water, but also eliminates back reflections from the conical reflecting surface of the space filler behind the quartz. The other end of the chamber is sealed by a sylphon bellows *A* which provides a reservoir of water to take up the slack arising from the compression of water in the chamber itself. These bellows are screwed on and sealed by a Neoprene washer.

All surfaces coming in contact with the water are of stainless steel except for the Neoprene washers and the gold-plated quartz crystal. The reflecting surface *B* is optically ground and polished stainless steel, flat within a wavelength of the mercury green line. Alignment is provided by the accurately machined shoulder in the echo plug against which the transducer is pressed by a spring.

MEASUREMENTS

The first data obtained in this experiment were isobaric curves in which it was hoped that the shift in the maximum velocity of sound as a function of temperature with increasing pressure could be directly observed. When the temperature of the maximum velocity was observed to increase with pressure and the corresponding discrepancy with Holton's data realized, it was decided to check the 30° and 50° curves isothermally. Further data were taken at other temperatures, some more complete than others, until a complete family of isobaric and isothermal curves was obtained as shown in Figs. 4 and 5. Direct plot of the present data with Holton's data (plotted points) is shown in Fig. 6. The data for these curves is given in Tables I and II

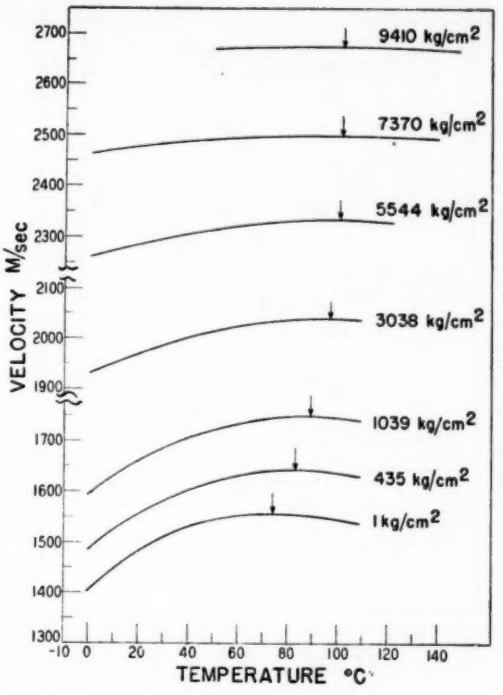

FIG. 4. The velocity of sound in water as a function of temperature at different pressures.

with corrections for the effect of the compressibility as a function of temperature and pressure included in the velocity shown, at most a 0.2 percent correction.

The apparatus as designed is more suitable for making observations of changes in the velocity of sound than in making an absolute determination of this ve-

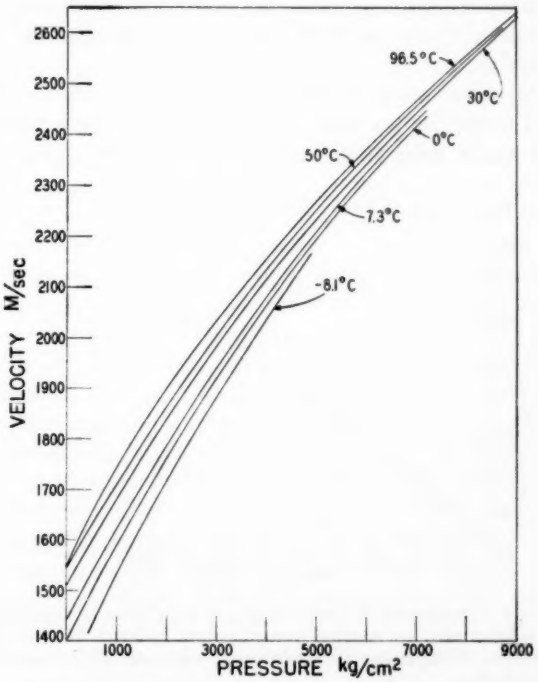

FIG. 5. The velocity of sound in water as a function of pressure at different temperatures.

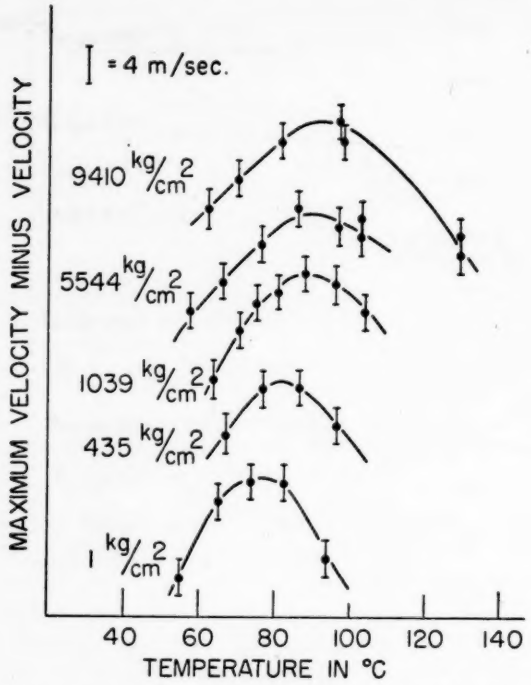

FIG. 6. Enlarged graphs showing relative variation of velocity of sound as a function of temperature near the maxima. The ordinate scale indicates only differences in velocity.

locity at each temperature and pressure. Therefore the velocity, 1510 m/sec, at 30°C and 1 atmosphere given by Willard[11] and other investigators was used as a reference velocity from which all velocities were calculated. An absolute determination of the velocity of sound in water, using the measured length of the echo chamber (1.583 cm) and an observed time interval gave a velocity at 30°C within 0.1 percent of the chosen value.

The water used in this experiment was doubly distilled water for the most part, although some readings were made with singly distilled water. No difference

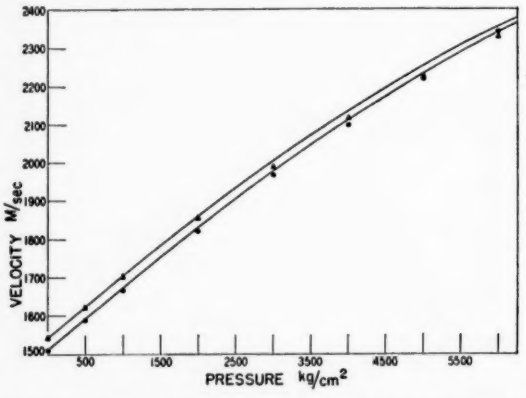

FIG. 7. Comparison of Holton's results with those reported here. The solid curves are plotted from the data in Table II; the solid circles and triangles are Holton's observations at 50°C and 30°C respectively.

[11] G. W. Willard, J. Acoust. Soc. Am. 19, 235 (1947).

was observed between the sets of data. No further effort was made to remove gas from the water.

The time interval between echoes was measured by observing the first four echoes and averaging the time interval between them. The input signal was too weak for parts of the temperature-pressure range to use more than four echoes. It is estimated that the time interval could be determined to ±0.1 percent. The calibration of the microsecond scale on the delay line of the 256D-A/R oscilloscope was checked against an internal crystal whose natural frequency gave 10μsec markers on the scale. The range markers were calibrated by beating against station WWV and are accurate to 1 part in 10^5.

TABLE I. The velocity of sound in water as a function of pressure determined isothermally at various temperatures.

T °C	P kg/cm²	u m/sec	T °C	P kg/cm²	u m/sec
−12.0	3467	1954	0.0	4619	2149
−12.0	4118	2065	0.0	5122	2221
−12.0	4311	2085	0.0	5136	2210
−8.1	1227	1576	0.0	5787	2289
−8.1	2169	1750	0.0	6447	2363
−8.1	3000	1889	7.3	11	1444
−8.1	3932	2023	7.3	1107	1639
−8.1	4861	2165	7.3	1892	1765
0.0	1	1403	7.3	3447	2006
0.0	1	1403	7.3	4672	2168
0.0	1	1402	7.3	5659	2290
0.0	36	1410	30.0	1	1510
0.0	256	1440	30.0	1989	1834
0.0	315	1468	30.0	3975	2110
0.0	474	1487	30.0	5963	2338
0.0	502	1478	50.0	1	1543
0.0	1011	1576	50.0	860	1684
0.0	1077	1565	50.0	1989	1861
0.0	1470	1666	50.0	2985	1999
0.0	1543	1675	50.0	3038	2011
0.0	1957	1744	50.0	3978	2129
0.0	2006	1761	50.0	5967	2351
0.0	2561	1848	96.5	1	1548
0.0	2562	1855	96.5	435	1638
0.0	3139	1939	96.5	1039	1747
0.0	3582	2014	96.5	5544	2333
0.0	3622	2016	96.5	7370	2506
0.0	4216	2097	96.5	9410	2678

RESULTS

From the reference velocity at 30°C and 1 atmosphere, the velocity calculated at 50°C and 0°C is found to be in good agreement with other investigators. Willard gives 1543 m/sec for 50°C, Randall[12] 1403 m/sec for 0°C. The only high-pressure work (about 800 kg/cm²) for comparison is that of Holton and is shown in Fig. 6.

The trend as seen from the curves in Fig. 4 is for the maximum of the velocity of sound *vs* temperature curve to move to higher temperature rather rapidly with initial rise in pressure, and approach a maximum displacement at about 94°C. In addition to this effect, there is a flattening out of the curve with increasing pressure. Thus the positive temperature coefficient at

[12] C. R. Randall, Bur. Standards J. Research 8, 94 (1932).

30° and 1 atmosphere (2.5 m/sec per °C) is about twice that at 30° and 5000 kg/cm² (1.2 m/sec per °C). Somewhere above 9500 kg/cm² it would appear that the temperature coefficient becomes zero over a range from the freezing temperature to about 100°C. All isothermal curves recorded would apparently cross at this pressure if extrapolated.

Referring to Fig. 6 again, where our results are compared with those of Holton, we observe that, while the two sets of data are in excellent agreement below about 3000 kg/cm², above this pressure Holton's two curves begin to converge until, at 5500 kg/cm², they have actually crossed. Our corresponding curves on the other hand are still converging very slowly. The implication of Holton's data is that pressure has displaced the maximum in the velocity of sound to lower temperatures. However, none of our more extensive data give any indication that this conclusion is correct but rather the contrary.

TABLE II. Velocity of sound as a function of temperature as determined isobarically for various pressures.

P kg/cm²	T °C	u m/sec	P kg/cm²	T °C	u m/sec
1	0.0	1403	1039	104.6	1744
1	22.5	1488	3038	48.8	2008
1	24.2	1494	3038	56.1	2024
1	26.6	1504	5544	0.0	2264
1	27.0	1505	5544	22.6	2290
1	27.6	1504	5544	57.4	2324
1	45.4	1539	5544	66.5	2327
1	55.1	1547	5544	76.3	2331
1	65.5	1555	5544	85.9	2335
1	74.7	1557	5544	96.1	2333
1	83.2	1557	5544	103.3	2334
1	93.8	1549	5544	103.4	2332
435	22.5	1563	7370	19.1	2485
435	57.6	1628	7370	42.8	2492
435	66.9	1637	7370	51.1	2491
435	77.0	1642	7370	63.4	2495
435	86.7	1642	7370	69.7	2495
435	96.5	1638	7370	84.0	2497
1039	26.5	1677	7370	95.6	2506
1039	44.2	1714	9410	56.5	2671
1039	55.4	1729	9410	62.4	2669
1039	63.4	1737	9410	70.2	2672
1039	70.5	1742	9410	82.7	2676
1039	75.5	1745	9410	97.4	2678
1039	80.4	1746	9410	98.4	2676
1039	88.1	1748	9410	128.9	2664
1039	96.4	1747	9410	129.0	2666

DISCUSSION OF EXPERIMENTAL RESULTS

It is not difficult to see why the two experiments lead to conflicting conclusions. The numerical discrepancies are small and any slight systematic error could easily account for the difference. *A priori*, it would be difficult to say which experiment is in error, or, in fact, if the difference did not arise from comparable errors in both experiments.

The principal sources of error in both Holton's experiment and ours are distortions of the wave form in successive pulses and the measurement of pressure.

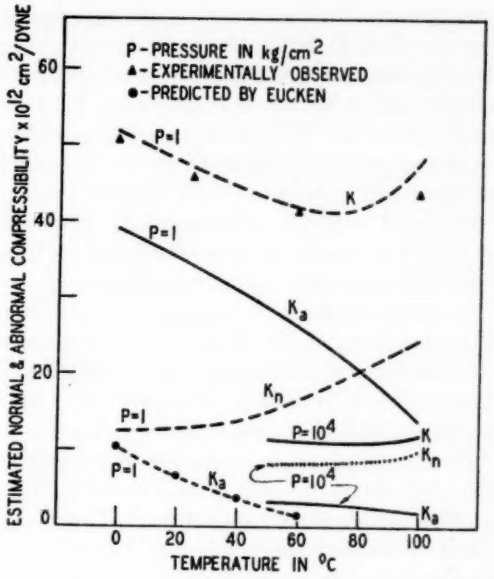

FIG. 8. Estimated contributions of the structural and normal components of the adiabatic compressibility of water. In this figure, K_a is the abnormal or structural component (denoted by K_s in the text), and K_n is the normal component.

With regard to the first source of error, it should be mentioned that one principal difference between Holton's technique and ours is the fact that Holton used up to 40 echoes in his measurements, while we used in many cases as few as four. The reason for this is that Holton applied over 1000 volts to the crystal while we worked with pulses of about 100 volts. In principle, the measurements are more precise with a larger number of echoes, but our experience indicated that, with our apparatus at least, at higher-voltage levels the distortion in the amplifier increased. The difference in echo times of successive pulses in our experiment was seldom greater than 0.3 percent and appeared to be random in distribution.

Holton does not discuss the calibration of his manganin gauge, but presumably his procedure was similar to ours. Differences in gauge calibration might cause small systematic discrepancies between the two sets of data but could not explain the crossover of Holton's two curves. A possible source of error in our experiment is the fact that our upper pressure vessel, containing the pressure gauge, was not thermostated. Consequently, during a run its temperature might have varied by several degrees. The effect on the pressure coefficient of resistance itself of such a temperature fluctuation would be negligible, but there would be an error owing to a hidden shift of the zero-pressure resistance of the gauge. We estimate that errors from this source in our experiment could not exceed 0.2 percent at 30°C and 50°C. Apparently, Holton's technique involves similar small errors.

One major source of error which could cause trouble is the possibility of change in gauge zero during a run owing to a sudden change in pressure. This source of

error was presumably eliminated in our experiments by rejecting any data in which the resistance at zero pressure of our gauge changed by more than ±0.01 ohm.

Another possible source of discrepancy between the two results is the fact that Holton used degassed water, while ours was merely distilled. However, the difference in velocity of sound between fully degassed water and water saturated with air at atmospheric pressure and 30°C is only 1 m/sec, and it is difficult to see how this error could increase with increasing pressure.

For the foregoing reasons the authors have examined the information available from other sources which might indicate in which direction the velocity maximum should be shifted by pressure. Such data are available in the form of isothermal compressibilities as a function of temperature and pressure from the investigations of Bridgman,[2] of Amagat,[13] and of Smith and Keyes.[14]

The following relations are pertinent. The velocity of sound u is related to the adiabatic compressibility K_a and the density ρ by the equation

$$u=(K_a\rho)^{-\frac{1}{2}}. \tag{1}$$

Thermodynamics relates the isothermal compressibility K_T to the thermal expansion coefficient α, the specific heat at constant pressure C_p, and K_a by the equation

$$K_T-K_a=\frac{TV\alpha^2}{C_p}. \tag{2}$$

Manipulation of Eq. (1) and Eq. (2) in the region of the maximum of the velocity of sound leads to the following conclusions. Corresponding to the maximum in the velocity of sound, both the isothermal and adiabatic compressibilities will exhibit minima as a function of temperature. Near zero pressure it may be shown that the minimum in the isothermal compressibility must occur at a lower temperature than the minimum in the adiabatic compressibility. Furthermore, the minimum in the adiabatic compressibility must occur at a lower temperature than the maximum in the velocity of sound. As an example, using Randall's[12] data for K_T and K_a, we may compute the various temperatures under consideration. At atmospheric pressure, we compute that the minimum in K_T will occur at 45°C, the minimum in K_a at 65°C, while the maximum in the velocity of sound will occur between 70°C and 74°C.

The conclusions of the preceding paragraph should be valid up to pressures of the order of magnitude of 6000 kg/cm² where a crossover occurs between curves of thermal expansion *vs* pressure for different temperatures. Above this pressure the minimum in K_a *vs* temperature will occur for a lower temperature than that for K_T.

If we pursue the reasoning of the preceding paragraphs, it becomes clear that if we can establish that the minimum of K_T *vs* temperature increases with increasing pressure, then the maximum in the velocity of sound must also increase, as found by our experiments.

Referring now to the behavior of the isothermal compressibility as a function of temperature and pressure, we find unfortunately that neither of Bridgman's experiments[2] on the PVT relations in water have been carried out with sufficient accuracy to provide an unambiguous answer to our question.

If, however, we examine the data of Amagat on K_T, we find that his results clearly indicate an increase of the minimum in K_T *vs* T with increasing pressure. Accordingly, his results lend weight to our conclusion that the maximum of u *vs* T increases with increasing pressure. To illustrate our point, we have incorporated Amagat's data in Table III. The same conclusion is indicated by the data of Smith and Keyes, whose data are reproduced in part in Table IV.

TABLE III. Abbreviated summary of Amagat's data on the isothermal compressibility of water as a function of temperature T and pressure P.

Pressure range kg/cm²	30°C	40°C	50°C	60°C	70°C
1–100	460	449[a]	449	455	462
100–200	436	429	425[a]	427	439
200 300	422	414	413[a]	415	425
300–400	413	407	402[a]	406	411
400–500	406	404	399	394[a]	398
500–600	392	390	390	388[a]	391

[a] Indicates minimum of K_T and illustrates how minimum shifts to higher T with increasing P. The units of K_T are in 10^{-13} dyne/cm².

[13] E. Amagat, Ann. chim. et phys. **29**, 68, 505 (1893).

[14] L. Smith and R. Keyes, Proc. Am. Acad. Arts. Sci. **69**, 285 (1934).

SELF-CONSISTENCY OF THE SOUND VELOCITY AND PRESSURE MEASUREMENTS

One of the most unsatisfactory aspects in precision investigations at high pressures is the lack of a uniform standard in the measurement of pressure. We have already touched briefly on the discrepancy between the determinations of Bridgman[9] and Michels[10] on the freezing point of CO_2. We do not propose to enter into a discussion of the complex of factors involved in this discrepancy, e.g., difference in observational techniques, purity of sample, etc.

The purpose of this section is to call attention to the fact that the measurement of the velocity of sound in a

TABLE IV. Abbreviated summary of the data of Smith and Keyes on the isothermal compressibility of water as a function of temperature and pressure (compressibility in arbitrary units).

Pressure range in bars	0°C	20°C	40°C	60°C	80°C
0–350	421	415[a]	418	429	450
350–1000	···	···	332	314[a]	331

[a] Indicates minimum of K_T and illustrstes how minimum shifts to higher T with increasing P. The units of K_T are in 10^{-13} dyne/cm².

TABLE V. Calculation of pressure from Eq. (4).[a]

P(kg/cm²)	V(cc/gm)	T(°K)	u(m/sec) Holton	u(m/sec) Authors	P from Eq. (4) kg/cm² Holton	P from Eq. (4) kg/cm² Authors
Based on Bridgman's H_2O data of 1935						
1	1.0046	303	1510	1510	1	1
500	0.9845	303	1588	1593	490	492
1000	0.9665	303	1667	1676	989	992
2000	0.9368	303	1822	1833	1978	1992
3000	0.9127	303	1968	1981	2969	2995
4000	0.8925	303	2100	2113	3967	4003
5000	0.8754	303	2222	2234	4954	5002
6000	0.8603	303	2344	2341	5955	6007
1	1.0120	323	1543	1543	1	1
500	0.9916	323	1623	1623	500	500
1000	0.9744	323	1703	1704	981	981
2000	0.9450	323	1856	1858	1965	1966
3000	0.9207	323	1990	2004	2962	2972
4000	0.9005	323	2118	2135	3944	3973
5000	0.8835	323	2227	2252	4906	4952
6000	0.8684	323	2334	2356	5877	5946
Based on Bridgman's H_2O data of 1912						
1	1.0041	303	1510	1510	1	1
500	0.9837	303	1588	1593	498	500
1000	0.9663	303	1667	1676	982	987
2000	0.9364	303	1822	1833	1978	1994
3000	0.9105	303	1968	1981	3046	3075
4000	0.8897	303	2100	2113	4077	4119
5000	0.8719	303	2222	2234	5089	5165
6000	0.8554	303	2344	2341	6203	6262
1	1.0118	323	1543	1543	1	1
500	0.9916	323	1623	1623	496	496
1000	0.9743	323	1703	1704	980	980
2000	0.9445	323	1856	1858	1978	1980
3000	0.9205	323	1990	2004	2965	2973
4000	0.8996	323	2118	2135	3987	4008
5000	0.8818	323	2227	2252	4998	5037
6000	0.8662	323	2334	2356	6007	6065

[a] Based on calibration of manganin resistance gauge using Bridgman's freezing point of Hg at 0°C and Michels' freezing point of CO_2 at 0°C.

liquid, the volume of the liquid as a function of pressure, and the pressure itself are not independent. In fact, for an imaginary fluid with no thermal expansion, the following relation between these three quantities must be valid:

$$P-P_0=\int_{V_0}^{V_P}\frac{M}{V^2}u^2dV. \tag{3}$$

For an actual fluid with a finite thermal expansion, it follows from Eq. (2) that the pressure, volume, and velocity of sound in a fluid must obey the relation

$$P-P_0=\int_{V_0}^{V_P}\frac{M}{V^2}u^2\left(1+\frac{u^2MT\alpha^2}{C_p}\right)^{-1}dV. \tag{4}$$

According to the preceding equation, if the volume of a fluid at some unknown pressure is ascertained, and the velocity of sound at the same pressure is determined, the pressure may then be calculated if rather crude values for the thermal expansion coefficient and the specific heat are available. The latter quantities need not be known very well because they represent a correction of from 3 percent to 6 percent. As a result of the integration the effect of an 8 percent error in α or C_p on P is reduced to about 0.2 percent.

TABLE VI. Dependence of calculations in Table V on gauge constant[a] at 30°C.

P(kg/cm²)	V(cc/gm)	Gauge constant[b] $\gamma=2.410\times10^{-6}$ (kg/cm²)⁻¹ u(m/sec)	Gauge constant[b] integral	Gauge constant[c] $\gamma=2.438\times10^{-6}$ (kg/cm²)⁻¹ u(m/sec)	Gauge constant[c] integral
1	1.0046	1510	1	1510	1
500	0.9845	1594	492	1593	492
1000	0.9665	1678	997	1676	992
2000	0.9368	1837	1999	1893	1992
3000	0.9127	1986	3007	1981	2995

[a] Pressure determined assuming gauge resistance varies as $R_p=R_0(1+\gamma P)$.
[b] Based on Bridgman's freezing point of CO_2 3400 kg/cm² at 0°C.
[c] Based on Michels' freezing point of CO_2 3439 kg/cm² at 0°C.

We are invited, therefore, to calculate the pressure from known PVT data and the velocity of sound from Eq. (4) and to compare the result with that determined by the manganin gauge using available pressure standards established by a free piston technique.

In making such a comparison, owing to various discrepancies in the experimental literature, several procedures are possible. The possibilities are denumerated according to whether we use (1) Bridgman's PVT data of 1912; (2) Bridgman's PVT data of 1935; (3) Holton's data on the velocity of sound; (4) The present data on the velocity of sound; (5) Bridgman's determination of the freezing point of CO_2; or (6) Michels' determination of the freezing point of CO_2.

Tables V and VI show the results of a number of the possible permuted comparisons. It is difficult to draw a cleancut conclusion from these calculations, but they may be summarized as follows. On the whole, both Holton's results and ours are in better agreement with Bridgman's PVT data of 1935 than those of 1912—this statement being particularly appropriate to the 1912 data at 30°C. Regardless of which set of data on the velocity of sound is employed in the calculation, the deviations between the pressures determined by the free piston technique and that calculated from the velocity of sound seldom exceed 2 percent—a remarkable result considering the lapse of years and the varied sources of the experimental data.

Table VI shows that the rough generalities drawn above are somewhat sensitive to the pressure standards used in the calibration of the resistance gauge. Table V is based on the use of the freezing point of mercury at 0°C as determined by Bridgman, and the freezing point of CO_2 as determined by Michels. If, on the other hand, we confine our comparison to pressures below 3000 atmospheres, we find that the consistency of the pressure data with ours is improved at 30°C by using Bridgman's data on the freezing point of CO_2. The arguments evoked in the selection between the two comparisons are so involved that we do not believe they may be resolved by our data. The suspicion is generated never-

theless that our absolute pressure standards are uncertain to about ½ percent in the range below 10 000 atmospheres.

COMPARISON OF THEORY AND EXPERIMENT

Although the differences between the results of Holton and ours seem minuscule from an experimental point of view, they have been emphasized because of their apparent importance in discriminating among the various theories of the structure of water. All of these theories incorporate as a basic postulate the concept that a considerable memory of the ice structure is retained in the liquid phase. Perhaps the first significant modern effort to interpret the properties of water was that of Bernal and Fowler,[15] who treated the water as a mixture of two types of H_2O complexes. One type of complex was considered to assume a quartz-like type of arrangement (normal water), while the other type was assumed to have a trydimite type of arrangement as in ice. To explain qualitatively the behavior of water near the ice point, Bernal and Fowler found it necessary to assume that approximately 70 percent of the molecules were ice-like even near the boiling point. Subsequent investigations of the structure of water using x-ray diffraction patterns indicated that this model was oversimplified and that the molecular rearrangements in the liquid state were more subtle. In particular, the investigations of Morgan and Warren,[16] and also of Katzhoff,[17] indicate that as the temperature was increased the major change in the structure could be ascribed to an increase in the number of neighbors in the successive shells of molecules surrounding any given molecular center. In an effort to circumvent this objection, Eucken[3] in a series of papers addressed himself to a somewhat different approach. He depicted water as composed of a mixture of polymers and considered the equilibrium between a system composed of monomers, dimers, quadrimers, and octomers. He then assumed the PVT data at 10 000 atmospheres to reflect the behavior of normal water. By empirically fitting an equation of state to this data, he predicted the behavior of normal water under atmospheric conditions. By differences between the observed and predicted values of the volume of water as a function of pressure, he deduced the number of abnormal molecules (octomers) as a function of temperature and by a rather elaborate structure was able to correlate this dependence with that of the specific heat and other physical properties. For the sake of completeness, we add that recently Gierer and Wirtz[18] have attempted to reconcile Eucken's theory with that of Bernal and Fowler.

If our experimental results be accepted at face value, it would seem that Eucken's assumption that water is behaving normally at 10 000 atmospheres is somewhat dangerous. Although the isothermal compressibility appears to be behaving in a normal fashion, the velocity of sound does not. A reexamination of these early theories, therefore, appears to be in order.

We digress temporarily to discuss a theory by Hall[19] which was developed to explain the anomolous absorption of sound in water. Hall assumes that a water molecule can exist in two states differing in free energy by an amount F. The molal volume V of water is then assumed to be given by

$$V=V_n(1-x_a)+V_ax_a=V_n+\Delta Vx_a, \tag{5}$$

where V_n is the molal volume of normal water, V_a the molal volume of abnormal water, x_n and x_a the corresponding concentrations of the two states assumed to be related by the simplest possible interaction, namely,

$$\frac{x_n}{x_a}=e^{-\Delta F/RT}. \tag{6}$$

It is now possible conceptually to separate the compressibility K of water into two components, the compressibility at infinite frequency K_∞ plus a structural component K_s, which is easily deduced to be given by the following expression:

$$K_s=K-K_\infty=+\frac{(\Delta V)^2}{2RTV\left[1+\cosh\frac{\Delta F}{RT}\right]}. \tag{7}$$

Estimates of K_∞ may be made from the compressibility of ice and calculations from known intermolecular potential functions. The estimates for K_∞ range between 12 and 24×10^{-12} cm²/dyne. Hall was able to obtain satisfactory agreement with sound absorption measurements by choosing K_∞ to be 18×10^{-12} cm²/dyne, ΔV equal to -8.4 cm³, and ΔF equal to 500 cal/mole.

We shall now investigate whether Hall's estimates of these quantities also give reasonable values for the compressibility, thermal expansion, and specific heat, and compare the resulting estimates with those obtained by Eucken.

We shall begin our analysis by commenting that the consistent application of thermodynamics to the Hall model leads to the conclusion that in addition to the structural compressibility K_s given by Eq. (7), concomitant structural effects also occur in the thermal expansion coefficient and the specific heat. These quantities are not completely independent, but are related by the following relations, regardless of the validity of Eq. (6):

$$\frac{T(\Delta V)^2c_s}{VK_s}=(\Delta H)^2 \tag{8}$$

and

$$\alpha_s=c_s\Delta V/V\Delta H, \tag{9}$$

[15] J. D. Bernal and R. H. Fowler, J. Chem. Phys. **1**, 515 (1933).
[16] J. Morgan and B. E. Warren, J. Chem. Phys. **6**, 666 (1935).
[17] S. Katzhoff, J. Chem. Phys. **2**, 841 (1934).
[18] A. Gierer and K. Wirtz, Z. Naturforsch. **5**, 577 (1950).
[19] L. Hall, Phys. Rev. **73**, 775 (1948).

where c_s is the structural contribution to the specific heat, α_s is the structural contribution to the thermal expansion coefficient, and ΔH is the difference in enthalpy between normal and abnormal water molecules.

Referring all our calculations for the moment to 0°C, we find from Eq. (7) by assuming ΔF is zero that the minimum value of ΔV is 8.0 cm³/mole if we use a value for $K_\infty = 12 \times 10^{-12}$ cm²/dyne. This value for ΔV compares favorably with the value of 8.4 cm³/mole assumed by Hall and is consistent with the difference between the observed density of water and that which it would acquire if water had the same structure as ice.

If the structure of water were completely ice-like, Pople[20] has estimated that its volume would differ from that of water at 0°C by 0.22 cm³/g, a difference which must be accounted for by the transition from abnormal molecules to a normal state. In accordance with this reasoning, assuming Eq. (6) is correct, we deduce that 0°C the fraction of normal molecules is 50 percent, a number intermediate to the predictions of Bernal and Fowler on the one hand and Eucken on the other.

Using the value of ΔV equal to 8.0 cm³/mole deduced above, and Eucken's estimate of 8.5 cal/mole for c_s, we find from Eq. (8) that we must take ΔH equal to 2600 cal/mole to be consistent. This value for ΔH falls within the range of the values assumed by Eucken for the dissociation of the various polymers in his model.

Using the value of ΔH deduced from Eq. (8), we now calculate from Eq. (9) that the consistent value of α_s at 0°C is 14.6×10^{-4}/°C. This value for α_s is eminently reasonable since the average expansion coefficient for methyl alcohol between 0°C and 100°C is about $+12 \times 10^{-4}$/°C and that for water at 0°C is -1.0×10^{-4}/°C.

Using Eq. (6) again, from the value of x_n at 0°C, we calculate that the value of x_n at 100°C should be 0.78. Thus, the increase of the normal component between the freezing and boiling points of water is 28 percent. If we take our value of 2600 cal/mole for ΔH, this implies an excess increase of the enthalpy of water between these two temperatures of 730 cal/mole. The value estimated by Eucken is approximately 785 cal/mole.

It is not difficult to verify from the above data that the minimum in the thermal expansion coefficient must occur in the neighborhood of 0°C. Thus, it must be concluded that the rather crude model used by Hall is in essential agreement with many of the thermodynamic properties of water.

Nevertheless, Hall's theory is subject to the following criticisms. Hall concluded that the difference between the two states assumed in this model was the breaking of a hydrogen bond. If so, the validity of Eq. (6) is open to question. Secondly, the value of ΔH found here is too small to account for the properties of water on this physical model. The heat of evaporation of ice, for instance, implies that the energy to break a hydrogen bond is at least twice the value of ΔH used here.

This dilemma may be resolved, perhaps, by considering the point of view of Pople[20,21] and Lennard-Jones.[21] According to their viewpoint the explanation of the anomalies in the behavior of water lies not in the breaking of bonds but in their flexibility. Thus, ΔH should not necessarily be considered as the energy required to break a hydrogen bond but probably as the energy required to bend one. Pople's theory seems to be consistent with the x-ray diffraction data.

Another insufficiency in Hall's model is its failure to describe satisfactorily the molal volume on data at higher pressures. Bridgman's PVT data indicate that this quantity goes through a minimum at successively lower temperatures as the pressure is raised and then at even lower temperatures through a maximum. These features are qualitatively described well by the equations given above. Quantitatively, however, the difference in molal volume between the maximum and minimum decreases rapidly with increasing pressure. In the theory this quantity is constant since the variations of ΔV and ΔS with temperature and pressure have been neglected. The theory requires considerable refinement before the fine experimental details can be adequately described.

We revert now to a comparison of the Hall theory with that of Eucken. According to Eq. (7), the structural bulk modulus should decrease somewhat more rapidly than the absolute temperature as the latter is increased. The behavior of the abnormal adiabatic compressibility, as predicted by Eq. (7), is shown in Fig. 8, where it is compared with that predicted by Eucken. As may be seen, the discrepancy is rather large. Although our measurements seem to support Hall's model, clearly more measurements and analysis are needed to select the preferable theory.

In conclusion, it should be noted that the arguments given above are not particularly sensitive to the form of Eq. (6) because $\Delta F/RT$ is relatively small.

ACKNOWLEDGMENT

It is a pleasure to acknowledge the partial support granted to this investigation by the U. S. Office of Naval Research.

[20] J. A. Pople, Proc. Roy. Soc. (London) **A205**, 163 (1951).

[21] Sir J. Lennard-Jones and J. A. Pople, Proc. Roy. Soc. (London) **A205**, 155 (1951).

The Thermal Conductivity of Organic Vapors. The Relationship between Thermal Conductivity and Viscosity, and the Significance of the Eucken Factor

R. G. VINES AND L. A. BENNETT
C.S.I.R.O., Division of Tribophysics, University of Melbourne, Australia
(Received September 21, 1953)

The thermal conductivities of thirty-one polar and nonpolar organic vapors have been determined at pressures up to one atmosphere, over a temperature range from 40 to 160°C. The relation between thermal conductivity and viscosity is discussed in terms of the expression:

$$\frac{K^0M}{\eta C_{v0}}=f=\frac{f_{\text{trans}}C_{v\text{trans}}+f_{\text{int}}C_{v\text{int}}}{C_{v0}}$$

where, following a suggestion by Eucken, the ratio f is divided into separate components f_{trans} and f_{int}, corresponding to the different rates of transfer of translational and "internal" (vibrational and rotational) energies.

Experimental values of f are not in accord with Eucken's original assumption that $f_{\text{int}}=1$. For nonpolar vapors f_{int} increases towards a high-temperature limit which is close to the theoretical value of 1.3. For polar vapors f_{trans} appears to be less than the theoretical value of 2.5, the decrease depending on the polar character of the molecule. These results are discussed with reference to energy exchanges occurring during collisions between complex molecules.

I. INTRODUCTION

THE thermal conductivity of an organic vapor varies with pressure and temperature. The variation with pressure is related to the corresponding change in specific heat.[1] The variation with temperature has been studied experimentally but no adequate theoretical treatment exists; before such a treatment is possible a knowledge of the relationship between conductivity and viscosity is required. In the present paper the results of extensive new thermal conductivity measurements are reported, and these, together with published values of viscosities and specific heats, have been used to investigate this relationship. The present results are complementary to those described recently;[1] the temperature range of the earlier measurements has been extended and further substances investigated.

The relation between thermal conductivity and viscosity may be discussed in terms of the dimensionless ratio

$$K^0M/\eta C_{v0}=f, \tag{1}$$

where K^0 is the conductivity at zero pressure (see Sec. III) and η, C_{v0}, and M are the viscosity, the molar heat at constant volume, and the molecular weight of the vapor. The theoretical studies of Chapman,[2] and Hirschfelder, Bird, and Spotz[3] have shown that for simple spherical molecules $f\approx 2.5$, the value being virtually independent of temperature; this has been confirmed experimentally for gases which possess only translational energy, e.g., the inert gases.[4] On the other hand, for polyatomic gases experiment shows that $f<2.5$. For these gases Eucken[5] suggested subdividing the conductivity into parts corresponding to the separate transport of translational and "internal" energies, *viz.*

$$K^0=\frac{\eta}{M}[f_{\text{trans}}C_{v\text{trans}}+f_{\text{int}}C_{v\text{int}}], \tag{2}$$

where $f_{\text{trans}}=2.5$ and $f_{\text{int}}=1$, and where $C_{v\text{trans}}$ and $C_{v\text{int}}$ are the translational and internal (vibrational and rotational) contributions to the total specific heat C_{v0}. From this it is easily shown[6] that

$$f_{\text{Eucken}}=1+4.47/C_{v0}, \tag{3}$$

where C_{v0} is in cal mole^{-1}.

Eucken's suggestion has no rigorous theoretical foundation. Chapman and Cowling,[7] and Schäfer[8] have pointed out that the transport of internal energy takes place by a diffusion mechanism, and on this basis the Eucken expression in Eq. (2) must be modified by the substitution $f_{\text{int}}=D\rho/\eta>1$, D being the self-diffusion coefficient and ρ the density of the vapor. It may be shown[7] that $D\rho/\eta=3A$, where A is a complicated function which depends upon the type of molecular interaction assumed. For the Lennard-Jones (12:6) potential, the values of A tabulated by Hirschfelder *et al.*[3] yield $D\rho/\eta=1.31-1.33$ over a large temperature range; for smooth elastic spheres $D\rho/\eta\approx 1.2$.[7]

The only molecular model with internal energy which has received rigorous theoretical treatment is the "rough sphere" discussed by Chapman and Cowling.[7] For this model, which possesses rotational but not vibrational

[1] R. G. Vines, Australian J. Chem. **6**, 1 (1953).
[2] S. Chapman, Phil. Trans. **A211**, 433 (1912).
[3] Hirschfelder, Bird, and Spotz, J. Chem. Phys. **16**, 968 (1948); Chem. Revs. **44**, 205 (1949).
[4] W. G. Kannuluik and E. H. Carman, Proc. Phys. Soc. (London) **B65**, 701 (1952).
[5] A. Eucken, Physik. Z. **14**, 324 (1913).
[6] P. M. Craven and J. D. Lambert, Proc. Roy. Soc. (London) **A205**, 439 (1951).
[7] S. Chapman and T. G. Cowling, *The Mathematical Theory of Non-Uniform Gases* (Cambridge University Press, Cambridge, 1939).
[8] K. Schäfer, Z. phvsik. Chem. **B53**, 149 (1943). See however J. Meixner, Z. Naturforsch. **8a**, 69 (1953).

energy, the modified Eucken expression holds strictly in the limiting case where the mass of the molecule is concentrated centrally. This, as Chapman and Cowling point out, implies negligible interchange of rotational and translational energy. For actual molecules it is thus considered that the modified Eucken expression is valid when translational/rotational energy interchange is infinitely slow, and a state of equilibrium exists between the various rotational modes, so that rotational/rotational exchange is infinitely rapid. There is no adequate model for molecules possessing vibrational energy, but by analogy it seems likely that the modified Eucken expression holds only when translational/vibrational interchange is negligible, and vibrational/vibrational (and vibrational/rotational) exchange is exceedingly fast. If $f_{int}=D\rho/\eta$ only under conditions approximating to these, then at low temperatures, where the rapid exchange of internal energy is reduced, the value of f_{int} may be smaller. However, at high temperatures as energy exchange is facilitated, f_{int} should increase towards $D\rho/\eta$; in fact, it might somewhat exceed this value if the relatively slow translational/rotational and translational/vibrational interchanges become appreciable.[9]

The validity of these conclusions will be examined in Sec. IV.

II. EXPERIMENTAL

The apparatus was of the compensated hot wire type and was similar to that used previously (for details see reference 1), but the design was improved so that the various parts of the conductivity cell could be assembled more easily. The new cell is shown diagrammatically in Fig. 1. The conductivity and compensating wires, 15 cm and 6 cm in length, respectively, were of platinum (diam $\frac{1}{10}$ mm) and were held centrally in holes (diam 2 mm) bored through a cylindrical block of aluminum bronze. The leads to the wires were of solid silver (diam $\sim$1 mm), and were insulated from the body of the apparatus by accurately ground glass sleeves, as shown in the diagram; to prevent strain on the wires all leads were brought to supporting terminals on a glass disk at the top of the cell. Fine tungsten springs were used to provide slight tension in the wires.

The assembly was contained in a brass tube silver-plated on the inside. At the top the tube was soldered with a high melting silver-tin solder to a metal/glass seal, and four tungsten seals in an adjoining glass bulb provided connections to the external electrical equipment. The unit could be immersed in a thermostat without the electrical leads coming into contact with the thermostat liquid.

The remainder of the equipment was identical with that of the earlier experiments, as also was the procedure

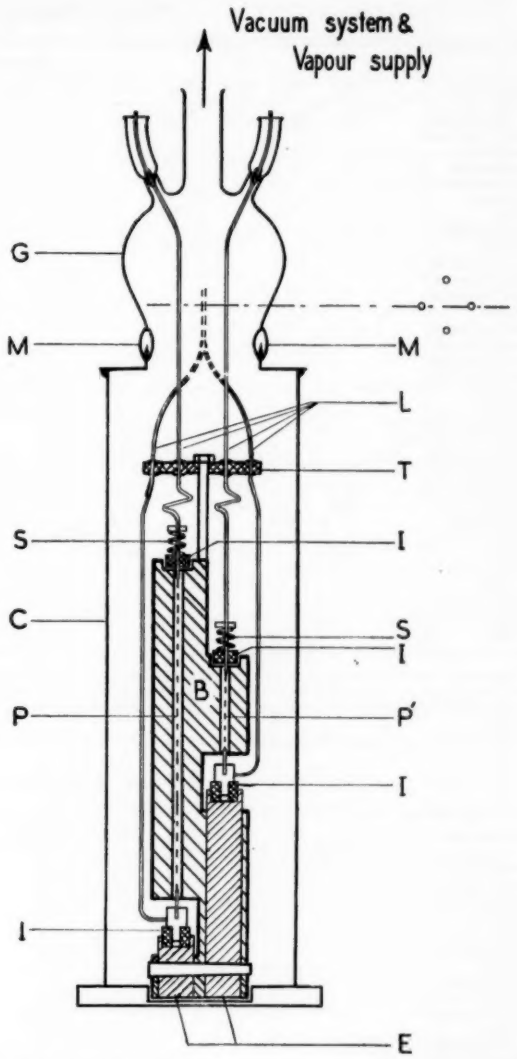

FIG. 1. Thermal conductivity apparatus. P, P' platinum wires; L silver leads; I glass insulators; T glass terminal support; S tungsten springs; B aluminum-bronze block; C metal container; G glass bulb; M metal/glass seal; E supports for lower electrodes.

involved in calibrating the apparatus and making measurements. The conductivities of the various vapors were compared with that of air at the same temperature and absolute values were calculated using Kannuluik and Carman's recent results for the conductivity of air.[10] Experiments were completed as rapidly as possible, since certain of the vapors (notably ethyl nitrate) appeared to decompose at the higher temperatures.

Experimental Accuracy

For accurate measurements the apparatus must be very carefully thermostated, and this proved difficult at 150 and 160°C. Furthermore, the effects of incomplete molecular accommodation in the apparatus become more pronounced with increasing temperature, and

[9] A more realistic model than the rough sphere has been discussed by Chapman and Hainsworth, Phil. Mag. **48**, 593 (1924). The treatment is not extensive, but again indicates that a decrease in f below the value given by the modified Eucken expression may be expected for real molecules.

[10] W. G. Kannuluik and E. H. Carman, Australian J. Sci. Research **A4**, 305 (1951).

TABLE I. Thermal conductivities of organic vapors.[a]

Temperature °C	$K^0 \times 10^6$ (cal cm^{-1} sec^{-1} deg^{-1}) 44.9	60.2	68.3	78.1	79.0	79.1	87.5	100.7	100.8	101.1	101.2	106.8	109.0	126.0	149.0	161.6	161.9
Air (Kannuluik and Carman)	65.3	67.9	69.2	70.8	71.0	71.0	72.4	74.6	74.6	74.7	74.7	75.4	75.8	78.4	81.8	83.6	83.7
Acetonitrile													34.1	36.8	41.7	(44.7s)	
Propionitrile														39.3s			
Nitromethane[b]														34.7	38.8		
Methanol[b]														59.1s	65.0	68.5	
Water											(56.6)		(58.2)	(62.2)	(68.5)		
Ethyl nitrate											38.3			43.6s	(49.0)		
Acetone[b]				37.1										47.7	53.3s	56.0	
Ethyl acetate[b]														47.8	53.5s	56.4s	
Methyl acetate[b]						37.7s		42.5						48.0	53.8s	57.2s	
Ethyl formate[b]								44.3						50.2s	56.3		
Dioxane								40.2s						46.3s	51.9		
Ethylene oxide											46.5			52.6s	59.6		
Acetaldehyde[b]														48.0			
Diethylamine[b]														59.7s	66.5s		
Triethylamine[b]														53.2s	59.6s		
Piperidine														(50.7s)			
Pyridine														(42.2)			
Ethylidene chloride[b]														35.4s			
Ethylene dichloride[b]														34.6			
Ethyl chloride[b]															50.9		
Methyl chloride	28.5		32.1s				35.3s										
Methyl bromide	20.3s		23.5				25.9s					29.1					
Methyl iodide	14.8		17.0				18.3s					20.2					
Chloroform[b]		20.3			22.2s									26.6s	29.1		
Ether[b]		43.2				47.6s		53.0						60.1	66.5		
Benzene[b]					34.7			39.5s						45.6s	51.1s		54.5s
Cyclohexane[b]														50.5s	57.8s	61.6	
Hexane[b]														54.9	61.6s		65.5
Cyclopropane									58.0s					66.8	74.4		
Propane										65.2s				73.8	81.7		
Ethane										75.5				84.5s	(~93)		

[a] Absolute conductivities were calculated using results for the conductivity of air recently obtained by Kannuluik and Carman (reference 10). Corrections have been made for accommodation effects in the apparatus [see Vines (reference 1) Appendix II]; the K^0 values determined by direct experiment have thus been decreased by about 0.3 percent at 60°C, 0.4 percent at 110°C, and 0.5 percent at 150°C, before being listed in Table I. The figures in parentheses are uncertain.

[b] Substances previously investigated at lower temperatures (see reference 1).

TABLE II. β values of organic vapors (percent atmos^{-1}).

Temperature °C	44.9	60.2	68.3	78.1	79.0	79.1	87.5	100.7	100.8	101.1	101.2	106.8	109.0	126.0	149.0	161.6	161.9
Acetonitrile													8.1s	5.5s	3.0	...	
Propionitrile														4.4			
Nitromethane[a]														4.0	(2.8s)		
Methanol[a]														3.1s	1.9	1.4	
Water											(3.2s)[b]		(2.9s)	(2.4s)	(1.6)		
Ethyl nitrate											2.2s			1.6s	(1.5)		
Acetone[a]				3.4s										1.4s	1.1s	0.9	
Ethyl acetate[a]														1.6	1.2s	...	
Methyl acetate[a]						2.2		1.8						1.4s	1.0	...	
Ethyl formate[a]								1.5s						1.1s	1.0s		
Dioxane								1.1						0.9	0.7		
Ethylene oxide											0.9			0.8s	0.5s		
Acetaldehyde[a]														0.8s			
Diethylamine[a]														0.8	0.7s		
Triethylamine[a]														0.5s	(0.6)		
Piperidine														0.7			
Pyridine														0.5			
Ethylidene chloride[a]														0.8			
Ethylene dichloride[a]														0.5			
Ethyl chloride[a]															0.3s		
Methyl chloride	0.6s		0.4				0.2s										
Methyl bromide	0.9s		0.6				0.3s					0.2					
Methyl iodide	1.4s		1.0				0.7					0.5					
Chloroform[a]		1.8s			1.4s									0.7	0.7		
Ether[a]		0.9s				0.9		0.8s						0.7s	0.7		
Benzene[a]					0.5s			0.4s						0.3s	0.3		(0.3)
Cyclohexane[a]														0.3	0.2s	...	
Hexane[a]														0.3s	0.3		(0.3)
Cyclopropane									0.2s					0.2	0.2		
Propane										(0.2s)				(0.2)	(0.1s)		
Ethane										(0.2)				(0.1s)	...		
Air[a]					0.3s			0.3s						0.4s	0.5	0.6	

[a] Substances previously investigated at lower temperatures (see reference 1).

[b] The figures in parentheses are uncertain—see Appendix.

although corrections for this can be applied, small errors inevitably remain. The estimated accuracy of the conductivity values is about ±1 percent. This includes the error due to radiation which, in the apparatus described, amounts to less than ½ percent even at 160°C. (Details for the calculation of the radiation correction are given by Kannuluik.)[11]

[11] W. G. Kannuluik, Proc. Roy. Soc. (London) **A131**, 328 (1931).

III. RESULTS

The thermal conductivities of the following substances were measured: ethane, propane, cyclopropane, hexane, cyclohexane, benzene, ether, chloroform, methyl iodide, methyl bromide, methyl chloride, ethyl chloride, ethylene dichloride, ethylidene chloride, pyridine, piperidine, diethylamine, triethylamine, acetaldehyde, ethylene oxide, dioxane, ethyl formate, methyl acetate,

ethyl acetate, acetone, ethyl nitrate, water vapor, methyl alcohol, nitromethane, propionitrile, acetonitrile. The results are of interest, independent of the discussion of f values given in Sec. IV, and are presented to show the dependence of conductivity on both pressure and temperature.

The variation of conductivity with pressure was found to be linear in all cases (see also references 1 and 12). Thus, at a given temperature,

$$K = K^0[1 + (\beta/100)p],$$

where K is the conductivity at pressure p (in atmospheres) and K^0 the (extrapolated) conductivity at zero pressure. β, the percentage increase in conductivity over a pressure range of one atmosphere, has a characteristic value for each vapor. Since typical measurements have already been reproduced in Figs. 2–6 of the previous paper,[1] the present results are not given in detail. Values of K^0 and β are summarized in Tables I and II; from these the conductivities of the various vapors at pressures up to one atmosphere may be computed.

The variation of K^0 with temperature is shown in Fig. 2, in which results of this and the earlier investigation have been collected. Where comparison is possible there is excellent agreement with the results of other workers.[12–14] It may be seen from Fig. 2 that, in general, the increase in conductivity of an organic vapor with temperature is steeper than linear (see reference 1, Appendix II).

IV. DISCUSSION

The extent to which the theoretical treatment outlined in the introduction agrees with the experimental results may be seen from Tables III and IV. "Observed" values of f (column VII) were obtained from Eq. (1) using K^0 values from Fig. 2, and published values of C_{v0} (column IV) and η (column V). Reliable figures for η and C_{v0} are scarce, and calculations are thus possible in only a few cases. Values of f_{Eucken} (see Eq. (3)) are shown in column VI.

It may be seen from Table III that, for *nonpolar vapors*, $f_{\text{obs}} > f_{\text{Eucken}}$; from this it follows that $f_{\text{int}} > 1$. Assuming $f_{\text{trans}} = 2.5$, values of f_{int} (column VIII) have been calculated from the experimental results using Eq. (2).

In Sec. I it was suggested that at lower temperatures $f_{\text{int}} < D\rho/\eta$, but should approach this value with increasing temperature as the exchange of internal energy becomes more rapid. Measurements of D for organic vapors are not available so that experimental values of $D\rho/\eta$ are unknown; however, experimental values of D for simple compounds yield $D\rho/\eta \approx 1.3$, the theoretical value for the Lennard-Jones (12:6) model. Since the intermolecular potential for nonpolar organic vapors is

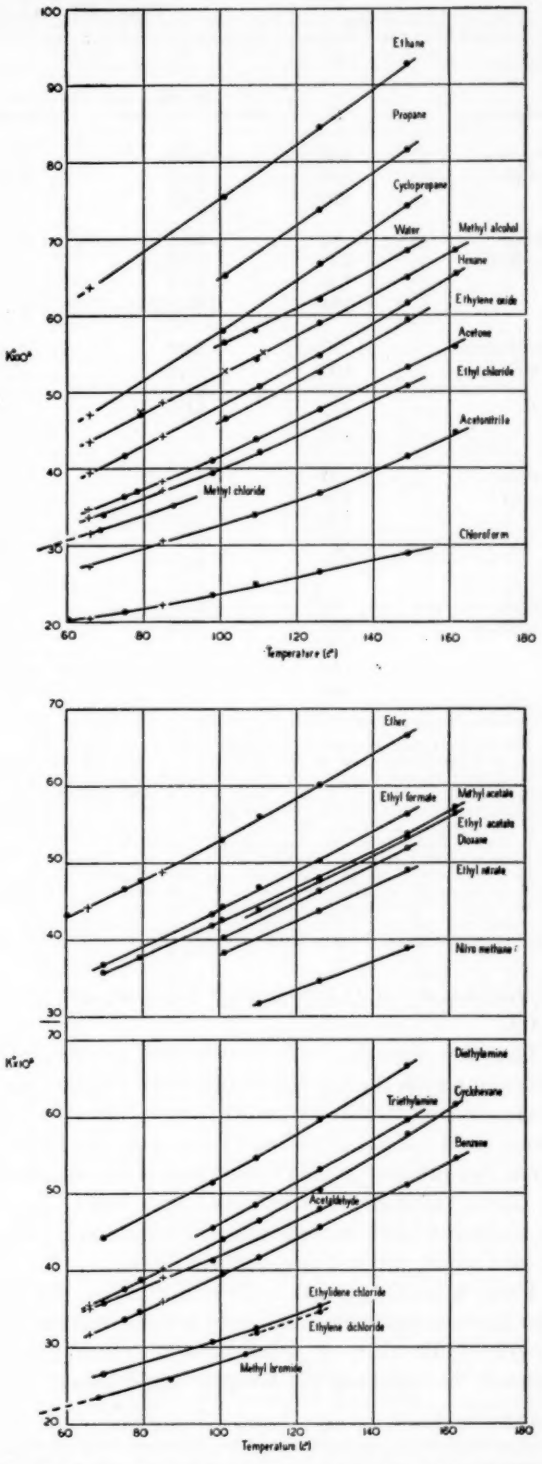

FIG. 2. The variation in the thermal conductivities of organic vapors with temperature. ● Present results and those of Vines (reference 1). + Results of Lambert, Staines, and Woods (reference 12) and Lambert and Scrivins (reference 13). × Results of Gazulla, Garcia, and Perez (reference 14). All results standardized by comparison with values for the conductivity of air given by Kannuluik and Carman (reference 10).

[12] Lambert, Staines, and Woods, Proc. Roy. Soc. (London) A200, 262 (1950).
[13] J. Scrivins, Ph.D. thesis (Oxford University, 1952).
[14] Gazulla, Garcia, and Perez, Z. Electrochem. 56, 569 (1952).

TABLE III. Values of f for nonpolar compounds.

I Substance	II T °C	III $K^0 \cdot 10^8$ cal cm^{-1} sec^{-1} deg^{-1}	IV C_{v_0} cal mole^{-1}	V $\eta \cdot 10^7$ g cm^{-1} sec^{-1}	VI $f_{\text{Eucken}} = 1 + 4.47/C_{v_0}$	VII $f_{\text{obs}} = K^0 M/\eta C_{v_0}$	VIII f_{int} [assuming $f_{\text{trans}} = 2.5$]
Propane	100	64.8	19.1$_5$[b]	1030[g]	1.23$_5$	1.45	1.25
$M = 44.1$	120	71.7	20.1	1080	1.22$_5$	1.45$_5$	1.27
	140	78.7	21.0$_5$	1130	1.21$_5$	1.46	1.29
Ethane	80	68.3	12.3$_5$[c]	1080[h,i]	1.36	1.54	1.24
$M = 30.0_5$	100	75.2	12.9$_5$	1140	1.34$_5$	1.53	1.24
	120	82.4	13.5$_5$	1195	1.33	1.52$_5$	1.25
	140	[89.6][a]	14.1$_5$	1255	1.31$_5$	1.51$_5$	1.25
Cyclohexane	80	38.9	[29.4][d]	830[g,h,j]	1.15	1.34	1.21
$M = 84.1_5$	100	43.9	31.3	870	1.14$_5$	1.35$_5$	1.24
	120	49.2	33.3	915	1.13$_5$	1.36	1.25
	140	54.8	35.2	960	1.12$_5$	1.36$_5$	1.26
	160	61.1	[37.1]	1005	1.12	1.38	1.28
Benzene	80	34.8	21.7$_5$[e]	900[h,j,k]	1.20$_5$	1.39	1.21
$M = 78.1$	100	39.4	23.2	950	1.19$_5$	1.39$_5$	1.23
	120	44.1	24.6	1000	1.18$_5$	1.40	1.25
	140	49.0	26.0	1045	1.17$_5$	1.40$_5$	1.27
	160	54.0	27.3	1095	1.16$_5$	1.41	1.28
Hexane	80	43.0	37.1$_5$[f]	745[k]	1.12	1.34	1.23$_5$
$M = 86.1_5$	100	48.0	39.0	790	1.11$_5$	1.34$_5$	1.25
	120	53.3	40.8	830	1.11	1.35$_5$	1.26$_5$
	140	59.0	42.5$_5$	875	1.0$_5$	1.36$_5$	1.28
	160	64.9	44.3	920	1.0	1.37	1.29

[a] The figures in brackets are less reliable than the other values.
[b] G. B. Kistiakowsky and W. W. Rice, J. Chem. Phys. **8**, 610 (1940).
[c] G. B. Kistiakowsky and W. W. Rice, J. Chem. Phys. **7**, 281 (1939); H. W. Thompson, Trans. Faraday Soc. **37**, 344 (1941).
[d] J. B. Montgomery and T. De Vries, J. Am. Chem. Soc. **64**, 2375 (1942); R. Spitzer and K. S. Pitzer, J. Am. Chem. Soc. **68**, 2537 (1946).
[e] Scott, Waddington, Smith, and Huffman, J. Chem. Phys. **15**, 565 (1947); J. B. Montgomery and T. De Vries, J. Am. Chem. Soc. **64**, 2375 (1942).
[f] G. Waddington and D. R. Douslin, J. Am. Chem. Soc. **69**, 2275 (1947).
[g] T. Titani, Bull. Chem. Soc. Japan **4**, 277 (1929); **5**, 98 (1930); **8**, 255 (1933).
[h] P. M. Craven and J. D. Lambert, Proc. Roy. Soc. (London) **A205**, 439 (1951).
[i] M. Trautz and K. G. Sorg, Ann. Physik. **10**, 81 (1931).
[j] A. G. Nasini, Proc. Roy. Soc. (London) **A123**, 686, 692, 704 (1929).
[k] McCoubrey, McCrea, and Ubbelohde, J. Chem. Soc. 1961 (1951). For hexane these measurements have been preferred to those of Craven and Lambert (reference h above) and Titani (reference g above), since the values of f_{int} obtained are more in keeping with the nonpolar character of the vapor. The latter measurements give abnormally low values, such as are found for polar vapors (see reference 6).

approximately of (12:6) form,[15] $D\rho/\eta$ should again be ~ 1.3.

The view that $f_{\text{int}} \rightarrow D\rho/\eta$ at higher temperatures is consistent with the results in Table III. In all cases f_{int} increases with temperature, the variation being from about (1.21−1.24) at 80° to (1.25−1.29) at 140°C. Of particular interest in this connection is the observation by Grilly[16] that at temperatures above 100°C $f_{\text{int}} \rightarrow 1.3$ for hydrogen, carbon monoxide, carbon dioxide, oxygen, nitrous oxide, nitric oxide, and methane.

There is another point to be noticed from Table III. The Eucken expression not only fails to reproduce the experimental values of f, but does not even reflect the trend of the values as the temperature is raised; except in the case of ethane, f_{obs} consistently increases with temperature whilst f_{Eucken} decreases. Together with the results above, this implies that at high temperatures there is considerable energy interchange in collisions between complex molecules. Ultrasonic measurements on organic vapors are in accord with this view.[17]

The increase in f_{obs} with temperature will not continue indefinitely. If f_{int} proceeds to a limit (possibly somewhat in excess of 1.3) the specific heat of the vapor will ultimately become the main factor determining the value of f; thus beyond a certain temperature f_{obs} should decrease. Such behavior has, in fact, been observed by Franck,[18] who has shown that the value of f exhibits a maximum for a number of simple gases.

The results for *polar vapors* are shown in Table IV. For strongly polar vapors (methyl alcohol, water, acetaldehyde, acetonitrile) the observed values of f are low; unlike the values for nonpolar compounds they are less than those calculated from Eq. (3). This is not because of a decrease in f_{int}, but is caused by the fact that for polar compounds f_{trans} falls below 2.5, the theoretical value for simple molecules. Schäfer[8] has shown that this

[15] This is shown, for example, by investigation of the reduced virial coefficients of nonpolar vapors (reference 1). It is true that agreement with experiment is here obtained only by assigning values for interaction energies and molecular diameters which have little physical significance; if more usual values are adopted deviations become apparent, particularly at lower temperatures (see E. A. Guggenheim, Revs. Pure Applied Chem. (Australia) **3**, 1 (1953); J. S. Rowlinson and J. R. Townley, Trans. Faraday Soc. **49**, 20 (1953)). Nevertheless, Rowlinson and Cook [Proc. Roy. Soc. (London) **A219**, 405 (1953)] have shown that these deviations are due primarily to orientation effects occurring in collisions between nonsymmetrical molecules, and that the prevailing intermolecular potential is still roughly of the (12:6) type.

[16] E. R. Grilly, Am. J. Phys. **20**, 447 (1952).

[17] J. D. Lambert and J. S. Rowlinson, Proc. Roy. Soc. (London) **A204**, 424 (1950).

[18] E. U. Franck, Z. Elektrochem. **55**, 636 (1951).

TABLE IV. Values of f for polar compounds.

I Substance	II T °C	III $K^0 \cdot 10^6$ cal cm^{-1} sec^{-1} deg^{-1}	IV Cv_0 cal mole^{-1}	V $\eta \cdot 10^7$ g cm^{-1} sec^{-1}	VI $f_{Eucken} = 1 + 4.47/Cv_0$	VII $f_{obs} = K^0M/\eta Cv_0$	VIII f_{int} [assuming $f_{trans} = 2.5$]	IX f_{trans} [assuming $f_{int} = 1.27$]	X "Reduced dipole energy" t
Ether	60	43.0	27.8$_5$[e]	840[m]	1.16	1.36	1.23	2.14	
$M = 74.1$	80	48.0	29.2	885	1.15$_5$	1.37$_5$	1.25	2.32	<0.2
	100	53.1	30.5	935	1.15	1.38	1.26	2.40	
	120	58.5	31.8	985	1.14	1.38$_5$	1.27	2.49	
Chloroform	60	20.1	14.5$_5$[d]	1160[n]	1.31	1.42	1.15	2.02	
$M = 119.4$	80	21.9	14.9$_5$	1225	1.30	1.43	1.17	2.07	
	100	23.9	15.3$_5$	1290	1.29	1.44	1.19	2.16	0.1
	120	26.0	15.7	1350	1.28$_5$	1.46	1.22	2.31	
	140	28.2	16.0$_5$	1415	1.28	1.48	1.25	2.43	
Ethyl chloride	40	28.7	12.9$_5$[e]	1020[o]	1.34	1.40$_5$	1.08	1.89	
$M = 64.5$	60	32.4	13.5	1080	1.33	1.43	1.13	2.02	
	80	36.2	14.1	1140	1.31$_5$	1.45	1.17	2.14	
	100	40.0	14.6$_5$	1205	1.30$_5$	1.46$_5$	1.20	2.24	0.2
	120	44.2	15.2$_5$	1265	1.29$_5$	1.48	1.23	2.34	
	140	48.5	15.8	1330	1.28$_5$	1.49	1.25	2.44	
Methyl chloride	40	27.8	8.00[d]	1140[n]	1.56	1.54	1.0	2.00	
$M = 50.5$	60	30.9	8.35[a]	1210	1.53$_5$	1.54	1.02	2.04	0.6
	80	34.0	8.70	1285	1.51$_5$	1.54	1.03	2.05	
Acetone	80	37.4	18.6[f]	900[m]	1.24	1.30	1.07	1.45	
$M = 58.0_5$	100	41.7	19.3	950	1.23$_5$	1.32	1.11	1.60	0.7
	120	46.2	20.1	1000	1.22$_5$	1.33$_5$	1.13	1.71	
	140	50.9	20.9$_5$	1050	1.21	1.34$_5$	1.15	1.79	
Methyl alcohol	80	47.3	9.53[g]	1165[m]	1.47	1.36$_5$	...	1.57	
$M = 32.0_5$	100	52.1	9.94	1230	1.45	1.36$_5$		1.59	
	120	57.2	10.34	1295	1.43$_5$	1.37		1.61	0.8
	140	62.5	10.75	1360	1.41$_5$	1.37		1.63	
	160	68.0	11.16	1425	1.40	1.37		1.64	
Water	100	[56.3][a]	6.14[h]	1220[p]	1.72$_5$	1.35	...	1.44	
$M = 18.0$	120	[60.8]	6.18	1295	1.72	1.36$_5$		1.47	1.2
	140	[65.9]	6.22	1370	1.71$_5$	1.39		1.52	
	100	[56.3]	6.14	1250[q]	1.72$_5$	1.32		1.38	
	120	[60.8]	6.18	1325	1.72	1.33$_5$		1.41	
	140	[65.9]	6.22	1405	1.71$_5$	1.36		1.45	
Acetaldehyde	40	30.1	11.5[i]	910[o]	1.39	1.26$_5$	...	1.27	
$M = 44.0_5$	60	34.0	12.0	970	1.37$_5$	1.28$_5$		1.35	
	80	37.9	12.5	1030	1.35$_5$	1.29$_5$		1.39	1.4
	100	42.0	13.0$_5$	1090	1.34	1.30		1.41	
	120	46.3	13.5$_5$	1150	1.33	1.31		1.46	
Acetonitrile	80	29.7	11.7[j]	850[o]	1.38$_5$	1.22$_5$	...	1.10	
$M = 41.0_5$	100	32.7	12.1$_5$	900	1.37	1.23		1.11	1.2
	120	35.8	12.5$_5$	950	1.35$_5$	1.23$_5$		1.12	
	140	[39.8]	13.0	1005	1.34$_5$	1.25		1.19	
Figures available at one temperature only									
Thiophene $M = 84.0$	110	[36.5][b]	20.1[k]	1075[r]	1.22	1.42	1.23	2.28	...
Ethyl acetate $M = 88.1$	137	50.4	[31.4][l]	1040[n]	1.14	1.36	1.24	2.37	...
Methyl acetate $M = 74.0_5$	137	51.0	[25.3][l]	1120[n]	1.17$_5$	1.33$_5$	1.18	1.81	...

[a] The figures in parentheses are less reliable than the other values.
[b] Conductivity value reported previously (see reference 1).
[c] W. H. Jennings and M. E. Bixler, J. Phys. Chem. **38**, 747 (1934). Experimental results corrected for gas imperfection (see Vines, reference 1). The values of Eucken and Franck (reference e below), which are uniformly ~1 cal higher, were taken as giving the correct temperature variation.
[d] R. D. Vold, J. Am. Chem. Soc. **57**, 1192 (1935).
[e] A. Eucken and E. U. Franck, Z. Electrochem. **52**, 195 (1948).
[f] Collins, Coleman, and De Vries, J. Am. Chem. Soc. **71**, 2929 (1949). Experimental results corrected for gas imperfection using equation $\log_{10}(-B) = 1.371 + 598.8/T$, where B, the second virial coefficient, is in cc/mole (Bennett, unpublished).
[g] J. S. Rowlinson, Nature **162**, 820 (1948).
[h] McCullough, Pennington, and Waddington, J. Am. Chem. Soc. **74**, 4439 (1952).
[i] K. S. Pitzer and W. Weltner, J. Am. Chem. Soc. **71**, 2842 (1949). See also C. F. Coleman and T. De Vries, J. Am. Chem. Soc. **71**, 2839 (1949).
[j] H. W. Thompson, Trans. Faraday Soc. **37**, 344 (1941).
[k] Waddington, Knowlton, Scott, Oliver, Todd, Hubbard, Smith, and Huffman, J. Am. Chem. Soc. **71**, 797 (1949).
[l] K. Bennewitz and W. Rossner, Z. Physik. Chem. **B39**, 126 (1938). Experimental results corrected for gas imperfection by the Berthelot equation.
[m] See references g and h of Table III.
[n] See reference g of Table III.
[o] See reference h of Table III.
[p] H. Braune and R. Linke, Z. Physik. Chem. **148**, 195 (1930). See also D. L. Timroth, J. Phys. U.S.S.R. **2**, 419 (1940).
[q] J. R. Partington, *An Advanced Treatise on Physical Chemistry. I* (Longmans Green and Company, New York, 1949), p. 859. See also H. Speyerer, Z. tech. Phys. **4**, 430 (1923).
[r] See reference j of Table III.
[s] From the Tables of Rowlinson (reference 20) and Craven and Lambert (reference 6).

results from configurational effects involved in the redistribution of translational energy in collisions between polar molecules, and that the decrease depends upon the dipole-moment, diameter, and moment of inertia of the molecules concerned. For the complex vapors considered here little reliance could be placed on calculations similar to those of Schäfer; however, values of f_{trans} have been obtained from the present experimental results, assuming as a rough approximation that $f_{int} = 1.27$ in all cases.[19] The results clearly show the over-all decrease in f_{trans} below the value of 2.5 (see the figures in Table IV, column IX for acetone, methyl alcohol, water vapor, acetaldehyde, and acetonitrile). The same effect, but less pronounced, may be observed in the results for weakly polar vapors (ether, chloroform, ethyl chloride, and methyl chloride).

Craven and Lambert[6] have shown that the decrease in f_{trans} corresponds roughly to the interaction between polar molecules as expressed by Rowlinson's "reduced dipole energy" t.[20] Comparison of values of t (column X) with those of f_{trans} shows that the present results are in agreement with this conclusion.[21]

As might be expected, the characteristics of weakly polar and nonpolar compounds are not very different. This is seen from Table IV (column VIII) where values of f_{int} for weakly polar compounds are given. These were calculated on the assumption that $f_{trans} = 2.5$, and may thus be compared with the corresponding results for nonpolar compounds in Table III. Since f_{trans} for polar vapors is undoubtedly <2.5, close agreement between the two sets of results is not to be expected. Nevertheless, at the higher temperatures the values for weakly polar vapors are not much lower than those for nonpolar vapors (compare $f_{int} = 1.25$ at 140°C for ethyl chloride and chloroform, with the average figure of 1.28 at 140°C in Table III).

It is clear that the results for both polar and nonpolar vapors can be interpreted qualitatively in this manner. However, the difficulties involved in any quantitative treatment would be serious and it is doubtful whether further extension along the present lines is warranted. The past success of the original Eucken formula [Eq. (3)] can now be fully understood. This was applied extensively at 0°C, at which temperature $f_{int} < D\rho/\eta$, being ~ 1 for many gases in accordance with Eucken's assumption. In view of the present results it seems unlikely that further work will lead to a simple formula relating thermal conductivities and viscosities, which will prove accurate over an appreciable temperature range.

[19] This value was chosen since f_{int} for nonpolar compounds is ~ 1.27 at 120°C (see Table III). The assumption is justified only as a very rough approximation since $D\rho/\eta$ for polar and nonpolar compounds may be somewhat different. Furthermore, the variation of f_{int} with temperature should also be considered, for f_{trans} is sensitive to the value of f_{int}, especially if C_{v0} is large (see reference 21).

[20] J. S. Rowlinson, Trans. Faraday Soc. **45**, 974 (1949).

[21] Since the variation of f_{int} with temperature has been neglected, the significance of this comparison is somewhat reduced. However, if it is assumed that f_{int} increases from ~ 1.23 at 80° to ~ 1.28 at 140°C as for nonpolar vapors, the variation with temperature in the calculated values of f_{trans} is correspondingly decreased; this emphasises the relationship between f_{trans} and t.

V. ACKNOWLEDGMENTS

The authors would like to thank Mr. J. D. Lambert for helpful comments in connection with this paper, and for permission to use unpublished conductivity results obtained in his laboratory by Dr. J. Scrivins. Special thanks are due Dr. J. S. Rowlinson for many valuable suggestions, and Dr. M. F. R. Mulcahy for useful advice regarding the presentation of the work.

APPENDIX: THE VARIATION OF CONDUCTIVITY WITH PRESSURE

For vapors of low molecular weight the effects of incomplete molecular accommodation are serious at high temperatures and persist even at pressures approaching one atmosphere. Thus the (very small) β values in Table II for ethane, propane, and cyclopropane could be in error by ± 50 percent. Similar considerations apply for methyl alcohol and water, but for these vapors the β values are large and the errors introduced negligible. With water vapor the electrical insulation of the apparatus appeared to fail even at 150°C; although the effect was very small at low pressures it is clear that the β values for water (and even the K^0 values which are obtained by extrapolation) may not be completely reliable. Nevertheless, the values given for K^0 are probably better than most others available at the present time. There was some indication that for water vapor the increase in conductivity with pressure might be more than linear at higher pressures. The effect was small and could possibly have been the result of the electrical breakdown mentioned above, a conclusion suggested by the fact that other authors[22,23] have observed a linear increase. On the other hand, the effect has a parallel in the behavior of methyl alcohol and other alcohols.[1,14] Furthermore, the variation in thermal conductivity with pressure is related to the variation in specific heat with pressure, which in the case of water vapor is definitely nonlinear.[24]

[22] S. W. Milverton, Proc. Roy. Soc. (London) **A150**, 287 (1935).

[23] Gazulla, Colomina, and Garcia, An. Soc. esp. Fis. Quim. B44, 1055 (1948).

[24] McCullough, Pennington, and Waddington, J. Am. Chem. Soc. **74**, 4439 (1952).

Electronic Structure of the Amylose-Iodine Complex

HIDEO MURAKAMI
Department of Chemistry, Faculty of Science, Osaka University, Osaka, Japan
(Received September 8, 1953)

The electronic structure of the amylose-iodine complex is studied on a different basis from that of the previous Stein-Rundle theory. First, the electron transfer from amylose oxygen to the iodine molecule is discussed from the viewpoint of Mulliken's intermolecular charge-transfer spectra. Then it is shown that the consideration of electronic interaction between neighboring iodine molecule ions and bond formation between oxygen and iodine gives a reasonable interpretation of bond number and absorption spectra. Last, the quantitative discussion of absorption spectra is performed by the application of the free-electron model to the system (I_4^{--}) which we consider to be the elemental unit in the polyiodine chain. The agreement between predicted and observed results is satisfactory if one considers the extreme simplification of the model.

INTRODUCTION

THE blue color of the starch-iodine complex is impressive and the nature of the complex has been studied numerous times since its discovery in 1812. Even at present, however, the problems of the starch-iodine complex are not completely solved. The most noticeable development in this field is the establishment of Hanes and Freudenberg's idea which postulates the helical structure of starch (amylose chain) and linear arrangement of iodine molecules in the internal channel of the helix. The experimental confirmation of this idea has been established by Rundle and his co-workers. The most important problem to be solved is the theoretical explanation of the nature of interaction in the complex. In order to explain the stability of the complex, Stein and Rundle postulated a cooperative effect which originated from dipolar interaction between induced dipoles in iodine molecules.[1] According to our quantitative analysis, however, Stein and Rundle's theory includes some unavoidable internal contradictions. Moreover, it is difficult to explain the observed interatomic distance between iodine atoms and the large intensity of absorption spectra from the standpoint of this theory.

Recently, Gilbert and Marriott carried out the new experiment of potentiometric titration in iodide solution and proved the entrance of the iodide ion together with the iodine molecule into the complex.[2] According to them, the predominant complex appears to be composed of groups of the type ($3I_2 \cdot 2I^-$) or (I_8^{--}). From this result, they suggested that the eight atoms might presumably be forming a linear resonating molecule which owed its characteristic powers of light absorption, and to some extent its stability, to the presence of two unlocalized electrons.

On the other hand, Rundle *et al.* discovered that the crystalline solid amylose could form the complex by absorbing the gaseous iodine molecules.[3] In this case, there is no room to consider the entrance of iodide ion, and it appears to contradict Gilbert's suggestion.

In the following, we discuss the electron transfer from oxygen atoms in amylose to iodine molecules, and Gilbert's suggestion is generalized to include the case of Rundle's solid complex. Considering electronic interaction between neighboring iodine molecule ions and the weak covalent bond formation between oxygen and iodine, the quantitative agreement between theoretical and experimental bond number is obtained. Moreover, by using the free-electron model, the satisfactory explanation of absorption spectra is given.

ELECTRON TRANSFER FROM AMYLOSE OXYGEN TO IODINE MOLECULE

When iodine is dissolved in ether or alcohol, a new strong absorption band appears in the near ultraviolet region. In relation to the study of the benzene-iodine complex, Mulliken postulated the complex formation between iodine and ether or alcohol, and explained this new band by the concept of intermolecular charge-transfer spectra.[4]

In the general theory of intermolecular charge-transfer spectra, developed by Mulliken, it is necessary to consider that a small amount of electron is transferred from one component to the other in the ground state.[5] This situation is expressed by writing the wave function of the ground state N of any molecular complex $A \cdot B$ as

$$\psi_N = a\psi_0 + b\psi_1. \tag{1}$$

Here, ψ_0 is a "no-bond" wave function with respect to covalent bonding, that is,

$$\psi_0 = \psi(A \cdot B), \tag{2}$$

and ψ_1 is a "dative" wave function corresponding to a transfer of an electron from B to A accompanied by the establishment of a weak covalent bond, that is,

$$\psi_1 = \psi(A^- - B^+). \tag{3}$$

In the present problem, iodine molecule corresponds to

[1] R. S. Stein and R. E. Rundle, J. Chem. Phys. **16**, 195 (1948).
[2] G. A. Gilbert and J. V. R. Marriott, Trans. Faraday Soc. **44**, 84 (1948).
[3] R. E. Rundle and D. French, J. Am. Chem. Soc. **65**, 558, 1707 (1943).
[4] R. S. Mulliken, J. Am. Chem. Soc. **72**, 600 (1950).
[5] R. S. Mulliken, J. Am. Chem. Soc. **74**, 811 (1952).

acceptor A, and ether or alcohol corresponds to donor B. Then, ψ_1 represents the structure in which an electron of the "lone pair" of the oxygen atom is transferred to iodine. In a loose complex such as alcohol-iodine or ether-iodine complex, the relation $a^2 \gg b^2$ is expected in Eq. (1), and the contribution of the structure as ψ_1 is rather small in the normal state.

As is well known, Mulliken's theory predicts the existence of an excited state which is expressed by the wave function

$$\psi_E = a^*\psi_1 - b^*\psi_0 \tag{4}$$

with $a^* \approx a$, $b^* \approx b$. Here, it is assumed that the coefficients a, b, a^*, b^* are chosen to satisfy the condition of normalization and orthogonality.

Using Eqs. (1) and (4), the dipole moment μ_{EN} of transition $N \rightarrow E$ is given by

$$\mu_{EN} = -e(\psi_E|r|\psi_N) \doteqdot a^*be(\bar{r}_B - \bar{r}_A) + (aa^* - bb^*)eS(\bar{r}_B - \bar{r}_{AB}), \tag{5}$$

where $\bar{r}_B$ and $\bar{r}_A$ denote, respectively, the average position of the electron in the B and A component, $\bar{r}_{AB}$ is situated midway between $\bar{r}_B$ and $\bar{r}_A$, and S is the overlap integral defined as

$$S = (\psi_0|\psi_1). \tag{6}$$

In the case of a loose complex, S may be exceedingly small.

Equation (5) enables us to estimate the order of magnitude of the transferred charge, if the experimental dipole moment is known. From the recent result by Ham, the observed oscillator strength f of charge-transfer spectra in t-butyl alcohol-iodine complex can be estimated as 0.36.[6] By using the well-known relation

$$f = 1.09 \times 10^{11} \nu Q_{EN}^2 \tag{7}$$

and $\nu = 42\,370\ \text{cm}^{-1}$, one obtains

$$\mu_{EN} = eQ_{EN} = 0.883e$$

as the experimental dipole moment.

In order to estimate the upper limit of transferred charge, we neglect the second term in the right-hand side of Eq. (5), that is,

$$\mu_{EN} \simeq a^*be(\bar{r}_B - \bar{r}_A) \tag{8}$$

or

$$Q_{EN} \simeq a^*b(\bar{r}_B - \bar{r}_A). \tag{8a}$$

As obtained above, $Q_{EN} = 0.883$, and we assume $a^* \simeq 1$, $\bar{r}_B - \bar{r}_A = 3.4\text{A}$ as reasonable values. Then it follows

$$b \simeq 0.26$$

or

$$b^2 \simeq 0.0676.$$

This result indicates that the upper limit of transferred charge in t-butyl alcohol-iodine complex is $0.0676e$ in the normal state. Of course, this value is not conclusive, since the experimental and assumed values of various parameters are not certain, though they are reasonable enough.

Now we return to the problems of the amylose-iodine complex. As it is easily inferred, if the iodine molecule enters the internal channel of the amylose helix, it may be surrounded by about six glucose residues. This situation has been confirmed by Rundle and his co-workers by using x-ray analysis.[3] At the present stage, however, the detailed form of the pyranose ring in the helical amylose is not determined. From the stereochemical point of view, we can consider the two chair forms and six boat forms. Freudenberg found that the two chair forms and only three boat forms could be used to construct the helical structure. From these five stereoisomers of helical amylose, Freudenberg picked out one structure which was constructed by one of the boat forms as shown in Fig. 1(a). In this model, the internal surface of amylose helix resembles a hydrocarbon in nature. According to Freudenberg, this situation explains the special affinity of amylose to the iodine molecule.[7]

As we mentioned in the foregoing, however, the oxygen atom also has a special affinity for the iodine molecule. From this point of view, Freudenberg's consideration is not conclusive. Moreover, the present knowledge about internal rotation predicts a large

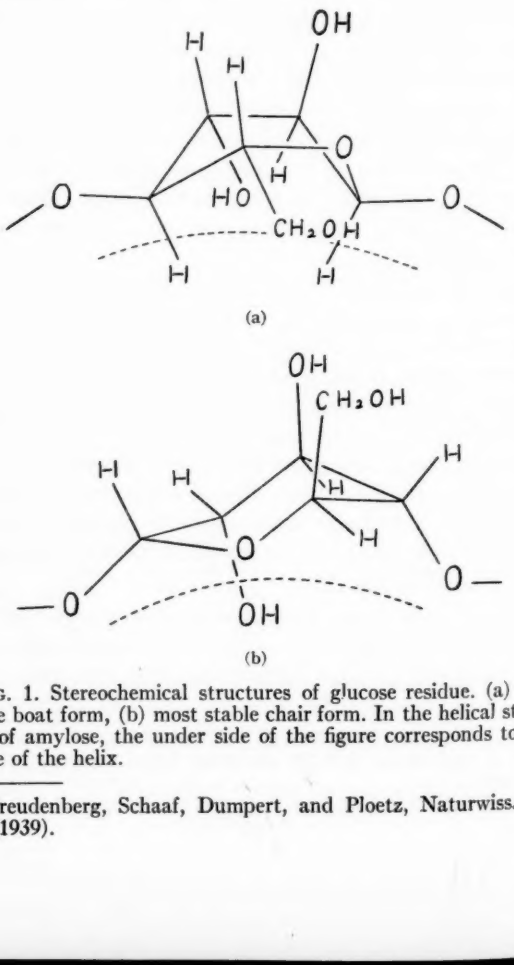

FIG. 1. Stereochemical structures of glucose residue. (a) Unstable boat form, (b) most stable chair form. In the helical structure of amylose, the under side of the figure corresponds to the inside of the helix.

[6] J. R. Ham, J. Chem. Phys. **20**, 1170 (1952).

[7] Freudenberg, Schaaf, Dumpert, and Ploetz, Naturwiss. **27**, 850 (1939).

instability of the boat form which includes the *cis*-configuration. In order to avoid this difficulty, we have to use the chair form of the pyranose ring which does not include the *cis*-configuration. According to the result of our examination, the most stable form of the glucose residue is the chair form which is shown in Fig. 1(b). In this structure, one of the hydroxyl groups projects into the channel of the helix. If the iodine molecule comes into this channel, the interatomic distance between hydroxyl-oxygen and iodine is about 3.2A. If we rotate the pyranose ring around the axis which connects the 1- and 4-carbon atoms, the distance mentioned in the foregoing may be lengthened somewhat; however, in compensating this loss, another bridge-oxygen atom in the pyranose ring comes nearer to iodine. In either case, we can expect the same situation as in alcohol-iodine or ether-iodine complex. Moreover, in the present case, iodine is surrounded by six or twelve oxygen atoms. Then, we can expect that a considerable amount of charge is transferred from the oxygen atoms of amylose to iodine. This situation probably corresponds to the concrete expression of residual affinity of bridge-oxygen, suggested by Barger.[8] Recently, Cramer also suggested in his study of "Einschlussverbindungen" that the internal channel of Schardinger dextrin might be "alkalisch" in quite a wide meaning.[9]

In order to estimate the upper limit of the transferred charge, we assume that every iodine molecule is surrounded by twelve oxygen atoms, and each oxygen atom donates electrons into the iodine molecule by the same amount as in the alcohol-iodine complex, that is, $0.0676e$. Then, the total charges which are transferred from amylose to iodine become $0.0676e \times 12 = 0.81e$ per iodine molecule. We must always remember that this value is rather an upper limit.

When the complex is formed in an iodide solution and iodide ions enter into the helix as is shown by Gilbert and Marriott, the amount of electron transferred from oxygen into the iodine may decrease considerably.

ELECTRONIC INTERACTION IN POLYIODINE CHAIN

It is well known that polyvinyl alcohol can form a complex with iodine which is similar in appearance and behavior to the amylose-iodine complex. (Polyvinyl alcohol has many hydroxyl groups!) In 1947, West studied the well-oriented polyvinyl alcohol-iodine complex together with some other polymer-iodine complexes by the x-ray method, and found the reflections characteristic of a one-dimensional lattice with period 3.10A.[10] According to West, this is the period of extended straight chains of iodine atoms which are lying parallel to the orientation of polymer. The interatomic distance 3.10A is much shorter than the unbonded separation of iodine atoms (4.3A) and somewhat greater than the single bond separation in an iodine molecule (2.67A). Considering these facts, West suggested that iodine atoms in the complexes mentioned in the foregoing might form bonds with each other at 180°, which are weaker than single covalent bonds but much stronger than van der Waals attractions, and called them linear polyatomic iodine or polyiodine for short.

Recently, Cramer studied the crystal of an α-dextrin (cyclohexaamylose)-iodine complex by using x-ray reflections, and came to almost the same conclusion as did West. The period 3.06A which is found by Cramer agrees with West's 3.10A within the experimental error.[11] Cramer found the same period 3.06A also in 2·6-diphenyl-pyrone-(4)-iodine complex. From these results, it may almost be sure that the iodine atoms are lying with a definite period 3.10A or 3.06A in the complexes mentioned in the foregoing and probably in amylose-iodine complex.

Now we examine the nature of interaction in these complexes (especially in the linear polyiodine chain) by using the concept of bond number. The experimental bond number is given by Pauling's empirical formula

$$R(1) - R(n) = 0.300 \log n, \tag{9}$$

where n is the bond number, $R(1)$ is the atomic radius in the case of a single bond, and $R(n)$ is the radius in the case of the bond in question.[12] Using $R(1) = 2.67\text{A}/2 = 1.335\text{A}$ and $R(n) = 3.10\text{A}/2 = 1.55\text{A}$ or $R(n) = 3.06\text{A}/2 = 1.53\text{A}$, we obtain $n = 0.192$ or $n = 0.224$. These results indicate that the experimental bond number is about 0.2, and iodine-iodine single bonding has nearly disappeared.

In Stein-Rundle's model, each iodine molecule should retain its original character (bond number, etc.) approximately, even in the internal channel of the amylose helix. Then, the equal spacing of the iodine atoms or the disappearing of single bond separation is rather surprising. Stein and Rundle pointed out, however, that if the complete resonance such as

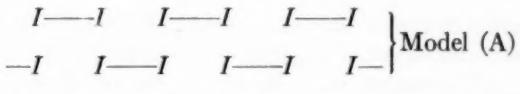

is assumed, equal spacing is not difficult to understand. According to Pauling's method, the bond number of any bond is defined as the number of shared electron pairs in it, and is expressed as a fraction corresponding to the existence of several bond diagrams when the concept of resonance is available. The foregoing definition predicts $n = 1.0/2 = 0.5$ for Model (A) of complete resonance, and the discrepancy between predicted and observed values is serious.

In order to exclude this difficulty, we construct the new model. According to the discussion in the last

[8] G. Barger, *Some Applications of Organic Chemistry to Biology and Medicine* (McGraw-Hill Book Company, Inc., New York, 1930).
[9] F. Cramer, Chem. Ber. **84**, 851 (1951).
[10] C. D. West, J. Chem. Phys. **15**, 689 (1947).
[11] F. Cramer, Chem. Ber. **84**, 855 (1951).
[12] L. Pauling, J. Am. Chem. Soc. **69**, 542 (1947).

section, we can expect the transfer of a considerable amount of the electron from the amylose oxygen to the iodine molecule. Then, as an idealized tentative model, we consider first the linear array of iodine molecule ions (I_2^-). The binding in the iodine molecule ion is due to a three-electron bond and, as is well known, its binding energy is approximately half of a single covalent bond.[13] Then, it is reasonable to assume that the effective bond number of the half-bond in (I_2^-) is 0.5. Now we consider the complete resonance such as

$$\left.\begin{array}{llll} I\text{---}I & I\text{---}I & I\text{---}I & \\ \text{--}I & I\text{---}I & I\text{---}I & I\text{--} \end{array}\right\}\text{Model (B)},$$

where I - - - I indicates (I_2^-). By this resonance effect, the bond number of any bond becomes $n=0.5/2=0.25$. This value is much closer to the experimental one ($\sim$0.20) than is the value (0.50) in Model (A). We must notice, however, that the predicted value is still slightly larger than the experimental one and that the assumed charge (1.00e per iodine molecule) exceeds the calculated upper limit of the transferred charge (0.81e).

In Model (B), the decrease of the charge on the iodine molecule causes the increase of the bond number. Then, in order to achieve the decrease of the charge and bond number simultaneously, we take into account the formation of weak covalent bonds between amylose oxygen atoms and iodine atoms. As the most promising one, we assume the model such as

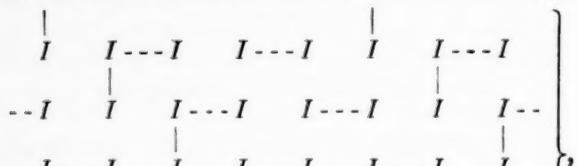

Model (C)

where I indicates the weak covalent bond formation between the amylose oxygen and the iodine atom and I - - - I indicates (I_2^-) in which we are expecting a three-electron half-bond as before. In Model (C), the transferred charge is 0.80e per iodine molecule (not to exceed the calculated upper limit!) and the bond number becomes $n=(0.5+0.5)/5=0.20$. (This agrees well with the experimental value!) As can be seen easily, the covalent bond between oxygen and iodine is very weak and resonating over all the oxygen atoms around the iodine chain. (Three-dimensional resonance!) Accordingly, there is no contradiction between this model and the experimental fact that the x-ray spacing of the halogen is unrelated to the fiber spacing of the polymer.

[13] L. Pauling, *Nature of the Chemical Bond* (Cornell University Press, Ithaca, 1940), see Chap. 8, Sec. 33a.

TABLE I. Data on the characteristic absorption band of the amylose-iodine complexes. (See reference 14.)

M	λ(A)	ΔE (ev)	ϵ
500	6280	1.964	43 000
450	6250	1.974	41 600
310	6220	1.983	41 400
250	6180	1.996	40 400
175	6050	2.039	40 100
85	5900	2.091	32 900
44	5800	2.127	25 400

M: Molecular size of amylose (number of glucose residues in amylose).
λ: Wavelength at absorption maximum.
$\Delta E=ch/\lambda$: Energy difference between excited and normal states.
ϵ: Molecular extinction coefficient per iodine molecule.

Oscillator strength per iodine molecule can be calculated by using the formula

$$f=4.32\times10^{-9}\int\epsilon_\nu d\nu\sim4.32\times10^{-9}\epsilon\Delta\nu.$$

If we use the largest value of ϵ in Table I and $\Delta\nu\sim6000$ cm^{-1} which is obtained from the absorption curve of Swanson (reference 23), it follows that

$$f\sim1.11.$$

Oscillator strength as a whole complex may be approximated by

$$f_c\sim f\times M/6.$$

Of course, this good agreement is rather fortuitous, because various electrostatic interactions are neglected, and, moreover, the contribution of electron configurations such as - - - - - - - $(5s)^2(5p)^5(6s)$ or - - - - - - - $(5s)^2(5p)^5(6p)$ is also neglected. We can infer, however, that the two factors mentioned in the foregoing tend to cancel with each other as concerns bond number, and the superiority of Model (C) will clearly be shown in the following discussion concerning absorption spectra.

QUALITATIVE DISCUSSION ON ABSORPTION SPECTRA

The absorption spectra of the amylose-iodine complexes have been studied experimentally by Rundle and his co-workers.[14] Their results are shown in Table I. They emphasize the shift of the absorption maximum towards red and the increase of the molecular extinction coefficient per iodine molecule with the increase of the chain length of the amylose. We emphasize, however, the following two points from the theoretical point of view.

(a) The variation of energy difference ΔE between the normal and excited states as the function of chain length is exceedingly small.

(b) The absolute value of absorption intensity per iodine molecule is very large, and comparable with those of organic dyes. Then, the total intensity for the whole complex—(intensity per iodine molecule)$\times$(number of iodine molecules in an amylose helix)—becomes exceedingly large.

Stein and Rundle considered that the characteristic absorption band of the amylose-iodine complex originates from the forbidden transition of the iodine molecule.[1] According to Mulliken, however, the absorption band of the iodine molecule in the visible region

[14] Baldwin, Bear, and Rundle, J. Am. Chem. Soc. 66, 111 (1944).

corresponds to the $N \rightarrow Q$ type transition, more precisely, ${}^1\Sigma_g^+ \rightarrow {}^3\Pi_0^+$. This transition is forbidden by the orthogonality of spin functions, and the observed intensity ($\epsilon \sim 1000$, $f \sim 0.015$) is explained as the effect of spin-orbit coupling.[15] In such a transition as this, it is very difficult to expect the large intensification of transition probability even if the electrostatic perturbation is as large as was expected by Stein and Rundle. (A strong electrostatic field tends to break up the spin-orbit coupling.) Accordingly, we postulate that the characteristic absorption band of the complex corresponds to the $N \rightarrow V$ type allowed transition.

First we consider Model (A). In this case, the electonic state is similar to that of a conjugated double bond system (for example, symmetrical cyanine dyes) except that the resonating electrons are rather σ electrons than π electrons. From the usual molecular orbital point of view, the secular equation for this system is given as follows:

$$\begin{vmatrix} W & \beta & & & & & \\ \beta & W & \beta & & & & \\ & \beta & W & \beta & & & \\ & & \beta & W & \beta & & \\ & & & \beta & W & \beta & \\ & & & & \beta & W & \\ & & & & & & \end{vmatrix} = 0, \qquad (10)$$

where β is the resonance integral and $W = \alpha - E$ in which α represents the Coulomb integral. When the iodine chain includes n iodine molecules, this equation gives $2n$ energy levels. Then the observed characteristic absorption band should be attributed to the electronic transition from level n to level $n+1$. In the case of polymethine or polyene, ΔE (or λ_{max}) of such a transition as the foregoing varies more remarkably than in the case of an amylose iodine complex as the function of chain length. This situation may probably indicate the inappropriateness of the assumed model.

Moreover, Kuhn and Kramers' sum rule predicts that the oscillator strength of this transition must not exceed 2, since only two electrons can exist in the molecular orbital of level n. (In this case, there is no degeneracy.) In fact, the experimental oscillator strength of the strongest band in polymethine or polyene seems to approach the upper limit ($2 \sim 3$) with an increase in chain length. On the other hand, the observed oscillator strength of the amylose-iodine complex as a whole molecule (total intensity) becomes larger with an increase in chain length, and there seems to be no upper limit. For example, when amylose is composed of about 500 glucose residues, the oscillator strength of the complex as a whole reaches about 90. This result seems decidedly to indicate the inappropriateness of the assumed model.

Next we consider Model (B). In this case also, one can expect an analogous secular equation. (Formally, there is no distinction.) Of course, the definition and numerical values of the Coulomb and resonance integrals change with the replacement of the single bond in Model (A) by a three-electron half-bond in Model (B). In the following, we call them the formal Coulomb integral and the formal resonance integral, respectively. Moreover, according to the existence of $3n$ σ electrons, one must consider the transition $3n/2 \rightarrow 3n/2+1$ or $(3n \pm 1)/2 \rightarrow (3n \pm 1)/2+1$. Even if these differences are taken into account, the same difficulties as those in Model (A) are inferred.

Now we consider Model (C). In this model, about $\frac{1}{5}$ of the total iodine atoms are forming weak covalent bonds with the oxygen atoms. That is, about $\frac{1}{5}$ of the total iodine atoms are chemically saturated on account of covalent bond formation with oxygen atoms. Then, in order to expect the electronic interaction between these iodine atoms and the neighboring iodine systems, one must consider the contribution of the $6s$ or $6p$ electrons. More precisely, one must take into account the electron configuration $\text{-------}(5s)^2(5p)^5(6s)$ or $\text{-------}(5s)^2(5p)^5(6p)$ in which one $5p$ electron is used for the covalent bond formation with oxygen atoms and an excess electron in the $(6s)$ or $(6p)$ orbital is available for the interaction with the neighboring iodine system.[16] We must notice, however, that the $(6s)$ or $(6p)$ orbital in the iodide ion mentioned in the foregoing spread extensively over the space, and the formal resonance integral γ between this orbital and the usual $(5p\sigma)$ orbital becomes much smaller than the formal resonance integral β in the case of model (B). Then, the secular equation for the iodine system becomes as follows:

$$\begin{vmatrix} \gamma & & & & & & & \\ \gamma & V & \gamma & & & & & \\ & \gamma & W & \beta & & & & \\ & & \beta & W & \beta & & & \\ & & & \beta & W & \beta & & \\ & & & & \beta & W & \gamma & \\ & & & & & \gamma & V & \gamma \\ & & & & & & \gamma & W \\ & & & & & & & \beta \end{vmatrix} = 0, \qquad (11)$$

[15] R. S. Mulliken, Phys. Rev. **57**, 500 (1940).

[16] We neglect the contribution of the electron configurations such as $\text{-------}(5s)^2(5p)^4(6s)$, $\text{-------}(5s)^2(5p)^4(6p)$ (excited states) or $\text{-------}(5s)^2(5p)^4$ (ionized state) since these states correspond to very high energy.

where $V=\alpha^*-E$ and α^* is the formal Coulomb integral because of the contribution of the excited orbitals mentioned in the foregoing.

If we put

$$\gamma=0$$

as an idealized limiting case, Eq. (11) is resolved into the classes of equations of the types as follows:

$$V=0$$

$$\begin{vmatrix} W_i & \beta_{i,i+1} & & \\ \beta_{i+1,i} & W_{i+1} & \beta_{i+1,i+2} & \\ & \beta_{i+2,i+1} & W_{i+2} & \beta_{i+2,i+3} \\ & & \beta_{i+3,i+2} & W_{i+3} \end{vmatrix}=0, \qquad (12)$$

where the suffix i is arbitrary. In the roughest approximation, the absorption spectra of the amylose-iodine complex can be discussed by Eq. (12). Strictly speaking, however, γ is not zero, though it may be small enough, and Eq. (11) will explain the very small variation of the energy difference ΔE between the normal and excited states as the function of the chain length. [Equation (10) will predict the much larger variation of ΔE as the function of the chain length.] We must remember that the suffix i in Eq. (12) is rather variable than constant, depending on the existence of a three-dimensional resonance; in other words, the covalent bond between the iodine atom and the amylose oxygen is moving from one position to the other. We can infer, however, that the speed of this movement is smaller than the speed of the electronic oscillation in the conjugated part of the polyiodine chain. This situation will probably justify the establishment of Eqs. (11) and (12).

According to the foregoing discussions, the whole system of the polyiodine chain can be approximated as an assemblage of rather small electronic systems which are expressed by Eq. (12). In this case, Kuhn and Kramers' sum rule is applicable to the individual small electronic system, and the total oscillator strength can become larger by any amount, depending upon the increase in chain length. (No upper limit!) This conclusion corresponds well with experimental results.

QUANTITATIVE DISCUSSION OF ABSORPTION SPECTRA

In the last section, we have shown that the electronic structure of the polyiodine chain can be approximated as an assemblage of elemental unit systems which are expressed by Eq. (12), that is, the systems (I_4^{--}). (In practice, there may be some degree of fluctuation, and it may contribute to the broadness of the absorption band together with nonuniformity of the amylose chain length.) Then we can infer that the main features of the absorption spectra are involved in Eq. (12). According to the previous experience, however, a simple molecular orbital method is not adequate for the quantitative study of spectroscopic problems. At least, it is necessary that the product of the molecular orbitals be antisymmetrized. Moreover, the evaluation of various integrals is rather complicated in the case of $5p$ orbitals. Accordingly, it is desirable to use a method which is independent of the actual form of each atomic orbital and which bears the quantitative consideration. The free-electron model which was developed by Bayliss,[17] Kuhn,[18] and others seems to be exceedingly suitable for this requirement.

Kuhn applied this model to the π-electron system of symmetrical polymethines such as the symmetrical cyanine dyes. To calculate the spectroscopic quantities, he assumed the one-dimensional potential box in which the potential was constant along the conjugated chain of length L and rose to infinity at the ends. The Schrödinger equation for the electron which is enclosed in this potential box can easily be solved, and the eigenvalue of energy is given as

$$E_n=\frac{h^2n^2}{8mL^2}, \qquad (13)$$

where n is the quantum number, h is Planck's constant, and m is the mass of the electron. Then, the wavelength of the transition $(n\rightarrow n+1)$ is given by

$$\lambda=\frac{8mc}{h}\frac{L^2}{2n+1}. \qquad (14)$$

The oscillator strength f of this transition is given as follows:

$$f=\frac{8}{3\pi^2}\frac{N^2(N+2)^2}{(N+1)^3}, \qquad (15)$$

where N is the number of electrons in the potential box.

If one remembers the exceeding simplicity of the assumed model, the excellent agreement between calculated and observed values is rather surprising. As for reasons which produce such agreement, we can probably enumerate the following situations which occur in symmetrical polymethine dyes. (1) π electrons of these dyes have a relatively low ionization potential, and consequently have large mobility. (2) In these dyes, the two principal resonance formulas in bond diagram are symmetrical; accordingly, all the bonds have equal bond numbers and the interatomic distances of these bonds are equal except for the differences in the radii of carbon and nitrogen. In the polyenes which are treated by Bayliss, this condition is not satisfied, and according to Kuhn, the model assumed in the foregoing of a simple potential box is no longer permissible.

Now we become aware that these conditions are satisfied also in the present problem except that the electrons are σ type instead of π type. We must notice, however, that even if these conditions are satisfied, electrons in the system are not as free as they are

[17] N. S. Bayliss, J. Chem. Phys. **16**, 287 (1948).
[18] H. Kuhn, J. Chem. Phys. **16**, 840 (1948); **17**, 1198 (1949).

assumed in Kuhn's model, and the effect due to the molecular core or to the interaction between electrons effectively diminishes the length L.[19] As is seen from Eq. (14), wavelength λ is very sensitive to the value of L, and we must estimate the reasonable effective length L before the application of Eq. (14) to the (I_4^{--}) system.

As a simple and intimate example, we consider the tri-iodide ion. According to Mooney, the (I_3^-) ion has a nearly linear configuration, and the two interatomic distances have slightly different values, that is $d_1=2.82$A and $d_2=3.10$A.[20] Then, L is expressed as follows:

$$L=d_1+d_2+\delta.$$

Considering the diminishing of effective length L, which was discussed in the foregoing, we assume a relatively small value for δ; i.e., $\delta=d_0/2=1.34$A where d_0 is the interatomic distance in the iodine molecule. This assumption gives us $L=7.26$A. Strictly speaking, the condition $d_1\neq d_2$ conflicts with the condition (2), mentioned in the foregoing, however, the difference between d_1 and d_2 is relatively small, and as a rough approximation, we apply Eqs. (14) and (15). The calculated value is $\lambda=3479$A, $f=1.24$, respectively, for $n=2$, $N=4$. According to the experimental result of Awtrey and Connick,[21] the (I_3^-) ion has two absorption bands in the near ultraviolet region:

$$\left.\begin{aligned}\lambda_1&=3530\text{A}\quad f_1=0.475\\ \lambda_2&=2875\text{A}\quad f_2=0.743\end{aligned}\right\}f=1.22.$$

The calculated values correspond relatively well with λ_1 and the total oscillator strength f. Recently, Friedman pointed out that the separation of the two peaks (6450 cm^{-1}) was roughly the difference in energy (7600 cm^{-1}) of the two lowest electronic states of the iodine atoms.[22] From this point of view, the agreement between calculated λ and observed λ_1 or between calculated f and observed total oscillator strength $f=f_1+f_2$ is reasonable enough.

Now, we calculate the wavelength of the system (I_4^{--}) which we consider the elemental unit in the polyiodine chain of the complex. By using Cramer's data $d=3.06$A and the same δ as before, we obtain

$$L=3d+\delta=10.52\text{A},$$

and then, from Eq. (14), $\lambda=5214$A for $n=3$. According to Swanson's experiment, which traces the absorption maximum during the hydrolysis of the amylose in the presence of iodine-iodide, the extrapolated wavelength for the shortest iodine chain becomes about 5200A.[23] This result agrees very well with the value calculated in the foregoing. For larger systems such as (I_6^{---}), (I_8^{--}), ----- the calculated wavelength becomes very large. Consequently, as a first approximation, the postulate of (I_4^{--}) as an elemental unit in the polyiodine chain may be a reasonable one.

Next, we consider the absorption intensity. In case of the system (I_4^{--}), Eq. (15) predicts $f=1.81$ for $N=6$. Remembering the construction of Model (C), one obtains $f_0=1.81\times 2/5=0.724$ as the oscillator strength per iodine molecule. On the other hand, the experimental value per iodine molecule is about 1.1 as is seen from Table I, and is considerably larger than the calculated value. If this excess is significant, it may be explained by considering the correction due to Lorentz and Lorentz' interaction between the neighboring elemental units in a polyiodine chain.[24] In the present model, the transition is allowed, with an electric vector which oscillates in the direction of the chain axis. This agrees with the experimental result of the double refraction of flow.[25]

From the foregoing discussions, it is expected that the absorption intensity per iodine molecule may be approximately constant regardless of the length of the polyiodine chain. According to the experimental result of Baldwin, Bear, and Rundle, however, the molecular extinction coefficient per iodine molecule is very sensitive to the change in the amylose chain length, especially in a relatively short chain.[14] We consider that this fact originates from the statistical situation in solution. In the foregoing experiment, the molecular extinction coefficients ϵ are determined for the total iodine molecules which are dissolved in water. (Experimental condition is $0.0001N$ with respect to iodine and 0.01 percent with respect to starch.) Therefore, we can infer that some portion of the iodine molecules is free from complex formation. If we express the number of iodine molecules of this portion by k and that of total iodine molecules by N, the apparent molecular extinction coefficients ϵ which correspond to the observed value may be given as follows:

$$\epsilon=\epsilon_c\cdot(N-k)/N, \tag{16}$$

where, ϵ_c is the true molecular-extinction coefficient. In this equation, the contribution of the weak absorption band of free iodine is neglected.

Now we consider the equilibrium between the free iodine and the complex. One of the simplest type of equilibrium is given by the following tentative model. We assume that each helix contains n molecules of I_2 (or corresponding $2I^-$) when it is completely filled. In the case of a solution, however, we can infer that $\alpha/2$ of I_2 (or $2I^-$) as a statistical mean, are escaping

[19] G. Araki and T. Murai, Prog. Theoret. Phys. (Japan) **8**, 639 (1952).
[20] R. C. L. Mooney, Z. Krist. **90**, 143 (1935).
[21] A. D. Awtrey and R. E. Connick, J. Am. Chem. Soc. **73**, 1842 (1951).
[22] H. L. Friedman, J. Chem. Phys. **21**, 319 (1953).
[23] M. A. Swanson, J. Biol. Chem. **172**, 825 (1948). (See Fig. 6 of this paper.)
[24] N. Q. Chako, J. Chem. Phys. **2**, 644 (1934).
[25] R. E. Rundle and R. R. Baldwin, J. Am. Chem. Soc. **65**, 554 (1943).

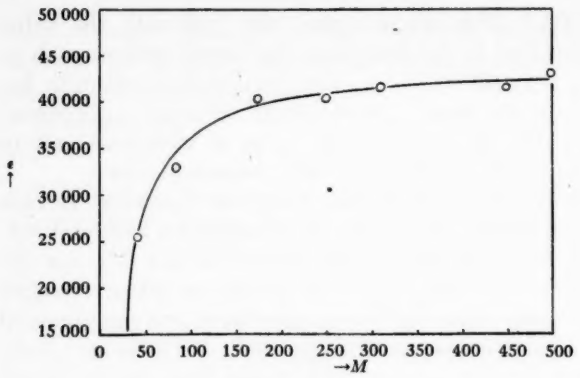

FIG. 2. Molecular extinction coefficient of the complex as the function of the amylose chain length. The full line is the theoretical curve and the small circles represent the experimental values. $\alpha=3$, $\epsilon_c=44\,000$, $n\simeq M/6$.

into the solution from both ends of the helix, respectively. Then we can expect the relation

$$k=\alpha N/n \qquad (17)$$

as long as the chain length of the amylose is uniform and all the amylose molecules are completely coiled into helices from one end to the other.[26] Introducing Eq. (17) into Eq. (16), it follows that

$$\epsilon=\epsilon_c\cdot(1-\alpha/n). \qquad (18)$$

The numerical result of this equation for $\alpha=3$ and $\epsilon_c=44\,000$ is shown in Fig. 2 together with observed values (see Table I). The agreement between the experimental and theoretical values is very good. The foregoing consideration may also give a reasonable explanation for the iodine activity as the function of chain length in the case of a potentiometric titration. A detailed study of this problem will be reported later.

The author wishes to express his sincere thanks to Professor S. Akabori for his encouragement and interest in the course of this study and also to Mr. B. Hagihara and Mr. E. Huwa for their valuable discussions.

[26] The latter condition may be true when the temperature is low enough or when the amylose helices are forming microcrystals in which both ends of the helices are contacting directly with the solution. If we assume the microcrystal formation of the completely filled amylose helices, the special stability of these completely filled helices may be explained without considering the cooperative effect which was discussed by Stein and Rundle. (See reference 1.)

Statistical Thermodynamics of Associated Solutions

J. A. BARKER AND F. SMITH
Division of Industrial Chemistry, Commonwealth Scientific and Industrial Research Organization, Melbourne, Australia

(Received July 16, 1953)

Thermodynamic data for the solutions chloroform+benzene, acetone+chloroform, ethanol+chloroform, ethanol+acetone, and ethanol+ether are discussed in the light of a model for associated solutions which has been described previously. The theory in its original form, previously found satisfactory for solutions of alcohols in nonpolar solvents, proves satisfactory for the first two of these systems. To interpret the data for the remaining more complicated systems it is necessary to generalize the model to allow for interaction free energies which depend on temperature (presumably because of changes in vibration frequencies). The necessary generalization of the theory is described, and a consistent set of interactions for the ethanol systems is derived. The generalized theory should apply, with the limitations inherent in lattice theories, to most nonaqueous associated solutions.

I. INTRODUCTION

SOLUTIONS of nonelectrolytes may be classified generally as (i) "nonpolar" solutions, characterized by spherically symmetrical interactions between molecules; (ii) "polar" solutions, characterized by orientation-dependent interactions which are not highly localized in the molecules, and which are often weak compared with kT; the dipole-dipole interaction is typical; (iii) "associated" solutions, characterized by strong, highly localized intereactions, of which the hydrogen bond is typical.

The theory of nonpolar solutions is highly developed,[1] and some progress has been made with the theory of polar solutions by treating the orientation-dependent interaction as a perturbation.[2] For associated solutions, with which we are concerned here, a simple model has been described and used previously.[3-6] A similar approach has been used by Tompa.[7] In this paper we interpret experimental data for five systems in terms of our model. Our purpose is to seek the limits of applicability of the model, and to determine how the model may usefully be modified.

In the model as originally described[3] a set of "contact points" on a given molecule were assumed to be in contact with similar points on neighboring molecules. Actually these points must move, or vibrate, about actual contact, and if there are changes in the extent of movement possible, or in the vibration frequencies, then there must be entropy changes in addition to those described by the original theory. One can take account of these facts phenomenologically by regarding the interactions U of reference 3 as free energies rather than as pure energies, thus permitting them to vary with temperature, but not with composition. This suggestion was first made by Guggenheim.[8] The formation of a given kind of intermolecular contact then involves a heat change H and entropy change S, given by

$$H=U-T\partial U/\partial T \tag{1}$$

$$S=-\partial U/\partial T. \tag{2}$$

For a hydrogen bond, for example, one would expect the entropy S to be negative, since the freedom of movement is reduced on forming the bond.

If this generalization is permitted, the formulas previously derived for H_x^M and TS_x^E must be modified, although that for G_x^E is unchanged. One finds*

$$G_x^E=\sum_A x_A\mu_A^E \tag{3}$$

$$\mu_A^E=RT[\sum_\mu Q_\mu^A \ln(X\mu^A/x_A X_\mu^{A1}) + (\tfrac{1}{2}z-1)r_A \ln(\sum_B r_B x_B/r_A)] \tag{4}$$

$$H_x^M=2\sum_A\sum_{\mu>\nu}(X_\mu^A X_\nu^A - x_A X_\mu^{A1} X_\nu^{A1})\eta_{\mu\nu}^{AA}H_{\mu\nu}^{AA} + 2\sum_{A\neq B}\sum_{\mu>\nu} X_\mu^A X_\nu^B \eta_{\mu\nu}^{AB}H_{\mu\nu}^{AB} \tag{5}$$

$$TS_x^E=H_x^M-G_x^E, \tag{6}$$

where $H_{\mu\nu}^{AB}$ is defined as in Eq. (1), and all other symbols are defined as before.[3] The quantities $\eta=\exp(-U/kT)$, formerly regarded as pure Boltzmann factors, are now to be regarded as partition functions for bending and stretching of intermolecular contacts.

We have introduced this generalization of the theory primarily because it is required by the experimental

[1] E. A. Guggenheim, Discussions Faraday Soc. **24**, 15 (1953).
[2] J. A. Pople, Discussions Faraday Soc. **15**, 35 (1953).
[3] J. A. Barker, J. Chem. Phys. **20**, 1526 (1952).
[4] Barker, Brown, and Smith, Discussions Faraday Soc. **15**, 142 (1953).
[5] J. A. Barker and W. Fock, Discussions Faraday Soc. **15**, 188 (1953).
[6] J. A. Barker, J. Chem. Phys. **21**, 1391 (1953).
[7] H. Tompa, J. Chem. Phys. **21**, 250 (1953).
[8] E. A. Guggenheim, Trans. Faraday Soc. **44**, 1007 (1948).

* Equation (5) is derived by differentiating (3) and (4) and the equations (see reference 3) defining X_μ^A; one uses the fact, which is readily established, that if variables X_i are determined by equations

$$X_i\sum_k \eta_{ik}X_k=Q_i,$$

where $\eta_{ik}=\eta_{ki}$, and η_{ik} and Q_i depend on a parameter ξ, then

$$\sum_i Q_i\partial \ln X_i/\partial\xi=\tfrac{1}{2}\sum_i \partial Q_i/\partial\xi-\sum_{i>k} X_iX_k\partial\eta_{ik}/\partial\xi.$$

facts. While the experimental data for chloroform +benzene and acetone+chloroform can be interpreted satisfactorily in terms of interactions U which do not depend on temperature, the data for the more complicated systems we have studied cannot be so interpreted, and we have therefore used the generalized theory for these three systems.

II. THE SYSTEM CHLOROFORM+BENZENE

(a) Experimental Data

The values of G_x^E, H_x^M, and TS_x^E at 25°C given by Kireev and Sitnikov[9] were used.

(b) Theory

As basic geometric model we assume that both chloroform and benzene molecules occupy 4 sites on a diamond lattice ($z=4$). This is a reasonable picture of chloroform, and we use the same picture for benzene since the molar volumes are roughly equal. Of the 10 contact points of chloroform we assume 1 to be hydrogen-like (H) and 9 to be chlorine-like (Cl). For benzene we assume that the electron-rich center of the ring is associated with 2 contact points (one on each side of the ring) which we label E. The remaining 8 contact points, assumed equivalent, are labeled B. We set all interactions between like molecules equal to zero, thereby neglecting any co-operative orientation in either pure component. The interaction energy between unlike molecules is assumed to have a small value U_2 (corresponding to the van der Waals interaction) except for contacts between chloroform hydrogen and the center of the benzene ring ($H-E$ contacts) which are assumed to have a relatively strong attractive interaction, called for convenience U_1+U_2. In summarized form all this may be written:

Lattice: $z=4$.

Benzene (B): $r_B=4$, $Q_E=2$, $Q_B=8$.

E is center of benzene ring, B is outer part of ring.

Chloroform (C): $r_C=4$, $Q_{Cl}=9$, $Q_H=1$.

Cl is chlorine, H is hydrogen.

Interactions:

$B-B$, $B-E$, $E-E$, Cl−Cl, Cl−H, H−H	zero
$B-$Cl, $B-$H, $E-$Cl	U_2
H$-E$	U_1+U_2.

We will not describe the calculation of G_x^E, H_x^M, TS_x^E for given values of U_1 and U_2, which involves straightforward application of the equations given previously[3] (or, in appropriate cases, of the modified equations given in the introduction). We will mention, however, a method of dealing with the small van der Waals interaction U_2, which has been used throughout this paper. It is found in practice that the effect of U_2 on TS_x^E is negligible, and that the contribution of U_2 to G_x^E and H_x^M is given with sufficient accuracy by

$$\Delta G_x^E=\Delta H_x^M=2(X_BX_{Cl}+X_EX_{Cl}+X_BX_H+\eta_1X_EX_H)U_2, \quad (7)$$

where X_B, X_{Cl}, etc., are calculated with $U_2=0$ [and therefore with $\eta_2=\exp(-U_2/kT)=1$]. Thus one may carry through the whole calculation with $\eta_2=1$, and afterwards add the contributions given by (7).

We determined first the value of U_1 which gave the correct value of TS_x^E for the equimolar mixture, and then the value of U_2 which gave the correct values of G_x^E and H_x^M for the equimolar mixture. The results were

$$U_1=-880 \text{ cal/mole}, \quad U_2=14 \text{ cal/mole}.$$

Theoretical values calculated with these interactions are compared with experimental data in Fig. 1.

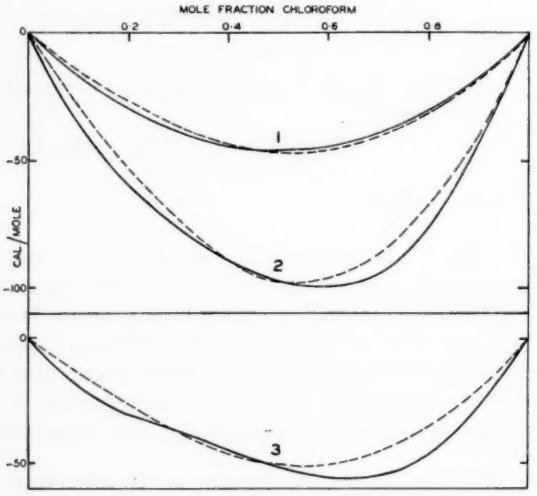

FIG. 1. Chloroform+benzene, 25°C. Solid lines experimental values, dotted lines theoretical.

1. G_x^E. 2. H_x^M. 3. TS_x^E.

Theoretical values calculated with $U_1=H_1=-880$ cal/mole, $U_2=H_2=14$ cal/mole.

(c) Remarks

The dissymmetry in the theoretical curves is in the same sense as that in the experimental curves, though not quite so marked. The agreement is generally satisfactory.

If we assume that the van der Waals interaction for the system benzene+carbon tetrachloride is the same as for benzene+chloroform, then our value $U_2=14$ cal/mole gives $G_x^E=36$ cal/mole for an equimolar mixture of benzene and carbon tetrachloride at 25°C. Scatchard's measurements[10] gave $G_x^E=20$ cal/mole. Thus our value of U_2 is at least of the right order of magnitude.

[9] V. A. Kireev and I. P. Sitnikov, J. Gen. Chem. U.S.S.R. **16**, 979 (1946).

[10] Scatchard, Wood, and Mochel, J. Am. Chem. Soc. **62**, 712 (1940).

III. THE SYSTEM ACETONE+CHLOROFORM

(a) Experimental Data

Values of G_x^E were calculated from the data of Zawidsky[11] at 35.2°C and of Rosanoff and Easely[12] at 68°C (actually the latter data were measured at constant pressure, but the temperature variation is small, and the average temperature 68°C is close enough for our purpose). Corrections for vapor nonideality were applied using virial coefficients for the components measured by Lambert *et al.*;[13] to estimate the mixture virial coefficient β_{12} it was assumed that $\delta_{12}=2\beta_{12}-\beta_{11}-\beta_{22}$ had the same value at the same temperature as that for the similar system chloroform+ether, for which measurements have been made by Fox and Lambert.[14] It was assumed that the temperature and concentration dependence of G_x^E could be expressed by the equation

$$G_x^E=x_1x_2[a+b(x_1-x_2)]$$

with

$$a=a_0+a_1T+a_2\ln T$$
$$b=b_0+b_1T+b_2\ln T$$

and the constants were determined to be consistent with the two sets of data mentioned above, as well as with Hirobe's[15] values of H_x^M at 25°C. Finally, values of G_x^E, H_x^M, TS_x^E at 25°C were calculated from the equation.

(b) Theory

The model for this system is identical with that for chloroform+benzene. Here the contact points labeled E represent hydrogen-bonding sites on the oxygen atom. With identical methods we found

$$U_1=-1930 \text{ cal/mole}, \quad U_2=72 \text{ cal/mole}.$$

Experimental and theoretical values of G_x^E, H_x^M, and TS_x^E are compared in Fig. 2.

(c) Remarks

The dissymmetry of the experimental curves is reproduced satisfactorily by the theoretical curves. The "hydrogen bond" interaction U_1 is stronger than the corresponding interaction with benzene, as one might have expected.

We have neglected the dipole interaction, and resulting state of co-operative orientation, in pure acetone. The dipole interaction may explain the unusually large value of the van der Waals interaction U_2.

[11] J. Zawidsky, Z. physik. Chem. **35**, 129 (1900).
[12] M. A. Rosanoff and C. W. Easeley, J. Am. Chem. Soc. **31**, 979 (1909).
[13] Lambert, Roberts, Rowlinson, and Wilkinson, Proc. Roy. Soc. (London) **A196**, 113 (1949).
[14] J. H. P. Fox and J. D. Lambert, Proc. Roy. Soc. (London) **A210**, 557 (1952).
[15] H. Hirobe, Tokyo Imp. Univ. J. Fac. Sci. **1**, 155 (1926).

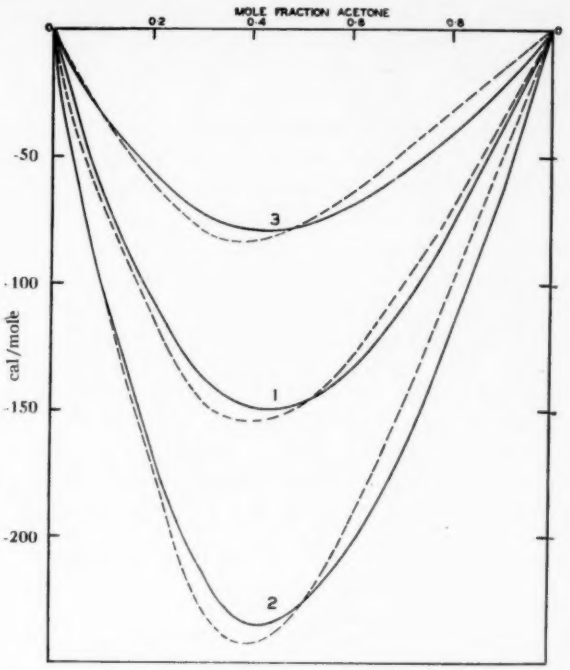

FIG. 2. Acetone+chloroform, 25°C. Solid lines experimental values, dotted lines theoretical.

1. G_x^E. 2. $\frac{1}{2}H_x^M$. 3. $\frac{1}{4}TS_x^E$.

Theoretical values calculated with $U_1=H_1=-1930$ cal/mole, $U_2=H_2=72$ cal/mole.

IV. THE SYSTEM ETHANOL+CHLOROFORM

(a) Experimental Data

The values of G_x^E at 55°C, 45°C, and 35°C given by Scatchard and Raymond[16] were extrapolated to give values at 25°C, which were used in conjunction with Hirobe's[15] values for H_x^M at 25°C. We have preferred to use Hirobe's calorimetric heats of mixing rather than those derived from the G_x^E measurements by Scatchard and Raymond.

(b) Theory

Lattice: $z=4$.

Ethanol (A): $r_A=3$, $Q_H=1$, $Q_O=2$, $Q_I=5$.

H is hydroxyl hydrogen, O is oxygen, I is hydrocarbon.

Chloroform (C): as before, but chloroform hydrogen labelled h.

Interactions:

H−I, O−I, H−H, O−O, I−I, Cl−Cl, Cl−h, h−h	zero
H−O	U_1
h−O	U_2+U_3
H−Cl, O−Cl, I−Cl, H−h, I−h	U_3.

[16] G. Scatchard and C. L. Raymond, J. Am. Chem. Soc. **60**, 1278 (1938).

Since U_1, U_2, U_3 were to vary with temperature it was desirable to determine them from G_x^E alone. The following procedure was tried. The quantity $5\mu_A^E|_{x_A=0} - 4\mu_C^E|_{x_C=0}$, as calculated from the theory, is independent of U_3. For a given value of U_1, we therefore determined U_2 to give the experimental value of this quantity, and then U_3 to give the experimental values of $\mu_A^E|_{x_A=0}$ and $\mu_C^E|_{x_C=0}$. We then attempted to determine U_1 to give the experimental value of G_x^E for the equimolar mixture. If this procedure was followed completely, the resulting value of U_3 was unreasonably large, so a compromise procedure assuming U_3 to be effectively zero was used (actually after U_1 and U_2 were determined a small, nonzero value of U_3 was determined by least squares to give the best fit of the G_x^E values; the additional labor required to determine U_1 and U_2 to make U_3 accurately zero would have been pointless). The values of U_1, U_2, and U_3 found in this way were

$$U_1=-2730 \text{ cal/mole}, \quad U_2=-1230 \text{ cal/mole},$$
$$U_3=3 \text{ cal/mole}.$$

Values of G_x^E, H_x^M, and TS_x^E calculated with these values of U_1, U_2, and U_3, *assuming them to be independent of temperature*, are compared with experimental data in Fig. 3. The fact that the experimental and theoretical TS_x^E values agree for the equimolar mixture is a coincidence which means that the values of U_1 and U_2 are very close to values that would have been determined by our previous methods of fitting to G_x^E, H_x^M, and TS_x^E. In fact the agreement between theory and experiment in Fig. 3 is as good as one can find with temperature-independent interactions.

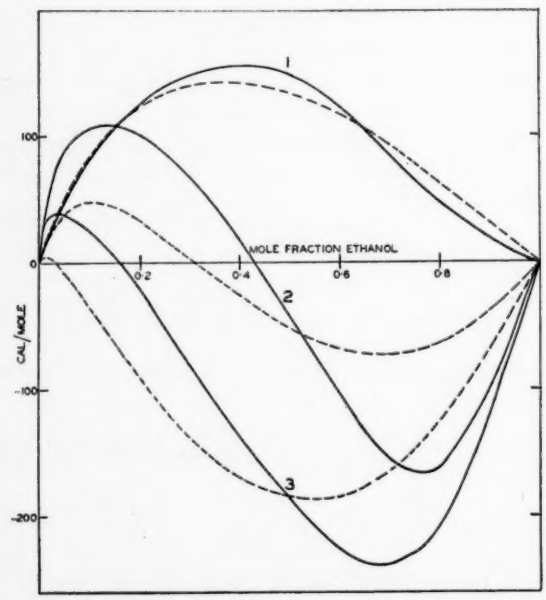

FIG. 3. Ethanol+chloroform, 25°C. Temperature-independent interactions. Solid lines experimental values, dotted lines theoretical.

1. G_x^E. 2. H_x^M. 3. TS_x^E.

Theoretical values calculated with

$$U_1=H_1=-2730 \text{ cal/mole}, \quad U_2=H_2=-2620 \text{ cal/mole},$$
$$U_3=H_3=3 \text{ cal/mole}.$$

If U_1 and U_2 may vary with temperature, then H_1 and H_2 become disposable constants. We have determined them by least squares to give the best fit of the experimental H_x^M values. The results were

$$U_1=-2730 \text{ cal/mole}, \quad H_1=-6740 \text{ cal/mole},$$
$$S_1=-13.5 \text{ cal/deg mole}.$$
$$U_2=-1230 \text{ cal/mole}, \quad H_2=-2620 \text{ cal/mole},$$
$$S_2=-4.7 \text{ cal/deg mole}.$$
$$U_3=H_3=3 \text{ cal/mole}.$$

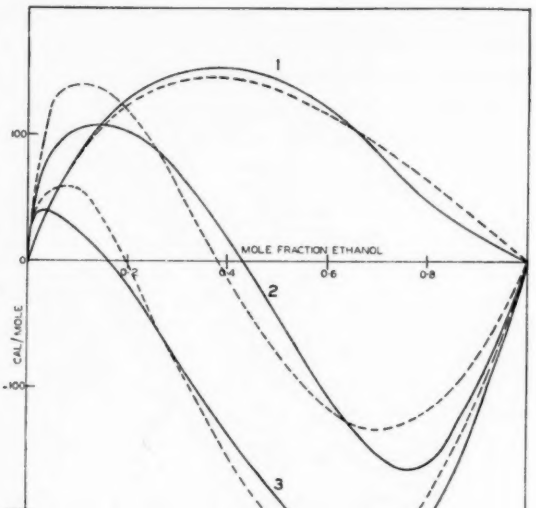

FIG. 4. Ethanol+chloroform, 25°C. Temperature-dependent nteractions. Solid lines experimental values, dotted lines theoretical. Theoretical values calculated with

$$U_1=-2730 \text{ cal/mole}, \quad H_1=-6740 \text{ cal/mole},$$
$$S_1=-13.5 \text{ cal/deg mole}.$$
$$U_2=-1230 \text{ cal/mole}, \quad H_2=-2620 \text{ cal/mole},$$
$$S_2=-4.7 \text{ cal/deg mole}.$$
$$U_3=H_3=3 \text{ cal/mole}, \quad S_3=0.$$

Values of G_x^E, H_x^M, and TS_x^E calculated with these interactions are compared with experimental data in Fig. 4.

(c) Remarks

The agreement between theory and experiment with temperature-independent interactions is most unsatisfactory. The agreement with temperature-dependent interactions, while not perfect, is a great deal better.

The hydrogen bond heat of formation $H_1=-6740$ cal/mole is comparable with other estimates; it seems more reasonable than the lower values one finds if U_1 is not permitted to vary with temperature. There is no direct method for comparing our value of S_1 with entropy changes on hydrogen bond formation derived

otherwise, e.g., from vapor compressibility measurements. We hope to devise an indirect method for making such a comparison.

A discussion of this system, in which the geometrical model was varied in an unsuccessful attempt to find a better fit of the experimental data with temperature-independent interactions, has been given previously.[3]

V. THE SYSTEM ETHANOL+ACETONE

(a) Experimental Data

Liquid-vapor equilibrium measurements for this system have been made by Gordon and Hines.[17] In view of the remarks made below in connection with ethanol+ether, only the total pressure measurements of these authors were used, and the assumption $\delta_{12}=0$ was made. Values of G_x^E at 32°C and 40°C were calculated and extrapolated to give values of G_x^E at 25°C. Values of H_x^M at 25°C measured by Hirobe[15] were used.

(b) Theory

The models for ethanol and acetone molecules have already been described. The interactions considered are the ethanol hydrogen bond (H−O), of strength U_1; interaction of hydroxyl hydrogen and acetone oxygen (H−E), of strength U_2; and the van der Waals interaction, of strength U_3.

If we assume that U_1, U_2, and U_3 are independent of temperature, then no set of values can give positive TS_x^E values as large as those found experimentally.† We therefore sought to determine U_1, U_2, and U_3 from the G_x^E values alone. For a given value of U_1, U_2, and U_3 were determined to give the experimental "end-values" of the excess chemical potentials (see Sec. IV). With these values of U_2 and U_3, the value of G_x^E for the equimolar mixture was substantially independent of U_1, so that the experimental data do not determine a value of U_1. We have adopted arbitrarily the value found for ethanol+chloroform, *viz.* $U_1=-2730$ cal/mole. The corresponding values of U_2 and U_3 were $U_2=-2450$ cal/mole, $U_3=27$ cal/mole.

Since the number of H−E contacts formed is very nearly equal to the number of H−O contacts broken, the experimental H_x^M data do not determine H_1 and H_2, but only H_1-H_2. We have therefore adopted the same value for H_1 as was found for ethanol+chloroform, giving $H_1=-6740$ cal/mole, $H_2=-5720$ cal/mole.

Theoretical values of G_x^E, H_x^M, TS_x^E calculated with these interactions are compared with experimental data in Fig. 5.

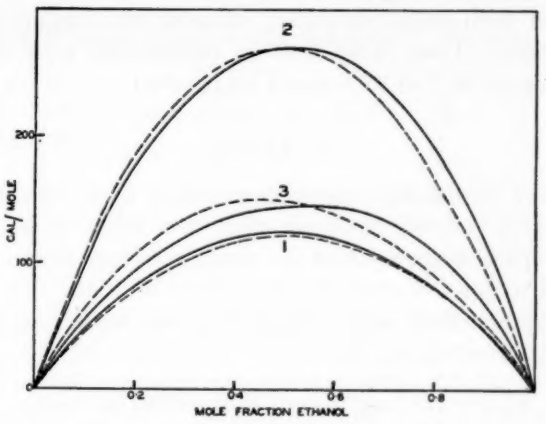

FIG. 5. Ethanol+acetone, 25°C. Solid lines experimental values, dotted lines theoretical.

1. G_x^E. 2. H_x^M. 3. TS_x^E.

Theoretical values calculated with

$U_1=-2730$ cal/mole, $H_1=-6740$ cal/mole,
$S_1=-13.5$ cal/deg mole.
$U_2=-2450$ cal/mole, $H_2=-5720$ cal/mole,
$S_2=-11.0$ cal/deg mole.
$U_3=H_3=27$ cal/mole.

(c) Remarks

The experimental data are fitted reasonably with temperature-dependent interactions; they cannot be fitted with temperature-independent interactions (TS_x^E for alcohol mole fractions greater than about 0.4 would have the wrong sign).

Here again we have neglected the dipole interaction in pure acetone; this would tend to produce positive values of TS_x^E.

VI. THE SYSTEM ETHANOL+ETHER

(a) Experimental Data

Liquid-vapor equilibrium measurements for this system have been made by Gordon and Hornibrook.[18] On calculating total pressures from vapor compositions by integration, using virial coefficients for ethanol derived from heats of vaporization[4] and for ether measured by Lambert *et al.*,[13] it was found that the total pressures and vapor compositions were consistent only if $\delta_{12}=2\beta_{12}-\beta_{11}-\beta_{22}$ had the value +5.2 liter. This is a most improbable value, since it requires β_{12} to be positive. One would expect β_{12} to be at least as negative as the virial coefficient for ether, which would mean that δ_{12} could not be more positive than +1.5 liter, and might well be negative. In the absence of measured values we have therefore assumed $\delta_{12}=0$. Since the method used by Gordon and Hornibrook suggests that their total pressures are more accurate than their vapor compositions, we have calculated values of G_x^E at 25°C

[17] A. R. Gordon and W. G. Hines, Can. J. Research **24B**, 254 (1946).

† With some modification of the geometrical model, TS_x^E can be made to take large positive values. This happens, for example, if the strong interaction U_2 occurs with *all* contact points of the acetone molecule, rather than with just two of them. For the present system this is unreasonable and it is not considered further.

[18] A. R. Gordon and W. S. Hornibrook, Can. J. Res. **24B**, 263 (1946).

from total pressures alone, following the method of Barker.[19] These were used in conjunction with the values of H_x^M at 25°C given by Hirobe.[15]

(b) Theory

The model for this system differs from that for ethanol+acetone only in that the ether molecule occupies one more lattice site than the acetone molecule, and so has two more contact points. With exactly the same procedures as for ethanol+acetone, we determined the interaction values

$$U_1=-2730 \text{ cal/mole}, \quad H_1=-6740 \text{ cal/mole},$$
$$S_1=-13.5 \text{ cal/deg mole}.$$
$$U_2=-1880 \text{ cal/mole}, \quad H_2=-6350 \text{ cal/mole},$$
$$S_2=-15.0 \text{ cal/deg mole}.$$
$$U_3=H_3=0.$$

Comparison of theoretical and experimental values of G_x^E, H_x^M, and TS_x^E is given in Fig. 6.

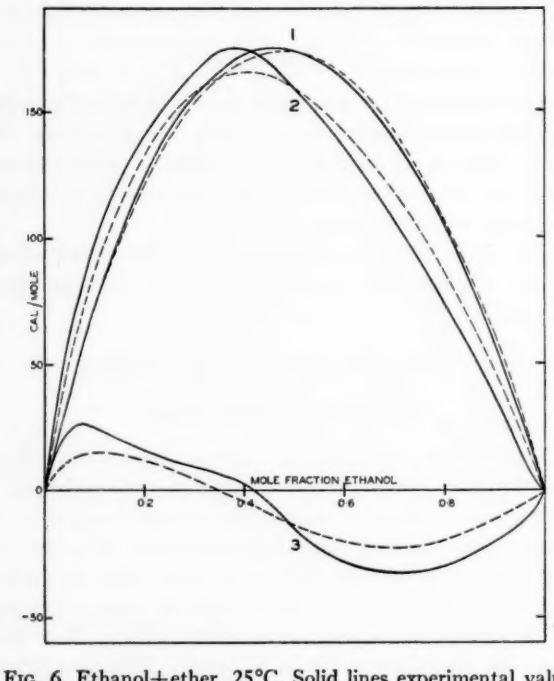

FIG. 6. Ethanol+ether, 25°C. Solid lines experimental values, dotted lines theoretical.

1. G_x^E. 2. H_x^M. 3. TS_x^E.

Theoretical values calculated with

$$U_1=-2730 \text{ cal/mole}, \quad H_1=-6740 \text{ cal/mole},$$
$$S_1=-13.5 \text{ cal/deg mole}.$$
$$U_2=-1880 \text{ cal/mole}, \quad H_2=-6350 \text{ cal/mole},$$
$$S_2=-15.0 \text{ cal/deg mole}.$$
$$U_3=H_3=0.$$

[19] J. A. Barker, Australian J. Chem. **6**, 207 (1953).

(c) Remarks

With temperature-dependent interactions, the theory reproduces the experimental data reasonably well. Here again the theory with temperature-independent interactions cannot give sufficiently positive values of TS_x^E, although the failure is much less serious than with ethanol+acetone.

The ethanol-ether "hydrogen bond" appears to be slightly weaker than the ethanol-ethanol bond ($-H_2<-H_1$) but at least as highly localized ($-S_2>-S_1$).

VII. GENERAL DISCUSSION

We have generalized a previous theory[3] to permit of temperature-dependent interaction free energies. For the systems chloroform+benzene and acetone+chloroform we have used, in the absence of other criteria, the *simplest* representation—*viz.*, that with temperature-independent interactions. For the three ethanol systems this was impossible, and temperature-dependent interactions were used. The interactions determined for the three ethanol systems are consistent in the sense that the same values of the free energy, heat, and entropy of formation of the ethanol hydrogen bond were used throughout. The values were $U=-2730$ cal/mole, $H=-6740$ cal/mole, and $S=-13.5$ cal/deg mole, respectively. The free energy and entropy values have meaning only with reference to our model (because of "standard state" difficulties), but the heat value H should be comparable with values derived otherwise (see for example Davies).[20]

The qualitative aspects of the relation between molecular interactions and thermodynamic functions have been discussed previously.[3] We make here a general remark on the tendency for the G_x^E curve to be more symmetrical than either H_x^M or TS_x^E curves. This is explained simply by the fact that positive values of H_x^M are generally due to breaking of bonds present in one pure component, and so are associated with gain of orientational freedom and a tendency to positive TS_x^E, while negative values of H_x^M are associated with formation of bonds between unlike molecules, loss of orientational freedom, and negative values of TS_x^E. Thus the dissymmetries in H_x^M and TS_x^E tend to cancel.

The systems studied here, together with these studied previously, form a representative selection of nonaqueous associated solutions (association in one pure component; association in solution but not in either component; and a combination of these effects). It seems reasonable to conclude that the theory in its generalized form should apply to most nonaqueous associated solutions. It is appropriate to mention here that extensive calculations have shown that the theory does not give satisfactory results when applied to aqueous solutions of nonelectrolytes.

[20] H. Davies, Chem. Soc. Ann. Repts. **43**, 5 (1946).

Relation between Bond Length and Stretching Frequency for the Carbonyl Group

M. MARGOSHES, F. FILLWALK, V. A. FASSEL, AND R. E. RUNDLE
Department of Chemistry and Institute for Atomic Research, Iowa State College, Ames, Iowa

(Received September 21, 1953)

A plot is shown of bond length *vs* stretching frequency of the carbonyl group in a series of compounds containing this group. For bond lengths ranging from 1.13 to 1.31A, the average distance of the points from a smooth curve is 0.013A.

THE success of Rundle and Parasol[1] and Lord and Merrifield[2] in correlating frequencies of infrared absorption bands with interatomic distances in hydrogen bonded systems has prompted us to make a test of this type of correlation with some other grouping. The carbonyl group was chosen because it occurs frequently enough for the results to be of some practical importance, considerable data is available on bond lengths, the carbonyl stretching vibration gives rise to a strong infrared band that is usually easily distinguished from other bands in the spectrum, and the group often enters into the formation of hydrogen bonds so it is possible to test the effect of such inter- and intramolecular forces on the correlation. A similar correlation of bond distance with stretching force constant has been shown by Walsh,[3] but the lack of knowledge of stretching force constants for the more complex compounds reduces the utility of Walsh's correlation.

Badger's rule[4] predicts a linear relation between the stretching force constant and $(r_e-d)^{-3}$, which is the basis for Walsh's correlation. In order to correlate bond lengths with stretching frequencies it is necessary to assume that the vibration involves only motion of the carbon and oxygen atoms relative to each other, with no other motion of the molecule. This will be a good assumption for most molecules, but will be extremely poor for carbon dioxide because of the splitting of the carbonyl stretching vibration into symmetric and asymmetric stretching vibrations, and may also be poor for the carboxylate ion.

Figure 1 shows how well these assumptions are justified in practice. The average distance of the points from the smooth curve is 0.013A, with the largest errors, of 0.0525A, being for *DL*-alanine and the carboxylate group of glycylglycine. This comparatively large deviation might be ascribed to the effect of hydrogen bonding, but this is not consistent with the fact that the points for *L*-threonine, hydroxy-*L*-proline, and salicylic acid all lie quite close to the curve and the point for urea is somewhat above the curve. The complexity of the spectra of amino acids in the 1500 to 1700 cm^{-1} region makes it difficult to assign a particular frequency to the carbonyl stretching vibration (we have plotted two possible frequencies for hydroxy-*L*-proline),

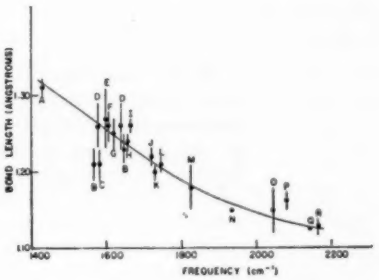

FIG. 1. Relation between bond length and stretching frequency for the carbonyl group. Vertical lines represent estimated error in bond-length determination.

Point	Compound	Bond length		Stretching frequency
A	Calcite	1.31 ±0.01A	(a)	1430 cm^{-1}
B	Glycylglycine	1.23 ±0.02	(b)	1650
		1.21 ±0.02	(b)	1570
C	*DL*-alanine	1.21 ±0.02	(c)	1580
D	Hydroxy-*L*-proline	1.26 ±0.03	(d)	1580 or 1640
E	Sodium formate	1.27 ±0.04	(e)	1600
F	Glycine	1.26 ±0.02	(f)	1605
G	*L*-Threonine	1.25 ±0.02	(g)	1620
H	Salicylic acid	1.24 ±0.01	(h)	1655
I	Urea	1.26 ±0.01	(i)	1665
J	Acetaldehyde	1.22 ±0.01	(j)	1720 (s)
K	Glyoxal	1.20 ±0.01	(k)	1730 (t)
L	Formaldehyde	1.21 ±0.01	(l)	1744 (u)
M	Phosgene	1.18 ±0.03	(m)	1827 (v)
N	Ketene	1.150	(n)	1935 (w)
O	Nickel carbonyl	1.15 ±0.03	(o)	2045
P	Carbonyl sulfide	1.16 ±0.01	(p)	2079 (x)
Q	Carbon monoxide	1.128	(q)	2143 (y)
R	Borine carbonyl	1.13 ±0.01	(r)	2164 (z)

[a] N. Elliott, J. Am. Chem. Soc. **59**, 1380 (1937).
[b] E. W. Hughes and W. J. Moore, J. Am. Chem. Soc. **71**, 2618 (1949).
[c] J. Donohue, J. Am. Chem. Soc. **72**, 949 (1950).
[d] J. Donohue and K. N. Trueblood, Acta Cryst. **5**, 419 (1952).
[e] W. H. Zachariasen, J. Am. Chem. Soc. **62**, 1011 (1940).
[f] G. Albrecht and R. B. Corey, J. Am. Chem. Soc. **61**, 1087 (1939).
[g] Schoemaker, Donohue, Schomaker, and Corey, J. Am. Chem. Soc. **72**, 2328 (1950).
[h] W. Cochran, Acta Cryst. **6**, 260 (1953).
[i] P. Vaughan and J. Donohue, Acta Cryst. **5**, 530 (1952).
[j] Stevenson, Burnham, and Schomaker, J. Am. Chem. Soc. **61**, 2922 (1939).
[k] J. E. LuValle and V. Schomaker, J. Am. Chem. Soc. **61**, 3520 (1939).
[l] Stevenson, LuValle, and Schomaker, J. Am. Chem. Soc. **61**, 2508 (1939).
[m] P. W. Allen and L. E. Sutton, Acta Cryst. **3**, 46 (1950).
[n] Bak, Knudson, Madsen, and Rastrup-Anderson, Phys. Rev. **79**, 190 (1950).
[o] Ladell, Post, and Fankuchen, Acta Cryst. **5**, 795 (1952).
[p] Townes, Holden, and Merritt, Phys. Rev. **74**, 1113 (1948).
[q] Gero, Herzberg, and Schmid, Phys. Rev. **52**, 467 (1937).
[r] Gordy, Ring, and Burg, Phys. Rev. **78**, 512 (1950).
[s] H. W. Thompson and G. P. Harris, Trans. Faraday Soc. **38**, 37 (1942).
[t] H. Thompson, Trans. Faraday Soc. **36**, 988 (1940).
[u] H. H. Nielson, Phys. Rev. **46**, 117 (1934).
[v] C. R. Bailey and J. B. Hale, Phil. Mag. **25**, 98 (1938).
[w] E. B. Wilson and H. Gershinowitz, J. Chem. Phys. **5**, 500 (1937).
[x] W. G. Penney and G. B. B. M. Sutherland, Proc. Roy. Soc. (London) **156**, 654 (1936).
[y] E. Amaldi, Z. Physik **79**, 492 (1932).
[z] R. D. Cowan, J. Chem. Phys. **18**, 1101 (1950).

[1] R. E. Rundle and M. Parasol, J. Chem. Phys. **20**, 1487 (1952).
[2] R. C. Lord and R. E. Merrifield, J. Chem. Phys. **21**, 166 (1953).
[3] A. D. Walsh, Trans. Faraday Soc. **43**, 60, 158 (1947).
[4] R. M. Badger, J. Chem. Phys. **2**, 128 (1934); **3**, 710 (1935).

but the two large discrepancies cannot be caused by this difficulty. Neither of the two compounds has an absorption band near 1720 cm^{-1}, the frequency that would correspond to the bond length of 1.21A.

In collecting the data for Fig. 1, care was taken that the frequencies used should be those of the compound in the same physical form as for the measurement of bond lengths. The one exception is for nickel carbonyl, where the distance is from a crystal structure and the frequency is that of the liquid. It is felt that the intermolecular forces in this case are too weak to affect the results appreciably.

THE JOURNAL OF CHEMICAL PHYSICS VOLUME 22, NUMBER 3 MARCH, 1954

Critical Phenomena in the Cyclohexane-Aniline System*

DOUGLAS ATACK AND O. K. RICE
University of North Carolina, Chapel Hill, North Carolina
(Received October 8, 1953)

Measurements have been made on the transition temperatures between one-phase and two-phase conditions in the cyclohexane-aniline system and on the densities of the coexisting phases, using an improved temperature control. The region of extreme cloudiness or wet fog, where the meniscus, if present, cannot be seen, and where density measurements are difficult because the density float cannot be seen, was investigated by means of a technique suggested by Zimm. In this procedure the temperature was raised, without stirring, to clear the wet fog without removing any density gradients which might have formed. The previous results of Rowden and Rice and Atack and Rice have been substantiated, and it is concluded with stronger evidence that there is an appreciable range of critical concentrations over which the transition temperature is constant.

DURING the past few years data have been accumulated in this laboratory on critical phenomena in the cyclohexane-aniline system. These studies have included measurements on the coexistence curve, vapor pressure,[1] density of coexisting phases, and interfacial tension between coexisting phases.[2] As one result of these studies it has been concluded that the coexistence curve has a finite horizontal top; in other words there is a range of compositions all of which can be called critical compositions.

When a solution in the critical range, whose temperature is higher than the critical temperature, is slowly cooled there appears quite suddenly a dense cloudiness or "wet fog," and this was found to persist over a range of 0.010° to 0.015°C. The temperature at which this wet fog appeared on cooling has been considered to be the critical temperature, T_c, in the belief that there were actually two phases present in very finely divided form, and the values of T_c for solutions of different composition were compared by placing these tubes in the bath simultaneously and observing the appearance of the wet fog.[1] In this way it was concluded that T_c was constant over a range of compositions. Actual appearance of the meniscus could not be observed on account of the wet fog.

On the other hand, measurements[2] which were made on the densities, ρ_1 (cyclohexane-rich phase) and ρ_2 (aniline-rich phase), of the coexisting phases in a mixture in the critical range of compositions, showed that $\rho_2-\rho_1$ was proportional roughly to $(T_c-T)^{\frac{1}{2}}$, up to the lower limit of the wet fog, i.e., up to the point where $T_c-T\sim0.010°$. This in itself might be taken as indicating that there was no flat part of the coexistence curve. However, since these density measurements were made with a quartz float suspended by a quartz helix, direct measurements could not be made when the wet fog was present because the bob and helix could not be seen. Observations made with the bob in the upper liquid layer and the helix in the vapor indicated a rather sharp drop in the density when T_c-T was equal to about 0.005°, the temperature at which the wet fog appeared on cooling being taken as T_c. This, we believed, might indicate that the true value of T_c lay 0.005° below the point previously supposed, in which case the coexistence curve would have a flat top, being truncated 0.005° below the original estimate of T_c.

It was suggested to us by Dr. B. H. Zimm that it might be possible to measure the density in the "no-man's-land" of the wet fog by raising the temperature very slightly without stirring. If any density differences had developed in the tube, these should persist, but the fog could be expected to clear. We found this technique extremely helpful, both in measuring the density, and in observing the formation of the meniscus, and it has been used in the present work, which is directed toward measuring the phenomena which occur in the wet-fog region.

* Work supported by the U. S. Office of Naval Research.
[1] R. W. Rowden and O. K. Rice, J. Chem. Phys. **19**, 1423 (1951); *Changements de Phases* (Compt rend. 2e Réunion Annuelle, Société de Chimie Physique, Paris, 1952), p. 78.
[2] D. Atack and O. K. Rice, Discussions Faraday Soc. **15**, 210 (1953).

EXPERIMENTAL

Materials

The materials used were the same samples of aniline and cyclohexane used in our most recently described work.[2] The critical temperature was reported as 29.587°C, which was slightly lower than the critical temperature of 29.61°, as found by Rowden and Rice[1] and corrected slightly as to scale. The difference undoubtedly arose from small amounts of impurity in one sample or the other. In all respects, however, they behaved very similarly, and we believe that these impurities will not affect the conclusions to be drawn from the results. The comparison of temperatures should be quite accurate, as the same set of Beckmann thermometers was used.

A recalibration of the resistance thermometer now gives 29.422°C as our corrected value of the critical temperature, and that of Rowden and Rice will correspondingly be reduced to 29.45°C.

For the density measurements the same mixture (hereafter called the "density sample") was used which had been used for the earlier density determinations. This had stood for several months in the tube with the quartz helix and bob, closed by a Teflon seal. It had exactly the same critical temperature as it had previously, and the same critical temperature as the other critical mixtures, by direct comparison. This was gratifying evidence of the tightness of the Teflon seal.

Coexistence Curve

Ten mixtures (including the density sample) of varying composition through the critical concentration range were prepared. They were exhaustively dried over fused calcium oxide, as before, all transfer of material after the mixtures were made up being done in vacuum. The transition temperatures were measured after each drying until that for each sample individually was constant. The tubes containing the final samples, with the exception of the density sample, were mounted on a circular frame and well inserted into a 15-gallon thermostat. By rotating the top of the frame each tube could be brought into the position previously occupied by any other tube. The thermostat could be controlled to ±0.001°C.

The procedure was to increase the bath temperature, stirring the contents of each tube until such time as the meniscus had disappeared in each tube and no heavy opalescence was present. Subsequently the bath was cooled at the rate of 0.005°C per hour until heavy opalescence began to appear in some of the tubes. The bath was held at this temperature for half an hour at least and then heated again until the opalescence disappeared. The lowest temperature was measured on a platinum resistance thermometer. No separation of the sample into two phases could be observed at the higher temperature and the color of the solution was homogeneous throughout. Again the temperature of the bath was lowered, this time to 0.001°C below the previous low temperature and the sample allowed to stand for half an hour at that temperature, before heating to clear the opalescence. This stepwise procedure was repeated, lowering the temperature each time 0.001°C below the previous low temperature and allowing at least half an hour standing time at this temperature, until on heating to clear the opalescence a meniscus persisted. In this manner it was possible reproducibly to measure the temperature of meniscus reappearance to 0.001°C. Moreover it was easy to compare the behavior of solutions of different composition precisely. The position of the tubes was changed and the entire procedure repeated; exactly the same results were obtained, as might have been expected as the bath water was extremely well circulated. The density sample was also compared with some of the other critical samples, and was found to have its transition at the same temperature.

TABLE I. Coexistence curve.

Mole fract. aniline	Temp. reappearance of meniscus	Temp. onset wet fog	Temp. first opalescence
0.390_2	29.377		
0.396_8	29.394		
0.406_4	29.414		29.423
0.420_0	29.420	29.422	29.426
0.429_6	29.422	29.426	29.436
0.437_6	29.422	29.425	29.433
0.445_1[a]	29.422	29.425	
0.448_0	29.422	29.425	29.430
0.457_4	29.422	29.425	29.430
0.465_6	29.422	29.425	29.428

[a] Density sample.

As the samples were only stirred once, at the beginning of the procedure described, they stood for some hours at a temperature just above the critical temperature, where, at final equilibrium, there would be some gradation of density in the gravitational field. However, diffusion in the liquid state is so slow and the driving force of gravity so small that the actual separation would be entirely negligible as long as the lowest temperature reached is above the critical.

The results of these measurements are given in Table I. We may remark that the meniscus appeared within the tube in the case of all the critical samples (mole fraction of aniline 0.4296 to 0.4656), as was to be expected, appearing near the bottom for those rich in cyclohexane and near the top for those rich in aniline. It seemed to come in at the bottom for those samples less than 0.4296-mole fraction aniline.

Through an inadvertance we failed to make up solutions stronger than 0.4656 in aniline, but we feel quite sure that this solution is at about the limit of the critical range, since the meniscus first appeared very close to the top of the tube.

The critical range as determined by Rowden and

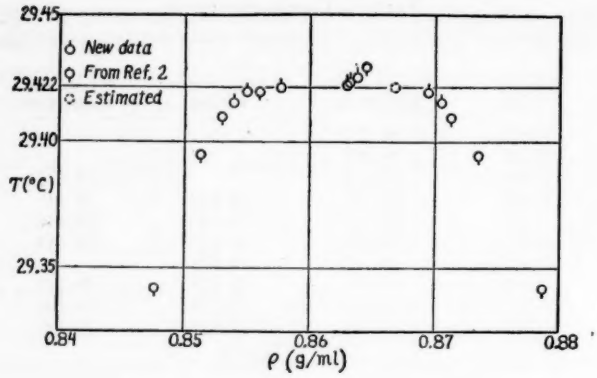

FIG. 1. Densities of coexisting phases.

Rice extended from about 0.418- to 0.462-mole fraction aniline, and thus appeared to be at a slightly lower concentration of aniline than we have found here.

Density measurements were made in exactly the same way as previously described,[2] and in the same tube previously used. In measuring the upper phase, the bob and quartz spiral were completely immersed in the phase, and were rendered visible when the dense fog formed by the technique described above. In measuring the lower phase the bob was in the phase measured, while the spiral was in the upper phase. The method of calculating the density from these measurements has been fully described.

Density measurements were made at temperatures closer to the critical than was previously possible by cooling to the required temperature, holding the solution at that temperature for half an hour, and then heating the solution until the opalescence cleared sufficiently so that the reference points of the quartz spiral were clearly defined in the cathetometer. The density thus measured was assumed to correspond to the lowest temperature reached, since settling out would occur much more rapidly than remixing. When measurements were made very close to the critical temperature (at 29.422°), it was necessary to raise the temperature almost 0.2°C in order to get the solution sufficiently clear to make the density measurements, and the sharp meniscus disappeared giving place to a dark brown line. The density values at this point may thus be in error rather more than the other values, but are, nevertheless, quite significant.

The data are given in Table II and plotted in Fig. 1.

It will be noted that the densities just above the critical temperature show a slight downward trend as the temperature is lowered. This is probably within the experimental error. Since the meniscus in the density sample disappeared near the middle of the tube, or perhaps a little below, the density of the homogeneous phase should be near or a little below the mean of the densities of the coexisting phases just below the critical temperature, and we believe that the new value at 29.424° must therefore be better than the one at 29.427° determined in the earlier work. It will also be seen from Table I that the meniscus appeared about 0.003° below the temperature of appearance of the wet fog, and from Table II we see that the sudden break in density occurred at the same temperature. In our earlier paper we stated that the sudden break in density occurred about 0.005° below the appearance of the dense fog, which probably agrees with the present result within error of observation of the earlier work.

Opalescence

The temperatures of the first visible appearance of opalescence on cooling and of the first appearance of the wet fog have been recorded in Table I. These observations, especially of the appearance of opalescence, naturally involve certain subjective judgments, since the opalescence actually appears gradually on cooling. The comparison between solutions of different composition will, however, be of some significance.

In addition, some observations of the opalescence in the density sample may be of some interest. The observations at 29.423°C were repeated several times in the following manner. The temperature of the bath was raised to about 29.6°C, and the contents of the tube thoroughly stirred. On lowering the bath temperature slowly, opalescence appeared simultaneously throughout the whole solution. The temperature was then lowered to 29.423°C very slowly and an extremely dense wet fog was present at this temperature. On raising the temperature to about 29.6°C the solution became clear with no visible inhomogeneity. This procedure was repeated several times without further stirring. On each successive occasion the volume of the solution through which opalescence first appeared became smaller, until on further repetition this volume appeared to be constant (about one-third the total volume of liquid). However, on lowering the temperature of the bath below that at which opalescence first appeared, the opalescence, in every case, spread throughout the contents of the tube and became uniform. When the wet fog was eventually formed it extended immediately throughout the entire content of the tube. The solution was allowed to stand in every case for about half an hour at 29.423°C but on raising the temperature a homogeneous solution was always obtained.

TABLE II. Densities of coexisting phases of cyclohexane-aniline system.

Temperature	Cyclohexane-rich phase	Aniline-rich phase
29.426	0.863_8[a]	0.863_3[a]
29.424	0.863_2[a]	0.863_2[a]
29.423	0.863[a]	0.863[a]
29.422	0.857_7	
29.420	0.855_0	0.869_5
29.416	0.854_0	0.870_5

[a] Single homogeneous phase, measured near top of tube.

DISCUSSION

This further study confirms in all essential details the conclusions drawn by Rowden and Rice regarding the existence of a range of critical concentrations. The slight difference in critical temperature and the slight shift of the flat portion of the coexistence curve to higher aniline concentrations, which we have found, do not affect the flatness of the coexistence curve, and the indications are that the impurity contents in both sets of samples, though slightly different, are extremely minute. Though the fluctuations of the thermostat were about ±0.001°, we believe that by careful simultaneous observations any one of the critical temperatures, judged by the appearance of the meniscus, of the six critical mixtures did not differ from any other by more than 0.001°. Special attention has been paid to this point in view of the recent criticism of Zimm.[3]

Although it now appears that the conversion occurs at a temperature about 0.003° lower than that of the appearance of the wet fog, the difference between the two reference points is, in every case but one, the same. It is a bit puzzling why, even after exhaustive purification, this slight difference should occur in one sample. If this should be interpreted as indicating that the coexistence curve does indeed have one highest point, it then would appear that the curve is not at all symmetrical and certainly does not have the classical form. However, it seems likely that the definite appearance of a meniscus provides a more accurate means of observation than a distinction between mists of various densities.

The density measurements are entirely consistent with the findings on the coexistence curve. In Fig. 2 we have plotted the density of the homogeneous solution, mole fraction aniline 0.4451, the density of pure aniline,[4] and the density of pure cyclohexane,[4] at a temperature just above the critical temperature, and have used them to estimate a density-composition curve. We have thus found the compositions corresponding to the highest density of the cyclohexane-rich phase below the critical temperature as given in Table II, and the lowest density of the aniline-rich phase (estimated from Table II, see Fig. 1). The range of critical concentrations thus estimated (which may be in error by 25 percent, or so) corresponds well with that obtained by direct measurement. This agreement would seem to support our belief that the appearance of a meniscus is a better criterion for the transition than the appearance of the wet fog, though the observation that the opalescence reappeared at first in only part of the tube after the temperature had been lowered to 29.423° and then raised without stirring might indicate that there was some settling at this temperature, which is 0.001° above that which we now report as the critical temperature. Such settling might possibly arise because the contents of the tube occasionally were cooled past the critical point on account of fluctuations of the bath temperature.

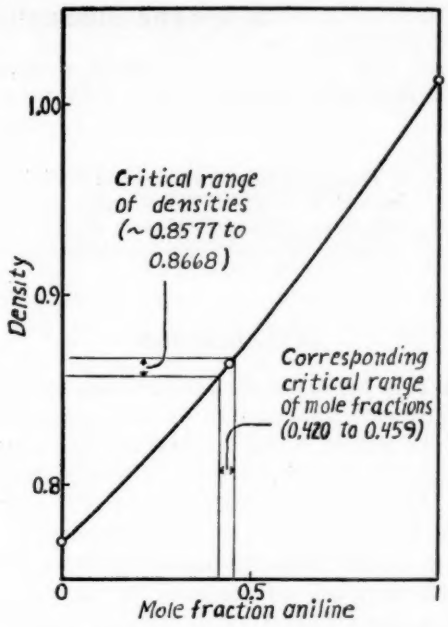

FIG. 2. Density against composition, showing critical range.

That we made an effort to close the gap in the densities between 0.863 and 0.8577 is indicated by the series of closely spaced temperature in Table II. The fact that we were unable to do so is of course consistent, as the calculation just made indicates, with the idea that the coexistence curve has a flat top. However, the fluctuations in temperature and the inherent difficulties in the density measurements may introduce some uncertainty in this respect, and we cannot finally say that it would be impossible to get an intermediate value, though we believe this to be the case.

We believe that we have now shown definitely that the coexistence curve is flat over a range from about 0.43- to 0.465-mole percent aniline to about 0.001°C. Thus there appears to be a considerable region of concentrations which can be called a critical region, over which the transition occurs at a constant temperature. We believe that the suggestion made by Zimm[3] that the coexistence curve is a cubic curve cannot be maintained.

[3] B. H. Zimm, J. Chem. Phys. **20**, 538 (1952).
[4] *International Critical Tables* (McGraw-Hill Book Company, Inc.).

Magnetic Susceptibilities of Np^{+6}, Np^{+5}, and Np^{+4}*

DIETER M. GRUEN AND CLYDE A. HUTCHISON, JR.
Institute for Nuclear Studies, Department of Chemistry and Argonne National Laboratory, University of Chicago, Chicago, Illinois
(Received August 26, 1953)

The magnetic susceptibilities of $NaNpO_2(CH_3COO)_2$, $NpO_2C_2O_4H\cdot H_2O$, and $KNpF_5$ have been measured from 14°K to 320°K. The magnetic susceptibilities of the ions Np^{+6}, Np^{+5}, and Np^{+4} have been compared with those calculated for ions in electronic states of f-electron configurations in the presence of electric fields of specific forms and with various amounts of spin-orbit coupling.

INTRODUCTION

THE only published data on the magnetic susceptibilities of compounds of Np are those of Howland and Calvin[1] and of Hutchison and Elliott.[2] These data were, however, obtained using solutions of compounds of Np in H_2O at room temperature only. It is of course desirable in connection with the interpretation of information on the magnetic susceptibilities in the light of possible electronic structures of the magnetic ions to have data over a wide temperature range on crystalline compounds, preferably of known structure. For these reasons we have measured the magnetic susceptibilities of $NaNpO_2(CH_3COO)_3$, $NpO_2C_2O_4H\cdot 2H_2O$, and $KNpF_5$ in crystalline form from 14.0 to 320°K. As has been pointed out previously[3] such information is of importance in determining the role played by f electrons in the ground states of the heavy metal ions. We have interpreted the data for these three compounds in which Np has the valences +6, +5, and +4, respectively, in terms of electronic states involving 1, 2, and 3 f electrons and of crystalline fields of specific forms.

EXPERIMENTAL PROCEDURES

Preparation of Compounds

a. Np(VI): $NaNpO_2(CH_3COO)_3$

The starting material for the preparation of the compounds of neptunium was a solution of Np^{237} (V) in 1M HCl. 7 cm³ of such a solution containing 3.6 mg of Np^{237} per cm³ was available from the Argonne National Laboratory for these experiments. The Np in this solution was precipitated with NH_3, redissolved in $HClO_4$ and oxidized with Cl_2 and $KBrO_3$. The $NaNpO_2(CH_3COO)_3$ was precipitated by addition of 5 cm³ of an 8M solution of $NaOOCH_3$. The precipitate was centrifuged from the supernatant solution and, after the surface was washed with water, it was dried in vacuum and transferred to the spherical capsule employed in the magnetic measurements.

b. Np(V): $NpO_2C_2O_4H\cdot 2H_2O$

A hexone extraction of Np in solution in HNO_3 was performed. Then the Np was extracted from the hexone into distilled H_2O. The Np was precipitated as hydroxide with NH_3 and then redissolved in 0.5M H_2SO_4. This solution was electrolyzed at a Hg cathode with an area of 3 cm² at 0.5 amp for 4 hr. The solution was then withdrawn from the cell and the hydroxide was precipitated with NH_3 and washed with H_2O. The hydroxide was dissolved in 0.05M HCl. Cl_2 gas was bubbled through the solution at 80°C for 0.5 hr and 0.1 g $NH_2OH\cdot HCl$ was added. The hydroxide (V) was precipitated with NH_3, washed with H_2O, and redissolved in 0.05M HCl. The hydroxide was again precipitated with NH_3 and washed with H_2O. It was then placed in contact with 5 cm³ t-butyl alcohol† containing 5-mole percent distilled H_2O and 0.1-g oxalic acid. The suspension was stirred with a platinum rod for several min. The suspension was centrifuged and washed with anhydrous ethyl ether. The precipitate was dried in air and then transferred to the spherical capsule employed in the magnetic measurements.

c. Np(IV): $KNpF_5$

The Np in a solution in HNO_3 was precipitated as the hydroxide using NH_3. The precipitate was washed with H_2O and redissolved in H_2SO_4. The solution was electrolyzed at a Hg cathode with an area of 3 cm² at 0.5 amp for 2.5 hr. Then the solution was withdrawn from the cell and the hydroxide was precipitated with NH_3, washed with H_2O and redissolved in constant boiling HCl. This solution was rapidly mixed with a 10 percent aqueous solution of KF. The resulting precipitate was washed with H_2O and dried in vacuum. This material was transferred to the spherical capsule used in the magnetic measurements.

Analysis of Compounds

a. $NaNpO_2(CH_3COO)_3$

* The compound was analyzed both before and after the magnetic measurements. $NH_2OH\cdot HCl$ was employed to reduce to Np(V) which was precipitated

* This work received support from the U. S. Office of Naval Research.

[1] J. J. Howland, Jr., and M. Calvin, J. Chem. Phys. **18**, 239 (1950).

[2] C. A. Hutchison, Jr., and N. S. Elliott, Abstracts of Papers, 113th Meeting, American Chemical Society, April 1948. Abstract No. 86, p. 52-O. Published in full as AEC Document-1896.

[3] C. A. Hutchison, Jr., and N. Elliott, J. Chem. Phys. **16**, 920 (1948).

† This procedure was suggested by L. I. Katzin of the Argonne National Laboratory.

with NH_3. The precipitates were heated in NO_2 for 0.5 hr at 325°C. The resulting Np_3O_8 was weighed and found in the sample taken before the measurements to be equivalent to 75.33 percent of the sample in the form $NaNpO_2(CH_3COO)_3$ and, in the sample taken after the measurements, to be equivalent to 75.27 percent. The Np was assumed to be all in the form $NaNpO_2(CH_3COO)_3$. The remainder of the sample was assumed to be $NaCH_3COO \cdot 3H_2O$. α counts on the supernatant solutions from the analysis showed that ~0.01-mg Np remained in them. Spectrographic analyses showed the $NaNpO_2(CH_3COO)_3$ to be of high purity and free of other possible paramagnetic elements. Pulse analysis of the emitted α's showed that the sample contained <0.01 percent Pu. X-ray analyses showed no compound other than $NaNpO_2(CH_3COO)_3$. This x-ray analysis would not be expected to show up the $NaCH_3COO \cdot 3H_2O$.

b. $NpO_2C_2O_4H \cdot 2H_2O$

A solution of the compound in 1M $HClO_4$ was subjected to α counting and spectrophotometric analysis. The data of Sjoblom and Hindman[4] for the extinction coefficient at 982μ were used after correcting them to the value $777 \cdot 10^6$ g^{-1} min^{-1} [5] for the rate of emission of α's. The spectrophotometric data showed that 2 percent of the Np was in the form Np^{+4}.

A solution of the compound in H_2SO_4 was titrated with 0.01 N $KMnO_4$ and the percent of oxalate was calculated after deducting a stoichiometrically proportionate amount for the oxidation of the Np.

Two samples of the compound were burned in a microcombustion apparatus and the C determined as CO_2 and the H and H_2O as H_2O. The analytical results may be summarized as follows:

			Theoretical for $NpO_2C_2O_4 \cdot 2H_2O$
Np	α count	60.80%, 60.50%	
	spectrophotometry	60.11%	60.15%
C_2O_4	titration	22.82%	22.33%
C	as CO_2	3.75%, 3.37%	6.09%
H_2O (including H)	as H_2O	11.29%, 11.51%	13.70%

c. $KNpF_5$

Three samples of the compound were dissolved in HNO_3 after the completion of the magnetic measurements and the hydroxide was precipitated with NH_3. The precipitates were heated at 500°C for 1.5 hr which converted them to NpO_2. The NpO_2 was weighed and the Np in the supernatant liquids was determined by α counting. The Np was assumed to be all in the form $KNpF_5$. The calculated amounts of $KNpF_5$ in the sample were found to be 91.53 percent, 92.66 percent, and 92.66 percent. The remainder of the sample was assumed to be $KF \cdot 2H_2O$. X-ray analysis showed the presence of no compound other than $KNpF_5$. This x-ray analysis would not be expected to show the presence of the $KF \cdot 2H_2O$.

d. $Fe(NH_4)_2(SO_4)_2 \cdot 6H_2O$

The $Fe(NH_4)_2(SO_4)_2 \cdot 6H_2O$ was analyzed for total Fe and Fe^{++} by volumetric procedures and the results were 99.85±0.07 percent of the theoretical amount and 99.75±0.09 percent of the theoretical amount, respectively.

e. $Mn(NH_4)_2(SO_4)_2 \cdot 6H_2O$

The $Mn(NH_4)_2(SO_4)_2 \cdot 6H_2O$ was analyzed for Mn gravimetrically and found to contain 97.56±0.05 percent of the theoretical amount.

Magnetic Measurements

The Faraday method was employed for the measurements of the magnetic susceptibilities. Since the amount of Np available was small, this method was suitable for the determinations. The samples were packed into a quartz sphere 0.4 cm in outside diameter and 0.05 cm in wall thickness with a neck 0.3 cm in length. The sphere was suspended by a chain from the arm of a beam microbalance. The cryostat and magnet were similar to those described by Hutchison and Elliott.[3] The sphere was located by means of a cathetometer in a precisely reproducible position 1.8±0.2 cm above the top edge of the vertical plane surfaces of truncated cone pole pieces. Weighings were made with magnet current on and off and these magnetic forces were compared with those exerted with the same current through the magnet when the same sphere was filled with a standard substance, $Fe(NH_4)_2(SO_4)_2 \cdot 6H_2O$. The molar susceptibility of the compound was assumed to be given by the expression,

$$M\chi_{Np} = M_{Np} \cdot \frac{F_{Np}}{{}_{300}F_{Fe}} \cdot \frac{W_{Fe}}{W_{Np}} \cdot {}_{300}\chi_{Fe}.$$

The molar susceptibility of the Np ion was assumed to be given by

$$M\chi_{Np\ ion} = M\chi_{Np} - M_{Np}(\mu_{Np\ ion} m_{Np} - \sum_i \chi_i m_i).$$

In these expressions:

$M\chi_{Np}$ is the molar susceptibility of the Np compound;

${}_{300}\chi_{Fe}$ is the gram susceptibility of the standard substance, $Fe(NH_4)_2(SO_4)_2 \cdot 6H_2O$ at 300°K calculated from the measurements of Jackson;[6]

χ_i is the diamagnetic gram susceptibility of the ith nonparamagnetic constituent in the compound;

[4] R. Sjoblom and J. C. Hindman, J. Am. Chem. Soc. **73**, 1744 (1951).

[5] L. B. Magnusson and T. J. LaChapelle, *National Nuclear Energy Series* (McGraw-Hill Book Company, Inc., New York, 1939) Vol. 14B, Paper 1.7.

[6] L. C. Jackson, Trans. Roy. Soc. (London) **A224**, 1 (1924).

$\mu_{Np\ ion}$ is the diamagnetic susceptibility of the Np ion calculated by the method of Angus;[7]

M_{Np} is the molecular weight of the Np compounds;

F_{Np} is the magnetic force on the Np compound in the sphere (force on container plus sample, minus force on container and minus force on impurity);

$_{300}F_{Fe}$ is the magnetic force on the $Fe(NH_4)_2(SO_4)_2 \cdot 6H_2O$ in the sphere at 300°K at the same magnetic current at which F_{Np} was measured calculated from our data near 300°K and the temperature coefficient of susceptibility as given by Jackson;[6]

W_{Fe} is the weight of $Fe(NH_4)_2(SO_4)_2 \cdot 6H_2O$ in the sphere;

W_{Np} is the weight of Np compound in the sphere as determined by analyses;

m_{Np} is the theoretical weight fraction of Np in the pure Np compound;

m_i is the theoretical weight fraction of the ith nonparamagnetic constituent in the pure Np compound.

The χ_i were either taken from the tabulations of Angus[7] or calculated by the method of Angus.[7] The corrections for the impurities were made by deducting from the measured magnetic forces at given magnet currents not only the previously determined forces on the container but also the forces on the impurity. The latter were read from an experimental curve for force on a sample of $NaCH_3COO \cdot 3H_2O$ *versus* magnet current in the case of $NaNp(CH_3COO)_3$ and from a similar curve for KF in the case of $KNpF_5$. The curves determined at room temperature were assumed valid at all temperatures. It was assumed that there was no impurity in the sample of $NpO_2C_2O_4H \cdot 2H_2O$.

The measurements were made in the vicinity of the following temperatures: 320°K obtained by circulating water in the Dewar jacket; room temperature; 274°K obtained by circulating water; 240°K obtained with NH_3 at atmospheric pressure; 195°K obtained with NH_3 at its triple point pressure; 185°K obtained with liquid C_2H_6 at atmospheric pressure; down to 131°K obtained with C_2H_6 at reduced pressures; 77°K obtained with liquid N_2 at atmospheric pressure; 62°K obtained with N_2 at its triple point pressure; 20°K obtained with liquid H_2 at atmospheric pressure; 14°K obtained with H_2 at its triple point pressure.

The temperatures higher than the H_2 temperatures were determined by means of copper-constantan thermocouples. The temperature was read from a curve of calibrations of couples made from the same spool of wire one of these having been calibrated by the National Bureau of Standards. Three couples were employed and were located at about 10-cm vertical intervals in the central gas space, the center one being about 1 cm below the sample container. The temperatures determined from the three couples agreed at the boiling point of N_2 within 0.1° with each other and with the temperature determined from the vapor-pressure measurements. The temperature of liquid hydrogen at atmospheric pressure was determined by measuring the atmospheric pressure and using the known data on vapor pressure *versus* temperature.[8] The triple point temperature was taken to be that given in the literature.[9] No measurable difference in temperature between two couples, one imbedded in a sample of salt in a glass tube in the weighing space and one located in the usual position of the center one mentioned above was observable down to the bp of H_2. Field strengths ranging from 2500 to 10 000 gauss were used in the experiments.

The force on the standard substance, $Fe(NH_4)_2(SO_4)_2 \cdot 6H_2O$, was determined as a function of voltage across a resistor in series with the windings of the magnet. The magnet core was always saturated first and then the current was lowered until the desired force was obtained. This procedure gave reproducible values of force at given voltage. The forces were reproducible for a given filling of the container to within 0.2 percent and for different fillings to within ±1 percent.

The total magnetic force (weight with current on minus weight with current off) on sample plus container plus impurity, if any, varied over the temperature and current range employed for $NaNpO_2(CH_3COO)_3$ from −0.3 to +10 mg; for $NpO_2C_2O_4H \cdot 2H_2O$ from +0.7 to +40 mg; for $KNpF_5$ from +2 to +34 mg. The container corrections varied from 0.4 to 1.0 mg for the currents employed. They were determined at room temperature, boiling point of liquid N_2 and at liquid H_2 boiling point. Curves were drawn through the room temperature and liquid H_2 boiling points and a linear interpolation was made for intermediate temperatures. The container correction did not vary more than about 10 percent between room temperature and the boiling point of liquid H_2 and the container correction was constant over a 12-month period.

The corrections for $NaCH_3COO \cdot 3H_2O$ in the sample of $NaNp(CH_3COO)_3$ were in the range 0.2 to 0.3 mg for the magnet currents employed. The corrections for $KF \cdot 2H_2O$ in the $KNpF_5$ in the range of magnet currents employed were in the range 0.05 to 0.1 mg.

EXPERIMENTAL RESULTS

Standardization

The ratio of the force per g on $Mn(NH_4)_2(SO_4)_2 \cdot 6H_2O$ to the force per g on $Fe(NH_4)_2(SO_4)_2 \cdot 6H_2O$ was computed at 6 widely differing magnetic field strengths from readings of the respective curves of forces at 300°K *versus* voltages across the resistor in series with the magnet windings. The average was 1.1413±0.0074. The value

[7] W. R. Angus, Proc. Roy. Soc. (London) **A136**, 569 (1932).

[8] Scott, Brickwedde, Urey, and Wahl, J. Chem. Phys. **2**, 454 (1934).

[9] F. C. Brickwedde, J. Research Natl. Bur. Standards **22**, 370 (1939).

given by Jackson's data[6,10] in conjunction with his measured temperature coefficients was 1.1406.

Np Compounds

A total of 279 measurements was made on the three compounds at the various temperatures and field strengths. No variation in susceptibility with field strength was observed in the range of 2500 to 10 000 gauss. The results were tabulated for reference[11] but the detailed tables containing magnet current readings, thermocouple readings, temperatures, measured forces, container and impurity corrections, forces per g, readings from the curve for the standard, molar susceptibilities of the salt, molar susceptibilities of the Np ion, and reciprocals of the molar susceptibilities of the Np ion are too extensive to reproduce here.

The results are summarized in this paper in the form of three graphs, Figs. 1, 2, and 3 in which $_M\chi^{-1}$, the reciprocal of the molar susceptibility, is plotted against T for $NaNpO_2(CH_3COO)_3$, $NpO_2C_2O_4H\cdot 2H_2O$ and

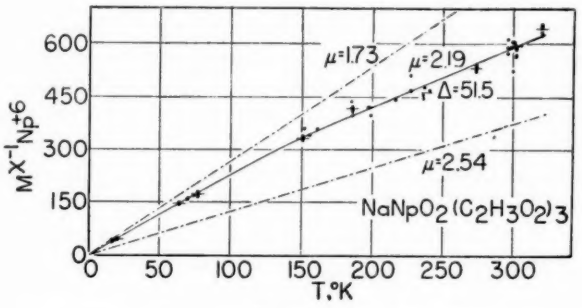

FIG. 1.

$KNpF_5$, respectively. The graphs were obtained as follows: (a) the tabulated values of $_M\chi^{-1}$ were plotted as ordinate *versus* T as abscissa; (b) points in the various temperature groups were corrected to the same temperature, averaged and the least-square straight lines were drawn through all the averages above 185°K for the data on $NaNpO_2(CH_3COO)_3$ and $KNpF_5$ and through all the averages for the data on $NpO_2C_2O_4H\cdot 2H_2O$; the equations for the straight lines were

$$_M\chi^{-1}_{Np^{+6}}=86.3+1.676T, \quad (A)$$

$$_M\chi^{-1}_{Np^{+5}}=0.041+0.796T, \quad (B)$$

$$_M\chi^{-1}_{Np^{+4}}=66.6+0.731T. \quad (C)$$

The averages are given by the centers of the short horizontal lines in the figures. (c) Smooth curves were drawn visually through the remaining points; (d) two other lines were drawn on each figure using the "spin only" equation,

$$_M\chi=\frac{N\beta^2 4S(S+1)}{3kT}$$

[10] L. C. Jackson, Proc. Roy. Soc. (London) **A104**, 671 (1923).
[11] For copy of these tables order from American Documentation Institute, Washington, D. C.

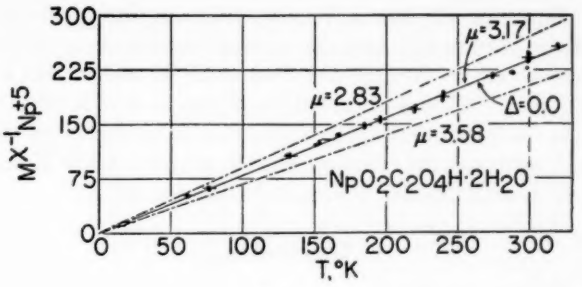

FIG. 2.

and the "free ion" equation,

$$_M\chi=\frac{N\beta^2 g^2 J(J+1)}{3kT}$$

in which S and J are taken for the Hund ground state in Russell-Saunders coupling; (e) for each graph a value of

$$\mu=[(3k/\beta^2 N_{Av})\sigma^{-1}]^{\frac{1}{2}}=\left(\frac{7.997}{\sigma}\right)^{\frac{1}{2}},$$

in which σ is the slope of χ^{-1} *versus* T, was calculated and a value of

$$\Delta=\frac{_{300}\chi^{-1}}{\sigma}-300,$$

in which $_{300}\chi^{-1}$ is the susceptibility at 300°K, was calculated. The values found for the μ's and Δ's were,

$NaNpO_2(CH_3COO)_3$,	$\mu=2.19$,	$\Delta=51.5$°K;
$NpO_2C_2O_4H\cdot 2H_2O$,	$\mu=3.17$,	$\Delta=0.0$°K;
$KNpF_5$,	$\mu=3.31$,	$\Delta=91.1$°K.

The measured susceptibilities can be represented to within ±3 percent by the equations:

$$_M\chi_{Np^{+6}}=\frac{0.425}{T}+0.24\cdot 10^{-3} \text{ from 14 to 320°K}; \quad (1)$$

$$_M\chi_{Np^{+5}}=\frac{1.257}{T} \text{ from 14 to 320°K}; \quad (2)$$

$$_M\chi_{Np^{+4}}=\frac{0.670}{T}+1.280\cdot 10^{-3} \text{ from 132 to 320°K}; \quad (3a)$$

$$_M\chi_{Np^{+4}}=\frac{0.499}{T}+2.54\cdot 10^{-3} \text{ from 14 to 77°K}. \quad (3b)$$

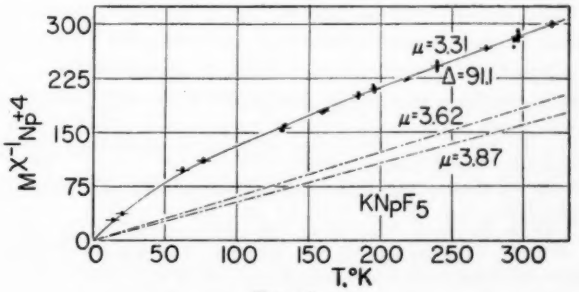

FIG. 3.

Equation (1) was derived by selecting the coefficient of the term in $1/T$ and the constant term so as to fit the smooth curve through the data at 20°K and at 200°K. Equation (2) was obtained by fitting at 300°K. Equation (3a) was obtained by adjusting the coefficient of the $1/T$ term and the constant term so as to fit at 300°K and 132°K and (3b) by fitting at 132°K and 14°K.

Discussion

We have compared the measured magnetic susceptibilities of the three salts of Np with magnetic susceptibilities calculated for 14 models of the situation, the models differing with respect to (a) ground electronic state of the ion, (b) symmetry of the electric field about the ion in the crystal, and (c) relative magnitudes of the perturbations caused by the spin-orbit interactions and by the crystalline field. These calculations were made by conventional methods using the crystalline field theory to the second order of perturbation theory.[12–14]

The unperturbed state was taken in each case to be the Hund ground state in Russell-Saunders coupling when all the electrons not in closed shells are f electrons. For f^1 (Np(VI) in $NaNpO_2(CH_3COO)_3$), the Hund ground state is ^2F; for f^2 (Np(V) in $NpO_2C_2O_4H\cdot 2H_2O$), it is ^3H; for f^3 (Np(IV) in $KNpF_5$), it is ^4I. The perturbations considered were those caused by spin-orbit coupling and by cubic or axial electrostatic fields in the crystal in addition to the magnetic perturbations.

The perturbation Hamiltonians employed were

$$\text{cubic field,}^{13}\ V_1=\sum_i D(x_i^4+y_i^4+z_i^4);$$

$$\text{axial field,}^{13}\ V_2=\sum_i A(x_i^2+y_i^2-2z_i^2);$$

$$\text{spin-orbit,}^{15}\ V_3=b\mathbf{L}\cdot\mathbf{S};$$

$$\text{magnetic field,}^{15}\ V_4=\beta\mathbf{H}\cdot(\mathbf{L}-2\mathbf{S}).$$

In the case of strong spin-orbit coupling the last becomes

$$V_4=g\beta\mathbf{H}\cdot\mathbf{J}.$$

The omission of the higher-order terms in the expansions of the crystalline fields does not of course affect the numbers and multiplicities of the levels obtained but does remove any freedom in the assignment of the relative spacings of levels.[16] The problem is thereby reduced to a one-parameter case.

The well-known matrix elements of these perturbations in the various systems of quantization were used. Calculations were made for cases S in which the spin-orbit coupling was small compared with the crystalline field splitting; L in which the spin-orbit coupling was large compared with crystalline field splitting; and M for intermediate cases in which the two were about the same size.

For the case S the matrix of the electric field perturbation on the ground state is, in the axial case, diagonal in the unperturbed system; for the cubic case the electric field perturbation was diagonalized. The spin-orbit plus magnetic perturbation was then transformed to the representation which diagonalized the electric perturbation and second-order perturbation theory was applied to the calculations of the energy levels. In this case S the spin-orbit perturbation was regarded as vanishingly small except in the one case noted. The susceptibility was calculated for only the lowest electric levels.

For the case L only the lowest multiplet component of the approximate Russell-Saunders term was considered. The electric perturbation was then written in diagonal form and the magnetic perturbation after transformation to the same representation was treated by second-order perturbation theory.

For the case M the sum of the electric field and spin-orbit perturbations was diagonalized and the energy levels were obtained for various values of the ratio of the spin-orbit coupling parameter to the electric field splitting parameter. A value of this ratio was then selected for which the splittings produced by the spin-orbit interactions and the crystalline fields were about equal. The spin-orbit plus electric perturbations were diagonalized for this value of the ratio and the magnetic perturbation was then transformed to the same representation and second-order perturbation theory was applied for calculation of the energy levels in the magnetic field.

After computing the energy levels, the molar susceptibility was calculated using the usual expression,[12]

$$M\chi=N_M\{\sum_{njm}[(W_{njm}^{(1)2}/kT)-2W_{njm}^{(2)}]\times\exp(-W_{njm}^{0}/kT)\}/\sum_{njm}\exp(-W_{njm}^{0}/kT).$$

In this expression W^0, $W^{(1)}$, and $W^{(2)}$ are the coefficients in the expansion

$$W_{njm}=W_{njm}^{0}+W_{njm}^{(1)}H+W_{njm}^{(2)}H^2.$$

In our experiments on powders we have observed the mean susceptibility. For purposes of comparison we calculated the mean susceptibility which is of course in the cubic case equal to the susceptibility in any direction and in the axial case is equal to $(1/3)(\chi_{\parallel}+2\chi_{\perp})$.

In addition to the symbols S, L, and M which denote the relative magnitudes of the spin-orbit and electric perturbations we have also employed the symbols F, H, and I to denote the corresponding Hund ground states and the symbols C and A to denote the cubic and axial symmetries.

[12] J. H. Van Vleck, *Electric and Magnetic Susceptibilities* (Oxford University Press, London, 1932).
[13] W. G. Penney and R. Schlapp, Phys. Rev. **42**, 662 (1932); **41**, 194 (1932).
[14] H. A. Kramers, Proc. Acad. Sci. (Amsterdam) **36**, 17 (1933).
[15] E. U. Condon and G. H. Shortley, *The Theory of Atomic Spectra* (Cambridge University Press, Cambridge, 1935).
[16] G. J. Kynch, Trans. Faraday Soc. **33**, 1402 (1937).

TABLE I.

Model State Field Spin-orbit	$\chi a/\beta^2 N_{Av}$		$\frac{\Lambda hc}{a}$	ukT/a	χ simplified
FCS	$u+0.40$		18	1	$(0.375/T)+(1.878/\Lambda)$
FCL	$g^2[(0.0145u-0.0309)e^{2u}+(0.0752u+0.0309)e^{-u}]\div[e^{2u}+2e^{-u}]$		144	48	$(0.192/T)-(0.853/\Lambda)$ $(0.533/T)-(0.427/\Lambda)$
FCM	$[(0.234u+0.182)e^{21.3u}+(2.680u-0.025)e^{11.5u}+(2.201u+0.958)e^{-3.81u}+(4.029u+1.112)e^{-12.0u}+(1.768u-2.260)e^{-16.5u}]\div[e^{21.3u}+2e^{11.5u}+e^{-3.81u}+2e^{-12.0u}+e^{-16.5u}]$		37.8	1	$(0.088/T)+(1.795/\Lambda)$ $(0.664/T)+(22.29/\Lambda)$
FAS	$(1/3)(3u+8)$	$a+$	27	1	$(0.375/T)+(18.78/\Lambda)$
	$(1/3)[(16u-1.333)e^{-1.5u}+(4u+1.333)e^{1.5u}]\div[e^{-1.5u}+e^{1.5u}]$	$a-$		b/a	$(0.500/T)+(0.157hc/b)$[a]
FAL	$(g^2/3)[(4.75u+2.67)e^{4u}+(2.25u-1.83)e^{u}+(6.25u-0.833)e^{-5u}]\div[e^{4u}+e^{u}+e^{-5u}]$		9	1	$(0.437/T)+(1.535/\Lambda)$ $(0.574/T)+(0.479/\Lambda)$
FAM	$(1/3)[(2.94u+1.14)e^{16.5u}+(2.94u+0.38)e^{10.5u}+(9.37u+1.64)e^{6u}+(1.65u+1.70)+(8.16u-3.85)e^{-1.5u}+(4.59u+0.14)e^{-12u}+(16u-1.16)e^{-19.5u}]\div[e^{16.5u}+e^{10.5u}+e^{6u}+1+e^{-1.5u}+e^{-12u}+e^{-19.5u}]$		36.0	1	$(0.368/T)+(3.569/\Lambda)$ $(2.002/T)+(3.632/\Lambda)$
HCS	$6.58u+0.063$	$a+$	1320	1	$(2.464/T)+(21.7/\Lambda)$
	$8.22u-0.022$	$a-$		1	$(3.078/T)+(7.6/\Lambda)$
HCL	$2g^2[(53/5760)e^{13u}+(1/30)e^{-2u}-(61/2688)e^{-7u}-(5/252)e^{-14u}+u(25e^{13u}+e^{-7u})/192]\div[3e^{13u}+2e^{-2u}+3e^{-7u}+e^{-14u}]$		1296	48	$(1.001/T)+(1.33/\Lambda)$ $+(8.59/\Lambda)$
HAS	$(1/3)(8u+20)$		75	1	$(1.000/T)+(130.4/\Lambda)$
HAL	$(g^2/3)[13.33e^{20u}+(2u-9.33)e^{17u}+(8u-2.13)e^{8u}+(18u-1.10)e^{-7u}+(32u-0.762)e^{-28u}]\div[e^{20u}+2e^{17u}+2e^{-7u}+2e^{-28u}]$		48	1	$+(35.61/\Lambda)$ $(1.281/T)+(1.018/\Lambda)$
ICS	$5u+K$		2880	1	$(1.877/T)+(K'/\Lambda)$
ICL	$2g^2[(5.018u+0.1483)e^{19.59u}+(5.076u+0.2396)e^{-9.11u}+(1.680u-0.3879)e^{-20.95u}]\div[2e^{19.59u}+2e^{-9.11u}+e^{-20.95u}]$		40.5	1	$(0.994/T)+(0.830/\Lambda)$ $(0.667/T)+(4.339/\Lambda)$
IAS	$(1/3)(15u+28)$		108	1	$(1.877/T)+(263/\Lambda)$
IAL	$(g^2/3)[(12.75u+24)e^{4u}+(2.25u-13.5)e^{3u}+(6.25u-5.16)e^{u}+(12.25u-3.08)e^{-2u}+(20.25u-2.25)e^{-6u}]\div[e^{4u}+e^{3u}+e^{u}+e^{-2u}+e^{-6u}]$		10	1	$(0.844/T)+(11.04/\Lambda)$ $(1.340/T)+(1.035/\Lambda)$

[a] This crystalline field result is, as pointed by by Elliot (reference 17), identical with that of his molecular treatment. In this case the spin-orbit coupling is not vanishingly small, and the temperature independent term arising from the electric field splitting is neglected in comparison with that resulting from the spin-orbit interaction.

The calculated mean susceptibilities are shown in Table I. In this table a is an electric field splitting parameter and is a suitable multiple of the electric field parameters appearing in the matrix elements for the electric splittings. It is to be expressed as an energy using the unit erg in these equations which give $_M\chi$ in the units $mole^{-1}$ cm^3. It is the only parameter which appears in the expressions for the susceptibilities except in the one case noted inasmuch as the electric perturbations contained only one parameter and in the cases in which the spin-orbit and electric perturbations were of approximately the same size, the spin-orbit parameter was taken to be a specific number times the crystalline field parameter. K and K' are constants.

Upon comparison of the calculated susceptibilities with the experimental ones it became apparent that no agreement could be obtained unless the electric field splittings were of the order of $3\cdot10^3$ to 10^4 cm^{-1}. Hence the susceptibility expressions simplify to the forms given in the last column of Table I. These forms then agree with the others to within 1 percent up to 350°K. In cases where there are two simplified expressions the first is for positive a and the second for negative a. In cases where there is only a single expression it is for positive a and the other case was not considered.

The parameter Λ in these simplified equations is equal to the separation of the highest and lowest levels in the electric field in the absence of the magnetic field. This separation is to be expressed as a wave number using the unit cm^{-1} in these equations which give $_M\chi$ in the units $mole^{-1}$ cm^3. Λ is always considered to be a positive number.

The comparison of the models with the experimental data may now be made by examining the agreement of

the simplified expressions of Table I for the theoretical susceptibilities with the experimental Eqs. (1), (2), and (3).

Np^{+6}

It is clear that, in order to obtain agreement at the lowest experimental temperatures between the experimental Eq. (1) and the simplified theoretical equations, it will be necessary that the coefficients of the $1/T$ terms in both be essentially equal. In the theoretical equations this coefficient is determined entirely by the model and there is no adjustable parameter. At the highest experimental temperatures the terms in Λ in the theoretical equations make a relatively large contribution and here the value of Λ may be chosen so as to give a fit. The agreement is therefore determined chiefly by the relative sizes of the coefficients of the $1/T$ terms.

Examination of the several theoretical equations reveals that the equation derived for the model *FAL* with *a* positive fits the data extremely well. The coefficient of the $1/T$ term is 0.437 as compared with the experimental value, 0.425. Thus the theory is in disagreement with the experiment at the lowest temperatures by only 3 percent. In order to secure agreement at 300°K the value of Λ, the separation between the highest and lowest of the states into which the ${}^2F_{\frac{5}{2}}$ level is split by the crystalline field, must be $7.7\cdot10^3$ cm^{-1}. This choice results in a maximum difference between the $_M\chi$'s of the theoretical and experimental equations of 3 percent.

The model *FAS* with *a* negative is seen to give disagreement of only 13 percent at the lowest temperatures. This case has been discussed by Elliott[17] using our data and employing a molecular model. He has stated that consideration of higher-order approximations has permitted considerably better agreement with our experimental data than is indicated by the simplified equation for χ in our table. In order to equate the temperature-independent term with that experimentally observed, b/hc must equal $6.6\cdot10^2$ cm^{-1}.† (Elliott has particularly emphasized the fact that the interactions of the 5*f* electrons with their surroundings may be quite large and that even a spin-only paramagnetism may be interpreted as arising from 5*f* electrons.)

Some of the other *F* models do not result in too bad disagreements. The models *FAS* with *a* positive and *FCS* are seen to give identical agreement with the experiment. The choice of Λ for agreement at 300°K must be different, of course, in the two cases, the choices $4.6\cdot10^4$ cm^{-1} and $4.6\cdot10^3$ cm^{-1}, respectively, giving maximum disagreements of 12 percent at the lowest temperatures.

The model *FAM* with Λ chosen equal to $8.3\cdot10^3$ cm^{-1} gives only slightly worse disagreement, namely, 13 percent at the lowest temperatures.

All the other models which were examined will be seen to give no agreement in any temperature range.

The structure of the compound $NaNpO_2(C_2H_3O_2)_3$ is known.[18,19] On the basis of x-ray and spectroscopic data it is known that the Np is surrounded by eight O atoms two of them closer than the others forming a linear NpO_2^{++} group. The electric field is thus known to be predominantly of axial symmetry. It therefore seems that the assumption of an *f* electron in the ground state of this ion adequately explains the magnetic properties in a way consistent with all the facts of the situation.

Moreover it is also seen that, in agreement with previous observations[3] on U, the Δ's are much larger than in the case of the rare earth elements. This is in agreement with a model of the electronic structures of these heavy elements in which the *f* electrons are much less deeply embedded than in the rare earths and in which, therefore, the perturbations by the crystalline fields are much more serious.

It is interesting to note that while all the axial models give some agreement with the experiments the *FAL* gives lower $_M\chi$'s and the *FAM* and *FAS* with *a* positive give higher. It might therefore be supposed that some intermediate value of the spin-orbit coupling might be found to be quite satisfactory. The particular *FAM* model chosen assumed the spin-orbit coupling to be $\frac{1}{4}$ of the electric field splitting, i.e., $2.1\cdot10^3$ cm^{-1}. One might therefore suppose that the spin-orbit coupling was considerably larger than this but not necessarily large compared with the crystalline field splitting as in the model *FAL*. This larger value would be in agreement with the observed multiplet separation of 2400 cm^{-1} [20] in Ce^{+3} which also has one *f* electron. In the heavy elements the spin-orbit coupling would be expected to be somewhat larger than this.

Np^{+5}

In this case the experimental results follow a straight line through the origin over the entire temperature range. It will be seen that the only model which gives any reasonable agreement is *HAL* and that this model gives excellent agreement. The theoretical and experimental terms in $1/T$ are in agreement to 2 percent which is within the error of the experimental equation. Any value of Λ therefore gives agreement with the measurements in this case.

It is to be noted that it is assumed in this model *HAL* that a degenerate state is lowest in contrast to the analogous case in the rare earths where Penney and Schapp[13] showed that a model with a nondegenerate state lowest was required.

† We wish to thank Professor M. H. L. Pryce for pointing out that this model *FAL* has the wrong sign for *a* on the basis of the charge distribution to be expected for a molecule NpO_2^{++}.

[17] R. J. Elliott, Phys. Rev. 89, 659 (1953).

[18] I. Fankuchen, Z. Krist. 91, 473 (1936).

[19] G. H. Dieke and A. B. F. Duncan, *Spectroscopic Properties of Uranium Compounds* (McGraw-Hill Book Company, Inc., New York, 1949).

[20] R. J. Lang, Phys. Rev. 49, 552 (1936).

The model *HAM* was not investigated but it would be interesting to see whether an intermediate spin-orbit coupling might not give very good agreement in this case also.

The assumption of the axial field is in agreement with the spectroscopic work of Sjoblom and Hindman[4] on Np^{+5} in solution. They interpret the structure of the visible band as arising from the vibrations of the NpO_2^+ molecule. The crystal structure of $NpO_2C_2O_4H\cdot 2H_2O$ has not been determined but it is to be expected that such molecules might also occur in these crystals.

It is also to be noted that there is a very great similarity between the magnetic behavior which we have observed for $NpO_2C_2O_4H\cdot 2H_2O$ and that of $NaPuO_2(C_2H_3O_2)_3$ as observed by Dawson.[21] The Pu in the latter compound also has two electrons not in closed shells. This strongly suggests that the situation is the same in both these cases as far as electric field symmetry and distribution of electronic states is concerned and is in agreement with the suggestion that the Np^{+5} exists as NpO_2^+ in the compound investigated.

The spectra of NpO_2^+ and PuO_2^{++} [22] have also been found to be similar in agreement with what would be expected on the basis of the foregoing remarks.

The assumption of f electrons is also seen in the case of Np^{+5} in the compound which we investigated to give a consistent interpretation of the magnetic data.

[21] J. K. Dawson, J. Chem. Soc. **1952**, 2705.
[22] D. M. Gruen, J. Chem. Phys. **20**, 1818 (1952).

Np^{+4}

The experimental data in this case do not obey a single relation of the form $\chi=(a/T)+b$ over the entire temperature range. *ICL* fits the data quite well at high temperatures when a is negative but disagrees greatly at the low temperatures. This compound is relatively more magnetically concentrated than the others and it is probably the case that exchange interactions play a very important role in the determination of the magnetic properties. The space group of the structure of this compound is known[23] and the locations of the Np^{+4} ions are known but the configurations of the F^- are unknown. It is quite possible that the field at the Np^{+4} might have cubic symmetry.

ACKNOWLEDGMENTS

We gratefully acknowledge the assistance of Charles M. Herzfeld in many phases of the experiments and of Jack Boardman in the calculations. We are also greatly indebted to the low-temperature laboratory of the Institute for the Study of Metals of the University of Chicago for the supply of the liquid H_2 and especially to J. W. Stout for his help with the low-temperature work. We wish to express our thanks to the Argonne National Laboratory for making available their facilities which were necessary to this research and particularly to J. J. Katz and W. M. Manning for their help and to J. C. Hindman for the loan of the Np. We thank Professor W. H. Zachariasen for x-ray analyses of several of the samples.

[23] W. H. Zachariasen, J. Am. Chem. Soc. **70**, 2147 (1948).

Some Ions of High Kinetic Energy in Mass Spectra of Polyatomic Molecules

FRED L. MOHLER, VERNON H. DIBELER, AND ROBERT M. REESE
National Bureau of Standards, Washington, D. C.

(Received April 17, 1953)

When the lighter-fragment ions of hydrocarbons and hydrocarbon derivatives are recorded with low-ion accelerating voltages, one observes satellite peaks on the high-mass side of the main peaks that come from ions with a fairly homogeneous high kinetic energy. Observations of the satellite peaks of CH_3^+ ions in mass spectra of 13 hydrocarbons and CH_3CF_3, are reported. The kinetic energies range from 1.5 to 3.4 ev and the relative intensities have a wide range of values but are less than the main peak except in benzene. The appearance potential of the satellite peak is roughly 30 volts in most cases while the main peak is observed above 20 volts. These high-energy ions are ascribed to doubly charged molecule ions that dissociate into two singly charged fragments. The kinetic energy of the pair of fragment ions is in most cases nearly equal to the Coulomb energy of two ions at a distance equal to the greatest distance between valence electrons in the molecule.

INTRODUCTION

IT has long been known that fragment ions from diatomic and polyatomic molecules often have excess kinetic energy.[1] The energy distribution of atomic ions from diatomic molecules has been the object of detailed study[2] and instances of atomic ions with a wide range of kinetic energies are satisfactorily explained in terms of the Frank-Condon diagrams of the normal state and the various ionized states.

Hustrulid, Kusch, and Tate[3] in a study of the mass spectrum of benzene found satellite peaks on the high mass side of the peaks of masses 26, 27, 12, 13, 14, and 15 but in the case of the mass-15 peak the "satellite" was larger than the main peak. Measurements with different magnetic fields and ion-accelerating voltages showed that these satellite peaks were ions of high kinetic energy. It was suggested that they came from the dissociation of doubly charged molecules into two singly charged fragments. The appearance potential of the satellite peaks was much higher than the main peaks, consistent with this explanation.

Hipple, Fox, and Condon[4] in a paper on metastable ions found that CH_3^+ of *n*-butane appeared as an incompletely resolved double peak. Their mass spectrometer could be operated with the collector at a positive potential relative to the analyser and, with a potential sufficient to stop all ions of zero initial velocity, the satellite peak alone was recorded showing that it came from ions with high initial velocity. Berry[5] has measured the velocity distribution of CH_3^+ ions of *n*-butane and of various other ions by deflecting the ion beam parallel to the magnetic field by an electric field. His results on CH_3^+ confirmed the result of Hipple *et al.* that there are two groups of ions, one with a roughly thermal distribution and one with high kinetic energy.

The authors first observed high kinetic energy satellite peaks in the mass spectrum of trimethyl-*n*-butyl lead. Ion peaks $C_4H_7^+$, $C_4H_8^+$, and $C_4H_9^+$ all had small satellite peaks and these were found to be ions of high kinetic energy. The satellite peaks had a high-appearance potential consistent with the theory of Hustrulid *et al.*[3] *viz.*, that they come from doubly charged molecules breaking into two singly charged fragments. This theory suggests that similar satellite peaks might be found in the mass spectra of many polyatomic molecules. They have escaped detection except in the instances noted above because under standard operating conditions of conventional mass spectrometers the ion accelerating voltage is too high to permit the resolution of ions with excess energy of 2 or 3 ev.

EXPERIMENTAL PROCEDURE

A model 21–103 Consolidated mass spectrometer was used in this research. This instrument has a "metastable suppressor" slit between the exit slit of the analyser and the ion collector which can be set at an adjustable positive potential to stop any ions which have lost kinetic energy while traversing the analyzer tube. This energy filter also has a focusing action and increases the resolving power of the instrument. The spectrum is recorded by varying the ion-accelerating voltage with a constant magnetic field and the normal range of voltage sweep is from 4000 to 500 volts. As the ion-accelerating voltage varies inversely as the mass of the ions, the resolving power in volts is given by the ion-accelerating voltage divided by the mass resolving power. This instrument had a mass resolving power of about 300 with the minimum setting of the suppressor voltage. If the ion accelerating voltage is reduced to 500 volts or less by reducing the magnetic field the satellite peaks described by Hustrulid *et al.*[3] become conspicuous in mass spectra of many compounds.

The satellite peaks are not completely resolved from the thermal energy peaks with 500 volts ion accelerating voltage and, for most of the compounds, measurements were repeated with an ion-accelerating voltage of 145 volts at mass 15. This gives very small ion currents and the sensitivity was increased by using 3 or 4 times the

[1] W. Bleakney, Phys. Rev. **35**, 1180 (1930).
[2] H. D. Hagstrum, Revs. Modern Phys. **23**, 185 (1951).
[3] Hustrulid, Kusch, and Tate, Phys. Rev. **54**, 1037 (1938).
[4] Hipple, Fox, and Condon, Phys. Rev. **69**, 347 (1946).
[5] C. E. Berry, Phys. Rev. **78**, 597 (1950).

normal gas pressure and maximum electron current. Under these conditions the "mass resolving power" is reduced but the voltage resolution is improved.

The voltage difference between the thermal energy peak and the satellite peak was measured by setting the ion-acceleratlng voltage manually on each peak and measuring the voltage with the potentiometer supplied with the instrument to calibrate the mass scale. It was also obtained by measuring on the spectrum record the intervals between the thermal energy mass 15 peak, the satellite peak and the msas 16 peak. Spectra were recorded with the minimum setting of the suppressor voltage and also with the suppressor voltage increased until the thermal energy peak was nearly equal to the satellite peak.

When ions of high initial energy are formed, the field in the ionization chamber exerts very little focusing action and only those ions are recorded which start out in a direction within the small solid angle determined by the slit system. Consequently, the measured kinetic energy distribution of these ions is nearly equal to the initial energy distribution, but the recorded intensity ratio of the satellite peak to the main peak is very much less than the true abundance ratio of high-energy ions to thermal energy ions. Ions contributing to the thermal energy peak are collected much more efficiently.

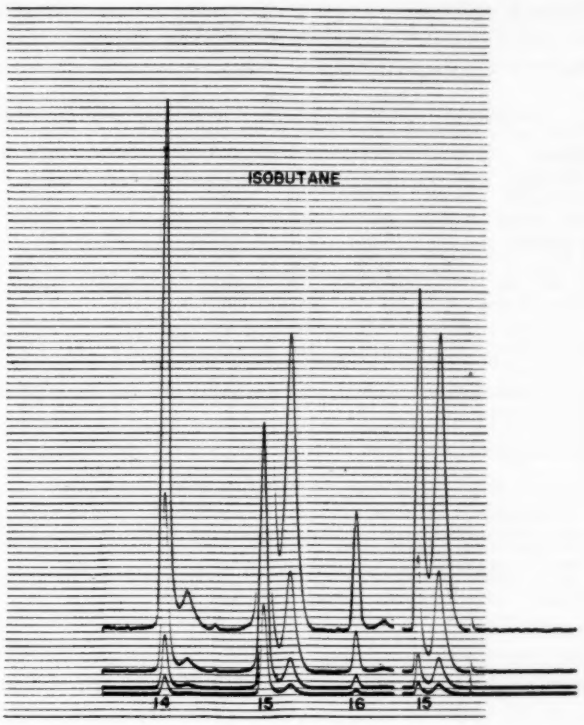

FIG. 1. Mass spectrum of peaks in the isobutane spectrum recorded with an ion-accelerating voltage of 144 volts at mass 15. This covers the range from mass 14 to mass 16 and mass 15 repeated with a high setting of the "metastable suppressor voltage."

RESULTS AND DISCUSSION

Figure 1 illustrates the mass spectrum of isobutane in the mass range 14 to 16 as recorded with minimum suppressor voltage, and on the right the mass 15 range is repeated with the suppressor voltage increased to make the intensity of the peaks nearly equal. The ion-accelerating voltage ranges from 155 volts at mass 14 to 135 volts at mass 16. The mass 15 peak on the left is recorded at one tenth of the full sensitivity.

The satellite peak on the right of the mass 15 peak is a prominent feature in these spectra. It is at an interval of 2.5 volts from the main peak. This peak is only slightly wider than the main peak and it is evident that it comes from ions of fairly homogeneous initial energy. There are also small satellite peaks associated with the peaks at mass 14 and mass 16.

Table I summarizes measurements of the CH_3^+ satellite peaks in fourteen hydrocarbons and CH_3CF_3. Column two gives the intensity of the satellite peak relative to the thermal energy peak as measured with 145 volts ion-accelerating voltage, 70 volts ionizing voltage, and minimum suppressor voltage except that for benzene and CH_3CF_3 the measurements were made with 500 volts ion accelerating voltage. This ratio depends markedly on the ion-accelerating voltage and on the ion-drawout voltage and the relative intensity is increased several fold at 500 volts ion-accelerating voltage.

The third column gives the voltage interval between the thermal energy peak and the satellite peak and most of the values are means of several measurements including direct voltage measurements and measurements from the recorded spectrum. They are probably accurate to ± 0.2 volts when the resolution and intensity are favorable. The peaks are not well resolved in nonane and for benzene and CH_3CF_3 the intensity is too low for good precision.

When the molecule ion dissociates, the two fragments have equal momenta and the kinetic energies are inversely proportional to the masses. On this basis the total kinetic energy of both fragments has been computed and is listed in the fourth column.

The appearance potential of the satellite peak is higher than that of the main peak. In all compounds it was verified that with an applied potential of 20 volts the main peak appeared without the satellite. In some cases, peaks were recorded at intervals of 2 or 5 volts and the data afforded a basis for a rough estimate of the appearance potential of the satellite peak. Values are included in the last column of Table II. These are uncorrected for electric fields in the ionization chamber except that for benzene a corrected value published by Hustrulid *et al.*[3] is given. The uncorrected values may be low by as much as 5 volts. For the hydrocarbons the appearance potential is roughly 28 volts in all cases.

The satellite peak is slightly wider than the thermal energy peak and this difference was measured on spectra recorded with the suppressor adjusted to give equal peak heights. In most cases the width of the satellite peak at

TABLE I. CH_3^+ ions of high kinetic energy in mass spectra of hydrocarbons and CH_3CF_3.

Compound	Relative[a] intensity	$K.E.$ of satellite	Total[b] $K.E.$	Max. charge separation, R	Coulomb energy
Ethane	0.03	2.3 ev	4.6 ev	2.57A	5.6 ev
Propane	0.076	2.2	3.3	3.86	3.7
n-butane	0.137	2.2	3.0	5.0	2.9
Isobutane	0.11	2.6	3.5	3.9	3.7
1-butene	0.11	2.2	3.0	4.8	3.0
1-butyne	0.08	2.2	3.0	4.7	3.06
n-pentane	0.11	2.0	2.5	6.36	2.26
Neopentane	0.17	2.4	3.0	3.8	3.8
n-hexane	0.09	1.8	2.2	7.6	1.9
n-heptane	0.07	1.7	2.0	8.9	1.6
n-nonane	0.05	1.4	1.6	11.7	1.2
2,2,3,3-me$_4$-butane	0.27	1.9	2.2	5.0	2.9
Cyclohexane	0.14	2.0	2.4	3.7	3.9
Benzene[c]	5.9	1.8	2.2	4.3	3.3
$CH_3 \cdot CF_3$[c]	0.01	3.4	4.1	2.5	5.7

[a] Intensity of high-energy peak relative to thermal energy peak. Measurements were made with 145 volts ion-accelerating voltage except as noted.
[b] Kinetic energy of both fragments of the molecule computed from column 3 on the basis of conservation of momentum.
[c] Measurements were made with 500 volts ion-accelerating voltage and intensity values are not comparable with other data.

half the maximum height is about 0.5 ev greater than that of the thermal energy peak. Extreme values range from 0.3 to 0.8 ev. The greater width of the satellite peak may be in part instrumental as the ion optics are more favorable for ions of zero initial energy.

In research on mass spectra of fluorocarbons[6] the CF_3^+ ions of many fluorocarbons were recorded on the low mass range with about 660 volts ion-accelerating potential and there was no evidence of satellite peaks. It is concluded that fluorocarbons differ from hydrocarbons in this respect.

The paper by Hustrulid *et al.*[3] does not give the kinetic energies of the satellite peaks of benzene but Fig. 8 of their paper and the known radius of curvature of their instrument afford a basis for computing the kinetic energies of the satellite peaks of $C_2H_2^+$ and $C_2H_3^+$ as about 1.5 ev. The total kinetic energy is about 2.2 volts and is consistent with the value derived from the CH_3^+ satellite in Table I.

The velocity distribution of CH_3^+ ions from *n*-butane as computed by Berry[5] is quite different from that found in this research for he finds a broad maximum at 1.6 ev instead of a sharp peak at 2.2 ev. This difference is ascribed to the fact that Berry's method measures the average component of velocity of ions moving in nearly random directions while this method records selectively the ions moving toward the slit.

The suggestion of Hustrulid *et al.* that these ions of high kinetic energy come from dissociation of doubly charged ions is an attractive one for it explains why the ions have a sharply defined kinetic energy rather than a wide range of energies. The minimum ionization potential for removing two electrons from a molecule will involve removing two valence electrons that are as far removed from each other as possible. The Coulomb repulsion of these two charges then can dissociate the molecule and most of this Coulomb energy will appear as kinetic energy of the fragment ions.

Table II, column 6, lists the Coulomb energy of two charges at the distance of the two most widely separated C—H bonding electrons (the distance between C—H and C—F bonds in CH_3CF_3). The distance R in angstrom units is based on accepted values[7] for the distances between atoms and the angles between bonds in these molecules. The Coulomb energy in ev is $14.4/R$. The values of the computed Coulomb energies are in many cases in good agreement with the observed kinetic energy but in other cases the differences are much greater than can be ascribed to experimental error.

Values either greater or less than the computed value can easily be understood. There is no obvious reason to exclude double ionization involving bonds closer than R of Table II. If we take R as the greatest distance between carbon atoms the computed energy is always too high. Bond strengths are undoubtedly weakened in the doubly ionized molecule ions but breaking bonds or rearrangements of atoms will involve some potential energy change and this will reduce the kinetic energy of the fragment ions.

It is interesting that high-energy CH_3^+ ions are observed in benzene and cyclohexane for in these molecules formation of CH_3^+ involves a rearrangement of H atoms in the ionization process. The disruption of the doubly charged molecule to give this ion is a process which involves several steps and it is not surprising that the observed kinetic energy is much less than the minimum Coulomb energy of a doubly charged ring. Probably the sequence of events is that the rings break with a rearrangement of H atoms and then the linear

TABLE II. Computed and observed appearance potentials for pairs of ions with the observed kinetic energy.

Compound	Computed potential	Reference	Observed potential
Ethane	29.3 ev	a	28±5 ev
Propane	25.3	a	...
n-butane	24.3	a	28±5
Isobutane	24.9	a	27±5
1-butene	24.7	b	...
n-pentane	24.0	a	...
Neopentane	25.0	a	27±5
n-hexane	23.2	a	...
Cyclohexane	23.9	c	...
n-heptane	22.3	a	...
Benzene	29.0	d	28±3[e]
CH_3CF_3	28.1	e	35±5

[a] M. B. Koffel and R. A. Lad, J. Chem. Phys. **16**, 420 (1948).
[b] V. H. Dibeler, J. Res. Natl. Bur. Standards **38**, 329 (1947).
[c] Kambara and Tyozo, Phys. Soc. Japan **1**, 2, 25 and 57 (1947).
[d] See reference 3.
[e] Dibeler, Reese, and Mohler, J. Chem. Phys. **20**, 761 (1952).

[6] Mohler, Dibeler, and Reese, J. Res. Natl. Bur. Standards **49**, 343 (1952).

[7] P. W. Allen and L. E. Sutton, Acta Cryst. **3**, 46 (1950).

ions dissociate. It may be significant that the observed kinetic energies for cyclohexane and benzene are not appreciably different from that observed for *n*-hexane.

It is possible to compute the minimum appearance potential for two ions with the observed kinetic energy for most of these molecules. The appearance potential for the fragment ion with a methyl radical removed, $A(R^+)$, is accurately known in most cases. The ionization potential of the CH_3 radical is 10.0 volts[8] and the minimum potential to give a pair of ions with the observed kinetic energy (KE) is: $A(R^+)+10+KE$. Table II lists the computed potentials and the observed potentials. The observed appearance potentials are in all cases consistent with the computed minimum appearance potentials within the wide range of uncertainty of the observed values.

CONCLUSION

It seems to be quite generally true that the lighter-fragment ions of hydrocarbons and hydrocarbon derivatives include ions of roughly thermal velocity and ions with a nearly homogeneous high kinetic energy. Measurements have been largely limited to CH_3^+ ions for intensity reasons. The magnitude of the kinetic energy of these high-velocity ions as well as their appearance potentials shows quite conclusively that they come from the dissociation of doubly charged molecules into two fragment ions. The kinetic energy is in many cases nearly equal to the Coulomb energy of two charges at a distance equal to the maximum separation of valence electrons in the molecule but this simple theory does not predict accurately all the observed values.

An earlier paper[9] gives a survey of doubly charged ions in mass spectra of hydrocarbons and it was shown that in paraffin hydrocarbons the doubly charged ion peaks are commonly only a few tenths of a percent of the maximum peak and the most abundant ions are ions with most of the H atoms removed. It was suggested that disruption of doubly charged ions to give two singly charged ions was a more probable process and this research confirms the prediction. In unsaturated hydrocarbons and aromatics doubly charged ions become much more abundant but even in these cases dissociation into singly charged ion pairs is conspicuous.

The phenomena deserve more detailed study both theoretically and experimentally, for the kinetic energy of these ions affords a new type of information on the ionization and dissociation process in polyatomic molecules.

[8] J. A. Hipple and D. P. Stevenson, Phys. Rev. **63**, 121 (1943).

[9] Mohler, Bloom, Wells, Lengel, and Wise, J. Res. Natl. Bur. Standards **42**, 369 (1949).

Markoff Random Processes and the Statistical Mechanics of Time-Dependent Phenomena. II. Irreversible Processes in Fluids*

MELVILLE S. GREEN
University of Maryland, College Park, Maryland
(Received March 10, 1953)

The procedures developed in a previous paper of the same main title are applied to the specific case of irreversible processes in fluids. The gross variables are chosen to be a finite number of the plane-wave expansion coefficients of the local particle, momentum and energy densities. As an example, the gross variables describing the local particle density are

$$\sum_{i=1}^{N} \exp i\mathbf{k}\cdot\mathbf{x}_i,$$

where $\mathbf{p}_i$ and $\mathbf{x}_i$ are the momentum and position of the ith molecule and N the total number. $\mathbf{k}$ runs over a finite number of values which are all small compared to the reciprocal mean distance between molecules. The phenomenonological equations are derived and expressions are given for the viscosity, diffusion, and heat conductivity in terms the autocorrelation coefficients of certain phase functions. These expressions are supposed to be valid for both liquids and gases. They are shown to coincide with the Chapman-Enskog expressions for dilute gases.

IN a previous paper of the same main title[1] the author has given a general statistical mechanical interpretation of the equations governing large scale time-dependent phenomena. The purpose of the present paper is to derive on this basis the phenomenonological equations for time-dependent phenomena in fluids, and to give explicit expressions for the coefficients of irreversible processes which appear in them.

The principles on which these equations are based, Stokes' expression for the stress tensor of viscous forces, Fourier's law of heat conductivity, Fick's law of diffusion have, of course, been known for a hundred years or more and their validity (and limitations) have been established from experience. Their interpretation from the molecular point of view, on the other hand, is not so well known except in certain special cases. For perfect or near perfect gases the Maxwell-Boltzmann kinetic theory gives a satisfactory explanation of these principles.[2] The theory of Born, and Green[3] gives an explanation for liquids based on the socalled superposition principle. Irving and Kirkwood have given a statistical mechanical derivation of the equations of fluid motion which is intended to be supplemented by Kirkwood's statistical mechanical theory of transport processes.[4] In the present paper we will give a derivation of the phenomenological equations of fluids based on assumptions which we suppose to be valid for perfect and near-perfect gases as well as for dense gases and liquids. As in recent work on the thermodynamics of irreversible processes we will find that the irreversible part of the rate of change of a state variable is naturally expressed in terms of the gradients of corresponding thermodynamic "forces."[5] As in Kirkwood's work[4] we will find that the viscosity, heat conduction, and diffusion coefficients are determined from the autocorrelation functions of certain random processes.

In Sec. A, we define a set of phase functions whose values determine the macroscopic state of the system, and in Sec. B, we derive exact expressions for their rates of change as well as convenient approximate expressions for these rates. Sections C and D are concerned with a fluid containing only one kind of molecule. In Sec. C, we derive as a first approximation the equations of motion of an inviscid fluid together with the corresponding equation of energy balance while in Sec. D, we demonstrate the existence of shear and volume viscosity terms in the equations of motion as well as heat conduction and viscous work terms in the energy balance equation. Also in Sec. D, we derive explicit expressions for the corresponding coefficients of the irreversible phenomena. In Sec. E, we discuss briefly and on the model of the discussion in Sec. D, time-dependent phenomena in a fluid containing two species of molecules. In Sec. F, we apply the formulas for the viscosity and heat conduction coefficients derived in Sec. D to the special case of a perfect gas, and show that the result is the same as that given by the Chapman-Enskog method.

A. THE COMPLETE SET OF GROSS VARIABLES

In paper I,[1] we defined a complete set of gross variables to be a set of functions of the phase of a dynamical system which is such that their present values completely determine their expected future values. This complete determination is supposed to hold for all future times separated from the present by more than a certain macroscopically inobservable interval. In the

* Supported by U. S. Office of Naval Research contract.
[1] M. S. Green, J. Chem. Phys. **20**, 1281 (1952).
[2] S. Chapman and T. G. Cowling, *The Mathematical Theory of Nonuniform Gases* (Cambridge University Press, Cambridge, 1939).
[3] M. Born and H. S. Green, *A General Kinetic Theory of Liquids* (Cambridge University Press, Cambridge, 1949).
[4] J. H. Irving and J. G. Kirkwood, J. Chem. Phys. **18**, 817 (1950). See also J. G. Kirkwood, J. Chem. Phys. **14**, 180 (1946).
[5] S. de Groot *The Thermodynamics of Irreversible Processes* (North Holland Publishing Company, Amsterdam, 1951).

notation of I, the gross variables are $a_i(X) i=1\cdots r$, where X is the phase of the system. With each of the gross variables is associated another phase function $v_i(X)$ which at any phase X is the rate of change of the corresponding gross variable whenever the phase of the system is X. Pointed brackets around any phase function are used to indicate the average value of this phase function in the region of phase space where the gross variables have certain fixed values and in general represents a function of these values. In the case that the deviations of the actual future values of the gross variables from their expected future values can be neglected the following differential equations for the expectation values were given:

$$\frac{da_i}{dt}=\langle v_i\rangle+\sum_{j=1}^{r}\xi_{ij}\frac{\partial}{\partial a_j}\log w+\sum_{j=1}^{r}\frac{\partial\xi_{ij}}{\partial a_j}, \tag{1}$$

where $w(a_1\cdots a_r)\Delta a_1\cdots\Delta a_r$ is the volume of the part of phase space where the values of the gross variables lie between a_1 and $\Delta a_1\cdots a_r$ and Δa_r and

$$\xi_{ij}=\int_0^\tau[\langle v_i(X)v_j(X_\sigma)\rangle-\langle v_i(X)\rangle\langle v_j(X_\sigma)\rangle]d\sigma. \tag{2}$$

X_σ is the phase into which the phase X goes after time σ under the motion of the system.

In paper I, it was argued that the integrand in Eq. (2) behaves in the following way: for times less than a certain microscopically inobservable interval θ, the integrand is large. For times greater than this interval, however, it drops down to a quite small value which varies slowly with σ. If this is so the integral (2) does not depend very sensitively on τ, so long as $\tau\gg\theta$.

In order to apply these ideas to irreversible phenomena in fluids, we must choose an appropriate set of gross variables. Let us do this first for a fluid consisting of one kind of molecule. We know from the phenomenonological equations that knowledge of the local density of particles, momentum and energy at all places in the fluid determine the future values of these quantities at all later times. An appropriate set of gross variable will then be a set of phase functions which represent these local densities everywhere in the fluid.

A first choice that comes to mind for, say, the gross variables which are to represent the density of particles is

$$\rho'(\mathbf{x})=\sum_{i=1}^{N}\delta(\mathbf{x}_i-\mathbf{x}), \tag{3}$$

where $\mathbf{x}$ is the position vector of a point in the fluid, $\mathbf{x}_i$ the position vector of the ith molecule, δ the three-dimensional Dirac delta "function," and N the total number of molecules. There are, however two difficulties with this first obvious choice. The first is that Eqs. (3) define a continuous infinity of phase functions; one, indeed, for each $\mathbf{x}$. The second is that they give a much finer description of the local density than that to which the phenomenonological equations refer.

In order to avoid these two difficulties and also to sidestep the problem of what happens at rigid boundaries, it will be convenient to assume that our fluid is contained in a three-dimensional toroidal space, that is to say in a cube of side a in which corresponding points on opposite faces are considered identical. Then a shift in the coordinate vector of each molecule of the fluid by a translation (la, ma, na), l, m, n integers, does not change the phase. Let us consider the Fourier expansion coefficients of $\rho'(\mathbf{x})$ in the toroidal space. These are the phase functions

$$\rho_{\mathbf{k}}=\sum_{i=1}^{N}\exp i\mathbf{k}\cdot\mathbf{x}_i, \tag{4}$$

where $\mathbf{k}$ is one of the vectors $(2\pi l/a, 2\pi m/a, 2\pi n/a)$, l, m, n integers. This discretely infinite set of functions (4) contains as much information as $\rho'(\mathbf{x})$. We can, however reduce the fineness of the description and at the same time obtain a finite set of functions by eliminating those Fourier coefficients for which $|l|$, $|m|$, $|n|$ is greater than M where M is some large integer. This will have the effect of ignoring variations in the local density which take place over distances smaller than a/M. If we choose M so that a/M is beyond the limit of macroscopic measurability, but still large enough so that a cube of volume a^3/M^3 contains on the average a large number of molecules, the set of gross variables will contain all information required, but no more than is required, for a complete macroscopic description of the local density. The local density itself will be

$$\begin{aligned}\rho(\mathbf{x})&=a^{-3}\sum_{\mathbf{k}}\rho_{\mathbf{k}}\exp-i\mathbf{k}\cdot x \quad |l|,|m|,|n|\leq M\\&=a^{-3}\sum_{i=1}^{N}\sum_{\mathbf{k}}\exp i\mathbf{k}\cdot(\mathbf{x}_i-\mathbf{x})\\&=\sum_{i=1}^{N}\varphi(\mathbf{x}_i-\mathbf{x}),\end{aligned} \tag{5}$$

where

$$\varphi(x,y,z)=\frac{\sin 2\pi x/a(M+\frac{1}{2})}{a\sin\pi x/a}\cdot\frac{\sin 2\pi y/a(M+\frac{1}{2})}{a\sin\pi y/a}\cdot\frac{\sin 2\pi z/a(M+\frac{1}{2})}{a\sin\pi z/a}.$$

In the same way we can define a set of phase functions which give a complete macroscopic description of the local momentum density

$$\mathbf{p}_{\mathbf{k}}=\sum_{i=1}^{N}\mathbf{p}_i\exp i\mathbf{k}\cdot\mathbf{x}_i \quad |l|,|m|,|n|\leq M. \tag{6}$$

The local momentum density itself is

$$\mathbf{p}(\mathbf{x})=\sum_{i=1}^{N}\mathbf{p}_i\varphi(\mathbf{x}_i-\mathbf{x}). \tag{7}$$

The gross variables which describe the local energy density are constructed on the same plan.

$$E_{\mathbf{k}}=\sum_{i=1}^{N} E_i \exp i\mathbf{k}\cdot\mathbf{x}_i,$$

where E_i is the energy of the ith molecule. For E_i we take, somewhat arbitrarily, the kinetic energy of the ith molecule plus half of its interaction energy with all other molecules of the system.

$$E_{\mathbf{k}}=\sum_{i=1}^{N} (\mathbf{p}_i^2/2m+\tfrac{1}{2}\sum_{j\neq i}^{N} V(\mathbf{x}_i-\mathbf{x}_j)) \exp i\mathbf{k}\cdot\mathbf{x}_i, \qquad |l|, |m|, |n|\leq M, \quad (8)$$

where $V(x_i-x_i)$ is the interaction energy between the ith and jth molecule and m the mass of a molecule. The local energy density itself is then

$$E(\mathbf{x})=\sum_{i=1}^{N} (\mathbf{p}_i^2/2m+\tfrac{1}{2}\sum_{j\neq i}^{N} V(\mathbf{x}_i-\mathbf{x}_j)\varphi(\mathbf{x}_i-\mathbf{x})). \quad (9)$$

The generalization of these formulas to systems which have more than one kind of molecule is straightforward, and we will simply state them explicitly for the case of two kinds, A and B.

$$\rho_{A\mathbf{k}}=\sum_{i=1}^{N_A} \exp i\mathbf{k}\cdot\mathbf{x}_i, \quad |l|, |m|, |n|\leq M \quad (10A)$$

$$\rho_A(\mathbf{x})=\sum_{i=1}^{N_A} \varphi(\mathbf{x}_i-\mathbf{x}) \quad (11A)$$

$$\rho_{B\mathbf{k}}=\sum_{i=1}^{N_B} \exp i\mathbf{k}\cdot\mathbf{y}_j \quad (10B)$$

$$\rho_B(\mathbf{x})=\sum_{i=1}^{N_B} \varphi(\mathbf{y}_j-\mathbf{x}), \quad (11B)$$

where $\mathbf{x}_i$ is the coordinate vector of the ith molecule of type A and $\mathbf{y}_j$ that of the jth molecule of type B, and N_A, N_B the total number of molecules of type A and B, respectively.

$$\mathbf{p}_{\mathbf{k}}=\sum_{i=1}^{N_A} \mathbf{p}_i \exp i\mathbf{k}\cdot\mathbf{x}_i+\sum_{j=1}^{N_B} \mathbf{q}_j \exp i\mathbf{k}\cdot\mathbf{y}_j, \quad (12)$$

$$\mathbf{p}(\mathbf{x})=\sum_{i=1}^{N_A} \mathbf{p}_i\varphi(\mathbf{x}_i-\mathbf{x})+\sum_{j=1}^{N_B} \mathbf{q}_j\varphi(\mathbf{y}_j-\mathbf{x}), \quad (13)$$

where $\mathbf{p}_i$ is the momentum of the ith molecule of type A, and $\mathbf{q}_j$ that of the jth molecule of type B.

$$E_{\mathbf{k}}=\sum_{i=1}^{N_A} (\mathbf{p}_i^2/2m_A+\tfrac{1}{2}\sum_{k\neq i}^{N_B} U(\mathbf{x}_i-\mathbf{x}_k) +\tfrac{1}{2}\sum_{l=1}^{N_B} V(\mathbf{x}_i-\mathbf{y}_l)) \exp i\mathbf{k}\cdot\mathbf{x}_i+\sum_{j=1}^{N_A} (\mathbf{q}_j^2/2m_B +\tfrac{1}{2}\sum_{k=1}^{N_B} V(\mathbf{y}_j-\mathbf{x}_k)+\tfrac{1}{2}\sum_{l\neq j}^{N_B} V(\mathbf{y}_j-\mathbf{y}_l)) \exp i\mathbf{k}\cdot\mathbf{y}_j \quad (14)$$

and similarly for $E(\mathbf{x})$. m_A is the mass of a molecule of type A and m_B that of one of type B. U, V, W are the interaction energies between two molecules of type A, one of type A and one of type B, and two of type B, respectively.

B. THE RATES OF CHANGE

The gross variables defined in the previous section were suggested by the phenomenonological theory of fluids. When we turn to the calculation of the corresponding rate of change functions, we will find that there is a more fundamental reason for choosing them. The phase functions given in Sec. A have an especially small rate of change. We will calculate these rates for systems having only one kind of molecule and then simply state the results for systems containing two types of molecules.

The dynamical equations of motion of the system are

$$(d\mathbf{x}_i/dt)=\mathbf{p}_i/m, \qquad (d\mathbf{p}_i/dt)=\sum_{j\neq i}^{N} -\nabla_{\mathbf{x}_i} V(\mathbf{x}_i-\mathbf{x}_j)=\sum_{j\neq i}^{N} \mathbf{F}_{ij}. \quad (15)$$

We have then

$$(d\rho_{\mathbf{k}}/dt)=i\mathbf{k}\cdot\sum_{i=1}^{N} (d\mathbf{x}_i/dt)_i \exp i\mathbf{k}\cdot\mathbf{x}_i =i\mathbf{k}\cdot\sum_{i=1}^{N} \mathbf{p}_i/m \exp i\mathbf{k}\cdot\mathbf{x}_i. \quad (16)$$

Similarly

$$(d\mathbf{p}_{\mathbf{k}}/dt)=\sum_{i=1}^{N} (i\mathbf{k}\cdot(d\mathbf{x}_i/dt)\mathbf{p}_i+(d\mathbf{p}_i/dt)) \exp i\mathbf{k}\cdot\mathbf{x}_i =i\mathbf{k}\cdot\sum_{i=1}^{N} \mathbf{p}_i\mathbf{p}_i/m \exp i\mathbf{k}\cdot\mathbf{x}_i+\sum_{i\neq j}^{N}\sum^{N} \mathbf{F}_{ij} \exp i\mathbf{k}\cdot\mathbf{x}_i.$$

Noting that $\mathbf{F}_{ji}=-\mathbf{F}_{ij}$, we can rewrite this in the form

$$(d\mathbf{p}_{\mathbf{k}}/dt)=i\mathbf{k}\cdot\sum_{i=1}^{N} \mathbf{p}_i\mathbf{p}_i/m \exp i\mathbf{k}\cdot\mathbf{x}_i +\tfrac{1}{2}\sum_{i\neq j}^{N}\sum^{N} \mathbf{F}_{ij}(\exp i\mathbf{k}\cdot\mathbf{x}_i-\exp i\mathbf{k}\cdot\mathbf{x}_j). \quad (17)$$

For $E_{\mathbf{k}}$ we have

$$(dE_{\mathbf{k}}/dt)=i\mathbf{k}\cdot\sum_{i=1}^{N} \mathbf{x}_i(\mathbf{p}_i^2/2m+\tfrac{1}{2}\sum_{j\neq i}^{N} V(\mathbf{x}_i-\mathbf{x}_j)) \times\exp i\mathbf{k}\cdot\mathbf{x}_i+\sum_{i=1}^{N} \{\mathbf{p}_i/m(d\mathbf{p}_i/dt) +\tfrac{1}{2}\sum_{j\neq i}^{N} [(d\mathbf{x}_i/dt)\nabla_{\mathbf{x}_i} V(\mathbf{x}_i-\mathbf{x}_j) +(d\mathbf{x}_j/dt)\nabla_{\mathbf{x}_j} V(\mathbf{x}_i-\mathbf{x}_j)]\} \exp i\mathbf{k}\cdot\mathbf{x}_i.$$

By the dynamical equations, and noting that

$$\nabla_{x_i} V(\mathbf{x}_i-\mathbf{x}_j)=-\nabla_{x_j} V(\mathbf{x}_i-\mathbf{x}_j)=-\mathbf{F}_{ij}=\mathbf{F}_{ji},$$

we obtain

$$(dE_{\mathbf{k}}/dt)=i\mathbf{k}\cdot\{\sum_{i=1}^{N}\mathbf{p}_i/m(\mathbf{p}_i^2/2m+\tfrac{1}{2}\sum_{j\neq i}^{N}V(\mathbf{x}_i-\mathbf{x}_j))\times\exp i\mathbf{k}\cdot\mathbf{x}_i\}+\tfrac{1}{2}\sum_{i\neq j}^{N}\sum^{N}(\mathbf{p}_i+\mathbf{p}_j)/2m\cdot\mathbf{F}_{ij}\times(\exp i\mathbf{k}\cdot\mathbf{x}_i-\exp i\mathbf{k}\cdot\mathbf{x}_j). \quad (18)$$

We note two features of Eqs. (16), (17), and (18). The first is that all the rates are zero when $\mathbf{k}=0$. This means of course that ρ_0, $\mathbf{p}_0$, and E_0 are all integrals of motion. They are in fact the total number of particles, the total momentum and the total energy, respectively. The second is that the rates of change are small when $\mathbf{k}$ is small. We can make this statement more explicit if we expand the last group of terms in Eqs. (17) and (18) in a power series. This expansion will be justified by the fact that each summand in the double sum contributes significantly only when the two molecules are within the range of molecular forces. Since $|\mathbf{k}|$ is small compared to the reciprocal of this range the two exponentials have practically the same value. We write their difference as

$$\exp i\mathbf{k}\cdot\mathbf{x}_i(1-\exp-i\mathbf{k}\cdot(\mathbf{x}_i-\mathbf{x}_j)=(i\mathbf{k}\cdot(\mathbf{x}_i-\mathbf{x}_j)+0(\mathbf{k}^2))\exp i\mathbf{k}\cdot\mathbf{x}_i$$

and obtain for Eq. (17)

$$(d\mathbf{p}/dt)_{\mathbf{k}}=i\mathbf{k}\cdot\sum_{i=1}^{N}[\mathbf{p}_i\mathbf{p}_i/m+\tfrac{1}{2}\sum_{j\neq i}^{N}(\mathbf{x}_i-\mathbf{x}_j)\mathbf{F}_{ij}]\times\exp i\mathbf{k}\cdot\mathbf{x}_i, \quad (19)$$

where the terms we have neglected are of the order $|\mathbf{k}|^2$ and higher. In the same way we obtain for Eq. (18)

$$(dE_{\mathbf{k}}/dt)=i\mathbf{k}\cdot\sum_{i=1}^{N}[\mathbf{p}_i/m(\mathbf{p}_i^2/2m+\tfrac{1}{2}\sum_{j\neq i}^{N}V(x_i-x_j)+\tfrac{1}{2}\sum_{j\neq i}^{N}(\mathbf{x}_i-\mathbf{x}_j)\mathbf{F}_{ij}\cdot(\mathbf{p}_i+\mathbf{p}_j)/2m]\times\exp i\mathbf{k}\cdot\mathbf{x}_i \quad (20)$$

to terms of the first order in $\mathbf{k}$.

If we examine the order of magnitude of these rates we see that each one can be expressed in the form $|\mathbf{k}|vA$, where v is a representative molecular velocity and A a quantity of the same order of magnitude as the gross variable in question. Thus the time for a gross variable to change by an appreciable fraction of itself $(|\mathbf{k}|v)^{-1}$. On the other hand the microscopic time scale is rv^{-1} where r is a measure of the molecular size. Since we have assumed that $|\mathbf{k}|^{-1}$ is large compared to r, the timescale for change of the gross variables is long compared to the microscopic time scale, longer, in fact, in proportion to the number of molecules contained in a macroscopically observable interval.

For the case of two kinds of molecules we have

$$(d\rho_{A\mathbf{k}}/dt)=i\mathbf{k}\cdot\sum_{i=1}^{N_A}\mathbf{p}_i/m_A\exp i\mathbf{k}\cdot\mathbf{x}_i, \quad (21A)$$

and

$$(d\rho_{B\mathbf{k}}/dt)=i\mathbf{k}\cdot\sum_{j=1}^{N_B}\mathbf{q}_j/m_B\exp i\mathbf{k}\cdot\mathbf{y}_j. \quad (21B)$$

To the first order in $|\mathbf{k}|$

$$(d\mathbf{p}_{\mathbf{k}}/dt)=i\mathbf{k}\cdot\{\sum_{i=1}^{N_A}(\mathbf{p}_i\mathbf{p}_i/m_A+\tfrac{1}{2}\sum_{k\neq i}^{N_A}(\mathbf{x}_i-\mathbf{x}_k)\mathbf{F}_{ik}+\tfrac{1}{2}\sum_{l=1}^{N_B}(\mathbf{x}_i-\mathbf{y}_l)\mathbf{G}_{il})\exp i\mathbf{k}\cdot\mathbf{x}_i+\sum_{j=1}^{N_B}(\mathbf{q}_j\mathbf{q}_j/m_B+\tfrac{1}{2}\sum_{k=1}^{N_A}(\mathbf{x}_k-\mathbf{y}_j)\mathbf{G}_{kj}+\tfrac{1}{2}\sum_{l\neq j}^{N_B}(\mathbf{y}_j-\mathbf{y}_l)\mathbf{H}_{jl})\exp i\mathbf{k}\cdot\mathbf{y}_j, \quad (22)$$

where $\mathbf{F}_{ik}$ is the force between two molecules of type A, $\mathbf{G}_{ik}$ that between one of type A and one of type B and $\mathbf{H}_{jl}$ that between two of type B.

$$(dE_{\mathbf{k}}/dt)=i\mathbf{k}\cdot\{\sum_{i=1}^{N_A}[\mathbf{p}_i/m_A(\mathbf{p}_i^2/2m_A+\tfrac{1}{2}\sum_{k\neq i}^{N_A}U(\mathbf{x}_i-\mathbf{x}_k)+\tfrac{1}{2}\sum_{l=1}^{N_B}V(\mathbf{x}_i-\mathbf{y}_l))+\tfrac{1}{4}\sum_{k\neq i}^{N_A}(\mathbf{x}_i-\mathbf{x}_k)\mathbf{F}_{ik}\cdot(\mathbf{p}_i/m_A+\mathbf{p}_k/m_A)+\tfrac{1}{4}\sum_{l=1}^{N_B}(\mathbf{x}_i-\mathbf{y}_l)\mathbf{G}_{il}\cdot(\mathbf{p}_i/m_A+\mathbf{q}_l/m_B)]\times\exp i\mathbf{k}\cdot\mathbf{x}_i+\sum_{j=1}^{N_B}[\mathbf{q}_j/m_B(\mathbf{q}_j^2/2m_B+\tfrac{1}{2}\sum_{k=1}^{N_A}V(\mathbf{x}_k-\mathbf{y}_j)+\tfrac{1}{2}\sum_{l\neq j}^{N_B}W(\mathbf{y}_l-\mathbf{y}_j))+\tfrac{1}{4}\sum_{k=1}^{N_A}(\mathbf{x}_k-\mathbf{y}_j)\mathbf{G}_{kj}\cdot(\mathbf{q}_j/m_B+\mathbf{p}_k/m_A)+\tfrac{1}{4}\sum_{l\neq j}^{N_B}(\mathbf{y}_j-\mathbf{y}_l)\mathbf{H}_{jl}\cdot(\mathbf{q}_j/m_B+\mathbf{q}_l/m_B)]\times\exp i\mathbf{k}\cdot\mathbf{y}_l\} \quad (23)$$

to the first order in $|\mathbf{k}|$.

C. THE FIRST APPROXIMATION

We will be concerned in this section and the next with the derivation of the phenomenonological equations of a one-component fluid, that is to say the Navier-Stokes

equations together with the equation of energy balance. In the present section we will consider the approximation which takes into account only the first term on the right in Eq. (1). In this approximation, the rate of change of the expectation value of a gross variable is simply the average of the corresponding rate over all phases for which the gross variables have the particular fixed values which define the gross state in which the system happens to be.

Because of the form of the rate functions we need to know only the distribution function of single particles and of pairs in order to calculate these averages. We will show in an appendix that to a sufficient approximation these are simply the equilibrium distributions corresponding to the local particle, momentum, and energy densities.

$$Nf_1(\mathbf{p}_i\mathbf{x}_i)=\rho(\mathbf{x}_i)(2\pi m\kappa T(\mathbf{x}_i))^{-\frac{3}{2}} \times\exp-(\mathbf{p}_i-m\mathbf{v}(\mathbf{x}_i)^2/2m\kappa T(\mathbf{x}_i) \quad (24A)$$

$$f_2(\mathbf{p}_i,\mathbf{x}_i;\mathbf{p}_j\mathbf{x}_j)=f_1(\mathbf{p}_i\mathbf{x}_i)f_1(\mathbf{p}_j\mathbf{x}_j)g(\mathbf{x}_i-\mathbf{x}_j), \quad (24B)$$

where $T(\mathbf{x})$ is the equilibrium temperature corresponding to the local internal energy[6] and particle densities at $\mathbf{x}$, $\mathbf{v}(\mathbf{x})$ is the local average velocity at $\mathbf{x}$, equal to $\mathbf{p}(\mathbf{x})/m\rho(\mathbf{x})$, and $g(\mathbf{x}_i-\mathbf{x}_j)$ is the equilibrium spacial distribution of pairs corresponding to the local conditions at some point representative of both $\mathbf{x}_i$ and $\mathbf{x}_j$. $g(\mathbf{x}_i-\mathbf{x}_j)$ is normalized so that $\lim_{|\mathbf{x}_i-\mathbf{x}_j|\to\infty}g(\mathbf{x}_i-\mathbf{x}_j)=1$.

For the mean of the rate of change of $\rho_\mathbf{k}$ we have

$$\langle(d\rho_\mathbf{k}/dt)\rangle=i\mathbf{k}\cdot\sum_{i=1}^{N}\int\mathbf{p}_i/mf_1(\mathbf{p}_i,\mathbf{x}_i)\exp i\mathbf{k}\cdot\mathbf{x}_i d\mathbf{p}_i d\mathbf{x}_i = i\mathbf{k}\cdot\int\rho(\mathbf{x})\mathbf{v}(\mathbf{x})\exp i\mathbf{k}\cdot\mathbf{x}d\mathbf{x}. \quad (25)$$

$$\langle(d\mathbf{p}_\mathbf{k}/dt)\rangle=i\mathbf{k}\cdot\{\sum_{i=1}^{N}\int\mathbf{p}_i\mathbf{p}_i/mf_1(\mathbf{p}_i,\mathbf{x}_i)d\mathbf{p}_i d\mathbf{x}_i +\tfrac{1}{2}\sum_{i\neq j}^{N}\sum^{N}\int(\mathbf{x}_i-\mathbf{x}_j)\mathbf{F}_{ij}f_2(\mathbf{p}_i\cdots\mathbf{x}_j)\times\exp i\mathbf{k}\cdot\mathbf{x}_i d\mathbf{x}_i\cdots d\mathbf{p}_j =i\mathbf{k}\cdot\int(m\rho(\mathbf{x})\mathbf{v}(\mathbf{x})\mathbf{v}(\mathbf{x})+\rho(\mathbf{x})\kappa T(\mathbf{x})\mathbf{I} +\tfrac{1}{2}\rho(\mathbf{x})^2\int\mathbf{RF}(\mathbf{R})g(\mathbf{R})d\mathbf{R})\exp i\mathbf{k}\cdot\mathbf{x}d\mathbf{x}. \quad (26)$$

In the second integral we have made use of the fact that $\rho(\mathbf{x})$ varies very slowly over the range of molecular forces and of the fact that $\mathbf{F}_{ij}$ is a function of R only. $\mathbf{I}$ is the unit dyadic. Since $\mathbf{F}(\mathbf{R})$ is in the direction of $\mathbf{R}$ and $g(\mathbf{R})$ is a function of the magnitude of $\mathbf{R}$ only, the third term in the integrand of Eq. (26) will be a multiple of the unit dyadic. The coefficient of the unit dyadic in Eq. (26) is simply the virial expression[4,7] for the equilibrium pressure $p(\mathbf{x})$ corresponding to the local state of the fluid. We can write Eq. (26) finally as

$$\langle(d\mathbf{p}_\mathbf{k}/dt)\rangle=i\mathbf{k}\cdot\int(m\rho(\mathbf{x})\mathbf{v}(\mathbf{x})\mathbf{v}(\mathbf{x})+p(\mathbf{x})\mathbf{I})\exp i\mathbf{k}\cdot\mathbf{x}d\mathbf{x}.$$

For $E_\mathbf{k}$ we obtain

$$\langle(dE_\mathbf{k}/dt)\rangle=\int\mathbf{v}(\mathbf{x})(\tfrac{1}{2}m\rho(\mathbf{x})\mathbf{v}(\mathbf{x})^2+(5/2)\rho(x)\kappa T(\mathbf{x}) +\tfrac{1}{2}\rho(\mathbf{x})^2\int V(\mathbf{R})g(\mathbf{R})d\mathbf{R} +\tfrac{1}{6}\rho(\mathbf{x})^2\int\mathbf{RF}(\mathbf{R})g(R)d\mathbf{R})\exp i\mathbf{k}\cdot\mathbf{x}d\mathbf{x}. \quad (27)$$

Now

$$\tfrac{1}{2}m\rho\mathbf{v}^2+\tfrac{3}{2}\rho\kappa T+\tfrac{1}{2}\rho^2\int Vgd\mathbf{R}$$

is very approximately equal to the average value of $E(\mathbf{x})$ [Eq. (9)] which, since $E(\mathbf{x})$ is a function of the gross variables, is of course equal to the constant value which $E(\mathbf{x})$ has throughout the ensemble in which we are averaging. On the other hand

$$\rho\kappa T+\tfrac{1}{6}\rho^2\int\mathbf{R}\cdot\mathbf{F}gd\mathbf{R}$$

is the local pressure so that we can write Eq. (27) as

$$\langle(dE/dt)_\mathbf{k}\rangle=i\mathbf{k}\cdot\int\mathbf{v}(\mathbf{x})(E(\mathbf{x})+\mathbf{p}(\mathbf{x}))\exp i\mathbf{k}\cdot\mathbf{x}d\mathbf{x}. \quad (28)$$

Formulas (25), (26), and (28) give a first approximation to the rates of change of the expectation value of the corresponding gross variables. We will be better able to see what they mean if we use them to calculate the expectation value of the local densities themselves. We have

$$\langle(d\rho(\mathbf{x})/dt\rangle=a^{-3}\sum_{\mathbf{k}\ |l|,\,|m|,\,|n|\leq M}\exp-i\mathbf{k}\cdot\mathbf{x}\langle(d\rho_\mathbf{k}/dt)\rangle$$

$$=a^{-3}\sum_{\mathbf{k}}i\mathbf{k}\cdot\int\rho(\mathbf{x}')\mathbf{v}(\mathbf{x}')\exp i\mathbf{k}\cdot(\mathbf{x}'-\mathbf{x})d\mathbf{x}$$

$$=\int\rho(\mathbf{x}')\mathbf{v}(\mathbf{x}')\cdot\nabla_{\mathbf{x}'}\varphi(\mathbf{x}'-\mathbf{x})d\mathbf{x}'$$

$$=-\int\nabla_{\mathbf{x}'}\rho(\mathbf{x}')\mathbf{v}(\mathbf{x}')\varphi(\mathbf{x}'-\mathbf{x})d\mathbf{x}'$$

$$=-\nabla_\mathbf{x}\rho(\mathbf{x})\mathbf{v}(\mathbf{x})$$

very approximately.

By similar calculations applied to the other local densities we have as the first approximation to the

[6] By the internal energy of a system we mean its energy as it would be determined by an observer moving along with its center of mass.

[7] H. Goldstein *Classical Mechanics* (Addison-Wesley Press, Cambridge, Massachusetts, 1950).

phenomenonological equations of a one component fluid[7]

$$\partial\rho/\partial t = -\nabla\cdot\rho\mathbf{v} \tag{29A}$$

$$\partial\mathbf{p}/\partial t = -\nabla\cdot(m\rho\mathbf{v}\mathbf{v}+p\mathbf{I}) \tag{29B}$$

$$\partial E/\partial t = -\nabla\cdot(E+p)\mathbf{v}. \tag{29C}$$

In Eqs. (29) ρ, $\mathbf{p}$, and E are to be taken as the expectation values of the phase functions (5), (7), and (9). Equations (29) are of course the familiar equations of motion of an inviscid fluid together with the equation of energy balance. The first approximation thus describes much of the behavior of fluids with the important exception of irreversible effects. This is a general feature of the first approximation.

D. IRREVERSIBLE EFFECTS IN A ONE-COMPONENT FLUID

We have seen that the first term in Eq. (1) does not give an account of the irreversible effects. In this section we will consider the second and third terms which contain these effects. Before we do this, however, it is necessary to remark that although the original theory was formulated for real gross variables we may use Eq. (1) without change for complex gross variables. This is due to the fact that the $5(2M+1)^3-1$ gross variables defined in Eqs. (4), (6), and (8) are linear combinations with constant coefficients of their $5(2M+1)^3-1$ distinct real and imaginary parts. If we use these real and imaginary parts to define both the region in which the averages are taken and w, its phase volume density, a simple calcultation shows that Eq. (1) has the same form for the complex gross variables as for their real and imaginary parts.

Let us first consider the function $\log w$ and its derivatives. We will show in the appendix that

$$\log w = \kappa^{-1}\int s(\epsilon(\mathbf{x}),\rho(\mathbf{x}))d\mathbf{x}, \tag{30}$$

where s is the equilibrium entropy density considered as a function of

$$\epsilon(\mathbf{x}) = E(\mathbf{x}) - \mathbf{p}(\mathbf{x})^2/2m\rho(\mathbf{x}),$$

the local density of intrinsic energy and $\rho(\mathbf{x})$ the local density of particles. $\log w$ is implicitly a function of the gross variables since $\epsilon(\mathbf{x})$ and $\rho(\mathbf{x})$ are. We have

$$\frac{\partial}{\partial\rho_\mathbf{k}}\log w = -\frac{1}{\kappa}\int\left(\frac{\partial s}{\partial\rho}+\frac{\mathbf{p}(\mathbf{x})^2}{2m\rho(\mathbf{x})}\frac{\partial s}{\partial\epsilon}\right)\frac{\partial\rho(\mathbf{x})}{\partial\rho_\mathbf{k}}d\mathbf{x}$$

$$\frac{\partial}{\partial\mathbf{p}_\mathbf{k}}\log w = -\frac{1}{\kappa}\int\frac{\mathbf{p}(\mathbf{x})}{m\rho(\mathbf{x})}\frac{\partial s}{\partial\epsilon}\frac{\partial\mathbf{p}(\mathbf{x})}{\partial\mathbf{p}_\mathbf{k}}d\mathbf{x}^8$$

$$\frac{\partial}{\partial E_\mathbf{k}}\log w = -\frac{1}{\kappa}\int\frac{\partial s}{\partial\epsilon}\frac{\partial\epsilon(\mathbf{x})}{\partial E_\mathbf{k}}d\mathbf{x}.$$

Now we know from phenomenonological thermodynamics that $\partial s/\partial\epsilon = T^{-1}$, $\partial s/\partial\rho = -\mu/T$, where μ is the chemical potential, while from Eqs. (5), (7), and (9),

$$\frac{\partial\rho(\mathbf{x})}{\partial\rho_\mathbf{k}} = \frac{\partial E(\mathbf{x})}{\partial E_\mathbf{k}} = \frac{1}{a^3}\exp -i\mathbf{k}\cdot\mathbf{x}, \quad \frac{\partial\mathbf{p}(\mathbf{x})}{\partial\mathbf{p}_\mathbf{k}} = \frac{\mathbf{I}}{a^3}\exp -i\mathbf{k}\cdot\mathbf{x}.$$

Substituting these values in the preceding equations and noting that $\mathbf{p}(\mathbf{x})/m\rho(\mathbf{x}) = \mathbf{v}(\mathbf{x})$ we obtain

$$\frac{\partial}{\partial\rho_\mathbf{k}}\log w = \frac{1}{\kappa a^3}\int\frac{-\mu(\mathbf{x})+\frac{1}{2}m\mathbf{v}(\mathbf{x})^2}{T(\mathbf{x})}\exp -i\mathbf{k}\cdot\mathbf{x}d\mathbf{x}, \tag{31A}$$

$$\frac{\partial}{\partial\mathbf{p}_\mathbf{k}}\log w = \frac{1}{\kappa a^3}\int\frac{-\mathbf{v}(\mathbf{x})}{T(\mathbf{x})}\exp -i\mathbf{k}\cdot\mathbf{x}d\mathbf{x}, \tag{31B}$$

$$\frac{\partial}{\partial E_\mathbf{k}}\log w = \frac{1}{\kappa a^3}\int\frac{1}{T(\mathbf{x})}\exp -i\mathbf{k}\cdot\mathbf{x}d\mathbf{x}. \tag{31C}$$

Each of these derivatives of $\log w$ is seen to be the Fourier expansion coefficient of a certain local property of the fluid. These local properties are the "forces" corresponding to $\rho(\mathbf{x})$, $\mathbf{p}(\mathbf{x})$ and $E(\mathbf{x})$ in the sense of the thermodynamics of irreversible processes.[5]

Let us turn now to the quantities in Eq. (1). It will be convenient in what follows sometimes to drop the Gibbsian dyadic and vector notation which we have been using until now and use instead an index notation in which Greek subscripts α, β, γ, δ, etc., take on the three values x, y, z and in which the convention of summing over two repeated subscripts is to be observed. Latin subscripts i, j, k, l, etc., will continue to refer to the different molecules. We propose to show that each ξ has the form

$$-k_\alpha k_\beta'\int T_{\alpha\beta}(\rho(\mathbf{x}),E(\mathbf{x}),\mathbf{p}(\mathbf{x}))\exp i(\mathbf{k}+\mathbf{k}')\cdot\mathbf{x}d\mathbf{x}, \tag{32}$$

where $T_{\alpha\beta}$ is an element of a Cartesian tensor of the second, third, or fourth rank, and $\mathbf{k}$, $\mathbf{k}'$ are the wave vectors of the two gross variables with which the particular ξ in question is concerned. We will take as an example a ξ which refers to the γ component of $\mathbf{p}_k$ and the δ component of $\mathbf{p}_{k'}$. We have

$$\xi(\mathbf{p}_{k\gamma},\mathbf{p}_{k'\delta})$$

$$= -k_\alpha k_\beta'\int_0^\tau d\sigma\sum_{i=1}^N\sum_{j=1}^N\Big\{\langle(p_{i\alpha}p_{i\gamma}/m+\tfrac{1}{2}\sum_{k\neq i}^N(x_{i\alpha}-x_{k\alpha})F_{ik\gamma})$$

$$\times(p_{j\beta}'p_{j\delta}'/m+\tfrac{1}{2}\sum_{l\neq j}^N(x_{j\beta}'-x_{l\beta}')F_{jl\delta}')\exp i(\mathbf{k}\cdot\mathbf{x}_i+\mathbf{k}'\cdot x_j')\rangle-\langle(p_{i\alpha}'p_{i\gamma}/m+\tfrac{1}{2}\sum_{k=i}^N(x_{i\alpha}-x_{k\alpha})F_{ik\gamma})\exp i\mathbf{k}\cdot\mathbf{x}_i)\rangle$$

$$\langle p_{j\beta}'p_{j\delta}'/m+\tfrac{1}{2}\sum_{i\neq j}^N(x_{j\beta}'-x_{l\beta}')F_{jl\delta}')\exp i\mathbf{k}'\cdot\mathbf{x}_j')\rangle\Big\}, \tag{33}$$

where we have used a dash ($'$) to indicate the value of a phase function at time σ considered as a function of the phase at time zero. It will be convenient to consider separately the summands in Eq. (33) with $i=j$ and those with $i\neq j$. We note first of all that during the interval $0\leq\sigma\leq\tau$ a molecule will probably not have diffused much from its original position so that we may put $\mathbf{x}_i'=\mathbf{x}_i$, $\mathbf{x}_j'=\mathbf{x}_j$. We may then write a term of the first kind as

$$N^{-1}\int\rho(\mathbf{x}_i)(\langle A_{i\alpha\gamma}A_{i\beta\delta}'\rangle_{\mathbf{x}_i}$$
$$-\langle A_{i\alpha\gamma}\rangle_{\mathbf{x}_i}\langle A_{i\beta\delta}'\rangle_{\mathbf{x}_i})\exp i(\mathbf{k}+\mathbf{k}')\cdot\mathbf{x}_i d\mathbf{x}_i$$
$$+N^{-1}\int\rho(\mathbf{x}_i)\langle A_{i\alpha\gamma}\rangle_{\mathbf{x}_i}\langle A_{i\beta\delta}'\rangle_{\mathbf{x}_i}\exp i(\mathbf{k}+\mathbf{k}')\cdot\mathbf{x}_i d\mathbf{x}_i$$
$$-N^{-2}\left[\int\rho(\mathbf{x}_i)\langle A_{i\alpha\gamma}\rangle_{\mathbf{x}_i}\exp i\mathbf{k}\cdot\mathbf{x}_i d\mathbf{x}_i\right]$$
$$\times\left[\int\rho(\mathbf{x}_i)\langle A_{i\beta\delta}'\rangle_{\mathbf{x}_i}\exp i\mathbf{k}'\cdot\mathbf{x}_i d\mathbf{x}_i\right],$$

where

$$A_{i\alpha\gamma}=p_{i\alpha}p_{i\gamma}/m+\tfrac{1}{2}\sum_{k=i}^{N}(x_{i\alpha}-x_{k\alpha})F_{ik\delta} \qquad (34)$$

and $\langle\ \rangle_{\mathbf{x}_i}$ means conditional average with all the gross variables *and* the position vector of the ith molecule fixed. We assert that the significant contribution to ξ comes from the first term. For small σ the conditional mean of the product is not in general equal to the product of the conditional means, but for σ long enough for a molecule to have made many collisions or vibrations in the space allowed it by its neighbors $\mathbf{A}_i'$ can be expected to be uncorrelated with its value at zero and the conditional mean of this product can be expected to be equal to the product of the conditional means. $\langle\mathbf{A}_i'\rangle_{\mathbf{x}_i}$ on the other hand is to a first approximation constant so that the second and third terms merely contribute terms proportional to τ.

We may write a term of the second kind as

$$N^{-2}\int\int\rho(\mathbf{x}_i)\rho(\mathbf{x}_j)[g(\mathbf{x}_i-\mathbf{x}_j)\langle A_{i\alpha\gamma}A_{j\beta\delta}'\rangle_{\mathbf{x}_i\mathbf{x}_j}$$
$$-\langle A_{i\alpha\gamma}\rangle_{\mathbf{x}_i}\langle A_{j\beta\delta}'\rangle_{\mathbf{x}_j}]\exp i(\mathbf{k}\cdot\mathbf{x}_i+\mathbf{k}'\cdot\mathbf{x}_j)d\mathbf{x}_i d\mathbf{x}_j, \qquad (35)$$

where $\langle\ \rangle_{\mathbf{x}_i\mathbf{x}_j}$ means conditional average with all the gross variables and $\mathbf{x}_i$ and $\mathbf{x}_j$ fixed. Now for molecule i far from molecule j we may expect $\mathbf{A}_j'$ to be statistically independent of $\mathbf{A}_i$ whether σ is large or small compared to the molecular time scale. The expression in square brackets in Eq. (34) will be zero unless $\mathbf{x}_i$ is close to $\mathbf{x}_j$. We may therefore replace $\mathbf{x}_j$ by $\mathbf{x}_i$ in Eq. (34) except in the square bracket and obtain

$$N^{-2}\int\rho(\mathbf{x}_i)^2\left\{\int[g(\mathbf{x}_i-\mathbf{x}_j)\langle A_{i\alpha\gamma}A_{j\beta\delta}'\rangle_{\mathbf{x}_i\mathbf{x}_i}$$
$$-\langle A_{i\alpha\gamma}\rangle_{\mathbf{x}_i}\langle A_{j\beta\delta}'\rangle]dx_j\right\}\exp i(\mathbf{k}+\mathbf{k}')\cdot\mathbf{x}_i d\mathbf{x}_i. \qquad (36)$$

Since there are N terms of the first kind and approximately N^2 of the second, Eq. (33) becomes

$$\xi(p_{k\gamma}p_{k'\delta})=-k_\alpha k_\beta\int T^{(4)}{}_{\alpha\beta\gamma\delta}\exp i(\mathbf{k}+\mathbf{k}')\cdot\mathbf{x}_i d\mathbf{x}_i \qquad (35)$$

with

$$T^{(4)}{}_{\alpha\beta\gamma\delta}(\mathbf{x}_i)=\rho(\mathbf{x}_i)\int_0^\tau d\sigma(\langle A_{i\alpha\gamma}A_{i\beta\delta}'\rangle_{\mathbf{x}_i}$$
$$-\langle A_{i\alpha\gamma}\rangle_{\mathbf{x}_i}\langle A_{i\beta\delta}'\rangle_{\mathbf{x}_i})+\rho(\mathbf{x}_i)^2\int_0^\tau d\sigma\int d\mathbf{x}_j$$
$$\times[g(\mathbf{x}_i-\mathbf{x}_j)\langle A_{i\alpha\gamma}A_{j\beta\delta}'\rangle_{\mathbf{x}_i\mathbf{x}_j}$$
$$-\langle A_{i\alpha\gamma}\rangle_{\mathbf{x}_i}\langle A_{j\beta\delta}'\rangle_{\mathbf{x}_j}]. \qquad (35A)$$

Now at $\sigma=0$ none of the molecules which make a significant contribution to $\mathbf{A}_i$ are far away from molecule i, and because the time for a molecule to diffuse a macroscopic distance is long compared to τ, this is true throughout the region of integration. In other words during the interval $0\leq\sigma\leq\tau$ none of the molecules whose behavior determines the value of $\mathbf{T}^{(4)}$ are outside a region where the local density of particles, momentum, and energy are substantially constant and equal to $\rho(\mathbf{x}_i)$, $\mathbf{p}(\mathbf{x}_i)$ and $E(\mathbf{x}_i)$. We may suppose therefore that $\mathbf{T}^{(4)}$ is independent of the values of ρ, p, E outside a small region surrounding $\mathbf{x}_i$, and replace the averages in Eq. (35A) by an average in which the total number of particles momentum and energy are fixed to be $\rho(\mathbf{x}_i)a^3$, $\mathbf{p}(\mathbf{x}_i)a_3$, and $E(\mathbf{x}_i)a^3$, respectively. $\mathbf{T}^{(4)}$ is thus a function of the local state at $\mathbf{x}_i$.

We can get a neater and more manageable form for $\mathbf{T}^{(4)}$ if we consider the autocorrelation matrix of the tensor phase function

$$A_{\alpha\gamma}=\sum_{i=1}^{N}A_{i\alpha\gamma}=\sum_{i=1}^{N}p_{i\alpha}p_{i\gamma}/m$$
$$+\tfrac{1}{2}\sum_{i\neq j}^{N}\sum^{N}(x_{i\alpha}-x_{j\alpha})F_{ij\gamma}. \qquad (37A)$$

$\mathbf{A}$ is the coefficient of $i\mathbf{k}$ in the rate function $\mathbf{p}_\mathbf{k}$ for $\mathbf{k}=0$. By the methods which were used to derive Eq. (35A), and remembering that any conditional average $\langle\ \rangle_{\mathbf{x}_i}$ or $\langle\ \rangle_{\mathbf{x}_i,\mathbf{x}_i+\mathbf{R}}$ is independent of $\mathbf{x}_i$ if we fix only the total number of particles, energy, and momentum, we see that

$$T^{(4)}{}_{\alpha\beta\gamma\delta}(N/a^3,\mathbf{p}_o/a^3,E_o/a^3)$$
$$=\int_0^\tau d\sigma a^{-3}(\langle A_{\alpha\gamma}A_{\beta\delta}'\rangle_{N,\mathbf{p}_o,E_o}$$
$$-\langle A_{\alpha\gamma}\rangle_{N,\mathbf{p}_o,E_o}\langle A_{\beta\delta}'\rangle_{N,\mathbf{p}_o,\mathbf{E}_o}), \qquad (37B)$$

where the subscripts N, $\mathbf{p}_0$, E_0 mean that the averages are to be taken in an ensemble where the total number of particles, momentum and energy are fixed. The integrand in Eq. (37B), unlike the similar expressions in the definition (2) of ξ, is an element of a true autocorrelation matrix of a stationary random process because N, $\mathbf{p}_0$, E_0 are integrals of motion.

The expression (37B) for $\mathbf{T}^{(4)}$ apparently depends on the quantities τ and a^3. In reality, however, $\mathbf{T}^{(4)}$ must be independent of both for constant densities of particles, momentum and energy. The most natural way of eliminating the apparent dependence on τ would be to extend the region of integration to infinity. We have no assurance, however, that this integral would converge for a finite number of degrees of freedom. If, on the other hand we take the limit of the integrand in (37B) as $a^3\to\infty$ with N/a^3, $\mathbf{p}_0/a^3$, E_0/a^3 fixed we obtain a quantity which is independent of a and depends only on the densities of particles, momentum, and energy and σ. There is reason to believe that this limit is integrable between 0 and ∞ with respect to σ.[9] We therefore write (37B) in the form

$$T^{(4)}{}_{\alpha\beta\gamma\delta}(\rho,\mathbf{p},E) = \int_0^\infty d\sigma \lim_{a\to\infty} a^{-3}(\langle A_{\alpha\gamma}A_{\beta\delta}'\rangle - \langle A_{\alpha\gamma}\rangle\langle A_{\beta\delta}'\rangle), \quad (37C)$$

where it is understood that the averages $\langle\ \rangle$ are taken with N, $\mathbf{p}_0$, E_0 fixed and that the limit $a\to\infty$ is taken with N, $\mathbf{p}_0=a^3\mathbf{p}$, $E_0=a^3E$.

We are now in a position to give expressions similar to Eqs. (37) for the other ξ's. We have

$$\xi(E_{\mathbf{k}},E_{\mathbf{k}'}) = -k_\alpha k_\beta' \int T^{(2)}{}_{\alpha\beta}(\rho(\mathbf{x}),\mathbf{p}(\mathbf{x}),E(\mathbf{x})) \times \exp i(\mathbf{k}+\mathbf{k}')\cdot\mathbf{x}\,d\mathbf{x}, \quad (38A)$$

where

$$T^{(2)}{}_{\alpha\beta}(\rho,\mathbf{p},E) = \int_0^\infty d\sigma \lim_{a\to\infty} a^{-3}(\langle B_\alpha B_\beta'\rangle - \langle B_\alpha\rangle\langle B_\beta\rangle) \quad (38B)$$

and

$$B_\alpha = \sum_{i=1}^N p_{i\alpha}/m(\mathbf{p}_i^2/2m + \tfrac{1}{2}\sum_{j\neq i}^N V(\mathbf{x}_i-\mathbf{x}_j)) + \tfrac{1}{2}\sum_{i\neq j}^N\sum^N (x_{i\alpha}-x_{j\alpha})\mathbf{F}_{ij}\cdot(\mathbf{p}_i+\mathbf{p}_j)/2m. \quad (38C)$$

For an ξ which has to do with $\mathbf{p}_\mathbf{k}$ and an $E_{\mathbf{k}'}$ we have

$$\xi(p_{\mathbf{k}\gamma},E_{\mathbf{k}'}) = -k_\alpha k_\beta' \int T^{(3)}{}_{\alpha\beta\gamma}(\rho(\mathbf{x}),\mathbf{p}(\mathbf{x}),E(\mathbf{x})) \times \exp i(\mathbf{k}+\mathbf{k}')\cdot\mathbf{x}\,d\mathbf{x}, \quad (39A)$$

where

$$T^{3}{}_{\alpha\beta\gamma}(\rho,\mathbf{p},E) = \int_0^\infty d\sigma \lim_{a\to\infty} a^{-3}(\langle A_{\alpha\gamma},B_{\beta}'\rangle - \langle A_{\alpha\gamma}\rangle\langle B_{\beta}'\rangle). \quad (39B)$$

$$\xi(E_{\mathbf{k}},p_{\mathbf{k}'\delta}) = -k_\alpha k_\beta' \int \bar{T}^{(3)}{}_{\alpha\beta\delta}(\rho(\mathbf{x}),\mathbf{p}(\mathbf{x}),E(\mathbf{x})) \times \exp i(k+k')\cdot\mathbf{x}\,d\mathbf{x}, \quad (40A)$$

where

$$\bar{T}^{(3)}{}_{\alpha\beta\delta} = \int_0^\infty d\sigma \lim_{a\to\infty} a^{-3}(\langle B_\alpha A_{\beta\delta}'\rangle - \langle B_\alpha\rangle\langle A_{\beta\delta}'\rangle). \quad (40B)$$

Equations (37)–(40) give expressions for all the ξ's which can be formed from the $\mathbf{p}_\mathbf{k}$'s and the $E_\mathbf{k}$'s. It is easily seen that the remaining ξ's which all have to do with at least one $\rho_\mathbf{k}$ are zero. This is due to the fact that the coefficient of $i\mathbf{k}$ in the expression (16) for $(d\rho/dt)_\mathbf{k}$ is $\mathbf{p}_0/m$ for $\mathbf{k}=0$. Since $\mathbf{p}_0$, unlike $\mathbf{A}$ and $\mathbf{B}$, is an integral of motion any autocorrelation matrix element between $\mathbf{p}_0$ and $\mathbf{p}_0$, $\mathbf{A}$ or $\mathbf{B}$ is zero.

We have in hand now all the means which we need to calculate the second and third terms in Eq. (1). We see immediately that these terms are zero for the rates of change of the expectation value of all the $\rho_\mathbf{k}$'s since the corresponding ξ's are zero. Let us look first at the contributions to the rate of $p_{\mathbf{k}\delta}$ from $\xi(p_{\mathbf{k}\gamma},p_{\mathbf{k}'\delta})$. For the second term this is

$$\kappa^{-1}a^{-3}\sum_\mathbf{k} -k_\alpha k_\beta'\Big[\int T^{(4)}{}_{\alpha\beta\gamma\delta}(\mathbf{x})\exp i(\mathbf{k}+\mathbf{k}')\cdot\mathbf{x}\,d\mathbf{x}\Big] \times\Big[\int\cdot -v(\mathbf{x}')/T(\mathbf{x}')\exp -i\mathbf{k}\cdot\mathbf{x}'d\mathbf{x}'\Big]$$
$$= ik_\beta'\int\int -T^{(4)}{}_{\alpha\beta\gamma\delta}(\mathbf{x})v_\gamma(\mathbf{x}')/\kappa T(\mathbf{x}') \times\exp i\mathbf{k}'\cdot\mathbf{x}\frac{\partial}{\partial x_\alpha}\varphi(\mathbf{x}-\mathbf{x}')d\mathbf{x}d\mathbf{x}'.$$

Performing the integration on $\mathbf{x}'$ this becomes

$$ik_\beta'\int\Big[-T^{(4)}{}_{\alpha\beta\gamma\delta}(\mathbf{x})\frac{\partial}{\partial x_\alpha}v_\gamma(\mathbf{x})/\kappa T(\mathbf{x})\Big]\exp i\mathbf{k}'\cdot\mathbf{x}\,d\mathbf{x}.$$

The contribution from the second term is

$$\sum_\mathbf{k} -k_\alpha k_\beta'\int\frac{\partial T^{(4)}{}_{\alpha\beta\gamma\delta}}{\partial p_{\mathbf{k}\gamma}}\exp i(\mathbf{k}+\mathbf{k}')\cdot\mathbf{x}\,d\mathbf{x}$$
$$=\sum_\mathbf{k} -k_\alpha k_\beta'\int\frac{\partial T^{(4)}{}_{\alpha\beta\gamma\delta}}{\partial p_\gamma}\frac{\partial p_\gamma(\mathbf{x})}{\partial p_{\mathbf{k}\gamma}}\exp i(\mathbf{k}+\mathbf{k}')\cdot\mathbf{x}\,d\mathbf{x}$$

which, by Eq. (5),

$$=a^{-3}\sum_\mathbf{k} -k_\alpha k_\beta'\int\frac{\partial T^{(4)}{}_{\alpha\beta\gamma\delta}}{\partial p_\gamma}\exp i\mathbf{k}'\cdot\mathbf{x}\,d\mathbf{x}.$$

[8] We use the notation of partial differentiation by a vector as an abbreviation.

[9] This conjecture is based on the behavior of similar quantities which appear in Peierls' theory of heat conductivity of crystals [Ann. Physik **3**, 1055 (1929)] and on the fact that in the quantum theory of scattering and of radiation, time-proportional transition probabilities are obtained only in the limit in which the size of the system goes to infinity.

Since the integral is independent of $\mathbf{k}$ this expression is proportional to $\sum_{\mathbf{k}} k_\alpha = 0$.

This conclusion is quite general. The contribution from the second term of Eq. (1) is zero. The other contributions from the first term may be calculated in the same way. We obtain thus the total contribution of these terms to the rate of the expectation value of $p_{\mathbf{k}\delta}$

$$ik_\beta \int \left(T^{(4)}{}_{\alpha\beta\gamma\delta} \frac{\partial}{\partial x_\alpha} - \frac{v_\gamma}{\kappa T} + \bar{T}^{(3)}{}_{\alpha\beta\delta} \frac{\partial}{\partial x_\alpha} \frac{1}{\kappa T} \right) \times \exp i\mathbf{k}\cdot x d\mathbf{x}. \quad (41A)$$

For $E_{\mathbf{k}}$ we obtain

$$ik_\beta \int \left(T^{(3)}{}_{\alpha\beta\gamma} \frac{\partial}{\partial x_\alpha} - \frac{v_\gamma}{\kappa T} + T^{(2)}{}_{\alpha\beta} \frac{\partial}{\partial x_\alpha} \frac{1}{\kappa T} \right) \times \exp i\mathbf{k}\cdot x d\mathbf{x}. \quad (41B)$$

The corresponding contributions toth e rates of $\mathbf{p}(\mathbf{x})$ and $E(\mathbf{x})$ are

$$-\frac{\partial}{\partial x_\beta} \left(T^{(4)}{}_{\alpha\beta\gamma\delta} \frac{\partial}{\partial x_\alpha} - \frac{v_\gamma}{\kappa T} + \bar{T}^{(3)}{}_{\alpha\beta\delta} \frac{\partial}{\partial x_\alpha} \frac{1}{\kappa T} \right) \quad (42A)$$

and

$$-\frac{\partial}{\partial x_\beta} \left(T_{\alpha\beta\gamma} \frac{\partial}{\partial x_\alpha} - \frac{v_\gamma}{\kappa T} + T^{(2)}{}_{\alpha\beta} \frac{\partial}{\partial x_\alpha} \frac{1}{\kappa T} \right). \quad (42B)$$

Expressions (42A) and (42B) have the same general form as the irreversible terms in the Navier-Stokes and energy balance equations of fluid motion. We will be able, by means of certain symmetry principles to specify $\mathbf{T}^{(2)}$, $\mathbf{T}^{(3)}$, $\bar{T}^{(3)}$, $\mathbf{T}^{(4)}$ more completely, and at the same time reduce expressions (42A) and (42B) to a more familiar form. We will first use the principle that the dynamical Eqs. (15) are invariant under a Gallilean transformation to determine the explicit dependence of these tensors on $\mathbf{p}$, or what is the same thing on $\mathbf{v}$, the local velocity. To do this we consider our system from a set coordinate axes moving with a velocity $\mathbf{v}=\mathbf{p}_0/mN$ with respect to the system which we have been using. In this system a phase point is represented by $\mathbf{p}_i{}^*=\mathbf{p}_i-m\mathbf{v}$, $\mathbf{x}_i{}^*=\mathbf{x}_i-\mathbf{v}t$, $i=1\cdots N$. Let us express in terms of the new coordinate system all the quantities which we need in order to calculate $\mathbf{T}^{(2)}\mathbf{T}^{(3)}$, $\bar{T}^{(3)}\mathbf{T}^{(4)}$.

$$\mathbf{p}_0=\sum_{i=1}^N \mathbf{p}_i=\sum_{i=1}^N \mathbf{p}_i{}^*+Nm\mathbf{v}=\mathbf{p}_0{}^*+Nm\mathbf{v}=Nm\mathbf{v}, \quad (43A)$$

since we have chosen our coordinate axes so that $\mathbf{p}_0{}^*=0$.

$$E_0=\sum_{i=1}^N (\mathbf{p}_i+m\mathbf{v})^2/2m+\tfrac{1}{2}\sum_{i\neq j}^N\sum^N V(\mathbf{x}_i-\mathbf{x}_j)$$
$$=E_0{}^*+\mathbf{p}_0{}^*\cdot\mathbf{v}+\tfrac{1}{2}Nm\mathbf{v}^2$$
$$=E_0{}^*+\tfrac{1}{2}Nm\mathbf{v}^2$$

$$\mathbf{A}=\sum_{i=1}^N (\mathbf{p}_i{}^*+m\mathbf{v})(\mathbf{p}_i{}^*+m\mathbf{v})/m + \tfrac{1}{2}\sum_{i\neq j}^N\sum^N (\mathbf{x}_i{}^*-\mathbf{x}_j{}^*)F_{ij} \quad (43B)$$
$$=\mathbf{A}^*+\mathbf{p}_0{}^*\mathbf{v}+\mathbf{v}\mathbf{p}_0{}^*+Nm\mathbf{v}\mathbf{v}$$
$$=\mathbf{A}^*+Nm\mathbf{v}\mathbf{v}$$

$$\mathbf{B}=\sum_{i=1}^N (\mathbf{p}_i{}^*+m\mathbf{v})/m((\mathbf{p}_i{}^*+m\mathbf{v})^2/2m + \tfrac{1}{2}\sum_{j\neq i}^N V(\mathbf{x}_i{}^*-\mathbf{x}_j{}^*))+\tfrac{1}{2}\sum_{i\neq j}^N\sum^N (\mathbf{x}_i{}^*-\mathbf{x}_j{}^*)\mathbf{F}_{ij}{}^* \cdot((\mathbf{p}_i{}^*+\mathbf{p}_j{}^*)/2m+\mathbf{v}) \quad (43C)$$
$$=\mathbf{B}^*+\mathbf{v}E_0{}^*+A^*\cdot\mathbf{v}+Nm\mathbf{v}\mathbf{v}^2. \quad (43D)$$

From the new point of view the ensemble where the total number, momentum and energy are fixed to be N, $\mathbf{p}_0$, and E_0 appears to be one in which the total number of particles is fixed to be N the total momentum $\mathbf{p}_0{}^*=0$ and the total energy $E_0{}^*=E_0-\frac{1}{2}Nm\mathbf{v}^2$. We therefore may replace averages $\langle\ \rangle_{N,\mathbf{p}_0E_0}$ with respect to the old variables by averages $\langle\ \rangle_{N,0,E_0}$ with respect to the new. We see then that

$$\mathbf{A}-\langle\mathbf{A}\rangle_{N,\mathbf{p}_0,E_0}=\mathbf{A}^*-\langle\mathbf{A}^*\rangle_{N,0,E_0}, \quad (44A)$$

and

$$\mathbf{B}-\langle\mathbf{B}\rangle_{N,\mathbf{p}_0,E_0}=\mathbf{B}^*-\langle\mathbf{B}^*\rangle_{N,0,E_0}+(\mathbf{A}^*-\langle\mathbf{A}^*\rangle_{N,0,E_0})\cdot\mathbf{v}, \quad (44B)$$

since there is no difference between $E_0{}^*$ and its average value. We have then

$$T^{(4)}{}_{\alpha\beta\gamma\delta}(\rho,\mathbf{p},E)$$
$$=\int_0^\infty d\sigma \lim_{a\to\infty} a^{-3}\langle(A_{\alpha\gamma}-\langle A_{\alpha\gamma}\rangle_{N,\mathbf{p}_0,E_0} \times(A_{\beta\delta}{}'-\langle A_{\beta\delta}{}'\rangle_{N,\mathbf{p}_0,E_0})\rangle_{N,\mathbf{p}_0,E_0}$$
$$=\int_0^\infty d\sigma \lim_{a\to\infty} a^{-3}\langle(A_{\alpha\gamma}{}^*-\langle A_{\alpha\gamma}{}^*\rangle_{N,0,E_0}) \times(A_{\beta\delta}{}^{*\prime}-\langle A_{\beta\delta}{}^{*\prime}\rangle_{N,0,E_0}\rangle_{N,0,E_0}$$
$$=T^{(4)}{}_{\alpha\beta\gamma\delta}(\rho,0,E-\mathbf{p}^2/2m\rho). \quad (45A)$$

In other words $\mathbf{T}^{(4)}$ is a function only of the particle density and the intrinsic energy density $\epsilon=E-\mathbf{p}^2/2m\rho$. Similarly we obtain

$$T^{(2)}{}_{\alpha\beta}(\rho,\mathbf{p},E)=T^{(2)}{}_{\alpha\beta}(\rho,0,\epsilon)+\bar{T}^{(3)}{}_{\alpha\beta\gamma}(\rho,0,\epsilon)v_\gamma + T^{(3)}{}_{\beta\alpha\gamma}(\rho,0,\epsilon)v_\gamma+T^{(4)}{}_{\alpha\beta\gamma\delta}(\rho,0,\epsilon)v_\gamma v_\delta. \quad (45B)$$

$$T^{(3)}{}_{\alpha\beta\gamma}(\rho,\mathbf{p},E)=T^{(3)}{}_{\alpha\beta\gamma}(\rho,0,\epsilon)+T^{(4)}{}_{\alpha\beta\gamma\delta}(\rho,0,\epsilon)v_\delta, \quad (45C)$$

$$\bar{T}^{(3)}{}_{\alpha\beta\delta}(\rho,\mathbf{p},E)=\bar{T}^{(3)}{}_{\alpha\beta\delta}(\rho,0,\epsilon)+T^{(4)}{}_{\alpha\beta\gamma\delta}(\rho,0,\epsilon)v_\gamma. \quad (45D)$$

Equations (45A)–(45D) permit the determination of the tensors $\mathbf{T}^{(2)}$ etc. by an average in an ensemble in

which the center of gravity of our system is at rest. We may use Onsager's symmetry relations to get further information about these quantities. In the form given in paper I[1] these relations show that $T^{(4)}{}_{\alpha\beta\gamma\delta}(\rho,0,\epsilon) = T^{(4)}{}_{\beta\alpha\delta\gamma}(\rho,0,\epsilon)$ while from the way it is constructed we know that this quantity is symmetric with respect to α, γ, and β, δ. We have also $T^{(3)}{}_{\alpha\beta\gamma}(\rho,0,\epsilon) = -\bar{T}^{(3)}{}_{\alpha\beta\gamma}(\rho,0,\epsilon)$ while from the way they are constructed $\mathbf{T}^{(3)}$, $\bar{\mathbf{T}}^{(3)}$ are symmetric in β, γ. Again, by Onsager's relations $T^{(2)}{}_{\alpha\beta}(\rho,0,\epsilon) = T^{(2)}{}_{\beta\alpha}(\rho,0,\epsilon)$. Now although we have chosen a cubic shape for our system with periodic boundary conditions, we should expect that in the limit $a\to\infty$ this particular shape and boundary conditions have no effect on the final result and that therefore the tensors $\mathbf{T}^{(2)}(\rho,0,\epsilon)$, etc., are isotropic. This means that we may write $\mathbf{T}^{(4)}(\rho,0,\epsilon)$ in the form

$$T^{(4)}{}_{\alpha\beta\gamma\delta}(\rho,0,\epsilon) = \kappa T(\eta'\delta_{\alpha\gamma}\delta_{\beta\delta} + \eta(\delta_{\alpha\beta}\delta_{\gamma\delta} + \delta_{\alpha\delta}\delta_{\beta\gamma})), \quad (46A)$$

where T is the equilibrium temperature corresponding to ρ and ϵ and η and η' are scalar functions of ρ and ϵ, or what is the same thing of ρ and T. Since there are no third rank tensors which are both isotropic and symmetric in a pair of indices $\mathbf{T}^{(3)}$ and $\bar{T}^{(3)}$ are both zero, while $\mathbf{T}^{(3)}$ must have the form

$$T^{(2)}{}_{\alpha\beta} = \kappa T^2 K \delta_{\alpha\beta}, \quad (46B)$$

where K is a scalar function of ρ and T. Substituting these expressions in Eqs. (45) we obtain

$$T^{(2)}{}_{\alpha\beta\gamma\delta}(\rho,\mathbf{p},E) = \kappa T[\eta'\delta_{\alpha\gamma}\delta_{\beta\delta} + \eta(\delta_{\alpha\beta}\delta_{\gamma\delta} + \delta_{\alpha\delta}\delta_{\beta\gamma}], \quad (47A)$$

$$T^{(3)}{}_{\alpha\beta\gamma}(\rho,\mathbf{p},E) = \kappa T[\eta' v_\beta\delta_{\alpha\gamma} + \eta(v_\gamma\delta_{\alpha\beta} + v_\alpha\delta_{\beta\gamma})], \quad (47B)$$

$$\bar{T}^{(3)}{}_{\alpha\beta\delta}(\rho,\mathbf{p},E) = \kappa T[\eta' v_\alpha\delta_{\beta\delta} + \eta(v_\delta\delta_{\alpha\beta} + v_\beta\delta_{\alpha\delta})], \quad (47C)$$

$$T^{(4)}{}_{\alpha\beta\gamma\delta}(\rho,\mathbf{p},E) = -\kappa T^2 K\delta_{\alpha\beta} + \kappa T[\eta' v_\alpha v_\beta + \eta(\mathbf{v}^2\delta_{\alpha\beta} + v_\alpha v_\beta)]. \quad (47D)$$

Returning now to the contributions to the rate of $p_\delta(\mathbf{x})$, $E(\mathbf{x})$ [Eqs. (42A) and (42B)] we obtain

$$\frac{\partial}{\partial x_\delta}\eta'\frac{\partial v_\alpha}{\partial x_\alpha} + \frac{\partial}{\partial x_\beta}\eta\left(\frac{\partial v_\delta}{\partial x_\beta} + \frac{\partial v_\beta}{\partial x_\delta}\right), \quad (48A)$$

$$\frac{\partial}{\partial x_\beta}v_\beta\eta'\frac{\partial v_\alpha}{\partial x_\alpha} + \frac{\partial}{\partial x_\beta}v_\gamma\eta\left(\frac{\partial v_\gamma}{\partial x_\beta} + \frac{\partial v_\beta}{\partial x_\gamma}\right) + \frac{\partial}{\partial x_\beta}K\frac{\partial T}{\partial x_\beta}. \quad (48B)$$

We see that terms in the stress tensor proportional to the temperature gradients have cancelled as we should expect from the principle of Gallilean relativity. In order to interpret our results we collect contributions to the rates of change of $\rho(\mathbf{x})$, $\mathbf{p}(\mathbf{x})$, and $E(\mathbf{x})$ [Eqs. (24) and (48)] and expressing them again in the Gibbs notation we obtain

$$\frac{\partial\rho}{\partial t} + \nabla\cdot\rho\mathbf{v} = 0, \quad (49A)$$

$$\frac{\partial\mathbf{p}}{\partial t} + \nabla\cdot\mathbf{pv} = \nabla\cdot[(-p+\eta'\nabla\cdot\mathbf{v})\mathbf{I} + \eta(\nabla\mathbf{v}+\mathbf{v}\nabla)], \quad (49B)$$

$$\frac{\partial E}{\partial t} + \nabla\cdot E\mathbf{v} = \nabla\cdot K\nabla T + \nabla\cdot[(-p+\eta\nabla\cdot\mathbf{v})\mathbf{I} + \eta(\nabla\mathbf{v}+\mathbf{v}\nabla)]\cdot\mathbf{v}. \quad (49C)$$

The quantity in square brackets in (49B) and (49C) can be interpreted as the stress tensor and η and $\eta'+\frac{2}{3}\eta$ as the coefficients of shear and bulk viscosity respectively. In Eq. (49C) we may interpret the second term as the work done per unit volume per second by this stress tensor. The quantity $K\nabla T$ can be interpreted as the heat current and K as the heat conductivity. The first term in (49C) is then, of course, the heat absorbed per unit volume per second.

E. DIFFUSION, THERMAL DIFFUSION AND THE DUFOUR EFFECT

In this section we will discuss irreversible effects in a fluid containing two species of molecules. These are besides those which occur in a fluid of one species, diffusion, thermal diffusion and its concomitant the Dufour effect. In the course of the discussion we will avoid repeating arguments which occur in the one species case.

The first approximation leads to two equations instead of Eq. (49A) which are obtained by averaging the rate functions (21A) and (21B) in the ensemble which represents the gross state of the fluid.

$$\frac{\partial\rho_A}{\partial t} = -\nabla\cdot\rho_A\mathbf{v} \quad (50A)$$

$$\frac{\partial\rho_B}{\partial t} = -\nabla\cdot\rho_B\mathbf{v}, \quad (50B)$$

where $\mathbf{v}(\mathbf{x}) = \mathbf{p}(\mathbf{x})/m_A\rho_A(\mathbf{x}) + m_B\rho_B(\mathbf{x})$. The rates of the expected local momentum and energy densities are the same as before with an appropriate redefinition of the local pressure.

We will show in the appendix that as before $\log w$ has the form

$$\log w = \kappa^{-1}\int s\,dx, \quad (51)$$

where s is the equilibrium entropy density corresponding to the intrinsic energy density

$$\epsilon = E - \mathbf{p}^2/2(m_A\rho_A + m_B\rho_B)$$

and the particles densities ρ_A, ρ_B.

$$\frac{\partial}{\partial\rho_{A\mathbf{k}}}\log w=\kappa a^{-3}\int(-\mu_A(\mathbf{x})+\tfrac{1}{2}m_A\mathbf{v}^2(\mathbf{x}))/T(\mathbf{x})\times\exp-i\mathbf{k}\cdot\mathbf{x}d\mathbf{x}, \quad (52A)$$

$$\frac{\partial}{\partial\rho_{B\mathbf{k}}}\log w=\kappa a^{-3}\int(-\mu_B(\mathbf{x})+\tfrac{1}{2}m_B\mathbf{v}^2(\mathbf{x}))/T(\mathbf{x})\times\exp-i\mathbf{k}\cdot\mathbf{x}d\mathbf{x}, \quad (52B)$$

where $\mu_A(\mathbf{x})$, $\mu_B(\mathbf{x})$ are the chemical potentials of species A and B, respectively. As before

$$\frac{\partial}{\partial\mathbf{p}_\mathbf{k}}\log w=\kappa a^{-3}\int-\mathbf{v}(\mathbf{x})/T(\mathbf{x})\exp-i\mathbf{k}\cdot\mathbf{x}d\mathbf{x}, \quad (52C)$$

$$\frac{\partial}{\partial E_\mathbf{k}}\log w=\kappa a^{-3}\int 1/T(\mathbf{x})\exp-i\mathbf{k}\cdot\mathbf{x}d\mathbf{x}. \quad (52D)$$

Proceeding now to the ξ's concerning the $\rho_{A\mathbf{k}}$ and $\rho_{B\mathbf{k}}$ we have

$$\xi(\rho_{A\mathbf{k}},\rho_{A\mathbf{k}'})=-\mathbf{k}\cdot\mathbf{k}'\int D_{AA}\exp i(\mathbf{k}+\mathbf{k}')\cdot\mathbf{x}d\mathbf{x}, \quad (53A)$$

$$\xi(\rho_{A\mathbf{k}},\rho_{B\mathbf{k}'})=-\mathbf{k}\cdot\mathbf{k}'\int D_{AB}\exp i(\mathbf{k}+\mathbf{k}')\cdot\mathbf{x}d\mathbf{x}, \quad (53B)$$

$$\xi(\rho_{B\mathbf{k}},\rho_{A\mathbf{k}'})=-\mathbf{k}\cdot\mathbf{k}'\int D_{BA}\exp i(\mathbf{k}+\mathbf{k}')\cdot\mathbf{x}d\mathbf{x}, \quad (53C)$$

$$\xi(\rho_{B\mathbf{k}},\rho_{B\mathbf{k}'})=-\mathbf{k}\cdot\mathbf{k}'\int D_{BB}\exp i(\mathbf{k}+\mathbf{k}')\cdot\mathbf{x}d\mathbf{x}, \quad (53D)$$

where the D_{AA} etc. are functions of the local state at $\mathbf{x}$.

$$D_{AA}\mathbf{I}=\int_0^\infty d\sigma\lim_{a\to\infty}a^{-3}(\langle\mathbf{C}_A\mathbf{C}_A'\rangle-\langle\mathbf{C}_A\rangle\langle\mathbf{C}_A\rangle), \quad (54A)$$

$$D_{AB}\mathbf{I}=\int_0^\infty d\sigma\lim_{a\to\infty}a^{-3}(\langle\mathbf{C}_A\mathbf{C}_B'\rangle-\langle\mathbf{C}_A\rangle\langle\mathbf{C}_B\rangle), \quad (54B)$$

$$D_{BA}\mathbf{I}=\int_0^\infty d\sigma\lim_{a\to\infty}a^{-3}(\langle\mathbf{C}_B\mathbf{C}_A'\rangle-\langle\mathbf{C}_B\rangle\langle\mathbf{C}_A\rangle), \quad (54C)$$

$$D_{BB}\mathbf{I}=\int_0^\infty d\sigma\lim_{a\to\infty}a^{-3}(\langle\mathbf{C}_B\mathbf{C}_B'\rangle-\langle\mathbf{C}_B\rangle\langle\mathbf{C}_B\rangle), \quad (54D)$$

where

$$\mathbf{C}_A=m_A^{-1}\sum_{i=1}^{N_A}\mathbf{p}_i \quad (55A)$$

$$\mathbf{C}_B=m_B^{-1}\sum_{j=1}^{N_B}\mathbf{q}_j. \quad (55B)$$

The limits in Eqs. (54) are to be taken with fixed particle, momentum and energy densities ρ_A, ρ_B, $\mathbf{p}$, E. It is easily seen, however, the D_{AA}, etc., have the same value if the average is taken in the ensemble with momentum density zero and energy density equal to the intrinsic energy density ϵ.

The four quantities D_{AA}, D_{AB}, D_{BA}, D_{BB} are not all independent and indeed are multiples of a single quantity. We note that

$$(m_AD_{AA}+m_BD_{BB})\mathbf{I}=\int_0^\infty d\sigma\lim_{a\to\infty}a^{-3}(\langle(m_A\mathbf{C}_A+m_B\mathbf{C}_B)\mathbf{C}_A'\rangle-\langle m_A\mathbf{C}_A+m_B\mathbf{C}_B\rangle\langle\mathbf{C}_A\rangle).$$

Now since $m_A\mathbf{C}_A+m_B\mathbf{C}_B$ is simply $\mathbf{p}_0$, the total momentum, and is therefore an integral of motion, the integrand on the right is identically zero and we have

$$m_AD_{AA}+m_BD_{BA}=0.$$

Similarly

$$m_AD_{AB}+m_BD_{BB}=0,$$

and

$$m_AD_{BA}+m_BD_{BB}=0$$
$$m_AD_{AA}+m_BD_{AB}=0.$$

These equations are satisfied if we set

$$D_{AA}=m_A^{-2}D,$$
$$D_{BA}=D_{AB}=-(m_Am_B)^{-1}D, \quad (56)$$
$$D_{BB}=m_B^{-2}D.$$

From Eqs. (52A), (52B), and (53) we see that the contributions to the rates of $\rho_A(\mathbf{x})$, $\rho_B(\mathbf{x})$ from the $\xi(\rho_{A\mathbf{k}},\rho_{B\mathbf{k}'})$, etc., are

$$-\nabla\{D_{AA}\nabla(-\mu_A+\tfrac{1}{2}m_A\mathbf{v}^2)/\kappa T+D_{BA}\nabla(-\mu_B+\tfrac{1}{2}m_B\mathbf{v}^2)/\kappa T\}$$
$$-\nabla\cdot\{D_{BA}\nabla(-\mu_A+\tfrac{1}{2}m_A\mathbf{v}^2)/\kappa T+D_{BB}\nabla(-\mu_B+\tfrac{1}{2}m_B\mathbf{v}^2)/\kappa T\}.$$

Using Eqs. (56) we see that these expressions become

$$\frac{1}{m_A}\nabla\cdot D\nabla\frac{1}{\kappa T}\left(\frac{\mu_A}{m_A}-\frac{\mu_B}{m_B}\right) \quad (57A)$$

$$-\frac{1}{m_A}\nabla\cdot D\nabla\frac{1}{\kappa T}\left(\frac{\mu_A}{m_A}-\frac{\mu_B}{m_B}\right). \quad (57B)$$

In the case of a dilute solution, i.e., when the number of molecules of type A is small compared to the number of type B, μ_A is approximately $\kappa T\log\rho_A+$ a constant while μ_B is constant. Formula (57A) becomes

$$\nabla\cdot D/m_A^2\rho_A\nabla\rho_A.$$

We see that

$$D/m_A^2\rho_A=D_{AA}/\rho_A$$

is the diffusion coefficient of a dilute solute. If we neglect contributions which come from the correlation of

the velocity of two different molecules,[10] Eq. (54A) for D_{AA} becomes

$$D_{AA}/\rho_A=\int_0^\infty d\sigma(\langle \mathbf{v}_i\mathbf{v}_i'\rangle-\langle \mathbf{v}_i\rangle\langle \mathbf{v}_i\rangle),$$

which coincides with the expression for the diffusion constant in the theory of Brownian motion.[11] ($\mathbf{v}_i$ is the velocity of a solute molecule.)

For an ξ concerning a $\rho_{A\mathbf{k}}$ or a $\rho_{B\mathbf{k}}$ and a $E_{\mathbf{k}'}$ we have the expressions

$$-\mathbf{k}\cdot\mathbf{k}'\int \kappa T^2 D_A \exp i(\mathbf{k}+\mathbf{k}')\cdot\mathbf{x}d\mathbf{x} \tag{58A}$$

$$-\mathbf{k}\cdot\mathbf{k}'\int \kappa T^2 D_B \exp i(\mathbf{k}+\mathbf{k}')\cdot\mathbf{x}d\mathbf{x}, \tag{58B}$$

where

$$\kappa T^2 D_A\mathbf{I}=\int_0^\infty d\sigma \lim_{a\to\infty} a^{-3}(\langle \mathbf{C}_A\mathbf{B}'\rangle-\langle \mathbf{C}_A\rangle\langle \mathbf{B}\rangle), \tag{59A}$$

$$\kappa T^2 D_B\mathbf{I}=\int_0^\infty d\sigma \lim_{a\to\infty} a^{-3}(\langle \mathbf{C}_B\mathbf{B}'\rangle-\langle \mathbf{C}_A\rangle\langle \mathbf{B}\rangle), \tag{59B}$$

and $\mathbf{B}$ is now the coefficient of $i\mathbf{k}$ in the expression (23) for $(d\mathbf{E}_\mathbf{k}/dt)$ for $\mathbf{k}=0$.

The corresponding contributions to the rates of ρ_A and ρ_B are

$$\nabla\cdot D_A\nabla T, \tag{60A}$$

$$\nabla\cdot D_B\nabla T. \tag{60B}$$

By the same reasoning that was used in Eqs. (56) we see that

$$m_A D_A+m_B D_B=0. \tag{61}$$

For the inverse ξ's we obtain expressions similar to (58A) and (58B) except that in Eqs. (59A) and (59B) the order of the $\mathbf{c}$'s and $\mathbf{B}$ is reversed. Since the $\mathbf{c}$'s and $\mathbf{B}$ are all antisymmetric variables and since the average may be taken in the ensemble with $\mathbf{p}=0$ this reversal makes no difference in the value of the ξ's.

For the contribution to the rate of $E(\mathbf{x})$ from these ξ's we obtain

$$\begin{aligned}&=\nabla\cdot\kappa T^2\{D_A\nabla(-\mu_A+\tfrac{1}{2}m_A\mathbf{v}^2)/\kappa T\\ &\qquad +D_B\nabla(-\mu_B+\tfrac{1}{2}m_B\mathbf{v}^2)/\kappa T\}\\ &=\nabla\cdot D'\nabla(\mu_A/m_A-\mu_B/m_B)/T,\end{aligned} \tag{62}$$

where D' is the common value of $m_A D_A T^2$ and $-m_B D_B T^2$. In case species A is a dilute solute (62) reduces to $\nabla D/m_A\rho\nabla\rho$ and $D/m_A\rho$ is the coefficient of the Dufour effect.

Finally in the case of a fluid of two species we have the same expressions for the viscosity and heat conduction coefficient except that the phase functions $\mathbf{A}$, $\mathbf{B}$ are now defined as the coefficients of $i\mathbf{k}$ in the expressions for $(d\mathbf{p}_\mathbf{k}/dt)$, $(dE_\mathbf{k}/dt)$ for $\mathbf{k}=0$ [Eqs. (22) and (23)].

F. VISCOSITY AND HEAT CONDUCTIVITY IN PERFECT GASES

The expressions which we have just presented for the coefficients of irreversible effects were derived without any assumption about the density or state of aggregation. In particular we do not assume that the density is small enough so that the kinetic theory of gases applies. In the present state of our knowledge, however, these formulas do not provide means actually to calculate irreversible coefficients. Indeed, in order to determine $\mathbf{A}'$, $\mathbf{B}'$, etc., we would need to know explicitly the solutions of the equations of motion. We wish to show in the present section that in those circumstances in which we already know how to calculate irreversible coefficients, i.e. in the limit of small densities our methods lead to the same results as the Chapman-Enskog theory.

In order to do this we will first give an interpretation of the Maxwell-Boltzmann differentio-integral equation in the terms which we have been using in this paper and in paper I. This equation may be considered to be the analogon of the Liouville equation for the phase space of the individual molecule, the μ space as opposed to the γ space, the phase space of the whole system. We wish to consider the Maxwell-Boltzmann equation to be analogous rather to the phenomenonological equations of grossly observable quantities although it gives a finer description of phenomena in perfect gases than is ordinarily observed with large-scale methods. The gross variables in this case are the local number density of molecules at each point of the μ space. The Maxwell-Boltzmann equation determines the future expected values of these gross variables if their present values are known. Fluctuations of the future values from their future expected values exist, but are presumably small.

Our present discussion will have to do only with cases in which the molecules are uniformly distributed spacially so that we may take our gross variables to be the local density in momentum space. More precisely we divide momentum space into small cells, Ω_ν, $\nu=1\cdots\infty$. $E_\nu(\mathbf{p})$ is the characteristic function of Ω_ν and V_ν its volume. The gross variables will then be the number density of molecules in each Ω_ν.

$$f_\nu(X)=V_\nu^{-1}\sum_{i=1}^{N} E_\nu(\mathbf{p}_i). \tag{63}$$

We will write $f_\nu(t)$ for the conditional expectation value of $f_\nu(X_t)$ when it is known that the $f_\nu(X)$ certainly had the values $f_\nu(0)$ at $t=0$. To determine the $f_\nu(t)$ under vitrious conditions is the object of the kinetic theory of gases. It is usual, however, to consider the expected local density as a function of a continuous

[10] These are proportional to ρ_A^2.

[11] S. Chandrasekhar, Revs. Modern Phys. **15**, 2 (1943). This expression is not explicitly derived but is easily verified from the explicit transition probabilities for the velocity given there.

variable $\mathbf{p}$ rather than of the discrete variable ν. We therefore define $f(\mathbf{p},t)$ to be equal to $f_\nu(t)$ when $\mathbf{p}$ is in Ω_ν. We can then write the Maxwell-Boltzmann equation as

$$\partial f(\mathbf{p},t)/\partial t=\Psi(f(\mathbf{p},t)), \tag{64}$$

where Ψ is a nonlinear functional of $f(\mathbf{p},t)$.

With this interpretation in hand we go on to the formulas for viscosity and heat conduction coefficients. In a gas of sufficiently small density we may neglect the contributions from the intermolecular forces in the expressions for $\mathbf{A}$ and $\mathbf{B}$. We are then able very approximately to express these quantities as functions of the gross variables f_ν.

$$A_{\alpha\gamma}=m^{-1}\sum_\nu p_{\nu\alpha}p_{\nu\delta}f_\nu(X)V_\nu, \tag{65A}$$

$$B_\alpha=(2m^2)^{-1}\sum_\nu p_{\nu\alpha}\mathbf{p}_\nu^2 f_\nu(X)V_\nu, \tag{65B}$$

where $\mathbf{p}_\nu$ is some representative value of $\mathbf{p}$ in Ω_ν.

In order to determine the viscosity and heat conduction coefficients we need to know the elements of the autocorrelation matrix of $\mathbf{A}$ and $\mathbf{B}$ in an ensemble in which the total number of particles is fixed to be N, the total momentum, to be zero, and the total energy, to be E. In such an ensemble the mean value of $f_\nu(X)$ is $f_0(\mathbf{p}_\nu)$ where

$$f_0(\mathbf{p})=N(2\pi mK T)^{-\frac{3}{2}}\exp-\mathbf{p}^2/2mK T \tag{66}$$

and therefore

$$\langle A_{\alpha\gamma}\rangle_{N,0,E}=m^{-1}\int p_\alpha p_\gamma f_0(\mathbf{p})d\mathbf{p}, \tag{67A}$$

$$\langle B_\alpha\rangle_{N,0,E}=(2m^2)^{-1}\int p_\alpha\mathbf{p}^2 f_0(\mathbf{p})d\mathbf{p}. \tag{67B}$$

We have for the $\alpha\beta\gamma\delta$ element of the autocorrelation matrix of $\mathbf{A}$

$$\langle(A_{\alpha\gamma}-\langle A_{\alpha\gamma}\rangle_{N,0,E})(A_{\beta\delta}'-\langle A_{\beta\delta}\rangle_{N,0,E})\rangle_{N,0,E}.$$

Taking into account Eqs. (66), we can write this expression as

$$m^{-2}\sum_{\mu\nu}p_{\nu\alpha}p_{\mu\beta}p_{\nu\gamma}p_{\mu\delta}\langle\Delta f_\nu\Delta f_\mu'\rangle_{N,0,E}V_\mu V_\nu \tag{68A}$$

where

$$\Delta f_\nu=f_\nu(X)-f_0(\mathbf{p}_\nu),\quad \Delta f_\mu'=f_\mu(X_\sigma)-f_0(\mathbf{p}_\mu).$$

Similarly we can write the $\alpha\beta$ element of the autocorrelation matrix of $\mathbf{B}$ as

$$(2m^2)^{-2}\sum_{\mu\nu}p_{\nu\alpha}p_{\mu\beta}\mathbf{p}_\nu^2\mathbf{p}_\mu^2\langle\Delta f_\nu\Delta f_\mu'\rangle_{N,0,E}V_\mu V_\nu. \tag{68B}$$

The procedure which we will use to calculate the means $\langle\Delta f_\nu\Delta f_\mu'\rangle_{N,0,E}$ will be first to calculate the conditional average with all of the phase functions $f_\mu(X)$ or what is the same thing, Δf_μ fixed. We will then average over the equilibrium distribution of the Δf_μ. Now according to our interpretation of the Maxwell-Boltzmann Eq. (64) the conditional average $\langle\Delta f_\nu\Delta f_\mu'\rangle f_1,f_2\cdots=\Delta f_\nu(f_\mu(\sigma)-f_0(\mathbf{p}_\mu)$, where $f_\mu(\sigma)$ is determined from the solution of Eq. (64) corresponding to the initial conditions $f_\mu(0)=f_\mu$ etc. Since we may expect the fluctuations of the $f_\mu(X)$ from their equilibrium values to be small on the average we may linearize Eq. (64) by setting

$$f(\mathbf{p},t)=f_0(\mathbf{p})(1+g(\mathbf{p},t)).$$

It is well known that for $g(\mathbf{p},t)$ we obtain the equation

$$\partial g(\mathbf{p},t)/\partial t=-\mathcal{g}g, \tag{69}$$

where $\mathcal{g}$ is a Hermitean positive semidefinite linear integral operator with respect to the weight function $w(\mathbf{p})=N^{-1}f_0(p)=(2\pi mK T)^{-\frac{3}{2}}\exp-\mathbf{p}^2/2mK T$. $\mathcal{g}g=0$ for $g=a+\mathbf{b}\cdot\mathbf{p}+c\mathbf{p}^2$, a, $\mathbf{b}$, c constants, and for no other functions. If $g(\mathbf{p},0)$ is orthogonal to all functions $a+\mathbf{b}\cdot\mathbf{p}+c\mathbf{p}^2$, i.e., if

$$\int g(\mathbf{p},0)(a+\mathbf{b}\cdot\mathbf{p}+c\mathbf{p}^2)w(\mathbf{p})d\mathbf{p}=0$$

for all a, $\mathbf{b}$, and c, Eq. (69) will have a solution which approaches zero for $\sigma\to\infty$ which we can write

$$g(\mathbf{p},\sigma)=\int K(\mathbf{p},\mathbf{p}',\sigma)g(\mathbf{p}',0)w(\mathbf{p}')d\mathbf{p}'. \tag{70}$$

In our case $g(\mathbf{p}',0)w(\mathbf{p}')=N^{-1}\Delta f_\lambda$, where Ω_λ is the cell in which $\mathbf{p}'$ is located. We have then, very approximately

$$\Delta f_\mu=f_0(\mathbf{p}_\mu)g(\mathbf{p},\sigma)=w(\mathbf{p}_\mu)\sum_\lambda K(\mathbf{p}_\mu,\mathbf{p}_\lambda,\sigma)\Delta f_\lambda V_\lambda,$$

where, as before, $\mathbf{p}_\mu$, $\mathbf{p}_\lambda$ are representative points in Ω_μ and Ω_λ, respectively. Multiplying by Δf_μ and averaging over the possible values of f_1, f_2, etc., we obtain

$$\langle\Delta f_\nu\Delta f_\mu'\rangle_{N,0,E}=w(\mathbf{p}_\mu)\sum_\lambda K(\mathbf{p}_\mu,\mathbf{p}_\lambda,\sigma)\langle\Delta f_\nu\Delta f_\lambda\rangle_{N,0,E}V_\lambda. \tag{71}$$

$\langle\Delta f_\nu\Delta f_\lambda\rangle_{N,0,E}$ is a quantity which we may calculate by the methods of equilibrium statistical mechanics.

Now

$$\Delta f_\nu=V_\nu^{-1}\sum_{i=1}^N E_\nu(\mathbf{p}_i)-NV_\nu^{-1}\int E_\nu(\mathbf{p})\rho_1(\mathbf{p})d\mathbf{p},$$

$$\Delta f_\lambda=V_\lambda^{-1}\sum_{i=1}^N E_\lambda(\mathbf{p}_i)-NV_\lambda^{-1}\int E_\lambda(\mathbf{p})\rho_1(\mathbf{p})d\mathbf{p},$$

where $\rho_1(\mathbf{p})$ is the equilibrium distribution of the momentum of a single molecule in the ensemble N, 0, E.

$$\begin{aligned}\langle\Delta f_\nu\Delta f_\lambda\rangle=&N\int E_\nu(\mathbf{p})E_\lambda(\mathbf{p})\rho_1(\mathbf{p})\delta(\mathbf{p}-\mathbf{p}')d\mathbf{p}d\mathbf{p}'\\&+N(N-1)\int E_\nu(\mathbf{p})E_\lambda(\mathbf{p}')\rho_2(\mathbf{p},\mathbf{p}')d\mathbf{p}d\mathbf{p}'\\&-N^2\int E_\nu(\mathbf{p})E_\lambda(\mathbf{p}')\rho_1(\mathbf{p})\rho_1(\mathbf{p}')d\mathbf{p}d\mathbf{p}',\end{aligned} \tag{72}$$

where $\rho_2(\mathbf{p},\mathbf{p}')$ is the distribution of the momenta of pairs of molecules in the ensemble N, 0, E.

If we were dealing with a canonical ensemble $\rho_1(\mathbf{p})$ would be equal to $w(\mathbf{p})$ and $\rho_2(\mathbf{p},\mathbf{p}')$, to $\rho_1(\mathbf{p})\rho_1(\mathbf{p}')$. In an ensemble in which total number momentum and energy are fixed this is true only if terms of order N^{-1} are neglected. Because of the factor N^2 in Eq. (72) these terms must be taken into account. We may then conveniently rewrite Eq. (72) as

$$\langle \Delta f_\nu \Delta f_\lambda \rangle V_\nu V_\lambda = N \int E_\nu(\mathbf{p}) E_\lambda(\mathbf{p}') \{ (\rho_1(\mathbf{p})\delta(\mathbf{p}-\mathbf{p}') - \rho_2(\mathbf{p},\mathbf{p}')) + N(\rho_2(\mathbf{p},\mathbf{p}') - \rho_1(\mathbf{p})\rho_1(\mathbf{p}')) \} d\mathbf{p} d\mathbf{p}'. \quad (73)$$

The exact expressions for $\rho_1(\mathbf{p})$ and $\rho_2(\mathbf{p},\mathbf{p}')$ in an ensemble with number of particles, momentum and energy fixed to be N, 0 and $E=3N\kappa T/2$ are

$$\rho_1(\mathbf{p}) = (2\pi m\kappa T)^{-\frac{3}{2}} (\tfrac{3}{2}(N-1))^{-\frac{3}{2}} \times \Gamma(\tfrac{3}{2}(N-1))/\Gamma(\tfrac{3}{2}(N-2)) \cdot (1-\mathbf{p}^2/3(N-1)m\kappa T)^{\frac{3}{2}(N-1)-1}, \quad (74A)$$

$$\rho_2(\mathbf{p},\mathbf{p}') = (2\pi m\kappa T)^{-\frac{3}{2}} ((9/4)N(N-2)^{-\frac{3}{2}} \times \Gamma(\tfrac{3}{2}(N-1))/\Gamma(\tfrac{3}{2}(N-3)) \times \{1-[\mathbf{p}^2+\mathbf{p}'^2+(\mathbf{p}+\mathbf{p}')^2/N-2]/3Nm\kappa T\}. \quad (74B)$$

Expanding these expressions in powers of N^{-1} with the aid of Stirling's formula for the gamma function, we obtain

$$\langle \Delta f_\nu \Delta f_\lambda \rangle V_\nu V_\lambda = N \int E_\nu(\mathbf{p}) E_\lambda(\mathbf{p}') \{ w(\mathbf{p})\delta(\mathbf{p}-\mathbf{p}') - w(\mathbf{p})w(\mathbf{p}')((5/2-(\mathbf{p}-\mathbf{p}')^2/2m\kappa T + \tfrac{1}{6}\mathbf{p}^2\mathbf{p}'^2/m^2\kappa^2T^2)\} d\mathbf{p} d\mathbf{p}' \quad (75)$$

$$= N \int E_\nu(\mathbf{p}) E_\lambda(\mathbf{p}') L(\mathbf{p},\mathbf{p}') w(\mathbf{p}) w(\mathbf{p}') d\mathbf{p} d\mathbf{p}'.$$

L will easily be recognized as the kernel of the operator which projects any function orthogonally onto the space of functions orthogonal to all $a+\mathbf{b}\cdot\mathbf{p}+c\mathbf{p}^2$.

By Eqs. (75), (71), and (68) (and substituting

$$\int \cdots d\mathbf{p} d\mathbf{p}' d\mathbf{p}'' \quad \text{for} \quad \sum_{\nu\mu\lambda} \cdots V_\nu V_\mu V_\lambda)$$

we obtain for the $\alpha\beta\gamma\delta$ element of the autocorrelation matrix of **A**

$$N \int m^{-2} p_\alpha p_\beta' p_\gamma p_\delta' L(\mathbf{p},\mathbf{p}') K(\mathbf{p}',\mathbf{p}'',\sigma) w(\mathbf{p}) w(\mathbf{p}') w(\mathbf{p}'') d\mathbf{p} d\mathbf{p}' d\mathbf{p}'', \quad (76A)$$

and for the $\alpha\beta$ element of the autocorrelation matrix of **B**

$$N \int (4m^4)^{-1} p_\alpha p_\beta' \mathbf{p}^2 \mathbf{p}'^2 L(\mathbf{p},\mathbf{p}') K(\mathbf{p}',\mathbf{p}'',\sigma) w(\mathbf{p}) w(\mathbf{p}') w(\mathbf{p}'') d\mathbf{p} d\mathbf{p}' d\mathbf{p}''. \quad (76B)$$

Now

$$\int m^{-1} p_\alpha p_\gamma L(\mathbf{p}\mathbf{p}') w(\mathbf{p}) d\mathbf{p} = m^{-1}(p_\alpha' p_\gamma' - \tfrac{1}{3}\mathbf{p}'^2\delta_{\alpha\gamma}),$$

while

$$\int (2m^2)^{-1} p_\alpha \mathbf{p}^2 L(\mathbf{p},\mathbf{p}') w(\mathbf{p}) d\mathbf{p} = (2m^2)^{-1} p_\alpha' (\mathbf{p}'^2 - 5m\kappa T).$$

Since $K(\mathbf{p}',\mathbf{p}'',\sigma)$, as a function of $\mathbf{p}'$ (and of $\mathbf{p}''$) is orthogonal to all linear combinations $a+\mathbf{b}\cdot\mathbf{p}+c\mathbf{p}^2$, we may rewrite our expressions for the elements of the autocorrelation matrices as

$$N \int m^{-1}(p_\alpha' p_\gamma' - \tfrac{1}{3}\mathbf{p}'^2\delta_{\alpha\gamma}) K(\mathbf{p}',\mathbf{p}'',\sigma) \times m^{-1}(p_\beta'' p_\delta'' - \mathbf{p}''^2\delta_{\beta\delta}) w(\mathbf{p}') w(\mathbf{p}'') d\mathbf{p}' d\mathbf{p}'', \quad (77A)$$

and

$$N \int (2m^2)^{-1} p_\alpha' (\mathbf{p}'^2 - 5m\kappa T) K(\mathbf{p}',\mathbf{p}'',\sigma) (2m^2)^{-1} \times p_\beta'' (\mathbf{p}''^2 - 5m\kappa T) w(\mathbf{p}') w(\mathbf{p}'') d\mathbf{p}' d\mathbf{p}''. \quad (77B)$$

If we set

$$g_{\beta\delta}(\mathbf{p}',\sigma) = \int K(\mathbf{p}',\mathbf{p}'',\sigma) \times m^{-1}(\mathbf{p}_\beta'' p_\delta'' - \mathbf{p}''^2\delta_{\beta\delta}) w(\mathbf{p}'') d\mathbf{p}'' \quad (78A)$$

and

$$g_\beta(\mathbf{p}',\sigma) = \int K(\mathbf{p}',\mathbf{p}'',\sigma)(2m^2)^{-1} \times p_\beta''(\mathbf{p}''^2 - 5m\kappa T) w(\mathbf{p}'') d\mathbf{p}'', \quad (78B)$$

we can express (77A) and (77B) as

$$N[m^{-1}(p_\alpha' p_\gamma' - \tfrac{1}{3}\mathbf{p}'^2\delta_{\alpha\gamma}), g_{\beta\delta}(\mathbf{p}',\sigma)] \quad (79A)$$

and

$$N[(2m^2)^{-1} p_\alpha' (\mathbf{p}'^2 - 5m\kappa T), g_\beta(\mathbf{p}',\sigma)], \quad (79B)$$

where the square brackets mean inner product with weight function $w(\mathbf{p}')$ in the sense of the theory of function spaces. $g_{\beta\delta}$, g_β are, of course, solutions of Eq. (69) corresponding to the initial conditions

$$g_{\beta\delta}(\mathbf{p}',0) = m^{-1}(p_\beta' p_\delta' - \mathbf{p}'^2\delta_{\beta\delta}) \quad (80A)$$

$$g_\beta(\mathbf{p}',0) = (2m^2)^{-1} p_\beta' (\mathbf{p}'^2 - 5m\kappa T). \quad (80B)$$

In order to determine the tensors $\mathbf{T}^{(4)}$, $\mathbf{T}^{(2)}$ we must divide the expressions, (79A) and (79B), by a^3, take the limit as $a\to\infty$ with $N/a^3=\text{constant}=d$ and integrate the result from $\sigma=0$ to infinity. These tensors depend on the functions

$$h_{\beta\delta}(\mathbf{p}')=\int_0^\infty g_{\beta\delta}(\mathbf{p}',\sigma)d\sigma, \quad h_\beta(\mathbf{p}')=\int_0^\infty g_\beta(\mathbf{k}',\sigma)d\sigma.$$

If we integrate both sides of Eq. (69) from $\sigma=0$ to infinity, we see that taking note of the initial conditions (80), $h_{\beta\delta}$, h_β satisfy the inhomogeneous integral equations

$$m^{-1}(p_\alpha' p_\delta' - \mathbf{p}'^2\delta_{\beta\delta})=\mathcal{g}h_{\beta\delta}(\mathbf{p}') \tag{81A}$$

$$(2m^2)^{-1}p_\beta'(\mathbf{p}'^2-5m\kappa T)=\mathcal{g}h_\beta(\mathbf{p}'). \tag{81B}$$

In terms of $h_{\beta\delta}$ and h_β we have

$$T^{(4)}{}_{\alpha\beta\gamma\delta}=\rho[m^{-1}(p_\alpha p_\gamma-\mathbf{p}^2\delta_{\alpha\gamma}), h_{\beta\delta}(\mathbf{p})] \tag{82A}$$

$$T^{(2)}{}_{\alpha\beta}=\rho[(2m^2)^{-1}p_\alpha(\mathbf{p}^2-5m\kappa T), h_\beta(\mathbf{p})]. \tag{82B}$$

By using symmetry and other properties of the operator $\mathcal{g}$ it may be shown that $\mathbf{T}^{(4)}$ and $\mathbf{T}^{(2)}$ are indeed isotropic and that the coefficient of volume viscosity vanishes. When translated into their notation Eqs. (82A) and (82B) yield the same values for the viscosity coefficients as are obtained in the book of Chapman and Cowling.[2]

This analysis also gives us an idea of the times for the functions $\mathbf{A}$, $\mathbf{B}$ to become uncorrelated. This is something like the time for a solution of Eq. (69) to approach equilibrium.

APPENDIX

In this appendix we will discuss certain theorems [stated in Eqs. (24), (30), and (51)] which belong essentially to time-independent statistical mechanics. These theorems answer the questions, what is the phase volume of a system in which the local temperature and density are not uniform and what are the local distributions of single particles and pairs. We will not prove these statements but will rather try to make them very plausible. We consider first the case of a single species.

We are seeking the phase volume density and the distribution of single particles and of pairs of the shell ensemble bounded by surfaces on which the $5(2M+1)^3-1$ phase functions given in Eqs. (4), (6), and (8), or rather their $5(2M+1)^3-1$ distinct real and imaginary parts, are constant. We can, however, describe the ensemble equally well by means of any $5(2M+1)^3-1$ independent functions of these phase functions provided we take account of the Jacobian of the transformation in calculating the phase volume density.

We consider the new phase functions

$$(a/2M+1)^3\rho(\mathbf{x}_{\lambda\mu\nu})=N_{\lambda\mu\nu}',$$
$$(a/2M+1)^3\mathbf{p}(\mathbf{x}_{\lambda\mu\nu})=\mathbf{p}_{\lambda\mu\nu}',$$
$$(a/2M+1)^3E(\mathbf{x}_{\lambda\mu\nu})=E_{\lambda\mu\nu}',$$

where $\mathbf{x}_{\lambda\mu\nu}=(a/2M+1)(\lambda,\mu,\nu)$, λ, μ, ν integers. Each of the points may be considered to be the center of one of the $(2M+1)^3$ cells of side $a/2m+1$ into which our volume a^3 may be divided, while the new phase functions may be considered to represent the total number, energy and momentum in each cell. As we should expect these functions are not all independent and in fact

$$\sum_{\lambda\mu\nu=-M}^{M}\sum N_{\lambda\mu\nu}'=N.$$

The $4(2M+1)^3$ cell momenta and cell energies and any $(2M+1)^3-1$ cell numbers may be used to define the surfaces which bound the region whose volume we wish to determine. The Jacobian of the transformation to this new set of functions will be a constant and moreover its logarithm will be negligible.

We have described the functions $N_{\lambda\mu\nu}'$, $\mathbf{p}_{\lambda\mu\nu}'$, $E_{\lambda\mu\nu}'$ as the total cell number momentum and cell energy, and they have many properties which justify these names. They have the defect however, the number, say, in cell $\lambda\mu\nu$ involves contributions from particles which are not actually in cell $\lambda\mu\nu$. One would, indeed, be more inclined to define these quantities as

$$N_{\lambda\mu\nu}=\sum_{i=1}^{N}E_{\lambda\mu\nu}(\mathbf{x}_i)$$

$$\mathbf{p}_{\lambda\mu\nu}=\sum_{i=1}^{N}\mathbf{p}_iE_{\lambda\mu\nu}(\mathbf{x}_i)$$

$$E_{\lambda\mu\nu}=\sum_{i=1}^{N}(\mathbf{p}_i^2/2m+\tfrac{1}{2}\sum_{j\neq i}^{N}V(x_i-x_j))E_{\lambda\mu\nu}(\mathbf{x}_i),$$

where $E_{\lambda\mu\nu}(\mathbf{x})$ is the characteristic function of cell $\lambda\mu\nu$. Now we know that the function $\varphi(\mathbf{x}-\mathbf{x}_{\lambda\mu\nu})$ is an approximation to the Dirac delta "function" and expressions such as

$$\int q(\mathbf{x})\varphi(\mathbf{x}-\mathbf{x}_{\lambda\mu\nu})d\mathbf{x}$$

or

$$\sum_{i=1}^{N}q_i\varphi(\mathbf{x}_i-\mathbf{x}_{\lambda\mu\nu})$$

have a value close to $q(\mathbf{x}_{\lambda\mu\nu})$ or to the mean value of q_i at $\mathbf{x}_{\lambda\mu\nu}$ *if the function* $q(x)$ *or the distribution of the quantity* q_i *is smooth enough.* We can expect that the particular quantities which enter into the definitions of $N_{\lambda\mu\nu}'$, $\mathbf{p}_{\lambda\mu\nu}'$, $E_{\lambda\mu\nu}'$ are very probably distributed uniformly enough for $N_{\lambda\mu\nu}'$ and $N_{\lambda\mu\nu}$, $\mathbf{p}_{\lambda\mu\nu}'$ and $\mathbf{p}_{\lambda\mu\nu}$, $E_{\lambda\mu\nu}'$ and $E_{\lambda\mu\nu}$ to be very closely equal. More precisely we

may expect that the volume of phase space where the unprimed quantities are significantly different from the primed is negligible. Needless to say a rigorous estimate of this volume, which we will not give, is necessary for an adequate proof. The $E_{\lambda\mu\nu}$ still cannot be described as the proper energy of a cell because the molecules j in their definition need not be in cell $\lambda\mu\nu$. We can, however, take into account the short range of the innermolecular forces and note that significant contributions to $E_{\lambda\mu\nu}$ come from molecules in cell $\lambda\mu\nu$ or in the six neighboring cells. Since each cell is supposed to contain many molecules and since only a few of these will be near enough to the cell surface to interact with a molecule in a different cell we may change the definition of the $E_{\lambda\mu\nu}$ so as to exclude contributions from such interactions. More precisely we assert (again without proof) that the phase volume in which these contributions are significant are negligible.

With these approximations we have reduced our problem to one with which we know how to deal. We have now to determine the phase volume in which the $4(2M+1)^3$ cell energies and momenta and $(2M+1)^3-1$ cell numbers have fixed values to within one unit. Since the cell numbers must be integers this means that we must fix all the $(2M+1)^3-1$ cell numbers exactly and determine the remaining one so that the total is N. For each particular assignment of molecules to cells the integral for this phase volume breaks up into a product of integrals each one of which refers to a single cell. Since there are $N!/\prod_{\lambda\mu\nu} N_{\lambda\mu\nu}$ such assignments we have for the phase volume density and expression of the form

$$w=N!\prod_{\lambda\mu\nu} w_{\lambda\mu\nu}/N_{\lambda\mu\nu}!,$$

where $w_{\lambda\mu\nu}$ is the volume of the $6N_{\lambda\mu\nu}$ dimensional phase space where the cell momentum and cell energy is fixed to be $\mathbf{p}_{\lambda\mu\nu}$ and $E_{\lambda\mu\nu}$ to within one unit. We have

$$\log w=\sum_{\lambda\mu\nu}\log(w_{\lambda\mu\nu}/N_{\lambda\mu\nu}!)+\log N!.$$

Now we can prove by the method of Gallilean transformations of section D that $w_{\lambda\mu\nu}$ is also the phase volume of the $6N_{\lambda\mu\nu}$-dimensional phase space where the cell momentum and cell energy is fixed to be 0 and $E_{\lambda\mu\nu}-\mathbf{p}_{\lambda\mu\nu}^2/2mN_{\lambda\mu\nu}$ to within one unit. If the momentum were not fixed to be zero $\log w_{\lambda\mu\nu}/N_{\lambda\mu\nu}!$ would be $\kappa^{-1}S(N_{\lambda\mu\nu},\ E_{\lambda\mu\nu}-\mathbf{p}_{\lambda\mu\nu}^2/2mN_{\lambda\mu\nu})$, where S is the total equilibrium entropy of a system containing $N_{\lambda\mu\nu}$ molecules and having energy $E_{\lambda\mu\nu}-\mathbf{p}_{\lambda\mu\nu}^2/2mN_{\lambda\mu\nu}$. The restriction of zero total momentum causes an error of order $1/N_{\lambda\mu\nu}$ which is negligible for our purposes. We have finally

$$\log w=\sum_{\lambda\mu\nu}(a/2M+1)^3 \times s(\rho(\mathbf{x}_{\lambda\mu\nu}),\ E(\mathbf{x}_{\lambda\mu\nu})-\mathbf{p}^2(\mathbf{x}_{\lambda\mu\nu})/2m\rho(\mathbf{x}_{\lambda\mu\nu})),$$

where s is the entropy density considered as function of the particle and intrinsic energy density. This expression is one of the approximating sums to the expression (30).

Since we have argued that our original ensemble is very approximately equivalent to a group of microcanonically distributed statistically independent cells, the one-particle distribution function will be proportional to the equilibrium one-particle distribution of the cell in which the particle is located. If the particles are in different cells, the two-particle distribution function will be proportional to the product of the equilibrium one-particle distribution functions corresponding to the two different cells. If they are in the same cell the two-particle distribution function is proportional to the equilibrium two-particle distribution function corresponding to that cell.

There is no essential complication of the above arguments for the case of two species.

Theory of Ignition Considered as a Thermal Reaction

BRUCE L. HICKS*
Ballistic Research Laboratories, Aberdeen Proving Ground, Maryland
(Received December 16, 1952)

The history of a family of exothermally reactive solids is studied theoretically with the help of analytical and numerical calculations. The different members of this family of nonisothermal solids are obtained, by changing scales and values of parameters, from the basic model which describes a zero-order reaction of a semi-infinite slab of material subjected at its surface to heat transfer from a gas.

For low initial temperatures of the solid, the heat transfer rate determines the ignition time while for high initial temperatures, this heating parameter is less important than the initial temperature, which controls the adiabatic ignition time. For the model used, the ignition time is generally quite sensitive to the duration of the external heating. Within the solid, it is found that the inner boundary of the region in which the chemical heat production is negligible moves inward along a diffusional type of path $x \propto t^{\frac{1}{2}}$ but that the point of maximum temperature, which develops after interruption of the external heating, follows a much different path. An analytical, approximate method of estimating minimum ignition time was tested by making comparison with numerical integrations and is probably accurate to 25 percent in the ignition time.

The computational side of the theory presented here may be regarded as essentially complete for practical purposes until greater accuracy and detail are required by more critical applications than are now in prospect. Meaningful utilization of the computations in practical applications will not however be possible until reliable measurements have been made of certain of the parameters for the solid—namely, activation energy, frequency factor and thermal conductivity—and for the external heating—namely, gas temperature and heat transfer coefficient.

In the course of the computations, many mathematical questions arose which are fundamental to the investigation of this and more realistic models of ignition but which remain to be answered.

SYMBOL LIST

Dimensional	Dimensionless	
x	ξ	distance from gas—solid interface
t	τ	time variable
$T(x, t)$	$U(\xi, \tau)$	temperature
h	H	heat transfer coefficient
c', K, q, f, E and R are defined in Table I.		
	ϕ	$(\xi/2\tau^{\frac{1}{2}})$
	ψ	$H\tau^{\frac{1}{2}}$
	α	$\exp(-1/U)/(\partial U/\partial\tau)$ discrimination parameter for cut-off of ξ-ward integration
	$F(\zeta)$	$e^{\zeta^2}erfc(\zeta)$
	m, n	integers such that $U(\xi, \tau) = U(m\delta\xi, n\delta\tau) = U_{m,n}$
	$\delta\xi, \delta\tau$	dimensions of mesh for numerical integration

Subscript	Denotes
a	adiabatic
c	critical
g	gas phase
i	ignition time
im	minimum ignition time
r	scaling unit
o	shutoff or end of heating time
1	starting value for numerical integration
α	value computed for a given value of α
ξ, τ	partial differentiation wrt these variables

Superscript	
L	result of a "linear" calculation
(0)	initial value
(1)	a subsequent value

* Now at the Control Systems Laboratory, University of Illinois, Urbana, Illinois.

1. INTRODUCTION

As part of a fundamental study of propellants at the Ballistic Research Laboratories, the theory of propellant ignition and combustion is being developed. In 1948 Alt's paper[1] on steady state burning appeared, in which a solid propellant was assumed to undergo a purely thermal reaction. We use the same assumption in the present paper but treat the ignition process.

The theory of steady reactions with or without spacewise propagation of the reaction zone requires the solution of *ordinary* differential equations which, except for isothermal reactions, are nonlinear because the reaction rate depends on the Arrhenius factor $\exp(-E/RT)$. Exact or approximate analytical solutions can often be obtained in the simpler cases.[2] The process of ignition can seldom be treated as steady state since by nature ignition is a transient process leading from one state, that of no reaction, to another, that of selfsustaining combustion. In thermal ignition the temperature is a function of position as well as of time. We see, therefore, that an exact thermal ignition theory will involve the solution of nonlinear *partial* differential equations. Exact analytical solutions will not now be expected, and approximate analytical treatments will be more difficult to construct than in steady burning theory because the nonlinear term is a function of two variables (x, t). Problems of this general mathematical type have

[1] F. L. Alt, Ballistic Research Laboratories Report No. 682 (1948).

[2] D. A. Frank-Kamenetzky, J. Phys. Chem. (U.S.S.R.) **13**, 738 (1939); P. V. Melentjev and O. M. Todes, Acta Physicochim. U.R.S.S. **14**, 27 (1941); O. K. Rice, J. Chem. Phys. **8**, 727 (1940); E. K. Rideal and A. J. B. Robertson, *Third Symposium on Combustion* (Williams and Wilkins, Baltimore, Maryland, 1949), p. 536; M. W. Evans, Technical Report No. 27, Project SQUID (Princeton, New Jersey, 1951)—a review of theories of steady-state flame propagation.

been examined by several investigators,[3,4] but not the specific one formulated here.

In the present paper, which is an amplification of reference 4, we shall give a fairly detailed account of an ignition process that is considered to be wholly thermal (i.e., no diffusion or consumption of material and no chain reactions).[5] Our purpose will be twofold: to give a thorough discussion heretofore unavailable, of the qualitative behavior of thermal ignition (thoroughness is possible because of the simple model chosen); and to display techniques that are useful in handling a nonlinear nonisothermal problem. We shall also attempt to evaluate briefly the adequacy of the computational methods. Since our method of evaluation is empirical rather than analytical, we have not considered local error nor its propagation quantitatively but have postponed these more detailed mathematical questions for future investigation. In the present state of the theory it is impossible to answer both quickly and precisely all questions that may be asked about an ignition process or about the validity of approximations made in the theory.

Some of our results have been summarized at various meetings of societies.[6]

2. THE MODEL

We shall suppose that the reacting medium[7] is bounded by a plane face, over which it is uniformly heated, and that for times of interest the effects of the heating penetrate only a small part of the thickness of the medium in the x direction perpendicular to the face. If the extent of the medium in directions parallel to the face is large and the material remains homogeneous throughout, we can take as our model simply a semi-infinite slab or rod (see Fig. 1). The partial differential equation describing the heat flow in such a volume which is undergoing exothermic reaction is

$$c'\frac{\partial T}{\partial t}=K\frac{\partial^2 T}{\partial x^2}+Q; \quad x\geqslant 0, \quad t>0, \tag{2-1}$$

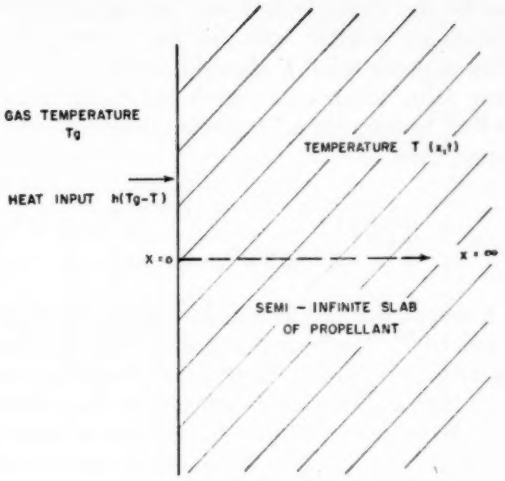

FIG. 1. The model.

in which $T(x, t)$ is the temperature at any point in the medium; c', K, Q are the parameters heat capacity per unit volume, thermal conductivity and rate of heat evolution (owing to the reaction) per unit volume. In our thermal theory, the reaction is assumed to be of zero order and the rate independent of concentrations; Q is therefore of the form

$$Q=qfe^{-E/RT}, \tag{2-2}$$

where q is the heat of reaction per unit volume, f the frequency factor, E the activation energy for the reaction, and R the gas constant.

We assume that the heat is transferred to the surface from a gas at temperature T_g with heat transfer coefficient h. Therefore one boundary condition is

$$-K\frac{\partial T}{\partial x}=h(T_g-T); \quad x=0, \quad t>0. \tag{2-3}$$

At infinity we assume that the heat flow vanishes because neither the internal heat source afforded by the chemical reaction nor the very distant heated surface can produce a gradient so far in the interior. The second boundary condition is thus

$$\frac{\partial T}{\partial x}\to 0; \quad x\to\infty, \quad t>0. \tag{2-4}$$

As an initial condition we take the temperature to be constant[8]

$$T=T^{(0)}; \quad x\geqslant 0, \quad t=0. \tag{2-5}$$

In practical ignition processes T_g would not be constant throughout the ignition process (nor would its variation be known with any degree of accuracy). We wish to have the model simulate ignition conditions,

[3] C. Lowener, NDRC Appl. Math. Panel Memos 131.1M and 131.2M, (1945); H. E. Goheen, J. Math. and Phys. **28**, 107 (1949); C. H. Bamford, J. Crank and D. H. Malan, Proc. Camb. Phil. Soc. **42**, 166 (1946); J. Crank and P. Nicolson, Proc. Camb. Phil. Soc., **43**, 50 (1947); D. Altman and A. F. Grant, Jr., *Abstracts of Papers for Fourth Symposium on Combustion* (Massachusetts Institute of Technology, 1952), p. 19.

[4] J. H. Frazer and B. L. Hicks, J. Phys. and Colloid Chem., **54**, 872 (1950).

[5] We have made extensive calculations, to be described elsewhere, of reaction models that allow for diffusion of a single reactant as well as of heat. The stability aspects of these calculations were discussed at the Pittsburgh meeting of the American Physical Society in 1951.

[6] J. H. Frazer, New York City Meeting of Am. Chem. Soc., September 15, 1947; B. L. Hicks and H. G. Landau, Math. Tables and Aids to Computation **3**, 207 (1948); B. L. Hicks, Phys. Rev. **76**, 166(A) (1949).

[7] The medium can be taken to be solid. We shall not consider here the ignition process after the surface begins to regress. [H. G. Landau, Quar. Appl. Math., **7**, 81 (1950).)] The medium could be liquid or gas if the density and position of all of its parts remain fixed.

[8] Any later temperature distribution developed by the internal and external heating in the propellant could likewise be considered to be an initial condition.

in a rocket for example, but also to introduce as few parameters as possible into this first treatment. We therefore suppose that T changes suddenly from one constant value to another (much lower) value at the end of the "heating time." If t_0 = duration of burning of an igniter, then

$$T_g = \begin{cases} T_g^{(0)}; & 0 < t \leqslant t_0 \\ T_g^{(1)} \ll T_g^{(0)}; & t_0 < t. \end{cases} \tag{2-6}$$

Thus t_0 marks the last instant for which the high gas temperature, $T_g^{(0)}$, affects the surface. Actually, during the heating time the gas temperature would normally be much higher than the temperature of the propellant surface. Accordingly, solution of the above equations for different values of h corresponds to ignition either with different heat transfer coefficients or, approximately, with different gas temperatures. The effects of variations with x or t of c', K, E, q, f, h, T_g, or $T^{(0)}$ could also be roughly estimated from results for our simple model in which all of these parameters are assumed constant. Actually not much is known about the variation of such of these parameters as are not constant. The assumed nonconsumption of the propellant and neglect of the regression of its surface perhaps restrict the validity of our description of ignition, relative to a more complete picture, more than does neglect of the variation of the parameters; and the effects of consumption and regression cannot be estimated directly from our zero-order thermal model.

Since temperature rise must be our criterion for ignition of the propellant as described by the model, we shall principally be interested in defining *ignition time* and calculating its value as a function of the parameters h, $T^{(0)}$, etc., and shall pay somewhat less attention relatively to the detailed variation of T with (x, t).

3. REDUCED VARIABLES

Not all the constant parameters need be retained explicitly in the analysis. We can simultaneously reduce the number of parameters and introduce new parameters and new variables that are dimensionless with the usual advantages of this property. The transformations introducing the new or reduced variables U, ξ, τ which we shall use are

$$T = (E/R)U = T_r U, \tag{3-1}$$

$$x = (KE/Rqf)^{\frac{1}{2}}\xi = x_r \xi, \tag{3-2}$$

$$t = (c'E/Rqf)\tau = t_r \tau. \tag{3-3}$$

The quantities U, ξ, and τ are then reduced variables of temperature, distance, and time. These transformations permit elimination of all but five parameters from the system of equations that must be solved to yield the desired information about the ignition process. Equations introducing the five parameters remaining, H, $U_g^{(0,1)}$, $U^{(0)}$, τ_0, are

$$h = (RKqf/E)^{\frac{1}{2}}H = h_r H, \tag{3-4}$$

$$T_g^{(k)} = T_r U_g^{(k)}, \tag{3-5}$$

$$T^{(0)} = T_r U^{(0)}, \tag{3-6}$$

$$t_0 = t_r \tau_0. \tag{3-7}$$

The equations to be solved then become:

$$\frac{\partial U}{\partial \tau} = \frac{\partial^2 U}{\partial \xi^2} + e^{-1/U}; \quad \xi \geqslant 0, \quad \tau > 0, \tag{3-8}$$

$$-\frac{\partial U}{\partial \xi} = H(U_g - U); \quad \xi = 0, \quad \tau > 0, \tag{3-9}$$

$$\frac{\partial U}{\partial \xi} \longrightarrow 0; \quad \xi \to \infty, \quad \tau > 0, \tag{3-10}$$

$$U = U^{(0)}; \quad \xi \geqslant 0, \quad \tau = 0, \tag{3-11}$$

where

$$U_g = \begin{cases} U_g^{(0)}; & 0 < \tau \leqslant \tau_0 \\ U_g^{(1)} \ll U_g^{(0)}; & \tau_0 < \tau. \end{cases} \tag{3-12}$$

Our mathematical problem will thus be to obtain a solution of the system (3-8) to (3-12) for the function $U(\xi, \tau; H, U_g^{(0)}, U_g^{(1)}, U^{(0)}, \tau_0)$.

Before methods of obtaining these solutions are discussed, it will be useful to note the range of variation of the various original and reduced variables and parameters and to give the physical interpretation of the transformations. Table I shows the range of values of the quantities of interest. We interpret the transformation to ξ, τ as usual in transient heat flow problems. The equation $t \sim (c'/K)x^2$ gives the approximate time for disturbances of temperature to diffuse the distance x. We therefore expect to find that the transformation factors in (3-2) and (3-3) differ only by the factor (K/c'), i.e., $(x/\xi)^2 = (K/c')(t/\tau) = (K/c')t_r$ where t_r is the unit of time. The unit of scaling in (3-1) is simply the temperature rise $T = (E/R)$. The scaling unit t_r for t can therefore be regarded as the time required to increase the temperature of the solid (of heat capacity c') by the amount T_r when it is heated at the rate of (qf) cal/cm^3 sec. The unit, t_r, is thus a measure of the (exponential) sensitivity of the (thermal) reaction rate to heating produced by the reaction in the solid. In terms of t_r we find that $h_r = (Kc'/t_r)^{\frac{1}{2}}H$. This is also the usual result since, once a time scale has been introduced, a heat transfer coefficient scales (in a transient heat flow problem) proportionally to $(Kc')^{\frac{1}{2}}$.

4. QUALITATIVE FEATURES OF THE IGNITION PROGRESS

The key to the general behavior of our model is to be found in its infinite extent. At infinity, although the heat flow vanishes, there always exists a finite positive heat source proportional to $\exp(-1/U)$. Since the sur-

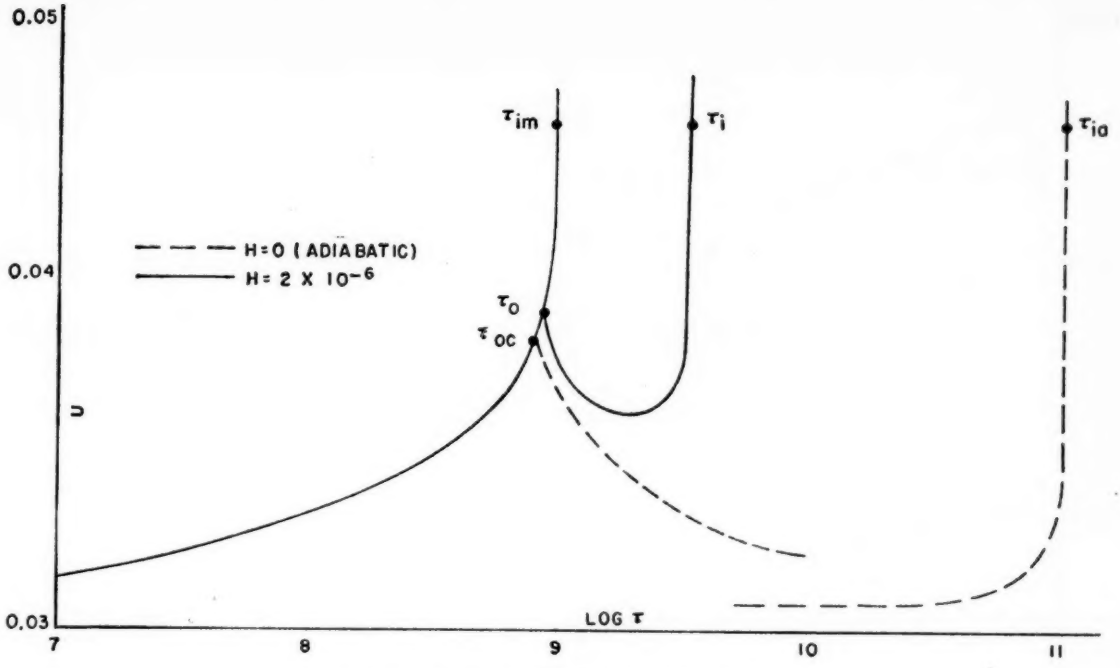

FIG. 2. $U^{(0)}=0.031$; $Ug^{(0)}=0.18$; $Ug^{(1)}=0.021$.

face boundary condition can have no influence on the behavior, at any finite time, at infinity we see that any assigned temperature will be attained at infinity in a finite time (though usually in a smaller finite time at some other point). Stated in physical terms, a propellant which behaves like the model will always eventually ignite (i.e., attain a high temperature and rate of reaction) and can never approach a steady state.[9] We find it convenient to say that the ignition has occurred when the reduced temperature at the surface first reaches the value of 0.045, and thus to define the reduced ignition time τ_i by

$$U(0, \tau_i)=0.045. \tag{4-1}$$

It simplifies matters to choose a common, rather high value such as 0.045, as the reduced ignition temperature in all cases. The value of 0.045 is somewhat above the values for which the model is realistic. For this reduced temperature, however, the reaction at the surface is very rapid for the whole range of parameters outlined in Table I, and even though the rapid temperature rise that takes place, once the exponential first takes hold, occurs at a temperature level which depends strongly on the initial temperature, the time to ignition is insensitive to the choice of reduced ignition temperature.

We similarly define τ_{ia}, which may be called the (reduced[10]) *adiabatic ignition time*, as the time for $U=U_a$ to reach 0.045 in a solid of uniform temperature

$$U_a(\tau_{ia})=U(\infty, \tau_{ia})=0.045. \tag{4-2}$$

The case of "adiabatic" self-heating is obtained when the heat transfer at the surface vanishes or when the remote interior of the solid is considered.

Under the influence of external heating which is "shut off" at time τ_0, the temperature at the surface of the propellent rises monotonically until τ_0, when, owing to discontinuity of the heat source at the boundary, $(\partial U/\partial\tau)/_{\xi=0}\rightarrow-\infty$ after which time there is cooling at the surface. Subsequently the temperature passes

TABLE I. Approximate range or values of variables and parameters.[a]

	Dimensional	Dimensionless
Depth to which reaction penetrates	Δx—10^{-5}–10^{3} cm	$\Delta\xi$—10^{2}–10^{10}
Time intervals	Δt—10^{-7}–10^{7} sec	$\Delta\tau$—10^{3}–10^{20}
Heating time	t_0—10^{-6}–10^{3} sec	τ_0—10^{4}–10^{16}
Temperature	T—200–600°K	U—0.010–0.050
Gas temperature (hot)	$T_g^{(0)}$—1500–3000°K	$U_g^{(0)}$—0.18, 0.20
Gas temperature (cooled)[b]	$T_g^{(1)}$—300–600°K	$U_g^{(1)}$—0.021
Initial propellant temperature	$T^{(0)}$—200–400°K	$U^{(0)}$—0.010–0.034
Ignition temperature	T_i—675–1250°K	U_i—0.045, 0.050
Heat transfer coefficient	h—10^{-6}–3×10^{-2} cal/cm² sec °C	H—10^{-10}–2×10^{-6}
Heat capacity/unit volume	c'—0.5–0.8 cal/cm³ °C	
Thermal conductivity	K—10^{-5}–10^{-2} cal/cm sec °C	
Heat of reaction/unit volume[c]	q—10^{2}–10^{3} cal/cm³	
Frequency factor	f—10^{13}–10^{16} sec^{-1}	
Activation energy	E—3.0–5.0×10^{4} cal/mole	

[a] The values in the second column are, for the most part, those encountered in practice. The values in the third column are those used in the numerical work for the present report.
[b] See Sec. 2 for significance of T_g (reference 1).
[c] In our treatment, q and f do not enter separately and only the product (qf) appears.

[9] We note that a steady state for a thermal, infinite model is possible when burning (with surface regression) rather than ignition of the propellant is considered. See reference 1.

[10] Except where there is a possibility of confusing the reduced (dimensionless) and the dimensional variables or parameters we shall generally omit the word "reduced" in the remainder of the paper.

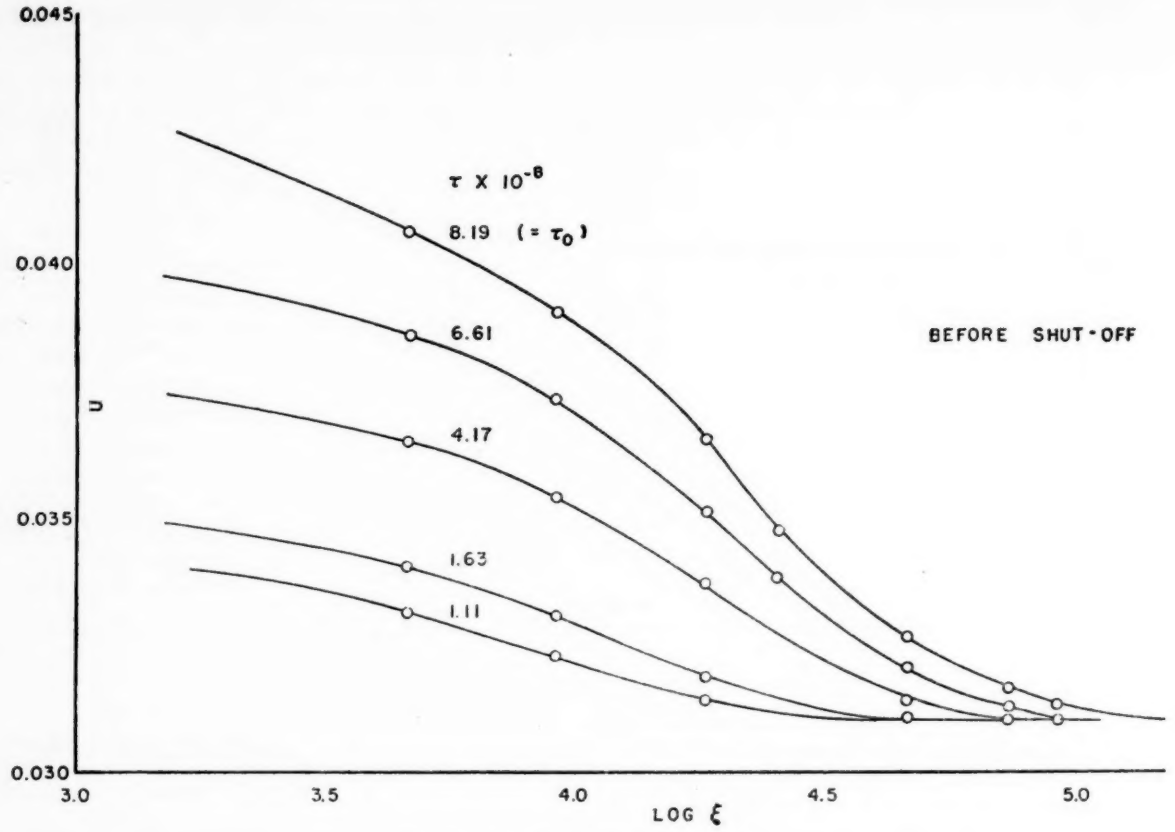

FIG. 3. $\tau<\tau_0$; $H=2\times10^{-6}$; $U^{(0)}=0.031$.

through a minimum and eventually rises again until the ignition condition is reached. The variations of the surface temperature with time, both for a positive value of the heat transfer coefficient H and for a zero value of H, are illustrated in Fig. 2. The effect of the surface heating in decreasing the ignition time τ_i from the adiabatic value τ_{ia} is evident. As the heating time τ_0 is increased, τ_0 and τ_i approach equality with one another and with τ_{im}, the *minimum ignition time*, or maximum heating time, for which the surface temperature at shutoff $U(0, \tau_0)=0.045$. The temperature distributions in space are illustrated for different values of $\tau<\tau_0$ (that is, before shutoff) for a typical case in Fig. 3.

We see that if the heating time τ_0 is decreased even slightly below the minimum ignition time τ_{im} then the ignition time τ_i increases very greatly. If the gas temperature $U_g{}^{(1)}$ is very much less than that of the surface of the solid $U(0, \tau)$, at a time after "shutoff," then if the heating time τ_0 is small enough the ignition time τ_i as defined above becomes greater than the adiabatic ignition time τ_{ia}. In general for these times after shutoff, moreover, the maximum temperature lies within the solid rather than at the surface and moves inward as τ increases (see Fig. 4). The value 0.045 will be reached at the point of maximum temperature somewhat sooner than at the surface, although the difference in ignition times is often not large. This point of maximum temperature moves toward infinity as the heating time τ_0 decreases, so that when the ignition time τ_i, as defined above in terms of the surface temperature, becomes equal to the adiabatic ignition time τ_{ia}, the temperature gradient is positive thoughout a considerable part of the solid. We define the *critical heating time* τ_{0c} to be that for which $\tau_{i/\xi=0}=\tau_{ia}$. In other words, if heat is supplied for time τ_{0c}, followed by cooling until ignition, the time for ignition will be the same as though the surface were always insulated. As illustrated in Fig. 2, the value of τ_{0c} is likely to be close to that of the minimum ignition time τ_{im}. We shall later describe most of the results of the calculations in terms of τ_{im}; less data are available for the ignition time τ_i and for the critical heating time τ_{0c}. These periods of heating τ_{0c} and τ_{im} represent the maximum and minimum periods of interest because the ignition time (as here defined) of a propellant is unchanged by external heating for $\tau_0=\tau_{0c}$ and is reduced to a minimum by the external heating when $\tau_0=\tau_{im}$.

For not too high values of the initial temperature (see Appendix) there will occur an extended initial phase of the heating process during which the nonlinear exponential term $\exp(-1/U)$ in Eq. (3-8) will be inappreciable. This is the period of "linear" heating. We shall measure the importance of the exponential

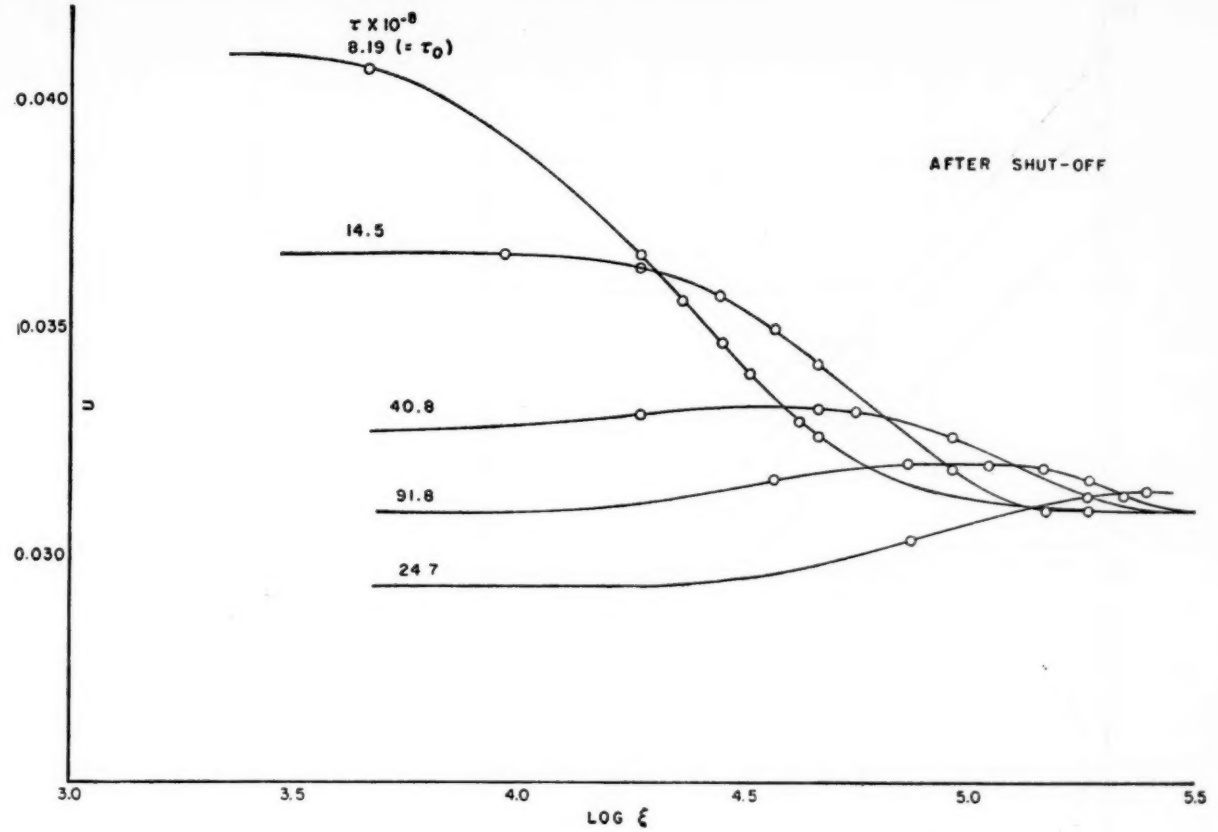

FIG. 4. $\tau > \tau_0$; $H = 2\times10^{-6}$; $U^{(0)} = 0.031$.

term by the parameter α where

$$e^{-1/U} = \alpha \partial U/\partial \tau. \tag{4-3}$$

α thus is a function both of ξ and of τ. A given value of $\alpha \ll 1$ will first be reached at the boundary $\xi = 0$ because $\exp(-1/U)$ is larger at the wall than elsewhere in the solid, and $\partial U/\partial \tau$ is smaller there than in the immediate neighborhood of the wall. Various quantities evaluated at $\xi = 0$ and for a given value of α will be marked by the subscript α. Quantities evaluated before the end of the "linear" heating will be marked by the superscript L.

The magnitude of the factor α is chosen differently, depending upon the purpose we have in mind. Thus, as the criterion for local "linearity" of the heating, we would take $\alpha \leqslant 0.05$. In numerical integrations of Eqs. (3-8 to 3-12) we shall want to know when, for a given desired accuracy of integration, the exponential term must first be considered. The value of α would then be small (say 5×10^{-4}). On the other hand, for many choices of the parameters $U^{(0)}$, $U_g{}^{(0)}$ and H it is found that the minimum ignition time τ_{im} is about equal to a quantity $\tau_\alpha{}^L$ (which is calculable without integration—see the Appendix) if α lies somewhere between 0.2 and 0.83. This property of the (approximately) "linear" part of the heating curves is valuable, for it is then possible in many cases to obtain useful approximations to the nonlinear problem by purely analytical means. Such approximations, even though somewhat crude, are of especial value in nonlinear problems such as the present one where they permit both concise representation of large ranges of numerical data and the construction of simple and of more generally powerful theoretical pictures.

5. NUMERICAL CALCULATIONS

A total of 70 different numerical integrations of the partial differential Eq. (3-8) were performed on desk computers and on the Bell Relay Computer and involved the following values of the parameters:

$$U^{(0)} = 0.010(7)0.034,^{11}$$
$$U_g{}^{(0)} = 0.18,\ 0.20,$$
$$H = 10^{-10}(6)2\times10^{-6}, \text{ and}$$
$$\tau_0 = 8.3\times10^{8}(37)3.3\times10^{16}.$$

Integrations were started at a time $\tau = \tau_\alpha{}^L$, different for each integration, with an initial temperature distribution given by $U^L(\xi, \tau_\alpha{}^L)$ (see Appendix). In this way proper allowance was made in each case for the "linear" phase of the heating of the solid, and the effect of the exponential term could be introduced smoothly when it first become appreciable. The formulas used for the

[11] To be read "seven values of which the smallest was 0.010 and the largest, 0.034."

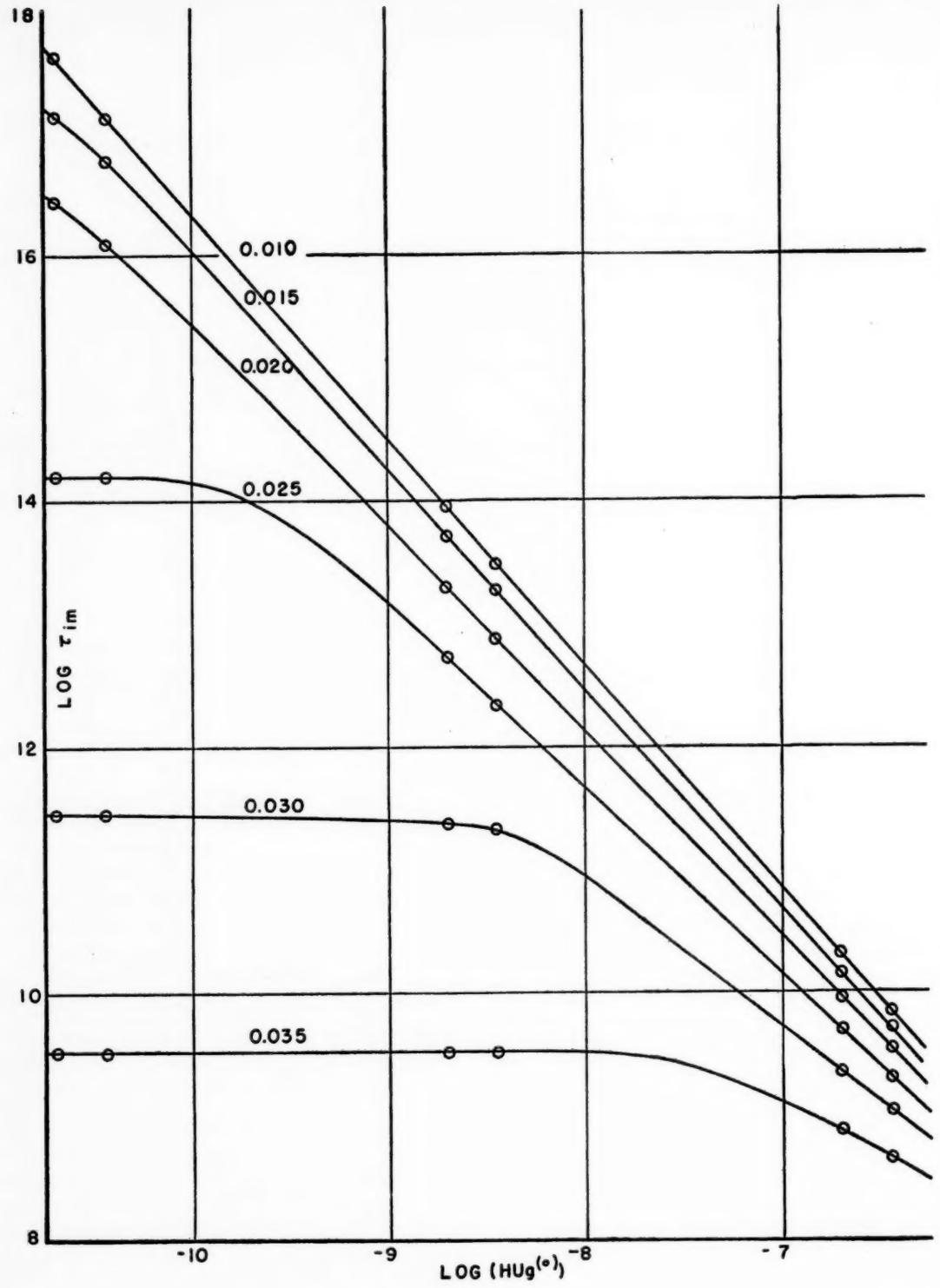

FIG. 5.

numerical integrations are given by Eqs. (A-18, 19, 20) in the Appendix.

For each of the numerical integrations, values of U_a and of τ_{ia} were computed from Eq. (A-3) and of U^L and of $\tau_a{}^L$ from the other equations in the Appendix and from Fig. 12.

6. RESULTS

Dimensionless Variables

The most complete data were obtained for the minimum ignition time τ_{im} corresponding to no shutoff. We recall that ignition is conveniently defined in terms of

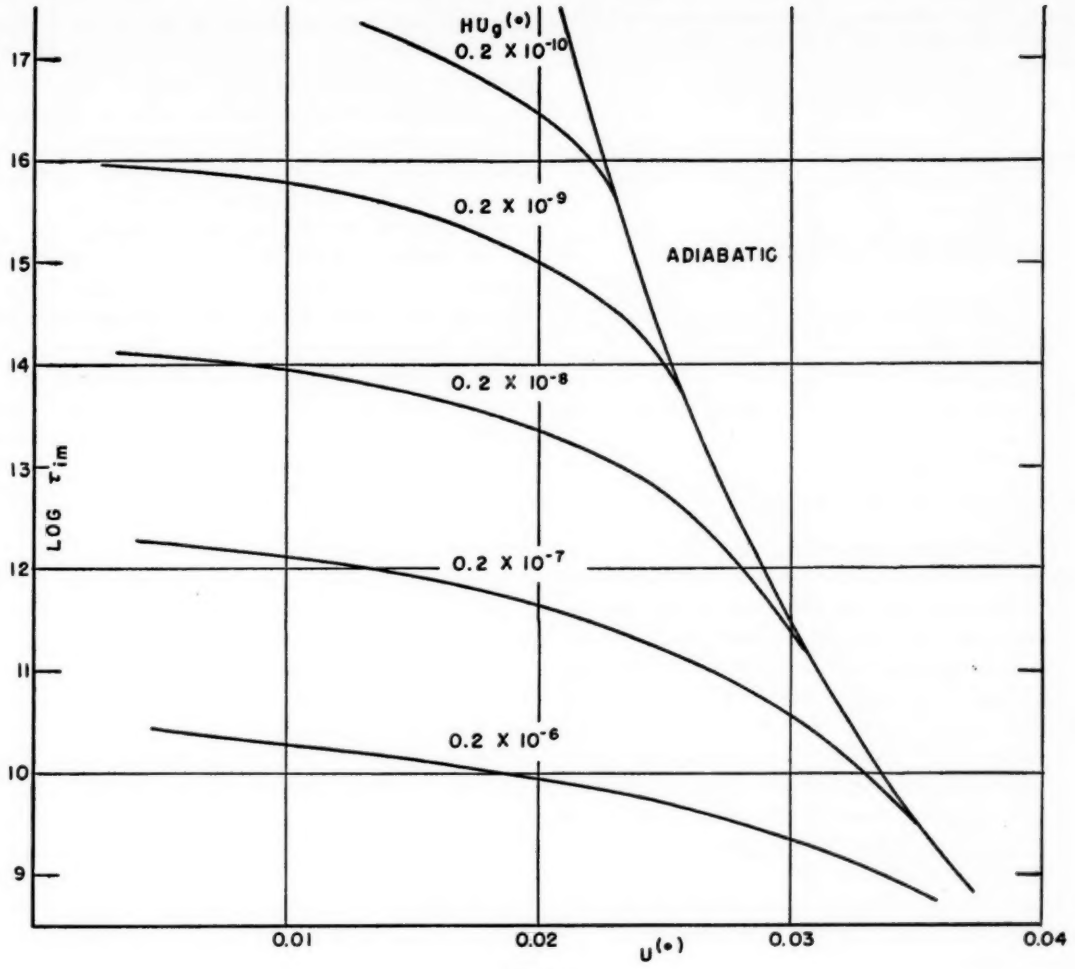

FIG. 6.

the temperature becoming equal to 0.045 at the surface; therefore the ignition involves the interior only indirectly. All of the data on τ_{im} resulting from the calculations described in Sec. 5 have been combined in Figs. 5 and 6, which were constructed as follows: the numerical integration data were extrapolated to lower and higher values of initial temperature $U^{(0)}$, interpolated for values of $U^{(0)}=0.015$ and 0.025, cross plotted and smoothed against $\log(HU_g^{(0)})$ in Fig. 5 and finally replotted against $U^{(0)}$ for even values of $(HU_g^{(0)})$ in Fig. 6. The close agreement between the points and curves of Fig. 5 shows the possibility of smoothing the calculated values of minimum ignition time τ_{im} from the various independent sets of numerical integrations but does not imply much as far as over-all accuracy of calculations is concerned. Correlation with $(HU_g^{(0)})$ (which is approximately the rate of heat transfer to the surface) seems to take the place of scanty data on the individual variations of τ_{im} with gas temperature $U_g^{(0)}$ and with heat transfer coefficient H. The adiabatic curve on Fig. 6, corresponding to no heat loss and to a uniform temperature of the solid, was calculated from Eq. (A-3) in the Appendix. On the basis of rather limited data pertaining to errors we estimate that the uncertainty in values of minimum ignition time τ_{im} obtained by numerical integration amounts to 10 to 20 percent. The discrepancy between these values and the values estimated by the linear approximation described in the Appendix are less than 10 percent in most instances and this figure could have been reduced if the value of α had been chosen to be smaller than 0.833. We therefore conclude that *for our model and the range of dimensionless parameters given in Table I, the minimum ignition time τ_{im} can probably be estimated within 25 percent by computing the quantity $\tau_{im}{}^{L}$ accurately by the analytical method (see Appendix) and combining this information with knowledge of the adiabatic ignition time τ_{ia}.* Physically speaking, therefore, the model can be replaced if the influence of external heating is not too small (i.e., $\tau_{im} \ll \tau_{ia}$) by an unreactive solid (of temperature $U^{L}(\xi, \tau)$ which by definition ignites under the effect of uninterrupted heating at the surface when the rate of heat production by the reaction becomes comparable at the surface to that supplied by external

TABLE II. Sensitivity of minimum ignition time to change of initial temperature and of rate of external heating.

$-\partial \log \tau_{im}/\partial \log U^{(0)} = -\partial \log t_{im}/\partial \log T^{(0)}$

$U^{(0)}$ \ $HU_g^{(0)}$	0	0.2×10^{-10}	0.2×10^{-8}	0.2×10^{-6}
0.01	100	2.0	0.81	0.69
0.02	50	8.3	5.8	1.6
0.03	33	33	24	5.9

$-\partial \log \tau_{im}/\partial \log (HU_g^{(0)}) = -\partial \log t_{im}/\partial \log (hT_g^{(0)})$

$U^{(0)}$ \ $HU_g^{(0)}$	0.2×10^{-10}	0.2×10^{-8}	0.2×10^{-6}
0.01	1.8	1.8	1.8
0.02	1.1	1.7	1.7
0.03	0	0.36	1.2

heating (i.e., when

$$\alpha^L = \exp(-1/U^L)/[\partial U^L/\partial\tau + \exp(-1/U^L)]$$

reaches 0.833, or slightly less, at the surface).[12]

Analysis of the data in Fig. 6 leads to a second conclusion. *The minimum ignition time, that is the time for the temperature at the surface to reach 0.045, is determined for low initail temperature $U^{(0)}$ primarily by the heat transfer coefficient H, while for higher $U^{(0)}$ or lower H it is determined primarily by $U^{(0)}$.* (See Tables II, III.) Since the value of α^L necessary to secure agreement with the numerical integration data seems to vary with $U^{(0)}$ and H, it appeared that ignition might better be defined in terms of a value of α rather than of $U^{(0)}$. The two criteria of ignition give curves of slightly different shape and position. It is not known at present which criterion would be more useful in comparing with experimental data.

The postponement of ignition is the most important phenomenon occurring as a result of the shutoff of the external heating at a time τ_0 which is less than the minimum ignition time τ_{im}. The shut-off data is rather fragmentary and uncertain partly because of computational difficulties. We recall that the propellant, as described by the model, always will ignite some time because of the distribution of heat sources, all positive, through the solid. It may be concluded, however, that *the time for ignition is quite sensitive to the length of the heating period, particularly for heating times near the minimum ignition time.* The sensitivity is probably less in the neighborhood of the adiabatic ignition process. Unification of the shut-off data by physical arguments is difficult because of the arbitrary though convenient definition of ignition time τ_i in terms of the surface temperature. In most cases of shutoff considered, an interior point will have the highest temperature and will ignite first. If the temperature at the surface at shut-off $U_0 = U(0, \tau_0)$ rather than the heating time τ_0 is used as the abscissa, however, the scattered data can be correlated to some extent as shown in Fig. 7. It should be remembered that the shape of the shut-off curve markedly influences ignition delays if they are short. It is probable that the ignition time τ_i depends sensitively on the surface temperature at shut-off when this temperature U_0 is in the neighborhood of $U_{0c} = U(0, \tau_{0c})$, i.e., of that at the critical heating time τ_{0c}.

For three of the integrations extending after shut-off it was possible to follow the point of maximum temperature. On the basis of these three cases it was found that *the movement of the point of maximum temperature within the propellant after shutoff does not even approximately follow a diffusional motion describable by $\xi \propto \tau^{-\frac{1}{2}}$*, and departs from this relation more the larger τ becomes. If the point of maximum temperature had been distinguishable in more of the runs, ignition time could have been more logically defined as the time for this point to reach 0.045.

The behavior of the interior of the propellant before shutoff may exhibit one of three patterns: the interior may heat almost uniformly (as in the adiabatic case); or as though there were no chemical reaction ("linear" case); or it may be affected by both chemical and external heating. Which pattern prevails is determined by the proximity, in the no shut-off case, of the point with coordinates $(U^{(0)}, H)$ to the adiabatic curve in a figure such as Fig. 6 and also by the values of ξ and τ. Thus if ξ is large enough, the adiabatic temperature level obtains; if τ is large enough the effect of the chemical production of heat will surely be felt. We have studied the extent of the "linear" region in various ways. The trajectory of the point where $\alpha = 0.05$ yields the interesting conclusion that *the regression inward of the inner boundary of the "linear" region follows approximately a diffusional type of path $\xi \propto \tau^{-\frac{1}{2}}$* in spite of the fact that the depth where the chemical heating will be negligible cannot be calculated by our present linearized theory. The outer boundary of this "linear" region moves inward more rapidly. In addition, it was found that at the surface the value of α for a given τ and initial temperature $U^{(0)}$ cannot be less than a minimum value that is independent of the heat transfer coefficient H.

The present theory gives the ignition time as a function of external heating rate and duration and of the initial temperature of the propellant, for a given choice of ignition temperature U_i. If U_i were prescribed

TABLE III. Typical conditions at ignition.[a]

h cal/cm²-sec-°C \ $T^{(0)}$°K	300		450	
	$\log t_{im}$-sec	$\log x_{1/5}$[b]-cm	$\log t_{im}$-sec	$\log x_{1/5}$-cm
0	6.21		−0.665	
2.58×10^{-6}	4.32	0.316	−0.665	
2.58×10^{-4}	1.22	−0.882	−0.745	−1.63
2.58×10^{-2}	−2.18	−2.34	−2.78	−2.69

[a] Calculated for the basic set of values of the parameters in Table IV.
[b] $x_{1/5}$ defines the position at which

$$T(x_{1/5}, t_{im}) - T^{(0)} = 0.2\,(T(0, t_{im}) - T^{(0)}).$$

[12] The less accurate linear method described by Altman and Grant (reference 3) appears to be satisfactory for correlating ignition data for a composite solid propellant. Our linear method may be required, however, when correlation of data for propellants whose parameters are considerably different is attempted.

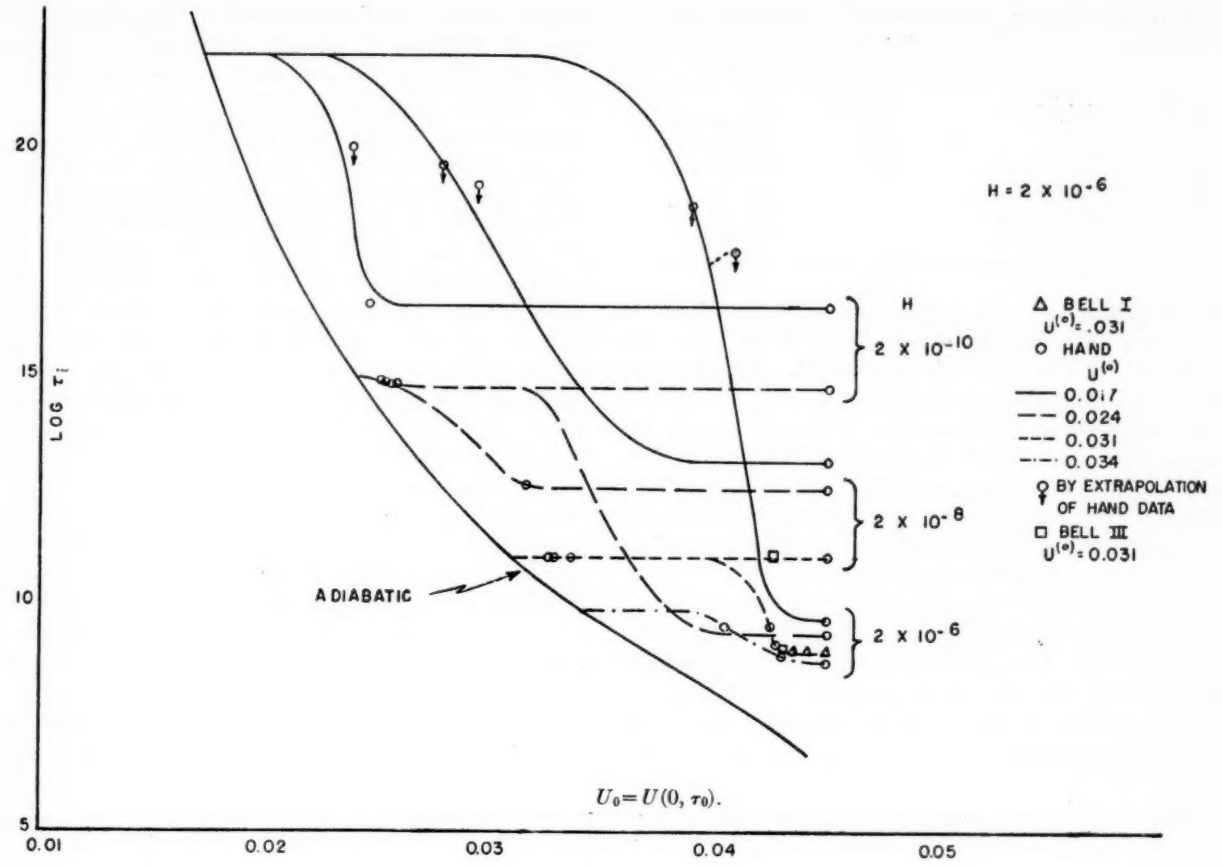

FIG. 7.

by a more complete theory or by experiment the methods of calculation of ignition time given here for our model would still suffice. Such a prescription would, in any case, be difficult because no adequate description has, to our knowledge, been given of the transition from the phase of ignition with fixed propellant boundary to the phase of stable burning with regressing boundary. Hence *there is no way at present to relate theoretically the parameters that characterize the two phases*, either in our theory or in that of Lewis and von Elbe.[13] Since their phenomenological approach has given a useful correlation of the characteristics of ignition and burning of gases, it may also succeed in the case of solid propellants. The theoretical predictions of Lewis and von Elbe would not agree with those of the present theory, primarily because the criterion for ignition is different in the two theories.

Dimensional Variables

It will be remembered that any of the plots in reduced variables U, ξ, τ, H (temperature, distance, time and heat transfer coefficient) are easily convertible into plots in terms of the original quantities T, x, t, h, by multiplication with suitable scale factors as discussed in Sec. 3. In the present Sec. we shall illustrate the interdependence of the reduced variables, the original variables and the parameters (E/R), (qf), K, and c'. The method used should be applicable to other ignition or flame propagation problems which also involve a great many parameters.

Five different sets of values of the four parameters will be picked in such a way that the effect of any changes in the parameters can be estimated by composition of the results obtained for each of the five sets individually.[14] The different sets are made up of values chosen from Table IV as follows:[15] first the basic set as shown in Table IV; then sets consisting, in turn,

[13] Bernard Lewis and Guenther von Elbe, J. Chem. Phys. **11**, 803 (1947). We note that their q must be taken to include both a chemical heat production term and a lateral heat loss if (see reference 1), the equation is to describe a stable combustion wave of constant velocity for an initial propellant temperature above absolute zero.

[14] It should be noted that accurate coverage in this way of the whole range of each of the original dimensional parameters requires that numerical integrations be performed for sets of the reduced (i.e., independent) parameters which cover the whole multidimensional space of variation of these parameters. This requirement is only partially satisfied by the data reported in the present paper.

[15] The parameters could also have been chosen to be (E/R), (K/c'), $(l_r = qf/c')$, (T_r), and $(Kc')^{\frac{1}{2}}$ (see Section 3) and would have somewhat different physical significance. These parameters have not been discussed separately here, however, because (E/R) and c' vary over a small range compared to (qf) and K.

TABLE IV. Values of parameters used in dimensional plots.

	Basic set	Altered values	
E/R	1.5×10^{4}	2.5×10^{4}	°K
qf	10^{16}	10^{18}	cal/cm³-sec
c'	0.50	0.70	cal/cm³-°C
K	10^{-3}	10^{-5}	cal/cm-sec-°C
x_r	3.873×10^{-8}		cm
t_r	7.500×10^{-13}		sec
h_r	2.582×10^{4}		cal/cm²-sec-°C

of one parameter value from among the altered values and the other three parameters from the basic set (for example $(E/R)=2.5\times10^{4}$, $(qf)=10^{16}$, $c'=0.50$ and $K=10^{-3}$). Temperature-time plots before shutoff are the ones chosen for illustration. The relationship between other variables in the ignition problem could in principle also be shown graphically but would be more difficult to construct from the computed data than the temperature-time plots because less of the required data would be immediately available.

The first plot of the dimensional variables (Fig. 8) was computed directly by multiplication with the appropriate scale factors of data from the Bell machine. For this run the reduced temperature $U^{(0)}=0.02$, and the reduced heat transfer coefficient $H=10^{-8}$. The variation of temperature T with time t is shown for two positions in the solid determined by the reduced variable of distance ξ, namely $\xi=0$ and $\xi=2.4\times10^{6}$. Corresponding to the value of the reduced distance $\xi=2.4\times10^{6}$, there will be different values of the distance x for the different sets of parameter values. These values of x are indicated on the figure. The adiabatic curve is not shown since the adiabatic temperature rise above the initial temperature is negligible for the longest periods of time shown in Fig. 8. In considering this figure, we should note that: only the activation energy (E/R) affects the temperature scale; (E/R) and the product (qf) affect each of the other three scales; the specific heat per unit volume c' affects only the time scale; and the thermal conductivity K affects only the scales of distance and of heat transfer coefficient h. For the given reduced initial temperature $U^{(0)}$ and reduced heat transfer coefficient H, the basic curve is shifted in some cases and not in others when one of the parameters is altered from its basic value. Furthermore, because we have restricted ourselves to constant values of H and ξ, the values of the heat transfer coefficients h (as noted above) and of the distance x are not, in general, the same for the various curves in Fig. 8 which correspond to a given value of ξ.

A second type of plot less easily derived from our numerical integrations and linearized theory but one

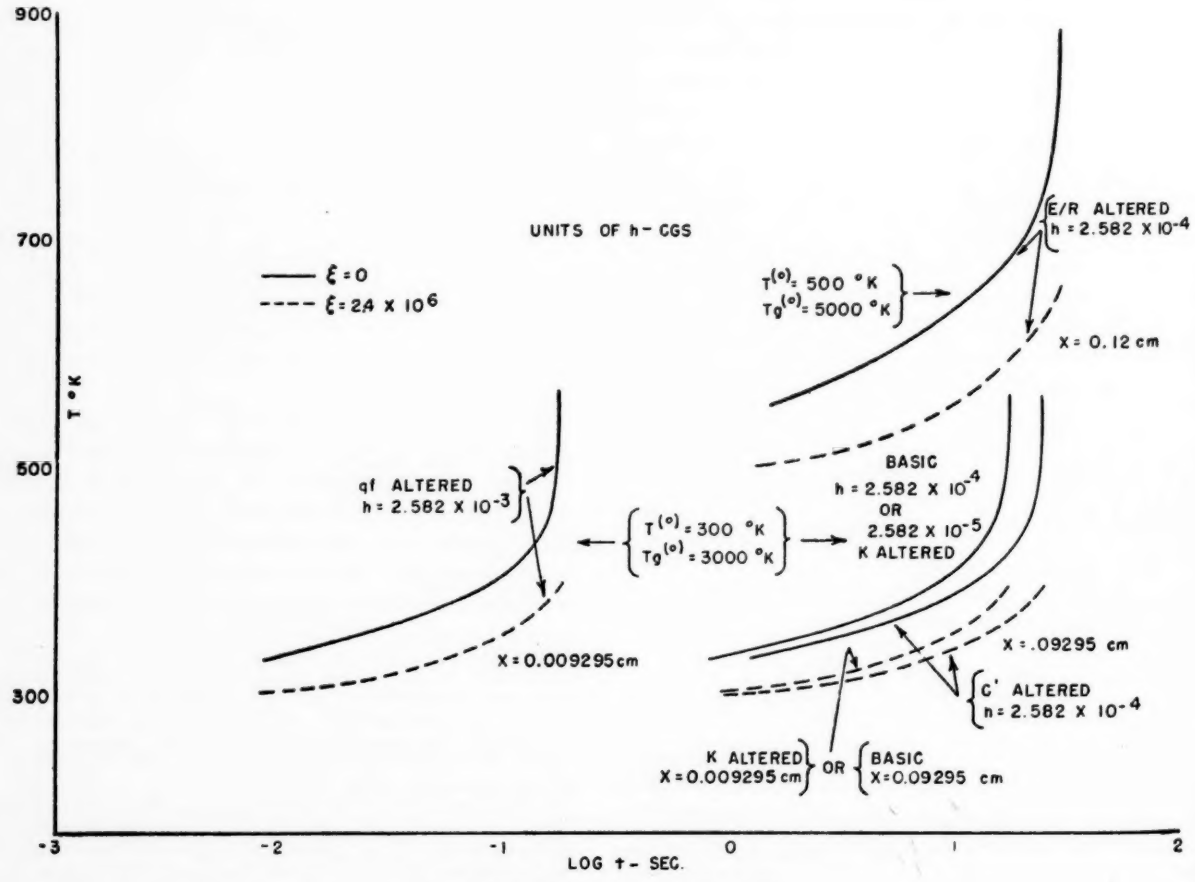

FIG 8. $U^{(0)}=0.02$; $H=10^{-8}$; $U_g=0.20$.

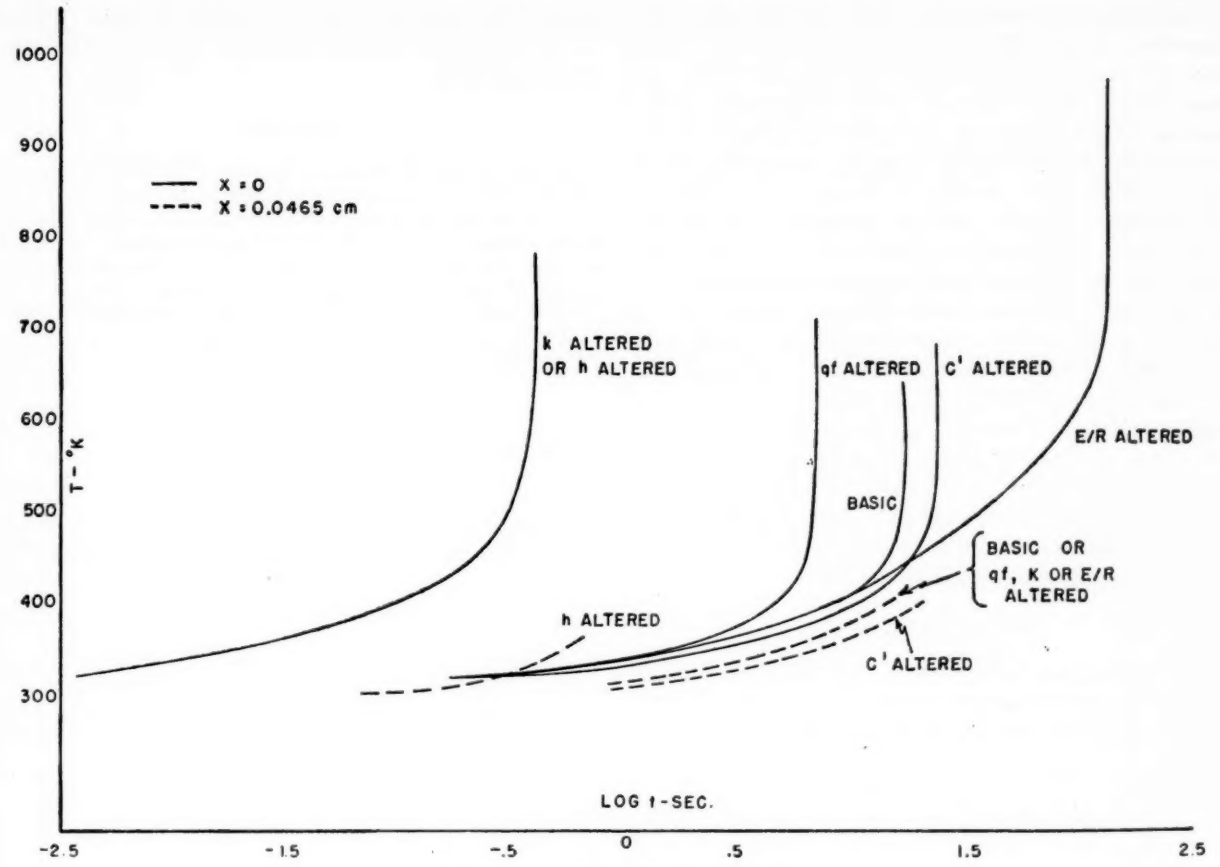

FIG. 9. $T^{(0)}=300°K$; $T_g=3000°K$.

that is more easily compared with experiment, is given in Fig. 9. Here the dimensional parameters, h and T_g, rather than the reduced ones, H and U_g, are held constant, and all curves for $x>0$ correspond to the value $x=0.0465$ cm rather than to a constant value of ξ. The basic curve for $x=0$ is the same as in Fig. 8. All curves for $x=0.0465$ were computed from the equation

$$T^L=(E/R)U^L[(KE/Rqf)^{-1}x, \quad (c'E/Rqf)^{-1}l, \quad (RKqf/E)^{-1}h] \quad (7\text{-}1)$$

where $U^L[\xi, \tau, H]$ is the function defined by Eq. (A-8). Calculations showed that this linear formula gave a good approximation to the values of reduced temperature U obtained by numerical integration for the corresponding reduced distance ξ. For the altered parameter sets at $x=0$ the method of construction used was the following: the ignition time t_{im} was obtained by interpolation of curves of reduced ignition time τ_{im} in Figs. 5 and 6; $T^L=T_rU^L$ was used for the lower part of each curve; and the middle portions of the curve were faired by hand.

Our calculations on the ignition model are partially incomplete in the respect that the parameter $U_g{}^{(0)}$, the reduced initial gas temperature, was not varied systematically or over a wide range. Accordingly, in Fig. 8 we note that the gas temperature T_g changes when $T^{(0)}$, the initial temperature of the solid, is altered. This was not a serious difficulty in preparing Fig. 9 because, particularly before shutoff, the gas temperature is much larger than the surface temperature, and therefore variation of the reduced gas temperature U_g is pretty well accounted for by approximately equivalent variation of the reduced heat transfer coefficient H. (See correlation used in Fig. 5.)

Possible conditions at ignition for the basic values of the parameters of Table IV appear in Table III.

If the theory is to be used for comparison with experimental ignition studies and for estimates of ignition time in weapons, it will be necessary to obtain reliable measurements of the parameters h, t_0, and T_g characterizing the heating process and of $T^{(0)}$, (E/R), K, c' and (qf) characterizing the propellant, in order that the differing effects of these various parameters can be clearly separated. This quantitative specification of the ignition process is especially needed because of the wide range permitted many of the parameters (see Table I).

7. CONCLUDING REMARKS

The first purpose of the calculations was to determine ignition times for a reasonable model based on a purely thermal phenomenon (i.e., no diffusion) for various conditions of external heating and initial temperature.

In the process of obtaining these ignition times, by numerical integration of the partial differential equation, the variation of the temperature with space and time was also found. Because of the complexities of the problem an interest in the mathematical aspects of the problem developed, leading to as yet incomplete use of big machines and studies of integration formulae, linearization methods, and the problem of estimating overall error. The question of how the theoretical results could best be compared with experimental findings suggested new theoretical investigations, which will be reported later, in which diffusion of reactive material is considered as well as the flow of heat. Although the investigations connected directly with the present model are incomplete and not fully reported here, their stimulus of related lines of inquiry have been to us as important as the specific results obtained for the present model. We believe that there now exists a rather broad basis for further numerical study of this and related models of a thermal ignition process.

ACKNOWLEDGMENT

The Computing Laboratory of the Ballistic Research Laboratories performed the computations for this ignition study, using desk calculators and the Bell Relay Computer. The author is also indebted to Mrs. Joanne Kelso who made a graphical analysis of the voluminous numerical data.

APPENDIX

In order to find the course of the temperature rise and in particular to find τ_i, τ_{im}, etc., as functions of the parameters $U^{(0)}$, τ_0, H in the heated reacting solid, it is necessary to integrate the system of Eqs. (3-8) to (3-12). In one important special case, which we shall discuss first, the integration is exact. Suppose that the heating at the surface is so gentle that $H\sim 0$ or $U\sim U(0, \tau)$, (i.e., we have the adiabatic case, denoted by subscript (a)). Then at no time will there be temperature gradients in the solid and (3-8) becomes

$$\frac{\partial U_a}{\partial \tau}=e^{-1/U_a}; \quad \tau \gtrless 0, \tag{A-1}$$

which integrates to

$$\tau=\int_{U^{(0)}}^{U_a} e^{1/V}dV. \tag{A-2}$$

The integral is expressible in terms of the integral exponential function, but for the range of U and $U^{(0)}$ of interest, the asymptotic series,

$$\tau=V^2e^{1/V}(1+2!V+3!V^2+\cdots)\Big|_{U_a}^{U^{(0)}} \tag{A-3}$$

is of adequate accuracy. For calculation of τ_{ia}, X_a is put equal to 0.045 in Eq. (A-3). Then only the terms in $U^{(0)}$ need be retained, which corresponds to the fact that the adiabatic ignition time depends (for $U^{(0)}$ not too close to 0.045) principally upon the ini-

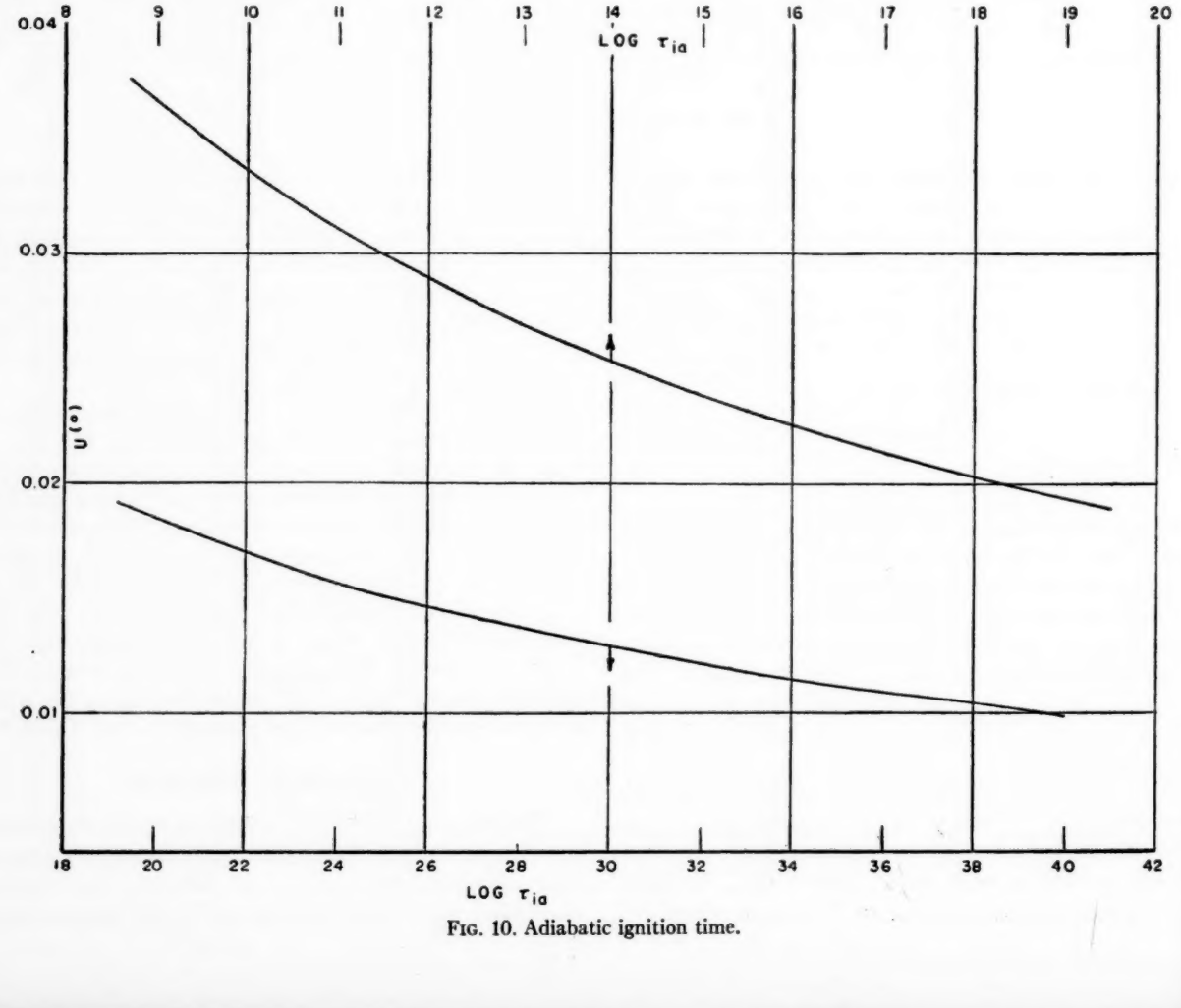

FIG. 10. Adiabatic ignition time.

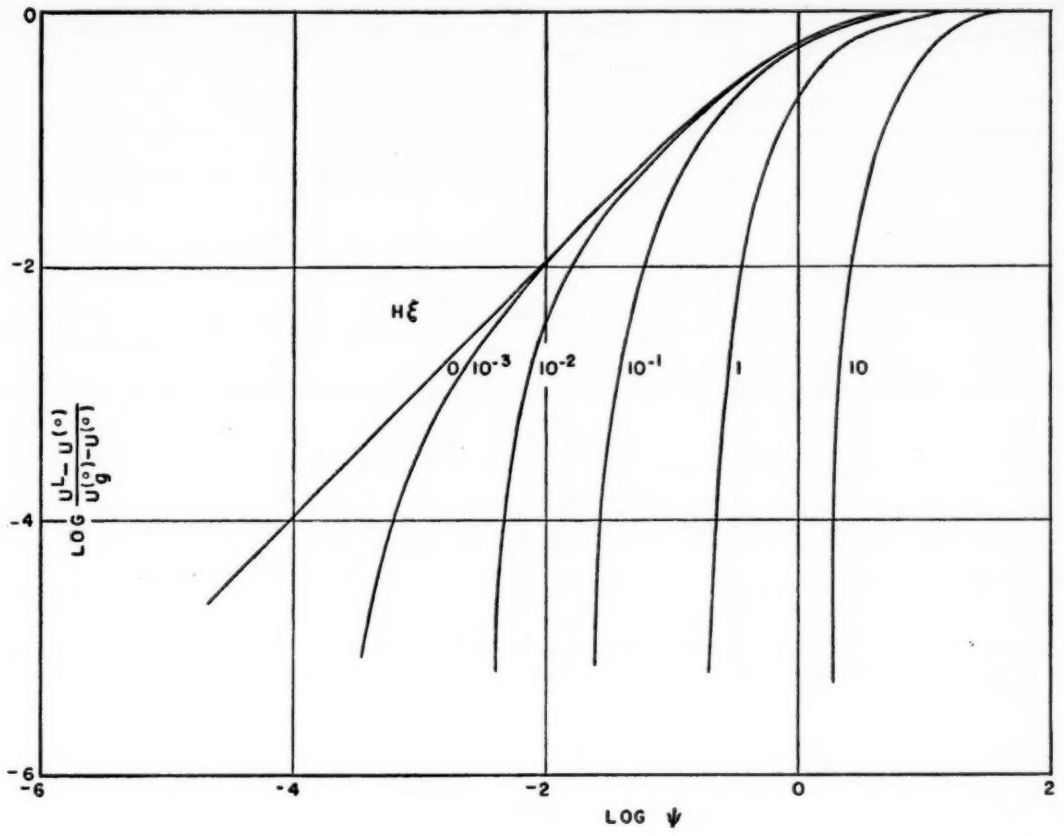

FIG. 11.

tial temperature $U^{(0)}$ and not upon the somewhat arbitrary choice of ignition temperature $U_i=0.045$. In Fig. 10, $U^{(0)}$, the initial temperature, is plotted as a function of $\log\tau_{i\alpha}$.

We shall next calculate the behavior of the propellant in the linear period of heating as defined by some suitably small value of α. In order to find the function $U^L(\xi,\tau)$ describing the behavior in this period we must solve the system:

$$\frac{\partial U^L}{\partial\tau}=\frac{\partial^2 U^L}{\partial\xi^2}; \qquad \xi\geqslant 0, \quad \tau>0 \qquad \text{(A-4)}$$

$$-\frac{\partial U^L}{\partial\xi}=H(U_g^{(0)}-U^L); \quad \xi=0, \quad \tau>0 \qquad \text{(A-5)}$$

$$\frac{\partial U^L}{\partial\xi}\to 0; \qquad \xi\to\infty, \quad \tau>0 \qquad \text{(A-6)}$$

$$U^L=U^{(0)}; \qquad \xi\geqslant 0, \quad \tau=0. \qquad \text{(A-7)}$$

The solution for U^L is,[16]

$$U^L=U^{(0)}+[U_g^{(0)}-U^{(0)}]e^{-\phi^2}[F(\phi)-F(\phi+\psi)] \qquad \text{(A-8)}$$

in which

$$F(\zeta)=\frac{2}{\sqrt{\pi}}e^{\zeta^2}\int_\zeta^\infty e^{-\eta^2}d\eta=e^{\zeta^2}erfc(\zeta) \qquad \text{(A-9)}$$

$$\phi=\xi/2\sqrt{\tau} \qquad \psi=H\sqrt{\tau} \qquad \text{(A-10)}$$

A table of $F(\zeta)$ to four figures is given in reference 16 (p. 373). The solution in the form $(U^L-U^{(0)})/(U_g^{(0)}-U^{(0)})$ is plotted as a function of $\log\psi$ in Fig. 11.[17] The time derivative which is needed in order that α may be computed is:

$$\frac{\partial U^L}{\partial\tau}=[U_g^{(0)}-U^{(0)}]H^2e^{-\phi^2}\left[\frac{1}{(\psi)\sqrt{\pi}}-F(\phi+\psi)\right]. \qquad \text{(A-11)}$$

In particular, at the surface of the propellant $\phi=\xi=0$, and Eqs. (A-8, 11) become, respectively,

$$U^L=U^{(0)}+[U_g^{(0)}-U^{(0)}][1-F(\psi)] \qquad \text{(A-12)}$$

$$\frac{\partial U^L}{\partial\tau}=[U_g^{(0)}-U^{(0)}]H^2\left[\frac{1}{(\psi)\sqrt{\pi}}-F(\psi)\right]. \qquad \text{(A-13)}$$

Values of $\tau_\alpha{}^L$ and $U_\alpha{}^L(0,\tau_\alpha{}^L)$ for which

$$\exp(-1/U^L)=\alpha^L[(\partial U^L/\partial\tau)+\exp(-1/U^L)]_{0,\ \tau_\alpha{}^L}$$

can be determined from simultaneous solution of this pair of equations and Eq. (4-3), together with a chosen value of α^L. The parameter $\tau_\alpha{}^L$ thus determined is plotted in Fig. 12 for $\alpha^L=0.833$ [18] as a function of $U^{(0)}$ and H. Such curves were used later for computing values of U at the starting time τ_1 of some of the numerical integrations ($\alpha^L=5\times10^{-4}$) and also approximate ignition times $\tau_{im}{}^L(\alpha^L=0.833)$. The quantities $U_\alpha{}^L$ do not have precise physical significance in the ignition problem for large α but were useful in estimating values of $\tau_\alpha{}^L$.

The behavior near the end of the period of linear heating can be discussed most simply in terms of approximate formulas. The

[16] H. S. Carslaw and J. C. Jaeger, *Conduction of Heat in Solids* (The Clarendon Press, Oxford, 1947), p. 55.

[17] If $\tau>\tau_0$ or if U_g were not constant for $\tau<\tau_0$, U^L could be obtained from Eq. (A-8) by integration. (See reference 16, Sec. 10 and p. 55.) If, in particular, U_g is constant for each of a number of intervals of τ separated by discontinuous jumps, then U^L can be found by addition of functions such as that in Eq. (A-8).

[18] In part of the calculations, an $\underline{\alpha}$ had been defined as $e^{-1/U}/U_{\xi\xi}$; $\underline{\alpha}^L$ was taken equal to 5×10^{-4}, 5×10^{-2} and 5.0 in finding $U_{\underline{\alpha}}{}^L$, $\tau_{\underline{\alpha}}{}^L$. The calculation of α from numerical integration data however is easier if it is defined as in Eq. (4-3). Since $U_{\xi\xi}{}^L+\exp(-1/U^L)$ is a good approximation to U_τ in the linear period of heating and $U_{\xi\xi}{}^L\equiv U_\tau{}^L$, we see that $\alpha^L=\underline{\alpha}^L(1+\underline{\alpha}^L)^{-1}$ leading, for the above values of $\underline{\alpha}^L$ to $\alpha^L=5\times10^{-4}$, 4.75×10^{-2} and 0.833, respectively.

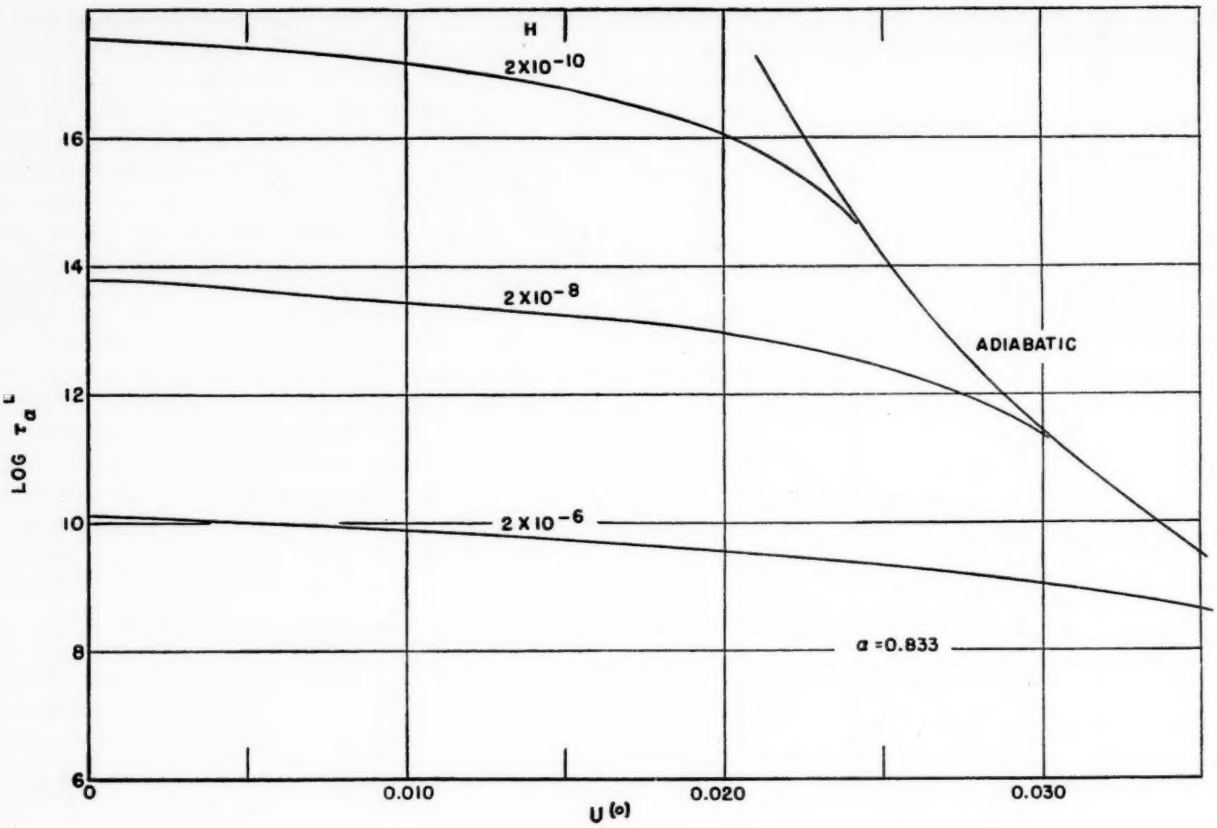

FIG. 12.

value of $\psi_\alpha{}^L = H(\tau_\alpha{}^L)^{\frac{1}{2}}$ for $\alpha^L = 5\times10^{-4}$ and values of $U^{(0)}$, $U_g{}^{(0)}$, H used in the numerical integration all lie below 0.2 making possible development of the following approximate expressions (i.e., first terms of series good near $\psi=0$):

$$U^L \sim U^{(0)} + [U_g{}^{(0)} - U^{(0)}]\frac{2}{\sqrt{\pi}}\psi^L \qquad \text{(A-14)}$$

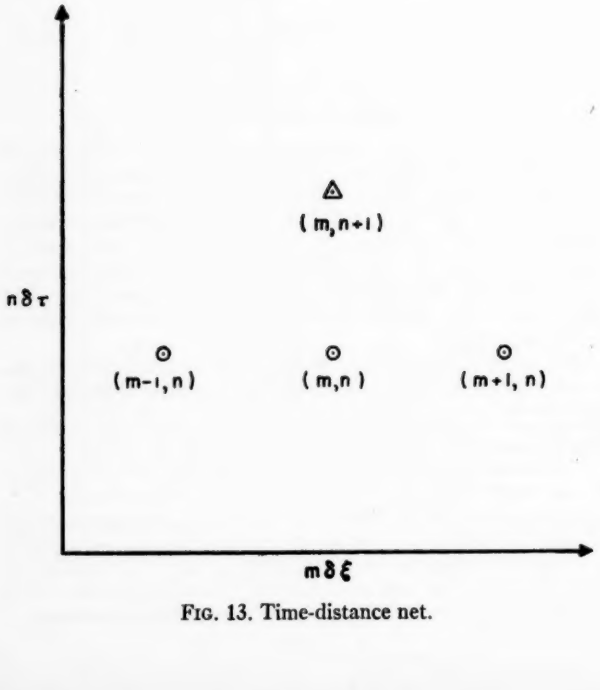

FIG. 13. Time-distance net.

and

$$\left.\frac{\partial U^L}{\partial \tau}\right|_{\xi=0} \sim H^2[U_g{}^{(0)} - U^{(0)}] \Big/ \psi^L\sqrt{\pi}. \qquad \text{(A-15)}$$

Elimination of ψ^L between Eqs. (A-14, A-15) gives, with Eq. (4-3), an implicit expression for $U_\alpha{}^L$, in first approximation,

$$[U_\alpha{}^L - U^{(0)}]\exp(-1/U_\alpha{}^L)\frac{2\alpha^L}{\sqrt{\pi}}H^2[U_g{}^{(0)} - U^{(0)}]^2. \qquad \text{(A-16)}$$

Substitution of the $U_\alpha{}^L$ obtained from Eq. (A-16) into (A-14) gives an approximate value of $\psi_\alpha{}^L$ and therefore of $\tau_\alpha{}^L$. Note that $U_\alpha{}^L$ and $\psi_\alpha{}^L$, in this approximation, depend upon the product $\alpha^L H^2$ and not upon α^L and H^2 individually. The behavior of α^L very near $\psi=0$ is given by the expression

$$\alpha^L = \sqrt{\pi}\exp[-1/U^{(0)}]\psi^L/H^2[U_g{}^{(0)} - U^{(0)}]. \qquad \text{(A-17)}$$

In addition to making the two special analytical calculations described, we obtained the solution of the system Eq. (3-8) to (3-12) from a direct numerical integration using simple finite difference approximations, Eqs. (A-18, 19), to the partial differential Eqs. (3-8, 3-9), expressed in terms of the values of $U_{m,n} = U(m\delta\xi, n\delta\tau)$ at the net points $(m\delta\xi, n\delta\tau)$ (see Fig. 13).

$$U_{m,n+1} = \tfrac{1}{2}(U_{m-1,n} + U_{m+1,n}) + \delta\tau\exp(-1/U_{m,n}),\ m \geqslant 1 \qquad \text{(A-18)}$$

$$U_{0,n+1} = U_{1,n} + H\delta\xi(U_g - U_{0,n}) + \delta\tau\exp(-1/U_{0,n}),\ m=0. \qquad \text{(A-19)}$$

In these formulae $\delta\tau = \delta\xi^2/2$. The boundary condition at infinity is automatically taken care of within a given degree of accuracy by choosing a value of M of m large enough for each n so that

$$|U_{M,n} - U_{M-1,n}| \leq \Delta. \qquad \text{(A-20)}$$

The value of Δ and of the method of approximating the jump in U_g at $\tau=\tau_0$ were chosen appropriately for each numerical integration. The formulas give $U_{m,n+1}$ in terms of quantities calculable from nth row information (i.e., at $\tau = n\delta\tau$) and thus permit for-

ward integration in time from $\tau=\tau_1$ to $\tau=\tau_i\sim n_i\delta\tau$. Calculations based on these finite difference formulae have been made by the Ballistic Laboratories' Computing Laboratory, both with desk calculators and with the Bell Relay Computer, about 35,000 net points being involved. The longterm stability of our method of integration is assured by the fact that $\delta\tau$ is not larger than $\delta\xi^2/2$.

As there was no analytical method of estimating the cumulative error in the integrations, essentially the same difference equations were used in numerical integrations on the *ENIAC* for $U^{(0)}=0.031$, $U_g^{(0)}=0.18$, $H=2\times10^{-6}$ for seven values of $\delta\xi$ for the full nonlinear equation and for four values of $\delta\xi$ for the linear equation obtained by omitting the exponential term. A total of more than 10^5 net points were involved in these integrations. A preliminary inspection of the results tends to substantiate the conservative estimate of errors given in Sec. 6. A detailed analysis, not as yet complete, of the extrapolation to zero net size of $\tau_i(\delta\xi)$ and other variables, should permit an estimate of the cumulative error both for the linear and the nonlinear cases.

THE JOURNAL OF CHEMICAL PHYSICS VOLUME 22, NUMBER 3 MARCH, 1954

The Infrared and Raman Spectra of Carbon Suboxide*

H. D. Rix
The Pennsylvania State University, State College, Pennsylvania
(Received June 15, 1953)

The infrared spectrum of C_3O_2 has been studied in the vapor phase from 2.2 to 20μ with a Perkin-Elmer double-pass spectrometer, and the Raman spectrum has been photographed in the liquid phase. A comparison of the Raman with the infrared spectrum shows definitely that the molecule has a center of symmetry as is required for the linear structure commonly assumed. However, the infrared spectrum cannot be explained on the assumption of a linear model; the envelopes of the principal absorption bands as well as those of the weaker combination bands have the wrong shape. It appears rather that the oxygen atoms are bent out of line with the carbons in a plane zig-zag configuration. From the rotational structure of one of the combination bands the O−C−C angle is computed to be approximately 158°.

INTRODUCTION

THE carbon suboxide molecule has commonly been assumed to have a linear symmetric structure,[1] the two oxygen atoms lying at either end of the chain of three carbons. Results of earlier Raman[2] and infrared[3] studies of the molecule were not inconsistent with this assumption, which appeared to be supported also by the electron diffraction evidence.[4] The previous Raman work was carried out under far from optimum conditions; also the infrared absorption was obtained with the use of only a KBr prism for the entire range investigated, from 500 to 4500 cm^{-1}. Hence it was considered advisable to repeat these experiments with the superior spectroscopic equipment that has been developed since the original work was done. The data obtained in the present investigation are not entirely consistent with the linear model hitherto assumed for C_3O_2; it now appears that the oxygen atoms on the average are bent out of line with the three carbon atoms but in such a fashion as to preserve a center of symmetry. In more recent electron diffraction work,[5] reported after the present study was begun, the authors favor a linear model but admit the possibility of a nonlinear one.

EXPERIMENTAL

Carbon suboxide was prepared by the pyrolysis of diacetyl tartaric anhydride at low pressure in a system similar to that used by Kobe and Reyerson.[6] Vapors from the pot containing the anhydride, which was maintained at a temperature of 150°C, passed through a 14-mm quartz tube enclosed in a cylindrical furnace at a temperature of 700°C. A series of liquid air traps was used to separate the various products of the reaction, the C_3O_2 being vacuum distilled before removal from the system.

The Raman spectrum was taken in a prism spectrograph[7] with a dispersion of 19A/mm at 4600A; the sample tube was of about 12-ml capacity. With the first sample studied, the temperature was held at −80°C for an exposure time of eight hours. Polarization measurements were made on this sample by the method of polarized incident light.[8] Later a new sample was prepared and the experiment repeated with an exposure time of eleven hours at a temperature of −70°C. On each occasion the sample was vacuum distilled into the Raman tube.

Preliminary infrared measurements were made with a Perkin-Elmer Model 12-C spectrometer using NaCl and KBr prisms. An 8-cm Pyrex cell with AgCl windows was employed after it was discovered that the vapor polymerized in a metal cell, yielding spurious absorption

* This research was assisted by support from the U. S. Office of Naval Research.
[1] L. Pauling, *The Nature of the Chemical Bond* (Cornell University Press, Ithaca, 1939 and 1941).
[2] W. Engler and K. W. F. Kohlrausch, Z. physik Chem. B **34**, 214 (1936).
[3] R. C. Lord, Jr., and N. Wright, J. Chem. Phys. **5**, 642 (1937).
[4] L. O. Brockway and L. Pauling, Proc. Natl. Acad. Sci. **19**, 860 (1933).
[5] H. Mackle and L. E. Sutton, Trans. Faraday Soc. **47**, 937 (1951).
[6] K. A. Kobe and L. H. Reyerson, J. Phys. Chem. **35**, 3025 (1931).
[7] Szasz, Sheppard, and Rank, J. Chem. Phys. **16**, 704 (1948).
[8] A. E. Douglas and D. H. Rank, J. Opt. Soc. Am. **38**, 281 (1948).

bands. Subsequently the infrared spectrum was remeasured with the Perkin-Elmer double-pass spectrometer, a LiF prism being used for the region above 2000 cm^{-1}.

Several attempts were made to obtain the photographic infrared spectrum of C_3O_2, in particular the combination of the second overtone of the strong infrared active fundamental at 2258 cm^{-1} with the Raman active fundamental at 2190 cm^{-1}. No spectrum was found with a 3-m path at a vapor pressure of about 60 cm, the dispersing element of the spectrograph being a 21-foot concave grating. A 2-m tube of the J. U. White type was constructed which made possible a path up to about 50 m. Utilizing a 5-m concave grating, a few weak lines representing the band in question were photographed and measured with third-order iron standards. Also photographs were taken with a Bausch and Lomb transfer plane grating and a 16-foot camera. With a vapor pressure as high as 71 cm, the silvered surfaces of the multiply reflecting mirrors were rendered useless in an hour's time by the action of the C_3O_2. When the vapor pressure was reduced to 50 cm, the freshly silvered surfaces deteriorated more slowly, but at such a rate as to make it impossible to obtain satisfactory exposures. With a much smaller vapor pressure, the resulting weaker absorption also yielded unsatisfactory plates.

OBSERVED SPECTRUM

The original Raman spectrum of C_3O_2 obtained by Engler and Kohlrausch[2] showed five certain and four doubtful lines. The first Raman spectrum photographed in this investigation with an 8-hr exposure included 11 lines of which five or six could be called certain. However, when the experiment was repeated with a new sample, an exposure of 11 hours yielded only four lines, one of which is apparently an overtone of one of the others. The Raman measurements are presented in Table I. Three of the lines observed in the 8-hour exposure can be identified as due to methyl acetylene, which is known to exist in the sample (as well as acetylene) from the photographic infrared plates. Of the four lines obtained on both plates, the one at 577 cm^{-1} is depolarized, the others being polarized. The line at 828 cm^{-1} is very broad and comparatively diffuse.

TABLE I. Raman spectrum of liquid carbon suboxide.

ν_{vac} cm^{-1}	Description[a]		Assignment	Engler and Kohlrausch cm^{-1}
577	m.	Dep.	ν_3	586
828	v.s., b.	P.	ν_2	843
1154	w.	P.	$2\nu_3$	1176
2190	s.	P.	ν_1	2200

Spurious or doubtful lines on first Raman plate: 335 (v.w.) (Me Ac): 519 (w.); 1084 (v.w.); 1127 (m.) (ketene ?); 1381 (w.) (Me Ac); 1642 (v.w.); 2132 (v.w.) (Me Ac).

[a] Abbreviations: v.s., s., m., w., v.w., b., Dep., P. = very strong, strong, medium, weak, very weak, broad, depolarized, polarized, respectively.

The infrared spectrum reported here is in substantial agreement with that of Lord and Wright[3] as to the number and positions of the bands, allowance being made for the difference in precision of measurement possible with the two spectrometers. However, with the superior resolving power of the Perkin-Elmer double-pass instrument, one can now distinguish the band envelopes much more clearly. A trace of the infrared spectrum in Fig. 1 shows that the prevailing band type for carbon suboxide with the resolution available consists of a strong central maximum. The principal exceptions to this in the NaCl region include a band of medium intensity at 1122.5 cm^{-1} with $P-Q-R$ structure, and at slightly lower frequency a series of peaks of varying intensity and separation. In the LiF region are found bands with a central minimum at 2154.5 and 2386 cm^{-1} suggesting $P-R$ structure and another at 3335 cm^{-1} with a very weak central maximum between much stronger side branches. The most informative band envelope in this region is that at 2386 cm^{-1} in which two strong maxima are accompanied on the short-wavelength side by a set of weak maxima of fairly regular separation. (The absence of these maxima on the long-wavelength side of the 2386 cm^{-1} band may be ascribed to the overlapping of this region by atmospheric CO_2 and by the very strong fundamental band at 2258 cm^{-1}.) The band at 4445 cm^{-1} is possibly also of this type, the resolution of the spectrometer not being great enough to separate the weak maxima. In Table II are given the measurements of the infrared bands along with those of Lord and Wright.

DISCUSSION OF THE SPECTRUM

Herzberg[9] has discussed three possible models for carbon suboxide: (I) O=C=C=C=O,

(II) 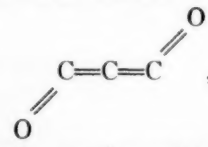 , (III) 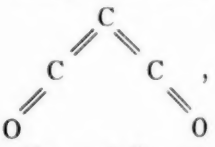 ,

belonging to the point groups $D_{\infty h}$, C_{2h}, and C_{2v}, respectively, and attempted vibrational assignments for Models I and III, his assignments for I differing in part from those of Lord and Wright. For Models I and II, which have a center of symmetry, only three of the fundamentals are Raman active, while for Model III all nine fundamentals are Raman active and eight are infrared active as well. From the Raman spectrum alone, which can best be analyzed as consisting of three fundamentals and one overtone, it would appear that Model III can be eliminated as a possible structure for carbon suboxide. This conclusion is strengthened by a comparison of the Raman and infrared spectra, for it turns out that there are no coincidences between them. A further reason for believing that the molecule has a

[9] G. Herzberg, *Infrared and Raman Spectra of Polyatomic Molecules* (D. Van Nostrand Company, Inc., New York, 1945).

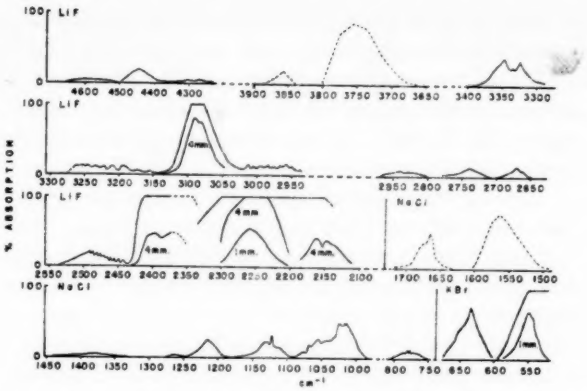

FIG. 1. Infrared absorption spectrum of C_3O_2 from 2.2 to 20μ at various vapor pressures. Bands distorted by atmospheric absorption are indicated by dotted lines.

center of symmetry is that there are no first overtones of the infrared fundamentals although the band at 1666 cm^{-1} can be reasonably interpreted as a second overtone. Likewise there are no binary combinations of infrared fundamentals but numerous binary combinations of infrared and Raman active vibrations.

It is not possible to choose between Models I and II on the basis of the Raman spectrum. For the linear model the Raman lines at 2190 and 828 cm^{-1} would be assigned to the two symmetric stretching modes of species Σ_g, while for the bent Model II these lines would be of species A_g. The line at 577 cm^{-1} should be due to the bending mode Π_g for the linear model and A_g for the zig-zag one. The polarization data (see Table I) might seem to favor Model I for which this last Raman line should be depolarized, whereas all three lines should be polarized for Model II. However, since for a totally symmetric vibration the degree of depolarization may vary between 0 and 6/7, Model II cannot be called inconsistent with the Raman spectrum. There remains to consider the evidence provided by the envelopes of the infrared bands.

Assuming the linear model, there are four infrared active fundamentals, two of which should be represented by parallel bands with a separation of about 11 cm^{-1} between the P and R branches, and two by perpendicular bands with P, Q, and R branches. The most probable assignments for these would be the strong bands at 2258 and 1570 cm^{-1} for the two stretching vibrations (of species Σ_u) and those at 635 and 551 cm^{-1} for the bending vibrations (Π_u). However, none of these bands has the required envelope; in fact, they all show just a strong central maximum with no side branches. All of the other bands shown in Fig. 1 with the exception of those at 779.5 and 1040 cm^{-1} could be accounted for as arising from these four fundamentals, nearly all being combinations of the infrared with the Raman active fundamentals. Aside from the previously mentioned band at 1666 cm^{-1}, which appears to be the second overtone of the infrared active fundamental at 551, and the band at 3335 cm^{-1}, which is probably a combination of the first overtone of this same fundamental with the highest-frequency fundamental at 2258 cm^{-1}, the remaining bands of the infrared spectrum can be explained as binary combinations involving one Raman and one infrared fundamental.

An examination of the band envelopes which have a more complicated structure than just a central maximum brings out the following discrepancies. The only one which shows definite PQR structure—at 1122.5 cm^{-1}—is a combination of the two bending modes at 577 and 551 and should consequently be of species Σ_u with P and R branches only. The band at 2154.5 cm^{-1}, which apparently has P and R branches with a separation of 14 cm^{-1} is presumably due to a combination of the 577 Raman active vibration with the infrared band at 1570 cm^{-1} and therefore of species Π_u. The band at 3335 cm^{-1}, being a combination of the fundamental 2258 and the first overtone of 551 should be of species Σ_u, and here we have the proper band contour if we assume that the weak central maximum is due to an impurity in the sample, namely, methyl acetylene. However, the P and R branch separation of 22 cm^{-1} is just twice what is expected if C_3O_2 is linear. The same comment can be made about the band at 2386 cm^{-1}, in which the separation of the P and R maxima is about 23 cm^{-1}. Furthermore this band has structure on the short-wavelength side which could not possibly arise from a

TABLE II. Infrared spectrum of carbon suboxide vapor from 2.2 to 20μ.

ν_{vac}(obs) cm^{-1}	Intensity[a]	Assignment	ν_{vac}(calc)[b] cm^{-1}	Lord and Wright cm^{-1}
				544
551	v.s.	ν_9		557
635	s.	ν_8		637
779.5	w.	ν_5		779
				889
				909
1050	m.	ν_4		1024
1122.5	m.	$\nu_3+\nu_9$	1128	1126
1215.5	m.	$\nu_3+\nu_8$	1212	1225
1375.5	v.w.	$\nu_2+\nu_9$	1379	1387
				1470
1570[c]	s.	ν_7		1570
1666[c]	m.	$3\nu_9$	1653	1670
1770[c]	v.w.			1760
				1850
				1980
2154.5	s.	$\nu_3+\nu_7$	2147	2190
2258	v.s.	ν_6		2290
2386[c]	s.	$\nu_2+\nu_7$	2398	2410
2670	w.	$\nu_7+2\nu_9$	2672	
2738	w.	$\nu_1+\nu_9$	2741	
2828	w.	$\nu_1+\nu_8$	2825	
2840	w.	$\nu_3+\nu_6$	2835	
3086	s.	$\nu_2+\nu_6$	3086	3150
3335	m.	$\nu_6+2\nu_9$	3360	3380
3756[c]	s.	$\nu_1+\nu_7$	3760	3790
3857[c]	w.	$\nu_1+3\nu_9$	3856	
4445	m.	$\nu_1+\nu_6$	4448	4590

[a] Abbreviations: v.s., s., m., w., v.w., =very strong, strong, medium, weak, very weak, respectively.
[b] Neglecting effect of anharmonicity.
[c] Band obscured or distorted by atmospheric absorption.

linear molecule. In view of all this evidence it seems necessary to abandon the assumption that carbon suboxide has a linear structure.

There remains to consider Herzberg's Model II. It is interesting to note that this type of structure was recently proposed for an excited electronic state of the normally linear molecule acetylene by King and Ingold,[10] who called it a "plane centro-symmetric zig-zag." This model for carbon suboxide requires in addition to the three Raman active fundamentals of species A_g mentioned previously six infrared fundamentals, four of them in the plane of the molecule (B_u) and two out of the plane (A_u). It has already been shown that this model is consistent with the observed Raman spectrum. As for the infrared spectrum, it may be noted first that the four vibrations of species B_u may be assigned to the same four bands considered above as fundamentals for the linear model. Since the model now under discussion is a slightly asymmetric top, the difficulty about the contours of these fundamentals is removed. The two infrared bands at 779.5 and 1040 cm^{-1} which could not readily be accounted for on the linear model can now be assigned as the A_u vibrations. The first of these two has been resolved into four rather weak maxima with an average separation of about 5 cm^{-1}. The other band is not so clear cut. It appears to consist of two maxima of medium intensity at 1015 and 1025 cm^{-1} and three weaker ones at 1055, 1068, and 1075, with two other barely resolved shoulders between these two groups at 1033 and 1045 cm^{-1}. Under the available resolution it is not clear whether this absorption represents only one band or more than one, and a further complication may arise from the fact that one of the weaker fundamentals of methyl acetylene is found in this same region. In view of these uncertainties the band is here given a wave number value of 1040, this being approximately the center of the absorption. The weak absorption of the 779.5-cm^{-1} fundamental may be explained thus: the vibration is believed to involve an out-of-plane motion of the two C—O groups against the central carbon with a consequently small change of dipole moment. A qualitative check on the assignment of these two fundamentals is provided by the fact that they should be pure perpendicular vibrations with no parallel component and this seems substantiated by the absence of the strong central absorption noted elsewhere in the infrared spectrum. A schematic representation of the vibrational modes for the zig-zag model is given in Fig. 2.

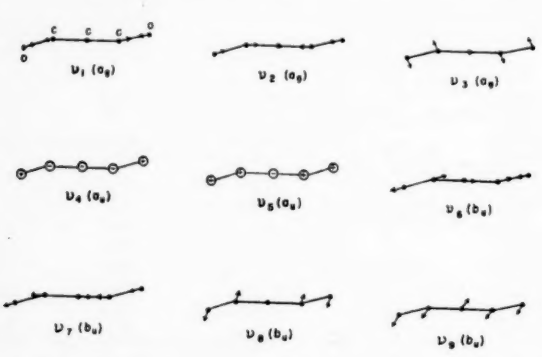

FIG. 2. Schematic representation of the fundamental modes of vibration of C_3O_2.

The fine structure on the short-wavelength side of the band at 2386 cm^{-1} has an average separation of about 5.5 cm^{-1}. This structure may be interpreted as due to the perpendicular component of a hybrid band, the parallel component being represented by the strong central maxima. If this interpretation is correct, the band in question provides the strongest kind of evidence for the nonlinearity of carbon suboxide. The similar structure on the long-wavelength side of the 3086 cm^{-1} band, which has an average separation of about 9.5 cm^{-1}, is almost certainly due to the ν_6 band of methyl acetylene, as the positions of the individual peaks check well with those reported in some recent work at higher resolution by Boyd and Thompson.[11] The irregularly spaced structure on the short-wavelength side of this band has an average spacing of 13 cm^{-1} and may be due to a combination of the perpendicular band at 1040 with the Raman band at 2190 cm^{-1}. Owing to the previously mentioned uncertainties with regard to the 1040 cm^{-1} band, this assignment is merely tentative. The unresolved background at the high-frequency end of this structure is no doubt due to the acetylene in the sample, but the eight or nine partly resolved weak maxima cannot readily be attributed to some other impurity. In Table II are found the assignments for the infrared spectrum along with the earlier data of Lord and Wright.

On the basis of force-constant calculations, Engler and Kohlrausch[2] postulated a low-frequency fundamental at about 200 cm^{-1}. From the analysis of the infrared spectrum given above it appears that the assumption of such a frequency is unnecessary. Recently, an examination[12] of the far infrared region of the carbon suboxide spectrum by the residual ray method has indicated weak absorption at 192 and 161 cm^{-1}. This is undoubtedly the difference band $\nu_2-\nu_8$. A somewhat stronger difference band should be found near 275 cm^{-1} for $\nu_2-\nu_9$, but apparently this region was not investigated.

As mentioned in the foregoing, two impurities in the sample of carbon suboxide used in this study that have been positively identified are methyl acetylene and acetylene. The $3\nu_1$ and $3\nu_3$ bands, respectively, of these two molecules were found in the photographic infrared with the rotational structure well resolved. In the near infrared region, the fundamental ν_5 of acetylene was observed as was also ν_3, the latter being overlapped by suboxide bands. A number of the fundamentals of methyl acetylene appeared including ν_1, ν_3, and ν_6; ν_9

[10] G. W. King and C. K. Ingold, Nature 169, 1101 (1952).

[11] D. R. J. Boyd and H. W. Thompson, Trans. Faraday Soc. 48, 493 (1952).

[12] J. K. O'Loane, J. Chem. Phys. 21, 669 (1953).

would be completely covered by the 635 cm^{-1} band of carbon suboxide, but $2\nu_9$ may be present. The possibility[5] that ketene may occur as an impurity in carbon suboxide produced by pyrolytic reaction could not be verified in this infrared study; however, the stronger infrared bands of ketene lie near regions of carbon suboxide absorption and may be obscured. In the first Raman plate, the line at 1127 cm^{-1} may be the ketene line reported by Kopper[13] at 1130 cm^{-1}, but if this is so it is not clear why the almost equally strong line at 2950 cm^{-1} was not observed. Since the doublet of medium intensity reported by Lord and Wright at 909–889 cm^{-1} was not found in this investigation, it is possibly an impurity in their sample. The same inference may be drawn concerning the group of bands they observed at 1760, 1850, and 1980 cm^{-1}, to which there corresponds in the present study only a very weak absorption near 1770 cm^{-1}.

DISCUSSION OF THE MOLECULAR CONSTANTS

As pointed out by Lord and Wright,[3] if the carbon suboxide molecule is linear it must have a moment of inertia of about 390×10^{-40} g cm^2, and this would give rise to a separation between the P and R branch maxima of a parallel band of about 11 cm^{-1}. Their failure to observe such a band was attributed to the low resolving power of their spectrometer. Since the Perkin-Elmer spectrometer employed in the present study can resolve bands separated by one wave number or a little less in the neighborhood of 2200 cm^{-1}, the failure to observe any splitting at all in the 2258 cm^{-1} band might alone be taken to indicate the nonlinear structure of the molecule. The combination bands $\nu_2+\nu_7$ and $\nu_3+\nu_7$ on either side of the fundamental ν_6 do exhibit a splitting suggestive of P and R branch envelopes, the separation of the maxima being 23 and 14 cm^{-1}, respectively. This latter value is, however, extremely dubious because the position of the supposed P branch of the band coincides with that of a strong band of methyl acetylene, and also the strongest infrared band of ketene falls in this same region. As pointed out previously, the strong maxima of the 3335 cm^{-1} band have a separation of about 22 cm^{-1}, which agrees well with the value observed for the band at 2386 cm^{-1}.

On the short-wavelength side of the $\nu_2+\nu_7$ band, the group of weak subsidiary bands ranging from about 2440 to 2490 cm^{-1} has an average separation of about 5.5 cm^{-1}. Taking this band envelope to represent a hybrid band of a slightly asymmetric top, this separation to a first approximation is given by $2(A'-B')$. Since the value of B (or C) for carbon suboxide is of the order of 0.07 cm^{-1}, we can compute a value of A' from this band of about 2.7 cm^{-1} and I_A as 10.4×10^{-40} g cm^2. The most recent electron diffraction measurements of carbon suboxide by Mackle and Sutton[5] give the C—C and C—O distances as 1.28 and 1.19A, respectively. Applying these values to the centrosymmetric zig-zag model discussed above, which seems required from the spectroscopic evidence, we obtain a value for the O—C—C angle of 158°. While these authors do not consider this model, they do discuss the possibility of a nonlinear model of point group C_{2v} (Herzberg's Model III). For such a structure they conclude that the minimum value of the O—C—C and C—C—C angles consistent with their data is 170° for each angle. A comparison of the spectroscopic and electron diffraction data can be made even though two different models are involved by computing the displacement of the oxygen atom from the C—C—C axis for the centrosymmetric model. For an angle of 158° this distance is 0.44A. From the electron diffraction data the corresponding distance would be 0.43A. Even though the electron diffraction values quoted here represent only one interpretation of the data (Mackle and Sutton prefer a linear model), the agreement with the spectroscopic data is noteworthy.

The evidence on molecular structure that can be obtained from the two bands in the NaCl region here assigned to the A_u vibrational species is less satisfactory than that just discussed. In the 1040 cm^{-1} band the apparent separation of the peaks ranging from 6 to nearly 15 cm^{-1} with an average value of 10 may be due either to incomplete resolution or the presence of an impurity. The four partly resolved peaks in the weak band at 789.5 cm^{-1} have an average separation of nearly 5 cm^{-1}, and since this is only a little less than that found in the combination band at 2386 cm^{-1}, it would seem to provide some support for the structural analysis given above.

The photographic infrared work yielded no results that would provide definite information about the structure of carbon suboxide. The only conclusions that can be drawn from the few weak lines obtained is that there was nothing to indicate a linear structure for the molecule and a slight suggestion that the spectrum could be due to an asymmetric top. It is hoped in the future to study the partly resolved bands which give some insight into the structure of carbon suboxide under higher resolution.

The author wishes to express his great indebtedness to Professor D. H. Rank for much assistance in preparing the compound and taking the spectra as well as to his former colleagues, Dr. R. E. Kagarise of the U. S. Naval Research Laboratory and Dr. E. R. Shull of the Research Laboratories of the Linde Air Products Company.

[13] H. Kopper, Z. physik. Chem. B **34**, 396 (1936).

THE JOURNAL OF CHEMICAL PHYSICS VOLUME 22, NUMBER 3 MARCH, 1954

The Lattice Constants of the Alkali Borohydrides and the Low-Temperature Phase of Sodium Borohydride*

S. C. ABRAHAMS AND J. KALNAJS
Laboratory for Insulation Research, Massachusetts Institute of Technology, Cambridge, Massachusetts
(Received December 4, 1953)

The lattice constants of sodium, potassium, rubidium, and cesium borohydrides have been measured at 25.0°C as 6.1635±0.0005, 6.7272±0.0005, 7.029±0.001, and 7.419±0.001A, respectively. All four crystals are face-centered cubic and have the sodium chloride structure. Below the transition point (−83°C) sodium borohydride becomes tetragonal with lattice constants of $a=4.354\pm0.005$ and $c=5.907\pm0.005$A at −195°C.

A RECENT letter by Stockmayer and Stephenson[1] pointed out that no reports of the properties of solid potassium, rubidium, and cesium borohydrides appear in the literature. They suggested that the cesium and possibly also the rubidium salt might possess a body-centered cubic structure at room temperature, as compared with the known face-centered cubic cell of sodium borohydride.[2] They further predicted, on the basis of the entropy change in sodium borohydride at the λ point and the heat capacity[3] below the transition, and also by analogy with the ammonium halides, that the structure below the λ point would be tetragonal. The present paper reports the lattice constants for sodium, potassium, rubidium, and cesium borohydrides at room temperature, and the symmetry of the sodium borohydride unit cell at −195°C. It is shown that the predicted behavior of this salt below the transition appears correct. The lattice constants of lithium borohydride have previously been reported.[4]

EXPERIMENTAL

The x-ray measurements were made with a Norelco high-angle diffractometer. The powdered crystalline salt (325 mesh) was mounted by pressing it into a polished flat stainless steel holder against a polished glass optical flat. While held in this position, the sample was annealed at 120°C for *ca* 4 h. The temperature of the sample was controlled to ±0.05°C using a cryostat previously described[5] in conjunction with a Hoeppler ultrathermostat.† The potassium, rubidium, and cesium salts‡ were stated by the manufacturer to be 99.3, 97.3, and 97.1 percent pure. The sodium salt‡ was recrystallized from liquid ammonia; no analysis of this material was made. Neither extra lines nor unusual line profile shapes were observed.

The room temperature experiments were made by carefully exploring the shape of the line profiles of the highest angle diffraction lines, using a counting method in which the statistical accuracy of each point was *ca* 1 percent. Readings were taken at intervals of 0.025° 2θ near the peak and 0.05° 2θ elsewhere. The center of gravity of the resultant profile was taken as the position of the reflecting angle. Several specimens were used in each set of measurements, and in no case was the difference obtained in the lattice parameter more than 0.0005A between specimens. The wavelength of CuKα_1 radiation was taken as 1.54050A.

The low-temperature work was carried out in a cryostat similar to that described by Calhoun and Abrahams.[6] This was modified to permit continuous rotation of the sample holder from 165° 2θ to 22° 2θ, by inserting into the entrance tube of the cryostat a closely fitting metal tube, provided with a washer at both ends. The cellophane windows previously used were replaced by Mylar,§ which is very transparent to copper x-rays, and very tough even at liquid nitrogen temperatures. The Styrofoam‖ end walls of the upper chamber were replaced by Mylar to enable lower angles to be recorded. The surface of the sodium borohydride was protected by a sheet of 1-mil Mylar polyester film to prevent hydration.

It was observed with sodium borohydride that purple color centers rapidly developed on exposure to x-rays. These faded slowly on subsequent exposure to daylight and rapidly on heating to 120°C. Faint blue color centers developed in the potassium salt, and none were observed visually in the other two salts.

LATTICE PARAMETERS AND CRYSTAL SYMMETRY AT 25°C

A survey of all reflections produced by each of the four cubic crystals with CuKα radiation indicated that the only systematic absences were in hkl for $h+k$, $k+l$, $l+h$ odd. Hence sodium, potassium, rubidium, and cesium borohydrides each belong to a face-centered cubic space group. The observed values of the reflecting angles of

* Sponsored by U. S. Office of Naval Research, the Army Signal Corps, and the Air Force under U. S. Office of Naval Research Contracts N5ori-07801 and N5ori-07858.
[1] W. H. Stockmayer and C. C. Stephenson, J. Chem. Phys. **21**, 1311 (1953).
[2] A. M. Soldate, J. Am. Chem. Soc. **69**, 987 (1947).
[3] H. L. Johnston and N. C. Hallett, J. Am. Chem. Soc. **75**, 1467 (1953).
[4] P. M. Harris and E. P. Meibohm, J. Am. Chem. Soc. **69**, 1231 (1947).
[5] Smakula, Kalnajs, and Sils, J. Opt. Soc. Am. **43**, 698 (1953).
† Carl Zeiss Company, Inc., New York, New York.
‡ Metal Hydrides, Inc., Beverly, Massachusetts (to be published).
[6] B. A. Calhoun and S. C. Abrahams, Rev. Sci. Instr. **24**, 397 (1953).
§ E. I. du Pont de Nemours and Company, Inc., Wilmington, Delaware.
‖ Dow Chemical Company, Midland, Michigan.

the smallest spacing planes, together with the resulting lattice parameters, are given in Table I. These parameters were obtained by extrapolating the spacings computed from these angles to 180° 2θ. In the case of the sodium and potassium salts the size of the graphically estimated error is ±0.0005A. For the rubidium and cesium salts, the degree of purity appears to justify an error of only ±0.001A.

STRUCTURE OF SODIUM BOROHYDRIDE BELOW THE λ POINT

The transition temperature of $NaBH_4$ is −83°C, and the low-temperature phase was examined at −195 ±5°C. Below the λ point, each cubic line was split into three lines if the cubic (hkl) had the property $h \neq k \neq l$; into two lines if $h \neq k = l$; and remained one line if $h = k = l$. This phase could thus readily be interpreted on the basis of a face-centered tetragonal cell, which could then be transformed by convention into a body-centered tetragonal cell, with $a = 4.354 \pm 0.005$A and

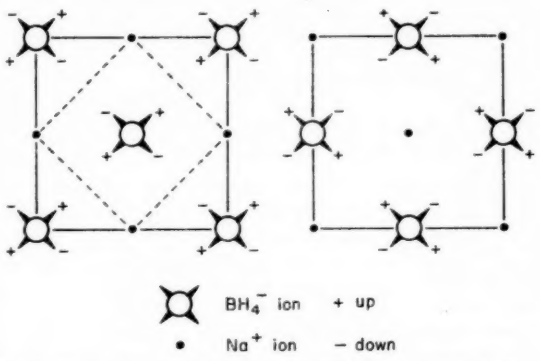

FIG. 1. Two successive layers in the $NaBH_4$ structure below the λ point. An outline of the body-centered tetragonal cell is shown dashed. The c axis is normal to these layers.

$c = 5.907 \pm 0.005$A. Table II gives the observed and calculated spacings based on this cell.

DISCUSSION

The lattice parameter of face-centered cubic sodium borohydride is identical with that reported by Soldate,[2] who gave $a_0 = 6.151 \pm 0.009$ kX. Taking the values for the radii of the sodium, potassium, rubidium, and cesium ions given by Pauling,[7] the corresponding values for the size of the borohydride ion, taking double repulsion effects into account, are 2.03, 2.02, 2.03, and 2.06A, respectively, for the four salts. It thus seems that the size of this ion is very close to 2.03A, i.e., between the radii of the bromide and iodide ions. The radius ratio of alkali to borohydride ion in these four salts is then 0.472, 0.656, 0.731, and 0.816, respectively. At values greater than 0.732, the coordination number generally changes from 6 to 8, and, hence, the unit cell from face-centered to body-centered cubic. The failure

[7] L. Pauling, *Nature of the Chemical Bond* (Cornell University Press, Ithaca, New York, 1940), p. 358.

TABLE I. Values of the largest reflecting angles θ and the lattice parameters ($CuK\alpha_1 = 1.54050$A).

hkl	$NaBH_4$	KBH_4	$RbBH_4$	$CsBH_4$
600/442	48.520° θ			
622	55.945			
640	64.279			
642	69.229	58.937° θ		
731/553		61.555	57.310° θ	
800		66.324		
820/644		70.745	64.635	58.870° θ
822/660		76.287	68.410	61.750
751/555			71.630	64.040
911/753				71.065
840			78.590	
842				72.095
$a_0^{25°}$	6.1635A	6.7272A	7.029A	7.419A

of cesium borohydride to become body-centered cubic may possibly be due to impurities in the sample but more likely represents a considerable departure from sphericity associated with the borohydride ion. Since the polarizability of the BH_4^- ion is very nearly equal to that of the Br^- ion,[8] the 6-coordination apparently cannot be the result of abnormally low dispersion forces.

Stockmayer and Stephenson suggested that no disorder is present in the low-temperature phase of sodium borohydride. However, if the ordered borohydride ion is operated on with the symmetry of a body-centered space group, no special direction can develop unless the hydrogen atom distribution is far from that of a regular tetrahedron. If a regular (or approximately regular) tetrahedral distribution of the boron-hydrogen bonds is assumed, then the cell should remain isotropic, which conflicts with the observation.

An alternative is that, while the sodium and boron atoms indeed form a body-centered tetragonal array, the hydrogens may lie on a primitive tetragonal lattice. No unambiguous indication of any line belonging to a primitive lattice was observed, but the intensity of a line with $h+k+l = 2n+1$ would be extremely weak and probably unobservable. In this case, there are several primitive tetragonal space groups which would allow the heavier atoms to form a body-centered lattice, and

TABLE II. Observed and calculated spacings for body-centered tetragonal sodium borohydride at −195°C.

hkl	d_{obs}	d_{calc}	hkl	d_{obs}	d_{calc}	hkl	d_{obs}	d_{calc}
101	[a]		204	1.222A	1.222A	116	0.939A	0.938A
110	3.09A	3.078A	321	1.184	1.183	413	0.931	0.930
002	2.97	2.954	303	1.170	1.168	422	0.924	0.924
200	2.184	2.177	105	1.142	1.140	305	[b]	0.916
112	2.138	2.131	400	1.089	1.088	206	0.897	0.897
211	1.853	1.849	224	1.067	1.066	404	0.877	0.876
103	1.797	1.794	411	1.039	1.039	431	0.861	0.861
202	1.755	1.752	323	1.028	1.029	510	0.854	0.854
220	1.541	1.539	330	1.025	1.026	334	0.844	0.843
004	1.478	1.477	402	1.023	1.021	223	0.830	0.829
301	1.410	1.409	215	1.013	1.010	107		0.828
213	1.386	1.384	314	1.007	1.007	512	0.820	0.820
310	1.378	1.377	006	0.985	0.985	424	0.813	0.813
222	1.366	1.365	410	0.974	0.973	316	0.801	0.801
114	1.333	1.332	332	0.970	0.969	521		0.801
312	1.248	1.248						

[a] Unobservable because of cutoff by the cryostat.
[b] Not observed.

[8] D. W. Rice (private communication, 1953).

the tetrahedral (regular or approximately regular) borohydride group to be arranged in antiparallel layers. Because it is not possible to distinguish among these space groups, the following models for the BH_4 group orientation may be considered: (a) as predicted by Stockmayer and Stephenson, in which the B—H bond points towards the second nearest sodium atoms; (b) one in which this bond points toward the nearest boron atoms; and (c) any other position for the bond. Models (b) and (c) seem to be precluded by the entropy change of $R \ln 2$ at the λ point, for they should give rise to a greater change. Model (a) (Fig. 1) shows the positions taken by the hydrogen atoms, below the transition. Above the λ point, there would be a 50-percent chance of pointing up or down for each hydrogen. Hence this model explains the observed entropy change at the transition and also the increase in the c axis (perpendicular to the planes in Fig. 1) on warming up through the transition, for, in the ordered form, each right square prism, defined by having alternately sodium and boron atoms at its vertices, contains two hydrogen atoms each with the same z coordinate. In the disordered form, this space would contain the equivalent of 4 half-atoms of hydrogen, involving two different z coordinates. It is very likely the increased repulsion between these hydrogen atoms that causes the c axis to expand.

ACKNOWLEDGMENT

We would like to thank Metal Hydrides, Inc., for having provided the samples of the alkali borohydrides, Professor W. H. Stockmayer and Professor C. C. Stephenson for stimulating discussions, and Professor A. R. von Hippel for his interest in this work.

THE JOURNAL OF CHEMICAL PHYSICS VOLUME 22, NUMBER 3 MARCH, 1954

Diffusion in CO_2-CH_4 Mixtures to 225 Atmospheres Pressure*

Q. R. JEFFRIES AND H. G. DRICKAMER
Department of Chemistry and Chemical Engineering, University of Illinois, Urbana, Illinois
(Received October 1, 1953)

Diffusion coefficients have been measured in two mixtures of CO_2 and CH_4. (1) 50 mole percent CO_2—50 percent CH_4; (2) 75 mole percent CO_2—25 mole percent CH_4. C^{14} tagged CO_2 was used, so that no gradient in chemical composition was necessary. For the first mixture the results agreed with Enskog's dense gas theory at all temperatures and pressures. For the 75 percent CO_2 mixture at 25°C there was a positive deviation from theory, corresponding to the increased importance of glancing collisions for CO_2 near saturation. The results are consistent with our previous data for self-diffusion in the two pure gases.

DIFFUSION measurements have been made in two mixtures of carbon dioxide and methane to 225 atmospheres, using the method previously described.[1] Each half of the cell was filled with a mixture of CO_2-CH_4 identical in composition, but some of the CO_2 on one side was C^{14} tagged. Thus all concentration effects were eliminated. The $C^{14}O_2$ was generated from $BaC^{14}O_3$ obtained from Oak Ridge National Laboratory.

The two mixtures studied contained 50 percent and 75 percent CO_2, respectively.

The kinetic theory of diffusion in dilute gases has

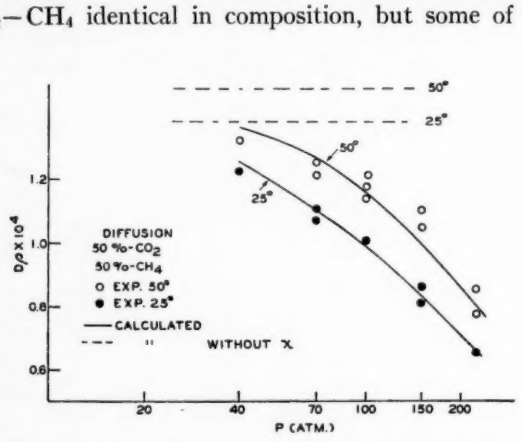

FIG. 1. Diffusion in 50 percent CO_2—50 percent CH_4.

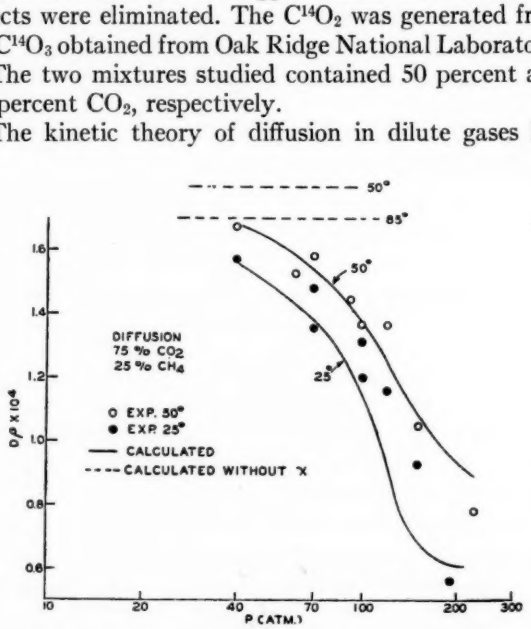

FIG. 2. Diffusion in 75 percent CO_2—25 percent CH_4.

* This work was supported in part by the U. S. Atomic Energy Commission.

[1] W. L. Robb, and H. G. Drickamer, J. Chem. Phys. **19**, 1504 (1951).

TABLE I. Diffusion data on 50 mole percent CO_2-CH_4 mixture.

T	P	ρ	χ	$D_{exp}\times10^3$	$D_{calc}\times10^3$
25°	40	0.0565	1.097	2.15	2.23
25°	70	0.1063	1.193	1.00	0.997
25°	70.5	0.108	1.197	1.02	0.995
25°	100	0.1785	1.35	0.562	0.572
25°	150	0.309	1.67	0.264	0.268
25°	150	0.309	1.67	0.278	0.268
25°	150	0.309	1.67	0.270	0.268
25°	225	0.435	2.065	0.150	0.1535
50°	40	0.0505	1.087	2.59	2.70
50°	70	0.094	1.167	1.33	1.35
50°	70	0.094	1.167	1.28	1.35
50°	100	0.146	1.276	0.815	0.796
50°	100	0.146	1.276	0.83	0.796
50°	100	0.146	1.276	0.78	0.796
50°	150	0.241	1.50	0.485	0.410
50°	150	0.241	1.50	0.455	0.410
50°	220	0.35	1.80	0.245	0.235
50°	225	0.36	1.83	0.225	0.224

TABLE II. Diffusion data on 75 mole percent CO_2—25 mole percent CH_4 mixture.

P	T	ρ	χ	$D_{exp}\times10^3$	D_{calc}
40	25°	0.073	1.102	2.15	2.12
70	25°	0.160	1.241	0.93	0.86
70	25°	0.160	1.241	0.85	0.86
100	25°	0.312	1.53	0.384	0.358
100	25°	0.312	1.53	0.420	0.358
120	25°	0.447	1.878	0.259	0.209
150	25°	0.582	2.183	0.160	0.134
190	25°	0.648	2.375	0.101	0.110
50	50°	0.064	1.084	2.60	2.62
60	50°	0.105	1.151	1.45	1.51
70	50°	0.1275	1.188	1.25	1.21
90	50°	0.181	1.278	0.80	0.79
100	50°	0.210	1.33	0.65	0.655
120	50°	0.280	1.467	0.490	0.445
150	50°	0.385	1.689	0.272	0.282
225	50°	0.540	2.073	0.143	0.164

been developed by Enskog[2] and the collision cross-section integrals for the Lennard-Jones model have been evaluated by Hirschfelder[3] *et al.* When Enskog's dense gas correction[4] is appended, the equation takes the form

$$D=\frac{3}{16}\left(\frac{kT}{\pi\mu}\right)^{\frac{1}{2}}\frac{1}{\gamma_0^2 W_{(1)}^{(1)} n\chi}, \qquad (1)$$

where μ = reduced mass, γ_0 = collision diameter, n = number of molecules per unit volume, $W_{(1)}^{(1)}$ = collision cross-section integral, $\chi=1+5/12n\sigma^3+0.1275(n\sigma^3)^2+\ldots$, and σ = collision diameter for solid elastic spheres—assumed equal to γ_0. (Actually, the form of χ for dense gas mixtures is somewhat more complex, but it reduces to this when the molecules have identical collision diameters. For the mixture CO_2-CH_4 this is reasonably satisfied: $\gamma_0(CO_2)=3.99$; $\gamma_0(CH_4)=3.88$).

The results are shown in Tables I and II. In Figs. 1 and 2. $D\rho$ is plotted *versus* pressure. The PVT data of Sage, *et al.*[5] were used, extrapolated where necessary. The solid lines are the theoretical curves plotted according to Eq. (1). The dotted curves were obtained from Eq. (1) without the dense gas correction.

For the 50 mole percent CO_2-50 mole percent CH_4 mixture the agreement with Eq. (1) is within experimental error throughout the pressure range. This is consistent with our previous results for self-diffusion in CH_4.[6]

In the 75 mole percent CO_2-25 mole percent CH_4 mixture, the results agree with theory at 50°. At 25° there is a positive deviation from theory in the pressure range 60–125 atmospheres, amounting to 22 percent at the maximum. Apparently, as one approaches the critical point for the mixture, glancing collisions become more important for CO_2 reducing the effective collision diameter. These results and conclusions are completely consistent with our previous results[1] for self-diffusion in CO_2.

Q. R. Jeffries would like to acknowledge financial assistance from the U. S. Atomic Energy Commission.

[2] S. Chapman and T. G. Cowling, *The Mathematical Theory of Non Uniform Gases* (Cambridge University Press, Cambridge, England, 1939).
[3] Hirschfelder, Bird, and Spotz, J. Chem. Phys. **16**, 968 (1948).
[4] Reference 2, pp. 273–295.
[5] Sage, Lacey, Reamer, and Olds, Ind. Eng. Chem. **36**, 88 (1944).
[6] Q. R. Jeffries and H. G. Drickamer, J. Chem. Phys. **21**, 1358 (1953).

The Yield of Oxidation of Ferrous Sulfate in Acid Solution by High-Energy Cathode Rays*

JEROME SALDICK AND AUGUSTINE O. ALLEN
Chemistry Department, Brookhaven National Laboratory, Upton, New York
(Received November 16, 1953)

An absolute determination of the yield of the ferrous sulfate radiation dosimeter has been made by delivering to the solution a measured charge of cathode rays at known energies of 1 or 2 Mev. Appropriate small corrections have been made for backscattering, window absorption and, bremsstrahlung. The result, $G=15.6\pm0.5$, is in complete agreement with Hochanadel's calorimetric determination of the yield, but disagrees by 30 percent with the most widely used value obtained by cavity ion chamber comparison.

AIR-SATURATED ferrous sulfate solution has in recent years come into wide use as a dosimeter for gamma rays and x-rays. A discrepancy, however, exists between calorimetric evaluation of this dosimeter, which according to Hochanadel and Ghormley[1] and Lazo, Dewhurst, and Burton[2] shows oxidation by gamma rays with a yield $G=15.6$ (atoms of iron oxidized per 100-ev energy input), and evaluation by comparison with cavity ionization chambers, which in several careful studies gave $G=20$.[3] The discrepancy between the two methods is not clear-cut, since Davison, Proctor, and Goldblith[4a] report a calorimetric value near 20, whereas by ion chamber measurements values of 16.7[1] (Co^{60} gamma rays), 17.4[4b] (Co^{60} gamma rays), and 16.8[4c] (Ra gamma rays) have recently been reported. The last three values were obtained, however, with the chamber placed close to the radiation source; with such geometry the Bragg-Gray conditions, basic to the use of cavity chambers, may not be completely fulfilled.[5,6] Hardwick has obtained values near 20 by using calibrated beta-ray sources dissolved in the ferrous sulfate solution,[7] but the accuracy of these results is now suspect[8] because of the possible presence of contaminating organic matter, which may increase the yield.[9] The discrepancy is of especial concern because intercomparison through ferrous sulfate provides one of the few practical methods for comparing the widely-used cavity chamber with any other absolute method for determining quantity of gamma radiation. We have therefore looked for a completely independent method of absolute evaluation of the ferrous sulfate yield and have studied the oxidation of air-saturated ferrous sulfate solutions in $0.8N$ H_2SO_4 by electron beams of 1- and 2-Mev energy obtained from an electrostatic generator. The chemical effects of such a beam must be the same as those of gamma rays, which transfer energy to an absorbing medium entirely through the agency of fast electrons. Determination of the absolute yield is in principle extremely simple; the beam is completely absorbed in the solution, and the integrated beam current and the beam voltage determine the energy input, which is compared with the amount of iron oxidized. The method also allows the yield to be followed as a function of radiation intensity to much higher intensities than in previous work.

Hochanadel[1] has described a determination similar to that reported here but which was subject to error because corrections for backscattering and conduction from sample to ground through ionized air were admittedly neglected.

EXPERIMENTAL

A 2-Mev horizontal Van de Graaff generator, constructed by the High Voltage Engineering Corporation, was the radiation source. The electron beam emerged from the generator through a 3-mil aluminum foil, and entered a cylindrical Pyrex glass cell, filled with solution, pictured in Fig. 1. A number of different cells were used, with volumes ranging from 16.4 to 24.7 ml. The front face of the cell was mica, 4 to 8 mg/cm² thick, cemented to the glass with a very thin layer of Araldite-101 or Apiezon W cement. The radius of the cell is appreciably greater than the maximum range of the electrons in the solution, so no electrons, even if scattered through 90°, could ever reach the glass. A platinum wire, dipping into the upper part of the solution, led the beam current through a shielded cable to the measuring instrument and thence to ground. The outside of the glass cell was coated with ceresin to help make the resistance of all alternate paths to ground orders of magnitude greater than that through the current measuring instrument. The whole front of the mica was coated with "dag," which was grounded. Thus the current measurement was unaffected by the low-energy secondary electrons which come off the surface when the beam enters the cell. (High-energy secondaries or backscatter coming

* Work performed under the auspices of the U. S. Atomic Energy Commission.
[1] C. J. Hochanadel and J. A. Ghormley, J. Chem. Phys. **21**, 880 (1953).
[2] R. Lazo, H. A. Dewhurst, and M. Burton (private communication).
[3] N. Miller and J. Wilkinson, Disc. Faraday Soc. **12**, 50 (1952).
[4a] S. Davison *et al.*, Nucleonics **11**, No. 7, 22 (1953).
[4b] Freeman, Van Cleave, and Spinks, Can. J. Chem. **31**, 448 (1953).
[4c] R. W. Hummel and J. W. T. Spinks, Can. J. Chem. **31**, 250 (1953).
[5] White, Marinelli, and Failla, Am. J. Roentgenology **44**, 889 (1940).
[6] N. Miller (private communication).
[7] T. J. Hardwick, Can. J. Chem. **30**, 39 (1952).
[8] T. J. Hardwick (private communication).
[9] H. A. Dewhurst, J. Chem. Phys. **19**, 1329 (1951).

from greater depths must be corrected for; see following.) The beam was defined by a $\frac{1}{4}$-in. hole in a $\frac{1}{4}$-in. thick Al plate mounted immediately before the cell.

Beam currents at 2 Mev ranged from 6×10^{-11} to 7×10^{-7} amp. Practically all the beam energy is dissipated in about 1 gram of solution, so that the mean intensity in the irradiated zone ranged from 1.2×10^{-4} to 1.4 watts/g, or 13 to 150 000 rep/sec, if 1 rep = 93 ergs/g. The maximum intensity is much higher; when the focused beam enters the solution, most of its energy lies in an area of 1 mm², and the rate of energy loss at 2 Mev is 1.76 Mev cm²/g. The maximum intensity is then about 88 watts/g per watt of total beam, and ranges in our experiments from about 0.01 to 120 watts/g, or from 1100 to about 1.4×10^{7} rep/sec. With x-rays, Miller[10] found that the $FeSO_4$ oxidation yield was constant up to an intensity of 1700 rep/sec. Our intensity range thus overlaps his.

With such high local intensity, local depletion of dissolved oxygen will begin to lower the yield before the mean concentration of ferrous ion in the whole solution has been appreciably lowered. Apparent values of G in unstirred solutions at 5×10^{-8} amp beam current decreased from 12 to 8 as the total dose was increased, showing that thermal convection was insufficient to prevent local depletion. The magnetic stirrer shown in Fig. 1 was thus required. It consisted of a glass paddle containing an iron bar, mounted on a glass bearing and rotated by a horseshoe magnet placed behind the cell and attached to the shaft of a variable speed motor. A stirring speed of a few hundred rpm was sufficient to bring the value of G up to the standard, and increase of stirring speed by a factor of 3 had no further effect on G.

The voltage of the beam was determined in the standard way by a generating voltmeter. Its output was calibrated several times during the course of the work, by determining the threshold voltage for production of neutrons from beryllium exposed to x-rays produced by allowing the beam to fall on a gold target. The correct threshold voltage was taken as 1.666 Mev.[11] Voltage calibration was good to ±0.5 percent, and the energy of the electrons in the beam is thought to be uniform to within 1 percent.

The beam currents were in general lower than ordinarily used with this type of generator, and it was not surprising to find that the currents were not very steady. A measuring device that would integrate the current received was necessary. Two meters were used. Below 10^{-9} amp, a battery-operated dc amplifier was used, with its output measured on a 25-mv range Brown recording potentiometer. Rapid fluctuations in input current were damped by condensers connected in parallel with the input resistors in the amplifier, giving time constants of 5–10 sec. The area under the recorder trace, corrected for a small zero drift, measured the total

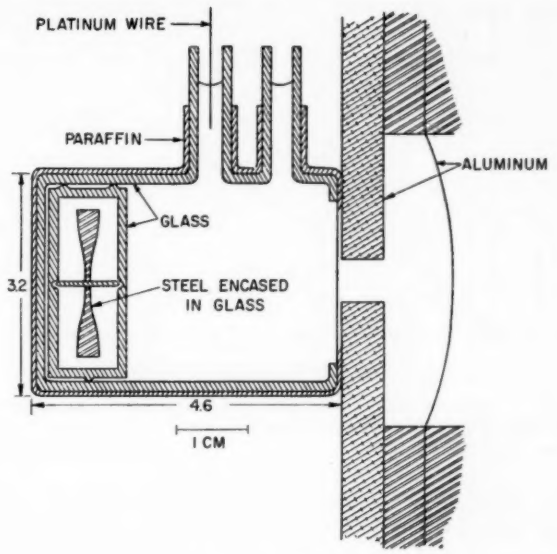

FIG. 1. Irradiation cell.

charge collected from the solution. At currents from 4×10^{-10} to 3×10^{-8} amp a line-operated current integrator described in the literature[12] was used. The amplified output of this instrument charges a condenser, which triggers a counter and is discharged whenever it reaches a preset voltage (100 v). The instruments were designed and constructed by W. Higinbotham, R. Chase, and S. Rankowitz, of the Brookhaven Electronics Department, to whom we are greatly indebted. For currents above 5×10^{-8} amp, where the runs were necessarily of short duration (<10 sec), the current integrator circuit was used in a different way. A 10^5-ohm and a 23-ohm resistor were connected in series between ground and the high-voltage side of the aforementioned condenser. The 25-mv Brown recording potentiometer measured the potential drop across the 23-ohm resistor. The circuit was set so that 10^{-6} coulombs input was required to charge the condenser to 100 v; the fraction of this voltage built up during the bombardment measured the total charge input.

So that an accurately measurable amount of chemical change might be obtained without approaching depletion in the cells used, charge inputs in the range 0.4–1.5 $\times10^{-6}$ coulomb were required. At the lowest currents, runs lasted two hours or more. In addition to the usual current fluctuations, the generator occasionally undergoes voltage breakdown, or "sparking," which results in a burst of charge entering the solution at a rate too fast for the measuring instruments to follow. All runs in which sparking occurred were rejected.

As a rough check on the current and voltage measurements, a calorimetric determination of the beam energy was made. The beam was allowed to fall on a small aluminum block, supported in the vacuum of the generator by wires of iron and constantan which acted

[10] N. Miller, Nature **171**, 688 (1953).
[11] Hornyak, Lauritsen, Morrison, and Fowler, Revs. Mod. Phys. **24**, 342 (1952).
[12] W. Higinbotham and S. Rankowitz, Rev. Sci. Instr. **22**, 688 (1951).

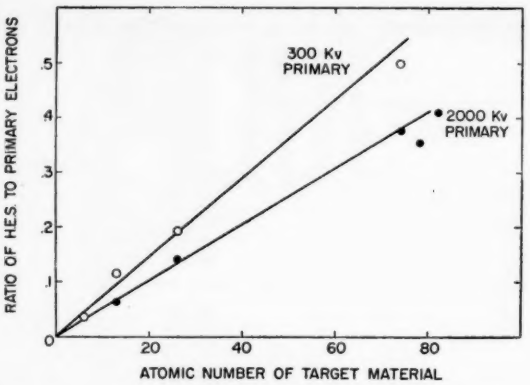

FIG. 2. Ratio of high-energy secondary to primary electrons as a function of atomic number of target material. Data for 300 kv taken from reference 13.

as a thermocouple and as current measurement leads. The charge collected was measured by the current integrator; immediately on interrupting the beam the leads were switched to a L and N recording potentiometer (2.5-mv range) which measured the temperature of the block as a function of time after irradiation. From the weight of the block, the specific heat of aluminum, and the temperature rise extrapolated back to the mid-time of the irradiation, the energy input was found and compared with that measured by the beam voltage and current corrected for backscattering (see below). In four determinations, the mean difference was only 2 percent, which is within the accuracy of the calorimetry.

All solutions were 10^{-3} molar in ferrous salt. They were made up in quadruply distilled water, using Eimer and Amend "Tested Purity" sulfuric acid and ACS reagent grade ferrous sulfate or ferrous ammonium sulfate (results were the same with either salt). In some runs, 10^{-3} M sodium chloride was added, without affecting the results.[9] After a run, the ferric sulfate concentration was determined by direct reading of the light absorption[3] at 305 mμ in a Beckman DU spectrophotometer, using 1-cm silica cells. The concentration of ferric ion in moles/liter was equal to the absorbancy (optical density) times 4.57×10^{-4}.

SOURCES OF ERROR AND CORRECTIONS

Backscattering

When a beam of electrons falls on a surface, the secondaries scattered back fall into a group of low energy (<30 ev), because of ionization of the surface atoms at the point of entrance, and a group having energies ranging up to that of the primary beam, because of collision backscattering of the primary electrons. The numbers of electrons in the two groups, as percentage of the primary beam, were determined by Trump and Van de Graaff[13] for primary energies up to 0.3 Mev. We determined these numbers for 2-Mev electrons with targets of various materials, by a similar method. Figure 2 shows the number in the high-energy group, plotted against the atomic number of the target material for 2 Mev, together with Trump and Van de Graaff's results at 0.3 Mev. The smaller amount of backscattering at the higher energy is consistent with the results of Miller.[14] The curves are approximately linear, as suggested by Wu,[15] and the percentage of primary electrons appearing as high-energy backscatter is 0.55 Z at 2 Mev and 0.68 Z at 0.3 Mev. For ferrous sulfate solution in 0.8N H_2SO_4, the effective value of Z was taken as $\Sigma n_i Z_i^2/\Sigma n_i Z_i$, where n_i is the concentration in the solution of atoms of number Z_i and the percentage high-energy backscatter at 2 Mev is 3.7. It is possible that we have slightly underestimated the percentage of high-energy secondary electrons backscattered because the scattering of the electrons by the materials between the accelerator and the solution causes some of them to enter at an angle different from the perpendicular, and hence to be subject to a somewhat greater degree of backscattering. The backscattered electrons deliver some of their energy to the solution but are not counted in the current reading. The mean fraction of energy lost by the scattered electrons before emerging is not precisely known, but Seliger[16] has shown that the mean energy of backscattered β rays from supports of low Z is much smaller than the mean energy of the primary rays, and we would guess from his results that in our case about 85 percent of the energy of the scattered electrons remains in the material. The correction to be added to our measured energy inputs in the ferrous sulfate solution at 2 Mev is therefore 0.85×3.7 percent, or 3.1 percent. For 1-Mev electrons, the high-energy backscattering was taken as 0.60 Z by rough interpolation between the 0.3- and 2.0-Mev curves, and the corresponding correction is 3.4 percent. In the calorimetric energy calibration, the low-energy as well as the high-energy secondaries must be included in the correction to the current reading; the percentage of low-energy secondaries from an aluminum target from our experiments is 2.6 percent.

Absorption in Windows

Trump, Van de Graaff, and co-workers[17] have published curves for cathode rays of 0.3 to 3.0 Mev, showing the relative ionization in a parallel-plate chamber intercepting the whole beam under various thicknesses of aluminum. The area under this curve is proportional to the energy loss in the absorber, and the total area under the curve, out to the extreme range of the beam, provides the normalizing factor. In most of our experiments, the beam traversed 20.6 mg/cm^2 of Al (3-mil generator window), 1.7 mg/cm^2 of air, and 1.5 mg/cm^2 of carbon

[13] J. G. Trump and R. J. Van de Graaff, Phys. Rev. **75**, 44 (1949).

[14] B. L. Miller, Rev. Sci. Instr. **23**, 408 (1952).
[15] C. S. Wu, Phys. Rev. **59**, 481 (1941).
[16] H. H. Seliger, Phys. Rev. **88**, 408 (1952).
[17] Trump, Wright, and Clarke, J. Appl. Phys. **21**, 345 (1950); Trump, Van de Graaff, and Cloud, Am. J. Roentgenol. Radium Therapy **43**, 728 (1940); J. G. Trump and R. W. Van de Graaff, J. Appl. Phys. **19**, 599 (1948).

plus 4 to 8 mg/cm² of mica (weighed cell window) before reaching the ferrous sulfate solution. The energy loss in mica, carbon, and air is not significantly different from that in the same weight of aluminum. From the published curves, the initial rate of energy loss is 1760 ev cm²/mg at 2 Mev and 2300 ev cm²/mg at 1 Mev. The total window absorption correction was 2.6 percent at 2 Mev and 6.9 percent at 1 Mev. There is some question as to the effect of the defining orifice on the absorption correction for the generator window, since those electrons that are deflected the most by the window and fail to pass the orifice might tend to differ in mean energy loss from those that are less deflected. This effect should be very small, since most of the large deflections arise from elastic collisions. A few runs made without the defining orifice gave results in good agreement with the others.

Bremsstrahlung

According to the data of Buechner *et al.*[18] the percentage of beam energy lost as bremsstrahlung from a target of the effective Z of $0.8N$ H_2SO_4 solution is 0.44 percent at initial energy of 2 Mev, 0.13 percent at 1 Mev. This correction must be subtracted from the measured energy input.

Combining the corrections for backscattering, absorption, and bremsstrahlung gives a net correction of 0.0 percent at 2 Mev and 3.6 percent at 1 Mev, the latter to be subtracted from the energy input. The probable error in the absolute yield due to uncertainty in these corrections should be less than 1.5 percent.

Current Leakage

The resistance between the solution and ground was determined by biasing the solution 280 volts positive with a battery and reading the resulting leakage current. The leakage resistance of a typical cell was 7.5×10^{10} ohms with no electron beam, and 2.5×10^{10} ohms when an electron beam of 10^{-8} amp was falling on the solution. These values are much higher than 10^9 ohms, which was the largest limiting resistance used with the current meters. Leakage was further minimized by the use of feedback built into the amplifiers of both current meters, which maintained the potential of the solution at a value differing from ground by less than 1 percent of the voltage drop across the limiting resistor, so that the leakage is less than 1 percent of what would be found with no feedback. Error due to current leakage is therefore negligible.

Scattering by the Orifice

A suggestion was made to us that electrons striking the edges of the orifice might be deflected into the solution after losing considerable energy. Part of the incoming current would then be of low energy and our value of G would be low. A focusing electromagnet on the generator extension tube allows the beam diameter at the window to be varied from about 8 mm at no focus to about 1 mm at optimum magnet current. With our arrangement, only about 50 percent of the 2-Mev beam passed through the orifice at no focus, while 90 percent passed through at optimum focus. The current density at the edges of the orifice was clearly an order of magnitude greater at no focus. But the mean value of G found in a long series of runs at no focus was the same as that found immediately after in a series at optimum focus (Table I). Also, as mentioned above, removing the orifice entirely in a few experiments (at optimum focus) showed no effect on G. The effect of scattering by the orifice must therefore be negligible.

[18] W. W. Buechner *et al.*, Phys. Rev. **74**, 1348 (1948).

TABLE I. Oxidation yield G of $0.001M$ $FeSO_4$ in air-saturated $0.8N$ H_2SO_4 by cathode rays.

Current (amp)	Energy (Mev)	Method[a]	G	Standard devn.	No. of detns.
$5\text{–}7\times10^{-7}$	2	2	15.15	0.57	8
$1\text{–}3\times10^{-7}$	2	2	16.12	0.36	14
$0.3\text{–}5\times10^{-8}$	2	1	14.85[b,c]	0.77	22
$0.6\text{–}1.0\times10^{-8}$	2	1	14.90[c]	0.06	7
$0.9\text{–}1.6\times10^{-8}$	2	1	15.40	0.12	13
7×10^{-10}	2	1	15.33		1
7×10^{-10}	2	3	15.57		1
$6\text{–}8\times10^{-11}$	2	3	15.52	0.08	4
$0.5\text{–}3\times10^{-8}$	1	1	15.92	0.35	21

[a] Method 1: current integrator.
Method 2: integrator used as pseudoballistic galvanometer.
Method 3: amplifier with recording potentiometer.
[b] Beam not focused. All other runs at optimum focus.
[c] Runs made before May 9, 1953, and given weight of 0.5 in calculation of best G.

Calibration of Current Measuring Instruments

The amplification of the meters is proportional to the limiting resistors, which are nominally 100 or 1000 megohms. Such resistors are likely to change by one or two percent in short periods of time. This fact was not realized until after the conclusion of the runs, when a recalibration of the current integrator showed most scales to have changed by 3 percent or more since the previous calibration, which had been made before the runs were started. It may be seen in Table I that a group of runs at about 10^{-8}-amp beam current, carried out before May 9, 1953, gave a 3.2 percent lower average value than a group done in precisely the same way after June 12, 1953, although the standard deviation within each group is less than 0.8 percent. The only explanation we can offer for this change is a change in the calibration of the current integrator. We believe this to be our largest source of uncertainty.

RESULTS AND DISCUSSION

The results of all runs are presented in Table I. Variation of the yield with current, over a 10 000-fold range, is less than 4 percent, and the yield may be taken as constant within the limits of error. The difference between the mean value of the yields at 1 Mev and 2

Mev is 2 percent, which is also regarded as less than the experimental error. (Any real effect on the yield of electron energy is expected to be in the opposite direction, i.e., the slower electrons should give if anything a slightly lower yield.)[19] Since the current meter calibrations used in calculating the yield values were made after the runs were finished, we believe greater weight should be given to the more recent runs. In averaging all runs to obtain a final best value, we have arbitrarily given runs made before May 9, 1953, a weight of $\frac{1}{2}$. The probable error in the absolute value we take as 3 percent; it arises largely from uncertainty in the current calibration. The final value of G is 15.6_2, with a probable error of 0.5.

The present results, in complete agreement with the calorimetric value of 15.6, and in disagreement with ion chamber comparisons, suggest that the question of interpretation of dose measurements for gamma rays by the cavity chamber method may require re-examination, although the latter now constitutes the "accepted" method of determining energy input to material irradiated by gamma rays.

[19] A. O. Allen, Radiation Research 1 (1954) (to be published).

THE JOURNAL OF CHEMICAL PHYSICS VOLUME 22, NUMBER 3 MARCH, 1954

The Microwave Spectrum of Hydrogen Peroxide*†

J. T. Massey and D. R. Bianco
Applied Physics Laboratory, The Johns Hopkins University, Silver Spring, Maryland
(Received August 17, 1953)

Nine absorption lines of H_2O_2 and some one hundred absorption lines of D_2O_2 and HDO_2 have been observed in the microwave frequency region using a flow system for sampling to overcome the decomposition of the peroxide at low vapor pressure. An analysis of the microwave spectrum of H_2O_2, using a symmetric top approximation, reveals that it is necessary to invoke hindered internal rotation to explain the experimental data. Using a sinusoidal approximation for the hindering potential yields a barrier height of about 113 cm^{-1}. From the Stark effect calculations, a value of dipole moment of 2.26 debye units is obtained. Some limiting conditions on the values of the molecular parameters are discussed.

INTRODUCTION

In 1934 Penny and Sutherland[1] applied the method of electron pairs to determine the most stable configuration for the atoms in the hydrogen-peroxide molecule. Their calculations indicated that the nonplanar structure of C_2 symmetry, shown in Fig. 1, was most probable and that a double minimum potential, restricting free rotation of the two O—H bars about the O—O bond, should exist and be of the form shown in Fig. 2. It was shown by the authors that this model gives a simple explanation of the large dipole moment of the H_2O_2 molecule. Later theoretical work[2,3] tended to confirm their conclusions.

Since 1934 experimental evidence has been accumulated from many sources. This tends to substantiate the theoretical work and to provide some structural parameters. The results of an x-ray examination of the compound "hyperol" [$CO(NH_2)_2 \cdot H_2O_2$] by Lu, Hughes, and Giguère[4] indicated that the structure shown in Fig. 1 was correct with the O—O distance = 1.46±0.03A, $\gamma = 78.5° \pm 2°$, and $\chi = 106.5° \pm 2°$. A more recent x-ray analysis of the hydrogen-peroxide crystal[5] again confirmed the nonplanar structure of Fig. 1 with the O—O distance = 1.49A, $\gamma = 83°$, and $\chi = 94°$. An electron diffraction study by Giguère and Schomaker[6] resulted in a value of 1.47±0.02A for the O—O bond distance.

The Raman[7] and infrared[8,9] spectra of the H_2O_2 molecule have been investigated many times and the assignment of the six fundamental vibrations has been made.[9] The lowest vibration frequency observed was an infrared band in the liquid at about 635 cm^{-1} which was tentatively assigned as the torsional vibration frequency. Lately this band has been studied in the 500–660 cm^{-1} region in the vapor state with better resolution by Giguère and Bain.[10] Since an examination of these data revealed that the two strongest Raman bands also occurred as infrared bands, the H_2O_2 molecule must not

* This paper is based in part on a dissertation presented by J. T. Massey in partial fulfillment of the requirements for the degree of Doctor of Philosophy in the Faculty of Philosophy of The Johns Hopkins University.

† This work was supported by the Bureau of Ordnance, U. S. Navy, under Contract NOrd 7386.

[1] W. G. Penny and G. B. B. M. Sutherland, J. Chem. Phys. **2**, 492 (1934).

[2] H. J. Lasettre and L. B. Dean, J. Chem. Phys. **17**, 317 (1949).

[3] N. W. Luft, J. Chem. Phys. **21**, 179 (1953).

[4] Lu, Hughes, and Giguère, J. Am. Chem. Soc. **63**, 1507 (1941).

[5] Abrahams, Collin, and Lipscomb, Acta Cryst. **4**, 15 (1951).

[6] P. A. Giguére and V. Schomaker, J. Am. Chem. Soc. **65**, 2025 (1943).

[7] F. Fehér, Ber. deut. chem. Ges. **72**, 1778 (1939).

[8] L. R. Zumwalt and P. A. Giguère, J. Chem. Phys. **9**, 458 (1941). (Note: other references to this work may be found in 7, 8, and 9).

[9] P. A. Giguère, J. Chem. Phys. **18**, 88 (1950).

[10] P. A. Giguère, private communication.

have a center of symmetry.[11] However, Giguère[9] stated that the fact that the O—O vibration gave the strongest Raman band but a very weak infrared band was further evidence for the C_2 (nonplanar) point group model. Badger's rule applied to the infared data gave 1.48A for the O—O bond length.

Investigation of the fine structure of two harmonic or combination bands of H_2O_2 revealed that these bands were of the hybrid type, thus ruling out a planar structure for the molecule since these models have a C_{2v} point group symmetry and should give pure parallel or perpendicular type bands. In addition, a doubling of these bands was observed and interpreted as arising from the double minimum character of the potential. Analysis of these bands yielded a value for the rotational constant A of about 9 cm^{-1}.

This investigation was undertaken to provide further confirmation for the nonplanar structure of the molecule and to determine values for the barrier height and molecular parameters.

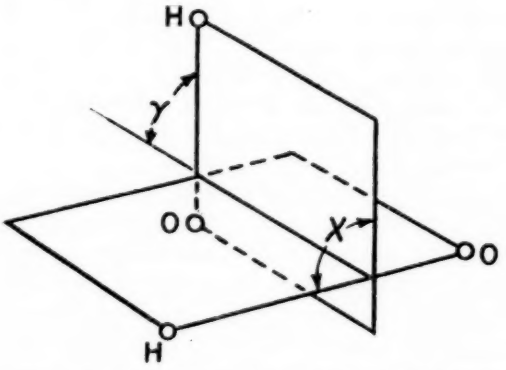

FIG. 1. Nonplanar molecular model for H_2O_2.

EXPERIMENTAL

The spectrometer used in this work was the standard Hughes-Wilson Stark modulated type. The Stark modulation was either a square wave voltage or a variable dc voltage plus a small ac sinusoidal modulation voltage at 100 kc/sec. The absorption cell was a 10-foot section of X-band RG 67/U wave guide.

Owing to the reactivity of H_2O_2 and the relatively large surface-to-volume ratio of the absorption cell, it was felt that some precautions were necessary to insure that a usable sample could be obtained for study. Based upon information concerning peroxide in the liquid state, the Stark cell was designed solely of aluminum and Teflon except for the mica windows, and the stopcock grease used was a fluorinated hydrocarbon. It was felt that these materials would allow minimum decomposition of H_2O_2 in the vapor state. Further, the inlet and outlet tubes to the cell were low copper content aluminum tubing, welded to the wave guide. Before assembling the

[11] G. Herzberg, *Infrared and Raman Spectra* (D. Van Nostrand Company, Inc., New York, 1945), p. 301.

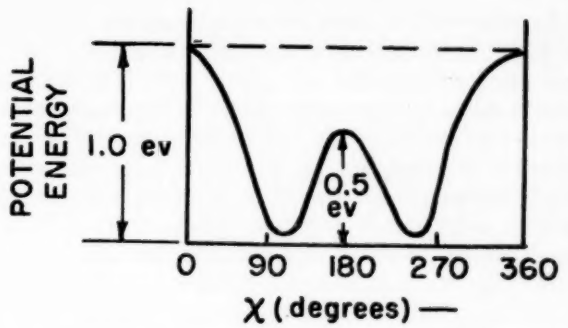

FIG. 2. Variation of potential energy with the angle χ for the model of Fig. 1.

absorption cell, the wave guide and Stark electrode were thoroughly washed numerous times with the following sequence of solutions: (1) sodium hydroxide in alcohol-water solution, (2) distilled water, (3) absolute ethanol. It was felt that this procedure removed all traces of grease and dirt.

A preliminary search of most of the frequency region from 21 000 Mc/sec to 36 000 Mc/sec using standard sampling techniques failed to reveal any absorption lines. This strengthened our belief that because of rapid decomposition of H_2O_2 at low vapor pressures in a metal system with a large surface-to-volume ratio it would be difficult, if not impossible, to observe the microwave absorption spectrum using standard microwave spectrometer sampling methods.

A continuous flow sampling system as shown in Fig. 3 was then devised. The sample of H_2O_2 was placed in a Pyrex glass sample tube which was immersed in a dry ice-acetone bath. The other end of the absorption cell was connected through a stopcock and vapor trap to a mechanical vacuum forepump. The sample tube was carefully cleaned with sodium hydroxide in an alcohol-water solution and rinsed thoroughly with distilled water before each use. The partial pressure of H_2O_2 in the absorption cell was controlled by maintaining the dry ice-acetone bath at the desired temperature. It was found that the temperature could be held to ± 1°C if the bath reservoir were large.

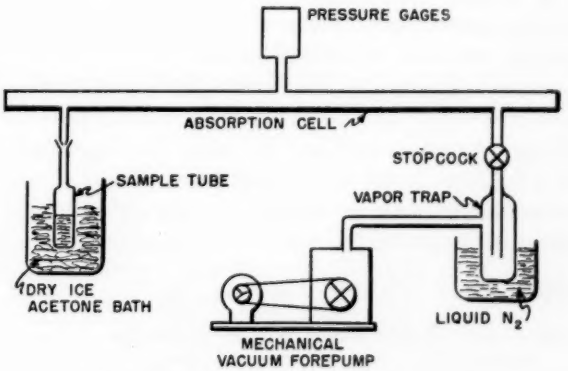

FIG. 3. Continuous flow sampling system.

In order to determine optimum sampling conditions with the continuous flow system, a series of carefully controlled experiments was conducted. The technique used in this study was as follows. A known mass, usually two to four grams, of H_2O_2 of known concentration was placed in the sample tube, and the temperature of the dry ice-acetone bath was then adjusted to secure the desired total vapor pressure. With the mechanical forepump on the outlet end of the system and with the vapor trap in a bath of liquid nitrogen, the peroxide was allowed to distill through the absorption cell and into the vapor trap. After a sufficient time (4 to 36 hours) which was determined by the necessity to trap an adequate sample, the vapor trap was removed and its contents analyzed for peroxide by the permanganate method.[12] The total vapor pressure range studied was from 10^{-2} mm Hg to 4 mm Hg.

By means of the above controlled experiments the percentage decomposition of H_2O_2 was studied as a function of total vapor pressure in the absorption cell. It was found that the amount of decomposition varied from about two percent at 4 mm Hg total vapor pressure to nearly 70 percent at 10^{-2} mm Hg total vapor pressure. These data together with the knowledge that the original sample contained about 95 percent by weight of H_2O_2 sufficed to substantiate the belief that at 10^{-2} mm Hg total vapor pressure, the amount of peroxide in the absorption cell was insufficient to permit observation of the absorption lines. Since an increase in vapor pressure results in line broadening, it was realized that a compromise must be made between vapor pressure and peroxide content in the absorption cell. An examination of the data resulted in a choice of 0.1 mm Hg as the optimum vapor pressure to use while searching for H_2O_2 absorption lines. On resuming the search, nine H_2O_2 and some one hundred D_2O_2 and HDO_2 absorption lines were discovered in the frequency region from about 9000 Mc/sec to 40 000 Mc/sec. At this pressure, however, the line widths were several Mc/sec. This made a detailed study of the Stark spectrum unusually difficult and limited the accuracy in frequency readings to ± 0.2 Mc/sec. This is, of course, not as good as normally secured in the microwave region.

A summary of the experimental microwave data on H_2O_2 is presented in Table I with some notations concerning ΔJ and J^* as obtained from the Stark data. Equations presenting the Stark splitting versus ϵ^2 for four of the lines are shown below. It was not possible to determine J^* unambiguously from the experimental data for lines 3 and 4, and as a result several equations are presented with the minimum allowable value of J^* corresponding to each.

Line 1 $\Delta\nu = 29.09\epsilon^2 \times 10^{-6}$ Mc/sec

Line 2 $\Delta\nu = (6.88 - 4.25m^2)\epsilon^2 \times 10^{-6}$ Mc/sec

Line 3 $\Delta\nu = (5.65 - 0.0874m^2)\epsilon^2 \times 10^{-6}$ Mc/sec $(J^* \geqq 8)$

$\Delta\nu = (6.07 - 0.0727m^2)\epsilon^2 \times 10^{-6}$ Mc/sec $(J^* \geqq 9)$

$\Delta\nu = (6.47 - 0.0623m^2)\epsilon^2 \times 10^{-6}$ Mc/sec $(J^* \geqq 10)$

Line 4 $\Delta\nu = (4.18 - 0.0537m^2)\epsilon^2 \times 10^{-6}$ Mc/sec $(J^* \geqq 8)$

$\Delta\nu = (4.49 - 0.0459m^2)\epsilon^2 \times 10^{-6}$ Mc/sec $(J^* \geqq 9)$

$\Delta\nu = (5.10 - 0.0356m^2)\epsilon^2 \times 10^{-6}$ Mc/sec $(J^* 1 \geqq 0)$,

where ϵ is in volts per cm and J^* is the larger of the two quantum numbers involved in the transition.

During the experimental phase of the problem, studies were made of the deuterated species, HDO_2 and D_2O_2. More than one hundred absorption lines were observed in the region 0.30 cm^{-1} to 1.34 cm^{-1}. A qualitative study of the Stark effect was made which revealed two points of interest. First, the Stark splitting and resolution were such as to indicate that quantitative Stark data could be obtained for about twenty-five of the lines. Secondly, transitions of the $|\Delta J| = 0$ type were present as well as those of $|\Delta J| = 1$ type.

Additional study of the data was made in an effort to determine if a series of lines, such as those found for methyl alcohol,[13] was present for the isotopic species. Such a series was not found, and the results of the present analysis indicate that this series for D_2O_2 would fall between 1.34 cm^{-1} and 1.67 cm^{-1}.

During the course of the experiments, an attempt was made to classify these lines according to their isotopic species. This attempt was unsuccessful for two reasons. First, the sample contained both HDO_2 and D_2O_2. This was established by a mass spectrographic analysis which revealed that the ratio of D_2O_2 to HDO_2 in the sample was about three to one. Secondly, concentration tests depend so critically on absorption cell contamination[14] that the application of this method led to unreliable results. Accordingly, the use of these data must await a method of isotopic assignment. It is hoped that this assignment may be made from a study of the Zeeman splitting.[15]

DISCUSSION OF THE MAIN FEATURES OF THE MICROWAVE SPECTRUM

In order to obtain a first approximation to the rotational spectrum of H_2O_2, the molecule will be assumed to be a symmetric top with the following values for the molecular parameters: O—O distance = 1.48A, $\gamma = 78°$, $\chi = 106°$, and an OH distance of 0.98A.[9] Calculations based on these parameters indicate that the top is only slightly asymmetric and, in fact, for a value of χ of 90° may be very nearly accidentally symmetric. The moments of inertia are $I_A = 2.81 \times 10^{-40}$ g cm^2 and $I_B = I_C = 33.7 \times 10^{-40}$ g cm^2 with the corresponding

[12] *Scott's Standard Methods of Chemical Analysis* (D. Van Nostrand Company, Inc., New York, 1939), Vol. 2, p. 2181.

[13] Hughes, Good, and Coles, Phys. Rev. **84**, 418 (1951).

[14] Jen, Bianco, and Massey, J. Chem. Phys. **21**, 520 (1953).

[15] C. K. Jen, Phys. Rev. **81**, 197 (1951).

rotational constants

$$A=\frac{h}{2(2\pi)^2c}\frac{1}{I_A}=9.96\ \text{cm}^{-1}$$

and

$$B=\frac{h}{2(2\pi)^2c}\frac{1}{I_B}=0.831\ \text{cm}^{-1},$$

where c is the velocity of light and h is Planck's constant. The term values of the symmetric top are represented by the formula

$$W_1=BJ(J+1)+(A-B)K^2,$$

where J and K are the usual quantum numbers. It is clear from the model of Fig. 1 that the C_2 axis is a principal axis and that the permanent dipole moment lies along this axis. As a result the selection rules require that $\Delta J=0,\ \pm1$ and $\Delta K=\pm1$. These selection rules allow only the transitions $J, K=0, 0\rightarrow1, 1$ and $1, 0\rightarrow1, 1$ (expressed as absorption lines) to explain line 1 of Table I. However, an examination of the energy level structure indicates that these transitions are of the order of nine to eleven wave numbers and consequently would not have been observed in the microwave region covered experimentally. Taking the actual asymmetry of the molecule into account does not change this argument. It is necessary, therefore, to investigate the possibility of hindered internal rotation in order to see if a rearrangement of the energy levels is brought about which will satisfactorily explain the observed spectrum.

Since the experimental data indicate that the change in the term values necessary to allow lines 1 and 2 is large, the effect of the hindered internal rotation may hardly be considered as a small perturbation. As a result certain simplifying assumptions will be made in order to obtain a wave equation which may be solved exactly. Similar assumptions have been used, with some success, by Koehler and Dennison[16] in an analysis of the methyl alcohol molecule. These assumptions are:

1. The H_2O_2 molecule will be assumed to be a symmetric top. This should suffice for an investigation of the main effects of hindered internal rotation upon the microwave spectrum since the top can be, at most, only very slightly asymmetric.

2. The molecule will be taken as rigid except for the hindered internal motion. This assumption should be good if the internal oscillation frequency is much lower than the next lowest vibrational mode so that the two are far out of resonance. The O—O vibration frequency is approximately 900 cm^{-1}. Since the large splitting required necessitates a rather low barrier, the torsional oscillation frequency should be small. This assumption is probably valid as will be brought out later.

3. The hindering potential will be assumed to be sinusoidal in form and will be represented by the equation

$$V=\frac{H}{2}(1+\cos2\chi).$$

If the potential deviates from this form in the manner predicted by Penny and Sutherland (see Fig. 2), it is possible that this effect could be studied by perturbation theory.

[16] J. S. Koehler and D. M. Dennison, Phys. Rev. **57**, 1006 (1940).

TABLE I. Microwave spectrum of H_2O_2.

Line	Frequency Mc/sec	Remarks
1	14 829.5±0.2	quadratic Stark effect $J^*=1$
2	37 517.6±0.2	quadratic Stark effect $J^*=2$
3	22 054.5±0.2	quadratic Stark effect $J_{\min}{}^*=7,\ \lvert\Delta J\rvert=1$
4	27 639.6±0.2	quadratic Stark effect $J_{\min}{}^*=7,\ \lvert\Delta J\rvert=1$
5	11 072.4±0.5	quadratic Stark effect probably high J
6	35 916±2	quadratic Stark effect high $J,\ \lvert\Delta J\rvert=1$
7	39 033±2	probably high J
8	39 495±2	probably high J
9	39 760±2	probably high J

All of these lines are of medium or strong intensity except lines 5, 6 and 7 which are relatively weak.

The analysis, based on these assumptions, will proceed along the same lines as for methyl alcohol. The expression for the kinetic energy is written down in an appropriate coordinate system and the Schrödinger wave equation is obtained in the usual manner. With an appropriate change of variable the equation is separable and results in the usual symmetric top rotation wave equation and the equation which describes the internal motion which is

$$\frac{d^2P}{d\chi^2}+[R-2\alpha\cos2\chi]P=0,$$

where

$$R=\frac{C}{\hbar^2}\left[W_2-\frac{H}{2}\right],$$

$$2\alpha=\frac{C}{\hbar^2}\frac{H}{2}$$

and

$$W=W_1+W_2,$$

where W_1 is the usual symmetric top energy. In this procedure the only changes from the Koehler and Dennison case are that $C_1=C_2=C=I_A/2$ and the potential is double minimum instead of triple minimum. The solution of this equation is

$$P(\chi)=e^{i\sigma\chi}\sum_{r=-\infty}^{+\infty}a_re^{ir\chi}\quad\text{where}\quad\sigma=-\frac{K}{2}$$

and the resulting expressions for the characteristic values, R, are equalities of infinite continued fractions which, however, converge rapidly enough to make computation feasible.‡ Therefore, R, and consequently

‡ There are some tables of characteristic values of the Mathieu equation for $K=0$ in the literature. The most comprehensive of these is *Tables Relating to Mathieu Functions, NBS* (Columbia University Press, New York, 1951).

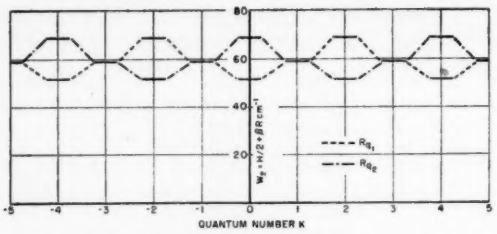

FIG. 4. Variation of W_2 with the quantum number K for the ground vibrational state ($n=0$).

W_2, is a function of the quantum number K, this being the connection between the internal motion and the usual rotation. In order to illustrate the effect of the internal motion the expression $W_2=H/2+\beta R$ where $\beta=\hbar^2/C$ is plotted in Fig. 4 as a function of K for a low barrier height. In Fig. 5, W_2 is plotted as a function of barrier height for $K=0$ and 1. Both of the above figures are for the ground vibrational state. In Fig. 6 is shown a curve of W_2 *vs* H for somewhat larger barrier heights and for $n=0$ and 1. It is seen that the symmetrical barrier used does not remove the degeneracy of the odd K levels, whereas the even K levels are widely split, and the splitting of the even K levels about the odd K levels is unsymmetrical, at least, for low barriers. The amount of splitting increases with decreasing barrier height and also with higher vibrational state as would be expected. It is desirable, as indicated in Fig. 5, to label the two types of levels by the quantities q_1 and q_2.

It can be seen from Fig. 5 that a sufficiently low value of the barrier height will produce the splitting necessary to explain the observed absorption lines 1 and 2 of Table I. These lines were assigned to the ground vibrational state because if assigned to the first or higher excited states, the splitting of the ground state will be very small and rotational transitions should have appeared which were not observed.

The selection rules for this molecular model are

$$\Delta J=0,\ \pm1$$
$$\Delta m=0,\ \pm1$$
$$\Delta K=\pm1$$
$$q_1\rightarrow q_1 \text{ or } q_2$$
$$q_2\rightarrow q_1 \text{ or } q_2.$$

These selection rules allow the following two transitions as possibilities to explain line 1 of Table I

$$J,\ |K|,\ q=1,\ 0,\ q_2\rightarrow 1,\ 1,\ q_1 \text{ or } q_2$$
$$J,\ |K|,\ q=0,\ 0,\ q_2\rightarrow 1,\ 1,\ q_1 \text{ or } q_2.$$

The first of these possibilities was not allowed because, in this case, the transitions

2, 0, $q_2\rightarrow$2, 1, q (where q represents q_1 and/or q_2)
3, 0, $q_2\rightarrow$3, 1, q
etc.

should also be observed, as in the case of methyl alcohol,[13,17] and such a series of lines was not observed experimentally. Thus, line 1 is assigned as follows (expressed as an absorption line)

$$1,\ 1,\ q\rightarrow 0,\ 0,\ q_2.$$

This order is necessary so that line 2 will fall within the microwave region as

$$1,\ 0,\ q_2\rightarrow 2,\ 1,\ q.$$

An examination of the term values illustrates explicitly how these transitions are brought about. From the expression for the energy

$$W=W_1+W_2=BJ(J+1)+GK^2+\frac{H}{2}+\frac{\hbar^2}{C}R,$$

where $G=(A-B)$, we obtain

$$W(0,\ 0,\ q_2)=\frac{H}{2}+\frac{\hbar^2}{C}R_{0,\,q_2},$$

$$W(1,\ 1,\ q)=2B+G+\frac{H}{2}+\frac{\hbar^2}{C}R_{1,\,q},$$

then

$$\nu(1,\ 1,\ q\rightarrow 0,\ 0,\ q_2)=\frac{\hbar^2}{C}(R_{0,\,q_2}-R_{1,\,q})$$
$$-2B-G=\Delta_2-2B-G,$$

where the subscripts on R indicate $R_{K,\,q}$ and Δ_2 is the splitting of the $K=0$, q_2 state relative to the $K=1$, q state. Similarly,

$$\nu(1,\ 0,\ q_2\rightarrow 2,\ 1,\ q)=4B+G-\Delta_2.$$

It is seen that in each case the hindered internal rotation term must shift the $K=0$ levels relative to the $K=1$ levels by a sufficient amount to bring these transitions within the microwave region. Further examination of the energy level structure reveals that other pairs of transitions such as these occur for higher J and K values. The pair which will arise as transitions between

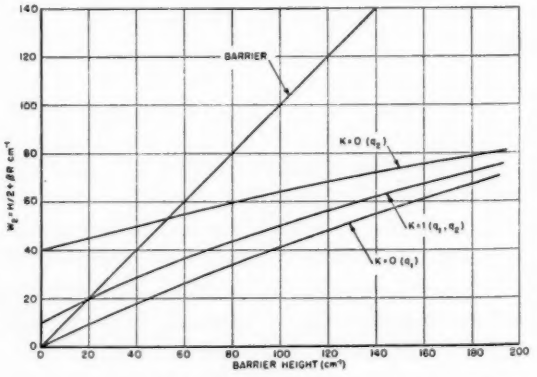

FIG. 5. Internal oscillation energy *vs* barrier height for the ground ($n=0$) state.

[17] D. G. Burkhard and D. M. Dennison, Phys. Rev. 84, 408 (1951).

the next lowest term values of the energy level table are

$$J, K, q=J+1, 0, q_1 \rightarrow J, 1, q$$
$$J, K, q=J+1, 1, q \rightarrow J+2, 0, q_1.$$

For the symmetric top approximation used here, the sum of the transition frequencies of the members of each pair is equal to $2B$.

Some thought may now be given to the possibility of obtaining an approximation for the rotational constants and an approximate value for the barrier height. From the assignments of lines 1 and 2 it is found that

$$\nu(1, 1, q \rightarrow 0, 0, q_2)+\nu(1, 0, q_2 \rightarrow 2, 1, q)=2B$$

and

$$\nu(1, 0, q_2 \rightarrow 2, 1, q)-\nu(1, 1, q \rightarrow 0, 0, q_2)=6B+2G-2\Delta_2.$$

Substituting the values from the experimental data gives

$$B=0.8725 \text{ cm}^{-1}$$

and

$$\Delta_2-G=2.2394 \text{ cm}^{-1}.$$

From a study of the Stark data, lines 3 and 4 were assigned as the pair of transitions

$$J+1, 0, q_1 \rightarrow J, 1, q$$
$$J+1, 1, q \rightarrow J+2, 0, q_1.$$

Substitution of the experimental data yields

$$B=0.8283 \text{ cm}^{-1}$$

and

$$\Delta_1+G=1.6565J+2.3917,$$

where the value $B=0.8283$ is used in computing the expression for Δ_1+G and Δ_1 is the splitting of the $K=0, q_1$ levels with respect to the $K=1, q$ levels. These results, together with analytic approximations of the R *vs* α curves may be used to obtain corresponding values of H and I_A for this model. The results are shown

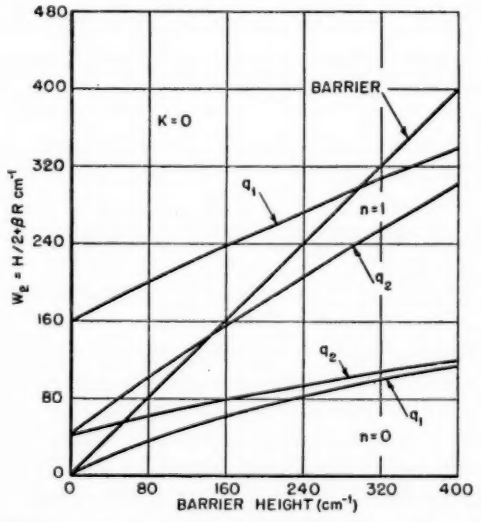

FIG. 6. Internal oscillation energy *vs* barrier height for $n=0$ and 1.

TABLE II.

J	α	H cm^{-1}	G cm^{-1}	$I_A \times 10^{40}$ g cm^2
7	0.697	111	7.600	3.304
8	0.708	113	8.587	2.959
9	0.720	115	9.561	2.675

in Table II. A study of the variation of I_A with γ and χ indicates that the most likely value of J is 8 and that the two higher J absorption lines may be assigned as follows.

Line 3 $\quad 9, 0, q_1 \rightarrow 8, 1, q$

Line 4 $\quad 9, 1, q \rightarrow 10, 0, q_1.$

It has been mentioned that the microwave lines occur in pairs such that the sum of the two transition frequencies is equal to $2B$. The lines five through nine of Table I may be accounted for in the following manner. From a study of the Stark effect it is probable that lines 5 and 6 form such a pair with $B=0.783$. Lines 7 through 9 are all near the high end of the microwave region searched and probably each is one member of such a pair, the other member being below the low end of the region covered. It is unlikely that any of these lines arise from excited torsional states since in these states the molecule is undergoing free (or slightly hindered) rotation. The two *OH* bars are spinning around rapidly and with such a motion the permanent electric dipole moment would become small. Calculation indicates that the line intensities would, for the excited state, be down by factors of 25 or more.

The three different values of B that were obtained from the experimental data are not explained by this model. There are several possible explanations. First, there is centrifugal distortion which makes B dependent upon J. Secondly, the effect of centrifugal distortion may alter the angle γ sufficiently to change the barrier height, thus making the splitting due to hindered internal rotation depend on J. Thirdly, the probable slight asymmetry of the molecule and the presence of a small product of inertia (unless $\gamma=0°$, 90°, or 180°) may produce perturbing elements in the Hamiltonian which will cause the effective B-value to depend on J as for methyl alcohol. It is likely that all of these effects will cause corrections to B that vary either as (J^2+J) or $(J^2+J)^2$. If so, the perturbing effect is less for the lower J values and the value $B=0.8725$ is likely close to the correct value. Interpreting this in the light of the molecular model with the O—O distance=1.48A and the OH distance=0.98A would mean that the angle, γ, must be close to 90° instead of the 78° as previously chosen. This also gives reasonable agreement for the small moment of inertia.

THE STARK EFFECT

The matrix elements for the Stark effect were derived for this model in order to determine the effect of hindered internal rotation. The evaluation of these

TABLE III. Dipole moments and ratios of B to A in the expression $\Delta\nu=(A-Bm^2)\epsilon^2$.

Line	Dipole moment μ debye units	Experimental B/A	Calculated B/A
1	2.26	—	−0.989
2	2.26	−0.618	−0.613
3	2.17	−0.0120	−0.0119
4	2.07	−0.0102	−0.0103

matrix elements indicated that the effect of the internal motion alters the value of the permanent dipole moment to be used depending upon whether the state under consideration was of q_1 or q_2 type. As a result, the actual numerical work was completed using the results already in the literature[18,19] taking care to use one-half the line strength since the inversion degeneracy has been removed for this case. The results are for $\Delta m=0$:

Line 1 $\Delta\nu=\mu^2\epsilon^2[5.70-5.64m^2]\times10^{-6}$ Mc/sec

Line 2 $\Delta\nu=\mu^2\epsilon^2[1.34-0.822m^2]\times10^{-6}$ Mc/sec

Line 3 $\Delta\nu=\mu^2\epsilon^2[1.29-0.0153m^2]\times10^{-6}$ Mc/sec

Line 4 $\Delta\nu=\mu^2\epsilon^2[1.05-0.0108m^2]\times10^{-6}$ Mc/sec

where the values for H and G for the case $J=8$ of Table II were used to calculate the energy differences not available from the experimental data.

It is necessary to compare these calculated results with the experimental data. For lines 1 and 2 there is no problem. For lines 3 and 4 the ratio of B/A in the expression $\Delta\nu=(A-Bm^2)\epsilon^2$ is to be used as a criterion of agreement with the experimental data. This criterion is best met by the following experimental equations for lines 3 and 4.

Line 3 $\Delta\nu=(6.07-0.0727m^2)\epsilon^2\times10^{-6}$ Mc/sec $(J^*\geqq9)$

Line 4 $\Delta\nu=(4.49-0.0459m^2)\epsilon^2\times10^{-6}$ Mc/sec $(J^*\geqq9)$.

The results of these calculations are presented in Table III along with the values of dipole moment obtained. Two points should be noted (1) the values of dipole moment agree favorably with the value of 2.13 debye units obtained by Linton and Maass from measurements on liquid solutions of H_2O_2 in dioxane, (2) the values of J^* for lines 3 and 4 obtained from the experimental data do not violate the assignments previously made from the theory as shown following Table II.

The approximate theory as developed here seems to explain the principal features of the microwave spectrum of H_2O_2. Further work is under way to complete the assignment of the observed microwave lines of HDO_2 and D_2O_2 to the proper isotopic species and to extend the frequency coverage in order to observe the series of D_2O_2 lines discussed previously. It is hoped that this work will allow determination of the details of the molecular model by the development of a less approximate theory.

ACKNOWLEDGMENTS

The authors wish to express their appreciation to their colleagues Dr. F. T. McClure, Dr. C. K. Jen, Dr. S. N. Foner, Dr. C. E. Feazel, and Mr. J. W. B. Barghausen for valuable assistance, and to Professor G. H. Dieke of the Physics Department for continued encouragement and stimulating discussions. Particular appreciation is due Miss K. Pace for her computational assistance. The samples of H_2O_2 used were supplied by the Buffalo Electrochemical Company, and the sample of D_2O_2 was supplied by Professor P. A. Giguère of Laval University. The latter sample was prepared by Mr. E. Anthony Secco.

[18] S. Golden and E. B. Wilson, J. Chem. Phys. **16**, 669 (1948).
[19] Cross, Hainer, and King, J. Chem. Phys. **12**, 210 (1944).

Ionic Components of Charge in the Electrical Double Layer

DAVID C. GRAHAME AND BARBARA A. SODERBERG
Department of Chemistry, Amherst College, Amherst, Massachusetts
(Received July 24, 1953)

The rate of change with concentration of the capacity of the electrical double layer on mercury has been measured. From this there have been calculated Γ_+, the excess of cations in the double layer, and Γ_-, the excess of anions. The latter has been subdivided into η_-^d, the excess of anions in the *diffuse* double layer, and η_-^i, the excess of anions in the inner part of the double layer. From these data it has also been possible to evaluate ψ^0, the potential of the outer Helmholtz plane.

It is found that fluoride ion remains unadsorbed on mercury at all potentials investigated, including potentials anodic to the e.c.max. Other anions are strongly adsorbed (chemisorbed) when the mercury is positively charged, and sometimes even when it is negatively charged. The "hump" in the capacity curves of salts of such anions as chloride, bromide, acetate, and nitrate, are found to be present in curves of C_-, the capacity attributable to anions alone. No chemisorption of monatomic cations could be detected.

The kinetic theory of the diffuse double layer with constant dielectric constant is found to fit the experimental results within the expected accuracy. This fit extends to electrolytes of the 1:2 and 2:1 types also.

A new method of evaluating salt adsorption at the potential of the electrocapillary maximum (e.c.max.) is described and results are given. Likewise a new method of determining C_+ at the e.c.max. is described and used.

INTRODUCTION

IT is possible by thermodynamic means to ascertain not only the charge on a mercury surface in contact with an inert electrolyte, but also the ionic components of that charge in the solution. These components, called Γ_+ and Γ_-, are the excess of cations or anions actually present over what would be present in a column of solution of unit cross section extending from the interface (assumed planar) into the interior of the solution, calculated on the assumption of no change of concentration at the interface. In brief, Γ_+ is the excess of cations in unit area of the electrical double layer, and Γ_- is the excess of anions.

The present paper is concerned with the evaluation of Γ_+ and Γ_- at the interface between mercury and an aqueous solution of various inert electrolytes such as potassium chloride or potassium nitrate. This has been done by the use of differential capacity measurements in a manner to be explained below. The results are of interest in that they provide a more detailed picture of the electrical double layer than had been obtained otherwise. In particular they provide quantitative data in support of concepts which had previously been understood only qualitatively.

The actual values of Γ_+ and Γ_- will depend upon one's choice of a boundary to represent the interface. It is convenient to let $\Gamma_{\text{solvent}}=0$, which amounts to fixing the boundary at a position such that the actual amount of solvent per square centimeter of interface equals that calculated on the assumption that all of the solvent (with its ordinary bulk concentration) lies on the solution side of the selected boundary, and none on the other. There is no theoretical advantage to be gained by setting Γ_{solvent} equal to anything different from zero, since it is only a problem in stoichiometry to convert values of Γ_+ and Γ_- obtained with one value of Γ_{solvent} to the corresponding values for any other value.[1] In what follows Γ_{solvent} is always set equal to zero. This obviously puts the selected boundary very close to the interface and gives rise to values of Γ_+ and Γ_- which have simple and exact thermodynamic meaning.

If the radius of curvature of the interface becomes comparable to the half-thickness of the electrical double layer, the interface cannot be regarded as planar and the theoretical treatment which follows would need to be modified. This complication does not arise in the experiments we are about to describe.

One of us (D.C.G.)[1] has computed Γ_+ for $0.3N$ NaCl using Gouy's electrocapillary data[2] for 0.1 and $1.0N$ solutions of that salt. This is not a very satisfactory procedure because the concentration difference is too great and the data are too sparse. The results are nevertheless in good agreement with those obtained by a method employing capacity data taken at the same two concentrations, and these results have already been presented.[1] An improved version of that method is described below. The necessary theory will be presented first.

THERMODYNAMIC PRELIMINARIES

The definitions, symbols, and sign conventions to be employed will be those already discussed in reference 1. The basic equations to be employed are[3]

$$\nu_+(\partial\sigma/\partial\mu)_{E^-} = -\Gamma_+, \tag{1}$$

$$\nu_-(\partial\sigma/\partial\mu)_{E^+} = -\Gamma_-, \tag{2}$$

where σ is the interfacial tension of a liquid metal in contact with an inert electrolyte, μ is the chemical potential of the electrolyte, $\nu_+(\nu_-)$ is the number of cations (anions) formed by the dissociation of one molecule of the electrolyte, and the subscript E^- denotes that the potential between the phases is to be

[1] D. C. Grahame, Chem. Revs. 41, 441 (1947).

[2] G. Guoy, Ann. chim. et phys. [7] 29, 145 (1903).

[3] Reference 1, Eq. 22.

maintained constant as measured in the ordinary way relative to an electrode reversible to the anion of the electrolyte in question. It is important to understand that the composition of the electrolyte in the reference electrode changes along with that of the solution under test, so that no liquid junctions arise, and that what is to be held constant is the relative potential of two pieces of wire of the same material, one attached to the reference electrode and one to the metallic phase under test.

Γ_+ and Γ_- are related through the equation

$$z_+\Gamma_+F+z_-\Gamma_-F=-q, \tag{3}$$

where z_+ is the "valence" of the cation, z_- that of the anion, including sign, and q is the surface charge density on the metallic phase. It is given in all cases by the Lippmann equation, namely,[4]

$$(\partial\sigma/\partial E)_\mu=-q \quad [=(\partial\sigma/\partial E^-)_\mu]. \tag{4}$$

Differentiation of Eq. (1) with respect to E^- at constant μ gives

$$\nu_+(\partial^2\sigma/\partial\mu\partial E^-)=-(\partial\Gamma_+/\partial E)_\mu. \tag{5}$$

The quantity on the right is proportional to what we propose to call C_+, which is that part of the total capacity attributable to the approach or departure of cations from the interface when the over-all potential is changed slightly. In order to keep C_+ a capacity in ordinary electrical units, we write

$$z_+F(\partial\Gamma_+/\partial E)_\mu=-C_+. \tag{6}$$

From Eqs. (4), (5), and (6)

$$z_+\nu_+F(\partial q/\partial\mu)_{E^-}=-C_+. \tag{7}$$

In a like manner, starting with Eq. (2)

$$\nu_-(\partial^2\sigma/\partial\mu\partial E^+)=-(\partial\Gamma_-/\partial E)_\mu=C_-/z_-F, \tag{8}$$

where we have let

$$C_-=-z_-F(\partial\Gamma_-/\partial E)_\mu. \tag{9}$$

Then from Eq. (4)

$$z_-\nu_-F(\partial q/\partial\mu)_{E^+}=-C_-. \tag{10}$$

By differentiation of Eq. (3)

$$(\partial q/\partial E)_\mu+z_+F(\partial\Gamma_+/\partial E)_\mu+z_-F(\partial\Gamma_-/\partial E)_\mu=0 \tag{11}$$

and

$$C-C_+-C_-=0, \tag{12}$$

a result to be expected in view of the significance of C_+ and C_- stated above.

Differentiating Eq. (7) with respect to E^- at constant μ gives

$$z_+\nu_+F(\partial^2q/\partial\mu\partial E^-)=-dC_+/dE. \tag{13}[5]$$

The ordinary differential capacity is defined as

$$C=dq/dE \quad [=dq/dE^-], \tag{14}$$

where the constancy of chemical potential is to be understood. Then with Eq. (13)

$$z_+\nu_+F(\partial C/\partial\mu)_{E^-}=-dC_+/dE. \tag{15}$$

In the same manner, starting with Eq. (10),

$$z_-\nu_-F(\partial C/\partial\mu)_{E^+}=-dC_-/dE. \tag{16}$$

These equations have the useful property that their left-hand members can be evaluated experimentally, thus giving entree to the calculation of dC_+/dE, C_+, Γ_+, and the corresponding quantities for anions.

Although dC_+/dE is of some interest on its own account, C_+ and Γ_+ are quantities easier to visualize, and it is therefore desirable to be able to calculate them. This can be done by integration, supposing $(\partial C/\partial\mu)_{E^-}$ known from experiment, the only complication being in the determination of the constants of integration. Thus

$$C_+=\int(dC_+/dE)dE+k \tag{17}$$

and

$$z_+F\Gamma_+=-\int C_+dE+k'. \tag{18}$$

The actual values of k and of k', of course, depend upon where one chooses to begin the evaluation of the definite integrals. When we speak of evaluating k or k', therefore, we shall usually mean nothing more than an evaluation of some one value of C_+ or of Γ_+.

The constant k may be obtained from a study of the rate of change with chemical potential of the potential of the electrocapillary maximum (e.c.max.) as follows: From Eq. (7)

$$z_+\nu_+F(\partial q/\partial E^-)_\mu(\partial E^-/\partial\mu)_q=C_+ \tag{19}$$

or from Eq. (14)

$$z_+\nu_+FC(\partial E^-/\partial\mu)_q=C_+. \tag{20}$$

At the potential of the e.c.max. q is zero and therefore constant. Hence one can write from Eq. (20),

$$z_+\nu_+FC^{\text{e.c.max.}}(\partial E^-/\partial\mu)^{\text{e.c.max.}}=C_+^{\text{e.c.max.}}, \tag{21}$$

and as the equation shows, a measurement of $\partial E^-/\partial\mu$ at the potential of the e.c.max. provides means for the calculation of $C_+^{\text{e.c.max.}}$ and hence, in effect, of the k in Eq. (17). It will be noted that this is a purely thermodynamic procedure, by contrast with another method to be presented below.

For the evaluation of k' by purely thermodynamic means, one must resort to electrocapillary measurements. The equation needed is[6]

$$(\partial\sigma/\partial\mu)^{\text{e.c.max.}}=-\Gamma_{\text{salt}}^{\text{e.c.max.}}=-\Gamma_+^{\text{e.c.max.}}/\nu_+=-\Gamma_-^{\text{e.c.max.}}/\nu_-, \tag{22}$$

[4] G. Lippmann, Ann. chim. et phys. [5] 5, 494 (1875).

[5] The constancy of μ in the expressions dC_+/dE and dC_-/dE is to be understood.

[6] Reference 1, Eqs. (20) and (21).

where $\Gamma_{salt}^{e.c.max.}$ is the superficial excess of the salt itself at the potential of the e.c.max. This symbol is appropriate because the anion and cation excesses are equivalent at this potential. The evaluation of $\Gamma_{salt}^{e.c.max.}$ through Eq. (22) provides a value of k' because it provides a value of Γ_+ at one potential. An alternative method of evaluating $\Gamma_{salt}^{e.c.max.}$ (and therefore k') will be presented below. This alternative method is nonthermodynamic in character because it employs certain results of the kinetic theory of the diffuse double layer. In the opinion of the authors this alternative method is far more exact than any experimental data with which it is every likely to be used, however, so that for all practical purposes it may be considered to be exact.

An entirely analogous situation exists with respect to the constant of integration k. C_+ can be obtained at the potential of the e.c.max. as already explained. But an alternative method of finding a value of C_+ (and therefore k) exists which uses chiefly the theory of the diffuse double layer. This method will be explained in the next section. For the present it will suffice to note that both k and k' can be determined by two methods, one thermodynamic and one based upon the theory of the diffuse double layer.

DIFFUSE DOUBLE LAYER THEORY

The kinetic theory of the diffuse double layer has already been presented in considerable detail,[1,7] and it only remains to be shown how the results can be applied to the present investigation. The object of this introduction of diffuse double layer theory is twofold. In the first place, diffuse double layer theory provides values of k and k', as stated above. In the second place it proves to be possible to compare certain of our experimental results with diffuse double layer theory, and this comparison serves at once as a check on the theory and provides direct information as to the presence or absence of specific adsorption of anions at any given potential.

Most of the equations which are of interest for these purposes have already been presented.[7] For purposes of illustration three will be cited. These are Eqs. (59), (61), and (63), respectively, in reference 7,[8]

$$\eta_+^d = A[v+(1+v^2)^{\frac{1}{2}}-1], \quad (1:1) \quad (23)$$

$$C_+^{de} = \frac{C^{de}}{2}\left[1+\frac{v}{(1+v^2)^{\frac{1}{2}}}\right], \quad (1:1) \quad (24)$$

$$\frac{dC_+^{de}}{dE} = \frac{C^{de}}{2(1+v^2)^{\frac{1}{2}}}\left[[(1+v^2)^{\frac{1}{2}}+v]\frac{dC^{de}}{C^{de}dE} - \frac{C^{de}}{2A(1+v^2)}\right]. \quad (1:1) \quad (25)$$

In these equations C^{de} is the differential capacity given by $d\eta^d/dE$, where η^d is the charge of the *diffuse* double layer only and E is the whole potential difference across the interface (not the potential across the diffuse double layer). Thus C^{de} is that part of the measured capacity attributable to the diffuse double layer alone. Similarly C_+^{de} is $d\eta_+^d/dE$, and is that part of the measured capacity attributable to cations in the diffuse double layer alone. v is $\eta^d/2A$, where

$$A = +(DD_0kTn_{0i}/2\pi)^{\frac{1}{2}}. \quad (26)$$

D is the dielectric constant, D_0 is a constant equal to 1.1128×10^{-12} coulomb-volt^{-1}–cm^{-1}, k is Boltzmann's constant, and n_{0i} is the number of ions of one kind per cm^3. Equations (23)–(25) are for 1:1 electrolytes. Corresponding equations have been derived for unsymmetrical electrolytes.[7] The significant feature of these equations is that they provide means for the calculation of C_+^{de} and dC_+^{de}/dE from a *single* differential capacity curve (C *vs* E) at a *single* concentration *provided one is allowed to assume the absence of specific adsorption.* The procedure is as follows: The observed differential capacity curve is numerically integrated once with respect to potential to give q, the surface charge density [Eq. (14)]. Where specific adsorption is absent, this is identical with η^d.[9] Hence one can find v as a function of E at potentials such that specific adsorption is absent. If specific adsorption is absent at some potential, C^{de} will be identical with the ordinary capacity C at that potential because $d\eta^d/dE$ and dq/dE are then identical. This makes it possible to evaluate η^d, C_+^{de}, and dC_+^{de}/dE from Eqs. (23), (24), and (25) and experimental data from a single capacity curve, as stated. C_+^{de} is wanted for the evaluation of k

[7] D. C. Grahame, J. Chem. Phys. **21**, 1054 (1953).

[8] In Eqs. (49) and (63) of reference 7, the sign joining the principal terms should be minus instead of plus. The constancy of μ in dC_+^{de}/dE is to be understood.

[9] It is sometimes supposed that there exists, in addition to the diffuse double layer, a compact layer of ions not specifically adsorbed. This is, in fact, a major point in the Stern theory of the electrical double layer. It arises, however, not as a consequence of any particular argument, but rather as a result of the mathematical form given to the theory. It now seems clear that positive ions, at least, do not form a layer at the interface over and above that which arises as a result of the existence of a diffuse double layer. The situation is a little less clear with respect to anions because of the evidence that these latter can often, if not always, move closer to the interface than can the cations (see reference 1). Thus there is a region between the inner and outer Helmholtz planes which is accessible only to anions, and the possibility exists that when the metallic surface is positively charged, a different kind of *diffuse* double layer may exist there, populated *only by anions* which are not held by other than simple Coulombic forces. The evidence against the view that this is an important part of the whole double layer consists primarily of the fact, to be demonstrated later, that fluoride ions are not adsorbed on positively charged mercury except as they are accompanied by the complement of positive ions predicted by ordinary diffuse double layer theory (see Fig. 14). When the anodic polarization becomes considerable, the outer Helmholtz plane loses its significance, and one should then regard ψ^0 in the theory as the potential of the inner Helmholtz plane. This whole question will be discussed quantitatively in a subsequent publication. For the present it has significance only in solutions of fluorides, because all of the other anions with which we are here concerned show specific adsorption on anodic polarization, and thus keep the potential of the inner Helmholtz plane negative, thereby repelling anions from the region in question.

in Eq. (17), $\eta_+{}^d$ is wanted for the evaluation of k', and $dC_+{}^{de}/dE$ is wanted for comparison with dC_+/dE obtained from an experimental evaluation of $(\partial C/\partial\mu)_E$ [with Eq. (15)]. These three matters will now be further discussed.

At sufficiently negative (cathodic) potentials, even such strongly adsorbed anions as iodide ion can be expelled from a mercury surface. This is evidenced, for example, by the convergence of the differential capacity curves of the potassium salts of different anions as the potential is made more cathodic.[10] At these potentials monatomic cations are not specifically adsorbed, however, as has been known for some time[1] and as we are about to prove anew.[11] Therefore it is possible to find values of $C_+{}^{de}$ from differential capacity data at a single concentration, and although these values are only valid at potentials sufficiently cathodic that no specific adsorption of anions is present, it is only necessary to pick a "most reliable" value of $C_+{}^{de}$, taking into account not only the demands of the theory but also the potential where the experimental data are believed to be most reliable. This "most reliable" value of $C_+{}^{de}$ gives in effect a value of k in Eq. (17).

The accuracy of Eq. (24) at the cathodic potentials in question is much greater than one might at first sight suppose. This comes about from the fact that $C_+{}^{de}$ differs only slightly from C^{de}, which is supposed to be known exactly,[12] and the difference is $C_-{}^{de}$. But $C_-{}^{de}$ can be computed with high absolute accuracy because it is nearly zero. Equation (24) then gives $C_+{}^{de}$ with this same absolute accuracy. It is for this reason that the diffuse double layer values of $C_+{}^{de}$ are preferred to the less well evaluated thermodynamic values of C_+ in the potential region where specific adsorption is known to be negligible and where the anions are known to be strongly repelled.

By the same argument it will be seen that $\eta_+{}^d$ is given by Eq. (23) with very high accuracy at sufficiently cathodic potentials because $\eta_-{}^d$ is practically zero and η^d is supposed exactly known. Then one picks a "most reliable" value of $\eta_+{}^d$ and this in effect gives the constant of integration k'.

The quantity dC_+/dE is known from experiment through Eq. (15). In the absence of specific adsorption, it is expected to be identical with $dC_+{}^{de}/dE$. Comparison of these two quantities can therefore be used as a criterion of specific adsorption. It is, in fact, the most direct and usable criterion of specific adsorption at our disposal.

For 1:2 electrolytes the necessary equations for the evaluation of $\eta_+{}^d$, $C_+{}^{de}$ and of $dC_+{}^{de}/dE$ have also been given [Eqs. (45), (47), and (49), reference 7].[8] In using these equations it is possible to evaluate all of the quantities demanded without employing any data other than a single capacity curve at a single concentration. The procedure is described in the reference cited. For 2:1 electrolytes the procedure is similar.

The quantity C_+/C has been denoted by τ_+ and called[13] the transference number of the cation in the double layer because it measures the fraction of the charge carried into or out of the double layer by cations alone. In the absence of specific adsorption it is expected to equal $\frac{1}{2}$ for symmetrical electrolytes at the potential of the e.c.max.[14] At sufficiently negative potentials it approaches unity, and at positive potentials it would approach zero in the absence of specific adsorption. However, because specific adsorption of negative ions usually occurs on a positively charged mercury surface, τ_+ is often negative at these potentials, and is sometimes negative even at the potential of the e.c.max.

EXPERIMENTAL DETAILS

In order to use the equations derived above it was necessary to evaluate $(\partial C/\partial\mu)_{E^+}$ or $(\partial C/\partial\mu)_{E^-}$ for suitable electrolytes at a metal-solution interface. The metal chosen was, of course, mercury, since this is the only metal for which adequate measurements of C can so far be made. For electrolytes we have chosen to employ principally aqueous tenth-normal solutions of potassium salts of representative types.

The solutions used were prepared from twice recrystallized A. R. salts dissolved in conductivity water. The measurements are not in any case much affected by minor impurities. Two concentrations were ordinarily employed, namely $0.12N$ and about $0.0835N$, the actual value of the latter concentration being chosen to make the mean chemical potentials of the two solutions the same as that of a tenth-normal solution. Activity coefficients for this calculation were mostly derived from Harned and Owen's tabulation.[15]

Measurements of the capacity of the electrical double layer at the mercury-solution interface were made at 25°C using the two concentrations of solution alter-

[10] Grahame, Poth, and Cummings, "Capacity and Surface Charge Density of the Mercury-Solution Interface in Tenth-Normal Aqueous Solutions of Potassium Salts at 25°C," Technical Report No. 7 to the U. S. Office of Naval Research, Dec. 13, 1951. Available at the Library of Congress or on request from the authors. An account of this work is to be found in the J. Am. Chem. Soc. **74**, 4422 (1952).

[11] Monatomic cations are held electrostatically, of course, but the forces involved are just those considered by the theory of the diffuse double layer. This is not called specific adsorption.

[12] In the absence of specific adsorption it is equal to the differential capacity C, which can be measured with good precision.

[13] D. C. Grahame, J. Chem. Phys. **16**, 1117 (1948).

[14] Because that part of the capacity associated with the inclusion of cations into the diffuse double layer equals the part associated with the removal of anions, as one can readily see by arguments of symmetry or from the theory of the diffuse double layer. For 1:2 or 2:1 electrolytes the corresponding figures are $\frac{1}{3}$ and $\frac{2}{3}$, respectively. This result can be verified by dividing Eq. (47) (reference 7) by Eq. (48) and noting that at the e.c.max. and in the absence of specific adsorption $g=\sqrt{3}$. Adsorption of the anion at the e.c.max. has the effect of depressing $\tau_+{}^{\text{e.c.max.}}$ very strongly and can even make it negative. The general expression for $\tau_+{}^{\text{e.c.max.}}$ in the absence of specific adsorption is ν_-/ν where $\nu=\nu_++\nu_-$.

[15] H. S. Harned and B. B. Owen, *The Physical Chemistry of Electrolytic Solutions* (Reinhold Publishing Corporation, New York, 1950).

nately. Instead of changing the reference electrode with each change of solution, as required by Eq. (15), the potential was changed by an amount just sufficient to give the *effect* of changing the reference electrode. This could be done with precision, since the necessary potential shift can be calculated without the introduction of nonthermodynamic assumptions. It is a far better procedure than an actual shift of electrodes would provide, because it frees one from the necessity of building exceedingly high-quality reference electrodes. Besides this, it makes it possible to use *in effect* electrodes which cannot in fact be built, such as a reversible nitrate electrode. A liquid junction will then be present, but this introduces no thermodynamic uncertainty because it can be left unaltered when the solutions are changed. There will be a second liquid junction between two concentrations of the same electrolyte, say potassium fluoride, but this introduces no thermodynamic uncertainty because it corresponds to a concentration cell with transference, whose emf can be calculated precisely if the necessary activity coefficients and transference numbers are known. Where the transference numbers were not available, they were computed with sufficiently accuracy from the equivalent conductances at infinite dilution, sometimes corrected with the aid of conductivity data at finite concentrations. Uncertainties in these quantities were of minor importance.

What was done was to measure $(\Delta C/\Delta\mu)_{E^-}$ or $(\Delta C/\Delta\mu)_{E^+}$ by measuring the differential capacity C at a given potential as precisely as possible, using the techniques previously described.[16] Since only the change in C was needed, no effort was made to obtain correct absolute values of C—only *the percentage change associated with a change of dilution* was measured. This percentage change was always small, never more than 10 percent and usually of the order of 2 or 3 percent, which indicates that ΔC itself could not be ascertained to better than about ± 5 percent or 0.02 mfd/cm^2, whichever was larger.

It is necessary that the percentage change in C be kept small, since otherwise one would not be entitled to set $\Delta C/\Delta\mu$ equal to $dC/d\mu$, as was done throughout. It would not have been advisable to attempt to compare more than two concentrations of solution at a time in this work because a slow drift in the rate of flow of the mercury, for instance, would more than offset any theoretical advantage to be gained.

In most of the measurements E^+ was held constant[17] at potentials more negative than the e.c.max. and E^- was held constant elsewhere. This has the advantage of keeping ΔC small, making the method more nearly a null method. It is easy to convert results obtained by either method to the corresponding result on the other (since dC/dE is the sum of dC_+/dE and dC_-/dE), and in presenting the results below this conversion has been made without comment wherever the presentation is thereby simplified.

The measurements made with potassium chloride were repeated many times and with several variants. For example, in one set of measurements the concentration range was about twice as great as indicated above. Measurements were made both at constant E^+ and constant E^- and also at constant E (i.e., with no change in the potentiometer reading, see reference 17). The latter is experimentally easy but requires more elaborate computation and is probably less desirable as an experimental technique. In all cases the results agreed to within the expected accuracy.

In order to evaluate the first constant of integration, k in Eq. (17), $(dE^-/d\mu)^{\text{e.c.max.}}$ was measured by the streaming electrode method. This method has been described in an earlier publication,[18] the particular method in question being there called Method VI.

METHODS OF COMPUTATION

The method of calculation finally adopted was not the obvious one represented by Eqs. (17) and (18) alone, since there are two ways of finding k and two ways of finding k'. In order to arrive at most probable or "best" values of C_+, and Γ_+ the following procedure was adopted:[19]

Observed values of $(\partial C/\partial\mu)_{E^-}$ were converted into the corresponding values of dC_+/dE by means of Eq. (15) and integrated with respect to E by Simpson's rule from $E=-1.2$ v (relative to the N calomel electrode) to the potential of the e.c.max. This gives the difference (to be called ΔC_+) between C_+ at -1.2 v and at the potential of the e.c.max. But this difference is also known independently from the fact that C_+ is known at -1.2 v from Eq. (24) and at the e.c.max. from Eq. (21). The two values of ΔC_+ naturally differed more or less, although the difference was never greater than could reasonably be attributed to errors in the experimental data. It was then assumed that whatever discrepancy existed arose wholly from errors in $(\partial C/\partial\mu)_{E^-}$. Accordingly a two-parameter *correction function* was set up, consisting of two straight lines, one starting from zero at -1.2 v and the other starting from the potential of the e.c.max. at an undetermined

[16] D. C. Grahame, Proc. Third Meeting International Committee on Thermodynamics and Electrochemical Kinetics, p. 330 (1952). Manfredi, Milan. Also available as Technical Report No. 6 to the U. S. Office of Naval Research, May 25, 1951. Essentially the same technique is described in J. Am. Chem. Soc. 71, 2975 (1949).

[17] This was accomplished, as explained above, by changing the potentiometer reading, when the solutions were changed from one concentration to the other, by an amount equal to the calculated emf of a cell composed of two identical electrodes, each reversible to the cation of the electrolyte, and differing only in the concentration of the electrolyte with which they are supposed in equilibrium.

[18] Grahame, Coffin, Cummings, and Poth, J. Am. Chem. Soc. 74, 1207 (1952).

[19] This method was devised by Professor W. T. Scott of the Smith College Department of Physics. The results are nearly identical with those obtained by an alternative but somewhat less objective method devised by ourselves. The authors take this opportunity to thank Professor Scott for his valued contribution to this work.

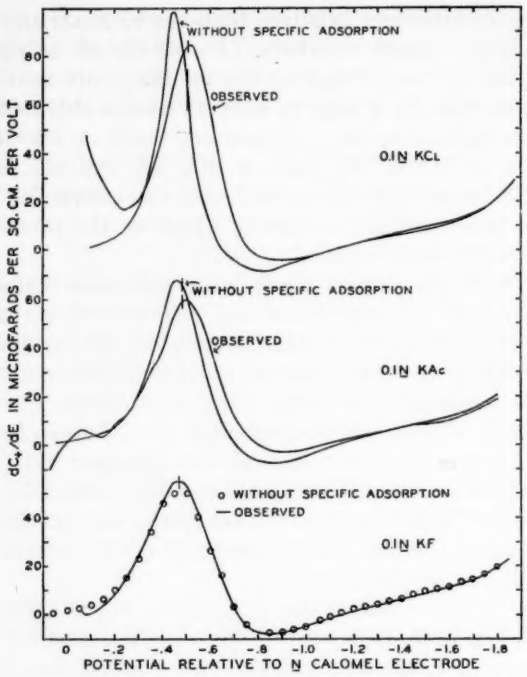

FIG. 1. Observed and calculated values of dC_+/dE. Calculated values assume the absence of specific adsorption.

ordinate A.[20] The two curves meet at a point of ordinate B. The *potential* at which they meet is selected somewhat arbitrarily near the middle of the range of potentials in question. This correction function is to be added to (or subtracted from) the observed function (dC_+/dE).

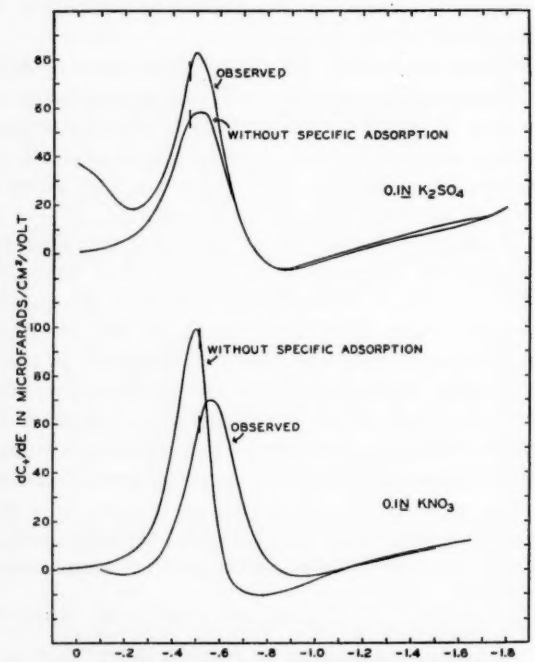

FIG. 2. Observed and calculated values of dC_+/dE. Calculated values assume the absence of specific adsorption.

[20] This A is not the A of Eqs. (23)–(25).

It is evident that the integral of the correction function $f(A,B)$ from -1.2 v to the e.c.max. must equal the discrepancy between the two values of ΔC_+ calculated above. This establishes one condition upon the function $f(A,B)$, making it essentially a one-parameter equation. We shall regard A itself as the parameter.

Limits of error are now set upon A and B corresponding to what we may regard as the probable limits of error in dC_+/dE at the two potentials in question (the e.c.max. and the potential where the two lines of the correction function were considered to meet). Now taking the upper limit of B puts a lower limit on A; likewise the lower limit of B puts an upper limit on A, so that A must fall between a pair of limits dependent upon the limits of B. But we have also an independently selected set of limits on A, and A is now required to lie within the *overlapping* region of the two sets of limits. Thus our correction function is now a one-parameter function in which the one parameter has a restricted range of values.

Taking the maximum allowed value of the parameter A, the *corrected* function dC_+/dE is integrated twice by Simpson's rule from $E=-1.2$ v to the e.c.max. to give $\Gamma_{salt}^{e.c.max.}-\Gamma_+^{-1.2}$. For the second integration $C_+^{-1.2}$ is taken from Eq. (24) [or from Eq. (43) or (47) in reference 7 for 1:2 or 2:1 electrolytes[21]]. The value of $\Gamma_+^{-1.2}$ is obtained from Eq. (23) or from the corresponding equations for 1:2 or 2:1 electrolytes.[21] This procedure assumes the absence of specific adsorption at a potential of -1.2 v, and gives a value of $\Gamma_{salt}^{e.c.max.}$. Taking the *minimum* allowed value of the parameter A gives another value of $\Gamma_{salt}^{e.c.max.}$. These two values are then averaged to give a "most probable" value and a set of limits.

In order to arrive at a "best" corrected function, dC_+/dE, the average correction function is smoothed to eliminate the discontinuity of slope at A and B. This procedure is not as arbitrary as it might seem because the smoothing must be done in such a way as to keep the area under the curve constant and also to keep the second integral constant. Except when B and A were both rather large and of opposite sign, which was unusual, the smoothing operation was quite satisfactory.

RESULTS AND DISCUSSION

Experimental values of $(dE^-/d\mu)^{e.c.max.}$ and the corresponding values of $C_+^{e.c.max.}$ are given in Table I. The results are of value chiefly in that they provide a constant of integration k for Eq. (17). For 1:1 electrolytes the expected value of $\tau_+^{e.c.max.}$ in the absence of specific adsorption is 0.5 and this is observed only with KF. Comparison of $\tau_+^{e.c.max.}$ for KF, KCl, KBr, and KI shows the expected falling off, although the decrease on going from KBr to KI is perhaps not as large as one would expect. Potassium nitrate and $KClO_4$

[21] The quantities b and g in those equations are evaluated by the use of Eq. (35) or (45). y is found from Eq. (5) or (20).

show about the same value as KCl, in agreement with the fact that nitrate, perchlorate, and chloride ions are adsorbed about equally at the potential of the e.c.max. Potassium acetate (KAc) shows a larger value of $\tau_+^{e.c.max.}$, suggesting that the acetate ion is less adsorbed than these, a fact which is borne out by the low value of the potential of the e.c.max. In the calculations which follow, these statements are given quantitative verification.

The 1:2 electrolytes K_2SO_4 and K_2CO_3 show values of $\tau_+^{e.c.max.}$ a little smaller than the theoretical value 0.333 for a nonadsorbed electrolyte. It is not known just how much uncertainty there is in these values of $\tau_+^{e.c.max.}$. It is just about certain, however, that the value 0.261 found for K_2SO_4 is significantly different from the theoretical value for a nonadsorbed electrolyte, 0.333. This difference would seem to indicate a certain amount of adsorption of sulfate ions at the potential of the e.c.max., a result which is further indicated

TABLE I. Quantities needed for the evaluation of C_+ at the potential of the electrocapillary maximum.

Salt	e.c.max. volts[a]	Tenth-normal solutions at 25°C $(\partial E^-/\partial\mu)^{e.c.max.}$ volts/volt	$\tau_+^{e.c.max.}$	$C^{e.c.max.}$ mfd/cm²	$C_+^{e.c.max.}$ mfd/cm²
KCl	0.506	0.205	0.205	29.9	6.12
KBr	0.574	−0.116	−0.116	41.9	−4.85
KI	0.732	−0.338	−0.338	60.0	−20.29
KNO_3	0.517	0.193	0.193	28.9	5.57
KAc	0.488	0.351	0.351	24.3	8.53
$KClO_4$	0.507	0.196	0.196	27.2	5.34
KF	0.471	0.50	0.50	20.8	10.4
$BaCl_2$	0.505	0.127	0.254	30.7	7.81
K_2SO_4	0.470	0.131	0.261	22.2	5.79
K_2CO_3	0.473	0.132	0.263	22.0	5.81

[a] Potentials in column 2 measured relative to normal calomel electrode with correction by Henderson's equation for the liquid junction potential between tenth-normal potassium chloride and the solution in question, but without correction for the liquid junction potential between tenth-normal and normal potassium chloride.

by a second line of evidence to be indicated presently. However, there are two additional pieces of evidence which seem to contradict the result, so that the question cannot be considered settled. It seems probable that the methods which indicate a positive adsorption of sulfate ion (both of which are qualitative in character) are simply more sensitive than the two quantitative methods which indicate a null result.

For $BaCl_2$ the "theoretical" value of $\tau_+^{e.c.max.}$ is 0.667, which is strikingly different from the observed value, 0.254. As with KCl, the difference is to be attributed to the specific adsorption of chloride ion.

Figures 1–4 show the experimental values (before the application of any correction function) of dC_+/dE together with calculated values of dC_+^{de}/dE obtained with the aid of Eq. (25) or the corresponding equations for other valence types. In the figures these calculated curves are labeled "without specific adsorption" but this is an oversimplification because the experimental capacity curve is used in the calculations. Thus the

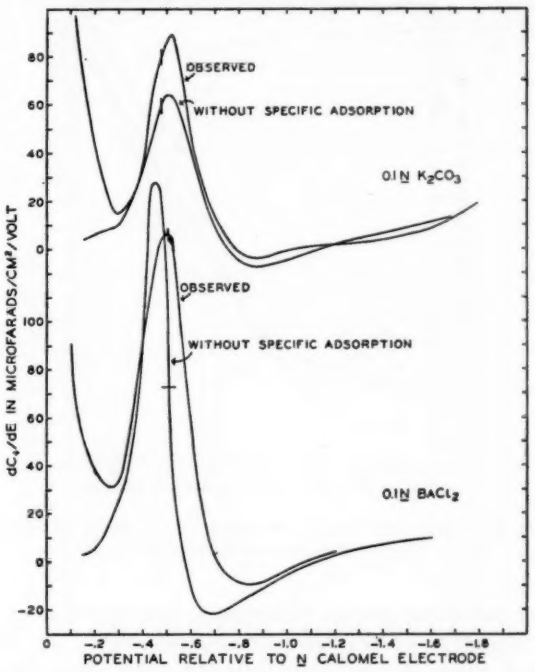

FIG. 3. Observed and calculated values of dC_+/dE. Calculated values assume the absence of specific adsorption.

calculated curves have meaning only in so far as specific adsorption is really absent. Where the observed and calculated curves agree, specific adsorption may be deemed absent, but the magnitude of any disagreement does not give a quantitative measure of the extent of the adsorption to which it corresponds.

The virtually exact agreement of the two curves for KF is strong direct evidence not only for the nonadsorption of fluoride ion over a large range of poten-

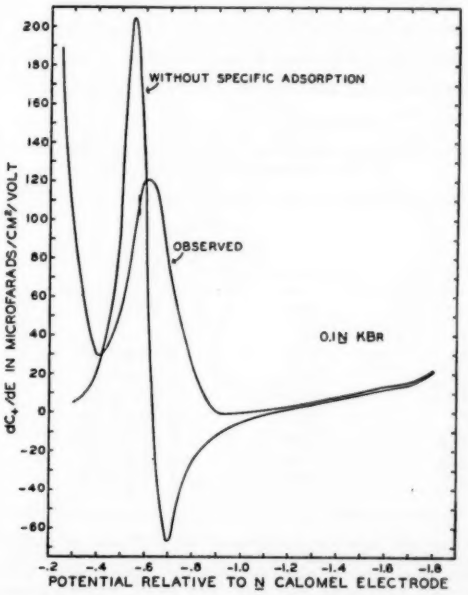

FIG. 4. Observed and calculated values of dC_+/dE. Calculated values assume the absence of specific adsorption.

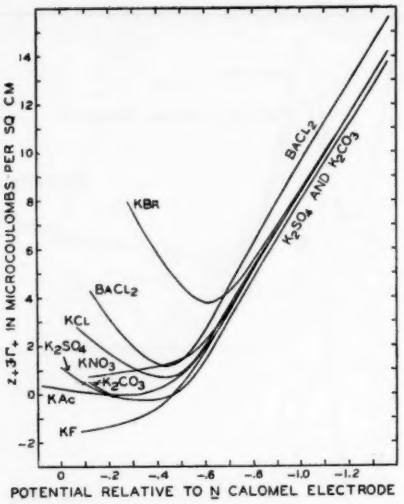

FIG. 5. Charge attributable to cations in the electrical double layer. Tenth-normal aqueous solutions at 25°C.

tials, including anodic potentials, but also speaks for the accuracy of the treatment upon which the theoretical curve is based. It means, among other things, that the kinetic treatment of the diffuse double layer in which the dielectric constant is considered constant is valid for the purposes for which we have employed it.

For all of the electrolytes investigated the curves in Figs. 1–4 converge at large negative potentials. This is direct evidence for the absence of specific adsorption of the cations under investigation. Since the capacity curves of salts of other monatomic cations are known to behave in almost exactly the same manner as those here investigated, it seems safe to conclude that other monatomic cations are also not specifically adsorbed on mercury.

The poorer agreement between the calculated and observed values of dC_+/dE at cathodic potentials obtained with K_2CO_3 is believed to be a result of the poor reproducibility of the capacity data obtained with that salt. This in turn is believed to be a consequence of the fact that we were not very successful in our attempts to purify potassium carbonate.

The curves for K_2SO_4 shown in Fig. 2 are separated at the potential of the e.c.max. (indicated by the short vertical line) by an amount which we regard as considerably larger than the probable error of the measurements. The disagreement is in the direction to be expected if there is a positive adsorption of sulfate ion at that potential, but one cannot estimate the magnitude of the adsorption from the separation of the curves for the reasons explained above.

Values of $\Gamma_{salt}^{e.c.max.}$ obtained in various ways are presented in Table II. Column 2 contains values obtained earlier[22] from electrocapillary data and are not believed to be very accurate. Column 3 contains values obtained by the integration method described above. Column 4 then gives what we regard as "best" values taking into account the relative reliability of the data in the two preceding columns and also noting that negative values are presumably impossible. Limits of error on these values are considered to be the same as those stated in column 3 except for the exclusion of negative values.

Even with our new method the absolute accuracy with which $\Gamma_{salt}^{e.c.max.}$ can be determined is still not high. For the purposes of the present paper, at least, this uncertainty is of minor importance because $\Gamma_{salt}^{e.c.max.}$, being a constant of integration, does not change the shape of the curve which it is used to determine and because, being small, its effect upon the absolute values of points on the curve not close to zero is necessarily small.

Figure 5 shows Γ_+, the charge attributable to cations in the double layer. These are obtained by double integration of the corrected dC_+/dE curves. Figures 6 and 7 show Γ_-, the charge attributable to anions in the whole double layer. These are obtained by difference between $-q$ and Γ_+.

Figure 5 shows the Coulombic adsorption (there being no specific adsorption) of cations and shows the additional feature of increasing adsorption of positive ions with increasing anodic polarization beyond a certain point. This behavior has already been noted for solutions of NaCl.[1] It is now shown to be fairly general but not universal, since KF and KNO_3 do not show it and KAc shows it to only a very slight degree.

The explanation has been given before and applies without change to the new instances here presented. Briefly, what is happening is that the anions are bound to the mercury by specific bonding forces (non-Coulombic in a simple sense), and these forces increase strongly as the mercury loses its negative charge or acquires a positive charge. The forces are surely analogous to ordinary chemical binding forces (the covalent bond), and it seems not inappropriate to refer

TABLE II. Salt adsorption on mercury at the potential of the electrocapillary maximum.[a]

Salt	$\Gamma_{salt}^{e.c.max.}$ microcoulombs per sq. cm. reference 12	this work	"best"
KCl	0.6[a]	1.01±0.13	0.9
	0.8		
KAc	0.4[a]	0.78±0.30	0.5
KBr	3.1[a]	3.95±0.25	3.7
K_2CO_3	−0.2[a,b]	0.20±0.13	0.0
KF	0.0	−0.09±0.15	0.0
KNO_3	1.8[a]	1.51±0.08	1.6
K_2SO_4	−0.3[a]	−0.07±0.15	0.0
$BaCl_2$	1.0[a]	1.42±0.10	1.3

[a] Tenth-normal aqueous solutions at 25°C except as marked by (*a*), where temperature was 18°C. The values marked with an (*a*) for KAc and K_2SO_4 were actually obtained with the corresponding sodium salts. No significant differences have ever been found between potassium and sodium salts in this connection.

[b] Estimated from electrocapillary data by Gouy at 1.0*N* and above together with data for 0.01*N* Na_2CO_3.

[22] D. C. Grahame, Record Chem. Progr. Kresge-Hooker Sci. Tib. **11**, 93 (1950).

to the adsorption as chemisorption. Because the chemisorption of anions takes place even after the charge of the anions equals the positive charge on the mercury (which may be thought of as being held fixed), an excess of positive ions must move in to equal the charge of this "excess" anion adsorption. This effect increases greatly as the positive charge on the mercury is made larger, and it is this effect which causes the curves of Γ_+ to turn upward.

Potassium fluoride does not show this effect because the fluoride ion is not chemisorbed. Potassium nitrate does not show it because the chemisorption of nitrate ion does not increase rapidly enough with increase of anodic polarization. Evidence for the chemisorption of nitrate ion comes not so much from these curves as from others to be presented below.

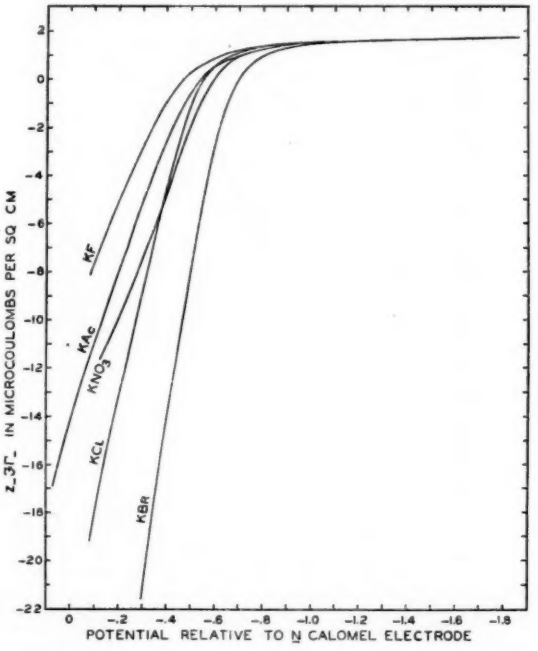

FIG. 6. Charge attributable to anions in the electrical double layer. Tenth-normal aqueous solutions at 25°C.

Figure 6 shows the expected result that the charge on the double layer is attributable largely to anions when the potential is anodic to the e.c.max. The order in which the curves fall is also as expected. Figure 7 shows how the valence type affects the limiting value of the charge attributable to anions when the metallic surface is negatively charged. This is a consequence of the kinetic theory of the diffuse double layer and can be understood qualitatively by a consideration of the fact that each ion has the same average kinetic energy regardless of its charge. If the diffuse double layer is thought of as an equilibrium state in which ions are moved in one direction by the electric field and in the other direction by the concentration gradient, then it is

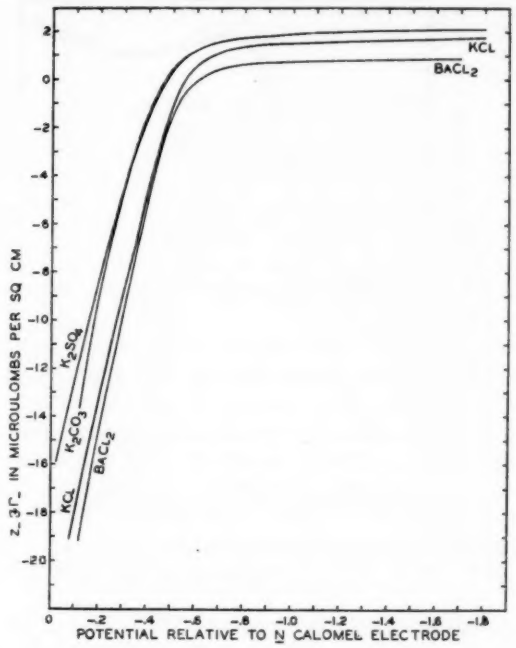

FIG. 7. Charge attributable to anions in the electrical double layer.

clear that the ions of greater charge will be able to sustain a greater concentration gradient than those of lesser charge. This has the effect of making a doubly charged ion more important than a singly charged ion in the sense that it has a greater influence on the diffuse double layer than an equivalent concentration of a singly charged ion. This argument does not apply to the compact part of the double layer, however, and it is known from experiment that a divalent cation is practically indistinguishable from a monovalent cation

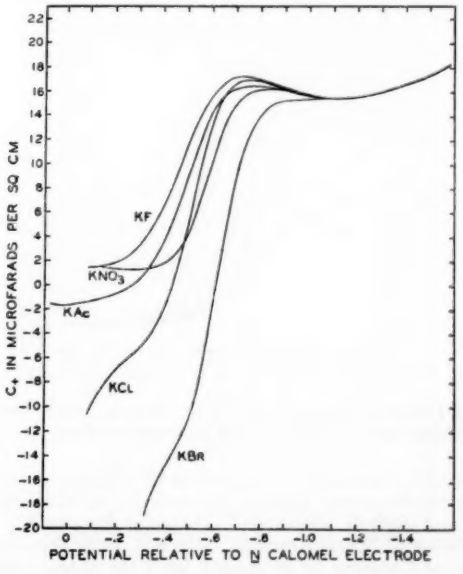

FIG. 8. Differential capacity attributable to cations in the electrical double layer. Tenth-normal aqueous solutions at 25°C.

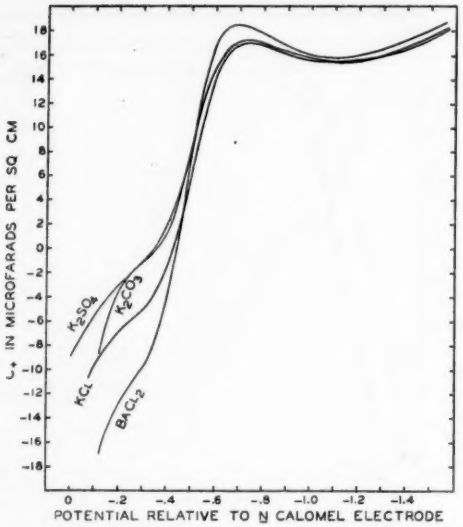

FIG. 9. Differential capacity attributable to cations in the electrical double layer. Tenth-normal aqueous solutions at 25°C.

in its electrocapillary properties.[2,23] This seeming contradiction arises from the fact that the capacity of the diffuse double layer is so large that it is of only minor importance in fixing the capacity of the whole double layer.[1]

Figures 8–10 are the slopes of the preceding curves and show how cations and anions individually contribute to the total observed capacity. The negative values of C_+ shown in Fig. 8 reflect the phenomenon just described. The "humps" in the ordinary capacity curves for chlorides, bromides, sulfates, acetates, and

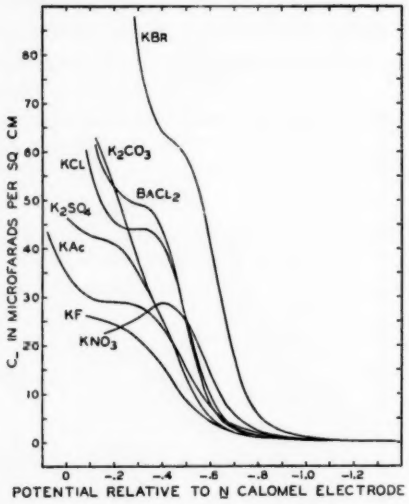

FIG. 10. Differential capacity attributable to anions in the electrical double layer. Tenth-normal aqueous solutions at 25°C.

[23] David C. Grahame, "Capacity of the mercury-solution interface in tenth-normal aqueous solutions of metallic chlorides at 25°C, and derived properties," Technical Report No. 1 to the U. S. Office of Naval Research, March 9, 1950. Available at the Library of Congress or on request from the author. An account of these results is to be found in J. Electrochem. Soc. **98**, 343 (1951).

nitrates are seen to be characteristics attributable to the anions, as one would expect; the rather small humps found on the C_+ curves occur at the wrong potentials to be held responsible for any part of the effect.

Potassium fluoride is seen to behave "ideally" in that C_- rises to a constant value of about 27 mfd/cm^2. In the older literature (and sometimes even in the current literature) it is usually mistakenly supposed that this type of behavior is characteristic of anions generally. Figure 10 shows that such behavior is very much the exception, not the rule.

The asymptotic approach of C_- to zero on cathodic polarization arises chiefly from the mode of calculation, in which this behavior is essentially assumed from the start. What is observed directly is the decrease of dC_-/dE [or $(\partial C/\partial\mu)_{E^+}$] to zero. Thus it is directly observed that C_- goes to a *constant* value and only

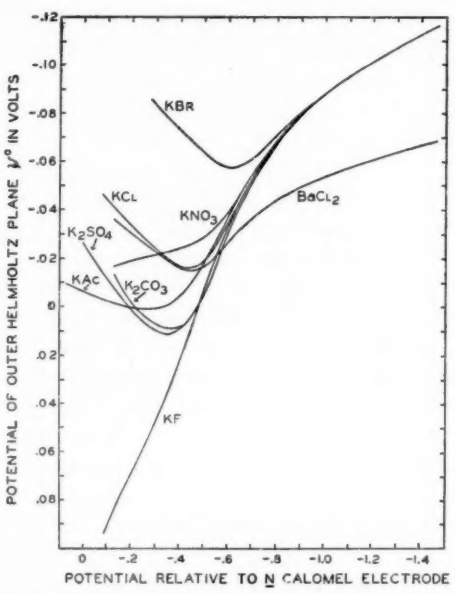

FIG. 11. Potential at the outer Helmholtz plane ψ^0 in volts. Tenth-normal aqueous solutions at 25°C.

roughly verified that this value is truly zero. However the theory of the diffuse double layer leads to this conclusion in so simple and positive a manner that no alternative assumption is readily imaginable.

Owing to the absence of specific adsorption of monatomic cations, these must belong to the diffuse double layer exclusively. Thus it becomes possible to calculate ψ^0, the potential of the outer Helmholtz plane, by means of equations already presented.[24] The results of the calculation are shown in Fig. 11. This may perhaps be regarded as the most important result of the present investigation since it constitutes an evaluation of a quantity which has rather often been sought by other investigators in this and related fields. It is related to the zeta potential in the field of electrokinetics since it

[24] Reference 7, Eqs. (36), (45), or (50) depending upon valence type.

is the most likely analog of the potential of the plane of shear.

The results shown in Fig. 11 supercede the very similar but not quite identical results obtained by us earlier[16] using the same experimental data but a less objective mathematical treatment.

The difference between the behavior of KF and that of all of the other electrolytes here investigated is very striking in Fig. 11 and is caused by the unique absence of chemisorption of fluoride ion on mercury, even when the latter is positively charged. It is worth remarking that the distinctive behavior of fluoride ion is believed to result from the fact that fluorine seldom if ever forms covalent bonds with metals. This, of course, is a consequence of its high electronegativity. The large hydration energy of the fluoride ion, associated with its small size in the unhydrated state, may also be a factor in its nonadsorption on mercury.

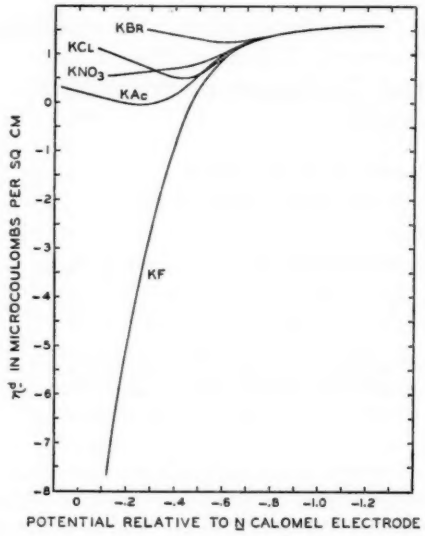

FIG. 12. Charge attributable to anions in the diffuse part of the electrical double layer. Tenth-normal aqueous solutions at 25°C.

Except in the case of fluorides, and over a small range of potentials with sulfates and carbonates, the potential of the outer Helmholtz plane is always negative. Potassium acetate dips very slightly into the region of positive values of ψ^0 also, however, according to Fig. 11, and thus constitutes another very slight exception to the rule. In more dilute solutions it is likely that ψ^0 more often goes positive.

Knowing the potential of the outer Helmholtz plane, we are in a position to calculate η_-^d, the contribution of anions to the *diffuse* part of the double layer. This is done by means of equations already presented elsewhere;[25] the results are given in Figs. 12 and 13. Again KF is unique in its behavior. With the exception of the fluoride ion, it is remarkable that the charge attributable

[25] Reference 7, Eqs. (35), (46), or (51) depending upon valence type.

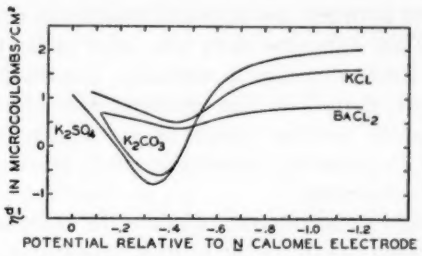

FIG. 13. Charge attributable to anions in the diffuse part of the electrical double layer. Tenth-normal aqueous solutions at 25°C.

to anions in the diffuse double layer seldom exceeds 1.5 microcoulombs/cm². Indeed, except for divalent anions and the fluoride ion, it almost never goes negative at all, which is to say that the contribution of anions to the diffuse double layer is almost always a *positive* charge resulting from their lower-than-normal concentration in the diffuse double layer. This is of course a direct consequence of the fact that ψ^0 is generally negative.

From our knowledge of Γ_- and η_-^d, it is clearly very easy to get η_-^i since

$$z_-F\Gamma_-=\eta_-^d+\eta_-^i. \tag{27}$$

η_-^i is the charge attributable to chemisorbed anions, or to be more exact, it is the charge attributable to anions which do not lie in the diffuse double layer. The results are shown in Fig. 14 and constitute our final objective in this work. These curves show, for example, that the nitrate ion is indeed adsorbed strongly and that the adsorption does not decrease, though it increases less rapidly, with increasing anodic polarization. The adsorption of nitrate ion seems rather different in kind from the adsorption of the other anions studied and is believed to be chiefly van der Waals adsorption.

The results here for KF are a little uncertain under anodic polarization because it is necessary to take the

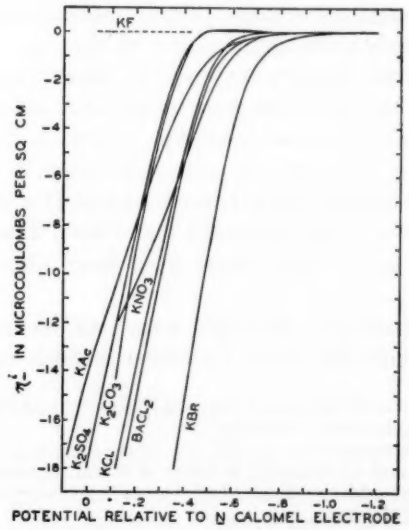

FIG. 14. Charge attributable to anions specifically adsorbed at the mercury surface. Tenth-normal aqueous solutions at 25°C.

difference between two large and essentially equal quantities. This difficulty does not arise with the other anions. Because of this uncertainty, the results for KF are shown dotted on the left-hand side of the curve. The slightly positive values of η_-^i shown for K_2SO_4 and K_2CO_3 at certain potentials are to be attributed to experimental error.

It would be of interest to carry the calculations one step further to obtain the specific adsorption potential of the adsorbed anions. Unfortunately this cannot be done in an unambiguous manner, since one has no way of knowing the potential of the inner Helmholtz plane. It now appears that these two quantities are not knowable separately, although their sum can be known if one is prepared to assume a value for the ionic radius. The equation for making the calculation has been given previously,[26] but the calculation is being held up pending a reexamination of the theoretical aspects of the problem.

From the data contained in this paper it is easy to calculate the transference numbers of cations and anions in the double layer. As stated above, these are denoted τ_+ and τ_- and are given by C_+/C and C_-/C, respectively. They have the qualitative characteristics enumerated above.

ACKNOWLEDGMENT

The authors are grateful to the U. S. Office of Naval Research for the continued support of the research program of which this work has been a part. They are also grateful to Professor William T. Scott for the assistance mentioned in reference 19.

[26] Reference 1, Eq. (85).

THE JOURNAL OF CHEMICAL PHYSICS VOLUME 22, NUMBER 3 MARCH, 1954

Rotation in Solid Mixtures of Neohexane and Cyclopentane from 20°K to Their Melting Points*†

J. G. Aston, Bouwe Bolger,‡ Ralph Trambarulo,§ and H. Segall
Department of Chemistry, Pennsylvania State University, State College, Pennsylvania

(Received October 5, 1953)

Studies of the broadening of the proton spin resonance line have been made for solid solutions of neohexane and cyclopentane.

A convenient apparatus for control of temperatures from 10°K to room temperature for such studies is described.

The "complex" of one mole of neohexane with two moles of cyclopentane rotates in the solid state down to 65°K. In solid solutions with cyclopentane in excess of the complex, the complex rotates independently of the cyclopentane down to 66°K. The complex has no effect on the lower rotational transition of the cyclopentane which apparently nucleates.

INTRODUCTION

THE solid-solid and solid-liquid equilibriums in the system neohexane-cyclopentane have been fairly exhaustively investigated above 90°K.[1]

The phase diagram as obtained from the thermal data is shown in Fig. 1. The pure components each have two transitions of the rotational type. These and the melting point are by a *curious coincidence* close to the same temperatures for the pair of compounds. It will be shown that the α to β rotational transitions, though comparable as to their heat, may bear little detailed similarity.

Unfortunately, although x-ray studies have been made above the upper transition in both compounds which there show complete freedom of rotation,[2] no measurements were made in the region between the two rotational transitions.

In keeping with the original nomenclature, for both compounds the form stable below the lower transitions will be denoted by α, that stable between the transitions by β, and that stable above the upper transition by γ. There is certainly little rotation for either compound in the α form. The natures of the rotational motions in the β forms of the two compounds and of the α to β transition are open to speculation.

There are two notable features about the condensed phase diagram as obtained from the thermal data. One of these is that there were no thermal transitions above 90°K in the solid for compositions richer in neohexane than corresponding to the "complex" of one neohexane molecule with two cyclopentane molecules. The first solid curve (marked *d*) in Fig. 1 shows the temperatures of the α to β transition. The other notable feature is the small variation in equilibrium temperature together with the decreasing heat of the α to β transition of cyclo-

* Contribution from the College of Chemistry and Physics of the Pennsylvania State University.

† This research was carried out under Contract N6 Onr-269 (T.O. III and X) of the U. S. Office of Naval Research.

‡ Present address: Kamerlingh-Onnes Laboratory, University of Leiden, Holland.

§ Present address: Physics Department, University of Delaware.

[1] Fink, Cines, Frey, and Aston, J. Am. Chem. Soc. **69**, 1501 (1947).

[2] Post, Schwartz, and Fankuchen, J. Am. Soc. **73**, 5113 (1951).

pentane as neohexane was added. From these it could be inferred that the α to β rotational transition involved only cyclopentane molecules not in the complex. This conclusion is strikingly verified by the fact that the heat of the transition is proportional to the amount of cyclopentane in excess of the compound. *Such an inference implies nucleation.*[3] It will take a careful study of the heat capacities below the α to β transition to tell if there is bulk phase separation.

Nuclear magnetic resonance has been used to study rotation in the solid state.[4a,b,c]

The present study by means of nuclear magnetic resonance follows previous methods. It has confirmed all conclusions from the thermal data and added to the knowledge of the extent of rotation in the solid system below the melting point.

EXPERIMENTAL

Nuclear Magnetic Resonance Apparatus

The apparatus is essentially that described by Pound and Knight.[5] It is shown as a block diagram in Fig. 2, which is self-explanatory.

The characteristics of the line were obtained from an oscillograph display with a 30-cps sinusoidal sweep on both the magnetic field and the horizontal axis of the oscillograph. Line widths were measured at half the height of the pattern appearing on the oscillograph face. In such a display the horizontal axis is linear in frequency (or magnetic field strength). This axis was calibrated in kilocycles per second from the positions of sharp lines in the liquid state for various settings of the oscillator frequency which was measured with a BC 221 frequency meter.

Relative intensity in the neighborhood of a transition could be obtained where desired by changing the vertical gain setting of the oscillograph to bring the peak to a previously chosen reference height. For very broad lines or for line shape derivative presentation, the oscillator was turned slowly through resonance by a clock motor and with a very small 280-cps modulation on the magnetic field. The derivative of the line shape is displayed on the recorder through the phase-sensitive lock-in amplifier in the limit of low magnetic modulation.

Magnet

A permanent magnet with a 2-in. gap between 6-in. pole faces giving a field of 5536 oersteds was used. This was manufactured specially by the Indiana Steel Company. By the use of three small iron strips on the raised rim of the pole faces, a region of 1 in.^{2} in the middle of the faces was obtained in which the field did not vary by more than 10^{-2} oersted. (The original variation on the same area was about 40×10^{-2} oersted.)

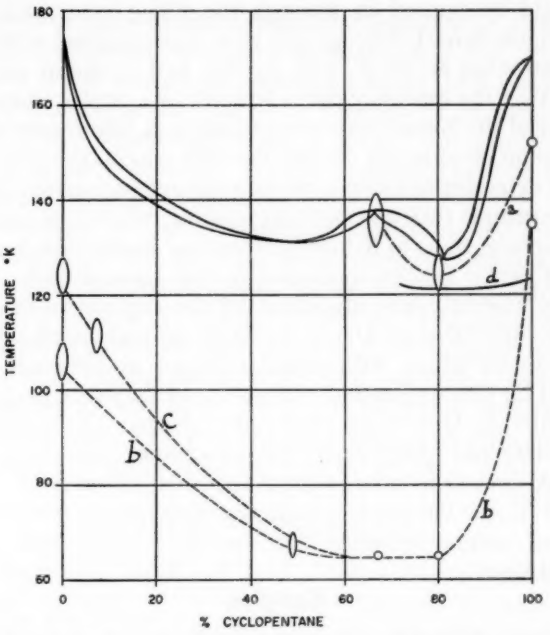

FIG. 1. Neohexane-cyclopentane condensed phase changes.

Cryostat and Temperature Measurements

The sample holder (6-cc capacity), *A* (see Fig. 3), was mounted in an evacuated chamber *B* to which small quantities of pure helium could be added for heat conduction. This was fastened to its cover by Woods metal. A copper-constantan thermocouple *C* made from the same spools as the laboratory standard thermocouples *S*-1 to *S*-8, passed down through the filling tube *D* with its junction at the bottom.[6] Where the wires passed out of the tube the insulation was removed so that they could be soldered to caps through which they passed. These caps closed two "Kovar" tubes sealed onto Pyrex side tubes *E*. The samples

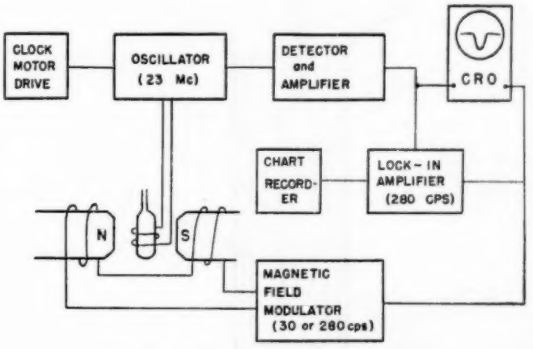

FIG. 2. Nuclear resonance assembly.

[3] R. Smoluchowski, *Phase Transformation in Solids* (John Wiley and Sons, Inc., New York, 1951), Chap. 5.

[4a] Bitter, Alpert, Poss, Lehr, and Linn, Phys. Rev. **71**, 738 (1947).

[4b] N. L. Alpert, Phys. Rev. **72**, 637 (1947).

[4c] H. S. Gutowsky and G. E. Pake, J. Chem. Phys. **18**, 162 (1950).

[5] R. V. Pound and W. D. Knight, Rev. Sci. Instr. **21**, 219 (1950).

[6] Aston, Willihnganz, and Messerly, J. Am. Chem. Soc. **57**, 1642 (1935).

could be poured in through the filling tube with a suitable funnel. The sample tube was equipped with a constantan heater *F*, with current and potential leads so that the assembly could be used as a crude calorimeter of the Nernst type or as a heat-leak calorimeter for cooling or warming curves. For this reason, the coil *G* for detecting absorption in the radio region, surrounded the sample tube as closely as possible, without actually touching, so as to reduce heat leak by conduction down the heavy copper conductor in the coaxial cable *H*. The assembly was supported by the cap which closed the strip-silvered Dewar *I*. This cap was fitted with tubes for filling with liquid nitrogen or hydrogen *J* and for evacuation and connection to the hydrogen gas holder *K*. One filling of liquid hydrogen (2 liters for cooling and filling) lasted for about four hours.

A deviation table, accurate to 0.10° from 20°K to 273°K, for the thermocouple was obtained by means of fixed points including the normal boiling point of hydrogen.

Samples

The cyclopentane was the same sample as used in the thermal studies.[1] The neohexane, kindly supplied by the Phillips Petroleum Company, was purified by fractional melting and contained probably no more than 0.3-mole percent impurity.

RESULTS

Line breadths in kc (4.26 kcps=1 gauss) obtained from the nuclear resonance along with thermal data

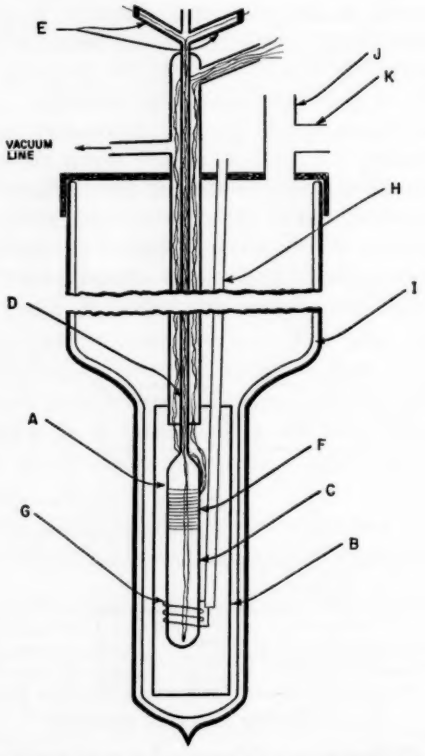

FIG. 3. Cryostat and cell for nuclear resonance.

TABLE I. Summary of data for system cyclopentane-neohexane.

Probable nature of transition	Transition temperature °K from heat capacity	Trans. in nucl. res. °K	Line width in kc
		Cyclopentane	
rot. tr. $\alpha\rightarrow\beta$	122.2	not found	not found
rot. tr. $\beta\rightarrow\gamma$	138.1	138.1	64.9– 6.6
?	not found	152.2	6.6– 5.5
γ to liquid	179.7	179.7	4.8– 4.4
		79.7 mole percent cyclopentane	
rot. tr.	...	65	50 –10
rot. tr.	...	101.5–105	10 – 7
rot. tr. $\alpha\rightarrow\beta$	121.3	gradual tr. from 121–128.5	7.1– 3.5
rot. tr. $\beta-\gamma$	128.0	...	3.5
γ to liquid	128.2–131.3	...	3.5
		66.7 mole percent cyclopentane (complex)	
rot. tr.	...	65	50.5–11
melting	136.5–137.7	130–141	11 – 3.5
		48.8 mole percent cyclopentane	
rot. tr.	...	66–70	30 –23
...	...	gradually from 70–126	23 –11
		7.1 mole percent cyclopentane	
rot. tr.	...	108–115	25 –10
...	...	gradually from 115–153	10 – 1.7
melting	149.5–152.8	...	1.7
		Neohexane	
?	...	range 102–110	82 –37
rot. tr. $\alpha\rightarrow\beta$	126.81	range 120–128	approximately 37 –10
rot. tr. $\beta\rightarrow\gamma$	140.88		
γ to liquid	174.16	gradually from 128–174	10 – 1.7

previously obtained are given for the pure compounds and mixtures in Table I. Widths below 23 kc (5.4 gauss) in the solid are considered unusually narrow as a result of rotation. For convenience, dotted lines *a*, *b*, and *c* on Fig. 1 connect points corresponding to narrowing of the resonance line between corresponding limits (i.e., relatively sharp changes in line width) which can be ascertained by reference to Table I. It is not implied that these curves represent (other than by pure guess) what is to be expected at unstudied compositions. Because the lines did not change width at definite temperatures but rather over ranges in temperature, these ranges are indicated by the vertical heights of ellipses drawn for the various concentrations studied. In addition to the curves shown, there was observed a slight (and only slight) narrowing of the lines upon melting. On the neohexane side of the "complex," warming curves were started at 20°K to be sure that no significant transitions were missed. The curve *a*, which exists only on the cyclopentane rich side of the "complex," corresponds to further narrowing of an already narrow line. This curve is to be associated with the α to β transition for cyclopentane found in the thermal data and shown in curve *d*. The temperature of the α

to β transition is hardly effected by composition. Since its heat depends on the amount of cyclopentane in excess of the complex,[1] only the excess cyclopentane is involved in it. This behavior must result from nucleation. That the α to β transition of the excess cyclopentane results in narrowing of a line already narrow because of rotation of the compound can be seen from Table I at 79.7-mole percent cyclopentane. At the β to γ transition of cyclopentane the line has become very narrow.

On the neohexane-rich side, curves *b* and *c* (insofar as they are defined by two compositions) change with composition with sufficient regularity to indicate no similar nucleation in neohexane. This is further shown by absence of the curve *a*. It is quite likely that the pseudosymmetry of the neohexane is the cause of this difference. Curve *b* extends over the entire diagram with a minimum at 66.7 percent cyclopentane. It corresponds to rotation setting in for the complex. On the cyclopentane side of the complex the nucleated cyclopentane apparently does not partake. The surprising fact brought out by this study (confirming a conclusion from the thermal data) is the persistance of rotation of the complex found at 66.7 percent cyclopentane down to at least a temperature of 65°K and its ability to lower the α to β transition of mixtures richer in neohexane. The transition at 65°K found by change in line shape for the compound at 66.7 percent cyclopentane was clearly shown by a flat in the cooling curve associated with heat evolution. Its heat will be measured as part of an investigation now in progress to study its zero-point entropy.

For compositions less than 67 percent cyclopentane, as well as for pure neohexane, line shapes showed hyperfine structure which became resolved at temperatures indicated by the lowest dotted curve *b* in Fig. 1. Recordings of the line-shape derivatives gave four peaks instead of the two which would be obtained for a line without hyperfine structure. Separations of the outer peaks of the derivatives were about 82 kc. This cannot be attributed to coupling of the protons in CH_3 groups which give separations of about 40 kc.[7] For compositions greater than 67 percent cyclopentane, these "wings" were not observed.

Inasmuch as this phenomenon occurs on the neohexane side of the diagram, one is tempted to associate this with the tertiary butyl group and/or the ethyl group. For pure cyclopentane the α to β transition results in no narrowing of the nuclear spin resonance line whereas for pure neohexane the main narrowing occurs at the α to β transition. Thus it is not likely that the α to β and β to γ transitions in the two compounds can be paired off logically in any simple fashion.

ACKNOWLEDGMENTS

We wish to thank Mr. L. F. Shultz for making the liquid hydrogen, Mr. F. Malloy for the construction of special Dewar vessels and other difficult glass work, and Mr. C. W. Brouse, Shop Superintendent of the School, for the construction of the cryostat. We are greatly indebted to Professor F. Bitter of the Massachusetts Institute of Technology and Professor R. V. Pound of Harvard University for advice and help in the design of the circuits and magnet and to the latter for this hospitality to one of us (B.B.) in allowing certain of the circuits to be tested in the magnet at Harvard.

A preliminary experiment showing complete rotation of the complex at 90°K was carried out by two of us (J.G.A. and B.B.) at the Kamerlingh-Onnes Laboratory, Leiden, Holland, whose hospitality J.G.A. enjoyed from September, 1951 to June, 1952 under a Fulbright grant.

[7] Gutowsky, Kistiakowsky, Pake, and Purcell, J. Chem. Phys. **17**, 972 (1949).

The Third Virial Coefficient of a Lennard-Jones Gas by Kihara's Method with Tables for the 6–9 Potential*†

LEO F. EPSTEIN, CELESTA J. HIBBERT, MARION D. POWERS, AND GLENN M. ROE
General Electric Company, Knolls Atomic Power Laboratory, Schenectady, New York

(Received July 16, 1953)

Kihara has shown that the third virial coefficient of a Lennard-Jones 6–9 gas can be expressed as a convergent power series of the form $\Sigma_j \beta_j(s)\theta^{(s-6)j/s}$ with $\theta=\epsilon/kT$. In this paper the coefficients $\beta_j(s)$, which are rather complicated double integrals, are developed and applied to the case $s=9$. For $j<20$ the coefficients are obtained by numerical quadrature, using high-speed computing equipment. Asymptotic formulas for arbitrary s are used to extrapolate the numerical results for $s=9$ into the range $20<j<100$. Values of the normalized third virial coefficient, $C_9^{(0)}(\theta)$ and its derivatives, computed from Kihara's series, are tabulated for the range $0<\theta<2$. An asymptotic expression for $C_s^{(0)}(\theta)$ is used to extend the tables to higher values of θ.

THE third virial coefficient of a gas $C(T)$ in the equation of state

$$PV/RT=1+B(T)/V+C(T)/V^2+\cdots \quad (1)$$

has been computed approximately by de Boer and Michels,[1] and Montroll and Mayer,[2] and more accurately by Bird, Spotz, and Hirschfelder[3] using the Lennard-Jones potential function

$$U_s(r)=\{\epsilon/(s-6)\}[6(r_0/r)^s-s(r_0/r)^6] \quad (2)$$

with $s=12$. Kihara[4,5] has shown that the triple integral for $C(T)$ can, for the LJ potential, be expanded in a power series in $\theta\equiv\epsilon/kT$ with the coefficients given by double integrals. His results may be written

$$C_s(T)=10v_0^2\sum_{j=0}^{\infty}\gamma_j(s)x_s^j, \quad (3a)$$

where

$$v_0=(\pi/6)Nr_0^3[6\theta/(s-6)]^{3/s} \quad (3b)$$

$$x_s=(s/12)[6\theta/(s-6)]^{(s-6)/s} \quad (3c)$$

and

$$\gamma_j(s)=(-72/5s)(2^j/j!)[(6j/s)-(6/s)-1]!I_j(s). \quad (3d)$$

In these equations

$$I_j(s)=2\int_0^1 dR\int_{1-R}^1 RTA_j'(R,T)dT, \quad (4a)$$

TABLE I. Definitions of δ_i and $\Phi_i(k)$.

i	δ_i	$\Phi_i(k)$
1	+1	$1+R^{-k}+T^{-k}$
2	−1	$1+R^{-k}$
3	−1	$1+T^{-k}$
4	−1	$R^{-k}+T^{-k}$
5	+1	1
6	+1	R^{-k}
7	+1	T^{-k}

TABLE II. $\gamma_j(9)$ for low j values.

j	$I_j(9)$	$\gamma_j(9)$	(Kihara's value)	% difference
0	+0.2425 66	+1.5595 67	(+1.561)	+0.09
1	+0.9186 65[a]	−2.9397 28	(−2.940)	+0.009$_2$
2	−0.2150 99	+0.9320 61	(+0.929)	−0.3
3	−0.3832 83	+0.7301 63	(+0.716)	−1.9
4	−0.4765 42	+0.5083 11	(+0.503)	−1.0
5	−0.4548 84	+0.2920 14	(+0.291)	−0.3$_5$
6	−0.2616 05	+0.1033 64	(+0.105)	+1.6
7	+0.1832 80	−0.0446 854	(−0.04)	−10
8	+0.9921 17	−0.1482 71	(−0.14)	−5.6
9	+2.3222 00	−0.2103 70	(−0.20)	−5.2
10	+4.3931 89	−0.2380 23	(−0.23)	−3.5
11	+7.5112 27	−0.2398 80	(−0.23)	−4.3
12	+12.1023 44	−0.2244 41		
13	+18.7587 11	−0.1990 04$_6$		
14	+28.3027 49	−0.1692 25		
15	+41.8759 82	−0.1390 74		
16	+61.0622 66	−0.1110 49		
17	+88.0587 88	−0.0864 902		
18	+125.9134 62	−0.0658 988		
19	+178.8547 22	−0.0492 324$_5$		
20	+252.7499 69	−0.0361 322		

[a] $\lim_{j\to 1}[\frac{1}{2}(j-1)]!I_j(9)$.

where

$$A_j'(R,T)=\sum_{i=1}^{7}\delta_i[\Phi_i(6)]^j[\Phi_i(s)]^{6(1-j)/s},\ (j\neq 1) \quad (4b)$$

$$\lim_{j\to 1}A_j'(R,T)[(6j/s)-(6/s)-1]!$$

$$=-\sum_{i=1}^{7}\delta_i\Phi_i(6)\ln\Phi_i(s),\ (j=1) \quad (4c)$$

* Operated for the United States Atomic Energy Commission by the General Electric Company Contract No. W-31-109 Eng. 52.

† This paper is an abbreviated version of a more detailed study which will be published by the Technical Information Service of the U. S. Atomic Energy Commission (Oak Ridge, Tennessee) as Document AECU-2731, and will be available shortly through the Office of Technical Services, Department of Commerce, Washington 25, D. C. The longer paper includes the derivations of many of the equations presented here, and a great many details of the computation.

[1] J. de Boer, and A. Michels, Physica **6**, 97 (1939).
[2] E. W. Montroll, and J. E. Mayer, J. Chem. Phys. **9**, 626 (1941).
[3] Bird, Spotz, and Hirschfelder, J. Chem. Phys. **18**, 1395 (1950).
[4] T. Kihara, J. Phys. Soc. Japan **3**, 265 (1948).
[5] T. Kihara, J. Phys. Soc. Japan **6**, 184 (1950); see also Revs. Modern Phys. **25**, 831 (1953).

TABLE III. The coefficients $\beta_j(9)$.[a]

j	$\beta_j^{(9)}$	j	$\beta_j^{(9)}$	j	$\beta_j^{(9)}$	j	$\beta_j^{(9)}$
0	+3.481 395 (0)	26	−2.140 (−3)	51	−2.019 (−9)	76	−5.619 (−17)
1	−6.200 988 (0)	27	−1.354 (−3)	52	−1.066 (−9)	77	−2.651 (−17)
2	+1.857 816 (0)	28	−8.475 (−4)	53	−5.595 (−10)	78	−1.246 (−17)
3	+1.375 254 (0)	29	−5.254 (−4)	54	−2.922 (−10)	79	−5.837 (−18)
4	+9.046 849 (−1)	30	−3.226 (−4)	55	−1.519 (−10)	80	−2.723 (−18)
5	+4.911 067 (−1)						
		31	−1.963 (−4)	56	−7.852 (−11)	81	−1.266 (−18)
6	+1.642 656 (−1)	32	−1.184 (−4)	57	−4.039 (−11)	82	−5.864 (−19)
7	−6.710 383 (−2)	33	−7.080 (−5)	58	−2.068 (−11)	83	−2.706 (−19)
8	−2.103 984 (−1)	34	−4.200 (−5)	59	−1.054 (−11)	84	−1.244 (−19)
9	−2.820 818 (−1)	35	−2.471 (−5)	60	−5.343 (−12)	85	−5.703 (−20)
10	−3.015 874 (−1)						
		36	−1.443 (−5)	61	−2.697 (−12)	86	−2.604 (−20)
11	−2.872 060 (−1)	37	−8.363 (−6)	62	−1.355 (−12)	87	−1.185 (−20)
12	−2.539 252 (−1)	38	−4.811 (−6)	63	−6.775 (−13)	88	−5.375 (−21)
13	−2.127 512 (−1)	39	−2.749 (−6)	64	−3.373 (−13)	89	−2.429 (−21)
14	−1.709 534 (−1)	40	−1.559 (−6)	65	−1.672 (−13)	90	−1.094 (−21)
15	−1.327 586 (−1)						
		41	−8.787 (−7)	66	−8.250 (−14)	91	−4.913 (−22)
16	−1.001 703 (−1)	42	−4.919 (−7)	67	−4.054 (−14)	92	−2.199 (−22)
17	−7.372 150 (−2)	43	−2.736 (−7)	68	−1.983 (−14)	93	−9.808 (−23)
18	−5.307 736 (−2)	44	−1.512 (−7)	69	−9.663 (−15)	94	−4.361 (−23)
19	−3.747 036 (−2)	45	−8.307 (−8)	70	−4.688 (−15)	95	−1.933 (−23)
20	−2.598 578 (−2)						
		46	−4.536 (−8)	71	−2.265 (−15)	96	−8.538 (−24)
21	−1.773 (−2)	47	−2.462 (−8)	72	−1.090 (−15)	97	−3.760 (−24)
22	−1.192 (−2)	48	−1.329 (−8)	73	−5.225 (−16)	98	−1.651 (−24)
23	−7.903 (−3)	49	−7.129 (−9)	74	−2.494 (−16)	99	−7.225 (−25)
24	−5.174 (−3)	50	−3.804 (−9)	75	−1.186 (−16)	100	−3.153 (−25)
25	−3.347 (−3)						

[a] The numbers in parentheses indicate the power of ten by which the tabulated values are to be multiplied, e.g., $\beta_{50}^{(9)} = -3.804 \times 10^{-9}$.

and $\Phi_i(k)$ is given in Table I. The form of Eq. (4a) differs somewhat from Kihara's original integral (3d) and is more convenient for numerical evaluation.

The case $s=9$ is of particular interest for reasons which have been discussed elsewhere.[6] The IBM computing equipment available at this laboratory has been used to recalculate Kihara's values for $\gamma_j(9)$ and to extend the results to $j=20$. The double integral (4a) was computed numerically, essentially using a biquadratic integration formula and the mesh size $\Delta R=\Delta T=0.025$. The results are given in Table II.

For large j, the double integral may be evaluated by the method of steepest descents to obtain an asymptotic expression for $I_j(s)$. It has been found in this study that

$$I_j(s)\cong+\{[2\pi/(s-6)]3^{(s-6)j/s+(6/s)-\frac{1}{2}}(1/j)\}$$
$$\times[1+\{(2s^2+33s+72)/18(s-6)\}(1/j)+\cdots]. \quad (5)$$

Kihara's formulation includes an extra factor of $\frac{3}{2}$ in the leading term, and omits the correction terms given above. In the range in which he used his asymptotic result ($s=12$, $12\leqslant j\leqslant 17$), the neglected correction terms amount to very nearly $\frac{3}{2}$. For larger j values however, Kihara's formula gives values of $I_j(s)$ which are too large.‡ For the computation of $I_j(9)$ for $j>20$, Eq. (5) did not provide the required accuracy and was replaced by

$$I_j(s)=[2\pi/(s-6)](1/j)3^{(s-6)j/s+6/s-\frac{1}{2}}F_s(j), \quad (6)$$

where $F_j(s)$ is a function which includes the correction term in (5), and in addition some higher terms empirically fitted to the values of $I_j(9)$ for $10\leqslant j\leqslant 20$.

The "normalized third virial coefficient" is defined by[3]

$$C_s^{(0)}(\theta)\equiv C_s(T)/(2\pi N\sigma_s^3/3)^2 \quad (7a)$$
$$=\sum_{j=0}^{\infty}\beta_j(s)\theta^{(s-6)j/s+6/s}, \quad (7b)$$

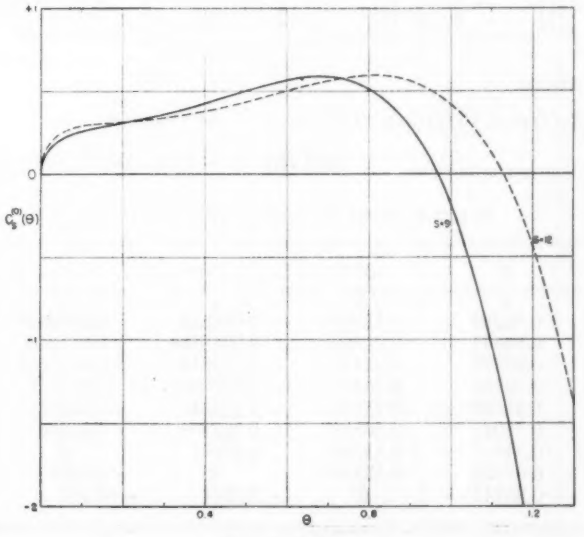

FIG. 1. $C_s^{(0)}(\theta)$.

[6] Roe, Epstein, and Powers, J. Chem. Phys. **20**, 1665 (1952).

‡ Professor Kihara has recently advised (private communication, November 20, 1953) that he has discovered a mistake of a factor of $\frac{3}{2}$ in his original article, so that his expression for the asymptotic form is now in complete agreement with the leading term of Eq. 5.

TABLE IV. Normalized third virial coefficient and its derivatives for a 6–9 gas.

θ	$C_9^{(0)}(\theta)$	$C_9^{(1)}(\theta)$	$C_9^{(2)}(\theta)$
0	0	0	0
0.0005	+ 0.018 909	− 0.011 626	+ 0.010 417
0.0010	+ 0.028 813	− 0.017 281	+ 0.026 925
0.0015	+ 0.036 666	− 0.021 586	+ 0.033 211
0.0020	+ 0.043 377	− 0.025 145	+ 0.038 274
0.0025	+ 0.049 325	− 0.028 208	+ 0.042 588
0.0030	+ 0.054 711	− 0.030 907	+ 0.046 193
0.0035	+ 0.059 661	− 0.033 325	+ 0.049 403
0.0040	+ 0.064 256	− 0.035 516	+ 0.052 248
0.0045	+ 0.068 556	− 0.037 519	+ 0.054 794
0.0050	+ 0.072 606	− 0.039 363	+ 0.057 086
0.0055	+ 0.076 439	− 0.041 070	+ 0.059 161
0.0060	+ 0.080 081	− 0.042 657	+ 0.061 048
0.0065	+ 0.083 555	− 0.044 139	+ 0.062 770
0.0070	+ 0.086 877	− 0.045 527	+ 0.064 345
0.0075	+ 0.090 063	− 0.046 831	+ 0.065 790
0.0080	+ 0.093 125	− 0.048 058	+ 0.067 116
0.0085	+ 0.096 074	− 0.049 215	+ 0.068 336
0.0090	+ 0.098 918	− 0.050 309	+ 0.069 459
0.0095	+ 0.101 666	− 0.051 344	+ 0.070 494
0.010	+ 0.104 325	− 0.052 326	+ 0.071 313
0.012	+ 0.114 181	− 0.055 787	+ 0.074 568
0.014	+ 0.123 002	− 0.058 639	+ 0.076 799
0.016	+ 0.130 992	− 0.061 012	+ 0.078 351
0.018	+ 0.138 296	− 0.063 000	+ 0.079 373
0.020	+ 0.145 023	− 0.064 670	+ 0.079 974
0.022	+ 0.151 254	− 0.066 076	+ 0.080 237
0.024	+ 0.157 056	− 0.067 257	+ 0.080 226
0.026	+ 0.162 480	− 0.068 247	+ 0.079 993
0.028	+ 0.167 568	− 0.069 072	+ 0.079 580
0.030	+ 0.172 358	− 0.069 755	+ 0.079 021
0.032	+ 0.176 878	− 0.070 313	+ 0.078 345
0.034	+ 0.181 155	− 0.070 764	+ 0.077 577
0.036	+ 0.185 210	− 0.071 119	+ 0.076 737
0.038	+ 0.189 063	− 0.071 392	+ 0.075 843
0.040	+ 0.192 730	− 0.071 591	+ 0.074 911
0.042	+ 0.196 227	− 0.071 726	+ 0.073 954
0.044	+ 0.199 566	− 0.071 806	+ 0.072 983
0.046	+ 0.202 758	− 0.071 836	+ 0.072 010
0.048	+ 0.205 815	− 0.071 823	+ 0.071 044
0.05	+ 0.208 746	− 0.071 772	+ 0.070 092
0.06	+ 0.221 783	− 0.071 121	+ 0.065 790
0.07	+ 0.232 673	− 0.070 121	+ 0.062 699
0.08	+ 0.241 968	− 0.069 084	+ 0.061 243
0.09	+ 0.250 053	− 0.068 219	+ 0.061 688
0.10	+ 0.257 209	− 0.067 674	+ 0.064 198
0.11	+ 0.263 649	− 0.067 553	+ 0.068 873
0.12	+ 0.269 540	− 0.067 935	+ 0.075 765
0.13	+ 0.275 011	− 0.068 874	+ 0.084 889
0.14	+ 0.280 167	− 0.070 410	+ 0.096 231
0.15	+ 0.285 095	− 0.072 570	+ 0.109 754
0.16	+ 0.289 864	− 0.075 372	+ 0.125 400
0.17	+ 0.294 534	− 0.078 826	+ 0.143 095
0.18	+ 0.299 153	− 0.082 933	+ 0.162 746
0.19	+ 0.303 761	− 0.087 692	+ 0.184 247
0.20	+ 0.308 394	− 0.093 093	+ 0.207 475
0.21	+ 0.313 080	− 0.099 125	+ 0.232 295
0.22	+ 0.317 842	− 0.105 770	+ 0.258 555
0.23	+ 0.322 701	− 0.113 007	+ 0.286 092
0.24	+ 0.327 674	− 0.120 812	+ 0.314 725
0.25	+ 0.332 773	− 0.129 156	+ 0.344 262
0.26	+ 0.338 009	− 0.138 009	+ 0.374 494
0.27	+ 0.343 391	− 0.147 335	+ 0.405 198
0.28	+ 0.348 924	− 0.157 097	+ 0.436 165
0.29	+ 0.354 613	− 0.167 252	+ 0.467 049
0.30	+ 0.360 460	− 0.177 757	+ 0.497 669
0.31	+ 0.366 464	− 0.188 563	+ 0.527 706
0.32	+ 0.372 624	− 0.199 620	+ 0.556 853
0.33	+ 0.378 939	− 0.210 872	+ 0.584 785
0.34	+ 0.385 403	− 0.222 261	+ 0.611 159
0.35	+ 0.392 011	− 0.233 727	+ 0.635 610
0.36	+ 0.398 756	− 0.245 204	+ 0.657 754
0.37	+ 0.405 630	− 0.256 623	+ 0.677 185
0.38	+ 0.412 624	− 0.267 912	+ 0.693 474
0.39	+ 0.419 727	− 0.278 995	+ 0.706 172
0.40	+ 0.426 928	− 0.289 791	+ 0.714 804
0.41	+ 0.434 212	− 0.300 217	+ 0.718 868
0.42	+ 0.441 567	− 0.310 183	+ 0.717 841
0.43	+ 0.448 978	− 0.319 597	+ 0.711 169
0.44	+ 0.456 427	− 0.328 362	+ 0.698 273
0.45	+ 0.463 897	− 0.336 377	+ 0.678 542
0.46	+ 0.471 370	− 0.343 534	+ 0.651 339
0.47	+ 0.478 827	− 0.349 722	+ 0.615 992
0.48	+ 0.486 245	− 0.354 825	+ 0.571 798
0.49	+ 0.493 603	− 0.358 721	+ 0.518 021
0.50	+ 0.500 879	− 0.361 283	+ 0.453 890
0.51	+ 0.508 046	− 0.362 380	+ 0.378 596
0.52	+ 0.515 081	− 0.361 872	+ 0.291 294
0.53	+ 0.521 955	− 0.359 616	+ 0.191 100
0.54	+ 0.528 642	− 0.355 462	+ 0.077 088
0.55	+ 0.535 111	− 0.349 253	− 0.051 711
0.56	+ 0.541 332	− 0.340 826	− 0.196 305
0.57	+ 0.547 272	− 0.330 012	− 0.357 753
0.58	+ 0.552 900	− 0.316 634	− 0.537 159
0.59	+ 0.558 179	− 0.300 509	− 0.735 674
0.60	+ 0.563 074	− 0.281 444	− 0.954 503
0.61	+ 0.567 548	− 0.259 243	− 1.194 90
0.62	+ 0.571 560	− 0.233 698	− 1.458 18
0.63	+ 0.575 072	− 0.204 593	− 1.745 70
0.64	+ 0.578 041	− 0.171 707	− 2.058 90
0.65	+ 0.580 424	− 0.134 808	− 2.399 25
0.66	+ 0.582 174	− 0.093 654	− 2.768 32
0.67	+ 0.583 246	− 0.047 997	− 3.167 70
0.68	+ 0.583 590	+ 0.002 425	− 3.599 10
0.69	+ 0.583 157	+ 0.057 879	− 4.064 25
0.70	+ 0.581 895	+ 0.118 646	− 4.564 99
0.71	+ 0.579 749	+ 0.185 016	− 5.103 22
0.72	+ 0.576 664	+ 0.257 289	− 5.680 91
0.73	+ 0.572 583	+ 0.335 778	− 6.300 12
0.74	+ 0.567 445	+ 0.420 806	− 6.963 01
0.75	+ 0.561 189	+ 0.512 709	− 7.671 80
0.76	+ 0.553 751	+ 0.611 833	− 8.428 81
0.77	+ 0.545 066	+ 0.718 541	− 9.236 47
0.78	+ 0.535 064	+ 0.833 205	− 10.097 3
0.79	+ 0.523 677	+ 0.956 212	− 11.013 8
0.80	+ 0.510 832	+ 1.087 96	− 11.988 9
0.81	+ 0.496 453	+ 1.228 88	− 13.025 2
0.82	+ 0.480 463	+ 1.379 38	− 14.125 7
0.83	+ 0.462 783	+ 1.539 91	− 15.293 6
0.84	+ 0.443 329	+ 1.710 95	− 16.531 9
0.85	+ 0.422 017	+ 1.892 95	− 17.843 9
0.86	+ 0.398 759	+ 2.086 43	− 19.233 1
0.87	+ 0.373 465	+ 2.291 89	− 20.702 9
0.88	+ 0.346 040	+ 2.509 85	− 22.257 2
0.89	+ 0.316 390	+ 2.740 88	− 23.899 7
0.90	+ 0.284 414	+ 2.985 52	− 25.634 4
0.91	+ 0.250 010	+ 3.244 38	− 27.465 4
0.92	+ 0.213 073	+ 3.518 06	− 29.397 0
0.93	+ 0.173 494	+ 3.807 18	− 31.433 7
0.94	+ 0.131 160	+ 4.112 40	− 33.580 0
0.95	+ 0.085 957	+ 4.434 38	− 35.840 7
0.96	+ 0.037 765	+ 4.773 82	− 38.220 9
0.97	− 0.013 539	+ 5.131 44	− 40.725 7
0.98	− 0.068 081	+ 5.507 97	− 43.360 3
0.99	− 0.125 991	+ 5.903 93	− 46.130 5
1.00	− 0.187 403	+ 6.320 89	− 49.041 8
1.05	− 0.551 979	+ 8.741 21	− 65.933 0
1.10	− 1.026 66	+ 11.808 6	− 87.347 8
1.15	− 1.633 30	+ 15.656 5	− 114.283
1.20	− 2.397 11	+ 20.441 3	− 147.928
1.25	− 3.347 11	+ 26.346 4	− 189.699
1.30	− 4.516 75	+ 33.586 8	− 241.282
1.35	− 5.944 40	+ 42.413 2	− 304.676
1.40	− 7.674 18	+ 53.118 9	− 382.252
1.45	− 9.756 63	+ 66.045 5	− 476.818
1.50	−12.249 7	+ 81.590 9	− 591.692
1.55	−15.219 6	+100.218	− 730.796
1.60	−18.742 4	+122.467	− 898.756
1.65	−22.904 7	+148.961	−1101.49
1.70	−27.805 6	+180.428	−1273.81
1.75	−33.558 3	+217.710	−2793.94
1.80	−40.292 1	+261.784	−1983.78
1.85	−48.154 2	+313.781	−2399.85
1.90	−57.313 0	+375.013	−2895.80
1.95	−67.960 0	+446.998	−3486.02
2.00	−80.313 5	+531.489	−4184.64

where

$$\beta_j(s) = -(9/s)(s/6)^{j+6/(s-6)}(6/s-6)^{(s-6)j/s+6/s} \times\{[(6j-6-s)/s]!/j!\}I_j(s) \quad (8)$$

TABLE V. Zeros and turning points in $C_9^{(n)}(\theta)$.

θ	$C_9^{(0)}(\theta)$	$-C_9^{(1)}(\theta)$	$C_9^{(2)}(\theta)$
0	0	0	0
0.02289	0.15389	0.066627	0.080262[a]
0.04635	0.20330	0.071836[a]	0.071840
0.08279	0.24434	0.068818	0.061168[a]
0.10758	0.26215	0.067539[a]	0.067539
0.41309	0.43648	0.30334	0.71912[a]
0.51047	0.50838	0.36239[a]	0.37479
0.54613	0.53263	0.35191	0
0.67954	0.58359[a]	0	−3.5786
0.96742	0	−5.0374	−40.067

[a] Extremum.

and

$$\sigma_s = r_0(6/s)^{[1/(s-6)]} \quad (9)$$

(so that $U_s(\sigma_s)=0$). The coefficients $\beta_j(9)$ for $0 \leqslant j \leqslant 100$ are given in Table III, and values of $C^{(0)}(\theta)$ and the derivative functions[3]

$$C_9^{(1)}(\theta) = (1/\theta)dC_9^{(0)}(\theta)/d(1/\theta) = -\sum_{j=0}^{\infty}[\beta_j(9)\cdot(j+2)/3]\theta^{(j+2)/3} \quad (10a)$$

and

$$C_9^{(2)}(\theta) = (1/\theta^2)d^2C_9^{(0)}(\theta)/d(1/\theta)^2 = +\sum_{j=0}^{\infty}[\beta_j(9)\cdot(j+2)(j+5)/9]\theta^{(j+2)/3} \quad (10b)$$

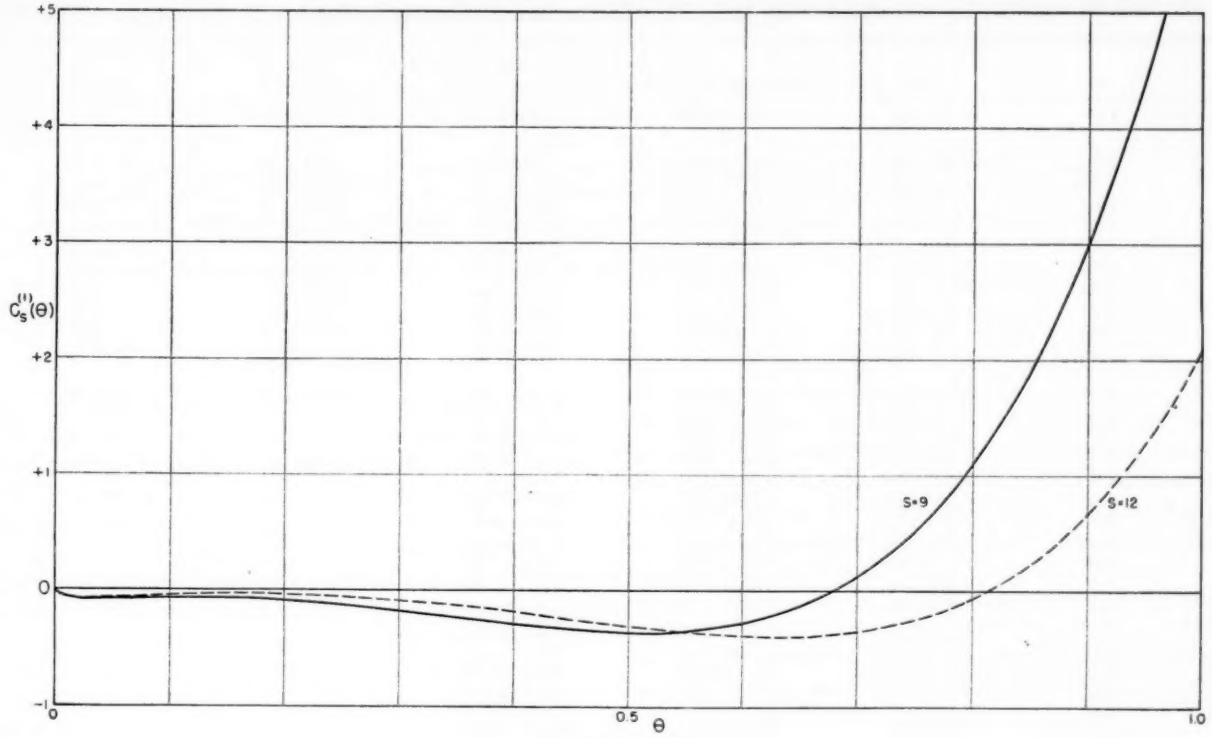

FIG. 2. $C_s^{(1)}(\theta)$.

are presented in Tables IV and V. For comparison with the results[3] for $s=12$ these quantities are plotted in Figs. 1 to 3.

For very low temperatures (θ large) the power series [Eq. (7b)] is useless for direct computation. However the limiting form for the coefficients for large j is known, and the sum can be replaced by an integral to yield an asymptotic result valid for large θ. It is found that

$$C_s^{(0)}(\theta)\cong -6(s/6)^{6/(s-6)}(\pi/3s)^{\frac{1}{2}}\theta^{-\frac{1}{2}}e^{+3\theta}F_s\{3s\theta/(s-6)\}$$
$$\times[1+(1/216s)(s^2+165s+900)(1/\theta)+f_s(\theta)], \quad (11)$$

where $f_s(\theta)$ is an empirical function fitted in the case $s=9$ to the region $1.5\leqslant\theta\leqslant 2$. Table VI gives the low-temperature virial coefficients computed from this relation.

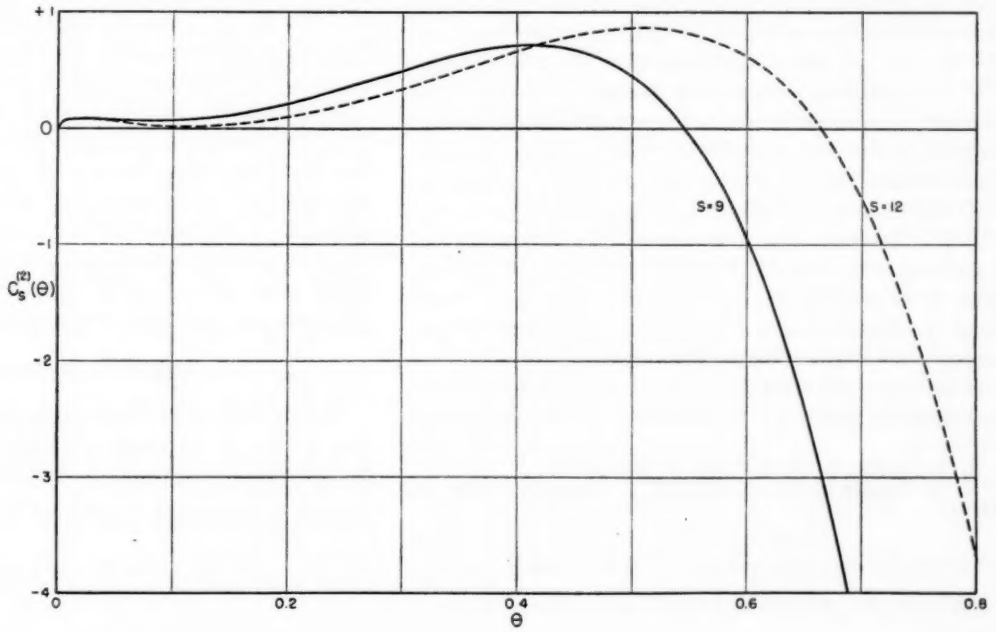

FIG. 3. $C_s^{(2)}(\theta)$.

TABLE VI. Low-temperature third virial coefficients for a 6–9 gas.

θ	$F_9(9\theta)$	$[\pi/6(\pi/3)^{\frac{1}{2}}](\theta^{-\frac{1}{2}}e^{+3\theta})$	$-C_9^{(0)}(\theta)$ (Eq. 11)	$-C_9^{(0)}(\theta)$ (Table IV)	% diff.
1.0	0.282 148	1.0762×10^{1}	1.381×10^{-1}	1.874×10^{-1}	+36
1.50	0.883 288	2.6254×10^{1}	1.209×10^{1}	1.225×10^{1}	+ 1.3
1.55	0.929 543	2.9039×10^{1}	1.514×10^{1}	1.522×10^{1}	+ 0.53
1.60	0.972 615	3.2170×10^{1}	1.873×10^{1}	1.874×10^{1}	+ 0.05
1.65	1.014 559	3.5690×10^{1}	2.299×10^{1}	2.290×10^{1}	− 0.39
1.70	1.053 282	3.9650×10^{1}	2.795×10^{1}	2.781×10^{1}	− 0.50
1.75	1.089 690	4.4106×10^{1}	3.376×10^{1}	3.356×10^{1}	− 0.60
1.80	1.123 448	4.9124×10^{1}	4.050×10^{1}	4.029×10^{1}	− 0.52
1.85	1.155 022	5.4776×10^{1}	4.833×10^{1}	4.815×10^{1}	− 0.37
1.90	1.183 908	6.1145×10^{1}	5.736×10^{1}	5.731×10^{1}	− 0.09
1.95	1.210 563	6.8326×10^{1}	6.777×10^{1}	6.796×10^{1}	+ 0.28
2.0	1.236 252	7.6425×10^{1}	7.984×10^{1}	8.031×10^{1}	+ 0.59
2.5	1.395 373	2.4508×10^{2}	3.55×10^{2}		
3.0	1.447 664	8.3557×10^{2}	1.38×10^{3}		
3.5	1.447 153	2.9717×10^{3}	5.14×10^{3}		
4.0	1.422 226	1.0901×10^{4}	1.89×10^{4}		
4.5	1.387 676	4.0942×10^{4}	6.945×10^{4}		
5.0	1.351 150	1.5667×10^{5}	2.58×10^{5}		
5.5	1.316 372	6.0859×10^{5}	9.69×10^{5}		
6.0	1.284 920	2.3938×10^{6}	3.69×10^{6}		
6.5	1.257 246	9.5145×10^{6}	1.42×10^{7}		
7.0	1.233 235	3.8155×10^{7}	5.54×10^{7}		
7.5	1.212 533	1.5419×10^{8}	2.18×10^{8}		
8.0	1.194 699	6.2726×10^{8}	8.67×10^{8}		
8.5	1.179 311	2.5668×10^{9}	3.48×10^{9}		
9.0	1.165 978	1.0558×10^{10}	1.40×10^{10}		
9.5	1.154 367	4.3634×10^{10}	5.71×10^{10}		
10.0	1.144 198	1.8107×10^{11}	2.33×10^{11}		
10.5	1.135 250	7.5423×10^{11}	9.60×10^{11}		
11.0	1.127 298	3.1524×10^{12}	3.96×10^{12}		

It is of interest to compare the leading terms in (11) with the corresponding expression for the low temperature second virial coefficient[6,7]

$$B_s^{(0)}(\theta)\cong-3(s/6)^{3/(s-6)}(\pi/3s)^{\frac{1}{2}}(\theta^{-\frac{1}{2}}e^{+\theta}) \quad (12a)$$

$$C_s^{(0)}(\theta)\cong-6(s/6)^{6/(s-6)}(\pi/3s)^{\frac{3}{2}}(\theta^{-\frac{1}{2}}e^{+\theta})^3. \quad (12b)$$

Note that, in this low-temperature form at least, $C_s^{(0)}(\theta)$ varies with temperature much more strongly than does $B_s^{(0)}(\theta)$, i.e., as the cube rather than the first power of $\theta^{-\frac{1}{2}}e^{+\theta}$. It has been pointed out previously that it is not possible from experiments over a limited temperature range to determine the value of the repulsive exponent s from measurements of the second virial coefficient;[8] from the results of this section, and the curves in Figs. 1 to 3, it appears that it would require extremely precise measurement to obtain s from third virial coefficient data. It is possible that if both the second and third virial coefficients are well known as functions of temperature, a better estimate of the value of s can be made.

In applying the relations for $C_s^{(0)}(\theta)$ for large θ above, care must be taken not to use them at temperatures so low that the assumption of a continuous energy spectrum, made in Eq. (2), is invalid. For extremely low temperatures, the fact that the energy levels are discrete rather than continuous must be taken into account, and proper quantum mechanical corrections applied. In the case of $B_s^{(0)}(\theta)$, these terms are nearly proportional to $(\theta/M\epsilon\sigma^2)$ or some power of this quantity,[9] and while important for light gases such as H_2, D_2, and He, will usually be negligible for materials of higher molecular weight M. The same kind of limitations can be expected to apply to $C_s^{(0)}(\theta)$.

It should also be emphasized that Eq. (2) and all of the subsequent equations in this paper assume that the potential field about each molecule is spherically symmetrical, and gross errors may result from the application of the results herein to polar molecules or to systems such as long chain hydrocarbons where the condition that the potential field is dependent only on distance, not on angles, would not be expected to apply.

ACKNOWLEDGMENTS

The authors wish to express their deepest appreciation to Dr. R. H. Stark and Mr. W. H. Howland for their invaluable assistance in this study.

[7] L. F. Epstein, J. Chem. Phys. **20**, 1670 (1952).
[8] L. F. Epstein and C. J. Hibbert, J. Chem. Phys. **20**, 752 (1952).
[9] L. F. Epstein and G. M. Roe, J. Chem. Phys. **19**, 1320 (1951).

The Development of a Quantum-Mechanical Model for the Lithium Fluoride Molecule†

G. C. BENSON AND B. M. E. VAN DER HOFF*
Division of Pure Chemistry, National Research Council, Ottawa, Canada
(Received July 30, 1953)

A quantum-mechanical model of the LiF molecule is developed using four different forms of wave functions. The most refined form (Sec. III, part iii) considers the transfer of electrons to an excited state of the F^- ion and possible covalency of the bond. This leads to values of the binding energy, internuclear distance, and dipole moment which are in reasonable agreement with available data. The inclusion of about 11 percent covalent character is essential for the success of the model proposed.

I. INTRODUCTION

A NUMBER of models to represent the properties of gaseous "ionic" diatomic molecules, such as the alkali halides, have been described in the literature. In most of these, a classical or semiempirical approach is adopted. The energy of interaction between the ions of the molecule is represented by certain forms which have been used in the Born-Mayer lattice theory of ionic crystals, with added terms to allow for the polarization energy of the ions. The expressions employed contain several adjustable parameters. Born and Heisenberg,[1] Verwey and de Boer[2] and others have identified the values of these parameters with those used in the calculation of the lattice energy of the crystalline solid, which in turn were chosen to give agreement with the observed lattice spacing and compressibility of the solid. In a later paper, Verwey and de Boer[3] describe an improved model in which the internuclear distance in the molecule as well as the crystal lattice spacing was used to determine the values of the parameters.

Recently, Rittner[4] has rejected the use of crystal data and employed the internuclear distance in the molecule, along with the force constant obtained from molecular spectra. In this way, a consistent picture can be given for most of the alkali halide molecules. Similar calculations have been made for the alkali hydrides.[5]

In all these "classical" models no attempt is made to portray directly the intramolecular electronic charge distribution. It is true that frequently terms are introduced to represent the polarization energy, but whether these are applicable in the inhomogeneous electric field occurring within a molecule is open to question. A more fundamental approach to the problem is to determine the wave functions representing the electronic charge density. A rigorous solution of such a problem is impossible at present because of computational difficulties. However, admitting certain approximations, it is possible to make some progress in this direction. The hydrogen halides have been treated quantum mechanically by a number of authors,[6–10] but very little work appears to have been done on the alkali halides. In the present paper, the successive steps in developing a simple quantum-mechanical model for the case of the LiF molecule are described.

As far as possible, the notation and assumptions used are consistent with a previous paper[11] on the LiF crystal. The essential features of that paper are summarized in the next section. Section III is divided into four parts. The first three of these demonstrate the effect on the binding energy, internuclear distance and dipole moment of successive refinements in the wave functions. The fourth part of this section deals with another possible intermediate form of wave function. In Sec. IV, the energy-internuclear distance curve for the best wave function (i.e., Sec. III, part iii) is considered in more detail. Finally, in Sec. V, the results of the calculations are compared with those of other authors and available experimental data.

II. DESCRIPTION OF THE MODEL

The structure of the LiF molecule is assumed to be mainly ionic, in the sense that it is considered to be derived from Li^+ and F^- ions having helium-like and neon-like quantum configurations, respectively. The coordinate system used in the description of the molecule is shown in Fig. 1, where the origin of a Cartesian set of axes is taken at the F^- nucleus and called position "a." The Li^+ ion is situated at position "b," a distance ρ along the $+z$ axis. Distances of any point P from the origin and the Li^+ ion are denoted by r_a and r_b. Atomic units[12] are used throughout the calculations unless otherwise stated.

Only the outer shell of electrons around the F^- ion is considered. Details of the inner structure are discarded and the F^- ion is simplified to a nucleus of charge $+5$

* National Research Council of Canada Postdoctorate Fellow 1951–1953; present address: Research and Development Division, Polymer Corporation Limited, Sarnia, Ontario, Canada.
† Issued as V.R.C. No. 3212.
[1] M. Born and W. Heisenberg, Z. Physik **23**, 388 (1924).
[2] E. J. W. Verwey and J. H. de Boer, Rec. trav. chim. **55**, 431 (1936).
[3] E. J. W. Verwey and J. H. de Boer, Rec. trav. chim. **59**, 633 (1940).
[4] E. S. Rittner, J. Chem. Phys. **19**, 1030 (1951).
[5] W. A. Klemperer and J. L. Margrave, J. Chem. Phys. **20**, 527 (1952).
[6] J. G. Kirkwood, Physik Z. **33**, 259 (1932).
[7] P. Gombas and T. Neugebauer, Z. Physik **92**, 375 (1934).
[8] D. Z. Robinson, J. Chem. Phys. **17**, 1022 (1949).
[9] D. Kastler, Compt. rend. **232**, 2323 (1951).
[10] J. I. Horvath, Z. Physik **129**, 56 (1951).
[11] G. C. Benson and G. Wyllie, Proc. Phys. Soc. (London) **64A**, 276 (1951).
[12] D. R. Hartree, Proc. Cambridge Phil. Soc. **24**, 89 (1928).

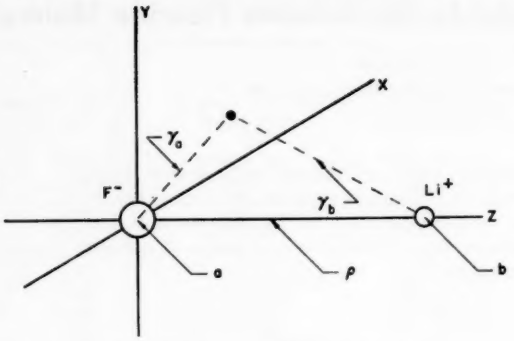

FIG. 1. The coordinate system.

surrounded by six $2p$ electrons. For a free F^- ion, these electrons are assigned in pairs with opposite spin to the orbitals

$$\psi_x = K_1 R(r_a) \sin\theta_a \cos\phi_a, \tag{1a}$$

$$\psi_y = K_1 R(r_a) \sin\theta_a \sin\phi_a, \tag{1b}$$

$$\psi_z = K_1 R(r_a) \cos\theta_a, \tag{1c}$$

where r_a, θ_a, and ϕ_a are the polar coordinates of an electron relative to the F^- nucleus at "a." The radial wave function $R(r_a)$ is given by

$$R(r_a) = r_a[A_1 \exp(-\alpha_1 r_a) + A_2 \exp(-\alpha_2 r_a)], \tag{2}$$

with

$$A_1 = 16.4459, \quad \alpha_1 = 3.29, \quad A_2 = 0.70387, \quad \alpha_2 = 1.18. \tag{3}$$

The method of selecting these values, using Hartree's self-consistent field data and Pauling's diamagnetic susceptibility for the F^- ion, has been described in reference 11. It can be shown that

$$\int_0^\infty [r_a R(r_a)]^2 dr_a = 1. \tag{4}$$

For normalization of the wave functions (1)

$$K_1 = (3/4\pi)^{\frac{1}{2}}. \tag{5}$$

In general, the Li^+ ion is treated as a point positive charge and account of the $1s$ electrons is taken only indirectly in the orthogonalization relations. For this latter purpose, an orbital of a $1s$ electron of the Li^+ ion at "b" is defined by the wave function

$$\phi = K_2 \exp(-\beta r_b), \tag{6}$$

where, for normalization,

$$K_2 = (\beta^3/\pi)^{\frac{1}{2}}. \tag{7}$$

In numerical calculations, $\beta = 2.69$[13,14] is used. The wave functions (1) and (6) are the same as those used successfully in reference 11 to calculate the cohesive energy, lattice spacing and compressibility of the LiF crystal.

[13] E. A. Hylleraas, Z. Physik **63**, 771 (1930).
[14] W. E. Duncanson and C. A. Coulson, Proc. Roy. Soc. (Edinburgh) **62A**, 37 (1944).

The Hamiltonian for a single $2p$ electron of the free F^- ion is

$$H = -\tfrac{1}{2}\nabla^2 + V(r_a), \tag{8}$$

in which $-V(r_a)$ expresses the average potential field acting on a $2p$ electron in the free ion. The wave functions (1) satisfy equations of the type

$$H\psi = \epsilon\psi. \tag{9}$$

If, by definition,

$$f(r_a) = V(r_a) - \epsilon, \tag{10}$$

it can be shown (reference 11, p. 280) that

$$f(r_a) = \frac{\alpha_1 A_1(\alpha_1 r_a - 4)\exp\{-\alpha_1 r_a\} + \alpha_2 A_2(\alpha_2 r_a - 4)\exp\{-\alpha_2 r_a\}}{2r_a[A_1 \exp\{-\alpha_1 r_a\} + A_2 \exp\{-\alpha_2 r_a\}]}. \tag{11}$$

The single electron Hamiltonian for a $2p$ electron of the F^- ion, when it is in the molecule, is assumed to be

$$H^M = H + v, \tag{12}$$

where v is the energy of the electron due to the potential field of the metal ion. Thus

$$v = -\frac{1}{r_b}. \tag{13}$$

In using H^M, changes in the electron-electron interaction due to the introduction of the Li^+ ion are neglected.

III. EQUILIBRIUM CONFIGURATION OF THE LiF MOLECULE

In this section, the use of a number of different forms of wave functions for the $2p$ electrons of the F^- ion in the molecule is considered.

i. Simple Orthogonalized Wave Functions

The importance of assigning the electrons of the F^- ion to orbitals which are orthogonal to the orbitals of the $1s$ electrons on the nearest neighbor Li^+ ions was noted in discussing the LiF crystal.[11] This suggests, for the LiF molecule, the use of the wave functions

$$\psi_x{}^M = \psi_x, \tag{14a}$$

$$\psi_y{}^M = \psi_y, \tag{14b}$$

$$\psi_z{}^M = C^M(\psi_z - S\phi), \tag{14c}$$

where

$$C^M = (1 - S^2)^{-\frac{1}{2}} \tag{15}$$

and S is the overlap integral between the orbitals ψ_z and ϕ,

$$S = (\psi_z|\phi). \tag{16}$$

Assigning the electrons to these orbitals, the energy of the molecule relative to that of the free ions is given by

$$U^M = 5/\rho + 2[\{(\psi_x{}^M|H^M|\psi_x{}^M) + (\psi_y{}^M|H|\psi_y{}^M) + (\psi_z{}^M|H^M|\psi_z{}^M)\} - \{(\psi_x|H|\psi_x) + (\psi_y|H|\psi_y) + (\psi_z|H|\psi_z)\}]. \tag{17}$$

This can be written as

$$U^M = 5/\rho + \Delta v(\rho) + 2h(\rho), \tag{18}$$

where

$$\Delta v(\rho) = 2[(\psi_x|v|\psi_x) + (\psi_y|v|\psi_y) + (\psi_z|v|\psi_z)] \tag{19}$$

and

$$h(\rho) = (C^M)^2 S[S\{\beta^2/2 - \beta + f(\rho) + (\psi_z|v|\psi_z)\} - 2(\psi_z|v|\phi)]. \tag{20}$$

The quantities S, $\Delta v(\rho)$, $(\psi_z|v|\psi_z)$, and $(\psi_z|v|\phi)$ are all two-center integrals and can be evaluated readily, as indicated in reference 11.

Curve i of Fig. 2 shows the variation of U^M with internuclear distance ρ. A polynomial in ρ was fitted to this curve and the minimum located by equating the slope to zero. The energy and internuclear spacing corresponding to the minimum are listed in Table I.

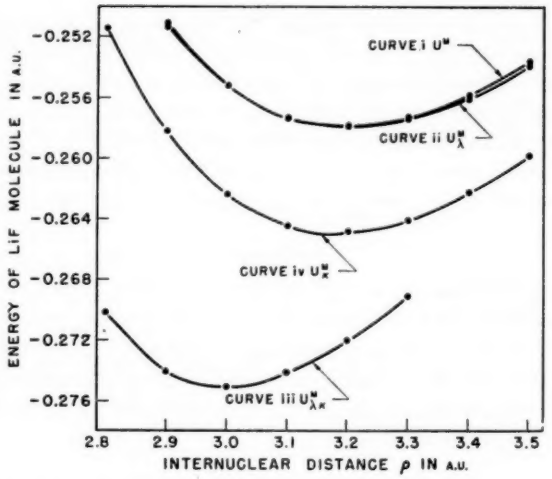

FIG. 2. Energy of the LiF molecule as a function of internuclear distance. The four curves correspond to the calculations described in parts i to iv of Sec. III.

The dipole moment of the molecule is given by

$$\mu = \rho + \mu^{el}. \tag{21}$$

The first term on the right-hand side is the contribution of a pure ionic bond, while the second term μ^{el} represents the dipole moment arising from the deviation of the $2p$ electron shell of the F^- ion from spherical symmetry. A positive value of μ^{el} therefore indicates a shift of the electrons in a direction away from the Li^+ ion.

From a consideration of the symmetry of the wave functions (14) it is apparent that only $\psi_z{}^M$ contributes to μ^{el}, thus

$$\mu^{el} = -2(\psi_z{}^M|z|\psi_z{}^M) = -2(C^M)^2 S[S\rho - 2(\psi_z|z|\phi)]. \tag{22}$$

The values of μ^{el} and μ corresponding to the minimum of curve i are given in Table I. It is not surprising that μ^{el} is positive since the distortion that has been allowed in the wave functions comes entirely from the orthogonalization. Thus it represents a repulsion of the electron cloud of the F^- ion by the $1s$ electrons of the Li^+ ion, as demanded by the Pauli principle.

From a classical consideration of a F^- ion polarized in the field of a positive charge, a negative value of μ^{el} might be expected. In the following parts of this section, several refinements of the wave function $\psi_z{}^M$ are introduced, in order to investigate their influence on the equilibrium configuration and in particular on the contribution of μ^{el} to the dipole moment of the molecule.

ii. Inclusion of an Excited State of the F^- Ion

In a recent paper developing equations to represent the interactions of closed shell ions, Montet, Keller, and Mayer[15] remark that "the energy of the alkali halide gas molecules will not be given adequately by such equations. The failure is due primarily to the failure of the assumption . . . that the one-electron functions of the assembly be made up of those of the isolated ions in their ground state." Thus it is of some interest to consider the possibility that in the presence of the Li^+ ion the p_z electrons of the F^- ion may be raised to a $3s$ state.

A simple form of wave function for the $3s$ state of a free fluorine ion has not been described in the literature. For the purpose of this paper a normalized orbital

$$\chi = \left[\frac{1}{4\pi} \times \frac{(2\gamma)^7}{6!}\right]^{\frac{1}{2}} r_a{}^2 e^{-\gamma r_a} \tag{23}$$

is assumed. This has the correct symmetry but the radial nodes have been compressed into the origin as in a Slater type of function. The method of selecting γ will be described at a later stage.

By analogy with (14c), an orthogonalized $3s$ orbital for the F^- ion in the molecule is defined as

$$\chi^M = E^M(\chi - U\phi) \tag{24}$$

with

$$E^M = (1 - U^2)^{-\frac{1}{2}} \tag{25}$$

and

$$U = (\chi|\phi). \tag{26}$$

χ^M is orthogonal to ϕ, $\psi_x{}^M$, and $\psi_y{}^M$. The overlap of χ^M with $\psi_z{}^M$ is

$$T = (\chi^M|\psi_z{}^M) = -C^M E^M S U. \tag{27}$$

In calculation of the energy of the LiF molecule, a linear combination of (14c) and (24)

$$\Psi_{z\lambda}{}^M = N_\lambda(\psi_z{}^M + \lambda\chi^M) \tag{28}$$

TABLE I. Values corresponding to the minima of the curves of Fig. 2.

Curve	$U_e{}^M$	ρ_e	λ	κ	μ^{el}	μ	$\mu^2 A$ esu² g cm⁴
(i)	−0.25784	3.195	···	···	0.033	3.228	1460×10^{-76}
(ii)	−0.25786	3.202	0.0064	···	0.021	3.223	1460×10^{-76}
(iii)	−0.27505	2.999	−0.2447	0.3903	−0.523	2.476	768×10^{-76}
(iv)	−0.26488	3.180	···	0.1478	−0.363	2.817	1100×10^{-76}

[15] Montet, Keller, and Mayer, J. Chem. Phys. **20**, 1057 (1952).

is used instead of (14c). The normalizing factor is

$$N_\lambda=[1+2\lambda T+\lambda^2]^{-\frac{1}{2}}. \quad (29)$$

The wave function $\Psi_{z\lambda}{}^M$ has cylindrical symmetry and allows for a varying degree of axial distortion, depending on the value of the parameter λ. Coulson[16] has discussed the use of this type of function for describing polarization effects.

The energy $U_\lambda{}^M$ of the molecule is

$$U_\lambda{}^M=U^M+2\delta_\lambda, \quad (30)$$

where

$$\delta_\lambda=(\Psi_{z\lambda}{}^M|H^M|\Psi_{z\lambda}{}^M)-(\psi_z{}^M|H^M|\psi_z{}^M). \quad (31)$$

For any ρ, the value of λ is selected to minimize δ_λ, or in other words the energy $U_\lambda{}^M$. It is easy to show that δ_λ and λ are solutions of

$$\delta_\lambda=\lambda[\{\psi_z{}^M;\chi^M\}-T\delta_\lambda] \quad (32)$$

and

$$\lambda=-\frac{[\{\psi_z{}^M;\chi^M\}-T\delta_\lambda]}{[\{\chi^M;\chi^M\}-\delta_\lambda]}, \quad (33)$$

where the bracket symbol† $\{\zeta;\xi\}$ for any two wave functions ζ and ξ is defined as

$$\{\zeta;\xi\}=(\zeta|H^M|\xi)-(\zeta|\xi)(\psi_z{}^M|H^M|\psi_z{}^M). \quad (34)$$

The two bracket symbols in Eqs. (32) and (33) may be written as

$$\{\psi_z{}^M;\chi^M\}=C^ME^M[SU(\beta^2/2+f(\rho)-\Delta\epsilon-\beta)+(\psi_z|v|\chi)-S(\chi|v|\phi)-U(\psi_z|v|\phi)]-T[(\psi_z|v|\psi_z)+h(\rho)], \quad (35)$$

$$\{\chi^M;\chi^M\}=(E^M)^2[(1-2U^2)\Delta\epsilon+U^2\{\beta^2/2+f(\rho)-\beta\}+(\chi|v|\chi)-2U(\chi|v|\phi)]-[(\psi_z|v|\psi_z)+h(\rho)]. \quad (36)$$

In these relations

$$\Delta\epsilon=(\chi|H|\chi)-(\psi_z|H|\psi_z) \quad (37)$$

and is identified with the energy of excitation $2p\rightarrow 3s$ for an electron in the free F^- ion. Bates[17] has estimated this energy to be 3.9 ev by an extrapolation of the ionization potentials of an isoelectronic series.‡

Before solving Eqs. (32) and (33) in general for δ_λ and λ, it is necessary to establish a value for the parameter γ. This is done by considering the solution of the problem for very large values of ρ. In that case, S, T, and U can be put equal to zero, and

$$\delta_\lambda=\lim_{\rho\ \text{large}}-\frac{\{\psi;\chi\}^2}{\{\chi;\chi\}}=\lim_{\rho\ \text{large}}-\frac{(\psi_z|v|\chi)^2}{\Delta\epsilon}. \quad (38)$$

This last expression has the form of a second-order perturbation term and on evaluation gives

$$\delta_\lambda=-\frac{30\,720\gamma^7}{\rho^4}\frac{}{\Delta\epsilon}\left[\frac{A_1}{(\alpha_1+\gamma)^7}+\frac{A_2}{(\alpha_2+\gamma)^7}\right]. \quad (39)$$

In a similar way,

$$U^M=\lim_{\rho\ \text{large}}\left[\frac{5}{\rho}+\Delta v(\rho)\right]=-\frac{1}{\rho}. \quad (40)$$

Hence,

$$U_\lambda{}^M=-\frac{1}{\rho}-\frac{2\times 30\,720\gamma^7}{\rho^4}\frac{}{\Delta\epsilon}\left[\frac{A_1}{(\alpha_1+\gamma)^7}+\frac{A_2}{(\alpha_2+\gamma)^7}\right]. \quad (41)$$

Equation (41) displays the energy of interaction for large values of ρ as the sum of a simple Coulomb term and a second which varies as the inverse fourth power of ρ. A value of $\gamma=0.7055$ is obtained by equating this last term to the classical polarization energy $-\frac{1}{2}(\alpha_F{}^-/\rho^4)$ and using a polarizability $\alpha_F{}^-=0.96\times 10^{-24}$ cm^3.[18–20]

Finally, δ_λ is calculated by solving the quadratic equation formed on elimination of λ from (32) and (33). The resulting energy $U_\lambda{}^M$ is shown in curve ii of Fig. 2. The second row of Table I gives values of $U_\lambda{}^M$, ρ, $\mu_\lambda{}^M$ etc., for the configuration corresponding to the minimum of this curve. For the purpose of calculating the dipole moment of the electrons, formula (22) is modified to

$$\mu_\lambda{}^{el}=-2(\Psi_{z\lambda}{}^M|z|\Psi_{z\lambda}{}^M). \quad (42)$$

A comparison of the first two rows of Table I shows that the energy has decreased very slightly and $\mu_\lambda{}^{el}<\mu^{el}$ but $\mu_\lambda{}^{el}$ is still positive. Apparently the Pauli principle is strong enough to keep the electrons away from the Li^+ ion even when the possibility of an excited $3s$ state of the F^- ion is considered.

iii. Inclusion of an Excited State of the F^- Ion and of Covalent Bond Character

A more drastic distortion of the electron distribution is envisaged in this part. The p_z electrons are assigned to a molecular orbital

$$\Psi_{z\lambda\kappa}{}^M=N_{\lambda\kappa}[\psi_z{}^M+\lambda\chi^M+\kappa\omega], \quad (43)$$

where

$$N_{\lambda\kappa}=[1+\lambda^2+\kappa^2+2\lambda T+2\kappa V+2\lambda\kappa W]^{-\frac{1}{2}} \quad (44)$$

and

$$\omega=\left(\frac{1}{4\pi}\right)^{\frac{1}{2}}N_4(r_b-0.878)e^{-0.720r_b}, \quad (45)$$

represents a $2s$ wave function for an electron in a lithium atom. The constants used in (45) are taken from the work of Coulson and Duncanson.[21] N_4 is a suitable normalizing factor, and V and W are overlap integrals

[16] C. A. Coulson, *Valence* (Oxford University Press, London, 1952), pp. 84, 207.

† No relation with Poisson brackets is implied here.

[17] D. R. Bates, Proc. Roy. Irish Acad. **51A**, 151 (1947).

‡ On the basis of a comparison of this energy with the electron affinity of fluorine given by Mayer and Helmholz, Bates concludes that the excited state is real in the free ion. However, in the light of recent work (see references 18 and 19) on the dissociation energy of F_2 and the experimental determination of the electron affinity, such a conclusion may be open to question.

[18] R. B. Bernstein and M. Metlay, J. Chem. Phys. **19**, 1612 (1951).

[19] P. W. Gilles and J. L. Margrave, J. Chem. Phys. **21**, 381 (1953).

[20] K. Fajans, Z. physik. Chem. **B24**, 118 (1934).

[21] C. A. Coulson and W. E. Duncanson, Proc. Roy. Soc. (London) **A181**, 378 (1943).

defined by

$$V=(\psi_z{}^M|\omega) \tag{46}$$

and

$$W=(\chi^M|\omega). \tag{47}$$

The inclusion of ω in (43) recognizes the possibility that the transfer of the electron from the Li atom to the F atom may not be complete in the molecule and that the bond may be partly covalent.

The values of λ and κ are chosen to minimize the energy

$$U_{\lambda\kappa}{}^M=U^M+2\delta_{\lambda\kappa} \tag{48}$$

for any given separation of the nuclei. Thus, λ, κ, and $\delta_{\lambda\kappa}$ must satisfy the equations

$$\delta_{\lambda\kappa}=\lambda[\{\psi_z{}^M;\chi^M\}-T\delta_{\lambda\kappa}]+\kappa[\{\psi_z{}^M;\omega\}-V\delta_{\lambda\kappa}], \tag{49}$$

$$\lambda[\{\chi^M;\chi^M\}-\delta_{\lambda\kappa}]+\kappa[\{\chi^M;\omega\}-W\delta_{\lambda\kappa}]+[\{\psi_z{}^M;\chi^M\}-T\delta_{\lambda\kappa}]=0, \tag{50}$$

$$\lambda[\{\chi^M;\omega\}-W\delta_{\lambda\kappa}]+\kappa[\{\omega;\omega\}-\delta_{\lambda\kappa}]+[\{\psi_z{}^M;\omega\}-V\delta_{\lambda\kappa}]=0. \tag{51}$$

The three new bracket symbols in these equations are written as

$$\{\psi_z{}^M;\omega\}=C^M(\psi_z|v|\omega)-V[(\psi_z|v|\psi_z)-h(\rho)], \tag{52}$$

$$\{\chi^M;\omega\}=E^M(\chi|v|\omega)+W\Delta\epsilon-W[(\psi_z|v|\psi_z)+h(\rho)], \tag{53}$$

$$\begin{aligned}\{\omega;\omega\}&=(\omega|H^M|\omega)-(\psi_z{}^M|H^M|\psi_z{}^M)\\&=\left(\omega\left|-\tfrac{1}{2}\nabla^2+V(r_a)-\frac{1}{r_b}\right|\omega\right)-\epsilon-[(\psi_z|v|\psi_z)+h(\rho)]\\&\approx\left(\omega\left|-\tfrac{1}{2}\nabla^2-\frac{1}{r_b}\right|\omega\right)+V(\rho)-\epsilon-[(\psi_z|v|\psi_z)+h(\rho)]\\&\approx\epsilon_{\mathrm{Li}}+f(\rho)-[(\psi_z|v|\psi_z)+h(\rho)].\end{aligned} \tag{54}$$

Derivations of these expressions are straightforward except in the case of $\{\omega;\omega\}$ where more detail is indicated. In the computations $(\omega|-\frac{1}{2}\nabla^2-(1/r_b)|\omega)$ is put equal to ϵ_{Li}, the ionization potential of the Li atom, and a numerical value of 5.37 ev[22] used.

Equations (49), (50), and (51) can be solved by iteration; the results are used to calculate $U_{\lambda\kappa}{}^M$ in curve iii, Fig. 2, whereas values for the minimum are listed in the third row of Table I. The new minimum falls below the results of parts i and ii. The dipole moment $\mu_{\lambda\kappa}{}^{el}$ is negative now, indicating a displacement of the electron cloud towards the Li^+ ion.

[22] R. F. Bacher and S. Goudsmit, *Atomic Energy States* (McGraw-Hill Book Company, Inc., New York, 1932).

iv. Inclusion of Covalent Character Alone

For the sake of completeness, the calculations are repeated using a wave function of the form

$$\Psi_{z\lambda\kappa}{}^M=[1+2\kappa V+\kappa^2]^{-\frac{1}{2}}[\psi_z{}^M+\kappa\omega] \tag{55}$$

in which the excited state χ^M is omitted. The work follows closely that outlined in the preceding parts of this section. The results are shown in the last curve iv of Fig. 2 and in Table I. The minimum of the energy plot is higher than that of curve iii but noticeably below the minima of the first two curves.

IV. THE EFFECT OF VIBRATIONAL MOTION

The minimum of the energy-internuclear distance curve calculated in Sec. III corresponds to the equilibrium configuration of the LiF molecule when there is no vibrational motion. In this section, a correction is made for the effect of vibrational energy on the molecular configuration. The calculations are carried out, only for the case of the orbital $\Psi_{z\lambda\kappa}{}^M$ (Sec. III, part iii), which gives the lowest energy. The values given in Table I corresponding to the minimum of this curve are repeated in more conventional units in Table II.

The energy $U_{\lambda\kappa}{}^M$, which is the sum of the nuclear and electronic interactions, acts as a potential function for the vibrational motion of the nuclei. An analytical expression

$$U_{\lambda\kappa}{}^M-U_e{}^M=\tfrac{1}{2}p(\rho-\rho_e)^2+C_3(\rho-\rho_e)^3+C_4(\rho-\rho_e)^4+C_5(\rho-\rho_e)^5 \tag{56}$$

is fitted to the energy curve around the minimum $U_e{}^M$. The coefficient of the quadratic term determines the force constant

$$p=\left[\frac{d^2U_{\lambda\kappa}{}^M}{d\rho^2}\right]_{\rho=\rho_e} \tag{57}$$

and the frequency ν_e of the harmonic oscillator with a reduced mass of 4.5700 MU corresponding to Li^6F^{19} is given in Table II.

The calculation of the effects of anharmonicity is described in standard texts on quantum mechanics. The

TABLE II. Correction for vibrational motion of Li^6F^{19} using potential curve iii.

$U_e{}^M=-7.4826$ ev $\quad \mu_A$ (reduced mass Li^6F^{19}) $=4.5700$ atomic weight units (physical)
$\rho_e=1.587$A $\quad \nu_e=3.1172\times10^{13}$ sec^{-1}

		Vibrational state $v=0$	Vibrational state $v=1$
Energy correction	harmonic term	0.0644 ev	...
	anharmonic term	−0.0006 ev	...
Corrected energy $[U_{\mathrm{LiF}(v)}]_v$		−7.4188 ev	...
Internuclear distance correction anharmonic term		0.013A	0.034A
Corrected internuclear distance $[\rho]_v$		1.600A	1.621A
Corrected dipole moment $[\mu]_v$		6.354 d	6.471 d
	$[\mu^2A]_v$	784×10^{-76} esu^2 g cm^4	834×10^{-76} esu^2 g cm^4
	$[\lambda]_v$	−0.2370	...
	$[\kappa]_v$	0.3827	...

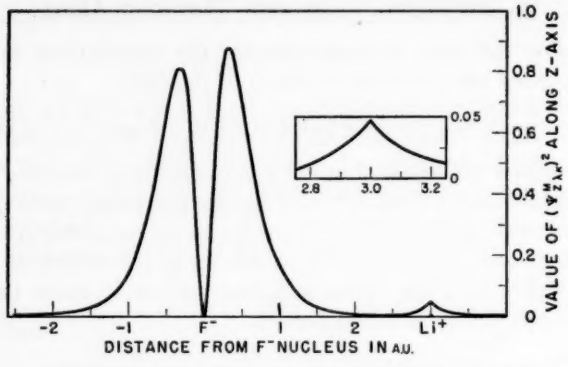

FIG. 3. Electron density along internuclear axis due to an electron in the orbital $\Psi_{z\lambda\kappa}{}^M$.

wave functions for the harmonic oscillator are Hermite functions. The last three terms of Eq. (56) are treated as a perturbation of this oscillator, and the average value of the energy and $(\rho-\rho_e)$ may be evaluated for any vibrational state. Table II shows the corrections obtained in this way for the vibrational quantum states $v=0$ and $v=1$.

A correction could also be introduced for the rotational motion of the molecule. However, the effect proves to be small for low rotational states and is not considered here.

V. DISCUSSION OF RESULTS

There is very little direct experimental information about the configuration of the LiF molecule. Neither the internuclear distance nor the dipole moment have been measured. However, Swartz, and Trischka,[23] using a molecular beam electric resonance method have obtained a value of

$$(\mu^2A)_0=(747.2\pm0.9)\times10^{-76}\ \text{esu}^2\ \text{g cm}^4$$

for Li^6F^{19} in the vibrational state $v=0$. A is the moment of inertia of the molecule in this state.

Values of μ^2A for configurations corresponding to the minima of the curves of Fig. 2 are given in the last column of Table I for comparison. Of the four forms of wave function considered, the most refined one, corresponding to curve iii, gives the best agreement with the observed result, as well as the lowest energy. In Table II the internuclear distance and dipole moment for this case are corrected for vibrational motion of the nuclei and used to calculate $(\mu^2A)_v$ for the first two vibrational states $v=0$ and $v=1$. The final value 784×10^{-76} esu^2 g cm^4 for $(\mu^2A)_0$ is about 5 percent higher than that measured by Swartz and Trischka. This agreement is quite good, in view of the fact that μ^2A varies approximately as the fourth power of the internuclear distance.

[23] J. C. Swartz and J. W. Trischka, Phys. Rev. **88**, 1085 (1952).

From Table II it follows that

$$\frac{(\mu^2A)_1-(\mu^2A)_0}{(\mu^2A)_0}=0.065.$$

Although this is somewhat larger than the value 0.043 $\pm$0.001 determined by Swartz and Trischka, it does indicate that the anharmonic character around the minimum of curve iii is approximately correct.

Recently Rittner[4] and Trischka[24] have discussed LiF from a theoretical point of view. Rittner, using an estimated value of 7.73 ev for the binding energy, calculated the internuclear distance in LiF^{19} to be 1.53A at 300°K and the dipole moment 5.04 d. These values give about 500×10^{-76} esu^2 g cm^4 for the quantity μ^2A. Trischka considered a classical model similar to that used by Rittner but introduced the experimental value of μ^2A. By comparing theoretical and measured results for other alkali halides, he estimated upper and lower limits for the internuclear distance ρ in the LiF molecule to be

$$1.44\text{A}<\rho<1.65\text{A}.$$

His calculations also indicated that probably the dipole moment should be greater than 6.0 d.

A check on the consistency of the present calculation on the LiF molecule with previous work on the LiF crystal is obtained by comparing the difference of the binding energy of the molecule $U_{\text{LiF}(g)}$ and the cohesive energy of the crystal $U_{\text{LiF}(c)}$ with the heat of sublimation S_{LiF}. The cohesive energy of the LiF crystal at 0°K is -10.32 ev. This is taken from Benson and Wyllie[11] with an added correction of 0.17 ev for the zero-point energy as given by Mayer and Helmholz.[25] Thus at 0°K

$$U_{\text{LiF}(g)}-U_{\text{LiF}(c)}=-7.42+10.32=2.90\ \text{ev}.$$

The heat of sublimation calculated from data in the compilation of Bichowsky and Rossini[26] is $S_{\text{LiF}}=2.76$ ev

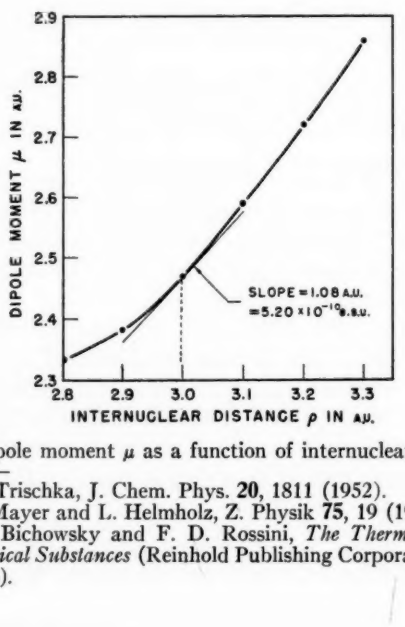

FIG. 4. Dipole moment μ as a function of internuclear distance.

[24] J. W. Trischka, J. Chem. Phys. **20**, 1811 (1952).
[25] J. E. Mayer and L. Helmholz, Z. Physik **75**, 19 (1932).
[26] F. R. Bichowsky and F. D. Rossini, *The Thermochemistry of the Chemical Substances* (Reinhold Publishing Corporation, New York, 1936).

at 291°K. Mayer and Helmholz estimated a value of $S_{LiF}=2.71\pm0.16$ ev at 0°K. Since energy calculations of the type described in the present paper may be subject to errors of the order of an electron volt or more (see reference 16, page 140) the result obtained for S_{LiF} is gratifying.

Although LiF is usually considered to be an "ionic" molecule, it is apparent that the inclusion of some covalent character is an essential feature of the present model. The electron density along the internuclear axis, due to an electron in the $\Psi_{z\lambda\kappa}{}^{M}$ orbital, is shown in Fig. 3 for a nuclear separation of 1.60A. The covalence of this orbital is approximately $[N_{\lambda\kappa}]^2=0.11$.

No measurements of infrared intensities have been made for LiF. However, the variation of the dipole moment with internuclear distance predicted by the present model may be of some interest and is given in Fig. 4. The slope of the curve at $\rho=1.60$A is 5.20 $\times10^{-10}$ esu.

Judged on the basis of the rather meager information available and summarized in this section, the model proposed in part iii of Sec. III gives a reasonably satisfactory representation of the LiF molecule.

ACKNOWLEDGMENT

The authors wish to thank Barbara A. Benson for assisting with the calculations.

THE JOURNAL OF CHEMICAL PHYSICS VOLUME 22, NUMBER 3 MARCH, 1954

A Quantum-Mechanical Calculation of the Surface Energy of Crystalline Lithium Fluoride*

B. M. E. VAN DER HOFF† AND G. C. BENSON
Division of Pure Chemistry, National Research Council, Ottawa, Canada

(Received July 30, 1953)

A quantum-mechanical model for calculating the surface energy of a LiF crystal is described. This work is an extension of previous papers on the energies of the LiF crystal and molecule. A simple form of distortion is permitted in the surface region. The value of the surface energy of a {100} face obtained from these computations is 557-erg cm^{-2} at 0°K and is appreciably higher than results based on classical considerations.

I. INTRODUCTION

IT is convenient to define the surface energy of a crystal in terms of the process of forming a new surface. Consider an infinite or "holo"-crystal at 0°K, composed of ions arranged on a NaCl-type lattice as indicated on the left side of Fig. 1. The energy of this system is denoted by U_{holo}. If the crystal is divided into two identical infinitely separated hemicrystals by a plane parallel to a {100} plane of the lattice, the energy of each part becomes U_{hemi}. The increase in energy $2U_{hemi}-U_{holo}$ is associated with the formation of two new {100} surfaces and is called the surface energy.

The lattice of the crystal after division is distorted in the region of the surface. Several forms of distortion have been assumed by previous authors. Madelung[1] and Glauberman[2] allowed the interplanar distance perpendicular to the surface to vary. It was shown that the change in lattice spacing decreases exponentially on proceeding inwards from the surface. The main contribution to the surface energy arising from this distortion is due to the change in spacing between the surface and the second layer. Models in which only this last change is considered have been investigated by Lennard-Jones and Dent[3] and Dent.[4] Different displacements perpendicular to the surface for positive and negative surface ions have been considered by Madelung[1] and Verwey.[5] Lateral displacements within

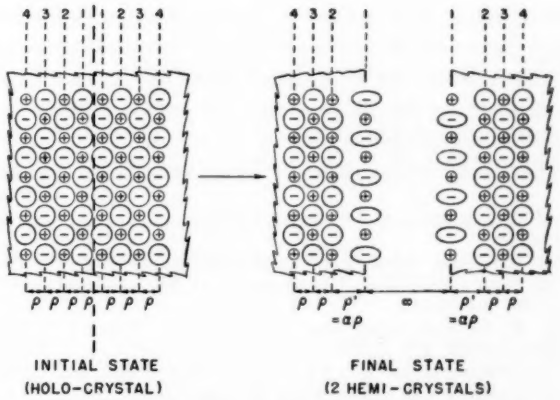

FIG. 1. Formation of two new surfaces by division of a holocrystal into two hemicrystals.

* Issued as N. R. C. No. 3211.
† National Research Council of Canada Postdoctorate Fellow, 1951–1953. Present address: Research and Development Division, Polymer Corporation Limited, Sarnia, Ontario, Canada.
[1] E. Madelung, Physik. Z. **20**, 494 (1919).
[2] A. E. Glauberman, Zhur. Fiz. Khim. **23**, 124 (1949).
[3] J. E. Lennard-Jones and B. M. Dent, Proc. Roy. Soc. (London) **A121**, 247 (1928).
[4] B. M. Dent, Phil. Mag. **8**, 530 (1929).
[5] E. J. W. Verwey, Rec. Trav. Chim. **65**, 521 (1946).

the surface layer have been treated by Molière, Rathje, and Stranski,[6] who found a tendency for ion-doublet formation. Recently Patterson[7] has disproved this picture for the alkali halides.

Another effect which has been considered by a number of authors,[3–7] is the change in polarization of the ions upon formation of the surface. In the holocrystal, the charge distribution of the ions may be approximated quite well by point charges. Creation of the surface results in a loss of symmetry and the point charge approximation requires modification since each ion now has a dipole moment.

Born and Stern,[8] Lennard-Jones and Taylor,[9] and Shuttleworth[10] have performed classical calculations of the surface energy $2U_{\text{hemi}}-U_{\text{holo}}$ by adding up the interactions of the ions before and after the division process and assuming certain forms for the laws of force. These forms usually contain two parameters which have been adjusted in calculations of the cohesive energy of the crystal to give the observed lattice spacing and compressibility. The application of these force laws which have been derived in the symmetrical field within the holocrystal to the surface region of a hemicrystal may be questioned. Some support of this criticism can be adduced from the extreme case of their application to single ionic molecules. Rittner[11] has calculated the energies of the alkali halide molecules "in the spirit of the Born-Mayer approximation" but has used properties of the molecules rather than of the crystalline state to adjust the parameters of the force laws. The parameters derived in this manner are different from those used in the crystal case.

Recently, several quantum-mechanical calculations of the cohesive energies of ionic crystals have been made.[12–15] In these the interactions between ions are related directly to the electronic structure of the ions and it is unnecessary to employ properties of the crystals to adjust force law parameters. It is of interest to consider a similar calculation of the surface energy of an ionic crystal. This is done in the present paper for LiF and forms an extension of previous quantum mechanical calculations on the energies of the LiF crystal,[13] and molecule.[16] As far as possible, the notation used will parallel these previous papers.

The model is described in the next section. An outline of the calculations is given in Sec. III, followed by a discussion of the results in Sec. IV.

II. DESCRIPTION OF THE MODEL

The main features of the model are similar to those described in references 13 and 16, and are mentioned only briefly here. The Li^+ ion is treated as a point charge. The F^- ion is represented as a nucleus of $+5$ with a shell of six electrons.

Two types of distortion at the surface of the hemicrystal are taken into account. The spacing $\alpha\rho$ between the surface and the second layer is allowed to vary and the electron distribution of F^- ions in the surface is permitted to deviate from spherical symmetry by introduction of an excited state and covalent bonding with the nearest neighbor Li^+ ions of the second layer. The asymmetry of the electron cloud of F^- ions in non-surface layers is neglected except that arising from the influence of the orthogonality relations. Polarization of the relatively small Li^+ ions is also neglected. On the right side of Fig. 1, the distortion of the hemicrystal due to polarization of surface F^- ions and change in lattice spacing has been indicated diagrammatically. A more general distortion of the hemicrystal is not considered since the computational work is unjustifiably increased.

The limiting classical form of the electrostatic field within the crystal is defined as that arising from unit positive and negative point charges arranged at the lattice points, together with the contributions from a set of dipoles. These latter, each with moment μ are situated at the F^- sites of the first layer and directed perpendicular to the surface, the inward normal being considered positive.

III. CALCULATIONS

A typical F^- ion of the nth layer, surrounded by its nearest neighbors is shown in Fig. 2. For any value of n, $\rho_1=\rho_2=\rho_3=\rho_4=\rho$. If $n=1$, $\rho_5=\rho'=\alpha\rho$ and $\rho_6=\infty$; if $n=2$, $\rho_5=\rho$ and $\rho_6=\rho'=\alpha\rho$. For all other layers $\rho_5=\rho_6=\rho$. A value

$$\rho=3.80 \text{ A.U.}\ddagger\ (=\tfrac{1}{2}\times 4.02\text{A})$$

taken from reference 13 is used for the crystal lattice spacing.

For the purpose of the present calculation each F^- ion is considered to be situated in a potential field $-V_-^{(n)}(x,y,z)$ due to the rest of the crystal and represented by its limiting classical form. Thus $-V_-^{(n)}(x,y,z)$ at position x,y,z relative to a negative ion site of the nth layer taken as origin, may be written as

$$-V_-^{(n)}(x,y,z)=P_-^{(n)}(x,y,z)+Q_-^{(n)}(x,y,z), \qquad (1)$$

where $P_-^{(n)}(x,y,z)$ and $Q_-^{(n)}(x,y,z)$ are the contributions arising from point charges at all other lattice sites and

[6] Molière, Rathke, and Stranski, Discussions Faraday Soc. **No. 5**, 21 (1949).
[7] D. Patterson, Trans. Faraday Soc. **48**, 877 (1952).
[8] M. Born and O. Stern, Physik-math. Kl. Sitzber. preuss. Akad. Wiss. **48**, 901 (1919).
[9] J. E. Lennard-Jones and P. A. Taylor, Proc. Roy. Soc. (London) **A109**, 476 (1925).
[10] R. Shuttleworth, Proc. Phys. Soc. (London) **62A**, 167 (1949).
[11] E. S. Rittner, J. Chem. Phys. **19**, 1030 (1951).
[12] P. O. Lowdin, dissertation, Uppsala (1948).
[13] G. C. Benson and G. Wyllie, Proc. Phys. Soc. (London) **A64**, 276 (1951).
[14] P. O. Lowdin, J. Chem. Phys. **19**, 1570 (1951).
[15] J. Yamashita, J. Phys. Soc. Japan **7**, 284 (1952).
[16] G. C. Benson and B. M. E. van der Hoff, accompanying paper.

‡ Atomic units are used throughout the calculations unless otherwise stated.

dipoles μ at F^- sites of the first layer, respectively. In the calculations it is convenient to write $P_-^{(n)}(x,y,z)$ as the sum of nearest neighbor contributions $-\sum^{(n)}v_i$ and $P_-^{(n)}(x,y,z)+\sum^{(n)}v_i$ arising from non-nearest neighbors. In this, the potential field at a distance r_b from a single isolated Li^+ ion, labelled "i" is written as $-v_i=1/r_b$, following the notation of reference 13. The non-nearest neighbor contribution and $Q_-^{(n)}(x,y,z)$ are approximated by the first two terms of their expansion in Taylor's series about the origin. Thus,

$$-V_-^{(n)}(x,y,z)=-\sum^{(n)}v_i+P_-^{(n)}(x,y,z)+\sum^{(n)}v_i$$
$$+Q_-^{(n)}(x,y,z)\approx-\sum^{(n)}v_i+P_-^{(n)}(0)-\sum^{(n)}1/\rho_i$$
$$+zp_-^{(n)}(0)+Q_-^{(n)}(0)+zq_-^{(n)}(0), \quad (2)$$

where $P_-^{(n)}(0)-\sum^{(n)}1/\rho_i$ and $-p_-^{(n)}(0)$ are the potential and electric fields at the origin arising from non-nearest neighbor charges. $Q_-^{(n)}(0)$ and $-q_-^{(n)}(0)$ are corresponding quantities arising from the dipoles μ. Hence,

$$V_-^{(n)}(x,y,z)=V_-^{(n)}(0)+\sum^{(n)}1/\rho_i+\sum^{(n)}v_i$$
$$-z[p_-^{(n)}(0)+q_-^{(n)}(0)], \quad (3)$$

where

$$V_-^{(n)}(0)=-[P_-^{(n)}(0)+Q_-^{(n)}(0)]. \quad (4)$$

By analogy, the potential field at a positive site is $-V_+^{(n)}(0)$, where

$$V_+^{(n)}(0)=-[P_+^{(n)}(0)+Q_+^{(n)}(0)]. \quad (5)$$

From the symmetry of the problem it can be seen that

$$P_-^{(n)}(0)=-P_+^{(n)}(0). \quad (6)$$

Using methods similar to those described by van der Hoff and Benson,[17] the following relations can be established—

$$P_+^{(1)}(0)-P_+^{(\infty)}(0)=\rho^{-1}[2S(1)-S(\alpha)], \quad (7)$$

$$P_+^{(n)}(0)-P_+^{(\infty)}(0)=(-1)^n\rho^{-1}[S(n-1)-S(n-1+\alpha)$$
$$-S(n-2+\alpha)], \text{ for } n\geq 2, \quad (8)$$

$$Q_+^{(1)}(0)-Q_-^{(1)}(0)=0, \quad (9)$$

$$Q_+^{(n)}(0)-Q_-^{(n)}(0)=(-1)^n\rho^{-2}\mu[D(n-1+\alpha)$$
$$+D(n-2+\alpha)], \text{ for } n\geq 2, \quad (10)$$

$$p_-^{(1)}(0)=\rho^{-2}[D(\alpha)-\alpha^{-2}], \quad (11)$$

$$q_-^{(1)}(0)=(2\sqrt{2}\rho^3)^{-1}\mu T, \quad (12)$$

where

$$S(u)=\sum_{k,l}^{\infty}{}_{-\infty}\sum_{m}^{\infty}{}_{0}(-1)^{k+l+m}[k^2+l^2+(m+u)^2]^{-\frac{1}{2}}$$

$$=8\sum_{\substack{k\ \text{odd}\\ l\ \text{odd}}}^{\infty}{}_{1}\frac{\exp[-\pi u(k^2+l^2)^{\frac{1}{2}}]}{(k^2+l^2)^{\frac{1}{2}}\{1+\exp[-\pi(k^2+l^2)^{\frac{1}{2}}]\}}, \quad \text{for } u>0 \quad (13)$$

$$D(u)=-\frac{dS(u)}{du}=8\pi\sum_{\substack{k\ \text{odd}\\ l\ \text{odd}}}^{\infty}{}_{1}\frac{\exp[-\pi u(k^2+l^2)^{\frac{1}{2}}]}{1+\exp[-\pi(k^2+l^2)^{\frac{1}{2}}]} \quad (14)$$

$$T=\sum_{k,l}^{'\infty}{}_{-\infty}(k^2+l^2)^{-\frac{3}{2}}=9.0336217$$

(see reference 17). (15)

The cohesive energy of a holo- or hemicrystal is regarded as made up from a classical electrostatic term plus a contribution associated with each F^- ion and representing the energy of the F^- ion in the crystal, in excess of that calculated from the classical treatment. Thus

$$U_{\text{hemi}}=\tfrac{1}{2}\sum_{n}^{\infty}{}_{1}[V_-^{(n)}(0)-V_+^{(n)}(0)]$$
$$+\sum_{n}^{\infty}{}_{1}[\epsilon_{F^-}{}^{(n)}{}_{(\text{quantal})}-\epsilon_{F^-}{}^{(n)}{}_{(\text{classical})}], \quad (16)$$

gives the energy of a hemicrystal relative to the free ions and stated per ion pair in the surface of the hemicrystal. Similarly,

$$U_{\text{holo}}=2[\tfrac{1}{2}\sum_{n}^{\infty}{}_{1}[V_-^{(\infty)}(0)-V_+^{(\infty)}(0)]$$
$$+\sum_{n}^{\infty}{}_{1}[\epsilon_{F^-}{}^{(\infty)}{}_{(\text{quantal})}-\epsilon_{F^-}{}^{(\infty)}{}_{(\text{classical})}]] \quad (17)$$

is the energy of a holocrystal relative to the free ions and stated per ion pair in a {100} plane. In Eqs. (16) and (17) $\epsilon_{F^-}{}^{(n)}{}_{(\text{quantal})}$ is the energy of a F^- ion in the nth layer, relative to a free F^- ion and calculated quantum mechanically while $\epsilon_{F^-}{}^{(n)}{}_{(\text{classical})}$ is the corresponding classical expression.

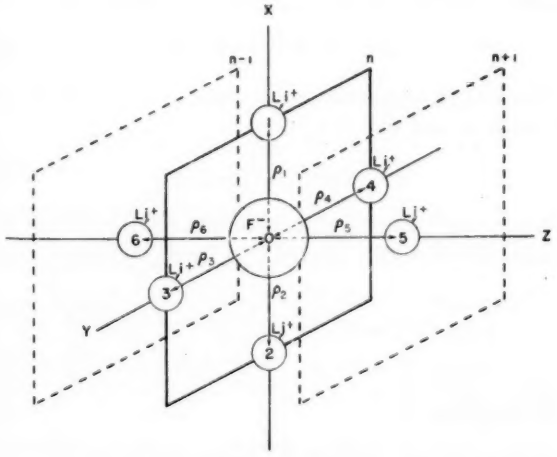

FIG. 2. Coordinate system of a F^- ion in the nth layer.

[17] B. M. E. van der Hoff and G. C. Benson, Can. J. Phys. **31**, 1087 (1953).

The surface energy per ion pair in the newly formed surface is $\frac{1}{2}(2U_{\text{hemi}}-U_{\text{holo}})$. The factor $\frac{1}{2}$ enters this expression because two new {100} surfaces are formed. Since the surface area occupied by an ion pair is $2\rho^2$, the surface energy per unit area is

$$\sigma=(2\rho^2)^{-1}[U_{\text{hemi}}-\tfrac{1}{2}U_{\text{holo}}]. \tag{18}$$

Using Eqs. (4), (5), (6), (16), and (17) gives

$$\begin{aligned}\sigma=(2\rho^2)^{-1}[\tfrac{1}{2}\sum_n^{\infty}{}_1\{&2(P_+^{(n)}(0)-P_+^{(\infty)}(0))\\&+(Q_+^{(n)}(0)-Q_-^{(n)}(0))\}\\&+\sum_n^{\infty}{}_1\{(\epsilon_{F^-}{}^{(n)}-\epsilon_{F^-}{}^{(\infty)})_{\text{(quantal)}}\\&-(\epsilon_{F^-}{}^{(n)}-\epsilon_{F^-}{}^{(\infty)})_{\text{(classical)}}\}].\end{aligned} \tag{19}$$

It can be shown that

$$\sum_n^{\infty}{}_1\,(P_+^{(n)}(0)-P_+^{(\infty)}(0))=\rho^{-1}[B+2(S(1)-S(\alpha))], \tag{20}$$

where

$$\begin{aligned}B&=\sum_n^{\infty}{}_1\,(-1)^{n+1}S(n)\\&=-\sum_{k,l}^{\infty}{}_{-\infty}\sum_m^{\infty}{}_1\{(-1)^{k+l+m}m(k^2+l^2+m^2)^{-\frac{1}{2}}\}\\&=8\sum_{\substack{k\text{ odd}\\l\text{ odd}}}^{\infty}{}_1\frac{\exp[-\pi(k^2+l^2)^{\frac{1}{2}}]}{(k^2+l^2)^{\frac{1}{2}}\{1+\exp[-\pi(k^2+l^2)^{\frac{1}{2}}]\}^2}\\&=0.06524647.\S\end{aligned} \tag{21}$$

Also,

$$\sum_n^{\infty}{}_1\,(Q_+^{(n)}(0)-Q_-^{(n)}(0))=\mu\rho^{-2}D(\alpha). \tag{22}$$

Hence,

$$\begin{aligned}\sigma=\frac{1}{2\rho^2}\Big[\frac{1}{\rho}&\{B+2(S(1)-S(\alpha))\}+\frac{\mu}{2\rho^2}D(\alpha)\\&+\sum_n^{\infty}{}_1\{(\epsilon_{F^-}{}^{(n)}-\epsilon_{F^-}{}^{(\infty)})_{\text{(quantal)}}\\&-(\epsilon_{F^-}{}^{(n)}-\epsilon_{F^-}{}^{(\infty)})_{\text{(classical)}}\}\Big].\end{aligned} \tag{23}$$

To calculate $\epsilon_{F^-}{}^{(n)}{}_{\text{(quantal)}}$ the six electrons of a F^- ion in the nth layer are assigned in pairs to the orbitals

$$\Psi_x^{(n)}=\psi_x^{(\infty)}=C^{(\infty)}[\psi_x-S\phi_1+S\phi_2], \quad \text{all } n, \tag{24a}$$

$$\Psi_y^{(n)}=\psi_y^{(\infty)}=C^{(\infty)}[\psi_y-S\phi_3+S\phi_4], \quad \text{all } n, \tag{24b}$$

$$\Psi_z^{(n)}=\psi_z^{(\infty)}=C^{(\infty)}[\psi_z-S\phi_5+S\phi_6], \quad \text{for } n\geqslant 3. \tag{24c}$$

§ B is the same as B_c''' defined in reference 10; however, the series of exponential terms given in the last part of Eq. (21) is a more convenient way of obtaining its value than the direct numerical summation used by Shuttleworth.

For $n=2$ the last orbital is replaced by

$$\Psi_z^{(2)}=\psi_z^{(2)}=C^{(2)}[\psi_z-S\phi_5+S'\phi_6'], \tag{24d}$$

while if $n=1$, the orbital used is

$$\Psi_z^{(1)}=N_{\lambda\kappa}[\psi_z^{(1)}+\lambda\chi^{(1)}+\kappa\omega_5'], \tag{24e}$$

where

$$\psi_z^{(1)}=C^{(1)}[\psi_z-S'\phi_5']. \tag{25}$$

In Eqs. (24), $C^{(n)}$, and $N_{\lambda\kappa}$ are appropriate normalizing factors. The wave functions ψ and ϕ represent $2p$ orbitals for F^- and $1s$ orbitals for Li^+ ions, respectively. The exact analytical forms of these are the same as used in the calculation of the cohesive energy (13) and are also summarized in reference 16. The orbital $\Psi_z^{(2)}$ used in the second layer is analogous to $\psi_z^{(\infty)}$ but has been modified to maintain orthogonality with the orbital ϕ_6' which now represents a $1s$-wave function for Li^+ in position "6" at a distance $\rho_6=\rho'=\alpha\rho$. The overlap integral S' is defined by

$$S'=\int\phi_5'\psi_z d\tau. \tag{26}$$

Orbitals (24a), (b), (c) give rise to no dipole moment for F^- ions in layers $n\geqslant 3$. In layer 2 $(\Psi_z^{(2)}|z|\Psi_z^{(2)})$ is not zero unless $\alpha=1$; however it is very small for values of α near 1 and hence the 2nd layer F^- ions are also considered as having no dipole moment. The use of $\Psi_z^{(1)}$ for F^- ions in the 1st layer is an attempt to allow for the polarization of the surface ions in the same way as in the LiF molecule.[16] Thus

$$\chi^{(1)}=E^{(1)}[\chi-U(\phi_1+\phi_2+\phi_3+\phi_4)-U'\phi_5'] \tag{27}$$

is an orthogonalized wave function based on the $3s$-excited state orbital χ for the free F^- ion, while ω is a $2s$ state for a Li atom and permits covalency of the bond. The expressions used for χ and ω are described in reference 16. The dipole moment of a surface F^- ion is

$$\mu=-2(\Psi_z^{(1)}|z|\Psi_z^{(1)}). \tag{28}$$

The Hamiltonian for an electron of a F^- ion in the nth layer is written as

$$H^{(n)}=H+V_-^{(n)}(x,y,z). \tag{29}$$

H is the single electron Hamiltonian for the free F^- ion as used in references 13 and 16.

$$\begin{aligned}\epsilon_{F^-}{}^{(n)}{}_{\text{(quantal)}}=&-5V_-^{(n)}(0)+2[(\Psi_x^{(n)}|H^{(n)}|\Psi_x^{(n)})\\&+(\Psi_y^{(n)}|H^{(n)}|\Psi_y^{(n)})+(\Psi_z^{(n)}|H^{(n)}|\Psi_z^{(n)})\\&-\{(\psi_x|H|\psi_x)+(\psi_y|H|\psi_y)+(\psi_z|H|\psi_z)\}].\end{aligned} \tag{30}$$

This simplifies to

$$\begin{aligned}\epsilon_{F^-}{}^{(n)}{}_{\text{(quantal)}}=&V_-^{(n)}(0)+6\textstyle\sum^{(n)}1/\rho_i\\&+4[(\psi_x^{(\infty)}|H+\textstyle\sum^{(n)}v_i|\psi_x^{(\infty)})-(\psi_x|H|\psi_x)]\\&+2[(\Psi_z^{(n)}|H+\textstyle\sum^{(n)}v_i|\Psi_z^{(n)})-(\psi_z|H|\psi_z)]\\&+\mu(p_-^{(1)}(0)+q_-^{(1)}(0))\delta(n-1),\end{aligned} \tag{31}$$

where δ is the usual Dirac function defined by

$$\delta(x)=0 \quad \text{for} \quad x\neq 0 \quad \text{and} \quad \delta(0)=1.$$

For n very large (31) becomes

$$\begin{aligned}\epsilon_{F^{-(\infty)}\,(\text{quantal})} &= V_{-}^{(\infty)}(0)+6\textstyle\sum^{(\infty)}1/\rho_i \\ &+4[(\psi_x^{(\infty)}|H+\textstyle\sum^{(\infty)}v_i|\psi_x^{(\infty)})-(\psi_x|H|\psi_x)] \\ &+2[(\psi_z^{(\infty)}|H+\textstyle\sum^{(\infty)}v_i|\psi_z^{(\infty)})-(\psi_z|H|\psi_z)]. \quad (32)\end{aligned}$$

Thus,

$$\begin{aligned}(\epsilon_{F^{-(n)}}-\epsilon_{F^{-(\infty)}})_{(\text{quantal})} &= V_{-}^{(n)}(0)-V_{-}^{(\infty)}(0) \\ &+6(\textstyle\sum^{(n)}1/\rho_i-\sum^{(\infty)}1/\rho_i) \\ &+4(\psi_x^{(\infty)}|\textstyle\sum^{(n)}v_i-\sum^{(\infty)}v_i|\psi_x^{(\infty)}) \\ &+2[(\Psi_z^{(n)}|H+\textstyle\sum^{(n)}v_i|\Psi_z^{(n)}) \\ &-(\psi_z^{(\infty)}|H+\textstyle\sum^{(\infty)}v_i|\psi_z^{(\infty)})] \\ &+\mu(p_{-}^{(1)}(0)+q_{-}^{(1)}(0))\delta(n-1). \quad (33)\end{aligned}$$

Similarly,

$$\begin{aligned}(\epsilon_{F^{-(n)}}-\epsilon_{F^{-(\infty)}})_{(\text{classical})} &= V_{-}^{(n)}(0)-V_{-}^{(\infty)}(0) \\ &+\frac{\mu}{2}\left(p_{-}^{(1)}(0)+q_{-}^{(1)}(0)+\frac{1}{(\alpha\rho)^2}\right)\delta(n-1). \quad (34)\end{aligned}$$

Combining (33) with (34) and summing over the index n gives

$$\begin{aligned}&\textstyle\sum_1^{\infty}[(\epsilon_{F^{-(n)}}-\epsilon_{F^{-(\infty)}})_{(\text{quantal})}-(\epsilon_{F^{-(n)}}-\epsilon_{F^{-(\infty)}})_{(\text{classical})}] \\ &=-\frac{6}{\rho}\left(\frac{2}{\alpha}-3\right)+4(\psi_x^{(\infty)}|\textstyle\sum^{(1)}v_i+\sum^{(2)}v_i \\ &-2\textstyle\sum^{(\infty)}v_i|\psi_x^{(\infty)})+2[(\Psi_z^{(1)}|H+\sum^{(1)}v_i|\Psi_z^{(1)}) \\ &+(\psi_z^{(2)}|H+\textstyle\sum^{(2)}v_i|\psi_z^{(2)}) \\ &-2(\psi_z^{(\infty)}|H+\textstyle\sum^{(\infty)}v_i|\psi_z^{(\infty)})] \\ &+\frac{\mu}{2}\left(p_{-}^{(1)}(0)+q_{-}^{(1)}(0)-\frac{1}{(\alpha\rho)^2}\right). \quad (35)\end{aligned}$$

Substituting (35) in (23) and using Eqs. (11) and (28) leads to the expression

$$\begin{aligned}\sigma=\frac{1}{2\rho^2}\Bigg[&\frac{1}{\rho}\left\{B+2(S(1)-S(\alpha))+6\left(\frac{2}{\alpha}-3\right)\right\} \\ &+4(\psi_x^{(\infty)}|\textstyle\sum^{(1)}v_i+\sum^{(2)}v_i-2\sum^{(\infty)}v_i|\psi_x^{(\infty)}) \\ &+2\{(\Psi_z^{(1)}|H+\textstyle\sum^{(1)}v_i-(p_{-}^{(1)}(0) \\ &+\tfrac{1}{2}q_{-}^{(1)}(0))z|\Psi_z^{(1)})+(\psi_z^{(2)}|H+\textstyle\sum^{(2)}v_i|\psi_z^{(2)}) \\ &-2(\psi_z^{(\infty)}|H+\textstyle\sum^{(\infty)}v_i|\psi_z^{(\infty)})\}\Bigg]. \quad (36)\end{aligned}$$

For any value of α the parameters λ and κ must be chosen to minimize σ. This means essentially that λ and κ are chosen to minimize

$$E=(\Psi_z^{(1)}|H+\textstyle\sum^{(1)}v_i-(p_{-}^{(1)}(0)+\tfrac{1}{2}q_{-}^{(1)}(0))z|\Psi_z^{(1)}). \quad (37)$$

Both $\Psi_z^{(1)}$ and $q_{-}^{(1)}(0)$ depend on λ and κ; however it can be shown that E will be a minimum if

$$\begin{aligned}\Delta=E&+(1/4)q_{-}^{(1)}(0)\mu-(\psi_z^{(1)}|H+\textstyle\sum^{(1)}v_i \\ &-(p_{-}^{(1)}(0)+q_{-}^{(1)}(0))z|\psi_z^{(1)}) \\ =&(\Psi_z^{(1)}|H+\textstyle\sum^{(1)}v_i-(p_{-}^{(1)}(0)+q_{-}^{(1)}(0))z|\Psi_z^{(1)}) \\ &-(\psi_z^{(1)}|H+\textstyle\sum^{(1)}v_i-(p_{-}^{(1)}(0)+q_{-}^{(1)}(0))z|\psi_z^{(1)}) \quad (38)\end{aligned}$$

is minimized with respect to λ and κ, with $q_{-}^{(1)}(0)$ treated as independent of λ and κ. Differentiating Δ partially with respect to λ and κ on this basis and equating the results to zero gives two equations which can be solved along with (38) to yield λ, κ, and Δ. Solution of this problem by iteration is similar to the calculations for the LiF molecule.[16] The matrix elements formed on expanding (38) are evaluated by the methods described in references 13 and 16. In general, integrals involving 3 centers are negligibly small but two, $(\psi_z|v_1|\omega_5')$ and $(\chi|v_1|\omega_5')$ are evaluated by suitable approximations.

Finally, the surface energy is given by

$$\begin{aligned}\sigma=\frac{1}{2\rho^2}\Bigg[&\frac{1}{\rho}\left\{B+2(S(1)-S(\alpha))+6\left(\frac{2}{\alpha}-3\right)\right\} \\ &+4(\psi_x^{(\infty)}|\textstyle\sum^{(1)}v_i+\sum^{(2)}v_i-2\sum^{(\infty)}v_i|\psi_x^{(\infty)}) \\ &+2\{(\psi_z^{(1)}|H+\textstyle\sum^{(1)}v_i|\psi_z^{(1)}) \\ &+(\psi_z^{(2)}|H+\textstyle\sum^{(2)}v_i|\psi_z^{(2)}) \\ &-2(\psi_z^{(\infty)}|H+\textstyle\sum^{(\infty)}v_i|\psi_z^{(\infty)})\} \\ &-2(p_{-}^{(1)}(0)+q_{-}^{(1)}(0))(\psi_z^{(1)}|z|\psi_z^{(1)}) \\ &-\tfrac{1}{2}q_{-}^{(1)}(0)\mu+2\Delta\Bigg]. \quad (39)\end{aligned}$$

In this expression, B/ρ is the usual classical Coulomb energy necessary to separate the two parts of the crystal when the spacing remains unchanged. The term $2(S(1)-S(\alpha))/\rho$ is a classical correction for the change in spacing at the surface. The remaining terms of (40) arise from the quantum-mechanical approach and replace the usual repulsive, dipole-dipole, . . . etc. contributions, found in classical calculations.

The surface energy σ is plotted as a function of $\rho'=\alpha\rho$ in curve i of Fig. 3. The minimum occurs at $\rho'=3.82$ A.U.$=2.02$A where $\sigma=0.01034$ A.U.$=557$ erg cm^{-2} and $\mu=0.031$ A.U.$=0.079$d.

DISCUSSION

The surface energy of LiF has not been determined experimentally. In the case of NaCl, experimental values‖ appear to be about 2 to 3 times larger than those predicted by classical calculations.[4,8–10]

‖ Lipsett, Johnson, and Maass [J. Am. Chem. Soc. **49**, 925 (1927)] obtained a value of 400-erg cm^{-2} at 25°C by measuring the difference in the heat of solution of coarse and fine salt. G. E. Boyd and W. D. Harkins [J. Am. Chem. Soc. **64**, 1190 (1942)] repeated these experiments and found 395 erg cm^{-2}. The surface areas of the fine salt in both of these sets of determi-

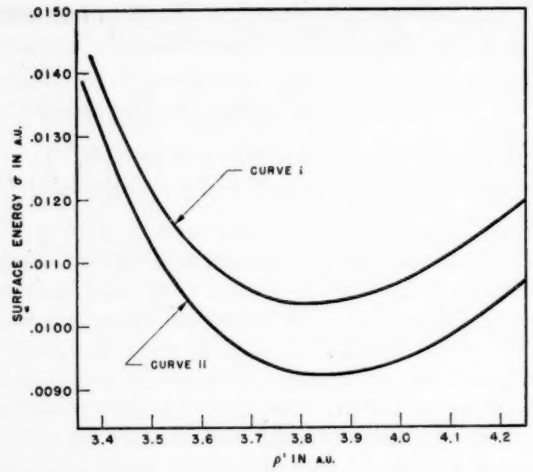

FIG. 3. Surface energy σ plotted as a function of the spacing $\rho'=\alpha\rho$ between the first and second layers. Curve i calculated as described in Sec. III. Curve ii calculated by putting $p_-^{(1)}(0)=q_-^{(1)}(0)=0$ in Eq. (33).

The surface energy 557-erg cm^{-2} obtained for LiF in Sec. III is 2.9 times larger than the value 194-erg cm^{-2} computed for this substance from a classical method used by Shuttleworth.[10]

An empirical method for calculating the surface free energy of liquids from the density and coefficient of thermal expansion has been given by Edser[18] and used by him for some solids.[19] According to Sutherland[20] application of this method to crystalline LiF yields a value of 570-erg cm^{-2} at 25°C. A positive energy term must be added to this value in order to compare it with the theoretical surface energy at 0°K.¶

nations were estimated by microscopic examination and are generally considered to be too small [G. E. Boyd, "Surface Chemistry," Publ. Am. Assoc. Advance Sci. **No. 21**, 128 (1943); see also reference 22]. In a preliminary experiment in our laboratory, a value of 290-erg cm^{-2} was obtained. The area of the fine salt used in this measurement was determined by low temperature nitrogen adsorption. It is unlikely that the discrepancy between experiment and classical theory can be explained by the difference of the temperature of the experiment from 0°K.

[18] E. Edser, Fourth Report on Colloid Chemistry, British Assoc. Advance Sci. Rept. (H.M.S.O. London, 1922), p. 40.

[19] E. Edser, reference 18, p. 263.

[20] K. L. Sutherland, Australian Chem. Inst. J. & Proc. **14**, 268 (1947).

¶ If γ is the surface free energy, then $\gamma_0=\gamma_{298}-\int_0^{298}(\partial\gamma/\partial T)dT$, where $-\partial\gamma/\partial T$ is the surface entropy. A crude estimate of the magnitude of this quantity for a crystalline solid can be obtained from the work of Jura and Garland [J. Am. Chem. Soc. **74**, 6033 (1952).] These authors state that the surface entropy of MgO at 298°K is 0.28-erg cm^{-2} deg^{-1}. This means that γ' may be about 80-erg cm^{-2} larger than γ_{298}.

The surface free energy of liquid LiF at the melting point 844°C is 255 erg cm^{-2}.[21] The temperature coefficient of this surface free energy is negative. Hence the value of the surface free energy (and surface energy) of liquid LiF at 0°K should be larger than 255-erg cm^{-2}. A questionable linear extrapolation of Jaeger's results to 0°K gives 396-erg cm^{-2}. To compare this value with that calculated in Sec. III and with the classical value (194-erg cm^{-2}) requires a knowledge of the difference in surface energy between the solid and liquid state. Conflicting estimates concerning even the sign of this difference occur in the literature. However, in making a similar comparison for NaCl Harkins[22] states "it is evident that there is a serious disagreement between (classically) calculated and experimental values . . . ."

The surface energy 557-erg cm^{-2} obtained in this paper appears reasonable and more in accord with the information presented in the above paragraphs than the classically calculated value.

The results of Sec. III also indicate a slight increase (0.5 percent) in the spacing between the surface and second layer, and a dipole moment which is opposite in sign to the classically calculated value of -0.33d. However, in view of the assumptions and approximations involved, too much significance should not be attached to these results, other than the facts that the distortion proves to be small and that the dipole moment of a surface F^- ion is considerably smaller than expected classically. Furthermore, the surface energy is not very sensitive to the magnitude of μ. This is illustrated in curve ii of Fig. 2, which shows the results of recalculating the surface energy with the second terms in the Taylor's series for $P_-^{(n)}(x,y,z)+\sum^{(n)}v_i$ and $Q_-^{(n)}(x,y,z)$ omitted (i.e. $p_-^{(1)}(0)$ and $q_-^{(1)}(0)$ are put equal to zero in Eq. (33.) The dipole moment in this case is -0.25d, but the surface energy has not been changed appreciably.

ACKNOWLEDGMENTS

The authors wish to express their indebtedness to Dr. J. A. Morrison and Dr. J. S. Dugdale of these laboratories for stimulating discussions and to Miss M. Menzies and Miss P. Maffett for assisting with the calculations.

[21] F. M. Jaeger, Z. anorg. u. allgem. Chem. **101**, 1 (1917).

[22] W. D. Harkins, *The Physical Chemistry of Surface Films* (Reinhold Publishing Corporation, New York, 1952), pp. 206–7.

Vibrational Intensities in Diatomic Infrared Transitions. The Vibrational Matrix Elements for CO*

ROBERT C. HERMAN AND KURT E. SHULER
Applied Physics Laboratory, The Johns Hopkins University, Silver Spring, Maryland
(Received August 17, 1953)

Second-order perturbation theory has been employed to obtain general formulas for the (rotationless) vibrational matrix elements of diatomic molecules in infrared transitions. The mechanical and electrical anharmonicities have been taken into account by expanding the potential function in a power series through quartic terms and the electric dipole moment through cubic terms in the internuclear separation. The formulas obtained in this manner are shown to be quite accurate for the fundamental and the first two overtones.

These expressions were then employed to evaluate the vibrational matrix elements for CO ($^1\Sigma^+$) up to $v'=4$ using the experimental integrated absorption coefficients as auxiliary data for the determination of the electric dipole moment expansion coefficients. A comparison of the vibrational matrix elements for CO involving the use of perturbed harmonic oscillator wave functions with those obtained using Morse wave functions with both linear and quadratic expansion of the electric dipole moment indicates that the Morse treatment is applicable through higher vibrational quantum numbers and higher transitions than the perturbation treatment. The comparison furthermore shows that the simple Morse expression with a linear expansion of the electric dipole moment yields vibrational matrix elements which would appear to be sufficiently accurate for many purposes.

The anharmonic oscillator wave functions obtained would also prove useful in the evaluation of vibrational matrix elements in electronic transitions if the array for the harmonic oscillator overlap integrals were extended through higher vibrational quantum numbers.

I. INTRODUCTION

THE calculation of vibrational transition probabilities in infrared transitions has assumed a renewed importance with the advent of improved experimental techniques for the accurate measurement of the intensities of vibration-rotation bands. A knowledge of the vibrational matrix elements in conjunction with accurate intensity measurements will permit, for instance, a detailed study of the distribution of the radiating or absorbing molecules among their vibrational energy levels and thus yield some information on the distribution and exchange of internal energy. The comparison of calculated vibrational intensities with those measured for equilibrium systems, such as hot gases in furnaces, leads to information regarding the variation of dipole moment with internuclear distance and is thus of interest in the fields of molecular structure and chemical valence.

The vibrational matrix element $\mathbf{R}^{v'v''}$ for infrared electric dipole transitions in diatomic molecules is given by

$$\mathbf{R}^{v'v''}=\int \Psi_{v'}^{*} M \Psi_{v''} d\tau,$$

where $\Psi_{v'}$ and $\Psi_{v''}$ are the wave function for the upper and lower vibrational states (in a given electronic state) and M is the (variable) dipole moment expressed as a function of the internuclear distance. This integral is usually evaluated by expanding M as a power series about r_e, the equilibrium internuclear distance, and representing the Ψ's either by Morse or by perturbed harmonic oscillator wave functions.

An approximate evaluation of $\mathbf{R}^{v'v''}$ for the $0\rightarrow1$ and $0\rightarrow2$ transitions using Morse wave functions and the linear term in the dipole moment expansion was first carried out by Dunham.[1] In a later paper, Dunham[2] extended these approximate calculations to include quadratic and cubic terms in the dipole expansion. An exact expression for $\mathbf{R}^{v'v''}$ for all transitions $v'\leftrightarrow v''$ using Morse wave functions with a linear variation of the dipole moment was derived by Rosenthal.[3] This paper also contains exact expressions for the vibrational matrix element with the quadratic term in the dipole expansion for certain specific transitions. Heaps and Herzberg[4] have recently re-evaluated $\mathbf{R}^{v'v''}$ with Morse wave function for both the linear and quadratic terms in the dipole expansion, the latter for the progressions with $v''=0$, 1, 2, and 3. They were able to reduce the Rosenthal triple summation for the matrix element with the linear dipole expansion term to a much simpler expression which can be evaluated more readily. An even simpler closed expression for this matrix element, which is equivalent to that found by Heaps and Herzberg has also been derived by us.[5] There have been so far no exact calculations for $\mathbf{R}^{v'v''}$ using Morse functions with higher than quadratic terms in the dipole moment expansion. It appears from an inspection of the above quoted papers that the inclusion of these higher terms

* This work was supported by the Bureau of Ordnance, Department of the Navy, under Contract NOrd-7386.

[1] J. L. Dunham, Phys. Rev. **34**, 438 (1929).
[2] J. L. Dunham, Phys. Rev. **35**, 1347 (1930).
[3] J. E. Rosenthal, Proc. Natl. Acad. Sci., U.S.A. **21**, 281 (1935); see also K. Scholz, Z. Physik **78**, 751 (1932).
[4] H. S. Heaps and G. Herzberg, Z. Physik **133**, 48 (1952).
[5] R. C. Herman and K. E. Shuler, J. Chem. Phys. **21**, 373 (1953).

would lead to formidable mathematical and computational difficulties.

The matrix elements $\mathbf{R}^{v'v''}$ were evaluated with perturbed harmonic oscillator wave functions by Dunham[2] for the specific transitions 0→1, 0→2, and 0→3 with the inclusion of the cubic term in the dipole expansion. His formulas for the fundamental and the 1st overtone include some second-order correction terms. This work was extended by Crawford and Dinsmore[6] who used a second-order perturbation treatment to derive general formulas for the intensities of the fundamental and the first two overtones through the cubic term in the dipole expansion. Eggers and Crawford[7] have also applied the perturbation treatment developed in the preceding paper[6] to calculate the intensities of some of the fundamental and overtone bands of the linear polyatomic molecules CO_2 and N_2O.

The work to be reported in the present paper is an extension of the previous perturbation treatments, a comparison of this treatment with that employing Morse wave functions, and an evaluation of the relative importance of the various terms in the electric dipole expansion. We have derived, by second-order perturbation methods, general expressions for the vibrational matrix elements of the fundamental and first two overtones using a power series expansion for the molecular potential function through the quartic term and a dipole moment expansion through the cubic term. These expressions contain second-order correction terms previously not evaluated. These formulas have been applied to the calculation of the matrix elements for the fundamental and first two overtone transitions of CO in the $^1\Sigma^+$ ground state and to the evaluation of the first three coefficients of the dipole moment expansion. It should be emphasized that the formulas obtained for the vibrational matrix elements in this paper are for transitions involving states with $J=0$ since vibration-rotation interactions have not been taken into account. We have finally discussed at some length the serious limitations on the use of perturbation methods with power series expansion of both the potential function and the dipole moment for the accurate calculation of vibrational transition probabilities for higher overtones and higher transitions in a given sequence.

II. THE ANHARMONIC OSCILLATOR WAVE FUNCTIONS

In order to evaluate the vibrational matrix elements $\mathbf{R}^{v'v''}$ with second-order corrections it is necessary to obtain the wave functions $\Psi_{v'}$ and $\Psi_{v''}$ for the anharmonic oscillator by means of second-order perturbation methods.

The second-order corrected wave function Ψ_v is given by the well-known expression

$$\Psi_v=\Psi_v^0+\sum_m{}' \frac{H'_{mv}}{(E_v^0-E_m^0)}\Psi_m^0 + \sum_k{}'\left[\sum_m{}' \frac{H'_{km}H'_{mv}}{(E_v^0-E_k^0)(E_v^0-E_m^0)} - \frac{H'_{vv}H'_{kv}}{(E_v^0-E_k^0)^2}\right]\Psi_k^0+\cdots, \quad (1)$$

where

$$H'_{mv}=\int \Psi_m^0(q)H'\Psi_v^0(q)dq, \quad (1a)$$

with $m\neq v$ and $k\neq v$. The potential function for the anharmonic oscillator may be written as a power series in terms of the dimensionless normal coordinate q as

$$U/hc=k_0q^2+\beta q^3+\gamma q^4+\cdots, \quad (2)$$

where

$$q=\alpha^{\frac{1}{2}}r_e\xi, \quad (2a)$$

$$\alpha=(4\pi^2\omega_e c\mu/h)\ \text{cm}^{-2}, \quad (2b)$$

and

$$\xi=(r-r_e)/r_e=u/r_e, \quad (2c)$$

r_e being the equilibrium internuclear separation.[8,9] The correction to the zero-order Hamiltonian, H', employed in Eq. (1a) is taken as

$$H'/hc=\beta q^3+\gamma q^4 \quad (3)$$

and the $\Psi_v^0(q)$ are the unperturbed harmonic oscillator wave functions given by

$$\Psi_v^0(q)=\alpha^{-\frac{1}{4}}\Psi_v^0(u)=\left\{\left(\frac{1}{\pi}\right)^{\frac{1}{2}}\frac{1}{2^v v!}\right\}^{\frac{1}{2}} \times H_v(q)\exp(-q^2/2). \quad (4)$$

The second-order perturbation calculation for the anharmonic oscillator wave functions gives

$$\Psi_v=\sum_{k=-8}^{+8} C_{v,v+k}\Psi_{v+k}^0, \quad (5)$$

[6] B. L. Crawford, Jr., and H. L. Dinsmore, J. Chem. Phys. **18**, 983, 1682, (1950).

[7] D. F. Eggers and B. L. Crawford, Jr., J. Chem. Phys. **19**, 1554 (1951).

[8] The constants α, β, and γ employed in Eq. (2) should not be confused with the spectroscopic rotational constants α_e, β_e, and γ_e.

[9] The coefficients in the potential function used in this paper [Eq. (2)] are related to the coefficients of the Dunham potential [J. L. Dunham, Phys. Rev. **41**, 721 (1932)],

$$U=hca_0\xi^2(1+a_1\xi+a_2\xi^2+a_3\xi^3+\cdots)$$

according to

$$k_0=a_0(\alpha^{\frac{1}{2}}r_e)^{-2}, \quad \beta=a_0a_1(\alpha^{\frac{1}{2}}r_e)^{-3}$$

and

$$\gamma=a_0a_2(\alpha^{\frac{1}{2}}r_e)^{-4}.$$

The coefficients a_0, a_1, and a_2 are related to the spectroscopic constants as follows [see J. L. Dunham, Phys. Rev. **41**, 713, 721 (1932) and H. M. Hulburt and J. O. Hirschfelder, J. Chem. Phys. **9**, 61 (1941)]:

$$a_0=(\omega_e^2/4B_e),$$
$$-a_1=1+(\alpha_e\omega_e/6B_e^2) \quad \text{and} \quad a_2=5a_1^2/4-(2x_e\omega_e/3B_e).$$

where the coefficients $C_{v,v+k}$ expressed in terms of the quantities

$$b \equiv \beta/\omega_e \quad \text{and} \quad g \equiv \gamma/\omega_e \tag{5a}$$

are given by:

$$C_{v,v-8}=\left[\frac{v!}{(v-8)!}\right]^{\frac{1}{2}}\frac{g^2}{512}$$

$$C_{v,v-7}=\left[\frac{v!}{(v-7)!}\right]^{\frac{1}{2}}\frac{bg}{96\sqrt{2}}$$

$$C_{v,v-6}=\left[\frac{v!}{(v-6)!}\right]^{\frac{1}{2}}\left\{\frac{b^2}{3}+\frac{g^2}{4}(6v-11)\right\}\cdot\frac{1}{48}$$

$$C_{v,v-5}=\left[\frac{v!}{(v-5)!}\right]^{\frac{1}{2}}\left\{\frac{bg}{480\sqrt{2}}(85v-104)\right\}$$

$$C_{v,v-4}=\left[\frac{v!}{(v-4)!}\right]^{\frac{1}{2}}\left\{g+\frac{b^2}{2}(4v-3)+g^2(2v^2-9v+7)\right\}\cdot\frac{1}{16}$$

$$C_{v,v-3}=\left[\frac{v!}{(v-3)!}\right]^{\frac{1}{2}}\left\{\frac{b}{3}+\frac{bg}{16}(21v^2-74v+29)\right\}\cdot\frac{1}{2\sqrt{2}}$$

$$C_{v,v-2}=\left[\frac{v!}{(v-2)!}\right]^{\frac{1}{2}}\left\{g(2v-1)+\frac{b^2}{4}(7v^2-19v+1)-\frac{g^2}{16}(2v^3+129v^2-107v+66)\right\}\cdot\frac{1}{4}$$

$$C_{v,v-1}=\left[\frac{v!}{(v-1)!}\right]^{\frac{1}{2}}\left\{3bv-\frac{bg}{16}(27v^3+398v^2+69v+90)\right\}\cdot\frac{1}{2\sqrt{2}} \tag{5b}$$

$$C_{v,v}=\left\{1-\frac{b^2}{144}(164v^3+246v^2+256v+87)-\frac{g^2}{256}(65v^4+130v^3+487v^2+422v+156)\right\}$$

$$C_{v,v+1}=\left[\frac{(v+1)!}{v!}\right]^{\frac{1}{2}}\left\{-3b(v+1)-\frac{bg}{16}(27v^3-317v^2-646v-392)\right\}\cdot\frac{1}{2\sqrt{2}}$$

$$C_{v,v+2}=\left[\frac{(v+2)!}{v!}\right]^{\frac{1}{2}}\left\{-g(2v+3)+\frac{b^2}{4}(7v^2+33v+27)-\frac{g^2}{16}(2v^3-123v^2-359v-300)\right\}\cdot\frac{1}{4}$$

$$C_{v,v+3}=\left[\frac{(v+3)!}{v!}\right]^{\frac{1}{2}}\left\{-\frac{b}{3}+\frac{bg}{16}(21v^2+116v+124)\right\}\cdot\frac{1}{2\sqrt{2}}$$

$$C_{v,v+4}=\left[\frac{(v+4)!}{v!}\right]^{\frac{1}{2}}\left\{-g+\frac{b^2}{2}(4v+7)+g^2(2v^2+13v+18)\right\}\cdot\frac{1}{16}$$

$$C_{v,v+5}=\left[\frac{(v+5)!}{v!}\right]^{\frac{1}{2}}\left\{\frac{bg}{480\sqrt{2}}(85v+189)\right\}$$

$$C_{v,v+6}=\left[\frac{(v+6)!}{v!}\right]^{\frac{1}{2}}\left\{\frac{b^2}{3}+\frac{g^2}{4}(6v+17)\right\}\cdot\frac{1}{48}$$

$$C_{v,v+7}=\left[\frac{(v+7)!}{v!}\right]^{\frac{1}{2}}\left\{\frac{bg}{96\sqrt{2}}\right\}$$

$$C_{v,v+8}=\left[\frac{(v+8)!}{v!}\right]^{\frac{1}{2}}\left\{\frac{g^2}{512}\right\}.$$

The wave functions Ψ_v given by Eq. (5) are normalized through terms in b^2 and g^2. A similar calculation was carried out by Hutchisson[10] through terms in b^2 and g. The results of Hutchisson have been extended in the above calculations to include higher-order correction terms in bg and g^2 in order to obtain more accurate wave functions for the evaluation of the matrix elements for both infrared and electronic transitions.[11]

III. MATRIX ELEMENTS FOR THE ANHARMONIC OSCILLATOR

The intensity of an emission line for the transition $v' \rightarrow v''$, $I_{em}{}^{v'v''}$, is given by

$$I_{em}{}^{v'v''} \sim \nu^4_{v'v''} |\mathbf{R}^{v'v''}|^2, \tag{6}$$

and the intensity of an absorption line for very thin absorbing layers for the transition $v'' \rightarrow v'$, $I_{\text{abs}}{}^{v'v''}$, is given by

$$I_{\text{abs}}{}^{v'v''} \sim \nu_{v'v''} |\mathbf{R}^{v'v''}|^2, \tag{6a}$$

where $\mathbf{R}^{v'v''}$, the vibrational matrix element of the electric dipole moment M, is given by

$$\mathbf{R}^{v'v''} = \int \Psi_{v'}{}^* M \Psi_{v''} d\tau \tag{6b}$$

and $\nu_{v'v''}$ is the frequency of the line. In order to evaluate the integral $\mathbf{R}^{v'v''}$ one must have, in addition to an

[10] E. Hutchisson, Phys. Rev. **37**, 45 (1931). It might be noted that in the coefficient $C_{v,v-2}$, given in this reference, the numerical factor 8 in front of $(2v-1)$ should read kc_4 and that the coefficients $C_{v,v\pm6}$ should have been listed in the approximation given because they contain terms in $c_3{}^2$.

[11] The integrals required in the above perturbation calculation can be obtained from the recursion formulas for the harmonic oscillator wave functions given in reference 10 or from the formulas given by E. Fues, Ann. Phys. **80**, 367 (1926).

adequate set of wave functions, an expression for the electric dipole moment as a function of internuclear distance. It has so far not proven possible to derive an analytical expression for the dependence of M on internuclear distance from independent quantum mechanical considerations.[12]

For the foregoing reason it has been customary[1,2,4,6] to approximate the dependence of the electric dipole moment on internuclear distance by a Taylor expansion about the equilibrium internuclear distance r_e. Such an expansion will give an adequate representation of the functional form of the dipole moment only in the immediate neighborhood of the equilibrium internuclear separation. The matrix elements calculated using this expansion will therefore be accurate only in the event that the contribution to $\mathbf{R}^{v'v''}$ arises mainly in this region. It is clear that this type of approximation will be best for molecules having small anharmonicity and large force constants as well as for transitions between low-lying vibrational states. This question is discussed in more detail in Sec. IV.

Since the analysis in the present paper is given in terms of the dimensionless normal coordinate q [see Eq. (2)], we expand the electric dipole moment, $p=M$, as

$$p=p(q)=p_0+p_1q+p_2q^2+p_3q^3+\cdots, \tag{7}$$

where p_0 is the equilibrium electric dipole moment and where the expansion coefficients p_i are to be determined from the experimental intensity measurements. Using Eq. (7) for the dipole moment and the wave functions of Eq. (5) in the vibrational matrix element given by Eq. (6b), one obtains[13]

$$\mathbf{R}^{v'v''}=\sum_{i=1} p_i\int \Psi_{v'}{}^*(q)q^i\Psi_{v''}(q)dq=\sum_{i=1} p_i\mathbf{R}_i{}^{v'v''}. \tag{8}$$

The matrix elements in Eq. (8) can be evaluated readily using the recurrence relations between the harmonic oscillator wave functions.[11] Writing Eq. (8) in the form

$$\mathbf{R}^{v'v''}=p_1\mathbf{R}_1{}^{v'v''}+p_2\mathbf{R}_2{}^{v'v''}+p_3\mathbf{R}_3{}^{v'v''}+\cdots, \tag{9}$$

one finds, using $s=v'-v''$ and replacing v'' by v for convenience, that

$$\mathbf{R}_1{}^{v+s,v}\equiv\int\Psi_{v+s}{}^*(q)q\Psi_v(q)dq$$

$$=\sum_{j=-8}^{8} C_{v+s,v+s+j}\left\{C_{v,v+s+j+1}\left(\frac{v+s+j+1}{2}\right)^{\frac{1}{2}}\right.$$

$$\left.+C_{v,v+s+j-1}\left(\frac{v+s+j}{2}\right)^{\frac{1}{2}}\right\}, \tag{9a}$$

$$\mathbf{R}_2{}^{v+s,v}\equiv\int\Psi_{v+s}{}^*(q)q^2\Psi_v(q)dq$$

$$=\sum_{j=-8}^{8} C_{v+s,v+s+j}\{C_{v,v+s+j+2}$$

$$\times[(v+s+j+1)(v+s+j+2)]^{\frac{1}{2}}$$

$$+C_{v,v+s+j}[2(v+s+j)+1]$$

$$+C_{v,v+s+j-2}[(v+s+j)(v+s+j-1)]^{\frac{1}{2}}\}, \tag{9b}$$

and

$$\mathbf{R}_3{}^{v+s,v}\equiv\int\Psi_{v+s}{}^{0*}(q)q^3\Psi_v{}^0(q)dq$$

$$=\left[\frac{(v+s)\,!v\,!}{2^{2v+s}}\right]^{\frac{1}{2}}\sum_{h=0}^{(3-s)/2}\frac{2^{v-h}}{(v-h)\,!}$$

$$\times\binom{3}{s+2h}\binom{s+2h}{s+h}K_{3-s-2h}, \tag{9c}$$

where

$$\left\{\begin{array}{l}K_n=[1\cdot3\cdot5\cdots(n-1)]/(2^{n/2}),\ n\text{ even}\\ \quad=0,\ n\text{ odd}\\ \quad=1,\ n=0.\end{array}\right\}$$

The coefficients $C_{v+s,v+s+j}$, etc., are given by Eqs. (5b). It should be pointed out that $\mathbf{R}_3{}^{v+s,v}$ is evaluated in Eq. (9c) with the unperturbed harmonic oscillator wave functions since the use of second-order wave functions for this matrix element leads to a very small correction which does not warrant the large amount of labor necessary for its evaluation.

It has been pointed out by Dunham[2] that for the transition $(0\rightarrow v')$ it is necessary in the perturbation calculation to evaluate terms up to and including $i=v'$ in Eq. (8). This result can be generalized into the statement that in Eq. (8), i must be taken up to s for all transitions $v'-v''=s$. Dunham[2] has also called attention to the necessity of employing a higher-order perturbation treatment as higher terms are included in the potential function and dipole moment expansion. In the second-order perturbation treatment given here the potential function was expanded through terms in q^4. Terms higher than q^4 in the potential function however should have been included to obtain all of the contributions in the second-order perturbation treatment but the coefficients of these higher terms in U/hc are not known at present. In view of the above discussions the results given in Eq. (9) will hold for $s=1$, 2, and 3 only.

Equations (9) can be rewritten in a more tractable form by introducing the values of the coefficients $C_{v+s,v+s+j}$ from Eq. (5b) and performing the indicated summations. For the transitions $s=1$, 2, and 3 one ob-

[12] For a discussion of this question see, for example, C. A. Coulson, *Valence* (Oxford University Press, London, 1953), pp. 102–105.

[13] Since the integral $\int\Psi^*(\tau)\Psi(\tau)d\tau$ is a dimensionless quantity the matrix element $\mathbf{R}^{v'v''}$ is always given in the same units as the electric dipole moment.

tains the following results:[14]

$s=1$:

$$\mathbf{R}_1^{v+1,v}=\left[\frac{(v+1)!}{v!}\right]^{\frac{1}{2}}\left\{\frac{1}{\sqrt{2}}-\frac{3}{2\sqrt{2}}(v+1)g+\frac{11}{4\sqrt{2}}(v+1)b^2\right\},$$

$$\mathbf{R}_2^{v+1,v}=\left[\frac{(v+1)!}{4v!}\right]^{\frac{1}{2}}\left\{-\frac{10}{\sqrt{2}}(v+1)b+\frac{269}{2\sqrt{2}}\left[(v+1)^2+\frac{83}{269}\right]bg-\frac{937}{72\sqrt{2}}\left[(v+1)^4+\frac{6725}{937}(v+1)^2+\frac{918}{937}\right]b^3\right\},$$

$$\mathbf{R}_3^{v+1,v}=3\left(\frac{v+1}{2}\right)^{\frac{1}{2}}=\left[\frac{(v+1)!}{v!}\right]^{\frac{1}{2}}\left\{\frac{3}{\sqrt{2}}\right\}.$$

$s=2$:

$$\mathbf{R}_1^{v+2,v}=\left[\frac{(v+2)!}{v!}\right]^{\frac{1}{2}}\left\{\frac{b}{2}-\frac{37}{8}(2v+3)bg+\frac{533}{2304}(2v+3)\left[(2v+3)^2-\frac{5933}{533}\right]b^3\right\}, \quad (10)$$

$$\mathbf{R}_2^{v+2,v}=\left[\frac{(v+2)!}{4v!}\right]^{\frac{1}{2}}\left\{1-\frac{5}{4}(2v+3)g+\frac{1}{8}(2v+3)b^2\right\},$$

$$\mathbf{R}_3^{v+2,v}\equiv 0.$$

$s=3$:

$$\mathbf{R}_1^{v+3,v}=\left[\frac{(v+3)!}{v!}\right]^{\frac{1}{2}}\left\{\frac{1}{4\sqrt{2}}g+\frac{3}{8\sqrt{2}}b^2\right\},$$

$$\mathbf{R}_2^{v+3,v}=\left[\frac{(v+3)!}{4v!}\right]^{\frac{1}{2}}\left\{\frac{2}{\sqrt{2}}b-\frac{42}{\sqrt{2}}(v+2)bg+\frac{1505}{144\sqrt{2}}(v+2)\left[(v+2)^2-\frac{781}{430}\right]b^3\right\},$$

$$\mathbf{R}_3^{v+3,v}=\left[\frac{(v+3)(v+2)(v+1)}{8}\right]^{\frac{1}{2}}=\left[\frac{(v+3)!}{v!}\right]^{\frac{1}{2}}\left\{\frac{1}{2\sqrt{2}}\right\}.$$

[14] It has been pointed out from general considerations that the results stated in Eq. (9) are valid for $s\lesssim 3$. The extent of the breakdown of this approximation for $s>3$ is demonstrated numerically in Sec. 4 using the following expressions for $s=4$ derived in the same manner as Eqs. (10):

$s=4$:

$$\mathbf{R}_1^{v+4,v}=\left[\frac{(v+4)!}{v!}\right]^{\frac{1}{2}}\left\{\frac{1}{4}bg+\frac{101}{288}\left[(2v+s)^2+\frac{151}{101}\right]b^3\right\},$$

$$\mathbf{R}_2^{v+4,v}=\left[\frac{(v+4)!}{4v!}\right]^{\frac{1}{2}}\left\{\frac{1}{2}g+\frac{5}{4}b^2\right\},$$

$$\mathbf{R}_3^{v+4,v}=0.$$

In the next section the above results are applied to the calculation of vibrational transition probabilities for the CO molecule in the $^1\Sigma^+$ ground state. In order to compare the results obtained with the above perturbation method using anharmonic oscillator wave functions with those obtained using matrix elements employing Morse wave functions, the necessary formulas for the latter method which have been derived by Heaps and Herzberg[4] are given below. If in Eq. (6b) one employs Morse wave functions designated by $\Psi(u)$, where $u=r-r_e$, and writes for the dipole moment an expression equivalent to that given in Eq. (7), namely,

$$M=M_0+M_1u+M_2u^2+\cdots, \quad (11)$$

one obtains [compare with Eq. (8)]

$$\mathbf{R}^{v'v''}=\sum_{i=1} M_i\int\Psi_{v'}^*(u)u^i\Psi_{v''}(u)du \quad (12)$$

$$=M_1\mathbf{S}_1^{v'v''}+M_2\mathbf{S}_2^{v'v''}+\cdots. \quad (12a)$$

It has been shown[4,5] that

$$\mathbf{S}_1^{v'v''}=(-1)^{v'+v''}\left[a(v'-v'')(k-v'-v''-1)\right]^{-1}\times\left\{\frac{v'!(k-2v'-1)(k-2v''-1)}{v''!\prod_{t=0}^{v'-v''-1}(k-v'+t)}\right\}^{\frac{1}{2}}, \quad (13)$$

where $ar_e=(\omega_e x_e/B_e)^{\frac{1}{2}}$ and $k=1/x_e$. In the approximation $(v'+v'')x_e\ll 1$ and taking $v'=v''+s$, and $v''=v$ as earlier, one obtains

$$|\mathbf{S}_1^{v+s,v}|^2\cong\frac{r_e^2B_ex_e^{s-1}}{\omega_e}\frac{(v+s)!}{s^2v!}(1+vx_e). \quad (13a)$$

According to Heaps and Herzberg[4] the matrix element $S_2^{v+s,v}$ is given by

$$\mathbf{S}_2^{v+s,v}=\frac{(-1)^{2v+s+1}}{\beta^2(v+s)!}\frac{2C'_{v+s,v}H'_{v+s,v}}{[1-(v+s+1)x_e]}, \quad (14)$$

where $C'_{v+s,v}$ and $H'_{v+s,v}$ are known expressions involving the quantum numbers and x_e.

In order to facilitate a comparison of results obtained by the perturbation and Morse treatments, the relationship between the electric dipole moment expansion coefficients in Eq. (7) and (11) is given below. Since $M(u)=p(q)$ one has[15]

$$M_i=p_i\alpha^{i/2}, \quad (15)$$

where α is defined in Eq. (2b).

[15] If the dipole moment is expanded as in reference 6, namely,

$$p(\xi)=p_e+p_e'\xi+(1/2!)p_e''\xi^2+(1/3!)p_e'''\xi^3+\cdots,$$

then

$$p_e'=\alpha^{\frac{1}{2}}r_ep_1,\quad p_e''=2\alpha r_e^2p_2,\quad p_e'''=6\alpha^{\frac{3}{2}}r_e^3p_3, \text{ etc.}$$

TABLE I. Molecular constants for CO ($^1\Sigma^+$).

ω_e(cm^{-1})	$\omega_e x_e$(cm^{-1})	B_e(cm^{-1})	α_e(cm^{-1})	r_e(A)
2169.84[a]	13.301[a]	1.93130[b]	0.017543[b]	1.1281[c]
a_0(cm^{-1})	a_1	a_2	$b=\beta/\omega_e$	$g=\gamma/\omega_e$
609,444[d]	−2.70088	4.53293	-5.69778×10^{-2}	4.02955×10^{-3}

[a] Reference 19.
[b] Reference 18. Values of B_v obtained from this paper also.
[c] Reference 20.
[d] See reference 9.

As mentioned earlier it has not yet proven possible to determine the coefficients in the electric dipole moment expansion, i.e., the electrical anharmonicity, by a direct quantum-mechanical calculation. These quantities must therefore be obtained from a comparison of experimental intensity data with the theoretical expressions obtained above for the vibrational matrix elements. This is in contradistinction to the mechanical anharmonicity which can be determined readily from the positions of the band origins.

It has been shown[6] that the total intensity or integrated absorption $A^{v'v''}$ of a vibration-rotation band is given by

$$A^{v'v''}=\sum_{J'J''}\alpha^{v'v''J'J''}=(8\pi^3N_{v''}/3hc)\tilde{\omega}^{v'v''}|\mathbf{R}^{v'v''}|^2, \quad (16)$$

where $\mathbf{R}^{v'v''}$ is given by Eq. (8), $\alpha^{v'v''J'J''}$ is the absorption coefficient, $N_{v''}$ is the concentration of molecules in the vibrational level v'', and

$$\tilde{\omega}^{v'v''}=[\omega^{v'v''}+(B_{v'}-B_{v''})(1+Z)]\times[1-\exp(-hc\omega^{v'v''}/kT)]+(B_{v'}+B_{v''})[1+\exp(-hc\omega^{v'v''}/kT)] \quad (16a)$$

with the rotational partition function Z expressed in the form

$$Z=\sum_{J=0}^{\infty}g_J\exp(-E_J/kT)\sim kT/hcB_{v''}. \quad (16b)$$

Since the integrated absorption coefficients can be determined experimentally[16,17] and the $\mathbf{R}_i^{v'v''}$ calculated, one can employ Eq. (16) to evaluate the dipole expansion coefficients p_i.

It should be noted that the above analysis can also be carried out for individual vibration-rotation lines rather than for an entire band. However, this necessitates obtaining spectra at high resolution and taking into account the effect of line shape on the line intensity. A detailed discussion of this question has been given by Wilson and Wells.[16]. The vibrational matrix elements $\mathbf{R}^{v'v''}$ as given in Eq. (9) have been calculated for the rotationless state $J=0$. Strictly speaking Eq. (16) should be modified so that the vibrational matrix element as well as the integrated absorption coefficient contain the influence of vibration-rotation interaction. This interaction should also be taken into account when dealing with the intensities of individual vibration-rotation lines.

In the next section the above formulas obtained for the vibrational matrix elements are applied to the particular case of the CO molecule in order to obtain both more accurate values of these matrix elements and to compare the results obtained using the perturbation and Morse treatments. This calculation also yields improved values for the electric dipole expansion coefficients which are of interest in connection with problems of molecular structure of the CO molecule.

TABLE II. Integrated absorption coefficients $A^{v',0}$ (cm^{-2} atmos^{-1}) for CO ($^1\Sigma^+$).

v'	1	2	3	4
$A^{v',0}$	237	1.64	9.3×10^{-3}	$\sim5\times10^{-5}$

IV. VIBRATIONAL INTENSITIES IN CO($^1\Sigma^+$)

The results developed in the foregoing sections are now applied to the CO molecule in the $^1\Sigma^+$ ground state. This molecule has been chosen because there exists relatively good intensity data for some of the vibration-rotation bands[17] and also because the fundamental spectroscopic constants are well known.[18–20] In addition a knowledge of vibrational matrix elements for the CO molecule is of great importance owing to the frequent occurrence of this molecule in various flame reactions. A knowledge of the relative vibrational transition probabilities is required in order to obtain information regarding questions of equilibrium and the equipartition of energy.[21]

The spectroscopic constants for the CO molecule employed in the present calculations are given in Table I. The experimental values of the integrated absorption coefficients $A^{v'v''}$ for the CO molecule are given in Table II. The coefficients $A^{1,0}$ and $A^{2,0}$ are those reported by Penner and Weber[17] and were obtained by measuring intensities of pressure broadened vibration-rotation bands. The value of the coefficient $A^{3,0}$ is that reported by Plyler, Benedict, and Silverman.[18] This coefficient was determined by a measurement of the relative intensity of resolved lines in the (0−3) and (0−2) bands of CO taken together with the value of the integrated absorption coefficient $A^{2,0}$ given by Penner and Weber. The value $A^{4,0}$ is a rough estimate made by us using the date of Herzberg and Rao.[22]

[16] E. B. Wilson, Jr., and A. J. Wells, Jr., J. Chem. Phys. **14**, 578 (1946).
[17] See for example, S. S. Penner and D. Weber, J. Chem. Phys. **19**, 807 (1951).
[18] Plyler, Benedict and Silverman, J. Chem. Phys. **20**, 175 (1952).
[19] K. E. McCulloh and G. Glockler, Phys. Rev. **89**, 145 (1953).
[20] G. Herzberg, *Spectra of Diatomic Molecules* (D. Van Nostrand Company, Inc., New York, 1950), second edition.
[21] See, for example, K. E. Shuler and H. P. Broida, J. Chem. Phys. **20**, 1383 (1952), and Benedict, Plyler and Humphreys, J. Chem. Phys. **21**, 398 (1953).
[22] G. Herzberg and K. N. Rao, J. Chem. Phys. **17**, 1099 (1949).

TABLE III.[a] Squares of the vibrational matrix elements, $|\mathbf{R}^{v'v''}|^2$ (debye)^2 and dipole moment expansion coefficients, p_i (debye), (3-constant fit) for CO ($^1\Sigma^+$) using anharmonic oscillator wave functions.

$v''-v'$	$\|\mathbf{R}^{v'v''}\|_a^2$	$\|\mathbf{R}^{v'v''}\|_b^2$	$\|\mathbf{R}^{v'v''}\|_c^2$	$\|\mathbf{R}^{v'v''}\|_d^2$	$\|\mathbf{S}^{v'v''}\|^2=x_e^{s-1}\frac{(v''+s)!}{s^2v''!}$
0–1[b]	1.074×10^{-2} (1.000)	1.074×10^{-2} (1.000)	1.074×10^{-2} (1.000)	1.074×10^{-2} (1.000)	(1)
1–2	2.134×10^{-2} (1.987)	2.359×10^{-2} (2.197)	2.320×10^{-2} (2.161)	2.096×10^{-2} (1.952)	(2)
2–3	3.177×10^{-2} (2.959)	3.907×10^{-2} (2.885)	3.784×10^{-2} (3.524)	3.066×10^{-2} (2.855)	(3)
3–4	4.196×10^{-2} (3.907)	5.853×10^{-2} (5.451)	5.594×10^{-2} (5.210)	3.976×10^{-2} (3.703)	(4)
0–2[b]	3.741×10^{-5} (3.484×10^{-3})	3.741×10^{-5} (3.484×10^{-3})	3.741×10^{-5} (3.484×10^{-3})	3.741×10^{-5} (3.484×10^{-3})	(3.065×10^{-3})
1–3	1.205×10^{-4} (1.123×10^{-2})	1.006×10^{-4} (9.374×10^{-3})	1.006×10^{-4} (9.366×10^{-3})	1.207×10^{-4} (1.124×10^{-2})	(9.195×10^{-3})
2–4	3.493×10^{-4} (3.253×10^{-2})	1.190×10^{-4} (1.109×10^{-2})	1.183×10^{-4} (1.012×10^{-2})	3.507×10^{-4} (3.267×10^{-2})	(1.839×10^{-2})
0–3[b]	1.423×10^{-7} (1.325×10^{-5})	1.423×10^{-7} (1.325×10^{-5})	1.423×10^{-7} (1.325×10^{-5})	1.423×10^{-7} (1.325×10^{-5})	(2.505×10^{-5})
1–4	6.657×10^{-7} (6.200×10^{-5})	1.143×10^{-8} (1.064×10^{-6})	1.974×10^{-6} (1.839×10^{-4})	4.956×10^{-7} (4.615×10^{-5})	(1.002×10^{-4})
0–4	1.505×10^{-6} (1.401×10^{-4})	1.621×10^{-6} (1.510×10^{-4})	1.225×10^{-6} (1.141×10^{-4})	1.124×10^{-6} (1.047×10^{-4})	(3.454×10^{-7})
p_1	1.470×10^{-1}	1.396×10^{-1}	1.409×10^{-1}	1.483×10^{-1}	
p_2	-1.307×10^{-3}	1.586×10^{-2}	1.592×10^{-2}	-1.244×10^{-3}	
p_3	-3.540×10^{-4}	1.450×10^{-3}	5.793×10^{-4}	-1.224×10^{-3}	
$A^{4,0}$(calc)	0.1303	0.1404	0.1060	0.09731	

[a] Certain apparent inconsistencies in the last place of the relative values of the squares of the matrix elements are caused by rounding after normalization
[b] The integrated absorption is known experimentally for these three transitions which have therefore been used as fitting points.

Table III which gives the results of the calculations of intensities for vibrational transitions of CO with a three constant fit in the electric dipole expansion has been constructed in the following manner. The quantities $\mathbf{R}_i^{v'v''}$ were evaluated using Eq. (10). The squares of the matrix elements $|\mathbf{R}^{v'v''}|^2$ in terms of the dipole coefficients p_i and the $\mathbf{R}_i^{v'v''}$ given by Eq. (9), were used in Eq. (16) together with the experimentally determined values of $A^{v'v''}$ for (0−1), (0−2), and (0−3) [see Table II] to evaluate the p_i. The values of p_1, p_2, and p_3 obtained in this fashion were then used in Eq. (9) to obtain the set $|\mathbf{R}^{v'v''}|^2$ given in Table III. The various sets of values for the $|\mathbf{R}^{v'v''}|^2$ in Table III arise because the solution of Eq. (16) for the p_i's involves solving i equations of second degree. For $i=3$, there are 4 independent sets of p_i, each of which is given in the appropriate column in Table III. The results given in Table IV for the anharmonic oscillator approximation have been obtained in the same manner for a two constant fit in $p(i=2)$. The results using Morse wave functions are also given in Table IV. These were obtained in an analogous manner using Eqs. (11–16). In both Tables III and IV we have given for comparison the quantity

$$|\mathbf{S}^{v'v''}|^2\equiv|S_1^{v'v''}|^2(\omega_e/r_e^2B_e)=x_e^{s-1}(v''+s)!/s^2v''!$$

from Eq. (13a) which is essentially the first term in the Morse treatment for $v''x_e\ll1$. The entries in parenthesis are relative values of $|\mathbf{R}^{v'v''}|^2$ normalized to the (0−1) transition. Finally, we have given the values of the integrated absorption coefficients $A^{3,0}$ and $A^{4,0}$ calculated from Eq. (16) using the appropriate values of $|\mathbf{R}^{v'v''}|^2$ as found in Tables III and IV.

Since both the foregoing theory and experimental results are not exact, one obtains a number of sets of values for the vibrational matrix elements given in Tables III and IV. This raises the question as to which set is most nearly correct. The most direct test would be given by comparison of calculated intensities with experimenally determined values of the $A^{v'v''}$ for a large number of transitions. In the absence of sufficient data of this type it is necessary to explore another criterion. One such criterion is the physical reasonableness of the

TABLE IV. Squares of the vibrational matrix elements, $|\mathbf{R}^{v'v''}|^2$ (debye),[2] and dipole moment expansion coefficients, p_i (debye), (2-constant fit) for CO ($^1\Sigma^+$) using Morse and anharmonic oscillator wave functions.

$v''-v'$	Morse wave functions $\lvert\mathbf{R}^{v'v''}\rvert^2$	Morse wave functions $\lvert\mathbf{R}^{v'v''}\rvert^2$	Anharmonic oscillator wave functions $\lvert\mathbf{R}^{v'v''}\rvert^2$	Anharmonic oscillator wave functions $\lvert\mathbf{R}^{v'v''}\rvert^2$	$\lvert S^{v'v''}\rvert^2=x_e^{s-1}\frac{(v''+s)!}{s^2v''!}$
0–1[a]	1.073×10^{-2} (1.000)	1.073×10^{-2} (1.000)	1.073×10^{-2} (1.000)	1.073×10^{-2} (1.000)	(1)
1–2	2.157×10^{-2} (2.009)	2.303×10^{-2} (2.145)	2.149×10^{-2} (2.001)	2.294×10^{-2} (2.137)	(2)
2–3	3.249×10^{-2} (3.026)	3.706×10^{-2} (3.452)	3.222×10^{-2} (3.001)	3.703×10^{-2} (3.449)	(3)
3–4	4.351×10^{-2} (4.052)	5.283×10^{-2} (4.920)	4.286×10^{-2} (3.992)	5.424×10^{-2} (5.052)	(4)
0–2[a]	3.741×10^{-5} (3.485×10^{-3})	3.741×10^{-5} (3.485×10^{-3})	3.741×10^{-5} (3.485×10^{-3})	3.741×10^{-5} (3.485×10^{-3})	(3.065×10^{-3})
1–3	1.134×10^{-4} (1.057×10^{-2})	1.069×10^{-4} (9.957×10^{-3})	1.206×10^{-4} (1.123×10^{-2})	1.028×10^{-4} (9.576×10^{-3})	(9.195×10^{-3})
2–4	2.294×10^{-4} (2.136×10^{-2})	2.042×10^{-4} (1.902×10^{-2})	3.489×10^{-4} (3.250×10^{-2})	1.178×10^{-4} (1.097×10^{-2})	(1.839×10^{-2})
0–3	3.291×10^{-7} (3.065×10^{-5})	1.198×10^{-6} (1.116×10^{-4})	4.675×10^{-7} (4.354×10^{-5})	7.739×10^{-7} (7.207×10^{-5})	(2.505×10^{-5})
1–4	1.339×10^{-6} (1.247×10^{-4})	4.766×10^{-6} (4.439×10^{-4})	2.022×10^{-6} (1.883×10^{-4})	5.815×10^{-6} (5.416×10^{-4})	(1.002×10^{-4})
0–4	4.822×10^{-9} (4.491×10^{-7})	2.988×10^{-8} (2.783×10^{-6})	1.676×10^{-6} (1.561×10^{-4})	9.914×10^{-7} (9.234×10^{-5})	(3.454×10^{-7})
p_1	1.462×10^{-1}	1.414×10^{-1}	1.465×10^{-1}	1.417×10^{-1}	
p_2	-4.861×10^{-4}	1.676×10^{-2}	-1.336×10^{-3}	1.597×10^{-2}	
$A^{3,0}$(calc)	2.150×10^{-2}	7.826×10^{-2}	3.055×10^{-2}	5.056×10^{-2}	
$A^{4,0}$(calc)	4.175×10^{-4}	2.587×10^{-3}	1.451×10^{-1}	8.585×10^{-2}	

[a] The integrated absorption is known best for these transitions which have therefore been used as fitting points in this case.

general behavior of the dipole expansions as given by the various sets of p_i in Tables III and IV. While it is true that the expansion $p=\sum_{i=0} p_i q^i$ is valid only in the vicinity of $r=r_e$, it might be expected that such an expansion through the cubic term, if valid, would at least approximate the known asymptotic behavior $p\to0$, when $r\to0$ and $r\to\infty$. However, it might be pointed out that the detailed behavior of the electric dipole moment as a function of internuclear separation is not known for any molecule at the present time.

We have examined the behavior of the various expansions obtained for p by using the four sets of p_i given in Table III. In Fig. 1 are given the four electric dipole moment expansions as a function of internuclear separation r as well as the potential curve for CO in the $^1\Sigma^+$ ground electronic state with the lower vibrational energy levels. Figure 2 shows the potential curve on an enlarged scale together with the portion of the dipole expansion curve (a) from Fig. 1 which lies in the vicinity of r_e. The potential function was obtained from the Dunham expansion[9] using the constants given in Table I. The magnitude of the permanent electric dipole moment, p_0, which is used to fix the curves was taken as -0.118 debye.[23] The sign of the moment was taken negative as suggested by Mulliken.[24] An examination of Fig. 1 indicates that curve (a) has the most reasonable physical behavior.[24] For this reason we believe that the corresponding values of $|\mathbf{R}^{v'v''}|_a^2$ given in the first column of Table III are perhaps the best. The other columns are given in the event that future experimental values of $A^{v'v''}$ may prove the above conclusion to be incorrect.

In Table IV the first columns for both the Morse and perturbation treatments are considered to give the better set of $|\mathbf{R}^{v'v'}|^2$. This suggestion is based on the fact that the set of p's in the first column for the perturbation trestments agrees most closely with the set of p_i's in the three constant fit in Table III.

An examination of Table IV shows that the results obtained using Morse wave functions and anharmonic oscillator wave functions are in very good agreement

[23] L. G. Wesson, *Tables of Electric Dipole Moments* (The Technology Press, Cambridge, Massachusetts, 1948).
[24] R. S. Mulliken, J. Chem. Phys. 2, 400 (1934).

for all transitions with $s \leqq 3$. It should furthermore be noted that the values of $|\mathbf{R}^{v'v''}|^2$ given in Table III (3-constant fit) also agree well with the values given in Table IV for transitions with $s \leqq 3$.

For transitions with $s>3$ the matrix elements calculated using the perturbation treatment give values of $A^{4,0}$ which are at great variance (factor 10^4) with the experimental values listed in Table II. On the other hand, the values of $A^{3,0}$ calculated with the two-constant fit (see Table IV) are in good agreement with experiment. This breakdown of the perturbation calculation for $s>3$ was predicted on theoretical grounds in Sec. III and is so complete as to vitiate the use of the formulas for $s=4$ given in footnote 14. On the other hand, inspection of the results in Table IV obtained with Morse wave functions shows that the $A^{v',0}$ calculated for both $v'=3$ and 4 are in moderately good agreement with the experimentally determined integrated absorption coefficients.

The quantities $|S^{v'v''}|^2$ listed in the last columns of Tables III and IV are the squares of the vibrational matrix elements for Morse wave functions and a linear dipole expansion normalized to the 0—1 transition. These values are to be compared with the normalized $|\mathbf{R}^{v'v''}|^2$ given in parentheses. It is evident that the agreement is quite good. Therefore, unless the experimental data required to determine the higher dipole expansion coefficients are very accurate, the labor required to compute the $|\mathbf{R}^{v'v''}|^2$ of Eqs. (8) and (12) is not justified considering the close agreement of $|S^{v'v''}|^2$ with $|\mathbf{R}^{v'v''}|^2$.. It would appear that for the lower-lying transitions the use of the simple form $|S^{v'v''}|^2$ will yield reasonable results of sufficient accuracy for many purposes.[25]

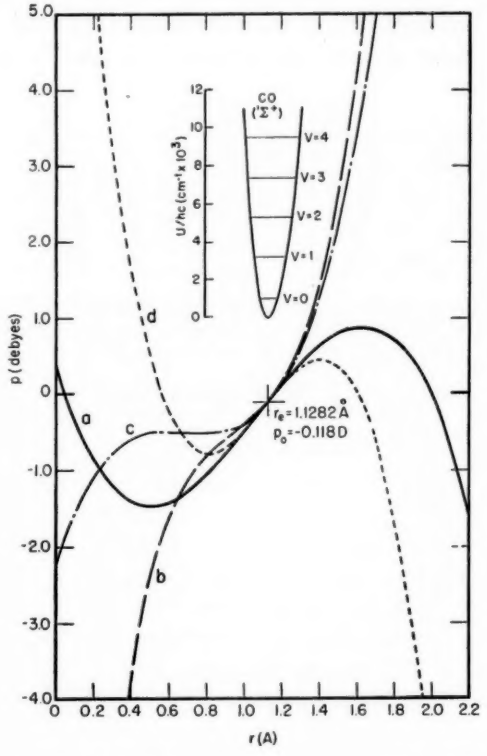

FIG. 1. Electric dipole moment expansions, $p=\Sigma p_i \alpha^{i/2}(r-r_e)^i$, as a function of internuclear separation r. The curves labeled a, b, c, and d correspond to the sets of p_i associated with the matrix elements $|\mathbf{R}^{v'v''}|_a^2$, etc., in Table III. The potential curve for CO in the $^1\Sigma^+$ ground electronic state is included to indicate the relative extent of the vibrational wave functions as compared with the essentially linear regions of the various dipole curves in the vicinity of r_e.

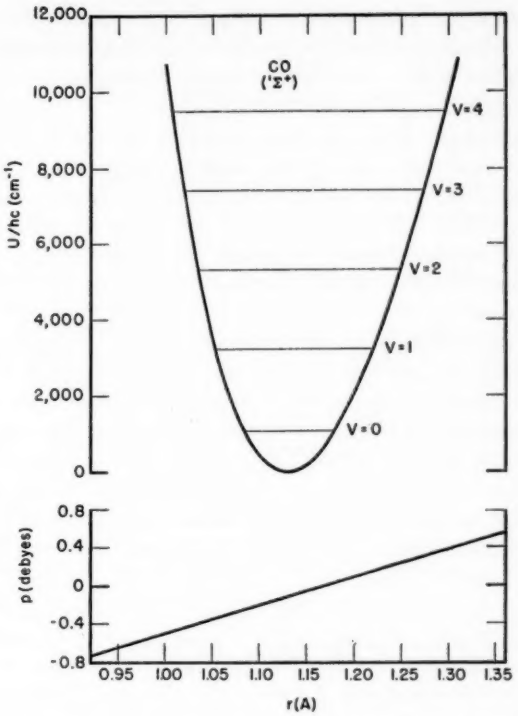

FIG. 2. The potential curve for CO in the $^1\Sigma^+$ ground electronic state and the electric dipole moment (curve a) in the vicinity of r_e on an enlarged scale.

V. DISCUSSION

It would appear that one of the principal needs in the field of intensity spectroscopy is extensive and accurate data on the intensities of vibration-rotation bands for many more diatomic molecules. These data should be obtained for equilibrium systems in order that they can be compared with theoretical calculations of relative intensities. In addition, data on transitions involving the higher vibrational quantum numbers would

[25] A comparison of $|S^{v'v''}|^2$ with $|\mathbf{R}^{v'v''}|^2$ obtained using Morse wave functions with a two constant fit [see Table IV] shows agreement to better than 1 percent for $s=1$ and $\sim$25 percent for $s=3$.

provide the information required to determine how well the Morse treatment represents the experimental intensities when the electric dipole expansion is carried through the quadratic term only.

Accurate data are also required to determine the electric dipole moment expansion coefficients, a study which may prove to be of interest for its own sake in connection with problems of molecular structure. It would prove highly desirable if it were possible to represent the electric dipole moment as an analytic function of the internuclear separation. Such an empirical function if properly chosen might make the matrix elements integrable in closed form for either the Morse or anharmonic oscillator treatments discussed above. While at present there are no experimental data bearing on this point it would appear from general considerations of the electronic structure of various diatomic molecules that such a function or functions would have to be capable of representing a wide variety of $p=f(r)$ curves.[26]

It may be noted that the wave functions for the anharmonic oscillator given in Eq. (5) can be used to evaluate some of the overlap integrals required in the study of vibrational intensities in electronic transitions. These wave functions are slightly improved over those employed by Hutchisson[10] in studying this problem. The overlap integral, $\mathbf{M}^{v'v''mn}$ required to evaluate the probability of a transition between the vibrational levels v' and v'' in the two different electronic states m and n is given by

$$\mathbf{M}^{v'v''mn}=\sum_{j=-8}^{8}\sum_{k=-8}^{8}C^{m}{}_{v',v'+j}C^{n}{}_{v'',v''+k}I^{0}{}_{v'+j,v''+k}, \quad (17)$$

where

$$I^{0}{}_{v'+j,v''+k}=\int_{0}^{\infty}\Psi^{0}{}_{v'+j,m}\Psi^{0}{}_{v''+k,n}d\boldsymbol{r}, \quad (17a)$$

the $C^{m}{}_{v',v'+j}$, etc., are given in Eq. (5b) and the Ψ^{0} are the harmonic oscillator wave functions. The evaluation of Eq. (17) is tedious but straightforward provided the integrals $I^{0}{}_{v'+j,v''+k}$ are known. Recently the harmonic oscillator overlap integrals $I^{0}{}_{v'+j,v''+k}$ were evaluated for a large number of diatomic molecules on the Mark I Calculator.[27] Unfortunately, these integrals were obtained only through $v'\leqq 7$ and $v''\leqq 7$. From Eq. (17) it is clear, however, that even for the 0,0 transition using second-order corrected wave functions one must have overlap integrals up to and including $I^{0}{}_{8,8}$, and in general for the transition $v'm\rightarrow v''n$ one requires overlap integrals evaluated through $v'+8$ and $v''+8$. Since the evaluation of the harmonic oscillator overlap integrals by the method suggested by Manneback[28] appears to be relatively simple for modern electronic computing machines[27] it is to be hoped that the results of the Harvard Computation Laboratory are extended to higher values of the vibrational quantum numbers. This extension will permit a comparison of the overlap integrals obtained using perturbed oscillator wave functions and those recently obtained by Wu[29] from Morse wave functions.

We wish to thank Mrs. Kathryn P. Stevenson for her invaluable assistance in carrying out many of the calculations and Dr. W. S. Benedict for several profitable discussions. In particular we thank Dr. G. Herzberg for his interest and a number of valuable suggestions.

Note added in proof.—The influence of the interaction of vibration and rotation on the vibrational matrix elements has been studied by Herman, Silverman, and Wallis and will form the subject of a future communication. See Bull. Am. Phys. Soc. **29**, 15 (1954).

[26] Some attempts along these lines which have been made by Mecke [see e.g., R. Mecke, Z. Elektrochem. **54**, 38 (1950) and previous papers quoted there] bear out the above analysis. See also reference 24 for the different behavior of $p(r)$ for the hydrogen halides at CO.

[27] H. Aiken, *et al.*, "Computation of the intensities of vibrational spectra of electronic bands in diatomic molecules," Problem Report No. 27, the Computation Laboratory, Harvard University (1951).

[28] C. Manneback, Physica **17**, 1001 (1951).

[29] T. Y. Wu, Proc. Phys. Soc. (London) **65A**, 965 (1952).

THE JOURNAL OF CHEMICAL PHYSICS VOLUME 22, NUMBER 3 MARCH, 1954

A Microwave Investigation of the Ionization of Hydrogen-Oxygen and Acetylene-Oxygen Flames*

KURT E. SHULER, *Applied Physics Laboratory, The Johns Hopkins University, Silver Spring, Maryland*

AND

JOSEPH WEBER, *U. S. Naval Ordnance Laboratory, White Oak, Maryland and Glenn L. Martin College of Engineering and Aeronautical Sciences, University of Maryland, College Park, Maryland*

(Received August 31, 1953)

The ionization of premixed hydrogen-oxygen and acetylene-oxygen flames burning at atmospheric pressure was studied by a microwave method. The attenuation of electromagnetic radiation by the flames was employed to determine the free electron concentration. To obtain a high sensitivity for these measurements, a microwave bridge operating slightly off balance was employed, with the flames positioned between two electromagnetic horns in one of the bridge arms. This method permits the determination of electron densities down to about $5 \cdot 10^8$ electrons per cm^3 at atmospheric pressure.

In interpreting the data obtained in this study it was found necessary to take a quantitative account of the "background ionization" resulting from the presence of alkali salts as contaminants in the air and the flame gases. After the appropriate background measurements and corrections were made, it was found that the ionization of the hydrogen-oxygen flames and of lean and stoichiometric oxy-acetylene flames was thermal and agreed well with the electron concentration values obtained from equilibrium calculations using the adiabatic flame temperatures. A complete equilibration and equipartition of the internal energy for H_2-O_2 flames is indicated by the good agreement between the effective ionization temperature and the rotational, vibrational, and electronic temperatures determined previously.

The background corrected ionization of the rich acetylene-oxygen flames ($C_2H_2/O_2 = 1.5/1$ to $4/1$) was found to be higher by a factor of 10 to 100 than that calculated for a purely thermal flame ionization. This can very plausibly be accounted for on the basis that the high electron concentration in these rich hydrocarbon flames is primarily due to the thermal evaporation of electrons from the carbon atom aggregates (soot particles) formed in these flames. A calculation showed that a work function of 8.5 ev for the small carbon particles in the flame accounts well for all the observed electron concentrations. This value stands in a reasonable relationship to the ionization potential of gaseous carbon atoms (11.265 ev) and the work function of graphite (4.35 ev).

It is suggested on the basis of these results that the ionization in hydrogen-oxygen and acetylene-oxygen flames, at least as far as the hot combustion gases are concerned, is an equilibrium process which can be accounted for by purely thermal considerations. Whether or not this holds true also for the reaction zone proper must remain open to question for the present, since the measurements described here pertain by necessity to an ionization density averaged over a rather extensive region of the flame.

I. INTRODUCTION

THERE exists now a voluminous and widely dispersed literature on the electric and magnetic properties of flames and on ionization in premixed burner flames. This literature, which has recently been reviewed and evaluated by Calcote[1] with special reference to the problem of ionization, appears to demonstrate that the concentration of ions (and thus of electrons) in flames is in general several orders of magnitude higher than would be expected from purely thermal considerations.

This result, if correct, is of considerable interest in connection with the general problem of the distribution of internal energy in fast reacting, high temperature systems of which flames are a conveniently studied example. Previous work on the rotational, vibrational, and electronic distribution of internal energy has shown that there exist in some flames nonequilibrium and/or nonequipartition distributions of energy in the various degrees of freedom.[2,3] It would thus appear not too surprising at first glance that similar conditions should obtain with regard to ionization. A factor which argues against the extension of previous arguments[3] to the case of excess ionization is the very large amount of energy required (about 9–11 ev) for the specific ionization of the various atomic and molecular species present in hydrocarbon and hydrogen-oxygen flames. It is difficult to see how this much energy, which compares with about 4 to 6 ev for electronic excitation, can be produced in combustion flames by elementary chemical reactions whose exothermicity in all but the most favorable case is only of the order of 4 to 6 ev.

We have, therefore, reinvestigated the extent of ionization in premixed and accurately metered oxy-hydrogen and oxy-acetylene flames of various fuel-oxygen ratios. We have attempted to obtain improved quantitative data for simple reaction systems whose thermal properties could readily be calculated for comparison with the experimental results.[4] These studies were carried out by directing a beam of microwaves through the flame and measuring the attenuation resulting from the free electrons with a microwave bridge.[5]

* This work was supported by the Bureau of Ordnance, Department of the Navy, under Contract NOrd 7386 and NOL FR-8.

[1] H. F. Calcote, Technical Paper No. 37, Project Squid, Princeton University, Princeton, N. J., June 15, 1948.

[2] See, e.g., A. G. Gaydon and H. G. Wolfhard, Proc. Roy. Soc. (London) **205A**, 118 (1952), and previous papers in this series; K. E. Shuler and H. P. Broida, J. Chem. Phys. **20**, 1383 (1952), and previous papers in this series.

[3] K. E. Shuler, J. Phys. Chem. **57**, 396 (1953).

[4] Calcote (reference 1) has characterized most of the previous work along these lines as being of "a qualitative nature only," and a study of the pertinent literature quoted in his review shows that this characterization is indeed an apt one.

[5] The attenuation of microwaves by free electrons was apparently first used for the study of ionization in flames by Andrew, Axford, and Sugden, Trans. Faraday Soc. **44**, 427 (1948).

This method gives a *direct* measure of the electron concentration without disturbing or distorting the flame and, in addition, eliminates many of the complications and uncertainties inherent in the more commonly used conductivity measurements.[6] It may be expected that the data obtained by this method will be sufficiently accurate to give, in conjunction with detailed calculations of the thermal equilibrium properties of the corresponding systems, more definite indications as to the nature and origin of the ionization in these flames.

II. THEORY OF THE MICROWAVE MEASUREMENTS

The concentration of free electrons in a flame can be determined from measurements of the absorption of electromagnetic radiation by the flame.[7] The presence of the free electrons introduces conductivity and affects the dielectric constant of the region occupied by the flame. It can be shown from classical electromagnetic theory[8] that the complex propagation constant for electromagnetic waves in a medium with conductivity σ is given by (in mks units)

$$\gamma=\{i\omega\mu[\sigma_r+i(\omega\epsilon+\sigma_i)]\}^{\frac{1}{2}}, \tag{1}$$

where γ is the propagation constant (meters^{-1}), ω is the angular radiofrequency, μ is the permeability, ϵ is the dielectric constant, σ_r is the real part of the conductivity (mho meters^{-1}), and σ_i is the imaginary part of the conductivity (mho meter^{-1}). If the conductivity is small, (1) may be written in the form

$$\gamma=(\sigma_r/2)(\mu/\epsilon)^{\frac{1}{2}}+i[\omega(\mu\epsilon)^{\frac{1}{2}}+(\sigma_i/2)(\mu/\epsilon)^{\frac{1}{2}}], \tag{2}$$

where the attenuation constant α and the phase constant β are given by

$$\alpha=(\sigma_r/2)(\mu/\epsilon)^{\frac{1}{2}};\quad \beta=\omega(\mu\epsilon)^{\frac{1}{2}}+(\sigma_i/2)(\mu/\epsilon)^{\frac{1}{2}}. \tag{3}$$

The real and imaginary parts of the conductivity, σ_r and σ_i, appearing in Eq. (3) have been evaluated for an ionized gas by Margenau,[9] who found that

$$\sigma_r=\frac{4e^2\lambda N_e}{3(2\pi mkT)^{\frac{1}{2}}}K_2(x), \tag{4}$$

$$\sigma_i=\frac{4e^2\lambda N_e}{3(2\pi mkT)^{\frac{1}{2}}}x^{\frac{1}{2}}K_{\frac{1}{2}}(x), \tag{5}$$

where e is the electronic charge, λ is the mean free path of the electrons, N_e is the number of electrons per unit volume, m is the electronic mass, k is Boltzmann's constant, T is the absolute temperature, and $x=m(\omega\lambda)^2/2kT$, where ω is the angular radio-frequency and where $K_2(x)$ and $K_{\frac{1}{2}}(x)$ are given by

$$K_2(x)=1-x-x^2e^xEi(-x), \tag{4a}$$

$$K_{\frac{1}{2}}(x)=(\tfrac{1}{2}-x)\pi^{\frac{1}{2}}+\pi x^{\frac{1}{2}}e^x[1-\mathrm{erf}(x)^{\frac{1}{2}}]. \tag{5a}$$

To determine N_e, the concentration of free electrons in the flame, one measures the attenuation constant α of the flame. Equation (3) is then used to find σ_r and Eqs. (4) and (4a) are used to evaluate N_e. In order to employ this procedure, λ, the mean free path of the electrons in the flame, must be known. This can be calculated if the collision diameters of the molecules in the flame have been measured previously. We have used in this study the values determined by Belcher and Sugden[7] for the collision diameters for coal gas-air flames. Even though our flames (oxy-hydrogen and oxy-acetylene) had a somewhat different composition from theirs, the use of the Belcher and Sugden collision diameters should be quite accurate for this purpose since it is known from kinetic theory data that the variation of the collision diameters is quite small among the various gases employed in these experiments.

The measurement of the attenuation constant α presented some difficulty since the attenuation of the flames used in this investigation was quite small, being only about $3\cdot10^{-4}$ neper for a hydrogen-oxygen flame with a 2-cm attenuation path. Various techniques of microwave spectroscopy have been developed in recent years which make it possible to measure attenuations as small and smaller than this. Most of these techniques are, however, not applicable here because the attenuation resulting from the free electrons in a flame is almost independent of frequency so that sweep detection methods, which show the contour of a narrow absorption line, cannot be used. Since it was considered undesirable to modulate the flame,[10] it was not possible to utilize various modulation techniques which could have enhanced the sensitivity of the measurements. The further requirement for an *absolute* value of the attenuation constant ruled out some other methods which may be employed when only relative attenuation measurements are required.

One simple way to measure the flame attenuation is to transmit microwaves over a path which includes the flame (see Fig. 1) and observe the change in detector current as the flame is moved in and out of the micro-

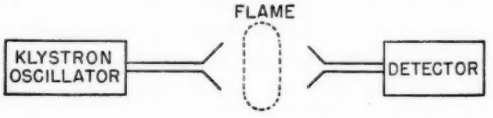

FIG. 1. Block diagram of simple apparatus for measuring large attenuation of microwaves by a flame.

[6] H. A. Wilson, Revs. Modern Phys. **3**, 156 (1931); *Modern Physics* (Blackie and Son, Ltd., London, 1944).

[7] H. Belcher and T. M. Sugden, Proc. Roy. Soc. (London) **201A**, 481 (1950).

[8] See, e.g., S. A. Schelkunoff, *Electromagnetic Waves* (D. Van Nostrand Company, Inc., New York, 1943), p. 243.

[9] H. Margenau, Phys. Rev. **69**, 508 (1946).

[10] Any mechanical modulation scheme which would have interacted directly with the flame, such as chopping the flame with a rotating sector disk, could conceivably have given rise to extraneous ionization in the flame by thermionic emission from the hot chopping disk. This could have seriously affected the accuracy of the desired data on flame ionization.

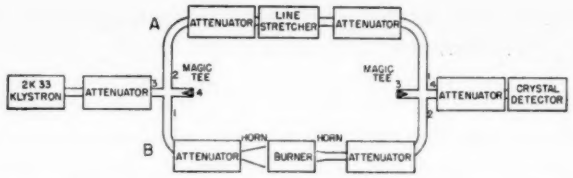

FIG. 2. Block diagram of microwave bridge used to measure attenuation in premixed burner flames.

wave beam. For small attenuation this change is, however, a relatively small one and a large amount of power would be required for its detection. Under these conditions the random fluctuations in the power output of the klystron mask the small changes in power resulting from introduction of a hydrogen-oxygen flame. In addition, the crystal noise is great when the power incident on the crystal detector is large.

These difficulties in measuring α can be overcome to a large extent by the microwave bridge illustrated in Fig. 2. Radiation from the klystron travels down the wave guide into the first magic tee, then divides among the two arms. If the bridge were approximately balanced, the amplitude and phase of the radiation from both bridge arms into the second magic tee on the right end of the bridge would be nearly the same, and there would be a small crystal current representing the difference of the outputs of the two bridge arms at the crystal detector. If the flame is now introduced in one arm, the attenuation of the microwaves in that arm will affect the balance of the bridge and change the crystal current. The detector reading will then depend only upon the difference of the electric fields in the two arms of the bridge. The klystron fluctuation will tend to balance out under these conditions as both arms are affected more or less equally. In addition, the power to the crystal, which is due to the difference in the fields in the two bridge arms, will always be small and the crystal noise will be reduced.[11] The two bridge arms will usually not be identical, so that random changes in klystron frequency and amplitude do not completely cancel. The over-all operation is, therefore, greatly improved by using a very well regulated power supply. An electronically regulated beam voltage supply was employed. In addition, 14 VR 150A tubes were connected in series across the beam voltage. Batteries were used for the reflector and focusing potentials, and a Sorenson regulator was employed for the 110 v supply. With this arrangement an attenuation of 10^{-4} neper could be detected with certainty and an order of magnitude measurement of the attenuation could be obtained. Larger attenuations could be measured with more precision.

[11] It will be shown later that it is desirable to operate the bridge slightly off balance in order to linearize its performance. This reduces to some extent the tendency of the fluctuations to balance out but improves the performance of the bridge by increasing its sensitivity.

The operation of the bridge is as follows. With the flame off, the attenuation in arm A is increased by means of an attenuator in arm A until virtually all of the observed crystal current is due to power transmitted through arm B. The crystal current i_0 is then given by

$$i_0=kE_B^n, \tag{6}$$

where E_B is the electric field at the center of the waveguide input of arm B to the second magic tee, n represents the power law of the crystal, and k is a constant of the apparatus. The attenuation in arm A is now decreased so that the bridge approaches a condition of balance. The line stretcher (phase shifter) is then adjusted to give a minimum crystal current corresponding to an out-of-phase combination of the electric fields at the magic tee. This minimum crystal current i_1 is given by

$$i_1=k(E_A-E_B)^n, \tag{7}$$

where E_A is the electric field at the center of the waveguide input of arm A to the magic tee. E_A is adjusted so that $E_A>E_B$.

The flame is now ignited. The free electrons in the flame will attenuate the radiation going down arm B and, to a lesser extent, also shift its phase. The crystal current will then change to a new value, i_2, given by

$$i_2=\{[E_A-E_B\exp(-\alpha l)\cos\Delta\varphi]^2 +[E_B\exp(-\alpha l)\sin\Delta\varphi]^2\}^{n/2}, \tag{8}$$

where α is the attenuation constant of the flame,[12] l is flame thickness (i.e., the path length through which the radiation is attenuated) and $\Delta\varphi=l\cdot\Delta\beta$ is the phase shift introduced by the flame. It will be noted from Eq. (3) that $\Delta\varphi$, the change in the phase due to the free electrons, is proportional to σ_i, the imaginary part of the conductivity of the flame. Since σ_i is also proportional to N_e, the electron density (Eq. (5)), it follows that $\Delta\varphi$ is proportional to the total attenuation αl, and by combining Eqs. (2) to (5) it can be shown that

$$\Delta\varphi=(\sigma_i/\sigma_r)\alpha l=C_1\alpha l, \tag{9}$$

where σ_i and σ_r are given by Eqs. (4) and (5). For $\alpha\ll1$ and $C_1>1$, which holds true for the flames employed in this investigation, Eq. (8) reduces to[13]

$$i_2=k\left\{E_A-E_B(1-\alpha l)+\frac{E_AE_BC_1^2(\alpha l)^2}{2[E_A-E_B(1-\alpha l)]}\right\}^n \tag{10}$$

after substitution of the value of $\Delta\varphi$ given in Eq. (9).

[12] Since a flame is not a homogeneous system but has concentration and temperature gradients across its dimensions, the attenuation constant as used above is an averaged quantity which is defined by the condition that the total attenuation equal $\alpha\cdot l$.

[13] In passing from Eq. (8) to (10) it is necessary to retain terms in $(\alpha l)^2$ in the trigonometric expansion in order to obtain a proper correction for the phase shift.

Combining Eqs. (6), (7), and (10) finally leads to

$$\alpha l=\frac{\tau-2\varphi\pm\{[2\varphi-\tau]^2-2\varphi[\varphi-\tau][C_1^2(1+\varphi)+2]\}^{\frac{1}{2}}}{[C_1^2(1+\varphi)+2]}, \quad (11)$$

where

$$\varphi=(i_1/i_0)^{1/n}, \quad \tau=(i_2/i_0)^{1/n},$$

and where i_0 is the crystal current with infinite attenuation in arm A, i_1 is the crystal current with the bridge slightly unbalanced and with the flame turned off, and i_2 is the crystal current with the bridge slightly unbalanced and with the flame present in arm B. Equation (11) was employed to calculate the attenuation αl for all the flames discussed in Sec. IV.

As was mentioned earlier, there are certain advantages in operating the bridge slightly unbalanced, particularly for the measurements of extremely small attenuations. For such small attenuations the terms in $(\alpha l)^2$ can be dropped. Equation (10) then reduces to

$$i_2=k[E_A-E_B(1-\alpha l)]^n, \quad (12)$$

and Eqs. (6), (7), and (12), when solved for αl, give

$$\alpha l=(i_2/i_0)^{1/n}-(i_1/i_0)^{1/n}. \quad (13)$$

If the bridge is now balanced so that i_1 is zero, then i_2, the unbalanced current arising from the introduction of the flame into arm B, is given by

$$i_2=i_0(\alpha l)^n, \quad (14)$$

where n represents the power law of the crystal. Since $n\sim 2$, it is evident that the current i_2 which has to be measured in these experiments is approximately quadratic in the attenuation. For very small attenuation this current is then too small to be measured conveniently and accurately. If the bridge is operated slightly unbalanced so that $i_1\neq 0$, then the change in the current i_2 for small flame attenuation can be made linear rather than quadratic in the attenuation. If i_1 is made sufficiently large so that i_2 is only slightly larger than i_1, Eq. (13) becomes

$$\alpha l=[(i_1+\Delta)/i_0]^{1/n}-(i_1/i_0)^{1/n}, \quad (14)$$

where Δ is the change in current resulting from the introduction of the flame into arm B. If Δ is small, Eq. (14) reduces to

$$\alpha l=(i_1/i_0)^{1/n}[\Delta/(ni_1)], \quad (15)$$

and the change in current, Δ, resulting from the introduction of the flame into the bridge is now seen to be linear in the attenuation αl.[14]

In the preceding discussion it has been assumed that the attenuation and phase shift brought about by the introduction of the flame into one arm of the bridge are due principally to the presence of free electrons in the flame. A phase shift accompanying the insertion of the flame into the microwave bridge could also be brought about by the change of the dielectric constant, magnetic permeability, and temperature, as the hot flame gases displace the air in the bridge arm. A calculation, assuming for the flame the extreme conditions of magnetic susceptibility equal to zero and electric susceptibility corresponding to that of an ensemble of dipoles with a moment of 1 debye at 3000°K, showed that the change of phase resulting from the above factors is too small to contribute significantly to the bridge balance.[15]

In deducing Eq. (11) it was furthermore assumed that the radiation traverses the transition region between the air and the flame without reflection. This is a reasonable assumption, since it is well known that no reflection normally occurs if the transition between two media of slightly different electrical properties is a gradual one. This is the case here, since there is a transition region of the order of a quarter-wavelength between the air at room temperature and the hot flame gases.

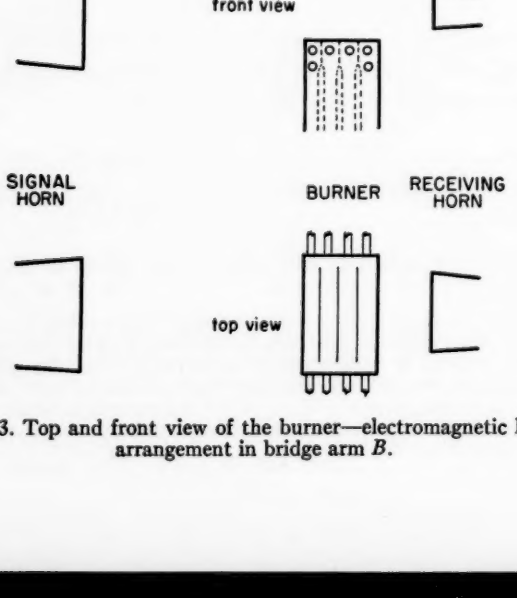

FIG. 3. Top and front view of the burner—electromagnetic horn arrangement in bridge arm B.

III. EXPERIMENTAL

Microwave Measurements

The microwave bridge was operated in the manner discussed in Sec. II. The arrangement of the electromagnetic horns and the burner shown schematically in Fig. 2 is shown in more detail (and to approximate scale) in Fig. 3. The dimensions of the horns (at the mouth) were $2\frac{1}{4}$ in. $\times 2\frac{1}{4}$ in. for the signal horn and 1 in. $\times\frac{1}{2}$ in. for the receiving horn. The distance between the horns was about 9 in., and the distance between the center of the burner and the receiving horn was about

[14] An alternative way to linearize a bridge is to employ two detectors, one in each arm of the bridge, and to subtract the detector currents. This method was tried but found to be unsatisfactory because of large output fluctuations. These large fluctuations were probably due to the high-power levels at which the detectors had to be operated.

[15] In making the measurements, care must be taken to burn the flame in such a way that no water films form on the burner. Since the electrical constants of water films are very different from those of air, the formation of such films affects the bridge balance much more than the introduction of a flame.

$1\frac{3}{4}$ in. The center of the receiving horn was about $\frac{1}{2}$ in. above the top of the burner. The final measurements were made by observing the crystal current with a sensitive mirror-type galvanometer. This type of detection system proved to be the most satisfactory of a number of techniques that were tried.

Since the klystron output changes slightly in the period between observations with the flame on and off it was necessary to minimize this interval between readings. This was achieved by measuring the galvanometer current initially with the flame on; the flame was then quickly turned off and the galvanometer was read again after it had come to rest in its new position. The time elapsed between the two readings was usually of the order of 2–5 sec.

It was found during the course of the experiments that the very small changes in the burner temperature occasioned by the ignition, the burning and the extinction of the flame during each run introduced some difficulties in obtaining an accurate measurement of the flame attenuation. The radiation arriving at the receiving horn may be considered to be the sum of the radiation which proceeds directly through the flame and that scattered by the burner. As the temperature of the burner changes during a cycle of flame off, flame on, flame off, there is a concomitant expansion and contraction in the burner dimensions. The effect of this change in burner dimensions is to change the amplitude and phase of the radiation scattered from the burner. Since the change in current observed on the galvanometer during each run is thus due both to flame attenuation and to the *change* in the radiation scattered from the burner, it was necessary either to account for or to eliminate the scattered radiation in order to obtain an accurate measurement of the attenuation.

This problem was solved in the following manner. First the scattering itself was minimized by placing a microwave absorber material around the burner to within a short distance of the burner slots. The effect of the change of burner temperature on the radiation scattered from the burner alone without a flame was then studied by observing the change in detector current as the circulating cooling water in the burner was changed from cold (~30°C) to hot (~80°C) and back to cold again. At some klystron frequencies the detector current increased when the burner temperature was increased; at other frequencies the current decreased with an increase in burner temperature. This implied that the change in the scattered radiation, depending upon its frequency, was sometimes in phase and sometimes out of phase with the direct radiation. Two frequencies were then chosen at which these effects were equal and opposite, i.e., for one frequency the effect of burner expansion on the bridge balance was in the same direction as the effect due to flame attenuation; for the other frequency the burner expansion effect was in the opposite direction to that of flame attenuation. By making all the measurements for each flame at both of these frequencies and then averaging the galvanometer deflections obtained, the effect of the burner expansion was reduced. The averaged change in the current is then a true measure of the attenuation of the radiation by the flame alone. It is believed that the probable error of these attenuation measurements is about ±25 percent.

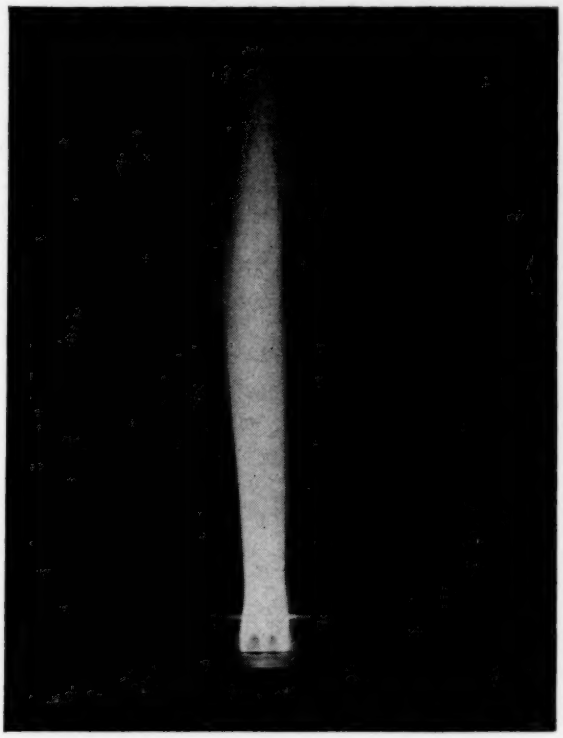

FIG. 4. Stoichiometric acetylene-oxygen flame issuing from the triple-slot burner.

Burner Construction and Flame Measurements

The burner used in this study was a slot burner designed to give a sufficiently long flame path for the attenuation measurements. It was machined out of brass and contained three parallel burning slots $1\frac{3}{4}$ in. long by 0.003 in. wide, spaced $\frac{3}{8}$ in. apart. The slot width was kept to this small dimension in order to prevent flashback. The burner was water-cooled by means of six cooling ducts drilled through the burner walls as shown in Fig. 3. The individual sheets of flame which issued from the three slots merge about $\frac{1}{4}$ to $\frac{1}{2}$ cm above the top of the burner (depending upon the flow rates and the fuel-oxygen ratio) to give a solid column of flame about 2 cm thick. This is illustrated in Fig. 4 which gives a front view of a stoichiometric oxy-acetylene flame issuing from the slot burner.

Commercial gases of high quality were used for this study without further purification. The hydrogen was specified by the supplier to be 99.9 percent pure (main impurity H_2O), the oxygen 99.7 percent pure (main impurities N_2, A and H_2O), and the acetylene 99.0 percent pure (main impurities are other hydrocarbons

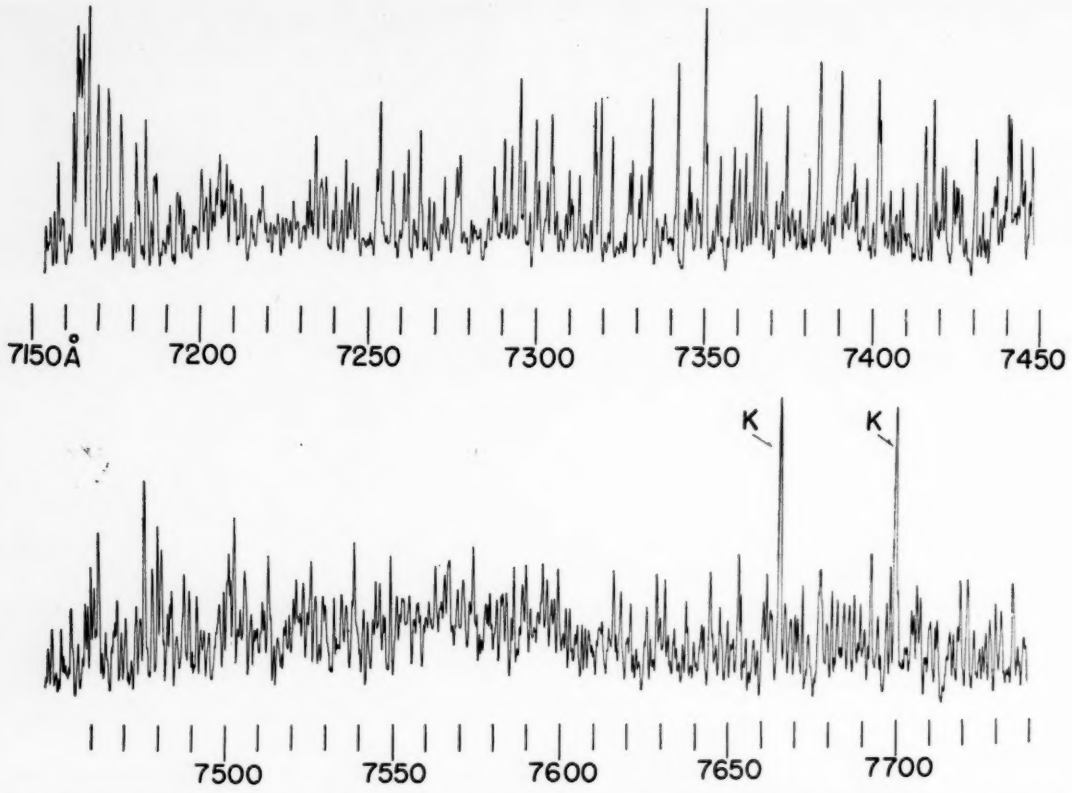

FIG. 5. Densitometer tracing of a portion of the vibration-rotation lines of water in an oxygen-methane flame showing the K doublet at 7665 and 7700A. (Courtesy of Dr. R. C. Herman.)

and 0.2 percent O_2). The gases were metered through accurately calibrated[16] rotameters and premixed in a commercial torch butt which was attached to the burner proper by means of a flexible hose.

As will be noted from Fig. 3 and from the dimensions given above, the signal and receiving horns cover a rather extensive area of the flame. *The results obtained for the flame ionization thus pertain to a region of the flame which contains both the inner cone (reaction zone) and parts of the outer cone (hot combustion gases).* Since flames are nonisotropic and nonhomogeneous reaction systems, a certain amount of such averaging and integration is unavoidable in measuring their properties even if the region under study is made quite small. The use of smaller electromagnetic horns would have been of no advantage in this connection since there would have been a large accompanying decrease of the directivity of the radiation as well as a loss of sensitivity in the measurements.[17]

In order to determine the concentration of the ions in the flame, it is necessary to know l, the length of the flame path through which the radiation is being attenuated. An unambiguous measurement of this quantity is rather difficult since the boundary between the air at room temperature and the hot attenuating flame gases is not a sharp one but rather a gradual transition region. Any measurement of the extent of the attenuation path l thus carries with it some arbitrariness. The result obtained depends to a large extent upon the method used to determine this parameter. This is, however, not too serious a problem since the critical factor in these experiments is the accuracy with which the total attenuation αl has been measured. Once this quantity has been determined accurately, an uncertainty of even 50 percent in the measurements of the flame path l would not significantly affect the order of magnitude of the electron concentration. We have chosen for the attenuation path l the thickness (i.e., the width) of the luminous part of the flame as measured from photographs of the type shown in Fig. 4. This procedure, which was employed to some extent on the basis of simplicity and convenience, can be justified on the grounds that the luminous part of the flame is presumably the hottest one and thus should contain most of the electrons which bring about the attenuation of the microwave beam.[18]

[16] The calibration were performed by the Fischer and Porter Company, Hatboro, Pennsylvania.

[17] The use of ion probes inserted into the flame would permit the study of very small regions so that the ionization in the flame could be studied as a function of the flame geometry. The interaction between the flame and the ion probes would, however, introduce other complications which would leave the interpretation of the results obtained in this manner open to considerable uncertainty.

[18] For another method of measuring the attenuation path see, e.g., L. Rudlin, National Advisory Committee for Aeronautics, NACA Research Memorandum E51G20, Washington, September, 1951.

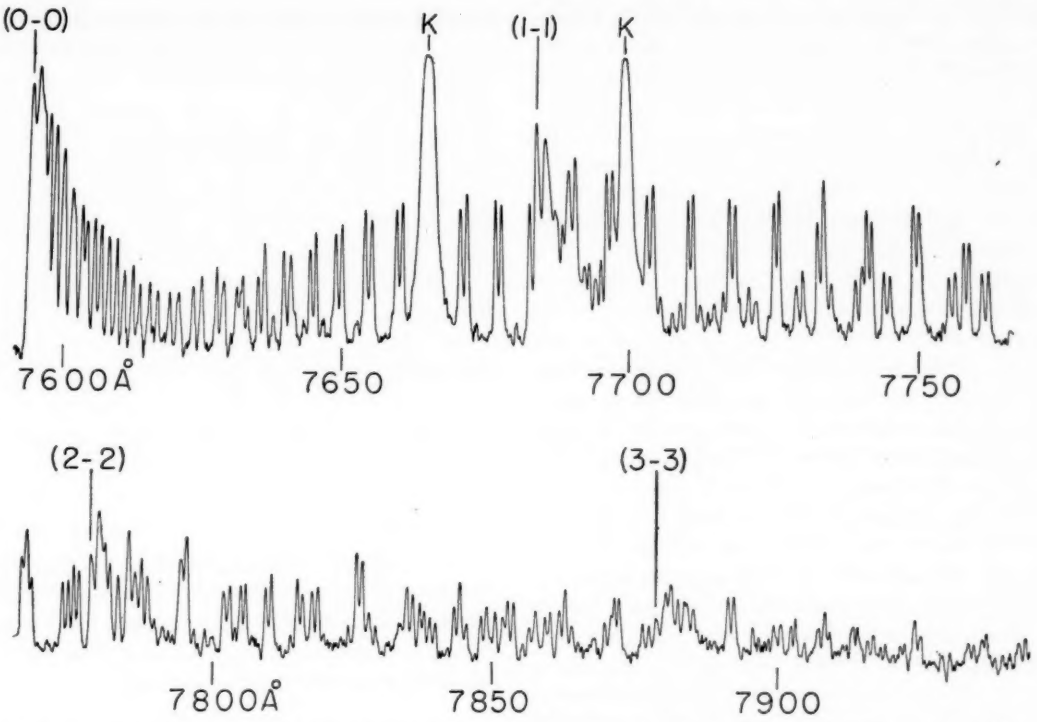

FIG. 6. Densitometer tracing of a portion of the atmospheric oxygen bands ($^1\Sigma_g^+-{}^3\Sigma_g^-$) in a carbon monoxide-oxygen flame showing the K doublet at 7665 and 7700Å. (Courtesy of Dr. R. C. Herman.)

OH Radicals in Flames

During the course of this work, the Columbia microwave group found the OH radical absorption lines at 23 826.9 Mc/sec and 23 818.2 Mc/sec.[19] This raised the question whether the attenuation observed in our experiments, which were carried out at a frequency of around 23 800 Mc/sec, might be due, at least in part, to the OH radicals in the flame rather than to the free electrons. In order to check this point, some of the measurements were repeated at a frequency of about 20 000 Mc/sec. These measurements gave substantially the same results as those obtained previously at 23 800 Mc/sec. This showed that the attenuation observed in our experiments is not due to the OH radicals in the flames. This is also in agreement with the theoretically predicted behavior, since a calculation indicates that the OH absorption in these flames should be at least an order of magnitude less than the absorption by the free electrons. Since the detection techniques employed in measuring absorption of microwaves in molecular transitions can be made quite selective and are distinct from those used to measure attenuation due to free electrons, there should be no difficulties in extending molecular microwave techniques to a study of the concentration of radicals in flames.

IV. "BACKGROUND" IONIZATION IN FLAMES

Before the results of this study can be properly evaluated it is necessary to consider a possible extraneous source of ions and electrons in flames which may increase the electron concentration above that calculated for the adiabatic flame. In spectroscopic studies of flames carried out at the Applied Physics Laboratory it has been noted that all spectra, regardless of the type of fuel, the fuel-oxygen ratio, and the burning condition, always show the K doublet at 7665A and 7699A as one of the most prominent features. This is illustrated in the tracings of hydrocarbon flame spectra shown here (Figs. 5 and 6) which were taken from the compilation of G. A. Hornbeck and R. C. Herman.[20] The corresponding Na doublet at 5890A has not been noted as such in the hydrocarbon flame spectra taken at our laboratory. This is most probably because they have been masked by the strong Swan bands of C_2 which fall in the same spectral region (4500A to 6500A). The occurrence of the Na doublet at 5890A in flames is quite common; as an example, one may refer to its strong appearance in the Bunsen flame spectrum shown in Plate 9 of Pearse and Gaydon's compilation of spectra.[21,22]

A rough calculation indicates that the observed in-

[19] Sanders, Schawlow, Dousmanis, and Townes, Phys. Rev. **89**, 1158 (1953).

[20] G. A. Hornbeck and R. C. Herman, Ind. Eng. Chem. **43**, 2739 (1951). We are very much obliged to Dr. Herman for making these tracings available to us.

[21] R. W. B. Pearse and A. G. Gaydon, *The Identification of Molecular Spectra* (John Wiley & Sons, Inc., New York, 1951), second edition.

[22] Evidence for the presence of considerable amounts of sodium in the air, and in gases obtained therefrom, such as N_2 and A, is also provided by shock tube experiments where a large part of the luminosity which accompanies the shock wave has been shown spectroscopically to be due to the sodium *D* lines. See, e.g., R. N. Hollyer, Jr., *et al.*, Nature **171**, 395 (1953).

tensity of the K lines relative to those of OH and H_2O in a flame at about 3000°K corresponds to a concentration of about $10^{10}-10^{12}$ K atoms/cm³. This concentration of potassium atoms (or its equivalent as alkali halide salts) would in turn give rise to an electron count of about 10^9 to 10^{10} per cm³ in a flame at about 3000°K. Since this concentration of electrons is of about the same order of magnitude as that produced by the thermal ionization of hydrogen-oxygen and acetylene-oxygen flames, it is clearly advisable to study this "background" ionization[23] in flames in somewhat more detail.

A study of the rather extensive literature on the concentration of alkali salts in the air[24] has shown that this concentration, recalculated for purposes of ready intercomparison in terms of Na atoms per cm³, is quite uniformly of the order of 10^{10} to 10^{12} Na atoms/cm³. The source of these alkali salts in the air is to be found in volcanic activity, industrial effluent including gasoline exhaust fumes, and in the action of the wind in carrying inland the salt sprays swept up in its passage across the ocean. The possible appearance of the salt particles in the flame gases may be attributed to (a) their presence in the oxygen, which is usually obtained by the liquefaction of air; (b) their presence as adsorbed particles on various surfaces such as hoses, valves, burners, etc., from which they may be swept along by the passing gas streams which feed into the flame; and (c) their diffusion into the flame from the air envelope which surrounds it. The concentration of these alkali salts (and that of other airborne nuclei) in the flame may thus be expected to be about equal to their concentration in the air within the laboratory.

We have determined the concentration of contaminant salts in the flame and the electron concentration produced by their ionization in the following manner. A previous study of the atmospheric pressure hydrogen-oxygen flame[25] has shown that equilibrium conditions obtain in the hot gaseous products of combustion which form the outer cone. It is reasonable to assume that this equilibrium behavior in the outer cone will also extend to the ionization of the combustion products. This is particularly true if the ionization measurements are made a distance of several centimeters above the inner cone reaction zone so that any excess concentration of ions which may have been produced in the reaction zone by chemi-ionization will have had a chance to return to a thermal distribution by recombination and other types of equilibrating collisions. We have measured the ionization in the outer cone of a 4/1 hydrogen-oxygen flame 13.5 cm and 27 cm above the burner by the method described in Secs. II and III and found that N_e, the number of electrons per cm³, was $2.53\cdot10^9$ and $1.94\cdot10^9$, respectively. The temperature of the hot combustion gases at these heights above the burner (and the inner cone) can be estimated from Broida's and Lalos' work on the gross temperature profile of flames[26] to be, at most, about 2400°K. At this temperature the thermal ionization of a 4/1 hydrogen-oxygen flame as calculated from the Saha equation[27] gives rise only to about 10^6 electrons/cm³, so that the observed flame ionization is in considerable excess (by a factor of 10^3) over that calculated for thermal equilibrium.

If the observed excess concentration of electrons is attributed to the thermal ionization of alkali salts in the flame, one finds that this ionization corresponds to a concentration of alkali salts, expressed in equivalents of Na atoms/cm³, of $5.0\cdot10^{10}$ Na atoms/cm³ at STP. The good agreement of this value with the above quoted data ($10^{10}-10^{12}$ Na atoms/cm³)[24] obtained by more conventional analytical methods in meteorological studies lends credence to the interpretation of the high electron concentration in flames in terms of contamination by airborne alkali salts. The data presented in the following section have all been corrected for background ionization using the aforementioned value of $5.0\cdot10^{10}$ Na atoms/cm³ at STP as the base figure.[28]

V. RESULTS AND DISCUSSION

The results of this study are presented in Tables I and II below. Table I gives the data for the hydrogen-oxygen flames and for the lean and stoichiometric acetylene-oxygen flames. Table II contains the results for some rich acetylene-oxygen flames which require, as will be evident below, a separate discussion.[29]

TABLE I. Electron concentrations (N_e=electrons/cm³) and ionization temperatures in hydrogen-oxygen and lean and stoichiometric acetylene-oxygen flames.

Fuel mixture	Electrons/cm³ N_e(calc.)	Electrons/cm³ N_e(exp.)	Electrons/cm³ N_e (corrected)	T(°K) adiabatic	T(°K) ionization
$H_2/O_2=2/1$	1.69×10^9	3.13×10^9	0.63×10^9	3000	2900
$H_2/O_2=4/1$	1.71×10^8	2.89×10^9	2.3×10^8	2850	2830
$H_2/O_2=6/1$	2.06×10^6	2.46×10^9	[a]	2420	[a]
$C_2H_2/O_2=1/4$	9.62×10^9	1.66×10^{10}	1.42×10^{10}	3210	3250
$C_2H_2/O_2=2/5$	2.12×10^{10}	1.89×10^{10}	1.66×10^{10}	3360	3320

[a] The background ionization corresponding to $T=2420$°K is 2.53×10^9 electrons/cm³. It is, therefore, not possible to determine N_e(corrected) for this flame within the sensitivity of our measurements.

[23] The term "background ionization" as used in the above context has, of course, no connection with the background ionization of the air due to the bombardment of cosmic rays or other nuclear radiation.

[24] R. M. Moyerman and K. E. Shuler, Science **118**, 612 (1953).

[25] H. P. Broida and K. E. Shuler, J. Chem. Phys. **20**, 168 (1952).

[26] H. P. Broida and G. T. Lalos, J. Chem. Phys. **20**, 1466 (1952).

[27] M. Saha, Proc. Roy. Soc. (London) **99A**, 135 (1921); consult the appendix for a more detailed discussion on the calculation of thermal ionization of flames.

[28] Somewhat more accurate results could probably have been obtained by continuous day-by-day monitoring during the performance of all the experiments. The small internal variation of the background concentration as a function of time, i.e., of atmospheric conditions, should, however, not seriously affect the results and conclusions of this study.

[29] It was not found possible to extend these measurements to lean hydrogen-oxygen flames since the flame path l for these flames was so small (<0.5 cm) that the attenuation αl could not be measured with our bridge.

Hydrogen-Oxygen Flames and Lean and Stoichiometric Acetylene-Oxygen Flames (Table I)

The values listed in the 2nd column of Table I are for the thermal electron concentrations (in electrons/cm³) calculated from the Saha equation using the adiabatic flame temperatures listed in column 5. These calculations and the data required to carry them out are given in the appendix. The experimentally determined electron concentrations are listed in the 3rd column. They were obtained from Eq. (11) in the manner discussed in Sec. II. These values were then corrected for background ionization and the corrected electron concentrations are to be found in column 4. Column 6 lists the "ionization temperatures" T_{ion}, obtained from the Saha equation under the assumption that the (corrected) electron concentration corresponds to thermal ionization.

In order to apply the background correction to the data of column 3, it is necessary to know the variation of the background ionization with temperature. If it is assumed, as a convenient basis for calculation, that the observed background ionization is entirely due to the thermal ionization of Na atoms, it is possible to calculate the temperature dependence by applying the Saha equation to the (single) ionization of Na. The results of this calculation are shown in Fig. 7, which is a plot of $\log(N_e)$ *vs* T for a range of sodium atom concentrations, N_A^0, at STP.[30] The base figure of $N_A^0 = 5.0 \cdot 10^{10}$ Na atoms per cm³ of air at STP (see Sec. IV) was used to obtain the appropriate background corrections from Fig. 7 which were then subtracted from the gross experimental data (column 3) to obtain the corrected electron concentrations for the uncontaminated flames.

The background correction obtained in this manner is subject to considerable uncertainty. In the first place, there may be daily and seasonal variations of the background which have not been taken into account here. Secondly, it is an oversimplification to attribute all the background ionization to that of Na, as has been done above in order to calculate the temperature dependence. It is felt, however, that the corrected electron concentrations listed in Table I are sufficiently accurate for purposes of interpretation and comparison, particularly as regards their order of magnitude. This belief is strengthened, *a posteriori*, by the result obtained for the 6/1 hydrogen-oxygen flame, where the background ionization accounts correctly for the observed electron concentration.

TABLE II. Electron concentrations (N_e = electrons/cm³) in rich acetylene-oxygen flames.

Fuel ratio C_2H_2/O_2	Electrons/cm³ N_e(calc.) (C as atoms)	Electrons/cm³ N_e(calc.) (C as graphite)	Electrons/cm³ N_e(exp)	Electrons/cm³ N_e(corrected)	T(°K) adiabatic
1.5/1	8.10×10^{8}	1.74×10^{14}	3.70×10^{10}	3.47×10^{10}	3285
1.75/1	...	1.45×10^{14}	3.55×10^{10}	3.32×10^{10}	3250
2/1	6.55×10^{8}	1.18×10^{14}	2.98×10^{10}	2.74×10^{10}	3210
2.25/1	...	1.09×10^{14}	1.66×10^{10}	1.42×10^{10}	3195
3/1	...	7.14×10^{13}	9.35×10^{9}	6.96×10^{9}	3135
4/1	2.12×10^{8}	6.03×10^{13}	8.88×10^{9}	6.44×10^{9}	3090

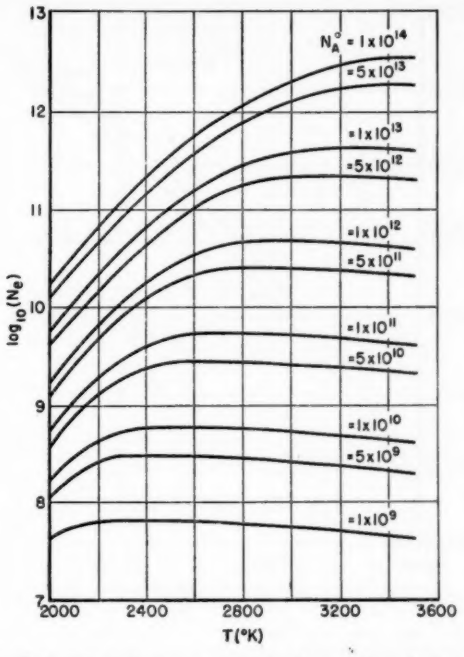

FIG. 7. Calculated electron concentrations (N_e = electrons/cm³) due to the thermal ionization of Na atoms as a function of temperature for a range of Na atom concentration at STP. N_A^0 = Na atoms/cm³ at STP.

The ionization temperatures T_{ion} were determined from the corrected electron concentrations and Figs. 8 and 9 which give calculated thermal electron concentrations as a function of temperature for the (uncontaminated) flames. The curves were obtained by applying the Saha equation to the data listed and referred to in the appendix.

It is interesting to note here the difference in the calculated temperature dependence of the thermal ionization curves for the uncontaminated flames (Figs. 8 and 9) as compared to that of the background (Fig. 7).[31] For the thermal ionization of an *uncontaminated* flame there should be a considerable variation of the electron

[30] The decrease of the electron concentration with increasing temperature appears at first to be a somewhat surprising result. This behavior (for single ionization) is brought about by two opposing temperature effects, namely, the increase in the fraction of atoms ionized with increasing temperature and the decrease in the concentration of the atoms as the temperature is increased at constant pressure. If the plot were made for the total number of electrons rather than for the electron concentration, i.e., number of electrons per unit volume, one would find that the total number of free electrons increases monotonically with the temperature.

[31] This difference in appearance over the temperature range investigated is primarily due to two factors (1) the higher ionization potentials of the flame constituents as compared to that for Na (10–12 ev *vs* 5.14 ev) and (2) the higher concentration of the atmospheric pressure flame constituents (fuel and oxygen) as compared to that of Na in the air (10^{18} molecules/cm³ *vs* 10^{11} atoms/cm³).

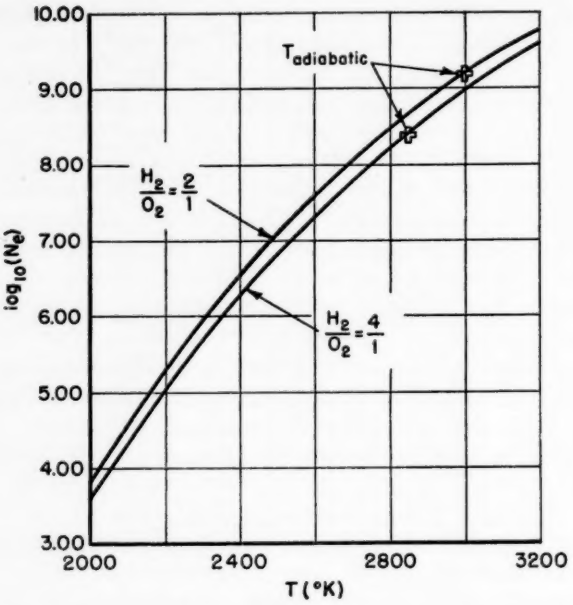

FIG. 8. Calculated electron concentrations (N_e = electrons/cm³) due to the thermal ionization of hydrogen-oxygen flames as a function of temperature.

concentration with temperature, as also shown in column 2 of Table I. It is found experimentally, however, that there is very little variation of electron concentration with temperature (column 3, Table I). While this experimentally observed lack of temperature dependence may be attributed to chemi-ionization, which would be largely independent of the adiabatic "temperature" of the flames, it is equally well accounted for by a thermal ionization of the background (with N_A^0 equal $5 \cdot 10^9$ to $1 \cdot 10^{11}$ atoms/cm³), as shown in Fig. 7. Since the reality of the background, i.e., the presence of a considerable concentration of alkali salts in the air, has been demonstrated repeatedly by various independent measurements,[24] we consider that the interpretation of our data in terms of these background effects is more firmly based on experimental evidence than is the alternative interpretation in terms of "chemi-ionization."[32]

A comparison of the data in columns 2 and 4 of Table I leads to the conclusion that there is a thermal concentration of ions and electrons in these (uncontaminated) flames. A similar comparison of the data in columns 5 and 6 bears out this result, the ionization temperatures T_{ion} being in good agreement both with the adiabatic flame temperatures and the rotational and vibrational temperatures determined in a previous investigation.[25]

[32] It may be noted in this connection that the temperature effects on the conductivity of flames (or rather the *lack* of these effects) quoted in Calcote's review (see, e.g., references 11, 87, and 106 quoted in reference 1 of this paper) can also readily be understood on the basis of background ionization involving the thermal ionization of species with low-ionization potentials.

Rich Acetylene-Oxygen Flames (Table II)

Column 2 in Table II contains the calculated thermal electron concentration for these flames obtained by using the Saha equation and the data listed and referred to in the appendix. These calculations were carried out on the basis that the carbon present in these fuel-rich flames is in the gaseous, atomic state with $I_C(g) = 11.265$ ev.[33] Column 3 lists the thermal electron concentrations calculated for $I_C(s) = 4.35$ ev, the work function of graphite, corresponding to the possible existence of the carbon particles in that form. The experimentally determined electron concentrations are listed in column 4; column 5 contains the experimental electron concentration as corrected for the background ionization. The adiabatic flame temperatures which were used for some of the above calculations are given in column 6.

It will be noted from columns 2 and 5 that the background-corrected electron concentration is larger by a factor of about 30 than that calculated for purely thermal ionization of the (uncontaminated) gaseous combustion products. This is in line with the observation of other investigators who found, as a general rule, that the ionization in rich hydrocarbon flames is much higher than in lean or stoichiometric ones.[34] A possible explanation for this apparently abnormally high ionization of rich hydrocarbon flames has been put forth by O. Stern.[34] One of the characteristic features of rich hydrocarbon flames is the presence of free carbon in the hot

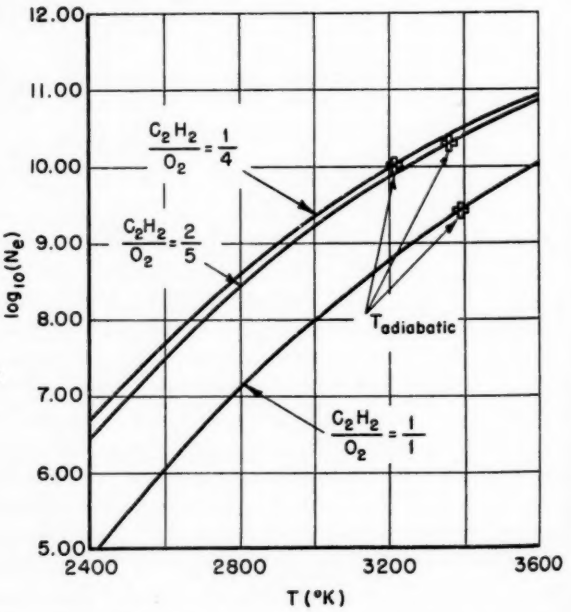

FIG. 9. Calculated electron concentrations (N_e = electrons/cm³) due to the thermal ionization of acetylene-oxygen flames as a function of temperature.

[33] No values for the thermal electron concentrations have been given for fuel-oxygen ratios for which the prerequisite thermodynamic data were not at hand. It is evident that they fall in the range of $2 \cdot 10^8$ to $8 \cdot 10^8$ electrons/cm³.

[34] See, e.g., B. Lewis and G. von Elbe, *Combustion, Flames and Explosions* (Academic Press, Inc., New York, 1951), p. 206.

combustion products. Studies of the size distribution and structure of carbon particles (soot) in flames have shown that they are submicroscopic aggregates with a diameter of between 100A to 1000A and a graphitic type of structure.[35] Since the ionization potential decreases from 11.265 ev for atomic carbon to 4.35 ev for graphite, which can be considered as an infinitely large aggregate of carbon atoms, it is reasonable to assume that the small carbon aggregates and polymers formed in flames will have a work function intermediate between the two above quoted values. If this is the case, it is quite possible that a large fraction, if not all, of the electrons found in rich, sooty hydrocarbon flames are produced by the thermal ionization of these carbon atom aggregates with relatively low work functions.

The experimentally determined values of the electron concentrations (as corrected for background ionization) are of the right order of magnitude to be in accord with the aforementioned hypothesis. If it is then assumed that the electrons in the rich oxy-acetylene flames are due to the thermal ionization of the carbon particles in the hot flame gases, it is possible to calculate the work function of these carbon aggregates. By a straightforward application of statistical mechanics it is found that for the equilibrium

$$C_n(s) \leftrightarrows C_n^+(s)+e \tag{16}$$

the number of electrons per cm³ is given by

$$N_e=\frac{2(2\pi m_e kT)^{\frac{3}{2}}}{h^3}\exp(-\chi/kT), \tag{17}$$

where χ is the work function of the carbon aggregate C_n. If it is now assumed that (a) χ is temperature-independent over small temperature intervals, and (b) independent of the state of aggregation, and thus independent of (or shows only a very small dependence on) the fuel-oxygen ratios over a rather wide range of burning conditions, one should obtain a straight-line relationship with slope equal to $(-\chi/k)$ when plotting $\ln(N_e/T^{\frac{3}{2}})$ *vs* $1/T$.

Such a plot of the data of columns 5 and 6 in Table II is shown in Fig. 10. The approximate straght-line relationship found by this analysis would seem to indicate that the above assumptions are valid and that the observed (corrected) electron concentrations can be explained on the basis of a thermal ionization of the carbon aggregates in these fuel-rich flames. The work function χ as determined by a least-square fit is 8.5 ev, a value which is quite reasonable in comparison with the ionization potentials of free carbon atoms and of graphite. It is interesting to note that Calcote[36] suggests

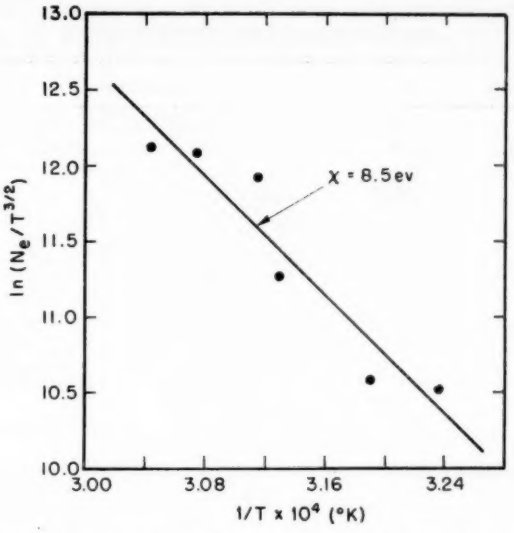

FIG. 10. A plot of $\ln(N_e/T^{\frac{3}{2}})$ *vs* $1/T$ to determine the work function χ of carbon particles in rich acetylene-oxygen flames. A least-square fit shows $\chi=8.5$ ev.

this same figure as an average ionization potential to account for the ion concentration in the outer cone of a coal gas-air flame.[37]

It is suggested on the basis of the results obtained in this study that the ionization of hydrogen-oxygen and acetylene-oxygen flames, at least as far as the hot combustion gases are concerned, is a purely thermal ionization in that the observed concentration of electrons in these flames can adequately be accounted for by the appropriate equilibrium calculations.

VI. ACKNOWLEDGMENTS

We wish to thank Dr. S. N. Foner, Applied Physics Laboratory, The Johns Hopkins University, for his constructive criticism and valuable suggestions in connection with several points raised in this paper.

APPENDIX

Calculation of the Equilibrium Ionization of Flames

For the single ionization of the atomic or molecular species A one can write, at equilibrium,

$$A \rightleftarrows A^+ + e. \tag{18}$$

The equilibrium constant K_i for ionization is then given by

$$K_i=\frac{[A^+][e]}{[A]}=\frac{F(A^+)F(e)}{F(A)}e^{-V_i/kT}, \tag{19}$$

[35] See, e.g., H. Senftleben and E. Benedict, Ann. Physik **60**, 297 (1919); U. Hofmann and D. Wilm, Z. Elektrochem. **42**, 504 (1936); H. G. Wolfhard and W. G. Parker, Proc. Phys. Soc. (London) **62B**, 523 (1949); W. G. Parker and H. G. Wolfhard, J. Chem. Soc. (London) 2038 (1950).

[36] See reference 1, p. 12.

[37] The treatment given above for the thermal ionization of the carbon aggregates is based on the assumption that the carbon particles are in temperature equilibrium with the hot flame gases. There is conflicting evidence regarding this point [see, e.g., H. G. Wolfhard and W. G. Parker, Nature **162**, 259 (1948); H. Behrens and F. Rössler, Z. Naturforsch. **5a**, 311 (1950)] which will have to be resolved before the treatment given here can be accepted as valid. The uncertainties inherent in the above method point up the need for independent and direct measurements of the work functions of small particles as a function of size and structure.

TABLE III. Ionization potentials of the combustion products of oxy-hydrogen and oxy-acetylene flames.

Species	I(ev)	Reference
H	13.595	(a) G. Herzberg, *Atomic Spectra and Atomic Structure* (Dover Publications, New York, 1944), p. 200.
$C_{gaseous}$	11.265	
O	13.615	(b) See reference (a).
H_2	15.922	(c) G. Herzberg, *Spectra of Diatomic Molecules* (D. Van Nostrand Company, New York, 1950), second edition, p. 459.
O_2	12.2	
OH	13.6	(d) Mann, Hustrulid, and Tate, Phys. Rev. **58**, 340 (1940).
H_2O	12.6	(e) W. C. Price, Chem. Revs. **41**, 257 (1947).
CO	14.1	(f) H. D. Hagstrum, Revs. Modern Phys. **23**, 185 (1951).
CO_2	13.85	(g) R. E. Honig, J. Chem. Phys. **16**, 105 (1948).
$C_{graphite}$	4.35	(h) G. Glockler and J. W. Sausville, J. Electrochem. Soc. **95**, 292 (1949).

where the F's are the partition functions per unit volume and V_i is the ionization energy. The evaluation of the partition functions of Eq. (19) within the quite accurate approximation

$$\frac{F_{tr}(A^+)F_{rot}(A^+)F_{vibr}(A^+)}{F_{tr}(A)F_{rot}(A)F_{vibr}(A)}\approx 1 \tag{20}$$

leads to

$$K_i=\frac{[A^+][e]}{[A]}=\frac{F_{el}(A^+)F_{el}(e)}{F_{el}(A)}\left(\frac{2\pi m_e kT}{h^2}\right)^{\frac{3}{2}}e^{-V_i/kT}. \tag{21}$$

Using

$$F_{el}=\sum_{el} g_{el}e^{-E_{el}/kT}, \tag{22}$$

where g_{el} is the electronic statistical weight, and making the further reasonable approximation that

$$\frac{F_{el}(A^+)F_{el}(e)}{F_{el}(A)}\approx\frac{g_{el}(A^+)g_{el}(e)}{g_{el}(A)}, \tag{23}$$

one can rewrite Eq. (21) in its final form as

$$K_i=\frac{[A^+][e]}{[A]}=\frac{2g_{el}(A^+)}{g_{el}(A)}\left(\frac{2\pi m_e kT}{h^2}\right)^{\frac{3}{2}}e^{-V_i/kT}, \tag{24}$$

where the factor 2 for $g_{el}(e)$ corresponds to the spin degeneracy of the electron.

The principal assumptions used in the above formulation of the ionization equilibrium are:

(1) The flame temperatures are of such an order of magnitude compared to the ionization potentials of the combustion products that secondary and higher ionization can be neglected.

(2) The flame gases can be considered as an ideal gas where the electrostatic interaction between the charged particles can be neglected. This presumes that the fraction of molecules which are ionized is rather small, i.e., $[A^+][e]/[A]\ll 1$. These conditions are well fulfilled for the flames under study so that the use of Eq. (24) for the calculation of the thermal ionization of flames will lead to quite accurate results.

The application of Eq. (24) to the calculation of the thermal ionization of a specific flame requires a knowledge of the equilibrium composition of the flame gases, the ionization potential of each species in the flame gas, and the adiabatic equilibrium temperature of the flame. The equilibrium composition and adiabatic temperatures for the hydrogen-oxygen flames were taken from the tables of Hottel, Williams, and Satterfield;[38] for the acetylene-oxygen flames the quantities were obtained from tables prepared at our request by the U. S. Bureau of Mines.[39] The values of the ionization potentials for the various flame constituents which were used in these calculations are listed below. All the flames reported on in this study were burned at atmospheric pressure.

Equation (24) was also used for calculating the thermal ionization of Na, as shown in Fig. 7. The values obtained in this calculation should be quite accurate since there is very little secondary ionization in the temperature region of 2000°K to 3000°K [$V_i(II)=47.292$ ev compared with $V_i(I)=5.138$ ev] and since ideal gas conditions probably obtain to a very good approximation for the highly attenuated Na atmosphere under study.

[38] Hottel, Williams, and Satterfield, *Thermodynamic Charts for Combustion Processes* (John Wiley and Sons, Inc., New York, 1949).

[39] "Flame temperatures and composition of the combustion products of oxy-acetylene flames." Report No. 3270, Project No. PX3-107, Explosives and Physical Sciences Division, Bureau of Mines, Pittsburgh, Pennsylvania (December 2, 1952). We are very much indebted to Dr. Stuart R. Brinkley, Jr., Head, Mathematical and Theoretical Physics Section, for his kind cooperation in furnishing us with these data.

The Near Ultraviolet Absorption Spectrum of *Para*-Difluorobenzene Vapor

C. DEWEY COOPER
Department of Physics, University of Georgia, Athens, Georgia
(Received September 8, 1953)

The vapor spectrum of *p*-difluorobenzene was obtained with a Bausch and Lomb Littrow spectrograph. The band at 36 843 cm^{-1} is assigned as the 0,0 band of the $A_g - B_{3u}$ electronic transition. Ground-state frequencies of 452, 860, and 1259 cm^{-1} with the corresponding excited-state frequencies of 408, 819, and 1250 cm^{-1} are assigned to totally symmetric vibrations. Also, an 841-cm^{-1} frequency is assigned to the ground state of a totally symmetric vibration. Many of the bands that are temperature dependent are shown to result from a transition that involves a 248-cm^{-1} ground-state vibration. This 248-cm^{-1} frequency is assigned as a β_{1g} fundamental. Most of the prominent bands are assigned to progressions or combinations of the above frequencies. The unusually large spectral shift produced by the two *para*-positioned fluorines is discussed.

INTRODUCTION

THIS study of the *p*-difluorobenzene spectrum was initiated as part of a program which is designed to investigate the near ultraviolet absorption spectra of several *para*-substituted benzenes. In this program, the spectral shifts produced by different substituents are studied; the electronic transitions are classified, and the ground- and excited-state vibrational frequencies are determined. A brief report on the ultraviolet vapor spectrum of 1,4 $C_6H_4F_2$ was published recently by Delsemme and Duchesne;[1] however, this is the first detailed report of the vapor spectrum. The solution spectrum has been obtained by Sponer and co-workers.[2] Both the Raman and infrared spectra have been published by Delsemme;[3] also, Nielsen and co-workers[4] have studied these spectra.

EXPERIMENTAL PROCEDURE

The spectrograms were obtained with a Bausch and Lomb Littrow Spectrograph with quartz optics. This instrument has a dispersion of 3.192 A/mm at 2700A. A low voltage hydrogen lamp of the Beckman type provided the ultraviolet continuum and a standard iron arc was used to supply a comparison spectrum. In obtaining the absorption spectrum, exposure times of 10 minutes were necessary with Eastman Kodak II-O plates. These plates were developed with uniform agitation in D-19 for 3 minutes. A comparator which is accurate to 0.001 mm was utilized to measure the spectrum.

The quartz absorption cell was 75 cm long and was made with a small reservoir attached at right angles to the main cell. With this cell the number of molecules in the light path depends upon the vapor pressure of the substance held in the reservoir. The temperature of the molecules in the light path was kept at either room temperature 27°C or the temperature of dry ice −79°C.

The sample of 1,4 $C_6H_4F_2$ used in this research was obtained from the Physics Department of Duke University. It was a commercial grade product which had been vacuum distilled and had a boiling point of 88°C.

Both the absorption cell and the break-seal tube containing the sample were sealed to a vacuum system, thoroughly outgassed, and the pressure lowered to 10^{-5} cm of Hg. Then the cell and sample were isolated from the pumping system, and by vacuum distillation about 2 grams of the compound were loaded into the cell. The cell was then sealed and removed from the system.

EXPERIMENTAL RESULTS

The vapor absorption spectrum of *p*-difluorobenzene between 2900 and 2350A was obtained for substance temperatures between −79°C and 30°C. There are about 600 bands in the spectrum. Many of the bands are sharp and have double heads 2 to 3 cm apart which are almost line-like in appearance. These bands appear in about thirty groups with some of these groups containing 30 to 40 band heads. Within the band groups the most pronounced separation between bands is 40 cm^{-1} with the separations of 6, 30, 60, and 100 cm^{-1} appearing also.

With the reservoir of the cell at −79°C the number of molecules in the 75-cm absorption path of 27°C is sufficient to produce twelve groups of bands. Of these bands the ones at 36 843, 37 662, 38 093, 38 480, and 38 908 cm^{-1} are the strongest. A few of the weaker bands are located at 36 595, 37 006, 37 251, 37 417, 37 843, and 38 237 cm^{-1}. When the temperature of the main cell is lowered to −79°C, all of the weak bands mentioned above except the one at 37 251 cm^{-1} disappear. The intensities of the weak band at 37 251 cm^{-1} and the stronger bands are found to be independent of temperature variations. The close-lying long wavelength companions of the strong bands (these make up the band groups) are found to diminish in number when the temperature is lowered. In fact, for a cell temperature of 27°C, bands are present that represent separa-

[1] A. H. Delsemme and J. Duchesne, Compt. rend. **234**, 612 (1952).
[2] Am. Petroleum Inst. Res. Project 44, Ultraviolet Spectral Data, Serial No. 493.
[3] A. H. Delsemme, J. Chem. Phys. **18**, 1680 (1950).
[4] Ferguson, Hudson, Nielsen, and Smith, J. Chem. Phys. **21**, 1457 (1953).

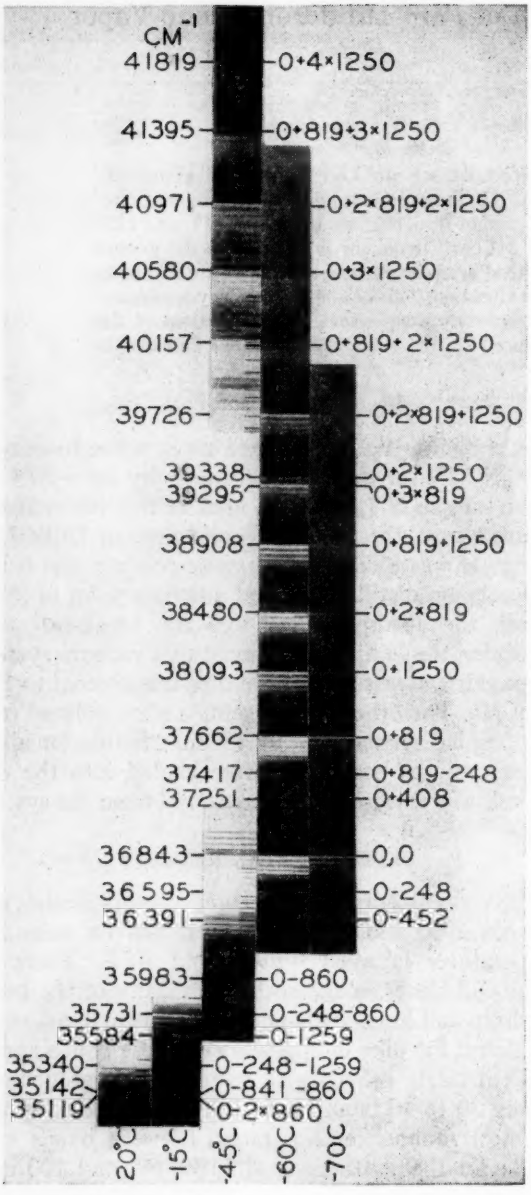

FIG. 1. Absorption bands of *para*-difluorobenzene vapor. The given temperature for each spectrogram represents the temperature of the reservoir which contained the sample. The 75-cm absorption path was maintained at 27°C.

tions of 40, 2×40, 3×40, 4×40, 100, and 40+100 cm^{-1}, while at a temperature of −79°C only bands representing separations of 40, 2×40, and 100 cm^{-1} are detectable.

The spectrograms obtained with the cell at room temperature and reservoir temperatures between −79°C and 30°C show more complexity for the higher temperatures (see Fig. 1). The reservoir temperature was varied in five degree steps. For temperatures above −25°C, complete absorption occurs in the 36 800–41 800 cm^{-1} region. Spectrograms obtained at these higher temperatures show many weak bands on the long wavelength side of the 36 843-cm^{-1} band.

The experimental data are presented for the most part in Table I. Here, the wavelengths are listed in column one, and the corresponding wave numbers are in column two. The wave numbers are accurate to within 2 or 3 cm^{-1}. Visually estimated intensities and the degree of diffuseness of the band heads for different reservoir temperatures are given in columns three, four, and five. The notations used in these columns have the following meanings: ew—extremely weak, vw—very weak, w—weak, mw—medium weak, m—medium, ms—medium strong, s—strong, vs—very strong, ed—extremely diffuse, vd—very diffuse, d—diffuse, sd—slightly diffuse, s—sharp, and vs—very sharp. Column six is used to record the wave number differences between each band and the 0,0 band at 36 843 cm^{-1}. Assignments are given in column seven.

DISCUSSION

The *p*-difluorobenzene molecules have D_{2h} symmetry. In this report the *z* axis is chosen perpendicular to the molecular plane (same as the choice made for benzene) and the *y* axis passes through the two fluorine bonds.* Then the symmetry notations used herein are the same as those given by Herzberg.[5] In *para*-di-substituted benzenes, the electronic transition which is expected to produce a spectrum in the 2600A region is the allowed $A_g - B_{3u}$ with the transition moment in the *x* direction.[6] Also vibrations of symmetries β_{1g} or β_{2g} may distort the benzene ring enough so that weak transitions are possible with their moments in the *y* or *z* directions, respectively.

The strong band at 36 843 cm^{-1} is chosen as the 0,0 band. This is the same choice made by Delsemme[1] and is supported by our assignments of ground and excited state frequencies. The strongest bands which appear on a spectrogram obtained with a reservoir temperature of −70°C can all be assigned to progressions or combinations of the 819- and 1250-cm^{-1} frequencies (see Table I). These values are associated with totally symmetric excited state vibrations. The corresponding ground-state frequencies are found to be 860 and 1259 cm^{-1}. Delsemme[1] has assigned the 860-cm^{-1} frequency to the totally symmetric carbon breathing vibration and the 1259-cm^{-1} value to the totally symmetric vibration which involves the stretching of the fluorine bonds. It is noted that the 1259-cm^{-1} value obtained from the ultraviolet vapor absorption data is slightly higher than the 1245-cm^{-1} value obtained from the Raman[3,4] spectrum of the liquid state, but the 860-cm^{-1} vapor spectrum value is practically the same as the 858.5-cm^{-1} Raman value. If we compare the frequencies of the totally symmetric carbon and hydrogen vibrations of

* *Note added in proof.*—The symmetry notation used in reference 4 differs from that used in this article because they chose the *z* axis to pass through the two fluorine bonds.

[5] G. Herzberg, *Infrared and Raman Spectra of Polyatomic Molecules* (D. Van Nostrand Company, Inc., New York, 1945), p. 108.

[6] H. Sponer, Revs. Modern Phys. **14**, 224 (1942).

Wavelength in A
2885.0
81.8
78.8
71.1
67.7
57.7
55.8
54.7
54.0
52.8
52.2
50.8
49.7
49.6
48.5
48.3
48.0
47.8
46.8
46.6
45.5
45.3
45.0
44.8
43.4
41.7
40.2
38.8
38.5
37.1
36.8
35.5
35.2
33.8
33.5
32.3
32.0
29.1
28.8
24.2
21.2
20.2
19.4
18.3
18.1
17.7
17.3
16.5
15.7
15.3
14.4
14.0
13.9
13.6
13.3
12.6
12.4
12.2
10.4
09.8
09.5
09.4
09.0
07.5
07.2
06.3
05.9
05.7

TABLE I. Absorption bands of *p*-difluorobenzene.

Wavelength in A	Wave numbers in cm^{-1}	Intensity 30°C	0°C	−25°C	Separation from 0,0 band	Assignments
2885.0	34 652	ew-vd			−2191	0−860−1259−2×40
81.8	690	ew-vd			−2153	0−860−1259−40
78.8	727	vw-d			−2116	0−860−1259
71.1	820	ew-vd			−2023	
67.7	861	vw-vd			−1982	
57.7	983	ew-d			−1860	0−2×860−2×40−60
55.8	35 006	ew-vd			−1837	0−2×860−3×40
54.7	020	vw-vd			−1823	0−2×860−40−60
54.0	028	vw-vd			−1815	0−2×841−860−3×40
52.8	043	vw-vd			−1800	0−2×860−2×40; 0−841−860−40−60
52.2	050	ew-ed			−1793	
50.8	068	ew-d			−1775	0−841−860−2×40
49.7	081	mw-d			−1762	0−2×860−40−3
49.6	082	m-d			−1761	0−2×860−40
48.5	096	ew-vd			−1747	
48.3	098	ew-vd			−1745	
48.0	102	m-d			−1741	0−841−860−40−3
47.8	105	w-vd			−1738	0−841−860−40
46.8	117	ms-s			−1726	0−2×860−3
46.6	119	ms-s			−1724	0−2×860
45.5	133	ew-sd			−1710	
45.3	135	ew-sd			−1708	
45.0	139	s-s			−1704	0−841−860−3
44.8	142	ms-s			−1701	0−841−860; 0−452−1259?
43.4	159	ew-ed			−1684	0−248−1259−3×40−60
41.7	180	vw-ed			−1663	0−248−1259−4×40
40.2	198	vw-ed			−1645	0−248−1259−2×40−60
38.8	216	w-d			−1627	0−248−1259−3×40−3
38.5	220	vw-ed			−1623	0−248−1259−3×40
37.1	237	mw-vd			−1606	0−248−1259−40−60−3
36.8	240	w-vd			−1603	0−248−1259−40−60
35.5	257	m-d			−1586	0−248−1259−2×40−3
35.2	261	mw-vd			−1582	0−248−1259−2×40
33.8	278	mw-sd			−1565	0−248−1259−60−3
33.5	282	m-sd			−1561	0−248−1259−60
32.3	297	s-d			−1546	0−248−1259−40−3
32.0	300	ms-d	vw-d		−1543	0−248−1259−40
29.1	337	vs-d			−1506	0−248−1259−3
28.8	340	vs-d	w-d		−1503	0−248−1259
24.2	398		ew-ed		−1445	0−1259−5×40?; 0−452−860−2×40−60
21.2	435		mw-d		−1408	0−1259−4×40; 0−452−860−40−60
20.2	448		mw-d		−1395	0−1259−2×40−60
19.4	458		mw-d		−1385	0−452−860−2×40
18.3	472		w-d		−1371	0−1259−3×40−3
18.1	474		w-d		−1369	0−1259−3×40; 0−452−860−60
17.7	480		vw-d		−1363	
17.3	485		mw-d		−1358	0−1259−100
16.5	494		vw-vd		−1349	0−452−860−40
15.7	505		ew-d		−1338	
15.3	510		mw-d		−1333	0−1259−2×40
14.4	521		ew-d		−1322	
14.0	526		ew-sd		−1317	0−1259−60?
13.9	527		ew-sd		−1316	
13.6	531		vw-d		−1312	0−452−860−3
13.3	535	$t=-19$°C	mw-d		−1308	0−452−860
12.6	544	ms-vd		ms-d	−1299	0−1259−40−3
12.4	546		s-d	vw-vd	−1297	0−1259−40
12.2	549		m-d		−1294	0−452−841
10.4	572		vw-vd		−1271	
09.8	579		w-vd		−1264	
09.5	583	vs-d	vs-d	vs-s	−1260	0−1259−3?
09.4	584	vw-sd	s-d	vw-vd	−1259	0−1259
09.0	589		ew-vd		−1254	0−248−860−2×40−60
07.5	608		w-d	ew-sd	−1235	0−248−860−3×40−3
07.2	612		w-d	ew-sd	−1231	0−248−860−3×40
06.3	624		ew-d	ew-sd	−1219	
05.9	629		w-sd	vw-sd	−1214	0−248−860−40−60−3
05.7	631		w-sd		−1212	0−248−860−40−60

Wavelength in A	Wave numbers in cm^{-1}	Intensity −19°C	0°C	−25°C	Separation from 0,0 band	Assignments
04.4	648	m-vd	vs-sd	m-sd	−1195	0−248−860−2×40−3
04.2	650	m-vd	vs-sd	m-sd	−1193	0−248−860−2×40
02.6	671		ew-sd		−1172	0−248−860−60
01.4	686		w-d	ew-vd	−1157	
01.2	688	ms-sd	vs-d	ms-s	−1155	0−248−860−40−3
01.0	691	ms-sd	vs-d	ms-s	−1152	0−248−860−40
		−19°C	0°C	−25°C		
2798.5	722		vs	vw-sd	−1121	
98.1	728	vs-s	vs	vs-sd	−1115	0−248−860−3
97.9	731	vs-s	vs	vs-sd	−1112	0−248−860
97.7	733		ms		−1110	
97.5	736		ew-d		−1107	
96.8	745		vw-sd		−1098	
96.5	748		vw-sd		−1095	
			−35°C	−45°C		
95.1	766	ew-d			−1077	0−860−4×40−60−3
95.0	768	ew-d			−1075	0−860−4×40−60
93.7	784	vw-vd			−1059	0−860−5×40?
91.9	807	vw-vd	ew-d		−1038	0−860−3×40−60−3
91.8	809	vw-vd			−1036	0−860−3×40−60
91.0	819	vw-vd			−1026	
90.9	820	ew-vd			−1025	
90.3	828	ew-vd			−1015	0−860−4×40−3
90.0	832	vw-vd			−1011	0−860−4×40
89.0	845	ms-sd	vw-vd	ew-d	−998	0−860−2×40−60−3
88.8	847	mw-d			−996	0−860−2×40−60
87.4	865	w-d			−978	
87.1	869	s-sd	vw-ed	ew-vd	−974	0−860−3×40−3
86.9	872	mw-d		vw-vd	−971	0−860−3×40
86.1	882	s-sd	vw-d	vw-sd	−961	0−860−40−60−3
85.9	884	ms-sd		vw-sd	−959	0−860−40−60
84.5	903	vs-d	ew-vd		−940	
84.2	906	vs-d	mw-sd	ew-sd	−937	0−860−2×40−3
84.0	909	vs-d	ew-d	ew-sd	−934	0−860−2×40
83.5	915	ew-sd			−928	
83.3	918	w-sd			−925	0−860−60−3
83.1	921	ew-sd			−922	0−860−60
81.7	939		ew-sd		−906	
81.3	944		s-s	ms-sd	−901	0−860−40−3
81.1	946		ms-s	m-sd	−897	0−860−40
80.8	950	ew sd			−893	
80.5	954	ew-d			−889	
78.5	980		vs-s	s-s	−863	0−860−3
78.3	983		vs-s	s-s	−860	0−860
78.2	984		ew-sd		−859	
77.0	999	ms-s	ew-sd	ew-d	−844	0−841−3
76.8	36 002	ms-s	ew-sd	ew-d	−841	0−841
75.4	020			ew-d	−823	
72.0	064		ew-ed		−779	0−248−452−2×40
69.1	102		ew-d		−741	0−248−452−40−3
68.9	105		ew-d	ew-d	−738	0−248−452−40
67.2	127		ew-d		−716	
67.0	130		ew-d	ew-d	−713	
65.9	144		w-d	vw-d	−699	0−248−452−3?
65.8	145		w-sd	vw-d	−698	0−248−452
			−45°C	−55°C	−70°C	
59.6	226	ew-d			−617	0−452−4×40
57.6	253	vw-d			−590	0−452−2×40−60
56.3	270	vw-sd			−573	
56.0	274	vw-sd			−569	
55.8	276	vw-sd			−567	0−452−3×40−3
55.6	279	ew-sd			−564	0−452−3×40
54.8	290	ew-sd			−553	0−452−40−60?
54.6	292	ew-sd			−551	0−452−40−60?
53.0	313	mw-d	vw-ed		−530	0−452−2×40−3
52.8	316	w-d			−527	0−452−2×40
52.0	326	vw-d			−517	0−452−30−40
50.5	346	vw-sd	w-d		−497	0−2×248?
50.2	350	ms-sd	w-d		−493	0−452−40−3
50.0	353	m-sd	w-d		−490	0−452−40

TABLE I—*Continued.*

Wave length in A	Wave numbers in cm^{-1}	Intensity −45°C	−55°C	−70°C	Separation from 0,0 band	Assignments
49.6	358	m-sd	vw-vd		−485	0−452−30−3?
49.4	361	mw-sd	ew-vd		−482	0−452−30?
47.3	389	vs-s			−454	0−452−3
47.1	391	vs-s		vw-vd	−452	0−452
45.7	410	vw-d			−433	0−248−3×40−60
44.3	428		ew-ed		−415	0−248−4×40−3
44.0	432	m-d	vw-vd		−411	0−248−4×40
42.7	450	ms-sd	vw-vd		−393	0−248−2×40−60−3
42.5	452	ms-sd	ew-vd		−391	0−248−2×40−60
41.7	463	ew-ed			−380	
41.4	467	ms-sd	ew-ed		−376	
41.2	470	s-sd	w-d	ew-ed	−373	0−248−3×40−3; 0−2×186?
40.9	474	m-sd	ew-d		−369	0−248−3×40
40.4	480	ew-d			−363	
40.2	483	ew-d			−360	
39.9	487	ew-d			−356	
39.6	491	s-sd	vw-d		−352	0−248−40−60−3
39.4	494	s-sd	vw-d		−349	0−248−40−60
39.3	495	vw-d			−348	
39.0	499	ew-d			−344	
38.7	503	ew-d			−340	
38.5	506	ew-d			−337	
38.4	507	mw-sd	ew-d		−336	
38.1	511	vs-vd	m-d		−332	0−248−2×40−3
37.8	515	vs-vd	mw-d	vw-vd	−328	0−248−2×40
36.4	534	ms-sd			−309	0−248−60−3
36.3	535	ms-sd			−308	0−248−60
35.1	551		s-sd		−292	0−248−40−3
34.9	554		s-sd		−289	0−248−40
34.3	562	m-sd			−281	0−248−30?
32.0	592		vs-s	m-sd	−251	0−248−3
31.8	595		vs-s	vw-sd	−248	0−248
30.4	614	vw-d			−229	
30.1	618	m-sd	vw-d		−225	
29.9	621	m-sd	vw-d		−222	
29.6	625	m-sd			−218	
29.4	627	m-sd			−216	
28.6	638		w-sd		−205	
28.4	641		vw-d		−202	
27.7	650		ew-vd		−193	
27.3	653		ew-ed		−190	
26.9	661		mw-vd		−182	0−3×40−60−3
26.7	664		w-ed	vw-d	−179	0−3×40−60
26.0	673		w-sd		−170	0−2×40−60−30
25.8	676		vw-d		−167	
25.2	684		m-vd		−159	0−4×40−3
24.9	688		mw-vd		−155	0−4×40
24.7	689		vw-vd		−154	
24.4	694		ew-d		−149	
24.2	697		vw-sd		−146	
24.0	700		ms-d	ew-d	−143	0−2×40−60−3
23.8	703		mw-d		−140	0−2×40−60
22.4	721		s-vd		−122	0−3×40−3
22.1	725		s-vd	w-d	−118	0−3×40
21.8	730		s-d	w-d	−113	
21.2	738		s-d	ms-s	−105	0−40−60−3
20.9	742		vs	m-s	−101	0−40−60
20.8	743		vw-d		−100	
19.3	763			m-s	−80	0−2×40−3
19.1	766			mw-s	−77	0−2×40
18.8	770		ew-s		−73	
18.6	773		s-sd	ew-ed	−70	0−30−40−3
18.4	775		s-sd	ew-ed	−68	0−30−40
17.1	793			ew-ed	−50	
16.8	797			ew-sd	−46	
16.5	801			s-s	−42	0−40−3
16.3	804			ms-s	−39	0−40
15.9	809		ew-d		−34	0−30−3
15.6	813		ew-d		−30	0−30
13.7	839			vs-vs	−4	0−3
13.4	843			vs-s	0	0,0
13.2	846		vs-d	ew-s	3	

Wave length in A	Wave numbers in cm^{-1}	Intensity −45°C	−55°C	−70°C	Separation from 0,0 band	Assignments
12.8	851	ew-d			8	
12.0	862	vw-vd			19	
10.9	877	ew-sd			34	
10.7	880	ew-sd			37	
10.4	884	ew-sd			41	0+408−248−3×40−3
10.2	887	ew-sd			44	0+408−248−3×40
08.2	914	m-d	vw-vd		71	
07.9	918	ew-ed			75	
07.6	922	mw-vd			79	0+408−248−2×40−3
07.3	926	ms-sd	vw-vd		83	0+408−248−2×40
05.4	956	ms-sd	w-sd		110	
05.2	955	ms-sd	w-sd		112	
04.9	959	s-sd	m-d		116	
04.6	963	s-sd	m-d		120	0+408−248−40−3
04.3	967	vw-d	ew-sd	ew-vd	124	0+408−248−40
03.6	977	ew-ed			134	0+408−248−30
02.4	993	vw-ed			150	
02.0	999	w-d			156	
01.7	37 003	s-d	mw-ed		160	0+408−248−3
01.5	006	s-d	w-vd	ew-vd	163	0+408−248
2699.0	040	ms-sd	vw-sd		197	
98.8	043	w-vd	ew-sd		200	0+200
98.5	047	ew-vd			204	
98.3	049	ew-vd			206	
97.0	067	ew-ed			224	
96.5	074	ew-d			231	
96.2	078	vw-sd	ew-vd		235	
96.0	081	ew-sd	ew-vd		238	
95.2	092	w-sd	vw-vd		249	0+408−4×40−3
95.0	095	ew-d	ew-vd		252	0+408−4×40
94.1	107		vw-ed		264	0+408−2×40−60−3
93.8	111	vs-vd	vw-ed		268	0+408−2×40−60
92.3	132		ew-ed		289	
92.0	136		ew-ed		293	0+408−3×40−3
91.7	140		ew-d		297	0+408−3×40
91.2	147		ew-sd		304	
90.9	151		w-d		308	
90.7	154		w-d		311	0+408−40−60
89.7	168		vw-ed		325	
89.6	169		vw-vd	ew-vd	326	
89.3	173		vw-vd		330	0+408−2×40−3
89.1	176		vw-vd		333	0+408−2×40
87.7	196		s-sd		353	
87.5	198		s-sd	vw-d	355	0+408−50−3
87.3	201			vw-d	358	0+408−50
87.0	205		ms-sd		362	
86.8	208		ms-sd		365	
86.6	211		ms-sd	vw-d	368	0+408−40−3
86.4	213		ms-sd	vw-d	370	0+408−40
84.1	245			ew-d	402	
83.9	248		vs-s	w-sd	405	0+408−3
83.7	251		vs-s	w-sd	408	0+408
81.0	288		ew-d		445	0+819−248−3×40−3
80.8	291		ew-d		448	0+819−248−3×40
79.5	309		ew-d		466	
79.3	312		ew-d		469	
78.4	325		ew-d		482	
78.3	326		ew-d		483	
78.1	329		vw-d		486	0+819−248−2×40−3
77.9	332		vw-d		489	0+819−248−2×40?
75.2	369		m-d		526	
75.0	372		m-d		529	
74.8	375		m-vd		532	0+819−248−3?
74.7	376		mw-vd	vw-ed	533	0+819−248−40
73.7	390		vw-sd		547	
73.2	397		vw-sd		554	
72.8	403		ew-sd		560	
72.6	406		ew-sd		563	
72.4	408		mw-sd		565	
72.2	411		ms-sd		568	0+819−248−6
72.0	414		ms-sd		571	0+819−248−3
71.8	417		ms-sd	w-ed	574	0+819−248
70.6	434		ew-d		591	

TABLE I—*Continued.*

Wave length in A	Wave numbers in cm^{-1}	Intensity −45°C	Intensity −55°C	Intensity −70°C	Separation from 0,0 band	Assignments
70.5	435		ew-d		592	
70.0	442		vw-d		599	0+819−4×40−60
69.1	455		ew-sd		612	
68.9	457		ew-sd		614	
68.8	459		ew-sd		616	
67.3	480		ms-sd		637	0+819−3×40−60−3
67.2	481		w-d	ew-vd	638	0+819−3×40−60
66.7	488		ew-d		645	
66.6	490		ew-d		647	
65.7	502		vw-sd		659	0+819−4×40−3
65.5	505		m-sd		662	0+819−4×40
65.3	508		w-sd		665	
65.1	511		ew-sd		668	
64.7	517		ms-sd		674	
64.5	519		ms-sd		676	
64.3	522			vw-ed	679	0+819−2×40−60
62.8	543			vw-sd	700	0+819−3×40
62.7	545			vw-sd	702	
62.4	549			ew-sd	706	
62.0	555			ew-sd	712	
61.7	559			vw-sd	716	
61.6	560			vw-sd	717	0+819−40−60
60.3	579			m-sd	736	0+819−2×40−3
60.1	581			mw-sd	738	0+819−2×40
59.9	584			w-sd	741	
59.6	588			ew-sd	745	
59.4	591			ew-sd	748	
57.7	615			ew-sd	772	
57.4	620			s-s	777	0+819−40−3
57.3	621			ms-s	778	0+819−40
55.7	644			w-vd	801	
55.3	649			w-vd	806	
55.1	652			w-vd	809	
54.8	656			vs-s	813	0+819−6
54.6	659			vs-s	816	0+819−3
54.4	662			ms-s	819	0+819
53.2	679		w-sd		836	0+876−40−3
53.1	681		w-sd		838	0+876−40
50.6	716		s-s	vw-d	873	0+876−3
50.4	719		s-s	ew-vd	876	0+876
49.0	739		ew-ed		896	
48.8	742		ew-vd		899	0+1250−248−40−60
48.2	750		ew-ed		907	
47.8	756		vw-vd		913	0+1250−248−2×40−3
47.6	759		vw-ed		916	0+1250−248−2×40
46.1	780		w-d		937	
45.8	785		m-sd		942	0+1250−248−60?
45.4	790		w-vd		947	0+1055−3×40
45.2	793		w-vd		950	
44.7	800		ew-ed		957	0+1250−248−40−3
44.6	802		ew-ed		959	0+1250−248−40
43.4	819		vw-d		976	0+1055−2×40−3
43.2	822		ew-d		979	0+1055−2×40
41.9	840		ms-d		997	
41.7	843		m-d	ew-ed	1000	0+1250−248
40.7	857		w-sd		1014	0+1055−40−3
40.6	859		ew-d	ew-vd	1016	0+1055−40
39.6	873		ew-ed	ew-ed	1030	
38.7	886		w-d		1043	
38.5	889		w-d		1046	
38.1	895		mw-d		1052	0+1055−3
37.9	898		mw-d	ew-vd	1055	0+1055
36.9	912		ew-vd		1069	
35.7	929		ew-vd		1086	
35.5	932		ew-vd		1089	
35.3	935		ew-d		1092	0+1250−4×40−3
35.1	939		ew-d		1096	0+1250−4×40
34.4	948		w-d		1105	0+408+819−3×40−3
34.2	951		w-d		1108	0+408+819−3×40
32.8	971		mw-vd		1128	
32.6	974		mw-vd		1131	0+1250−3×40−3
32.4	977		w-vd		1134	0+1250−3×40
31.9	984		ew-d		1141	0+408+819−2×40−3
31.7	987		ms-sd		1144	0+408+819−2×40
31.6	988		vw-sd	ew-ed	1145	0+1250−40−60?
29.8	38 014		s-vd	vw-sd	1171	0+1250−2×40−3
29.7	016		m-d	ew-sd	1173	0+1250−2×40
29.6	017		ew-sd		1174	
29.3	022		s-vd	ew-sd	1179	0+408+819−40−3
29.1	025		s-vd	ew-sd	1182	0+408+819−40
28.8	029		ew-sd		1186	0+1250−60−3
28.7	030		ew-sd		1187	0+1250−60
27.2	052			m-d	1209	0+1250−40−3
27.1	053		vs	m-d	1210	0+1250−40
26.8	058		ew-ed		1215	
27.7	059		ew-ed		1216	
26.3	065		ms-sd		1222	
26.2	066		ms-sd		1223	0+408+819?
24.5	091			s-s	1248	0+1250−3
24.4	093		w-sd	s-s	1250	0+1250
24.1	097		ew-d		1254	
20.2	154		ew-vd		1311	
18.9	173		ew-vd		1330	
18.7	176		ew-vd		1333	
18.2	183		ew-vd		1340	
18.1	184		ew-vd		1341	
17.6	192		vw-d		1349	
17.4	194		w-d		1351	0+2×819−248−40−3
17.3	196		ew-d		1353	0+2×819−248−40
16.2	212		ew-d		1369	
16.1	213		ew-d		1370	
14.9	231		ew-d		1388	
14.7	233		ms-sd		1390	0+2×819−248−3
14.5	237		ms-sd		1394	0+2×819−248
11.2	285		ew-vd		1442	
11.0	288		ew-vd		1445	
10.7	292		ew-vd		1449	
10.4	297		ew-vd		1454	0+2×819−3×40−60
08.6	323		mw-d		1480	0+2×819−4×40−3
08.4	326		mw-d		1483	0+2×819−4×40
07.9	334		vw-d		1491	
07.6	338		m-sd		1495	
07.5	339		vw-d		1496	0+2×819−2×40−60
06.1	360		ms-d		1517	0+2×819−3×40−3
05.9	363		ms-d	vw vd	1520	0+2×819−3×40
05.3	372		vw-sd		1529	
05.1	375		m-d		1530	
04.9	378		m-d	vw-vd	1535	0+2×819−40−60
04.8	379		ew-sd		1536	
04.1	391			ew-vd	1548	
03.2	403			mw-vd	1560	0+2×819−2×40
01.6	426			ew-ed	1583	
00.9	437			m-sd	1594	0+2×819−40−3
00.7	440			mw-sd	1597	0+2×819−40
00.6	441			ew-d	1598	
2598.9	466			vw-ed	1623	
98.7	469			ew-ed	1626	
98.4	473			m-s	1630	0+2×819−6
98.2	477			ms-s	1634	0+2×819−3
98.0	480			m-s	1637	0+2×819
97.9	481		ms-d		1638	
97.5	487		vw-d		1644	0+819+876−40−3
97.3	490		vw-d		1647	0+819+876−40
96.7	499		vw-vd		1656	0+408+1250−3
96.5	502		vw-vd		1659	0+408+1250
95.6	515		vw-d		1672	
95.4	518		vw-d		1675	
95.2	521		ew-d		1678	
94.9	526		ms-s		1683	0+819+876−3
94.7	529		ms-s	ew vd	1686	0+819+876?
92.3	564		ew-ed		1721	
91.5	576		ew-ed		1733	
90.7	588		ew-ed		1745	
89.8	601		vw-d		1758	
89.6	604		ew-vd		1761	
89.3	609		m-sd		1766	

TABLE I—*Continued.*

Wave length in A	Wave numbers in cm^{-1}	Intensity −45°C	−55°C	−70°C	Separation from 0,0 band	Assignments
89.1	612	ew-vd			1769	
88.3	624	ew-ed			1781	0+819+1250−40
85.6	664	ms-vd			1821	0+819+1250−248?
82.7	708	vw-ed			1865	
82.1	717	vw-ed			1874	0+819+1250−5×40
81.3	729	vw-ed			1886	0+819+1250−3×40−60
80.7	738	vw-ed			1895	
80.0	748	vw-ed			1905	
79.5	756	vw-vd			1913	0+819+1250−4×40
79.3	759	vw-vd			1916	
78.9	765	mw-vd			1922	0+819+1250 −2×40−60−3
78.7	768	w-vd			1925	0+819+1250−2×40−60
77.3	789	ms-ed			1946	0+819+1250−3×40−3
77.0	793	ms-ed			1950	0+819+1250−3×40
76.7	798	mw-ed			1955	
76.3	804	ms-d			1961	0+819+1250 −40−60−3?
76.2	805	ms-d			1962	0+819+1250−40−60
74.8	826	ms-ed			1983	0+819+1250−2×40−3
74.5	831	s-ed			1988	0+819+1250−2×40
74.0	838	vw-ed			1995	
73.7	843	w-d			2000	
73.6	844	w-d			2001	0+819+1250−60?
72.0	869			m-vd	2026	0+819+1250−40−3
71.8	872			m-vd	2029	0+819+1250−40
71.5	876	ew-ed			2033	
71.0	883	ew-ed			2040	
70.6	890	vw-ed			2047	0+876+1250−2×40
69.5	906			ms-sd	2063	0+819+1250−3
69.4	908			m-sd	2065	0+819+1250
69.1	912	ms-vd			2069	
68.1	928	vw-vd			2085	0+876+1250−40
65.6	966	w-vd			2123	0+876+1250−3?
65.5	967	w-vd			2124	0+876+1250
60.4	39 045	ew-vd			2202	
59.9	052	ew-vd			2209	
59.8	054	ew-vd			2211	
58.8	069	ew-ed			2226	
57.6	087	ew-ed			2244	
56.3	107	vw-vd			2264	
55.6	118	ew-ed			2275	
54.8	130	ew-ed			2287	
53.8	146	w-ed			2303	
50.6	195	vw-vd			2352	
49.9	205	vw-vd			2362	
49.8	207	vw-vd			2364	
49.4	213	vw-vd			2370	
49.1	218	vw-vd			2375	
49.0	219	vw-vd			2376	0+2×1250−3×40
47.5	242	mw-sd			2399	
47.3	245	ms-sd			2402	
47.2	247	mw-sd		w-ed	2404	
46.9	252	w-sd		ew-ed	2409	0+3×819−40−3
46.7	255	mw-d			2412	0+3×819−40
46.6	256	mw-d		vw-ed	2413	0+2×1250−2×40−3
46.4	259	vw-vd			2416	0+2×1250−2×40
45.8	269			vw-ed	2426	
44.9	282	s-sd			2439	
44.7	286	s-sd		w-ed	2443	
44.5	289	vw-vd		mw-d	2446	
44.3	292	s-sd		mw-d	2449	0+3×819−3
44.1	295	s-sd		mw-d	2452	0+3×819
44.0	296	ms-d			2453	0+2×1250−40−3
43.9	298	ms-ed		mw-d	2455	0+2×1250−40
42.0	327	m-vd		ew-vd	2484	
41.5	335	s-sd			2492	0+2×1250−3
41.3	338	ms-sd		mw-vd	2495	0+2×1250
41.1	341	vs-vd		ew-vd	2498	
40.8	346	w-vd			2503	
40.0	358	vw-ed			2515	
38.9	375	vw-ed			2532	
38.4	383	w-d			2540	0+2×819+1250 −248−40−60
38.3	385	vw-vd			2542	
37.8	392	vw-d			2549	
37.3	400	ew-ed			2557	
36.6	411	ew-vd			2568	
36.2	417	w-d			2574	
36.0	420	vw-vd			2577	
35.7	425	mw-vd			2582	0+2×819+1250 −248−60
35.5	428	w-ed			2585	
34.4	445	vw-vd			2602	0+2×819+1250 −248−40
31.9	484	vs-vd			2641	0+2×819+1250−248
31.3	494	ew-ed			2651	
30.9	500	ew-ed			2657	
29.4	523	vw-ed			2680	
28.8	533	m-ed			2690	
21.3	650			vw-vd	2807	0+2×819+1250−2×40
19.1	685			vw-vd	2842	0+2×819+1250−40−3
18.9	688			vw-vd	2845	0+2×819+1250−40
16.7	723			w-d	2880	0+2×819+1250−3
16.5	726			w-d	2883	0+2×819+1250
15.9	735	s-vd			2892	
15.1	748	ew-ed			2905	
14.6	756	ew-ed			2913	
14.2	762	vw-ed			2919	
13.4	775	s-d			2932	0+819+876+1250
12.5	789	ew-ed			2946	
11.2	810	vw-ed			2967	0+819+2×1250 −248−40−60
10.8	816	ew-ed			2973	
10.2	825	vw-ed			2982	0+819+2×1250 −248−2×40
09.6	835	ew-vd			2992	
09.1	843	ew-vd			3000	
08.3	856	vw-vd			3013	
08.0	860	w-vd			3017	
07.5	868	vw-ed			3025	0+819+2×1250 −248−40
06.9	878	ew-ed			3035	
06.3	887	ew-ed			3044	
05.0	908	w-vd			3065	0+819+2×1250−248
04.5	916	ew-ed			3073	
04.1	922	ew-ed			3079	
02.6	946	ew-vd			3103	
02.1	954	mw-d			3111	0+819+2×1250−2×100
01.5	965	ew-ed			3121	
01.0	972	ew-ed			3129	
00.0	988	s-ed			3145	
2498.5	40 012	ew-ed			3169	
97.6	026	ew-ed			3183	
95.9	054	m-ed			3211	0+819+2×1250−40−60
94.5	076	m-ed			3233	0+819+2×1250−2×40
93.5	092	ms-ed			3249	
92.9	102	ms-ed			3259	
92.1	115	ms-ed			3272	0+819+2×1250−40
91.6	123	ms-ed			3280	0+4×819?
91.0	132	ew-d			3289	
90.9	134	ew-vd			3291	
90.3	144	ew-ed			3301	
89.5	157	vs-ed			3314	0+819+2×1250
88.6	171	vw-ed			3328	0+876+2×1250−40
88.1	179	ew-ed			3336	
86.6	203	vw-ed			3360	
86.2	210	w-vd			3367	0+876+2×1250
84.3	241	vw-ed			3398	
83.1	260	ew-vd			3417	
80.5	302	vw-vd			3459	
80.2	307	ew-vd			3464	
78.4	336	ew vd			3493	
77.5	351	ew-vd			3508	
75.5	384	ew-vd			3541	

TABLE I—*Continued.*

Wave length in A	Wave numbers in cm^{-1}	Intensity −45°C −55°C −70°C	Separation from 0,0 band	Assignments
75.1	390	ew-vd	3547	
74.4	402	ew-vd	3559	
72.8	428	ew-vd	3585	
72.0	441	ew-ed	3598	
71.6	447	ew-ed	3604	
71.1	456	vw-vd	3613	
70.8	460	vw-vd	3617	
70.4	467	vw-ed	3624	
68.9	492	s-vd	3649	
68.5	498	m-d	3655	
68.1	505	s-vd	3672	0+2×1250−2×40
66.5	531	vs-vd	3688	
66.2	536	m-vd	3693	
65.8	543	vs-vd	3700	0+3×819+1250; 0+3×1250−40
64.1	570	ms-vd	3727	
63.5	580	ms-vd	3737	0+3×1250
60.8	625	vw-vd	3782	
60.4	632	ew-ed	3789	
57.9	673	ew-ed	3830	
54.8	724	ew-ed	3881	
54.4	731	vw-ed	3888	
54.1	736	ew-ed	3893	
53.0	754	ew-d	3911	
52.5	762	ew-d	3919	
52.1	769	vs-sd	3926	
49.4	814	ew-ed	3971	
48.7	826	ms-ed	3983	
47.9	839	m-ed	3996	
44.8	891	m-ed	4048	0+2×819+2×1250−2×40
43.3	916	ms-vd	4073	
42.5	929	ms-vd	4086	0+2×819+2×1250−40
41.0	954	vw-ed	4111	
40.3	966	vs-ed	4123	
40.0	971	s-vd	4128	0+2×819+2×1250
37.5	41 013	w-d	4170	0+819+876+2×1250?
26.7	196	ew-d	4353	
26.2	204	ew-d	4361	
22.5	267	ew-d	4424	
19.2	323	ew-ed	4480	0+4×819+1250−40
18.6	334	vw-vd	4491	
17.8	347	w-d	4504	
17.3	356	w-d	4513	0+819+3×1250−40
16.9	363	w-d	4520	0+4×819+1250
15.0	395	ms-d	4552	0+819+3×1250
00.7	642	vw-ed	4799	
2399.9	656	vw-ed	4813	
96.7	711	vw-ed	4868	0+3×819+2×1250−2×40
94.7	746	mw-ed	4903	0+3×819+2×1250−40
92.5	785	ms-ed	4942	0+3×819+2×1250
90.5	819	ew-ed	4976	0+4×1250

benzene obtained from the vapor spectrum with those obtained from the liquid spectrum, we find that the carbon vibration has the same value in both the liquid and vapor spectrum, but the hydrogen frequency is lower in the liquid spectrum.[7] If we assume that the forces in the liquid would lower the frequency of the totally symmetric fluorine bond stretching vibration in much the same manner as they do the hydrogen vibrations of benzene then this is additional support for the assignment given above for the 1259-cm^{-1} frequency.

The relatively weak bands at 37 251 and 36 391 cm^{-1} represent frequencies of 408 and 452 cm^{-1} and are assigned to the respective excited and ground-state frequencies of another α_g vibration. This vibration corresponds to the totally symmetric component of the 606 ϵ_g^+ benzene vibration and the assignment agrees with that made by Delsemme.[1]

Still another α_g vibration is correlated with the weak band at 36 002 cm^{-1}. This band represents a ground-state frequency of 841 cm^{-1} which is identical with the polarized Raman line of 841 cm^{-1} reported by Nielsen.[4] The 841-cm^{-1} frequency does combine with the 860-cm^{-1} frequency to produce the ultraviolet band at 35 142 cm^{-1}. It is not known whether there is a transition which involves the excited state of the 841 vibration because such a band would be indistinguishable from the $v-v$ transitions that accompany the 819-cm^{-1} band.

Two other excited-state frequencies of 876 and 1055 cm^{-1} are represented by the weak bands at 37 719 and 37 898 cm^{-1}, respectively. Bands were not found in the ultraviolet spectrum which could be assigned as the ground-state values of these fundamentals. The 1055-cm^{-1} value is probably the excited-state frequency of the 1142 cm^{-1}, β_{1g}, fundamental reported in the Raman spectra. The 876-cm^{-1} frequency combines with both the 819- and 1250-cm^{-1} frequencies; however, the most likely Raman value which could be correlated with this frequency is the weak 889-cm^{-1} line which Nielsen has assigned as a β_{3g} fundamental. A transition which combines a β_{3g} vibration with the A_g-B_{3u} electronic transition is forbidden by symmetry so the above correlation is untenable if the Raman assignment is correct. Possibly, the 876-cm^{-1} frequency represents two quanta of an excited-state β_u vibration since such a transition would be allowed even though transitions involving only one quantum of a β_u vibration are forbidden.

As has been pointed out in the previous section, the weak bands at 36 595, 37 006, 37 417, 37 843, and 38 237 cm^{-1} are temperature dependent. Each of the transitions involved here start from a 248-cm^{-1} ground-state level, and their respective assignments are 0−248, 0+408−248, 0+819−248, 0+1250−248, and 0+2×819−248. Also this 248-cm^{-1} frequency is found in combination with the ground-state frequencies 452, 860, and 1259 cm^{-1}. The excited-state value of the 248-cm^{-1} fundamental may be either 163 or 200 cm^{-1} as represented by the bands at 37 006 and 37 043 cm^{-1}; however, since the 37 006-cm^{-1} band has another assignment, the excited state is chosen to be 200 cm^{-1}. The assigning of this 248-cm^{-1} frequency as a fundamental gains little support from past assignments of Raman data. Nielsen and co-workers report an extremely weak

[7] See reference 5, p. 535.

Raman frequency of 239 cm^{-1}; but they are inclined to attribute this value to an impurity. A better assignment would be to associate the 248-cm^{-1} value above with the 239 Raman value and assign them to a β_{1g} fundamental. According to the assignments of both Delsemme and Nielsen this would give one more β_{1g} fundamental than is allowed. Such a difficulty is dissolved if we do not assign the 507-cm^{-1} Raman line to a β_{1g} fundamental as was done in the reports on the Raman spectra. Actually, since the Raman values were obtained for the liquid state, and liquid forces may cause a partial breakdown of selection rules, it is possible that this extremely weak 507-cm^{-1} line is produced by the 508-cm^{-1}, β_{1u}, fundamental which is very strong in the infrared spectrum.

The complexness of the *p*-difluorobenzene spectrum is due primarily to the double or triple appearance of some band heads and the large number of long wavelength companions that accompany each band. The multiple band heads are thought to be rotational fine structure. The companion bands are attributed to $v-v$ transitions, but at the present time there are not sufficient data to provide definite assignments for these bands. Companion bands which appear 40, 2×40, 3×40, and 4×40 cm^{-1} on the red side of the main bands represent the 1–1, 2–2, 3–3, and 4–4 transitions of some low-lying vibration. With the absorbing molecules at −79°C, bands are present which are separated by 40 and 2×40 cm^{-1}. Although microphotometer tracing of these bands have not been made, rough intensity measurements indicate that the vibration involved should be below 200 cm^{-1}. The ϵ_u^+ 404 cm^{-1} vibration of benzene has been shown to account for some of the strong $v-v$ transitions of benzene. This vibration is no longer degenerate for D_{2h} symmetry and it splits into two vibrations of symmetry β_{1u} and α_{1u}. Delsemme and Nielsen have assigned somewhat arbitrarily a value of about 186 cm^{-1} to the β_{1u} frequency. This frequency may be the one involved in the above $v-v$ transitions. In fact, in the spectrum reported here the band at 36 470 cm^{-1} represents a frequency of 373 cm^{-1} which could result from a transition involving two ground-state quanta of the 186-cm^{-1} fundamental; however, this band can also be assigned as a $v-v$ transition starting from the 248-cm^{-1} ground level.

By using combinations and progressions of the frequency values discussed above most of the prominent bands have been assigned as in Table I. In making these assignments the effects of anharmonicity have been neglected. The overlapping and diffuseness of the bands above 39 000 cm^{-1} introduces uncertainties in the assigning of some of these bands.

The position of the 0,0 band in the *p*-difluorobenzene spectrum is shifted 1246 cm^{-1} toward longer wavelengths relative to the calculated 0,0 band of benzene. This shift is more than four times the 270-cm^{-1} shift produced by the fluorine substituent in monofluorobenzene. Previous experimental results have shown that *para*-substitution of like substituents on the benzene ring generally shifts the spectrum a little more than twice the amount produced by one substituent. The unusually large shift produced by the *para*-positioned fluorines is probably connected with the inductive effect of fluorine. A simple explanation of the observed shifts is obtained if we assume that the inductive effect of one fluorine produces a violet spectra shift and that the resonance effect produces a red shift. If the inductive effects of two *para*-positioned fluorines cancel, and the resonance effects add,[8] then a qualitative explanation of the spectrum of *para*-substituted benzenes is obtained if the substitutents are all *ortho-para* directing. However, this hypothesis breaks down when the spectral shifts produced by *meta*-directing substituents such as CF_3 or CN are studied. This leaves the subject of spectral shift as a problem for further theoretical study.

[8] A. L. Sklar, J. Chem. Phys. **10**, 135 (1942).

Nuclear Quadrupole Couplings in Solid Bromides and Iodides*

HUGH ROBINSON,† H. G. DEHMELT, AND WALTER GORDY
Department of Physics, Duke University, Durham, North Carolina

(Received October 13, 1953)

From measurements of pure nuclear quadrupole transitions at 77°K the following coupling constants (in Mc/sec) and asymmetry parameters have been obtained: for I^{127} $|eQq|=1765.846$, $\epsilon^2=0.00078$ in CH_3I; $|eQq|=1897.368$, $\epsilon^2=0.00736$ in CH_2I_2; $|eQq|=2046.634$, $\epsilon^2=0.00033$ in $CHI_3\cdot 3S_8$; $|eQq|=2130.33$ for CI_4; $|eQq|=2069.17$ for CF_3I; $|eQq|=1324.788$ and 1333.313, $\epsilon^2=0.000082$ and ≤ 0.000010 for the two nonequivalent I's in unit cell of SiI_4; $|eQq|=1484.339$ and 1500.577, $\epsilon^2=0.000087$ and ≤ 0.000005 for the two nonequivalent I's in unit cell of GeI_4; $|eQq|=1384.424$ and 1394.190, $\epsilon^2=0.000085$ and ≤ 0.000016 for the two nonequivalent I's in unit cell of SnI_4; $|eQq|=1517.07$, $\epsilon^2=0.00008$ in $AsI_3\cdot 3S_8$; $|eQq|=1226.35$, $\epsilon^2=0.00101$ in $SbI_3\cdot 3S_8$. The coupling values of Br are: $|eQq(Br^{79})|=437.27$ and 441.15; $|eQq(Br^{81})|=365.272$ and 368.514 for the two nonequivalent Br's in unit cell of PBr_3 ($T=87\pm 4$°K); $|eQq(Br^{79})|=329.000$ and 345.920; $|eQq(Br^{81})|=274.856$ and 288.980 for the two nonequivalent Br's in unit cell of $SbBr_3$. From these coupling values the number of unbalanced p electrons in the atoms was calculated. The latter quantity was found to be closely related to chemical bond properties such as ionic character, and was found to vary systematically with chemical constitution. A cross bonding mechanism involving d orbitals is proposed to account for the iodine coupling in certain solids.

EXPERIMENTAL METHOD

ALL lines reported here were observed by the method of superregenerative detection with a spectrometer similar to that described by Dehmelt.[1] The sample, in most cases of the order of one cubic centimeter in volume, was placed at one end of a $\lambda/2$- or λ-length Lecher line. The line was driven by two triodes in push-pull operating at a length of about $\lambda/4$ from one end of the line. Sixty-cycle sine wave sweep frequency modulation was employed. Following the oscillator was an audio-frequency amplifier, serving both to amplify the resonance signal and to attenuate the unwanted quench signal and 60-cycle oscillator-mode signal. The resonance was displayed on an oscilloscope using 60-cycle sine wave horizontal sweep. Measurements were accomplished by means of a Gertsch Model FM-3 frequency meter.

RESULTS

In Table I are listed the observed frequencies, and in Table II the coupling constants and asymmetry parameters obtained for I^{127}. Similar data are given for Br^{79} and Br^{81} in Tables III and IV.

The stable bromine isotopes both have spins of 3/2. For this spin value there is only one pure quadrupole transition, and the asymmetry in the electric field gradient about the nucleus cannot be obtained from a measurement of the quadrupole resonance frequency alone. If a cylindrically symmetric field gradient is assumed, the quadrupole coupling eQq for $I=3/2$ is equal to two times the resonance frequency. Even for a very large deviation of axial symmetry corresponding to $\epsilon=0.5$ the value obtained for the coupling constant by doubling the transition frequency would be only 4 percent too high.[2] This assumption was made here in the calculation of the coupling constant of Br^{79} and Br^{81}. It is possible, however, to ascertain the asymmetry parameter for the case of a 3/2 spin from the Zeeman effect in a single crystal.[3]

The I^{127} nucleus (spin 5/2) exhibits two resonant frequencies corresponding to the transitions $M_I=\pm 1/2 \leftrightarrow \pm 3/2$ and $M_I=\pm 3/2 \leftrightarrow \pm 5/2$. When both transitions are measured, the asymmetry parameter can be evaluated and an accurate evaluation of the coupling made. To fourth order, the frequencies are given by perturbation theory as,

$$\nu_1=3/20|eQq|(1+1.0926\epsilon^2-0.634\epsilon^4) \quad (1)$$

$$\nu_2=3/10|eQq|(1-0.2037\epsilon^2+0.162\epsilon^4). \quad (2)$$

For all iodine compounds studied, except CI_4 and CF_3I, we were able to observe both transitions. An

TABLE I. Observed frequencies for I^{127}.

Molecule	T(°K)	$\nu_1(\pm 1/2 \leftrightarrow \pm 3/2)$ (Mc)	$\nu_2(\pm 3/2 \leftrightarrow \pm 5/2)$ (Mc)
CH_3I	77	265.102±0.008	529.670±0.013
CH_2I_2	77	286.883±0.023	568.362±0.025
$CHI_3\cdot 3S_8$	77	307.106±0.004	613.949±0.014
CI_4	77	319.549±0.043	···
CF_3I	83±4	310.375±0.055	···
SiI_4 I_1	77	198.736±0.003	397.430±0.010
SiI_4 I_2	77	199.999±0.003	399.993±0.010
GeI_4 I_1	77	222.672±0.003	445.294±0.012
GeI_4 I_2	77	225.088±0.003	450.173±0.010
SnI_4 I_1	77	207.683±0.003	415.320±0.012
SnI_4 I_2	77	209.133±0.003	418.257±0.010
$AsI_3\cdot 3S_8$	77	227.582±0.007	455.114±0.015
$SbI_3\cdot 3S_8$	77	184.155±0.017	367.830±0.050

* The work has been supported by a contract with the Ordnance Corps, Department of the U. S. Army. It will be submitted by Mr. H. Robinson in partial fulfillment of the requirements for the Ph.D. degree at Duke University.

† National Science Foundation Fellow.

[1] H. G. Dehmelt, Z. Physik **130**, 356 (1951).

[2] H. Krueger, Z. Physik **130**, 371 (1951).

[3] C. Dean, Phys. Rev. **86**, 607 (1952).

TABLE II. Observed coupling constants for I^{127}.

Molecule	$\lvert eQq\rvert$ (Mc)	$\epsilon^2=\left\lvert\frac{q_{xx}-q_{yy}}{q_{zz}}\right\rvert^2$
CH_3I	1765.846±0.045	0.00078 ∓0.00004
CH_2I_2	1897.368±0.095	0.00736 ∓0.00010
$CHI_3\cdot 3S_8$	2046.634±0.044	0.00033 ∓0.00003
CI_4	2130.33 ±0.29	···
CF_3I	2069.17 ±0.36	···
SiI_4 I_1	1324.788±0.031	0.000082∓0.000027
SiI_4 I_2	1333.313±0.031	0.000010∓0.000028
GeI_4 I_1	1484.339±0.037	0.000087∓0.000033
GeI_4 I_2	1500.577±0.033	0.000005∓0.000031
SnI_4 I_1	1384.424±0.037	0.000085∓0.000034
SnI_4 I_2	1394.190±0.033	0.000016∓0.000029
$AsI_3\cdot 3S_8$	1517.07 ±0.05	0.00008 ∓0.00005
$SbI_3\cdot 3S_8$	1226.35 ±0.16	0.00101 ∓0.00018

unsuccessful search was made for the upper line of CI_4; it proved too weak for detection with our spectrometer. The lower lines of these compounds were abnormally broad, and it is undoubtedly the large width which made the upper line difficult to detect.

During the course of our work, measurement of the lower frequency of CH_2I_2 was reported by Zeldes and Livingston.[4] Earlier, the lines in CH_3I and SnI_4 were observed by Dehmelt.[5] The measurement of the upper transitions in the present work allows the asymmetry parameters to be evaluated and thus provides a more accurate value of $|eQq|$. Values for the Br couplings in PBr_3 were also reported by Kojima, Tsukada, Ogawa, and Shimauchi[6] while our work was in progress. Our values agree approximately with theirs.

The structure of CI_4 is quoted in the literature as different from that of SiI_4, GeI_4, and SnI_4. This is borne out by the fact that only one line per transition was observed for CI_4, whereas for SiI_4, GeI_4, and SnI_4 a doublet structure was observed. A doublet structure is also observed for the Br resonances in PBr_3. The line doubling can be interpreted as due to the existence of two nonequivalent members in the unit cell. At dry ice temperature several closely spaced lines were observed for CH_2I_2; the number and intensity of these lines were found to depend upon the rate and length of time of cooling.

No lines were observed in a sample of pure CHI_3. However, in the molecular addition compound[7] $CHI_3\cdot 3S_8$ strong sharp lines were found. The narrow lines which were obtained are evidence for a high degree of regularity in the crystal lattice. The employment of molecular addition compounds to facilitate the observation of nuclear quadrupole resonance might also prove helpful in other cases where it is desirable to separate the otherwise strongly interacting molecules by more inert "fillers," S_8 molecules in our case. The negligible difference in the frequencies measured for SnI_4 and $SnI_4\cdot 4S_8$ appears to prove the inertness of the S_8 molecule in addition compounds of this type.

TABLE III. Observed frequencies for Br^{79} and Br^{81}.

Molecule	T(°K)	$\nu_1(\pm 1/2\leftrightarrow\pm 3/2)$
PBr_3^{79} Br_1	83±4	220.575±0.010
PBr_3^{79} Br_2		218.635±0.010
PBr_3^{81} Br_1		184.257±0.10
PBr_3^{81} Br_2		182.636±0.011
[a]$SbBr_3^{79}$ Br_1	77	172.960±0.013
[a]$SbBr_3^{79}$ Br_2		164.500±0.008
$SbBr_3^{81}$ Br_1		144.490±0.008
$SbBr_3^{81}$ Br_2		137.428±0.009

[a] The pure quadrupole spectrum of Sb^{123}, Sb^{121} in $SbBr_3$ has been observed and assignments made; results will be published in a later paper.

[4] H. Zeldes and R. Livingston, J. Chem. Phys. **21**, 1418 (1953).
[5] H. G. Dehmelt, Naturwiss. **37**, 398 (1950); see also R. Livingston and H. Zeldes, Phys. Rev. **90**, 609 (1953).
[6] Kojima, Tsukada, Ogawa, and Shimauchi, J. Chem. Phys. **21**, 1415 (1953).

REGULARITIES IN THE HALIDE COUPLINGS

Because the halide atoms are found in numerous combinations in which they form a single bond, they offer the most promise for investigation of chemical bond properties with nuclear quadrupole resonance. Furthermore, the atomic coupling has now been accurately measured in the three halides which have quadrupole moments: Cl, Br, and I. With the coupling per p electron in the atom known, the number of unbalanced p electrons U_p in the bonded atom can be obtained immediately from its observed coupling. The latter quantity depends upon such chemical bond properties as ionic character, bond orbital hybridization and bond resonance. Because it allows comparison of results obtained from different atoms, a correlation of

$$|U_p| = |(eQq)_{\text{mol.}}|/2|(eQq)_{\text{atom}}| \ddagger \qquad (3)$$

with other properties has a broader significance than a simple comparison $(eQq)_{\text{molecule}}$ with such properties. Values of U_p determined in the present study together with those on related solids investigated by others are given in Table V.

It has been shown,[8] mainly from couplings in gases, that where bond orbital hybridization and double bond characters are small, the effective number of unbal-

TABLE IV. Observed couplings for Br^{79} and Br^{81}.

Molecule	$\lvert eQq\rvert_{Av}$ (Mc)	$\left(\frac{Q^{79}}{Q^{81}}\right)_{Br_1}$	$\left(\frac{Q^{79}}{Q^{81}}\right)_{Br_2}$
PBr_3	439.21	1.19711±0.00012	1.19711±0.00013
$SbBr_3$	337.46	1.19703±0.00015	1.19699±0.00014

[7] E. Hertel, Z. physik. Chem. **15**, 51 (1931).

‡ The field gradient q_{zz} generated by a p bond is approximately equal to that of a p electron in the magnetic substate $m_l=0$ with decoupled electron spin in the free atom. The latter quantity is equal to $-(l+1)/(2l-1)=-2$ times the field gradient for the substate $m_j=j$ for which the atomic couplings are usually given.

[8] (a) W. Gordy, J. Chem. Phys. **19**, 792 (1951); (b) Gordy, Smith, and Trambarulo, *Microwave Spectroscopy* (John Wiley and Sons, Inc., New York, 1953), Sec. 7.1.

anced p electrons (U_p) in the halides bears a simple relation to the electronegativity difference of the bonded atoms. This relation is of the form

$$|U_p| = \frac{|(eQq)_{\text{mol.}}|}{2|(eQq)_{\text{atom}}|} = a + b(x_{\text{Hal}} - x) \approx 1 - (x_{\text{Hal}} - x)/2 \quad (4)$$

in which $(x_{\text{Hal}} - x) \leq 2$ and $x_{\text{Hal}} > x$.

It indicates that

$$\text{ionic character} \approx \frac{|x_A - x_B|}{2}, \quad (5)$$

and that the bond is almost completely ionic for $|x_A - x_B| > 2$.

TABLE V. Comparison of couplings and unbalanced p electrons in related halides.

Molecule	eQq in solid (Mc)	Observed $\|U_p\| = \frac{\|(eQq)_{\text{molecule}}\|}{2\|(eQq)_{\text{atom}}\|}$ Solid	Gas	$x_{\text{Hal}} - x_A$
	$Cl^{35}(2(eQq)_{\text{atom}} = +109.74$ Mc)[α]			
Cl_2	−108.95[a]	0.993		
CH_3Cl	−68.4[a]	0.623	0.686[b]	
CH_2Cl_2	−72.47[a]	0.660		
$CHCl_3$	−76.98[a]	0.701		
CCl_4	−81.85[a]	0.746		0.5
CF_3Cl	−77.58[a]	0.707	0.711[b]	
CCl_4	−81.85[a]	0.746		0.5
$SiCl_4$	−40.8[f]	0.372		1.2
$GeCl_4$	−51.3[a]	0.467		1.3
$SnCl_4$	−48.2[f]	0.439		1.3
PCl_3	−52.3[a]	0.477		0.9
$AsCl_3$	−50.5[a]	0.460		1.0
$SbCl_3$	−40.4[a]	0.368		1.2
	$Br^{79}(2(eQq)_{\text{atom}} = -769.62$ Mc)[β]			
Br_2	765[b]	0.994		
CH_3Br	529[g]	0.687	0.750[b]	
CH_2Br_2	563[e]	0.732		
$CHBr_3$	601[e]	0.781		
CF_3Br	604[e]	0.785	0.804[b]	
$SnBr_4$	382[d]	0.496		1.1
PBr_3	439[e]	0.570		0.7
$SbBr_3$	337[e]	0.438		1.0
	$I^{127}(2(eQq)_{\text{atom}} = +2292.439$ Mc)[γ]			
I_2	−2153[b]	0.939		
CH_3I	−1766[e]	0.770	0.844[b]	
CH_2I_2	−1897[e]	0.828		
$CHI_3 \cdot 3S_8$	−2047[e]	0.893		
CI_4	−2130[e]	0.929		0.0
CF_3I	−2069[e]	0.903	0.938[b]	
SiI_4	−1329[e]	0.580		0.7
SnI_4	−1389[e]	0.606		0.8
GeI_4	−1492[e]	0.651		0.8
$AsI_3 \cdot 3S_8$	−1517[e]	0.662		0.5
$SbI_3 \cdot 3S_8$	−1226[e]	0.535		0.7

[α] V. Jaccarino and J. G. King, Phys. Rev. **83**, 471 (1951).
[β] J. G. King and V. Jaccarino (private communication).
[γ] Jaccarino, King, and Stroke (private communication).
[a] R. Livingston, as quoted in reference h, p. 366.
[b] H. G. Dehmelt, Naturwiss. **37**, 398 (1950), p. 367.
[c] H. Zeldes and R. Livingston, J. Chem. Phys. **21**, 1418 (1953).
[d] S. Kojima *et al.*, J. Chem. Phys. **21**, 1415 (1953).
[e] Present work.
[f] Reference a. See also H. G. Dehmelt, J. Chem. Phys. **21**, 380 (1953).
[g] Reference b. See also reference c.
[h] Gordy, Smith, and Trambarulo, *Microwave Spectroscopy* (John Wiley and Sons, Inc., New York, 1953); value of $(eQq)_{\text{molecule}}$ from Table A.6 in Appendix.

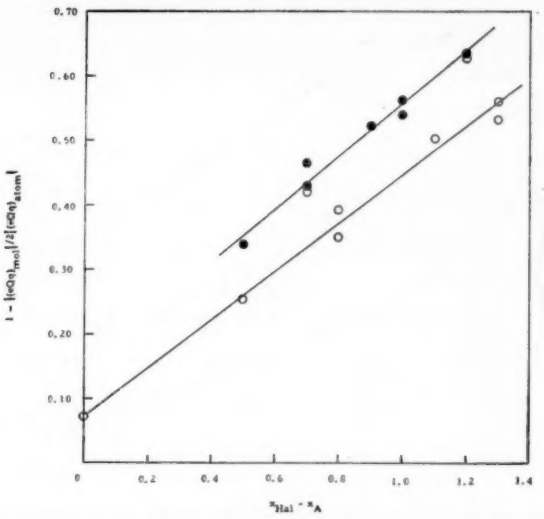

FIG. 1. Plot of $(1-|U_p|)$ *versus* electronegativity difference of the bonded atoms. $|U_p| = |(eQq)_{\text{molecule}}|/2|(eQq)_{\text{atom}}|$ represents the number of unbalanced electrons on the halogen. Black dots represent $A(\text{Hal})_3$ compounds; open circles represent $A(\text{Hal})_4$ compounds. Solid state.

A plot of all the halide data (which are now numerous) on solids as well as gases reveals that the points scatter, about equally, on either side of the line determined by the above Eq. (4). However, the data obtained in the present study taken with earlier data show individual group trends. This is indicated in Fig. 1 where it is apparent that the P, As, and Sb halides (black dots) fall along a different line from those of the C, Si, Ge, and Sn halides (open circles). Note that the point for $SiCl_4$ departs most from the group trend. This is evidence for double bond character in $SiCl_4$, already emphasized.[9]

For the former group (P, As, Sb) the correlation is expressed approximately by

$$|U_p| = \frac{|(eQq)_{\text{mol.}}|}{2|(eQq)_{\text{atom}}|} = 0.88 - 0.44(x_{\text{Hal}} - x_A), \quad (6)$$

and for the latter group (C, Si, Ge, Sn) by

$$|U_p| = \frac{|(eQq)_{\text{molecule}}|}{2|(eQq)_{\text{atom}}|} = 0.93 - 0.37(x_{\text{Hal}} - x_B). \quad (7)$$

The coupling of Cl^{35} in NCl_3, not yet measured, is predicted by Eq. (6) to be −97 Mc. As soon as the chemical can be obtained we plan to search for the resonance which should occur at about 49 Mc. We have already searched without success for the resonance in CBr_4, for which a Br^{79} coupling of 670 Mc is predicted by Eq. (7). Our failure is believed to result from lack of sufficient uniformity in the crystalline fields of the sample used. A more persistent attempt to find the line will be made later.

Figure 2 compares the behavior of different carbon halides with increasing substitutes of H on the carbon. Note that the lines for Cl, Br, and I are almost straight

[9] Gordy, Smith, and Trambarulo, reference 8b, Sec. 8.3b.

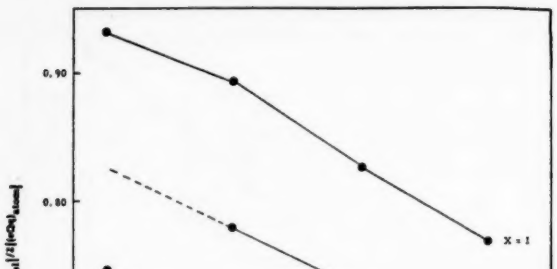

FIG. 2. Variation of number of unbalanced p electrons on the halogen ($|U_p| = |(eQq)_{\text{molecule}}|/2|(eQq)_{\text{atom}}|$) with H substitution on carbon. Solid state.

and almost parallel. The value for CBr_4 can be predicted by extrapolation of the center curve, and pleasingly this result agrees with that already predicted from Fig. 1. Previously, regularities have been noted in the couplings of the separate chloride and bromide groups by Livingston.[10,4]

The value in the CX_4 compounds may be considered as normal since their observed U_p agrees closely with that predicted from the electronegativity difference. With increasing substitutions of H, the observed U_p decreases. This decrease might be ascribed, partly at least, to a decrease in the effective electronegativity of the C. To attribute the entire change to this effect would require the C in CH_3 to have an electronegativity of 2.3 instead of the average value of 2.5 for C.

The behavior of CH_3(Hal) and CF_3(Hal) in gases and solids are compared in Fig. 3. Interestingly, the CF_3(Hal) compounds which have essentially normal coupling as predicted by Eq. (4) have almost identical coupling in the gaseous and the solid state. The CH_3(Hal) compounds which deviate widest from Eq. (4) also differ most in the solid and gaseous state. The latter differences have a simple explanation in the small size of the H atoms which makes it possible for the CH dipole to approach closely to, and thus interact strongly with, the negatively charged halogen.

The failure of the projected curves of Fig. 1 to pass through zero could be explained by assumption of s admixtures in the halogen bonding orbital, 7 percent for one group and 12 percent for the other. There is no such evidence, however, for hybridization in Cl_2 and Br_2. These elements have couplings which are within one percent of those expected for one unbalanced p electron, and the coupling of I_2 is within 6 percent of that for one unbalanced p electron. The simplest interpretation is that the bonding in the elementary halides is with nearly pure p orbitals. Nevertheless, the existence of s admixture is not excluded since it is possible for the effects of s admixture (which would decrease the coupling) to be offset by an accompanying d admixture (which would increase the coupling because the complementary pd hybrid would be unoccupied). It would not be possible to detect such composite hybridization from the quadrupole coupling alone since there would then be more parameters than observables. From a combination of coupling data and bond angle, evidence for both s and d hybridization in the bonding orbitals of S in H_2S has been obtained.[11] One is tempted to interpret the coupling in I_2 as indicating 6 percent s character in the bonding orbitals. Nevertheless, this would not account for the large asymmetry in the coupling[5,12] ($\epsilon = 0.173$), and the lowered coupling and the asymmetry in the coupling probably are related. Both effects are accounted for by the bonding mechanism proposed below.

NATURE OF IODINE BONDING IN SOLIDS

The quadrupole coupling in crystalline I_2 might merit some discussion. In this case the lattice consists of plane sheets of I_2 molecules, their axes falling in the plane of the sheets. Although the sheets are stacked over each other with fairly wide spacing, the atoms of neighboring molecules within individual sheets approach each other considerably closer than double the Van der Waals radius, suggesting some stronger interaction. To explain this intermolecular bonding, switching of the molecular p bond has been postulated.[13] An attractive alternative is to treat the molecules in one sheet as belonging to a macromolecule, which resonates between two structures A, B (see Fig. 4). While A contains isolated molecules formed from monovalent I atoms in the $5s^25p^5$ configuration, structure B consists

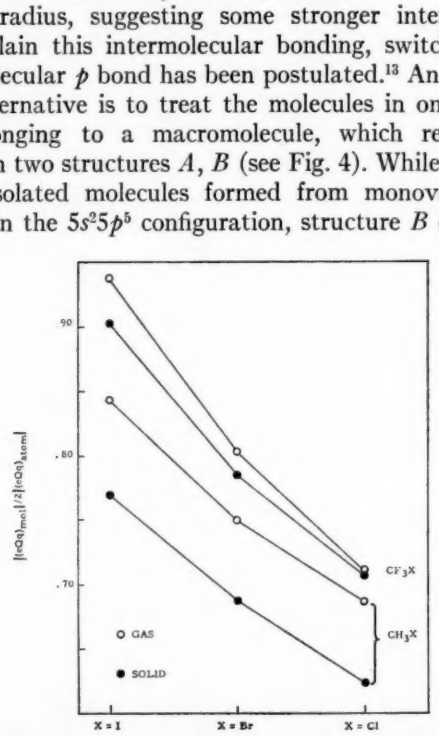

FIG. 3. Variation of the number of unbalanced p electrons ($|U_p| = |(eQq)_{\text{molecule}}|/2|(eQq)_{\text{atom}}|$) on the halogen with chemical constitution.

[10] Ralph Livingston, J. Chem. Phys. **19**, 1434 (1951).

[11] C. A. Burrus and W. Gordy, Phys. Rev. (to be published).

[12] T. Kamei, J. Phys. Soc. Japan **7**, 649 (1952).

[13] C. H. Townes and B. P. Dailey, J. Chem. Phys. **20**, 35 (1952).

of trivalent atoms in the $5s^25p^45d$ configuration forming an infinite network. The T-like planar structure observed[14] for ClF_3 is likewise explained by the promotion of a $3p$ electron of Cl to form the trivalent $3s^23p^43d$, configuration. With the p-bond switching mechanism[13] it is difficult to account for the preference of the I_2 molecules to arrange themselves in plane sheets.

The comparison of the quadrupole coupling measured in the I_2 crystal with that of the free atom and especially the correct interpretation of the large asymmetry of the field gradient observed in the crystal provides a certain test, to which the two alternative models can be subjected. Our model gives for structure A an axially symmetric field gradient equivalent to that of an unbalanced atomic p electron, whose axis falls in the plane of the sheet. Concerning structure B we need only to know that the two atomic p orbitals used for bonding must lie in the plane of the sheet, since the direct contribution of the d orbital to the field gradient is negligible. This leads to an axially symmetric field gradient equivalent to that of a p electron, however, with opposite sign, whose axis is perpendicular to the sheet. If we place the z axis in the I_2 molecular axis and the x axis perpendicular to the sheet, the components of the field gradient tensors are as shown in Table VI (the unit being the q_{zz} component of an unbalanced p electron). Denoting the fractional contribution of structure B by $2b$, the gradient components for the compound structure are given in the last column. The relation for the contribution of structure B, $2b$, and the asymmetry parameter $\epsilon=|q_{xx}-q_{yy}|/q_{zz}$ comes out $\epsilon=3b/(1-b)$. With this formula, the coupling per unbalanced p electron can now be calculated from the measured values $eQq_{zz}=2156$ Mc/sec[5,12] and $\epsilon=17.3$ percent and compared with the atomic beam value, as shown in Table VII. The agreement is excellent for our model, and the required amount of contribution of trivalent configuration, $2b=11$ percent, is not unreasonable.

The cross bonding proposed above could occur between iodine atoms in the same molecule and might indeed account largely for the lowered coupling in CI_4 ($U_p=0.93$ with $x_I-x_C=0$) which is almost identical to that in I_2 ($U_p=0.94$ with $x_I-x_I=0$). Because

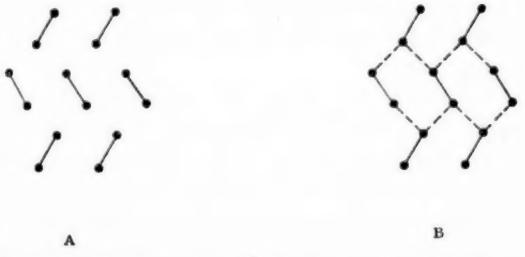

FIG. 4. The diagrams A and B represent the two structures between which the macromolecule formed by the I atoms in one layer of the iodine crystal lattice is assumed to resonate.

[14] D. F. Smith, see reference 8b, Table A.9.

TABLE VI.

Component \ Structure	A	B	$(1-2b)A+2bB$
q_{zz}	1	$+\frac{1}{2}$	$1-b$
q_{xx}	$-\frac{1}{2}$	-1	$-\frac{1}{2}-b$
q_{yy}	$-\frac{1}{2}$	$+\frac{1}{2}$	$-\frac{1}{2}+2b$

TABLE VII.

	Switching p bonds[13]	Macro-molecule	Atomic beam experimental value
Coupling per p-electron $eQq_{zz}(p)$ Mc/sec	2480	2280	2292

of symmetrical arrangement of the four iodines, it would not cause an asymmetry in the coupling however. Although the asymmetry parameter has not been measured for CI_4, it is expected to be zero as the occurrence of only one quadrupole line shows that the lattice sites of the 4 I atoms in the tetrahedral molecule are equivalent. Simple valence forces have been found inadequate to account for the vibrational spectra of AB_4 molecules of this type, and Urey and Bradley[15] have used successfully modified valence force functions in which terms are included to account for strong interaction of the supposedly nonbonding B atoms.

The electrons which are exchanged between the I's in cross bonding of AI_4 compounds may be considered to be in molecular orbitals which spread over the surface of the spherically symmetric AI_4 molecule. When the spherical symmetry is destroyed as in HAI_3 the cross bonding is evidently reduced. This would account for the bend in the top curve of Fig. 2 at HCI_3. In the molecular orbital representation there would be strong localized bonds between the C and I atoms in addition to the much weaker nonlocalized bonds linking the I atoms.

Likewise, the cross bonding electrons in structure B for I_2 mentioned above might be regarded as in molecular orbitals which are spread over the entire plane sheet. These nonlocalized molecular orbitals can be represented approximately by linear combinations of atomic orbitals of all the I atoms in the macromolecule. The macromolecule would then be represented by structure B alone if the solid lines indicate localized σ bonds between the closest I's, and the dots represent the much weaker nonlocalized bonds which spread throughout the molecular sheet. This picture is simpler than the valence bond representation since it requires no resonance between A and B. The molecular orbital treatment of I_2 is similar to the Bloch molecular orbital treatment of metals except in I_2 we have both localized and nonlocalized bond, whereas in ordinary metals all the bonding electrons are presumably in delocalized orbitals.

[15] H. C. Urey and C. A. Bradley, Phys. Rev. **38**, 1969 (1931).

The Microwave Spectrum of Vinyl Cyanide*

W. S. WILCOX † AND J. H. GOLDSTEIN, *Department of Chemistry*

AND

J. W. SIMMONS, *Department of Physics, Emory University, Emory University, Georgia*

(Received November 20, 1953)

The rotational spectrum of the slightly asymmetric top, vinyl cyanide, has been investigated in a microwave spectrograph employing Stark effect modulation and in a direct absorption cell. The rotational constants $a=49\,076.2$ Mc/sec, $b=4971.33$, and $c=4514.05$ were computed from the observed frequencies of the $J=2\rightarrow3$ transitions. From measurements of the Stark effect, the components of the dipole moment were found to be $\mu_a=3.68D$, $\mu_b=1.25$, $\mu=3.89$. Partial resolution of the hyperfine structure of certain lines gave the value -3.0 Mc/sec for the χ_{aa} component of quadrupole coupling.

INTRODUCTION

VINYL cyanide, or acrylonitrile, is of interest because of its similarity to the vinyl halides, some of which have been investigated previously by microwave spectroscopic techniques.[1-3]

The high sensitivity of the microwave spectrograph employing Stark effect modulation permits ready location and measurement of the lines in the rotational spectrum as well as a quantitative study of the Stark effect. On the other hand, the somewhat superior resolution of the direct absorption spectrograph makes possible the observation of the closely spaced hyperfine components of some of the lines.

The direct absorption spectrograph used in this work has been described previously.[4] The Stark spectrograph has as the absorption cell a nine-foot section of copper K-band wave guide. The central electrode is a brass strip supported and insulated from the wave guide by Teflon runners. The modulation source is a 100 kc/sec, variable voltage, zero-based square-wave generator. The absorption signal is amplified by a National HRO receiver and displayed on an oscilloscope screen. Frequency measurements are made with a crystal-controlled frequency standard which is monitored by comparison with the 10-megacycle signal from station WWV.

TABLE I. Vinyl cyanide $J=2\rightarrow3$ rotational spectrum.

Transition	Frequency
$2_{12}\rightarrow3_{13}$	27 767.45±0.10 Mc/sec
$2_{02}\rightarrow3_{03}$	28 441.60±0.10
$2_{21}\rightarrow3_{22}$	28 457.1 ±0.2
$2_{20}\rightarrow3_{21}$	28 470.7 ±0.2
$2_{11}\rightarrow3_{12}$	29 139.27±0.10

ROTATIONAL SPECTRUM

The frequencies of the $J=2\rightarrow3$ lines are given in Table I.

Tentative identification of the lines was made by computation of a predicted spectrum, using the following molecular parameters estimated on the basis of known values in analogous molecules: C−H=1.09A, C−C=1.46, C=C=1.38, C≡N=1.16, all angles 120°. Principal moments of inertia of 20, 169, and 189×10^{-40} g-cm² are thus obtained. The observed spectrum is nearly identical in pattern with the predicted spectrum, being displaced as a whole toward higher frequency by about 400 Mc/sec. Qualitative observations of the relative intensities were in agreement with the tentative assignment. It was observed that all lines listed in Table I were intensified when the wave guide containing the gas sample was cooled to dry ice temperature, while other lines appearing at room temperature in this frequency range became less intense or disappeared. Positive identification was made by using two of the observed frequencies, together with the assumption that the molecule is planar, to calculate the frequencies of the remaining lines.

TABLE II. Vinyl cyanide rotational constants.

$a=49\,076.2$ Mc/sec	$I_a=17.09463\times10^{-40}$ g-cm²
$b=4971.33$	$I_b=168.7555$
$c=4514.05$	$I_c=185.8507$
$\kappa=-0.979477$	$I_a+I_b=185.8501$
$\delta=0.0102615$	

In Table II are listed the rotational constants, moments of inertia, and asymmetry parameters. The constants appearing in the table were calculated from the spectrum without the assumption of planarity and disregarding the small quadrupole effect. Since for a rigid planar molecule the sum of the two in-plane moments is equal to the third moment, the close agreement of I_a+I_b with I_c confirms the validity of a planar model of the molecule.

* This work was sponsored in part by the Office of Ordnance Research, U. S. Army.

† Present address: Southern Research Institute, Birmingham, Alabama.

[1] J. H. Goldstein and J. K. Bragg, Phys. Rev. **75**, 1453 (1949).
[2] C. D. Cornwell, J. Chem. Phys. **18**, 1118 (1950).
[3] J. K. Bragg and A. H. Sharbaugh, Phys. Rev. **77**, 148 (1950).
[4] J. W. Simmons and J. H. Goldstein, J. Chem. Phys. **20**, 122 (1952).

STARK EFFECT

The Stark effect for the $2_{12}\rightarrow 3_{13}$, $2_{02}\rightarrow 3_{03}$, and $2_{11}\rightarrow 3_{12}$ lines is second order. That for the $2_{21}\rightarrow 3_{22}$ and $2_{20}\rightarrow 3_{21}$ lines is strong—probably approximately linear since these transitions arise from near-degenerate energy levels.[5] Quantitative Stark effect measurements were made on the $2_{12}\rightarrow 3_{13}$ and $2_{11}\rightarrow 3_{12}$ lines, the $m=\pm 1$ and $m=\pm 2$ components of each line being observed at various fields. The maximum separation from the undisplaced line for which measurements were made was about 135 Mc/sec for the $m=\pm 2$ component and about 80 Mc/sec for $m=\pm 1$. The Stark components were fairly sharp, and the error in measuring the separation was probably not more than 1 percent of the observed frequency difference in most cases. The field applied to the gas sample was measured with a peak-reading voltmeter which was calibrated against a 60-cy source. The calibration was checked by observation of the Stark effect for OCS, the dipole moment of which is accurately known.[6] The final field measurements were accurate to about 2 percent, and consequently the uncertainty in the value of the field is the limiting factor in the accuracy of the dipole moment determination.

The dipole moment was computed by the method of Golden and Wilson.[5] Since the components of the moment along the principal axes of inertia are obtained, the orientation as well as the magnitude of the moment μ can be determined. Calculation based on the Stark effect for the $2_{11}\rightarrow 3_{12}$ and $2_{12}\rightarrow 3_{13}$ lines yielded the following average values for the dipole moment and its components for the molecule in its ground vibrational state: $\mu=3.89\pm 0.08d$, $\mu_a=3.68$, $\mu_b=1.25$. The value of μ agrees very closely with that of 3.88 obtained by Hurdis and Smyth[7] from dielectric constant measurements on the vapor. Their measurement of course includes the effect of vibrational excitation of some of the molecules, but it is not surprising that the effect on the average dipole moment should be less than the experimental error in the present result. The fact that the observed moment of vinyl cyanide is only 0.11 less than the value of 4.00 reported for ethyl cyanide,[7] appears to confirm the conclusion of Hurdis and Smyth that the resonance structure which places positive charge on the nitrogen atom is of less importance than the similar vinyl chloride structure which places positive charge on the chlorine. Vinyl chloride[8] has a dipole moment of 1.44 compared with 1.98 for ethyl chloride.[9]

The use of comparative values of dipole moments to draw conclusions concerning resonance involving a particular bond must be viewed with some caution if, as in the case of the vinyl compounds, the dipole moment is not required by molecular symmetry to coincide in direction with the bond under consideration. The present result can be used to show that in the case of vinyl cyanide such a comparison with the moment of ethyl cyanide is justifiable. The principal moment calculation fixes the angle between the axis of least moment of inertia and the C≡N bond direction as 17°. This is probably within ±2° of the true value in view of the close similarity of the observed and predicted spectra. The calculated components of the dipole moment fix the angle between the axis of least moment of inertia and the dipole moment as 18.5° with an uncertainty of about ±3°. Thus it may be concluded that, within the limits of experimental error, the direction of the dipole moment coincides with that of the C≡N bond.

[5] S. Golden and E. B. Wilson, J. Chem. Phys. **16**, 669 (1948).
[6] R. G. Shulman and C. H. Townes, Phys. Rev. **77**, 500 (1950).
[7] E. C. Hurdis and C. P. Smyth, J. Am. Chem. Soc. **65**, 89 (1943).
[8] Hugill, Coop, and Sutton, Trans. Faraday Soc. **34**, 1518 (1938).
[9] J. G. Jelatis, Technical Report **7**, Office of Naval Research Contract N5 ori-78 T. O. 1. Laboratory for Insulation Research, Massachusetts Institute of Technology (1947).

TABLE III. Vinyl cyanide hyperfine structure.

Hyperfine component	$2_{21}\rightarrow 3_{22}$	$2_{20}\rightarrow 3_{21}$
2→3	+0.95±0.08 Mc/sec	+0.9±0.1
1→2	−1 (approx)	

HYPERFINE STRUCTURE

The first four lines listed in Table I were observed in the direct absorption cell, and the hyperfine structure of the $2_{21}\rightarrow 3_{22}$ and $2_{20}\rightarrow 3_{21}$ lines was partly resolved. The $F=3\rightarrow 4$ component, which is strongest, and the $2\rightarrow 3$ component, which is next strongest, could be seen for each line and their separation measured. The $1\rightarrow 2$ component of line $2_{12}\rightarrow 3_{13}$ was detected but was too indistinct for measurement. Table III gives the separation of the F component indicated in the first column from the $F=3\rightarrow 4$ component of the line.

Some information about the quadrupole coupling can be obtained from these separations, following the method previously described in the case of vinyl chloride.[1] The term χ_{bb} contributes negligibly to the observed hyperfine splitting of the $2_{21}\rightarrow 3_{22}$ line. The value of χ_{aa}, the quadrupole coupling in the direction of the axis of least moment of inertia, is found to be -3.0 ± 0.3 Mc/sec. The additional observation of a pair of peaks of the $2_{20}\rightarrow 3_{21}$ line does not permit a satisfactory determination of χ_{bb}, because its contribution to this splitting also is very small. The information obtained from the observed hyperfine structure is not sufficient for a computation of the quadrupole coupling in the bond direction. It is of interest to note the reported bond-coupling constants of −4.35 for methyl cyanide[10] and −4.20 for cyanoacteylene,[11] although a direct comparison with the present result is not possible.

The value found for χ_{aa} serves to confirm the validity of measuring the frequencies and calculating the rotational constants without regard to the quadrupole

[10] Ring, Edwards, Kessler, and Gordy, Phys. Rev. **79**, 54 (1950).
[11] A. A. Westenberg and E. B. Wilson, J. Am. Chem. Soc. **72**, 199 (1950).

effect. The $F=3\rightarrow4$ component is strongest for each line, and the observed peak of the unresolved line should very nearly coincide with the $3\rightarrow4$ hyperfine peak. This peak for the $2_{21}\rightarrow3_{22}$ line is displaced from ν_0 by -0.10 Mc/sec and by about the same amount for the $2_{20}\rightarrow3_{21}$ line. For the other lines, the hyperfine structure of which was not observable even in the direct absorption cell, the separation from ν_0 is less than half as great, as indicated by a symmetric top approximation to the quadrupole coupling.

ACKNOWLEDGMENT

The authors wish to express their appreciation to the University Center in Georgia for grants which assisted materially in the prosecution of the research described above.

THE JOURNAL OF CHEMICAL PHYSICS VOLUME 22, NUMBER 3 MARCH, 1954

Electronic Structure, Infrared Absorption, and Hall Effect in Tellurium*

HERBERT B. CALLEN, *Department of Physics, University of Pennsylvania, Philadelphia, Pennsylvania*

(Received November 16, 1953)

An analysis of the band structure of tellurium is based on the symmetry properties of a drastically simplified model of its crystal structure. These symmetry considerations lead to suggestions of the physical mechanisms underlying a variety of experimental facts in this material.

I. INTRODUCTION

SELENIUM and tellurium are intrinsic semiconductors which crystallize in hexagonal lattices. They share column VI_b of the periodic table with oxygen, sulfur, and polonium, and their free-atom configurations are $4s^2\,4p^4$ and $5s^2\,5p^4$, respectively. The crystal structure of selenium and tellurium is illustrated[1] in Fig. 1 and the lattice constants are given in Table I.

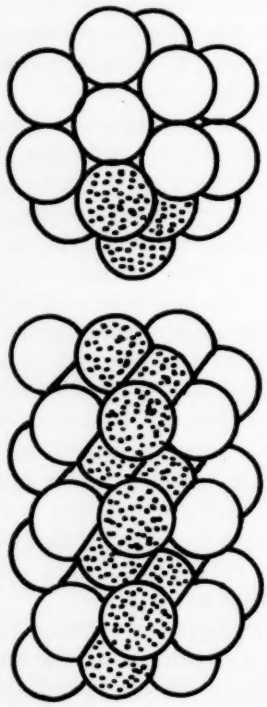

FIG. 1. Crystal structure of selenium and tellurium, after A. R. von Hippel (see reference 4).

The infrared absorption spectrum of Te, as measured by J. Loferski,[2] is indicated in Fig. 2. It will be noted that the absorption spectrum depends markedly on the polarization of the incident radiation. In particular the absorption commences at a lower frequency for radiation polarized with the electric vector perpendicular rather than parallel to the hexagonal axis.

A second significant and unique phenomenon obsevred in tellurium is the reversal in sign of the Hall coefficient, occurring at about 230°C. This reversal is distinct from the low-temperature reversal which is connected with the transition from the extrinsic to the intrinsic range; the high-temperature transition is an intrinsic property of the material. Tellurium shows a negative Hall coefficient below 230°C and a positive coefficient above this temperature.

In this paper we present a simplified discussion of the electronic band structure and thence of the optical absorption phenomena and the high-temperature Hall reversal in Te. The simplification made is the replacement of the actual hexagonal structure by a closely related tetragonal structure. The tetragonal structure contains only one atom per unit cell rather than three, and the space group consists only of translations and rotations rather than of these plus screw axes. The analysis is thereby simplified and the underlying mechanism may be more easily visualized. A more thoroughgoing analysis on the basis of the correct crystal structure is presently in progress.

The pertinent feature of the structure of selenium and tellurium is that the crystals consist of long chains of atoms, the interatomic spacing along the chains being much smaller than the interchain separation. The chains are actually puckered, with bond angles of 105.5°

* This work was supported by the U. S. Office of Naval Research under Contract Nonr 698(00).

[1] A. R. von Hippel, J. Chem. Phys. **16**, 372 (1948).

[2] J. J. Loferski, Phys. Rev. **93**, 707 (1954); see also Phys. Rev. **87**, 905 (1952).

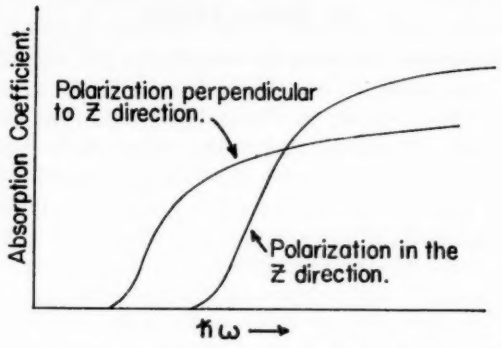

FIG. 2. Infrared absorption in tellurium (schematic).

and 102.6°, and are arranged with hexagonal symmetry in the plane perpendicular to their axes (the z axis). For simplicity we treat the chains as straight and as being arranged with square symmetry. Thus, the true crystal structure is replaced by a simple tetragonal structure.

We briefly consider the conceptual synthesis of the crystal by a quasi-static reduction of the lattice constant from some initial very large value. When the lattice constant is very large, the electronic eigenfunctions are just those of the isolated atoms. As the lattice constant is reduced, the energy eigenvalues of the isolated atoms broaden into bands, and the proper wave functions become Bloch-type linear combinations of the isolated-atom functions. The selection rules for optical transitions in the isolated atom are essentially maintained for the corresponding band-band transitions in the solid, forbidden transitions in the atoms corresponding to small band-band transition probabilities in the solid. The selection rules, in fact, are maintained precisely at the band edges (which determine the infrared absorption edge) although only approximately through the center of the band. In addition, a new selection rule appears, permitting only vertical transitions in the reduced band scheme.

II. THE POINT GROUP

The point group of the tetragonal crystal is D_{4h}; a group of order sixteen containing ten classes. The generating elements of the group are: C_4^z, a fourfold rotation about the z axis; C_2^x, a twofold rotation about an axis perpendicular to the z axis; and i, the inversion. The character system of the group is given[3] in Table II, in which the sixteen elements are classified into ten classes, heading the ten columns of the table. The ten irreducible representations fall into two types, those indicated by a subscript g, which are even under the inversion operation, and those indicated by a subscript u, which are odd under the inversion operation. There are eight one-dimensional irreducible representations and two two-dimensional irreducible representations (E_g and E_u).

TABLE I. Crystalline parameters of selineum and tellurium.

	Se	Te
a; distance between like atoms in adjacent chains	4.34 A	4.44 A
c; distance between like atoms along a chain axis	4.95 A	5.92A
distance between successive atoms in a chain	2.32 A	2.86A
bond angle	105.5°	102.6°

III. THE p BANDS

We shall now consider the manner in which the partially filled p levels of the isolated atoms broaden into bands, and, in particular, the manner in which these bands give rise to the insulating properties of selenium and tellurium. Ignoring the spin degeneracy, which plays no role in our analysis, the isolated-atom p state is threefold degenerate. From the point of view of the degeneracies determined by the point group D_{4h}, which predicts only singly or doubly degenerate levels, part of this threefold degeneracy is to be viewed as "accidental." As the lattice constant is diminished, the threefold degeneracy will be destroyed.

The angular dependence of the isolated-atom functions is known, being simply the spherical harmonics, so that these functions can easily be associated with the irreducible representations to which they belong. One of the p functions (that with azimuthal quantum number $m=0$) belongs to the irreducible representation A_{2u}; the other two belong to the two-dimensional representation E_u. Thus, the threefold degenerate p level

TABLE II. The character system of the point group D_{4h}.

	E	$(C_4^z)^2$	C_4^z $(C_4^z)^3$	C_2^x $C_2^x(C_4^z)^2$	$C_2^{x'}C_4^z$ $C_2^{x'}(C_4^z)^3$	i	$i(C_4^z)^2$	iC_4^z $i(C_4^z)^3$	iC_2^x $iC_2^x(C_4^z)^2$	$iC_2^{x'}C_4^z$ $iC_2^{x'}(C_4^z)^3$
A_{1g}	1	1	1	1	1	1	1	1	1	1
A_{1u}	1	1	1	1	1	−1	−1	−1	−1	−1
A_{2g}	1	1	1	−1	−1	1	1	1	−1	−1
A_{2u}	1	1	1	−1	−1	−1	−1	−1	1	1
B_{1g}	1	1	−1	1	−1	1	1	−1	1	−1
B_{1u}	1	1	−1	1	−1	−1	−1	1	−1	1
B_{2g}	1	1	−1	−1	1	1	1	−1	−1	1
B_{2u}	1	1	−1	−1	1	−1	−1	1	1	−1
E_g	2	−2	0	0	0	2	−2	0	0	0
E_u	2	−2	0	0	0	−2	2	0	0	0

[3] Eyring, Walter, and Kimbel, *Quantum Chemistry* (John Wiley and Sons, Inc., New York, 1944).

splits into a nondegenerate and a doubly degenerate level as the lattice constant is decreased. Furthermore, this splitting occurs before the $\psi_p(E_u)$ levels become appreciably broadened into bands. That this latter statement is true may be seen by considering the sequence of events as the lattice constant is decreased. The isolated-atom wave functions maintain their form until the wave functions of neighboring atoms begin to overlap. This first occurs for the $\psi_p(A_{2u})$ functions, which are elongated along the z axis, as indicated in Fig. 3. Because of the very close spacing of atoms along the chains relative to the spacing of atoms perpendicular to the chains, the overlap of the $\psi_p(E_u)$ levels is negligible even when the overlap of the $\psi_p(A_{2u})$ functions has become appreciable. Thus the $\psi_p(E_u)$ band remains very narrow even after the $\psi_p(A_{2u})$ band has split off and has itself begun to broaden appreciably. This situation is indicated schematically in Fig. 4.

At the true lattice spacing the doubly degenerate $\psi_p(E_u)$ band evidently lies below, and is separate from the $\psi_p(A_{2u})$ band. The four p electrons per atom completely fill the $\psi_p(E_u)$ band, whereas the $\psi_p(A_{2u})$ band, and the various d bands, are completely empty. Thus, the insulating property of these crystals can be understood on the basis of the symmetry properties of the crystal structure.

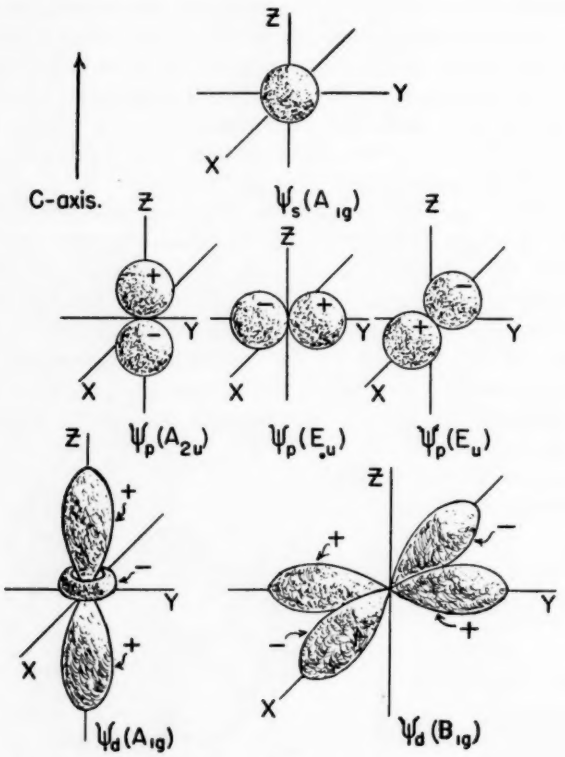

FIG. 3. Symmetry properties of the isolated atom wave functions. $\psi_d(B_{2g})$ is similar to $\psi_d(B_{1g})$, but is rotated $-45°$ about the z axis. The two $\psi_d(E_g)$ functions are similar to $\psi_d(B_{2g})$, but lie in the $x-z$ and $y-z$ planes rather than in the $x-y$ plane.

IV. THE d BANDS

Having now analyzed the behavior of the p bands, we turn our attention to the empty d bands which lie above. The d levels in the isolated atom are fivefold degenerate. Consideration of the appropriate spherical harmonics associated with the isolated atom functions yields their symmetry behavior under the generating elements of D_{4h}. The functions are illustrated in Fig. 3. Thus, one function belongs to the irreducible representation A_{1g}, one function to B_{1g}, one to B_{2g}, and a pair of functions belong to the two-dimensional representation E_g. The fivefold degenerate d level, therefore, splits into three nondegenerate bands and one doubly degenerate band. These d bands certainly overlap in the real crystal, and almost certainly overlap also with $\psi_p(A_{2u})$ band. They apparently do not overlap the $\psi_p(E_u)$ band.

V. THE SELECTION RULES

The transition probability between an initial state ψ_i and a final state ψ_f induced by an incident light wave with electric vector in the direction of the unit vector $\boldsymbol{\varepsilon}_0$ is proportional to $|\langle\psi_f|\,\boldsymbol{\varepsilon}_0\cdot\nabla\,|\psi_i\rangle|^2$. The integrand belongs to the direct product of the representations of ψ_f, ψ_i and of the operator $\boldsymbol{\varepsilon}_0\cdot\nabla$. This direct product will generally be a reducible representation, and the integral will vanish unless it contains the totally symmetric irreducible representation A_{1g}. Alternatively stated, the matrix element of a transition will vanish unless the direct product of the representations of ψ_i and $\boldsymbol{\varepsilon}_0\cdot\nabla$ contains that representation to which ψ_f belongs.

We shall be particularly interested in the transition probabilities induced by light polarized in the z direction and by light polarized perpendicular to the z direction. For light polarized in the z direction the operator $\boldsymbol{\varepsilon}_0\cdot\nabla$ has the symmetry of the z coordinate, and consequently belongs to the representation A_{2u}. For light polarized perpendicular to the z axis the operator $\boldsymbol{\varepsilon}_0\cdot\nabla$ has the symmetry of x or y and consequently belongs to the representation E_u.

For transitions in which an electron is excited from the highest filled band to one of the empty conduction bands, the initial state is $\psi_p(E_u)$. The direct product of E_u and A_{2u} is E_g, whereas the direct product of E_u and E_u is $A_{1g}+A_{2g}+B_{1g}+B_{2g}$. Thus, light polarized in the z direction can excite an electron from the $\psi_p(E_u)$ state to a final state belonging only to the representation E_g, that is, only to the state $\psi_d(E_g)$. Light polarized perpendicular to the z direction can excite an electron from the $\psi_p(E_u)$ state to a final state belonging to any of the representations A_{1g}, A_{2g}, B_{1g}, or B_{2g}, that is, to the states $\psi_d(A_{1g})$, $\psi_d(B_{1g})$, or $\psi_d(B_{2g})$. It is interesting to note that the empty $\psi_p(A_{2u})$ band cannot be reached by either polarization of the incident light.

As the above selection rules indicate that the electron is excited into entirely different d bands by the two polarizations of the incident light, the dependence of

absorption on polarization indicated in Fig. 2 is readily explained. The fact that the absorption commences at a lower frequency for light polarized perpendicular to the z axis indicates that at least one of the three nondegenerate d bands lies lower than the doubly degenerate $\psi_d(E_g)$ band. Inspection of the forms of the various d orbitals, as shown in Fig. 3, indicates that the nondegenerate $\psi_d(A_{1g})$ band may, in fact, be expected to be the lowest lying of the d bands. Two of the nondegenerate d functions have the form of four coplanar lobes lying in the $x-y$ plane; the doubly degenerate orbitals have the form of four coplanar lobes lying in the $x-z$ and $y-z$ planes; the $\psi_d(A_{1g})$ orbital is elongated along the z axis. Because of these shapes the overlap of the $\psi_d(A_{1g})$ orbitals may be expected to be particularly large, and the $\psi_d(A_{1g})$ band may be expected to be particularly wide. Thus, the lower limit of the various overlapping d bands is evidently determined by the $\psi_d(A_{1g})$ band. The fact that the infrared absorption edge for x polarization lies at a lower frequency than that for z polarization is a direct consequence of this band structure.

VI. THE EFFECT OF TEMPERATURE ON THE BAND STRUCTURE

The coefficient of thermal expansion of crystalline tellurium has been measured by P. Bridgman.[4] The coefficient is anisotropic and has a value of -1.6×10^{-6}/°C parallel to the z axis and a value of 27.2×10^{-6}/°C perpendicular to the z axis. Thus, the crystal expands perpendicularly to the z axis on heating, and suffers only a negligible anomolous contraction along the z axis. As the temperature is raised, we may, therefore, expect a narrowing of those bands which arise from orbitals elongated perpendicular to the z axis, and a negligible change in the width of those bands arising from functions elongated parallel to the z axis. In particular, the filled p band and the upper d bands will narrow, whereas the empty p band and the low-lying $\psi_d(A_{1g})$ band will remain essentially unaffected.

The thermal activation energy of tellurium appears to be equal to the lower of the two optical activation energies,[5,6] although the experimental evidence is not definitive on this point. We may, consequently, assume that at room temperature the $\psi_d(A_{1g})$ band is the lowest-lying conduction band. It follows then, from our discussion above, that the thermal activation energy should increase with temperature, and this prediction is indeed in agreement with experiment.

VII. THE EFFECT OF PRESSURE ON THE BAND STRUCTURE

Bridgman[4] has measured the compressibility of tellurium under hydrostatic pressure and has found an anomalous expansion parallel to the z axis and a normal contraction perpendicular to the z axis. Along the z axis the linear compressibility is $^{\Delta l}/_{l})_z=4.137\times10^{-7}p-9.6\times10^{-12}p^2$ (p in kg/cm^2), whereas perpendicular to the z axis the linear compressibility is $^{\Delta l}/_{l})_x=-27.48\times10^{-7}p+52.7\times10^{-12}p^2$. Thus an increase in pressure widens the filled p band and the upper d bands and narrows the empty p band and the low-lying d band. In terms of Fig. 4 the effect of pressure is to translate to the left as far as the filled p band is concerned and to translate to the right as far as the $\psi_d(A_{1g})$ band is concerned. We thus predict a decrease in the thermal activation energy with increasing pressure, and this again is in agreement with experiment.[7]

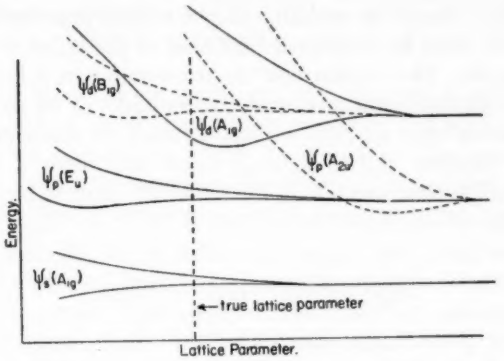

FIG. 4. Schematic energy band structure. The $\psi_d(B_{2g})$ and $\psi_d(E_g)$ bands are not shown, but are roughly like the $\psi_d(B_{1g})$ band.

VIII. THE HIGH-TEMPERATURE REVERSAL OF THE HALL COEFFICIENT

As the temperature is increased, the Hall coefficient of tellurium is observed to change from a negative to a positive sign at about 230°C. The reversal occurs entirely within the intrinsic temperature range and does not seem to be associated with impurities (which cause a second reversal at lower temperatures). The effect is not observed in selenium, which melts before becoming intrinsic.

The sign of the Hall coefficient is determined by the sign of the carrier with the largest mobility, or smallest effective mass. Thus, if the effective mass of the electron is smaller than that of the hole, the electronic mobility will predominate and the Hall coefficient will be negative. This is apparently the case below 230°C. We then seek a mechanism whereby the mobility of the hole will be increased relative to that of the electron as the temperature increases, the hole mobility exceeding the electronic mobility above about 230°C.

We have seen that an increase of temperature causes the filled p band to narrow. As this is the band in which the holes move, we therefore see that increasing temperature increases the effective mass of the holes and decreases their mobility. This effect, of course, is opposite to that required to explain the high-temperature Hall reversal.

[4] P. W. Bridgman, Proc. Am. Acad. Arts Sci. **60**, 303 (1925).
[5] V. E. Bottom, Science **115**, 570 (1952).
[6] T. Fukoroi, Tohoku Univ. Research Inst. Sci. Repts. **A3**, 175 (1951).
[7] J. Bardeen, Phys. Rev. **75**, 1777 (1949).

The change in mobility of the conduction electrons, which must be compared with that of the holes, is more complex. The conduction electrons move in a band of complicated structure, and the mobility of an electron depends upon its position in the band. An electron near the bottom of the $\psi_d(A_{1g})$ band will have a larger mobility than one which is sufficiently high to be in the region of overlap with the other d bands. As the temperature increases, a greater fraction of the electrons will exist in the upper portions of the d band, and the average electronic mobility will consequently decrease. This effect presumably dominates the aforementioned decrease in the hole mobility and leads to the high-temperature Hall reversal.

The above-mentioned mechanism has been previously suggested by Fukuroi and Tanuma[8] on a phenomenological basis.

[8] T. Fukuroi and S. Tanuma, Tohoku Univ. Research Inst. Sci. Repts. A4, 353 (1952).

IX. THE EFFECT OF PRESSURE ON THE HALL REVERSAL TEMPERATURE

As a means of further testing of the ideas developed in this paper, the author suggested to Mr. A. Nussbaum the desirability of measurement of the dependence on pressure of the temperature of the Hall reversal. The prediction of our model is clear. Increasing pressure widens the filled p band and thereby increases the hole mobility. On the other hand, the application of pressure narrows the $\psi_d(A_{1g})$ band and decreases the electron mobility. These effects tend to make the Hall effect positive at a given temperature, or to lower the temperature of the Hall inversion. In a paper to be published in *The Physical Review*, Mr. Nussbaum describes the results of the pressure measurements, which do exhibit a reduction of the Hall inversion temperature in agreement with our predictions.

THE JOURNAL OF CHEMICAL PHYSICS VOLUME 22, NUMBER 3 MARCH, 1954

The Intermolecular Potentials of Helium and Hydrogen*

EDWARD A. MASON† AND WILLIAM E. RICE‡
Naval Research Laboratory, Department of Chemistry, University of Wisconsin, Madison, Wisconsin
(Received October 8, 1953)

The parameters for helium and hydrogen of the "exp-six" potential,

$$\varphi(r)=\frac{\epsilon}{1-6/\alpha}\left[\frac{6}{\alpha}e^{\alpha(1-r/r_m)}-\left(\frac{r_m}{r}\right)^6\right],$$

have been calculated by use of experimental values of the second virial coefficients and viscosity coefficients. Because of the uncertainty of the quantum corrections, no low temperature data were used in determining the parameters. The exp-six potential is able to reproduce both the second virial and the viscosity coefficients within experimental error, and is thus an improvement over the simpler Lennard-Jones (12-6) potential. In addition, other transport properties are accurately predicted. A combination rule is suggested for calculation of the exp-six potential between two unlike molecules from the potentials between two pairs of like molecules, and is used to calculate a number of properties of helium-hydrogen mixtures with satisfactory results.

I. INTRODUCTION

RECENTLY, the transport property collision integrals and the second virial coefficients have been evaluated[1,2] for gases whose molecules obey an "exp-six" intermolecular potential

$$\varphi(r)=\frac{\epsilon}{1-6/\alpha}\left[\frac{6}{\alpha}e^{\alpha(1-r/r_m)}-\left(\frac{r_m}{r}\right)^6\right], \quad (1)$$

where $\varphi(r)$ is the potential energy of two molecules at a separation distance r, ϵ is the depth of the potential energy minimum, r_m is the position of the minimum, and α is a parameter which is a measure of the steepness of the repulsion energy. The form of this potential has some theoretical justification in that the inverse sixth power term represents the leading term in the expression for the attractive London dispersion potential, and the exponential term is indicated by quantum-mechanical calculations of the repulsive potential between molecules. The representation of the total intermolecular potential by Eq. (1) is, however, probably to be considered semiempirical at best. The parameters ϵ, r_m, and α may be determined for a particular gas by comparison of the experimentally observed transport properties and second virial coefficients with the theoretical tabulations given in references 1 and 2. The best previous potential

* This work was supported in part by contract N7onr-28511 with the U. S. Office of Naval Research.
† National Research Fellow, 1952–1953. Present address: Department of Chemistry, Pennsylvania State University, State College, Pennsylvania.
‡ Present address: Experiment Incorporated, Richmond, Virginia.
[1] E. A. Mason, J. Chem. Phys. **22**, 169 (1954).
[2] W. E. Rice and J. O. Hirschfelder, J. Chem. Phys. **22**, 187 (1954).

for which similar theoretical calculations have been performed is of the Lennard-Jones (12-6) form

$$\varphi(r)=\epsilon\left[\left(\frac{r_m}{r}\right)^{12}-2\left(\frac{r_m}{r}\right)^{6}\right], \tag{2}$$

where $\varphi(r)$, ϵ, and r_m are as defined in connection with Eq. (1). This potential has had some success in correlating transport properties and compressibilities of simple gases, but has not been completely satisfactory for a number of gases. Two particular cases are helium and hydrogen, in which it appears that the intermolecular repulsion is actually "softer" than indicated by an inverse twelfth power. In the present paper we report the analysis of the available experimental data on these two gases to determine the appropriate values of the parameters of Eq. (1), and a discussion of the ability of this potential form to correlate the properties of these gases.

II. DETERMINATION OF POTENTIAL PARAMETERS

Several different methods are available for the determination of the potential parameters from experimental results on compressibilities[3–6] and transport properties.[6–9] The method we have used is an adaptation of the Keesom and Lennard-Jones procedure[3] for the second virial coefficient. It is simple, accurate, and permits the simultaneous fit of several different gas properties with relatively little calculation. We have applied this method to experimental second virial coefficient and viscosity data to evaluate the potential parameters for helium and hydrogen. Data are also available on the other transport properties of thermal conductivity, self-diffusion, and thermal diffusion, but these data are usually rather scanty and of poor accuracy compared with those on viscosity, and we have not used them directly in assigning potential parameters. However, they serve as a check on the parameters determined from the second virial coefficient and viscosity.

The method used is as follows:

The second virial coefficient $B(T)$ of a pure gas is given by

$$B(T)=b_m B^*(\alpha,T^*), \tag{3}$$

with

$$b_m=(2\pi N_0/3)r_m^3, \tag{4}$$

and

$$T^*=kT/\epsilon, \tag{5}$$

where N_0 is the Avogadro number, k is the Boltzmann constant, T is the absolute temperature, and α, r_m, and ϵ are the parameters given in Eq. (1). The quantity $B^*(\alpha,T^*)$ is tabulated in reference (2) as a function of T^* for several values of α. Taking logarithms of Eqs. (3) and (5), we obtain

$$\log B(T)=\log B^*(\alpha,T^*)+\log b_m, \tag{6}$$

$$\log T=\log T^*+\log(\epsilon/k). \tag{7}$$

A plot of the tabulated quantities $\log B^*(\alpha,T^*)$ *vs* $\log T^*$ yields a family of curves, one for each value of α. From Eqs. (6) and (7) it is seen that a plot of the experimental quantities $\log B(T)$ *vs* $\log T$ should be superposable by parallel translation of axes on one of the theoretical curves, and that $\log b_m$ is directly determined by the amount of translation parallel to the B axis, and $\log(\epsilon/k)$ by the amount of translation parallel to the T axis. The parameter r_m is then found from Eq. (4), and the third parameter α has of course already been determined by the decision to superpose the experimental plot on a particular one of the family of theoretical curves.

An analogous procedure may be used to determine α, r_m, and ϵ from experimental viscosity measurements. In practical units, the viscosity η of a pure gas is given by

$$10^7\eta=\frac{266.93(MT)^{\frac{1}{2}}}{r_m^2}\,\frac{f_\eta^{(3)}(\alpha,T^*)}{\Omega^{(2,2)*}(\alpha,T^*)}, \tag{8}$$

where η is the viscosity in grams-cm^{-1}-sec^{-1}, M is the molecular weight, r_m is in angstroms, and $f_\eta^{(3)}(\alpha,T^*)$ and $\Omega^{(2,2)*}(\alpha,T^*)$ are dimensionless functions which may be obtained from the tabulations in reference 1. Taking logarithms of Eqs. (8) and (5), we obtain

$$\log\frac{10^7\eta}{(MT)^{\frac{1}{2}}}=\log\frac{f_\eta^{(3)}}{\Omega^{(2,2)*}}+\log(266.93)-2\log r_m, \tag{9}$$

$$\log T=\log T^*+\log(\epsilon/k).$$

As with the second virial coefficient, a plot of the theoretical quantities $\log[f_\eta^{(3)}/\Omega^{(2,2)*}]$ *vs* $\log T^*$ yields a family of curves, over one of which may be superposed by parallel translation of axes the plot of the experimental quantities $\log[10^7\eta/(MT)^{\frac{1}{2}}]$ *vs* $\log T$. The amount of translation along the η axis determines $\log r_m$, the amount of translation along the T axis determines $\log(\epsilon/k)$, and the decision to superpose on a particular theoretical curve determines α.

The above procedures were carried out for helium and hydrogen. Most of the experimental viscosity values were determined relative to the viscosity of air, and it was necessary to reduce them to a common basis. For this purpose the viscosity of air was taken as $\eta=1833.0$

[3] W. H. Keesom, Leiden Comm. Suppl. No. **25**, (1912); J. E. Lennard-Jones, Proc. Roy. Soc. (London) **A106**, 463 (1924).
[4] R. A. Buckingham, Proc. Roy. Soc. (London) **A168**, 264 (1938).
[5] W. H. Stockmayer and J. A. Beattie, J. Chem. Phys. **10**, 476 (1942).
[6] Hirschfelder, Curtiss, Bird, and Spotz, *The Molecular Theory of Gases and Liquids*. (John Wiley and Sons, Inc., New York, 1954), Chapters 3 and 8.
[7] H. R. Hassé and W. R. Cook, Phil. Mag. **3**, 977 (1927); Proc. Roy. Soc. (London) **A125**, 196 (1929).
[8] E. Whalley and W. G. Schneider, J. Chem. Phys. **20**, 657 (1952).
[9] Amdur, Ross, and Mason, J. Chem. Phys. **20**, 1620 (1952).

$\times 10^{-7}$ g-cm^{-1}-sec^{-1} at 23°C, following Johnston and McCloskey.[10] None of the necessary corrections were as large as one percent. It should be pointed out that neither the viscosity data nor the second virial coefficient data alone are sufficient to determine three potential parameters uniquely for either helium or hydrogen, but that both properties must be considered together. For example, the parameter α may be assigned uniquely on the basis of the viscosity results, but a number of different pairs of values of the parameters ϵ and r_m would serve equally well to fit the experimental points. On the other hand, the second virial coefficients have not been measured accurately over a sufficiently wide temperature range to enable a unique assignment of the parameter α to be made.

The determination of the potential parameters for helium and hydrogen is complicated by the fact that these gases exhibit large quantum deviations. Even at room temperature the quantum correction to the second virial coefficient of hydrogen amounts to several percent. Kirkwood[11] and Uhlenbeck and Beth[12] have shown that for the second virial coefficient the quantum deviations may be expressed as an infinite series in powers of h^2, where h is Planck's constant. For the exp-six potential, the expression for the second virial coefficient including quantum corrections may be written as

$$\begin{aligned} B(T) &= B_{cl}(T)+h^2B_I(T)+h^4B_{II}(T)+\cdots, \\ &= b_m[B^*(\alpha,T^*)+(\Lambda^2/T^*)B_I^*(\alpha,T^*) \\ &\quad +(\Lambda^2/T^*)^2B_{II}^*(\alpha,T^*)+\cdots], \end{aligned} \tag{10}$$

where $B(T)$, b_m, $B^*(\alpha,T^*)$, and T^* are as defined in connection with Eqs. (3)–(5), Λ is the dimensionless group $h/[r_m(m\epsilon)^{\frac{1}{2}}]$, where m is the mass of one molecule, and $B_I^*(\alpha,T^*)$ and $B_{II}^*(\alpha,T^*)$ are integrals involving the intermolecular potential, $\varphi(r)$. The convergence of this series is poor except when (Λ^2/T^*) is small and hence it cannot be used at low temperatures for helium and hydrogen. The integrals B_I^* and B_{II}^* have not been evaluated for the exp-six potential, but B_I^* has been calculated for the Buckingham-Corner potential.[13] This potential differs from Eq. (1) only for $r<r_m$, in which region the inverse sixth power term is multiplied by an exponential term to prevent $\varphi(r)$ from becoming negative for very small values of r. Thus, in the region of the minimum, the exp-six and the Buckingham-Corner potentials are nearly identical, and since this portion of the potential contributes strongly to $B(T)$ at temperatures low enough for quantum deviations to be appreciable, it seems reasonable to use the tables of Buckingham and Corner to determine the first quantum correction, $b_m(\Lambda^2/T^*)B_I^*$, for the exp-six potential. The first quantum correction is tabulated in reference (13) as the function $F_1(\alpha,x)$, given as

$$F_1(\alpha,x)=(2\pi/3)B_I^*(\alpha,T^*), \tag{11}$$

where $x=1/T^*$.

Inclusion of the quantum correction necessitates a small change in the curve-fitting procedure outlined above for determining the potential parameters ϵ, r_m, and α from experimental values of $B(T)$. The quantity Λ is first assumed to be zero, and the method of translation of axes applied to obtain a first approximation to ϵ, r_m, and α. From these values a first approximation to Λ is calculated, which is substituted into Eqs. (10) and (11), and the entire procedure repeated to obtain second approximations to ϵ, r_m, and α. A new value of Λ is then calculated, and the procedure repeated until Λ no longer varies appreciably. It turns out that the first quantum corrections for helium and hydrogen calculated in this way are very nearly equal to those calculated for these gases by de Boer and Michels[14] according to the Lennard-Jones (12-6) potential given in Eq. (2). It therefore seems reasonable to make the assumption that the second quantum corrections, $b_m(\Lambda^2/T^*)^2B_{II}^*$, are also nearly equal for the two potentials, and to take the small values of the second quantum corrections from the tabulations of de Boer and Michels. The lack of exact values for the second quantum correction limits the usable temperature region to values above 60°K for helium and above 120°K for hydrogen.

The quantum deviations for the transport properties may also be expressed as a power series in h^2, as shown by de Boer and Bird.[15,16] In this case, unfortunately, very few numerical calculations have been made, so the best we can do at present is to obtain a rough estimate of the temperature range for which quantum deviations from the transport properties are negligible. The reduced collision integral for viscosity, $\Omega^{(2,2)*}(\alpha,T^*)$, which is given in Eq. (8), may be modified to include quantum effects as follows:

$$\begin{aligned} \Omega^{(2,2)*}(\alpha,T^*) &= \Omega_{cl}^{(2,2)*}(\alpha,T^*) \\ &\quad +(\Lambda^2/T^*)\Omega_I^{(2,2)*}(\alpha,T^*)+\cdots, \end{aligned} \tag{12}$$

where $\Omega_{cl}^{(2,2)*}$ is the classical contribution to the total reduced collision integral, tabulated in reference 1, Λ and T^* are as previously defined, and $\Omega_I^{(2,2)*}$ is a very complicated integral involving the intermolecular potential. The only potential for which $\Omega_I^{(2,2)*}$ has been evaluated[16] is

$$\varphi(r)=\epsilon\left(\frac{r_m}{r}\right)^{12}, \tag{13}$$

which is the form assumed by the Lennard-Jones (12-6) potential of Eq. (2) when there is no intermolecular attraction. Since in helium and hydrogen the intermolecular attraction is small, it seems reasonable to use Eq. (13) to obtain a rough estimate of the quantum

[10] H. L. Johnston and K. E. McCloskey, J. Phys. Chem. 44, 1038 (1940).
[11] J. G. Kirkwood, Phys. Rev. 44, 31 (1933).
[12] G. E. Uhlenbeck and E. Beth, Physica 3, 729 (1936).
[13] R. A. Buckingham and J. Corner, Proc. Roy. Soc. (London) A189, 118 (1947).
[14] J. de Boer and A. Michels, Physica 5, 945 (1938).
[15] J. de Boer and R. B. Bird, Phys. Rev. 83, 1259 (1951).
[16] See reference 6, Chapter 10.

corrections, using the values of ϵ and r_m for the Lennard-Jones (12-6) potential found by de Boer and Michels[14] from analysis of second virial coefficients. In this way it is found that the quantum deviations of the viscosity, thermal conductivity, and self-diffusion are less than about 0.6 percent for temperatures above 200°K and 250°K for helium and hydrogen, respectively.

The values of the potential parameters of the exp-six potential and the quantum-mechanical parameter Λ for helium and hydrogen found by the above procedure are given in Table I. Also included are the values of these quantities for the Lennard-Jones (12-6) potential as found by de Boer and Michels[14] and revised by Lunbeck.[17] These Lennard-Jones parameters have been shown to give reasonable agreement with experiment on helium for very low temperature second virial coefficients,[18] viscosities, and thermal conductivities,[19] and for higher temperature viscosities and thermal conductivities,[20] as well as reasonable agreement on hydrogen for very low temperature second virial coefficients and viscosities,[21] and higher temperature viscosities.[20] Thus, these are probably the best Lennard-Jones parameters available for helium and hydrogen.

III. COMPARISON WITH EXPERIMENT

A check on the validity of using the parameters determined for the exp-six potential to calculate the first quantum correction for the second virial coefficient from the tables for the Buckingham-Corner potential may be obtained from a consideration of hydrogen and deuterium. Since the intermolecular potential for hydrogen is the same as that for deuterium,[14,22,23] the virial coefficients of hydrogen and deuterium differ only because of quantum effects, and we therefore obtain from Eq. (10) the relation

$$B(H_2)-B(D_2)=(b_m/T^*)[\Lambda^2(H_2)-\Lambda^2(D_2)]B_I^*(\alpha,T^*)+\cdots, \quad (13)$$

TABLE I. Potential parameters for the exp-six and Lennard-Jones (12-6) potentials for helium and hydrogen, and the quantum-mechanical parameter $\Lambda=h/[r_m(m\epsilon)^{\frac{1}{2}}]$.

	Helium		Hydrogen	
	Exp-six	L.-J. (12-6)	Exp-six	L.-J. (12-6)
α	12.4	...	14.0	...
r_m, A	3.135	2.869	3.337	3.287
ϵ/k, °K	9.16	10.22	37.3	37.0
Λ	2.305	2.385	1.512	1.541

[17] R. J. Lunbeck, dissertation, Amsterdam (1951), has revised the parameters found by de Boer and Michels to take account of more recent values of the fundamental constants k, N_0, and h. See reference 6 for a compilation of these revised parameters.

[18] J. de Boer and A. Michels, Physica **6**, 409 (1939).

[19] J. de Boer, Physica **10**, 348 (1943).

[20] J. de Boer and J. van Kranendonk, Physica **14**, 442 (1948).

[21] R. Miyako, Proc. Phys.-Math Soc. (Japan) **24**, 852 (1942).

[22] A. B. van Cleave and O. Maass, Can. J. Research **B13**, 384 (1935).

[23] Woolley, Scott, and Brickwedde, J. Research Natl. Bur. Standards **41**, 379 (1948), have summarized most of the evidence for this conclusion.

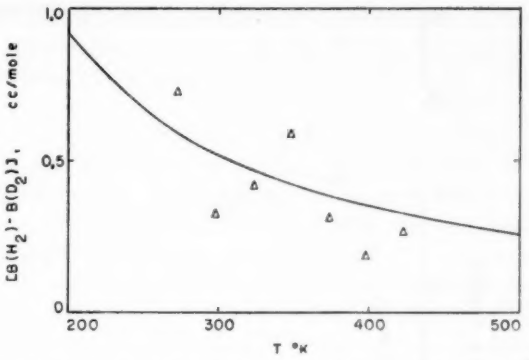

FIG. 1. Comparison of experimental and theoretical values of the quantum correction to the second virial coefficient of hydrogen. The experimental points are from the data of Michels and Goudeket (reference 24); the calculated curve is from the tables of Buckingham and Corner (reference 13) using the parameters of Table I.

where $B(H_2)$ and $B(D_2)$ are the second virial coefficients, and $\Lambda(H_2)$ and $\Lambda(D_2)$ are the quantum-mechanical parameters for hydrogen and deuterium. In Fig. 1 we plot the values of $[B(H_2)-B(D_2)]$ as a function of temperature as found from the compressibility measurements of Michels and Goudeket,[24] along with the theoretical curve obtained from Buckingham and Corner's tables by using the exp-six potential parameters in Table I. The agreement between theory and experiment provides some justification for our procedure. It is true that the theoretical curve was obtained under the assumption that hydrogen and deuterium could be considered as spherical molecules, but de Boer[25] has shown that the values of $[B(H_2)-B(D_2)]$ calculated in this way do not differ significantly from the values obtained when hydrogen and deuterium are treated as nonspherical diatomic molecules.

A. Helium

To illustrate the suitability of the exp-six form for describing the intermolecular potential of helium, we have used the potential parameters listed in Table I to calculate a number of properties of gaseous helium for comparison with experimental results. Second virial coefficients of helium have been compared from 65.2° to 1473.2°K. Figure 2 shows a comparison of calculated and experimental[26] values; also shown in the figure is the

[24] A. Michels and M. Goudeket, Physica **8**, 347, 353 (1941). We have used the second virial coefficients obtained by fitting the experimental PV values between 9 and 32 atmos with a quadratic series in the density.

[25] J. de Boer, Physica **10**, 357 (1943).

[26] J. D. A. Boks and H. K. Onnes, Leiden Comm. **170a** (1924); L. Holborn and J. Otto, Z. Physik **10**, 367 (1922); **23**, 77 (1924); **33**, 1 (1925); **38**, 359 (1926); G. P. Nijhoff and W. H. Keesom, Leiden Comm. **188b** (1927); Nijhoff, Keesom, and Iliin, **188c** (1927); Gibby, Tanner, and Masson, Proc. Roy. Soc. (London) **A122**, 283 (1929); A. Michels and H. Wouters, Physica **8**, 923 (1941); W. G. Schneider and J. A. H. Duffie, J. Chem. Phys. **17**, 751 (1949); J. L. Yntema and W. G. Schneider, **18**, 641 (1950). The results of Gibby, Tanner, and Masson are not shown in Fig. 1 because they are essentially duplicated by those of Michels and Wouters.

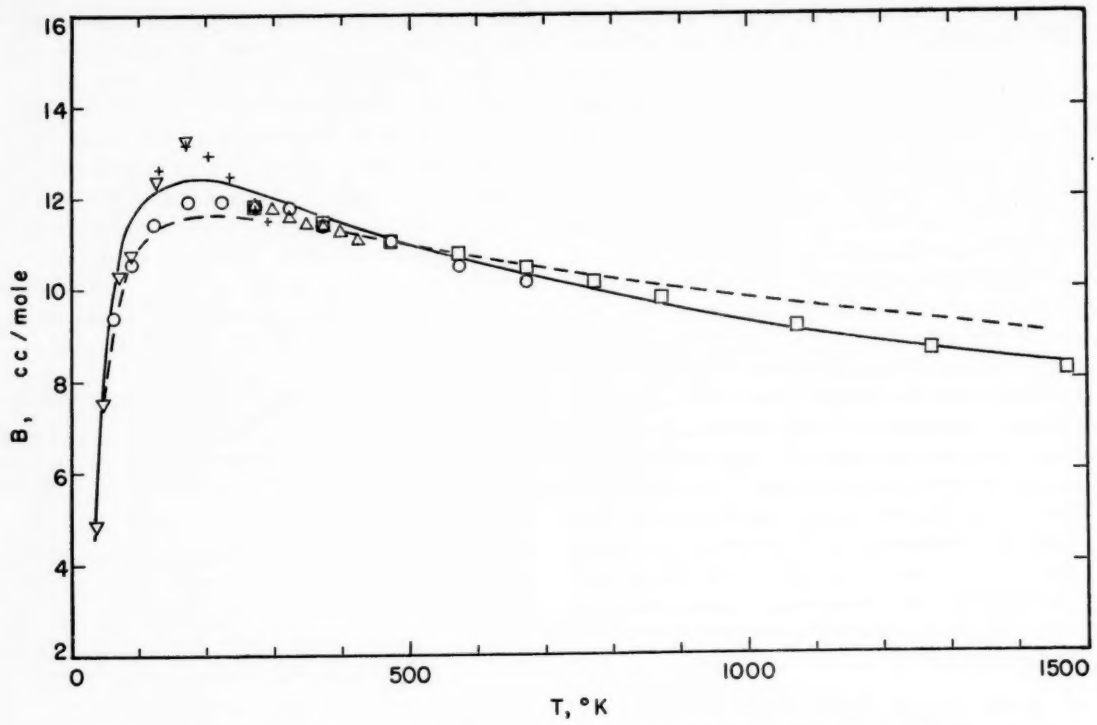

FIG. 2. Comparison of observed and calculated values of the second virial coefficient of helium. Solid line: exp-six potential; broken line: Lennard-Jones (12-6) potential. Observed values: + Boks and Onnes; ▽ Nijhoff, Keesom, and Iliin; ⊙ Holborn and Otto; △ Michels and Wouters; ⊡ Schneider, Duffie, and Yntema.

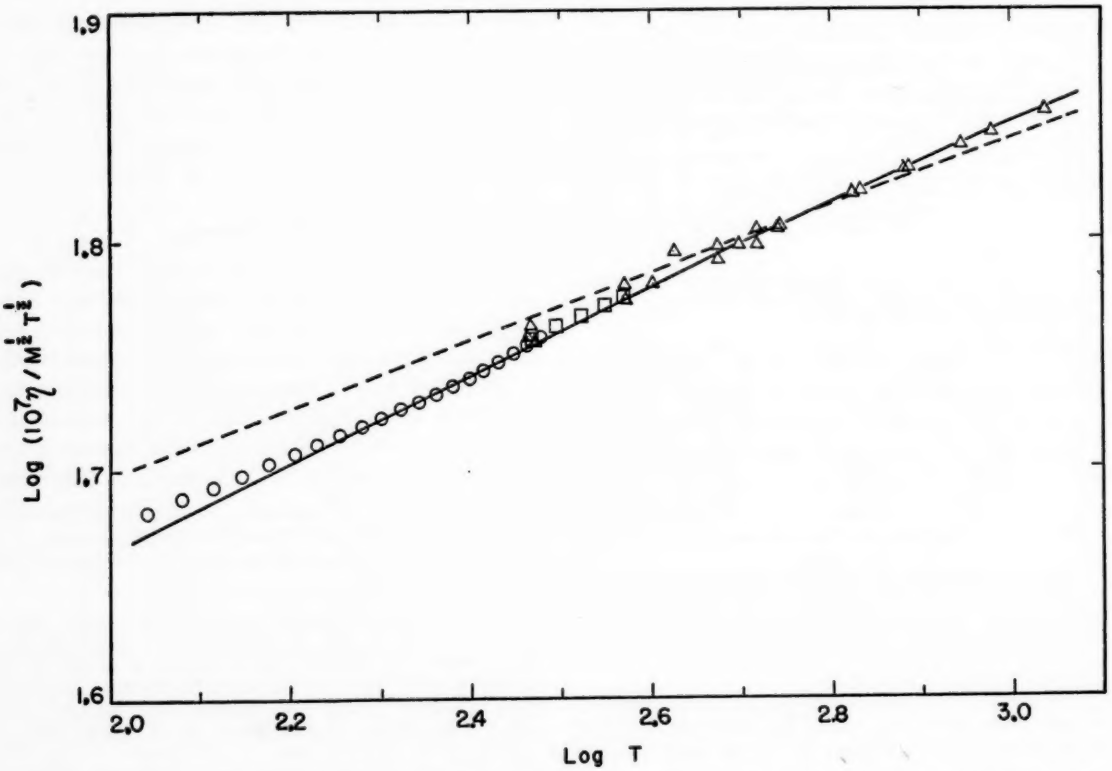

FIG. 3. Comparison of observed and calculated values of the viscosity of helium. Solid line: exp-six potential; broken line: Lennard-Jones (12-6) potential. Observed values: △ Trautz *et al.*; ⊡ Wobser and Müller; ⊙ Johnston and Grilly.

TABLE II. Comparison of observed second virial coefficients of helium with those calculated for the exp-six potential.

T, °K	$B(T)$, cc/mole Calc	Obs	Deviation, cc/mole
273.2	12.11	11.86[a]	−0.25
		11.87[b]	−0.24
		11.77[c]	−0.34
298.2	11.99	11.74[b]	−0.25
323.2	11.86	11.74[a]	−0.12
		11.58[b]	−0.28
348.2	11.73	11.43[b]	−0.30
373.2	11.60	11.39[a]	−0.21
		11.35[b]	−0.25
		11.42[c]	−0.18
398.2	11.48	11.24[b]	−0.24
423.2	11.36	11.07[b]	−0.29
473.2	11.12	11.07[a]	−0.05
		11.08[c]	−0.04
573.2	10.71	10.50[a]	−0.21
		10.76[c]	+0.05
673.2	10.33	10.14[a]	−0.19
		10.45[c]	+0.12
773.2	9.99	10.14[c]	+0.15
873.2	9.68	9.82[c]	+0.14
		9.80[d]	+0.12
1073.2	9.11	9.17[d]	+0.06
1273.2	8.69	8.66[d]	−0.03
1473.2	8.33	8.19[d]	−0.24

[a] L. Holborn and J. Otto, Z. Physik **10**, 367 (1922); **23**, 77 (1924); **33**, 1 (1925); **38**, 359 (1926).
[b] A. Michels and H. Wouters, Physica **8**, 923 (1941).
[c] W. G. Schneider and J. A. H. Duffie, J. Chem. Phys. **17**, 751 (1949).
[d] J. L. Yntema and W. G. Schneider, J. Chem. Phys. **18**, 641 (1950).

theoretical curve for the Lennard-Jones (12-6) potential of Table I. Below 273.2°K the experimental values are in poor agreement, and the exp-six and Lennard-Jones (12-6) potentials do about equally well in fitting the data, but at high temperatures the exp-six gives a definitely superior fit; helium atoms are clearly "softer" than indicated by the (12-6) potential. The agreement between experimental values and those calculated from the exp-six potential is shown in more detail in Table II for temperatures above 273.2°K. The maximum deviation is 0.34 cc/mole, and the average absolute deviation is 0.18 cc/mole. This is satisfactory agreement, since experimental second virial coefficients are seldom more accurate than this.[24,27]

Figure 3 shows a similar comparison of calculated and experimental[28] viscosities for helium. Only the data of Trautz and Binkele, Trautz and Zink, Trautz and Heberling, Trautz and Husseini, Wobser and Müller, and Johnston and Grilly are shown; values obtained by other workers are in satisfactory agreement with these. The agreement is excellent at higher temperatures; the deviations below about 200°K are presumably due to quantum effects. Calculations for the Lennard-Jones (12-6) potential are also shown in the figure; here again it is seen that the inverse twelfth power repulsion is too steep for helium. Table III gives a more detailed comparison between calculated and experimental values for temperatures above 200°K; in all cases the agreement is within the consistency of the experimental data.

If the exp-six potential is to be considered satisfactory, it should be able to predict other properties than second virial coefficients and viscosities. For helium, experimental results suitable for comparison with theoretical calculations are available for the properties of thermal conductivity and thermal diffusion. The thermal con-

TABLE III. Comparison of observed viscosities of helium with those calculated for the exp-six potential.

T, °K	$10^7\eta$, g-cm^{-1}-sec^{-1} Calc	Obs	% dev.
200	1491	1496[a]	+0.34
210	1542	1546[a]	+0.26
220	1593	1594[a]	+0.06
230	1644	1644[a]	0
240	1692	1692[a]	0
250	1740	1740[a]	0
260	1789	1788[a]	+0.05
270	1837	1838[a]	+0.05
280	1884	1888[a]	+0.21
290	1929	1937[a]	+0.41
291.8	1937	1956[b]	+0.98
293	1943	1951[c]	+0.41
		1953[d]	+0.51
293.2	1944	1984[e]	+2.06
		1960[f]	+0.82
294.6	1950	1960[b]	+0.51
300	1975	1987[a]	+0.61
313.2	2034	2051[f]	+0.84
333.2	2123	2139[f]	+0.75
353.2	2211	2225[f]	+0.63
371.2	2288	2300[f]	+0.52
373	2295	2297[d]	+0.09
373.2	2296	2320[e]	+1.57
400	2409	2416[e]	+0.29
423.2	2504	2565[e]	+2.44
473	2702	2687[d]	−0.56
473.2	2703	2729[e]	+0.96
500	2805	2806[c]	+0.04
523	2893	2871[d]	−0.76
523.2	2894	2918[e]	+0.83
550	2997	2992[e]	−0.17
554	3012	3013[b]	+0.03
555	3015	3007[b]	−0.26
665	3408	3405[b]	−0.09
680	3460	3453[b]	−0.20
759	3728	3724[b]	−0.11
767	3754	3748[b]	−0.16
879	4115	4107[b]	−0.19
881	4121	4113[b]	−0.19
949	4334	4324[b]	−0.23
955	4353	4338[b]	−0.34
1088	4753	4726[b]	−0.57
1090	4760	4736[b]	−0.50

[a] H. L. Johnston and E. R. Grilly, J. Phys. Chem. **46**, 948 (1942).
[b] M. Trautz and R. Zink, Ann. Physik **7**, 427 (1930).
[c] M. Trautz and R. Heberling, Ann. Physik **20**, 118 (1934).
[d] M. Trautz and I. Husseini, Ann. Physik **20**, 121 (1934).
[e] M. Trautz and H. E. Binkele, Ann. Physik **5**, 561 (1930).
[f] R. Wobser and F. Müller, Kolloid-Beih. **52**, 165 (1941).

[27] Hirschfelder, McClure, and Weeks, J. Chem. Phys. **10**, 201 (1942).

[28] Y. Ishida, Phys. Rev. **21**, 550 (1923); M. N. States, Phys. Rev. **21**, 662 (1923); A. G. Nasini and C. Rossi, Gazz. chim. ital. **58**, 433, 898 (1928); M. Trautz and H. E. Binkele, Ann. Physik **5**, 561 (1930); M. Trautz and R. Zink, **7**, 427 (1930); M. Trautz and R. Heberling, **20**, 118 (1934); M. Trautz and I. Husseini, **20**, 121 (1934); M. Trautz and H. Zimmerman, **22**, 189 (1935); A. van Itterbeek and W. H. Keesom, Physica **5**, 257 (1938); A. van Itterbeek and O. van Paemel, Physica **7**, 265 (1940); R. Wobser and F. Müller, Kolloid-Beihefte **52**, 165 (1941); H. L. Johnston and E. R. Grilly, J. Phys. Chem. **46**, 948 (1942); van Itterbeek, van Paemel, and van Lierde, Physica **13**, 88 (1947).

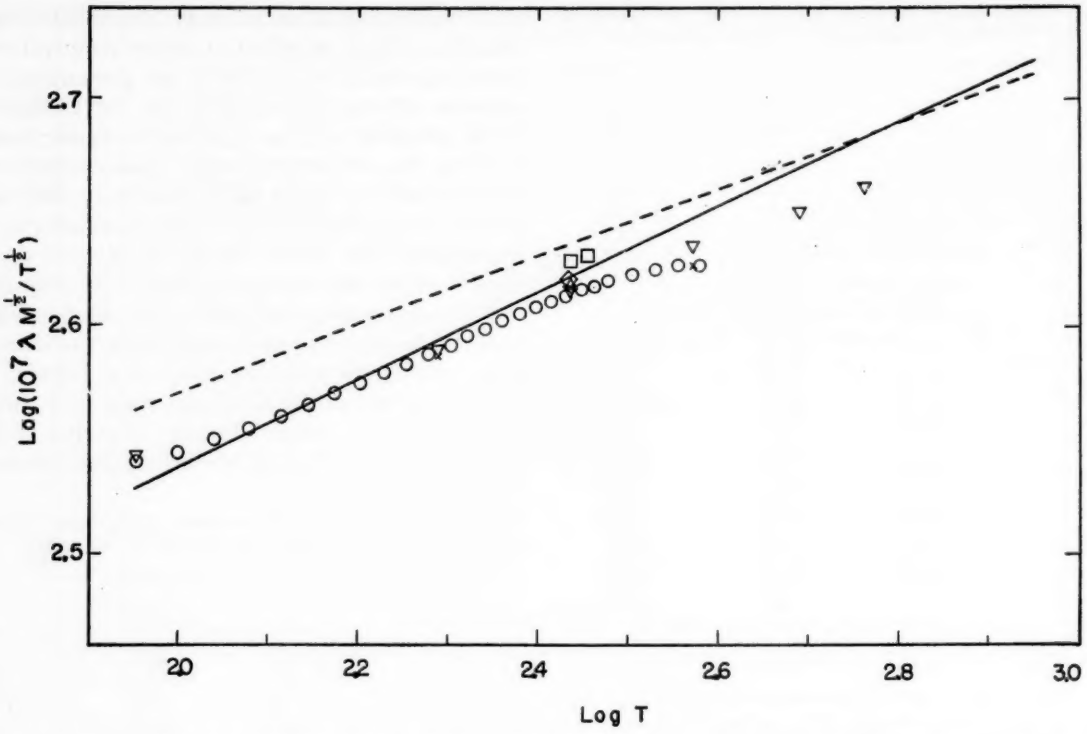

FIG. 4. Comparison of observed and calculated values of the thermal conductivity of helium. Solid line: exp-six potential; broken line: Lennard-Jones (12-6) potential. Observed values: × Eucken; ◇ Weber; ⊡ Dickins; △ Kannuluik and Martin; ⊙ Johnston and Grilly; ▽ Kannuluik and Carman.

ductivity of a monatomic gas may be written as

$$\lambda=\frac{5}{2}\eta\frac{C_v}{M}\frac{f_\lambda^{(3)}}{f_\eta^{(3)}}, \tag{14}$$

where λ is the thermal conductivity, η is the viscosity as given by Eq. (8), C_v is the molar heat capacity of the gas, M is the molecular weight, and $f_\lambda^{(3)}$ and $f_\eta^{(3)}$ are functions tabulated in reference 1. The ratio $(f_\lambda^{(3)}/f_\eta^{(3)})$ is very close to unity. Figure 4 shows a comparison between experimental[29] thermal conductivities and those calculated from Eq. (14) for the exp-six and Lennard-Jones (12-6) potentials. The exp-six potential gives somewhat better results, but the agreement between theory and experiment is certainly not outstanding, the discrepancies being usually larger than the estimated experimental error. However, it should be pointed out that the discrepancies are not the fault of the potential, but rather of the basic theory itself, since measured values of λ, η, and C_v are not consistent with Eq. (14) for any reasonable values of the f's. This disagreement between experiment and the fundamental theory, if real and not due to unexpectedly large experimental errors, is certainly surprising.

A property which is quite sensitive to the intermolecular potential is the thermal diffusion factor. Different theoretical expressions are available for this quantity, depending on the approximation procedures used. According to the procedure of Chapman and Cowling,[30] the mth approximation to the thermal diffusion factor of a binary gas mixture, $[\alpha_T]_m$, is given by the expression

$$[\alpha_T]_m=\frac{5}{2}\times\frac{x_1\left(\frac{M_1+M_2}{2M_1}\right)^{\frac{1}{2}}\mathfrak{A}_{01}^{(m)}+x_2\left(\frac{M_1+M_2}{2M_2}\right)^{\frac{1}{2}}\mathfrak{A}_{0-1}^{(m)}}{x_1x_2\mathfrak{A}_{00}^{(m)}}, \tag{15}$$

where x_1 and x_2 are the mole fractions of gas 1 and gas 2 of the binary mixture, and M_1 and M_2 are the molecular weights. The three terms of the form $\mathfrak{A}_{ij}^{(m)}$ are minors of a $(2m+1)$-order determinant $\mathfrak{A}^{(m)}$. The general element of $\mathfrak{A}^{(m)}$ is a_{ij}, where i and j range from $-m$ to m, and is a complicated function of the composition of the mixture, the molecular weights of the component gases, and the intermolecular forces. The minor $\mathfrak{A}_{ij}^{(m)}$ is obtained from $\mathfrak{A}^{(m)}$ by deleting the row and column containing a_{ij}. Expressions for the a_{ij} for $m=2$ are

[29] A. Eucken, Physik. Z. **12**, 1101 (1911); **14**, 324 (1913); S. Weber, Ann. Physik **54**, 437 (1917); B. G. Dickins, Proc. Roy. Soc. (London) **A143**, 517 (1934); W. G. Kannuluik and L. H. Martin, Proc. Roy. Soc. (London) **A144**, 496 (1934); H. L. Johnston and E. R. Grilly, J. Chem. Phys. **14**, 233 (1946); W. G. Kannuluik and E. H. Carman, Proc. Phys. Soc. (London) **B65**, 701 (1952).

[30] S. Chapman and T. G. Cowling, *The Mathematical Theory of Non-Uniform Gases* (Cambridge University Press, Teddington, England, 1952), second edition, p. 149.

given in reference 1, as well as tables for evaluating the a_{ij} for the special case of the exp-six potential. For $m=1$, Eq. (15) may be written in the handier form,

$$[\alpha_T]_1=(6C^*-5)\frac{x_1S_1-x_2S_2}{x_1^2Q_1+x_2^2Q_2+x_1x_2Q_{12}}, \quad (16)$$

where

$$S_1=\frac{M_1}{M_2}\left(\frac{2M_2}{M_1+M_2}\right)^{\frac{1}{2}}\left[\frac{\Omega_{11}^{(2,2)*}}{\Omega_{12}^{(1,1)*}}\right]\left[\frac{(r_m)_{11}}{(r_m)_{12}}\right]^2 -\left[\frac{4M_1M_2}{(M_1+M_2)^2}\right]A^*-\frac{15M_2(M_2-M_1)}{(M_1+M_2)^2},$$

$$Q_1=\frac{2}{M_2(M_1+M_2)}\left(\frac{2M_2}{M_1+M_2}\right)^{\frac{1}{2}}\left[\frac{\Omega_{11}^{(2,2)*}}{\Omega_{12}^{(1,1)*}}\right]\left[\frac{(r_m)_{11}}{(r_m)_{12}}\right]^2 \times\left[3M_2^2+\left(\frac{5}{2}-\frac{6}{5}B^*\right)M_1^2+\frac{8}{5}M_1M_2A^*\right],$$

$$Q_{12}=\frac{15(M_1-M_2)^2}{(M_1+M_2)^2}\left(\frac{5}{2}-\frac{6}{5}B^*\right) +\frac{4M_1M_2}{(M_1+M_2)^2}\left(11-\frac{12}{5}B^*\right)A^*+\left(\frac{8}{5}\right)\frac{M_1+M_2}{(M_1M_2)^{\frac{1}{2}}} \times\left[\frac{\Omega_{11}^{(2,2)*}}{\Omega_{12}^{(1,1)*}}\right]\left[\frac{\Omega_{22}^{(2,2)*}}{\Omega_{12}^{(1,1)*}}\right]\left[\frac{(r_m)_{11}(r_m)_{22}}{(r_m)_{12}^2}\right]^2,$$

and A^*, B^*, C^*, and the $\Omega^{(l,n)*}$ are functions tabulated in reference 1. The subscripts refer to the molecular species, and the relations for S_2 and Q_2 are obtained from those for S_1 and Q_1 by an interchange of subscripts. The subscripts on the $\Omega^{(l,n)*}$ and the r_m refer to the three different molecular interactions which must be considered in a binary gas mixture, two involving like molecules (1,1) and (2,2), and the third involving unlike molecules (1,2). For isotopes, the distinction does not arise, since intermolecular forces are presumably the same between different isotopic species.

Kihara[31] observed that the elements a_{ij} are small unless $i=j$, and performed an expansion of Eq. (15) in powers of the a_{ij}, keeping no terms of order higher than $a_{ij}^2(i\neq j)$. In this way he arrived at an expression for the first approximation to α_T of the same form as Eq. (16), but with the following expressions for the Q's:

$$Q_1=\frac{2}{M_2(M_1+M_2)}\left(\frac{2M_2}{M_1+M_2}\right)^{\frac{1}{2}}\left[\frac{\Omega_{11}^{(2,2)*}}{\Omega_{12}^{(1,1)*}}\right] \times\left[\frac{(r_m)_{11}}{(r_m)_{12}}\right]^2\left[M_1^2+3M_2^2+\frac{8}{5}M_1M_2A^*\right],$$

$$Q_{12}=\frac{15(M_1-M_2)^2}{(M_1+M_2)^2}+\left[\frac{32M_1M_2}{(M_1+M_2)^2}\right]A^* +\left(\frac{8}{5}\right)\frac{M_1+M_2}{(M_1M_2)^{\frac{1}{2}}}\left[\frac{\Omega_{11}^{(2,2)*}}{\Omega_{12}^{(1,1)*}}\right] \times\left[\frac{\Omega_{22}^{(2,2)*}}{\Omega_{12}^{(1,1)*}}\right]\left[\frac{(r_m)_{11}(r_m)_{22}}{(r_m)_{12}^2}\right]^2. \quad (17)$$

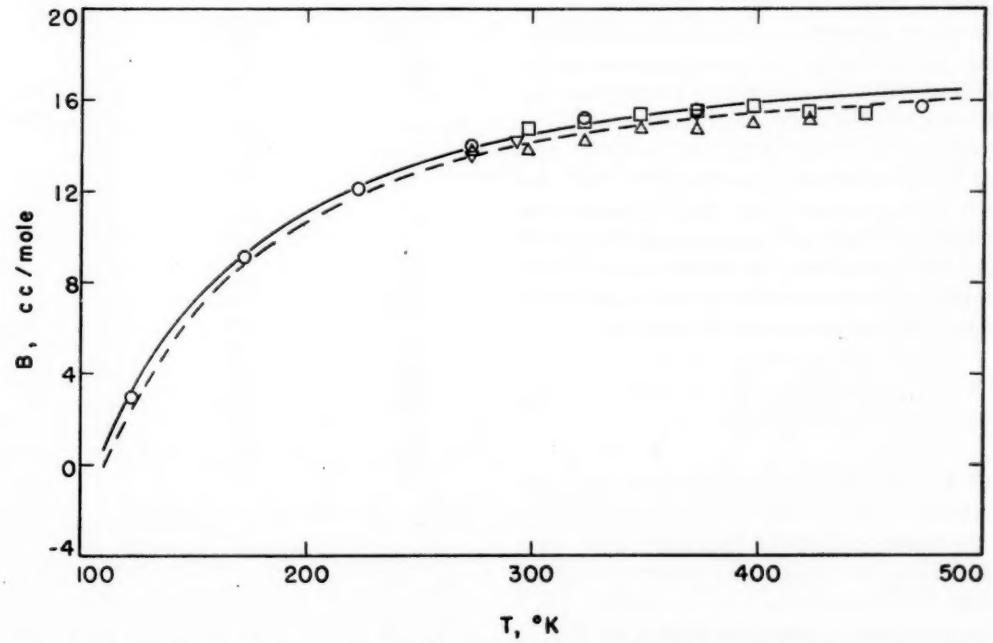

FIG. 5. Comparison of observed and calculated values of the second virial coefficient of hydrogen. Solid line: exp-six potential; broken line: Lennard-Jones (12-6) potential. Observed values: ⊙ Holborn and Otto; ▽ Nijhoff and Keesom; ⊡ Gibby, Tanner, and Masson; △ Michels and Goudeket.

[31] T. Kihara, *Imperfect Gases* [originally published in Japanese (Asakusa Bookstore, Tokyo (1949)) and translated into English by the U. S. Office of Air Research, Wright-Patterson Air Force Base].

TABLE IV. Comparison of observed second virial coefficients of hydrogen with those calculated for the exp-six potential.

T, °K	$B(T)$, cc/mole Calc	Obs	Deviation, cc/mole
123.2	3.34	2.95[a]	−0.39
173.2	9.27	9.15[a]	−0.12
223.2	12.24	12.10[a]	−0.14
273.2	13.93	14.00[a]	+0.07
		13.58[b]	−0.35
		13.71[c]	−0.22
293.2	14.41	14.16[b]	−0.25
298.2	14.51	14.71[d]	+0.20
		13.81[e]	−0.70
323.2	14.97	15.17[a]	+0.19
		15.04[d]	+0.07
		14.21[e]	−0.76
348.2	15.34	15.37[d]	+0.03
		14.76[e]	−0.58
373.2	15.63	15.58[a]	−0.04
		15.39[b]	−0.24
		14.72[e]	−0.91
373.5	15.64	15.54[d]	−0.10
398.2	15.88	14.94[e]	−0.94
398.4	15.88	15.74[d]	−0.14
423.2	16.07	15.10[e]	−0.97
423.3	16.07	15.51[d]	−0.56
448.2	16.24	15.39[d]	−0.85
473.2	16.38	15.71[a]	−0.67

[a] L. Holborn and J. Otto, Ann. Physik **63**, 674 (1920); Z. Physik **23**, 77 (1924); **33**, 1 (1925); **38**, 359 (1926).
[b] G. P. Nijhoff and W. H. Keesom, Leiden Comm. **188d** (1927).
[c] A. Michels and M. Goudeket, Physica **8**, 347 (1941).
[d] Gibby, Tanner, and Masson, Proc. Roy. Soc. (London) **A122**, 283 (1929).

The relation for Q_2 is obtained from that for Q_1 by an interchange of subscripts.

Three expressions are thus available for the thermal diffusion factor: the first and second approximations of Chapman and Cowling, hereafter denoted, respectively, as $[CC]_1$ and $[CC]_2$, and the first approximation of Kihara, hereafter denoted as $[K]_1$. For helium, the thermal diffusion factor has been determined by McInteer, Aldrich, and Nier[32] by measuring the thermal separation of a He^3-He^4 mixture between 273° and 613°K. Over this temperature range, they found a mean value of the thermal diffusion factor, $\bar{\alpha}_T=0.059\pm0.005$, the He^3 being present in only a trace concentration. According to Brown,[33] this should be equal to the actual value of α_T at a mean temperature $\bar{T}$, given by

$$\bar{T}=\frac{TT'}{T'-T}\ln\frac{T'}{T}, \tag{18}$$

where T and T' are, respectively, the low and high temperatures involved in the thermal separation. Taking $\bar{T}=398$°K, the values calculated from the three theoretical formulas from the exp-six parameters of Table I are as follows: $[CC]_1=0.0532$, $[CC]_2=0.0599$, $[K]_1=0.0594$. The agreement is excellent except for $[CC]_1$, which is a little low. The value of $[K]_1$ is better than $[CC]_1$, a feature which has previously been noted for the special case of thermal diffusion in a binary mixture of heavy isotopes.[1]

[32] McInteer, Aldrich, and Nier, Phys. Rev. **72**, 510 (1947).
[33] H. Brown, Phys. Rev. **58**, 661 (1940).

B. Hydrogen

The parameters of Table I have been used to calculate a number of properties of gaseous hydrogen for comparison with experimental results. Experimental values of the second virial coefficient which lie in the temperature range where comparisons are possible have been measured from 123.2° to 473.2°K. Figure 5 is a plot of experimental[34] and calculated values for both the exp-six

TABLE V. Comparison of observed viscosities of hydrogen with those calculated for the exp-six potential.

T, °K	$10^7\eta$, g-cm^{-1}-sec^{-1} Calc	Obs	% dev.
200	680	681[a]	+0.15
210	704	704[a]	0.00
220	727	727[a]	0.00
230	749	749[a]	0.00
235.2	761	758[b]	−0.39
240	771	771[a]	0.00
250	793	792[a]	−0.13
260	815	814[a]	−0.12
270	836	835[a]	−0.12
280	857	856[a]	−0.12
289.9	877	872[c]	−0.57
290	878	876[a]	−0.23
292.2	882	878[b]	−0.45
293	884	879[d]	−0.57
	884	880[e]	−0.45
293.2	884	879[f]	−0.57
	884	881[g]	−0.34
300	898	896[a]	−0.22
313.2	924	922[g]	−0.22
323.2	944	942[f]	−0.21
333.2	964	960[g]	−0.41
353.2	1002	999[g]	−0.30
371.2	1036	1031[g]	−0.48
373	1039	1036[e]	−0.29
373.2	1040	1035[b]	−0.48
	1040	1034[f]	−0.58
400	1090	1092[d]	+0.18
423.2	1132	1131[f]	−0.09
473	1219	1221[e]	+0.16
	1219	1216[e]	−0.25
473.2	1219	1218[b]	−0.08
	1219	1217[f]	−0.16
500	1265	1255[d]	−0.79
523	1303	1303[e]	0.00
523.2	1303	1304[b]	+0.08
	1303	1303[f]	0.00
550	1348	1352[d]	+0.30
572	1384	1388[e]	+0.30
685	1561	1562[e]	+0.06
763	1678	1680[e]	+0.12
874	1839	1838[e]	−0.05
986	1994	1992[e]	−0.10
1098	2143	2148[e]	+0.23

[a] H. L. Johnston and K. E. McCloskey, J. Phys. Chem. **44**, 1038 (1940).
[b] M. Trautz and P. B. Baumann, Ann. Physik **2**, 733 (1929).
[c] M. Trautz and R. Zink, Ann. Physik **7**, 427 (1930).
[d] M. Trautz and R. Heberling, Ann. Physik **20**, 118 (1934).
[e] M. Trautz and I. Husseini, Ann. Physik **20**, 121 (1934).
[f] M. Trautz and H. E. Binkele, Ann. Physik **5**, 561 (1930).
[g] R. Wobser and F. Müller, Kolloid-Beih. **52**, 165 (1941).

[34] L. Holborn and J. Otto, Ann. Physik **63**, 674 (1920); Z. Physik **23**, 77 (1924); **33**, 1 (1925); **38**, 359 (1926); G. P. Nijhoff and W. H. Keesom, Leiden Comm. **188d** (1927); Gibby, Tanner, and Masson, Proc. Roy. Soc. (London) **A122**, 283 (1929); A. Michels and M. Goudeket, reference 24.

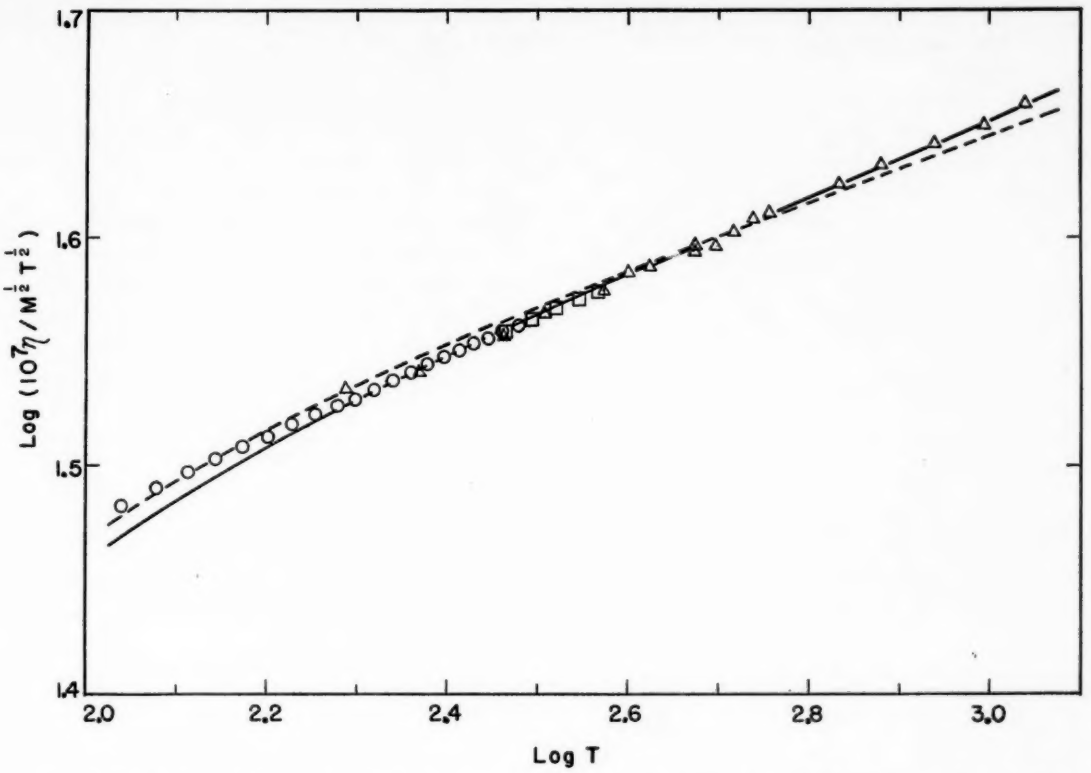

FIG. 6. Comparison of observed and calculated values of the viscosity of hydrogen. Solid line: exp-six potential; broken line: Lennard-Jones (12-6) potential. Observed values: △ Trautz *et al.*; ⊡ Wobser and Müller; ⊙ Johnston and McCloskey.

and Lennard-Jones (12-6) potential; the agreement is seen to be satisfactory for both potentials. Unlike those for helium, the data do not extend to high enough temperatures to show the "softness" of the repulsion energy. A more detailed comparison is given in Table IV; the maximum deviation is 0.97 cc/mole, and the average absolute deviation is 0.40 cc/mole. Thus, the agreement between theory and experiment is about as good as the agreement among different observers.

Figure 6 shows a similar comparison of experimental[35] viscosities and those calculated for the exp-six and Lennard-Jones (12-6) potential. Only a sampling of the available data is plotted; other values are in satisfactory agreement. Here we can see that hydrogen is "softer" than an inverse twelfth power repulsion, although the discrepancy is not as marked as in the case of helium. The deviations at temperatures below about 200°K are presumably due to quantum effects. Table V gives a more detailed comparison between theory and the experimental values shown in Fig. 6 for temperatures above 200°K; the agreement is within the consistency of the experimental data.

Other properties of gaseous hydrogen which have been measured include thermal conductivity, self-diffusion, and thermal diffusion. Since a hydrogen molecule can transport energy in its internal degrees of freedom, the calculation of the thermal conductivity is quite uncertain, and we have not attempted to make any comparison between theory and experiment for this property.

The coefficient of self-diffusion of a gas may be written

$$D_{11}=\frac{2.6280\times10^{-3}T^{\frac{3}{2}}}{pM^{\frac{1}{2}}r_m^{\,2}}\frac{f_D^{(3)}(\alpha,T^*)}{\Omega^{(1,1)*}(\alpha,T^*)}, \qquad (19)$$

where D_{11} is the self-diffusion coefficient in cm²/sec, p is the pressure in atmospheres, $f_D^{(3)}(\alpha,T^*)$, and $\Omega^{(1,1)*}(\alpha,T^*)$ are dimensionless functions which may be obtained from the tabulations in reference 1, and the other quantities are as previously defined. The self-diffusion

[35] Y. Ishida, Phys. Rev. **21**, 550 (1923); P. Günther, Z. physik. Chem. **110**, 626 (1924); M. Trautz and P. B. Baumann, Ann. Physik **2**, 733 (1929); M. Trautz and F. W. Stauf, **2**, 737 (1929); M. Trautz and K. F. Kipphan, **2**, 743 (1929); M. Trautz and W. Ludewigs, **3**, 409 (1929); M. Trautz and H. E. Binkele, **5**, 561 (1930); M. Trautz and A. Melster, **7**, 409 (1930); M. Trautz and R. Zink, **7**, 427 (1930); M. Trautz and F. Kurz, **9**, 981 (1931); M. Trautz and K. G. Sorg, **10**, 81 (1931); M. Trautz and R. Heberling, **10**, 155 (1931); B. P. Sutherland and O. Maass, Can. J. Research **6**, 428 (1932); M. Trautz and R. Heberling, Ann. Physik **20**, 118 (1934); M. Trautz and I. Husseini, **20**, 121 (1934); M. Trautz and H. Zimmerman, **22**, 189 (1935); A. van Itterbeek and A. Claes, Nature **142**, 793 (1938); Physica **5**, 938 (1938); A. van Itterbeek and O. van Paemel, Physica **7**, 265 (1940); H. L. Johnston and K. E. McCloskey, J. Phys. Chem. **44**, 1038 (1940); R. Wobser and F. Müller, Kolloid-Beih. **52**, 165 (1941); van Itterbeek, van Paemel, and van Lierde, Physica **13**, 88 (1947); de Troyer, van Itterbeek, and Rietveld, **17**, 938 (1951); J. W. Buddenberg and C. R. Wilke, J. Phys. Coll. Chem. **55**, 1491 (1951).

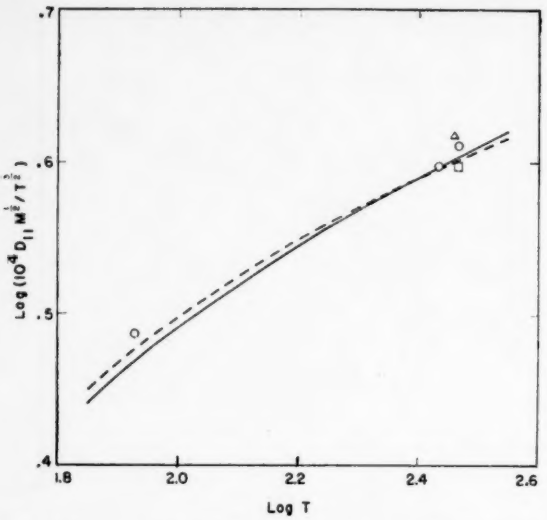

FIG. 7. Comparison of observed and calculated values of the self-diffusion coefficient of hydrogen. Solid line: exp-six potential; broken line: Lennard-Jones (12-6) potential. Observed values: ⊙ Harteck and Schmidt; △ Heath, Ibbs, and Wild; ⊡ Waldmann.

coefficient for hydrogen has been measured by following the diffusion of *ortho*hydrogen and *para*hydrogen,[36] and of deuterium and hydrogen.[37,38] Table VI compares the measured values with those calculated for the exp-six potential. All values refer to a pressure of 1 atmosphere. The values for the system D_2-H_2 have been corrected to refer to an ideal system in which all molecules have the same mass as normal hydrogen by multiplying by the square root of the ratio of the reduced mass of the experimental system to that of the ideal system. The correction factor is equal to 1.155 in the present case. The values are also shown in Fig. 7, together with the theoretical values for the exp-six and Lennard-Jones (12-6) potentials. Within the experimental error both potentials are satisfactory.

The thermal diffusion factor, α_T, has been measured a number of times for the system D_2-H_2. The best data

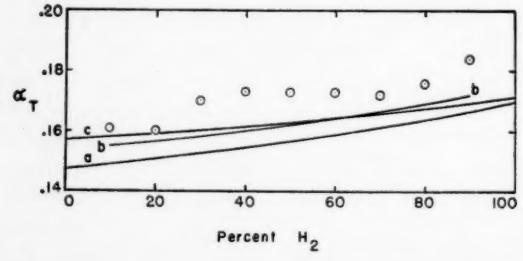

FIG. 8. Comparison of observed values of the thermal diffusion factor α_T for the system D_2-H_2 with those calculated for the exp-six potential. Curves *a*, *b*: first and second approximations of Chapman and Cowling; curve *c*: first approximation of Kihara. Here $T=327°K$.

[36] P. Harteck and H. W. Schmidt, Z. physik. Chem. **B21**, 447 (1933).

[37] Heath, Ibbs, and Wild, Proc. Roy. Soc. (London) **A178**, 380 (1941).

[38] L. Waldmann, Naturwiss. **32**, 223 (1944); Z. Naturforsch. **1**, 59 (1946).

appear to be those of Heath, Ibbs, and Wild,[37] who measured thermal separations between 288° and 373°K. The same method has also been used by Grew,[39] Murphey,[40] and de Troyer, van Itterbeek, and Rietveld.[41] The value of α_T has also been determined from the diffusion thermoeffect by Waldmann.[38] Within the scatter of the experimental values, which is large, the various workers are in agreement with Heath, Ibbs, and Wild. The results of the latter are compared with the theoretical calculations in Table VII where T has been taken as 327°K, according to Eq. (18). Three theoretical expressions are available, as discussed in connection with the thermal diffusion of helium. The values in Table VII are plotted in Fig. 8, in which the trend of α_T with composition is more easily seen. The agreement between theory and experiment is excellent, and higher approximations to the theoretical value should even improve the agreement. It is remarkable that the simple first approximation of Kihara gives results which are as good as those given by the very complicated second approximation of Chapman and Cowling.

TABLE VI. Comparison of observed values of the self-diffusion coefficient of hydrogen with those calculated for the exp six potential.

	D_{11} (1 atmos), cm²/sec		
T °K	Calc	Obs	% dev.
85	0.162	0.169±0.008[a]	+4.3
273	1.257	1.26 ±0.04[a]	0.0
288.2	1.379	1.43[b]	+3.6
293	1.418	1.442±0.0026[a]	+1.7
293.2	1.420	1.40[c]	−1.4

[a] P. Harteck and H. W. Schmidt, Z. physik. Chem. **B21**, 447 (1933). These values have been recalculated to avoid an uncertain extrapolation over a temperature range performed in the original article.
[b] Heath, Ibbs, and Wild, Proc. Roy. Soc. (London) **A178**, 380 (1941).
[c] L. Waldmann, Naturwiss. **32**, 223 (1944); Z. Naturforsch. **1**, 59 (1946).

C. Helium-Hydrogen Mixtures

The properties of gaseous mixtures depend to some extent on the forces between unlike molecules. In principle these forces could be calculated from experimental results on mixtures, but in practice the accuracy required of the experimental measurements is too great, since the dependence of a property on the forces between unlike molecules is partly masked by the dependence on the forces between the like molecules in the mixture. It would, therefore, be very helpful to be able to predict the interaction for unlike molecules from the known interactions for the like molecules. In this way properties of gaseous mixtures could be calculated from data on the pure components. Combining rules for the exp-six potential can be obtained by writing Eq. (1) in the form

$$\varphi(r)=Ae^{-br}-C/r^6. \tag{20}$$

[39] K. E. Grew, Proc. Roy. Soc. (London) **A178**, 390 (1941).

[40] B. F. Murphey, Phys. Rev. **72**, 834 (1947).

[41] de Troyer, van Itterbeek, and Rietveld, Physica **17**, 938 (1951).

Zener[42] has shown from theoretical considerations that the parameter b for an unlike interaction may be obtained from the relation

$$b_{12}=\tfrac{1}{2}(b_{11}+b_{22}), \tag{21}$$

where b_{12} refers to the unlike interaction, and b_{11} and b_{22} refer to the like interactions. The theory of the dispersion energy leads to the following combining rule[43] for the parameter C:

$$C_{12}=(C_{11}C_{22})^{\frac{1}{2}}. \tag{22}$$

Unfortunately no combining rule for the parameter A is forthcoming from theory, and we must proceed empirically. Since the parameters A and C appear in Eq. (20) in a similar way, it is tempting to write the relation

$$A_{12}=(A_{11}A_{22})^{\frac{1}{2}}. \tag{23}$$

We could also proceed by analogy with Eq. (21) for the parameter b, letting $A=e^a$, and

$$a_{12}=\tfrac{1}{2}(a_{11}+a_{22}). \tag{24}$$

Eqs. (23) and (24) are entirely equivalent, however, as may be shown by substitution of the relation $a=\ln A$ into Eq. (24). We have, therefore, taken this empirical relation as our third combining rule.

The combining rules, Eqs. (21)–(23), are more complicated in terms of the parameters ϵ, r_m, and α. The parameter $(r_m)_{12}$ for the unlike interaction first is found from the transcendental equation,

$$(GH)(r_m)_{12}^7=\exp[(G)(r_m)_{12}], \tag{25}$$

where

$$G=\frac{1}{2}\left[\frac{\alpha_{11}}{(r_m)_{11}}+\frac{\alpha_{22}}{(r_m)_{22}}\right],$$

$$H=(\alpha_{11}\alpha_{22})^{-\frac{1}{2}}[(r_m)_{11}(r_m)_{22}]^{-3}\exp[(\alpha_{11}+\alpha_{22})/2].$$

The parameters α_{12} and ϵ_{12} are then calculated from the relations

$$\alpha_{12}=(G)(r_m)_{12}, \tag{26}$$

$$\epsilon_{12}=(\epsilon_{11}\epsilon_{22})^{\frac{1}{2}}\left[\frac{(\alpha_{12}-6)^2}{(\alpha_{11}-6)(\alpha_{22}-6)}\right]^{\frac{1}{2}} \times\exp\left(\frac{\alpha_{11}+\alpha_{22}-2\alpha_{12}}{2}\right). \tag{27}$$

Substitution of the exp-six potential parameters in Table I leads to the following values for the interaction between a helium atom and hydrogen molecule:

$$\alpha=13.22,$$
$$r_m=3.244\text{A}, \tag{28}$$
$$\epsilon/k=18.27^\circ\text{K}.$$

[42] C. Zener, Phys. Rev. **37**, 556 (1931).

[43] J. A. Beattie and W. H. Stockmayer, *States of Matter* (D. van Nostrand Company, Inc., New York, 1951, H. S. Taylor and S. Glasstone, Editors), pp. 350–352.

TABLE VII. Comparison of observed values of the thermal diffusion factor for the system D_2-H_2 with those calculated for the exp-six potential.

% H_2	Thermal diffusion factor, α_T $[CC]_1$	$[CC]_2$	$[K]_1$	Obs
10	0.1491	0.1552	0.1579	0.161
20	0.1507	0.1567	0.1590	0.160
30	0.1525	0.1584	0.1602	0.170
40	0.1544	0.1602	0.1614	0.173
50	0.1565	0.1622	0.1628	0.173
60	0.1588	0.1643	0.1643	0.173
70	0.1612	0.1666	0.1658	0.172
80	0.1638	0.1691	0.1675	0.176
90	0.1665	0.1718	0.1693	0.184

A check on the suitability of the combining rules may be obtained by using these parameters to calculate properties of helium-hydrogen mixtures for comparison with available measurements.

The second virial coefficient of a binary mixture, B_m, is given by

$$B_m=x_1^2B_{11}+x_2^2B_{22}+2x_1x_2B_{12}, \tag{29}$$

where x_1 and x_2 are the mole fractions of the components, B_{11} and B_{22} are the virial coefficients of the pure components, and B_{12} is the virial coefficient of a hypothetical pure gas whose molecules interact according to the potential law for (1,2) interactions. Second virial coefficients for helium, hydrogen, and a 50–50 mixture have been measured by Gibby, Tanner, and Masson.[24] Table VIII compares the experimental values of B_{12} as obtained from Eq. (29) with the values calculated from the parameters of Eq. (28). A small quantum correction has been applied to the calculated values, taking the molecular weight of the hypothetical (1,2) gas to be equal to $[2M_1M_2/(M_1+M_2)]$. The agreement is of the same order as that obtained for the pure components using the parameters of Table I.

The viscosity of a binary mixture, η_m, is given by

$$\eta_m=\frac{1}{X}\left[\frac{1+Z}{1+(Y/X)}\right], \tag{30}$$

TABLE VIII. Comparison of observed values of the second virial coefficient interaction term, B_{12}, for $He-H_2$ mixtures with those calculated from the combining rule for the exp-six potential.

T, °K	B_{12}, cc/mole Calc	Obs	Deviation, cc/mole
298.2	14.66	15.60	+0.94
323.2	14.74	15.66	+0.92
348.2	14.71	15.24	+0.53
373.5	14.70	15.61	+0.91
398.4	14.68	14.39	−0.29
423.3	14.64	15.81	+1.17
448.2	14.60	14.55	−0.05

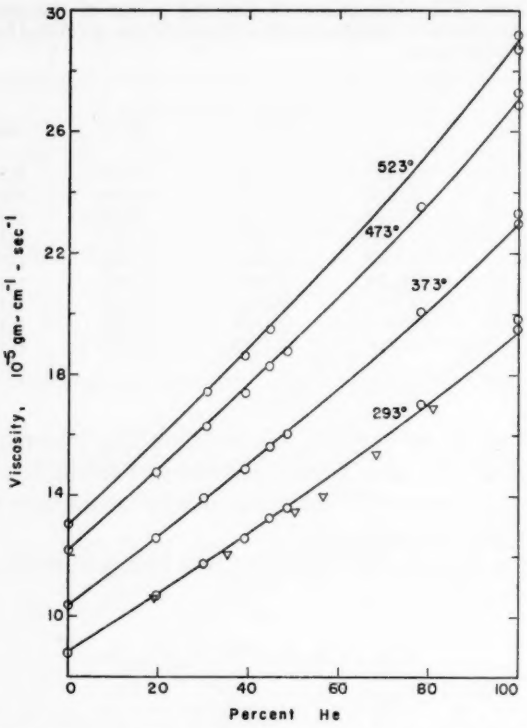

FIG. 9. Comparison of observed and calculated values of the viscosity of helium-hydrogen mixtures. Curves are calculated for the exp-six potential using the combining rules, Eqs. (25)–(27). Observed values: ⊙ Trautz *et al.*; ▽ van Itterbeek, van Paemel, and van Lierde (291.7°K).

where

$$X=\frac{x_1^2}{\eta_1}+\frac{x_2^2}{\eta_2}+\frac{2x_1x_2}{\eta_{12}},$$

$$Y=\frac{3}{5}A_{12}^*\left\{\frac{x_1^2}{\eta_1}\left(\frac{M_1}{M_2}\right)+\frac{2x_1x_2}{\eta_{12}}\times\left[\frac{(M_1+M_2)^2}{4M_1M_2}\right]\left(\frac{\eta_{12}^2}{\eta_1\eta_2}\right)+\frac{x_2^2}{\eta_2}\left(\frac{M_2}{M_1}\right)\right\},$$

$$Z=\frac{3}{5}A_{12}^*\left\{x_1^2\left(\frac{M_1}{M_2}\right)+2x_1x_2\times\left[\frac{(M_1+M_2)^2}{4M_1M_2}\left(\frac{\eta_{12}}{\eta_1}+\frac{\eta_{12}}{\eta_2}\right)-1\right]+x_2^2\left(\frac{M_2}{M_1}\right)\right\},$$

and η_1 and η_2 are the viscosities of the pure components as given by Eq. (8). The term η_{12} is the viscosity of a hypothetical pure gas whose molecules interact according to the potential law for (1,2) interactions, and whose molecular weight is $[2M_1M_2/(M_1+M_2)]$. The term A_{12}^* is a function of α_{12} and $T_{12}^*(=kT/\epsilon_{12})$ tabulated in reference 1. Figure 9 shows a plot of η_m for $He-H_2$ mixtures at several temperatures as calculated from Eq. (30). The agreement with the available experimental data[44] seems satisfactory, since it is of the same order as the agreement for the pure components.

A more serious test of the combination rules for the exp-six potential is given by the thermal diffusion factor, since this quantity depends strongly on the forces between unlike molecules, and only weakly on interactions between like molecules. The thermal diffusion factor for the system $He-H_2$ has been measured by the thermal separation method by a number of workers,[45] whose results are in reasonable accord with one another. The scatter of the experimental results is greater than the difference between Kihara's first approximation and Chapman and Cowling's second approximation, and we have, therefore, used Kihara's expression since the second approximation of Chapman and Cowling requires very tedious calculations. Figure 10 shows a comparison between calculated and experimental values of the thermal diffusion factor, α_T, as a function of composition for three different values of the mean temperature, $\bar{T}$, as given by Eq. (18). We have not ex-

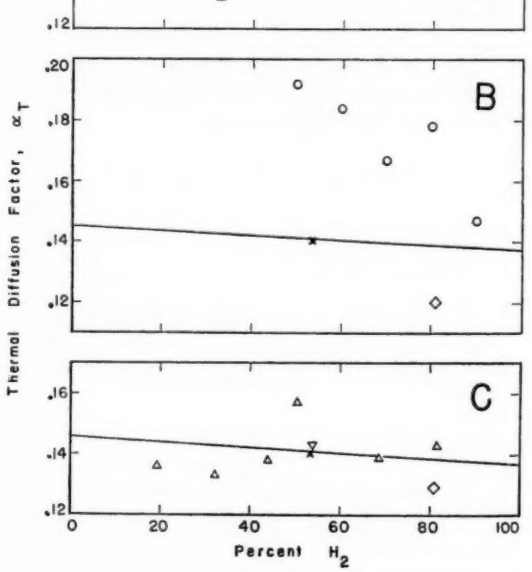

FIG. 10. Comparison of observed values of the thermal diffusion factor α_T for the system $He-H_2$ with those calculated for the exp-six potential according to Kihara's approximation. A. $\bar{T}=436°K$; B. $\bar{T}=327°K$; C. $\bar{T}=153°K$. Observed values: ⊡ Elliot and Masson; ⊙ Heath, Ibbs, and Wild; △ van Itterbeek, van Paemel, and van Lierde; ◊ Murphey; × Grew; ▽ de Troyer, van Itterbeek, and Rietveld.

[44] M. Trautz and K. F. Kipphan, Ann. Physik **2**, 743 (1929); M. Trautz and H. E. Binkele, **5**, 561 (1930); M. Trautz and I. Husseini, **20**, 121 (1934); van Itterbeek, van Paemel, and van Lierde, Physica **13**, 88 (1947).

[45] G. A. Elliot and I. Masson, Proc. Roy. Soc. (London) **A108**, 378 (1925); Heath, Ibbs, and Wild, reference 37; van Itterbeek, van Paemel, and van Lierde, Physica **13**, 231 (1947); B. F. Murphey, reference 40; K. E. Grew, Proc. Phys. Soc. (London) **B62**, 655 (1949); de Troyer, van Itterbeek, and Rietveld, reference 41.

tended the comparison to mean temperatures in which one bulb of the separation system was at a temperature below 90°K because of the uncertainty of the quantum corrections at low temperatures. The agreement is within the experimental error in all cases. Within the experimental error the calculated value of α_T is independent of temperature over this range, in agreement with the observations of Grew.[45]

Thermal diffusion in the system D_2—He is of particular interest since the observed separation cannot depend on the difference in mass, but must arise from the law of force. Figure 11 is a comparison of the measured[40] and calculated values of α_T for D_2—He as a function of temperature at a composition of 20 percent deuterium. The agreement is probably satisfactory, in view of the rather large experimental errors involved in measuring thermal separations for this system.

In summary, the agreement between theory and experiment for second virial coefficients, viscosities, and thermal diffusion factors for mixtures of helium and hydrogen greatly increases our confidence in the accuracy of the combining rules, Eqs. (25)–(27), for the exp-six potential.

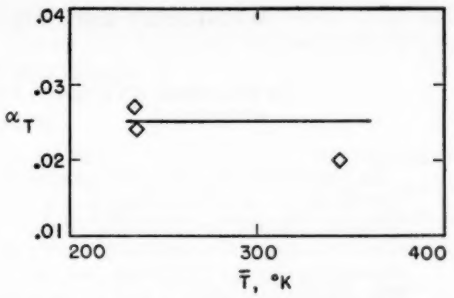

FIG. 11. Comparison of observed and calculated values of the thermal diffusion factor α_T as a function of temperature for the system D_2—He at a composition of 20 percent D_2.

ACKNOWLEDGMENTS

The authors wish to express their thanks to Dr. J. O. Hirschfelder for many helpful discussions and suggestions throughout the course of the work. For help with most of the calculations they are indebted to the computing group of the Naval Research Laboratory, under the direction of Catherine Denton and Elaine Petersen, and including Judith Aronow, Lois Brittenham, Peggy Kossow, Eva Silversmith, and Clarice Wruck.

Symmetry and Stability in Diborane and in Borine

G. W. CASTELLAN
The Department of Chemistry, The Catholic University of America, Washington, D. C.
(Received November 30, 1953)

On the basis of the electronic state of diborane in the ethane structure proposed by Mulliken, a group theoretical theorem due to Jahn and Teller shows that the ethane structure is not a possible structure for diborane; a nontotally symmetric vibration will move the molecule to a more stable configuration of lower symmetry. Any of the common bridge structures on the other hand are possible structures for diborane. The ethane structure is a permissible structure for $B_2H_6^{--}$. The argument is applied to the hypothetical molecule BH_3, but the conclusion is that the instability of this molecule is not due to symmetry.

ALTHOUGH the controversy over various proposed structures of diborane has passed its height, it is not out of place to call attention to an additional piece of evidence which from the theoretical standpoint may be regarded as decisive in excluding the "ethane-like" structure as a possible structure for the compound, diborane. At present, the generally accepted structure for B_2H_6 is the bridge structure or the protonated-double-bond structure. The treatment here will show that the bridge structure is an admissible structure while the ethane-like structure which, until ten years ago, was assumed to be correct, is not an admissible structure in the light of the present theoretical knowledge of diborane.

The calculation of the energy levels in diborane has been done by Mulliken, using the molecular orbital method. Originally, Mulliken[1] used the ethane-like structure as a basis for the calculation; later he extended the calculation to the bridge structure.[2] The measurements of Price[3] on the infrared spectrum of diborane were then considered conclusive in establishing the ethylene-type (bridge-type) structure. The experimental evidence favoring the ethane structure is based on the electron diffraction studies of Bauer[4] who is responsible for many of the earliest investigations of the hydrides of boron. Hedberg and Schomaker[5] have recently made electron diffraction study of diborane and conclude that the ethane structure is definitely eliminated by their work.

The arguments here will be based on two pieces of theoretical evidence: Mulliken's calculation of the molecular orbital energies for the ethane-like model of B_2H_6, a group-theoretical theorem due to Jahn and Teller[6] and an extension of the theorem by Jahn.[7] The combination of these two theoretical treatments shows that diborane in the ethane structure is unstable with respect to unsymmetrical vibrations of the nuclei and hence cannot exist in this structure. On the other hand, there is in the bridge structure no possibility of instability because of symmetry. (The structure could be unstable because of being too highly energetic.) Mulliken's application of the MO method to the bridge structure[2] shows that this structure is acceptable on energetic grounds.

The electronic structure of the ethane model of diborane is calculated by Mulliken to be $(1s)^2(1s)^2(\sigma_g)^2(\sigma_g)^2(\sigma_u)^2(\pi_u)^4(\pi_g)^2$.* Thus, the molecule has two electrons in the outermost π_g orbital, exists in a triplet state, and should be paramagnetic. (Experiment shows the compound to be diamagnetic.) In this configuration the electronic structure of diborane is formally similar to that of diatomic oxygen, an isostere of diborane.

The second piece of evidence is the theorem of Jahn and Teller which may be stated in these words: "A configuration of a polyatomic molecule for an electronic state having orbital degeneracy cannot be stable with respect to all displacements of the nuclei unless in the original configuration the nuclei all lie on a straight line." The proof of the theorem consists in showing that if the perturbation produced by the nontotally symmetric vibrations is expanded in terms of nontotally symmetric displacements of the unperturbed configuration, then the elements of the perturbation matrix, which are linear in these displacements, will not vanish if the function product $\phi_a V_r \phi_b$ contains in its reduced form the totally symmetric representation A_1. ϕ_a and ϕ_b are two wave functions which are solutions of the Hamiltonian for the unperturbed configuration; V_r is the expansion coefficient for the rth nontotally symmetric displacement in the linear term of the expansion of the perturbation energy in terms of these displacements. V_r is a function of the coordinates and has the symmetry of the nontotally symmetric vibrations of the nuclei. Unless these matrix elements do vanish, the perturbation energy will be a linear function of the nontotally symmetric displacement and hence motion along one of these coordinates will move the molecule into a more stable configuration of lower symmetry. The authors then show for the various finite symmetry groups that if ϕ_a and ϕ_b belong to any doubly-degenerate

[1] R. S. Mulliken, J. Chem. Phys. **3**, 635 (1935).
[2] R. S. Mulliken, Chem. Revs. **41**, 207 (1947).
[3] W. C. Price, J. Chem. Phys. **16**, 894 (1948).
[4] S. H. Bauer, J. Am. Chem. Soc. **59**, 1096 (1937).
[5] K. Hedberg and V. Schomaker, J. Am. Chem. Soc. **73**, 1482 (1951).
[6] H. A. Jahn and E. Teller, Proc. Roy. Soc. (London) **A161**, 220 (1937).
[7] H. A. Jahn, Proc. Roy. Soc. (London) **A164**, 117 (1938).

* The notation is that of Mulliken, reference 2.

representation (E) the direct product of E^2 with any nontotally symmetric representation will contain the representation A_1. In this way they complete the proof of the theorem.

In the light of this theorem, the fact that in the ethane structure the outermost pair of electrons in diborane are in an orbitally degenerate state of symmetry E is sufficient evidence to classify the ethane structure as an impossible structure for the compound. The symmetry species of the normal vibrations of the ethane structure are $4A_1+2A_2+6E$. The molecule in the ethane structure would then be unstable with respect to any of the fourteen vibrations $2A_2+6E$.

One could object to this and argue that since the molecular orbital method is necessarily an approximate method, the calculation may be inaccurate and that the ground state of the ethane structure might turn out to be nondegenerate in an exact calculation. This structure would in such a case not be an impossible structure. Although it is true that an exact calculation of the energy of the ground state of diborane would displace each energy level downward, it is unlikely that such a calculation would shift the order of the energy levels. In this connection it should be noted that the species $B_2H_6^=$,[2] C_2H_6, and $N_2H_6^{++}$ form an isoelectronic series, all have the same (ethane-like) electronic structure and geometrical configuration. The theorem considered here would admit the ethane structure for $B_2H_6^=$ since the addition of two more electrons to ethane-like B_2H_6 would fill the π_g level and produce a nondegenerate state. The chemical evidence supports the ethane structure for $B_2H_6^=$.

The extension of the theorem to include the effect of spin has been done by Jahn.[7] The theorem in this case shows that spin degeneracy in a nonlinear molecule will also cause instability except in the case of the twofold degeneracy which arises when the molecule has an odd number of electrons. (However, the spin effect is much smaller than in the case of orbital degeneracy and is insufficient to cause instability of an orbitally stable state.) It is possible that an orbitally unstable state may be stabilized by the spin property but for this to occur, it is necessary that the spin-orbit coupling be large (see Jahn). It is possible to conclude that the triplet-singlet splitting of the degenerate state will not alter the argument presented here. In fact, if the triplet state lies lower than the singlet, the orbital instability and spin instability reinforce each other.

For the instability of the symmetrical arrangement of nuclei to have practical consequences, that is, for the molecule to be incapable of existing in the supposed configuration, it is necessary that the electrons in the degenerate states be essential to the binding in the molecule. This is the case in diborane. With regard to the bridge structures, the theorem would predict no instability caused by symmetry since for these structures of symmetry V_h (symmetrical bridge) and C_{2v} (unsymmetrical bridge) the set of eigenfunctions does not include any degenerate functions. (The accidental degeneracy of two normally nondegenerate levels will not produce instability.)†

BORINE

It is tempting to ask if the Jahn-Teller theorem can be applied to explain the nonexistence of the molecule BH_3. Mulliken[8] has listed the electronic structure for this aggregate as

$$K,\ a_1')^2\ e')^4\ \ddagger \quad (D_{3h};\ \text{triangular, plane}),$$
$$K,\ a_1)^2\ \ e)^4 \quad (C_{3v};\ \text{pyramidal}).$$

In each case this order of levels yields a filled orbital and there is no orbital degeneracy. Unless this ordering of the levels is incorrect, either of these structures is acceptable. However, for purposes of argument, suppose that the structure is not that one given above but one which interchanges the order of the e' level or the e level with the next higher lying level, the structure would then be

$$K,\ a_1')^2\ a_2'')^2\ e')^2 \quad D_{3h},$$
$$K,\ a_1)^2\ \ a_2)^2\ \ e)^2 \quad C_{3v},$$

Neither of these structures could be stable, but there would be here a clear reason for the stability of such a molecule as $BH_3{:}C{::}O$. The additional pair of electrons from the carbon monoxide molecule would be sufficient to fill up the e level in the pyramidal model and produce stability in a structure of the same symmetry. (A curious sidelight is to note that borine carbonyl has much the same type electronic structure as CO_2.) This would provide an explanation of this type of addition reaction which occurs quite commonly with diborane. Such molecules as trimethyl amine, pyridine, methyl nitrile, dimethyl ether, etc., readily form addition products containing pyramidal BH_3 groups. The ready addition of H^- to form the borohydride ion would fall into the pattern; however, it is to be noted that one would compare the electronic structure of BH_4^- with that of CH_4 or NH_4^+, all of which presumably have the same electronic structure.

The acceptance of the first structure rules out the possibility that the instability is due to symmetry and places the blame on simple energetic factors. Indeed, although the considerations in the above paragraph are

† S. H. Bauer [p. 56 of Chem. Revs. **31**, 43 (1942)] states that Mulliken drew attention to the Jahn-Teller theorem in connection with the structure of diborane—apparently in a private communication. Without giving any reason, Bauer dismissed this argument against the ethane structure by saying that the instability due to symmetry might be overcome by movement to a displaced configuration only slightly different from the normal structure. For an example of a case in which the theorem has been applied and the effect is large, see J. O. Hirschfelder's treatment of H_3 in the triangular and linear configurations: J. Chem. Phys. **6**, 795 (1938). In addition, investigations in this laboratory confirm that the effect is large: see publications by V. Griffing and by A. Macek, now in preparation.

[8] R. S. Mulliken, J. Chem. Phys. **1**, 492 (1933).

‡ The configuration here is written simply in terms of the symmetry species to which the MO belong. K indicates a filled ($1s$) level on the boron atom.

tempting, such an explanation may raise more questions than it answers. For example, it would then be difficult to account for the observation in the mass spectrometer of the ion CH_3^+ (isoelectronic with BH_3) in large amounts in the methane spectrum. Alternatively, one could ask that the levels shift their order again in CH_3^+, or that the ion peak ascribed to CH_3^+ be actually due to the species $C_2H_6^{++}$ with a diborane structure. The first alternative is *ad hoc* but possible; as for the second, for such a dimeric species to occur in the methane mass spectrum under the conditions existing in the mass spectrometer is more than unlikely. One concludes that BH_3 has the structure proposed by Mulliken and the instability is not due to symmetry.

ACKNOWLEDGMENT

The author wishes to express his thanks to Dr. V. Griffing for directing his attention to the Jahn-Teller theorem and to both Dr. V. Griffing and Dr. J. T. Vanderslice for many helpful discussions.

THE JOURNAL OF CHEMICAL PHYSICS VOLUME 22, NUMBER 3 MARCH, 1954

Equilibrium Theory of Unimolecular Reactions*

J. Calvin Giddings and Henry Eyring
University of Utah, Salt Lake City, Utah
(Received July 20, 1953)

This paper develops an equilibrium theory of unimolecular reactions, and shows how this theory is related to other theories, such as the Rice-Ramsperger-Kassel treatment. Unimolecular decomposition reactions and isomerization reactions are described in terms of statistical mechanics and quantum mechanics (potential energy surfaces). The nature of the transmission coefficient is discussed in detail.

I. INTRODUCTION

IT is frequently erroneously stated that the theory of unimolecular reaction rates cannot be described by usual equilibrium methods. It is true that we are unable to predict, *a priori*, experimental reaction rates, but this is true of reactions of any molecularity. We will show that the theory of unimolecular reactions lends itself easily to a statistical mechanical description, and that the problem, as in the case of bimolecular reactions, is complete when the correct potential energy surfaces are given.

II. THE TRANSMISSION COEFFICIENT AT HIGH PRESSURES

The high-pressure rate of any reaction is given by the expression,

$$k_\infty' = \kappa \frac{kT}{h} \exp(\Delta S^\ddagger/R) \exp(-\Delta H^\ddagger/RT), \qquad (1)$$

in which usual reaction rate terminology has been used. Since the transmission coefficient κ will be important to this development it is well to point out that κ is not a function alone of the coordinates of the potential energy surface; it is an average of individual transmission coefficients, properly weighted, representing paths of reaction through every possible quantum state of the activated complex. Considering, for example, the association reaction of two triphenyl methyl radicals, the rate equation, strictly written, is

$$k_\infty' = \sum_t \kappa_t \frac{kT}{h} \frac{\omega_t}{F_i} e^{-\epsilon_t/kT}, \qquad (2)$$

where ω_t is the degeneracy of the activated state t, and F_i the partition function of the reactant. The subscript t represents a particular activated state with energy ϵ_t. κ_t may be strongly dependent upon the state t of reaction and therefore be pressure and temperature dependant. This is generally the case for unimolecular processes. Two effects militate against achieving a long lived association complex from two radicals. First, there is a slowness of energy transfer from the reaction coordinate to the internal vibrations. Second, since the internal energy levels of hexaphenylethane are discrete, the fitting of the continuous spectrum of the colliding radicals to this discrete spectrum will only occasionally be of such a nature as to lead to a long lived intermediate. If the levels of the discrete spectrum are closely spaced, and if κ_t is not notably different for low- and high-energy levels, then we have

$$k_\infty' = \bar{\kappa} \frac{kT}{h} \sum_t \frac{\omega_t}{F_i} e^{-\epsilon_t/kT} = \bar{\kappa} \frac{kT}{h} \frac{F_0^\ddagger}{F_i} e^{-\epsilon_0/kT}, \qquad (3)$$

where $\bar{\kappa}$ will have little temperature dependence. We may assume for most bimolecular reactions of the type $A+B \rightarrow C+D$ that for all t's, $\kappa_t \sim 1$, so that $\bar{\kappa} \sim 1$. For the recombination of triphenylmethyl radicals, however, evidence shows that $\bar{\kappa} \sim 0.1$.[1] Thus for the inverse

* This research was carried out under a U. S. Air Force grant, Contract Number 33(038)-20839.

[1] Giddings, Cagle, Ree, and Eyring (to be published).

reaction, the unimolecular dissociation of hexaphenylethane, we must also have $\kappa \sim 0.1$.

III. DECOMPOSITION REACTIONS

The rate of a unimolecular reaction, following Eq. (2), is conveniently written as the sum of the rate of all possible reaction paths. The reaction scheme for a reaction of the type $A \rightarrow B+C$ is,

$$A+A \underset{k_{-i}}{\overset{k_i}{\rightleftarrows}} A_\epsilon^*+A \tag{4}$$

$$A_\epsilon^* \overset{k_\epsilon}{\rightarrow} A\ddagger \rightarrow B+C. \tag{5}$$

An unnecessarily involved discussion of this situation has appeared recently.[2] Evans and Rushbrooke[3] consider a rate constant for the reaction $A\ddagger \rightarrow A^*$. There is little reason to expect this reflection back into the active molecule A^* to be significant. It is to be remembered that the equilibrium postulate of rate theory concerns only the concentration of forward moving systems (see Wynne-Jones and Eyring).[4] The rate constant k_{-i} is usually written as λZ in which λ is an efficiency factor and Z is the collision number of the active species. Nothing can be said about the value of λ without considering the potential energy surface for the deactivation process. These considerations lead to the equation

$$k_{-i}=\frac{\sum_{a\cdots n}\left(\sum_{a'\cdots n'}\kappa_{a\cdots n}^{a'\cdots n'}\right)\frac{1}{2}\frac{ah}{2\delta^2 m\ddagger}\exp\left(-\frac{\epsilon_a{}^1+\cdots+\epsilon_n{}^N}{kT}\right)}{F_{A\epsilon}{}^* F_A}. \tag{6}$$

This is, again, a summation over all processes that lead to deactivation. The N quantum numbers of the critical collision complex involving A and $A_\epsilon{}^*$ have the values $a\cdots n$. The quantum numbers of the final state, in which the molecule is deactivated, are given as $a'\cdots n'$. When the process does not lead to deactivation, it is not considered, since the transmission coefficient is zero. $F_{A\epsilon}{}^*$ and F_i are the partition functions of the active and normal molecule, respectively. δ is the extension of the critical complex along the reaction coordinate. The first summation to the right is the sum of all transmission coefficients proceeding from the state, $a\cdots n$, to all final states $a'\cdots n'$. The first summation involves the transmission coefficient and the frequency of passage through the critical state, $ah/2\delta^2 m\ddagger$ (a is the quantum number representing this translation). The rest of the expression (6) gives the chance that an activated complex will be found in a state represented by quantum numbers, $a\cdots n$. This chance is the exponential term divided by the partition functions, $F_{A\epsilon}{}^*$ and F_A. The summation is then over all possible states of the critical collision complex. The factor $\frac{1}{2}$ is necessary since only half of the critical complexes are moving in the forward direction along the reaction coordinate. The rate constant k_i is simply $K_\epsilon k_{-i}$ where K_ϵ is the equilibrium constant per unit energy range leading to the active molecule $A_\epsilon{}^*$ (4). The nature of k_ϵ will be discussed below.

Consider the equilibrium of each active molecule having energy between ϵ and $\epsilon+\delta\epsilon$, where $\epsilon \geq \epsilon_0$, the minimum energy of reaction. The fraction of molecules with energy ϵ, per unit energy range, is

$$F_\epsilon = a_\epsilon K_\epsilon, \tag{7}$$

where K_ϵ is the equilibrium constant k_i/k_{-i} and a_ϵ is a nonequilibrium constant with value,

$$a_\epsilon = \frac{k_{-i}A}{k_{-i}A+k_\epsilon}, \tag{8}$$

A is the concentration of reactant. The rate, written as a sum (we use here the integral) of reactions, is

$$k' = \int_{\epsilon=0}^{\epsilon=\infty} F_\epsilon k_\epsilon d\epsilon = \int_{\epsilon=0}^{\infty} \frac{k_\epsilon k_i A}{k_\epsilon + k_{-i}A} d\epsilon. \tag{9}$$

This clearly shows the nature of the pressure dependence of k'. We may also write,

$$k' = a\kappa \frac{kT}{h} \exp(\Delta S\ddagger/R) \exp(-\Delta H\ddagger/RT). \tag{10}$$

We let a equal the transmission coefficient due to low pressure effects. The relation of a to a_ϵ, is

$$a = \int_0^\infty k_\epsilon a_\epsilon K_\epsilon d\epsilon \Big/ \int_0^\infty k_\epsilon K_\epsilon d\epsilon, \tag{11}$$

which shows a as the weighted average of a_ϵ. a is of course pressure dependent.

IV. EQUILIBRIUM THEORY OF k_ϵ

In a recent paper by Rosenstock, Wallenstein, Wahrhaftig, and Eyring,[5] the concept of equilibrium used in absolute reaction rate theory was extended to include an

[2] S. W. Benson and A. E. Axworthy, Jr., J. Chem. Phys. **21**, 428 (1953).

[3] M. G. Evans and G. S. Rushbrooke, Trans. Faraday Soc. **41**, 621 (1945).

[4] W. F. K. Wynne-Jones and H. Eyring, J. Chem. Phys. **3**, 492 (1935).

[5] Rosenstock, Wallenstein, Wahrhaftig, and Eyring, Proc. Natl. Acad. Sci. **38**, 667 (1952).

evaluation of k_ϵ. Assuming a transmission coefficient of unity, k_ϵ can be written exactly, for any system, as

$$k_\epsilon=\frac{1}{h}\int_0^{\epsilon-\epsilon_0}\frac{\rho^\ddagger(\epsilon,\epsilon_0,\epsilon_t)}{\rho(\epsilon)}d\epsilon_t. \tag{12}$$

$\rho^\ddagger(\epsilon,\epsilon_0,\epsilon_t)$ and $\rho(\epsilon)$ are energy densities of the activated complex and normal molecule, respectively. ϵ_t is the translational energy across the saddle point of the activated complex. If it be assumed that both the excited molecule and the activated complex contain classical harmonic oscillators only, Eq. (12) yields

$$k_\epsilon=\frac{\prod^{s}\nu_i}{\prod^{s-1}\nu_i^\ddagger}\left(\frac{\epsilon-\epsilon_0}{\epsilon}\right)^{s-1}. \tag{13}$$

s equals the number of oscillators in the excited molecule. If k_ϵ in Eq. (12) is averaged over a thermal distribution of molecules to give k', the result is the usual absolute reaction rate expression, as it must be, since both equations are derived from equilibrium considerations. The proof of this has been shown by Magee.[6] If there is not a thermal (high-pressure) distribution K_ϵ, but a distribution F_ϵ, the rate constant at any pressure is simply

$$k'=\frac{1}{hF_A}\int_0^\infty a_\epsilon\rho(\epsilon)e^{-\epsilon/kT}d\epsilon\int_0^{\epsilon-\epsilon_0}\frac{\rho^\ddagger(\epsilon,\epsilon_0,\epsilon_t)}{\rho(\epsilon)}d\epsilon_t, \tag{14}$$

in which a_ϵ is described by Eq. (8).

V. THE RICE-RAMSPERGER-KASSEL TREATMENT

In order to arrive at the Rice-Ramsperger-Kassel results, a definite molecular model must be used. We must assume that (a) the molecular species are composed of classical harmonic oscillators, (b) there can be no bond extension so as to affect rotational partition functions, (c) the activated molecules must be in some sort of equilibrium with the active molecules, and (d) $k_{-i}=Z$, the collision number. For classical oscillators, statistical mechanics gives us the formula,

$$K_\epsilon=\frac{\epsilon^{s-1}}{(kT)^s\Gamma(s)}e^{-\epsilon/kT}. \tag{15}$$

This is equivalent to assumption (a). Assumption (c) as given by the original authors[7] is in the form

$$k_\epsilon=\bar{\nu}\left(\frac{\epsilon-\epsilon_0}{\epsilon}\right)^{s-1}. \tag{16}$$

$\bar{\nu}$ will be identified presently. Use of Eq. (9) now leads identically to the Kassel equation,[7]

$$k'=\frac{\bar{\nu}e^{-\epsilon_0/kT}}{\Gamma(S)(kT)^s}\int_0^\infty\frac{e^{-x/kT}dX}{\dfrac{1}{X^{s-1}}+\dfrac{\bar{\nu}/ZA}{(X+\epsilon_0)^{s-1}}}, \tag{17}$$

where use has been made of the substitution $X=\epsilon-\epsilon_0$.

At high pressures, evaluation of the integral leads to,

$$k_\infty'=\int_0^\infty K_\epsilon k_\epsilon d\epsilon=\bar{\nu}e^{-\epsilon_0/kT}. \tag{18}$$

This rate must also equal

$$k_\infty'=\kappa\frac{kT}{h}\frac{F^*}{F_A}e^{-\epsilon_0/kT}. \tag{19}$$

For the model employed (assumptions (a) and (b)),

$$k_\infty'=\kappa\frac{\prod^{s}\nu_i}{\prod^{s-1}\nu_i^\ddagger}e^{-\epsilon_0/kT}, \tag{20}$$

which identifies the quantities,

$$\bar{\nu}=\kappa\frac{\prod^{s}\nu_i}{\prod^{s-1}\nu_i^\ddagger}. \tag{21}$$

The difference between Eqs. (21) and (13) is found in the assumption that the transmission coefficient of (12) is unity. If it is not, Eq. (12) should be multiplied on the right side by κ. Since the only assumption made in deriving (12) was that $\kappa=1$, the expression is now completely general, and will lend itself to further modification of the expression k_ϵ. This equation has been used in a more general case,[5] that in which the decomposing molecule consists of η classical internal rotators. Other applications are possible.

It is to be noted that under any circumstances the high-pressure reaction rate of common reactions cannot exceed the value given by Eq. (1) with $\kappa=1$, except as tunneling makes $\kappa>1$. A recent paper[8] that uses Slater's results[9] replaces kT/h by a molecular constant, which, at least at low temperatures, is larger than kT/h. This of course means more than an equilibrium concentration of activated complexes; a contradiction of rigorous statistical mechanics. Slater's paper deals with classical oscillators, and the results derived therewith form a special case of the general absolute reaction rate theory.

VI. ISOMERIZATION REACTIONS

Application of absolute reaction rate theory to unimolecular isomerization reactions involves several new

[6] J. L. Magee, Proc. Natl. Acad. Sci. **38**, 764 (1952).
[7] L. S. Kassel, *Kinetics of Homogeneous Gas Reactions* (Chemical Catalog Company, Inc., New York, 1932).
[8] S. W. Benson, J. Chem. Phys. **20**, 1064 (1952).
[9] N. B. Slater, Proc. Roy. Soc. (London) **A194**, 112 (1948).

considerations. In the racemization of ethylene derivatives there is apparently competition between normal passage over the barrier of the reaction coordinate and an electronic reorganization which allows passage through the barrier at a lower level.[10] The two competing rates are given approximately by the following expressions:

$$k \sim 10^{4} e^{-25\,000/RT} \text{ sec}^{-1};$$

and

$$k \sim 10^{11} e^{-45\,000/RT} \text{ sec}^{-1}.$$

A quantum-mechanical approach has been made in agreement with experimental values. A complete discussion is found elsewhere.[10]

Consider a sterically hindered biphenyl that has just passed through the activated state. The molecule could possibly continue to rotate until deactivated, or, if the second barrier is higher than the first, the system might be reflected back through the same activated complex, repeatedly, and this may continue until the molecule is deactivated. The process of deactivation allows for several alternatives, all of which depend upon the pressure and certain molecular constants. The molecular constants are a function of the potential energy surface, and real progress must consist in their evaluation. The rate of reaction is given, again, at high pressures, by the absolute reaction rate expression. The transmission coefficient at these pressures has been shown to probably equal unity.[11] At lower pressures the transmission coefficient depends upon both the pressure and the previously mentioned molecular constants. The evaluation of the transmission coefficient is always easily made in terms of the molecular constants, all of which represent rate of internal energy transfer.

We will now define two molecular entities involved in the isomerization reaction $A \rightarrow B$. A^+, we shall define as having the spatial configuration of A, but with sufficient energy in the reaction coordinate to spontaneously rearrange to B. We define B^+ in the same manner. A^*, with the configuration of A, is defined as having sufficient internal energy distributed within its internal coordinates to cross the potential barrier. B^* is analogously defined. The latter two are usually referred to as active molecules. Consider the process of deactivation for the above reaction. This may involve collision with either B^* or B^+, with resulting deactivation. In fact, at low pressures, B^* and B^+ may be in dynamic equilibrium, and the rate controlling step probably involves collision with that species having the longer lifetime. Since the adjacent groups are so large in sterically hindered biphenyls, B^* will have a much

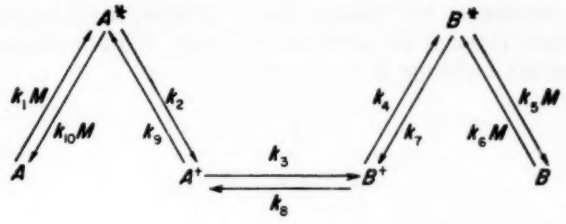

FIG. 1.

greater lifetime than B^+, so that its deactivation will be rate controlling. This will also be true for the smaller ethylene derivatives. In fact, the lifetime, τ_2, of B^* relative to τ_1, of B^+, is

$$\frac{\tau_2}{\tau_1} \sim \left(\frac{\epsilon - \epsilon_0}{\epsilon}\right)^{s-1},$$

where ϵ_0 is the energy of reaction. If B^+ rotates several times when formed, then the transmission coefficient, which will be multiplied into Eq. (12), will be small. At high pressures, B^+ will be deactivated immediately after reaction by collision. The transmission coefficient will then be unity. The path of reaction involving the larger transmission coefficient will, in general, determine the rate of reaction.

As mentioned, the transmission coefficient is easily solved for in principle. We will illustrate the method of solution when deactivation of B^* is rate controlling (low-pressure region). Figure 1 gives the scheme for reaction. M is the concentration of any species that may deactivate either A^* or B^*. The activated complex lies midway between A^+ and B^+. The rate of reaction can be written,

$$k' = \langle \kappa_1 \kappa_2 \rangle_{Av} \frac{kT}{h} \exp(\Delta S^{\ddagger}/R) \exp(-\Delta H^{\ddagger}/RT). \quad (22)$$

The transmission coefficient κ is composed of two separate coefficients, κ_1, the nonequilibrium coefficient and κ_2, the reflection coefficient. κ_1 we define as being that concentration of forward moving activated complexes when there is no product B divided by their concentration at complete equilibrium. Since forward moving activated complexes result directly from the rearrangement of A^+, κ_1 is equal to the concentration of A^+ when there is no B divided by the equilibrium concentration of A^+. The result follows directly after solving the steady state equations for A^*, A^+, B^+, and B^*. The value of κ_1 is

$$\kappa_1 = \frac{k_1 k_2 (k_7 k_8 + k_5 k_8 M + k_4 k_5 M) M}{k_1 k_2 (k_7 k_8 + k_5 k_8 M + k_4 k_5 M) M + \dfrac{k_1 k_2 k_3 k_4 k_5}{k_9 k_{10}} (k_2 + k_{10} M) M}. \quad (23)$$

[10] Glasstone, Laidler, and Eyring, *Theory of Rate Processes* (McGraw-Hill Book Company, Inc., New York, 1941).
[11] F. W. Cagle, Jr., and H. Eyring, J. Am. Chem. Soc. **73**, 5628 (1951).

κ_2 represents the chance that a system, after having passed through the activated complex, will remain as a product molecule B. κ_2 is equal to,

$$\kappa_2=\frac{k_4k_5M}{k_4k_5M+k_5k_8M+k_7k_8}. \tag{24}$$

The product of κ_1 and κ_2 is the total transmission coefficient, κ.

$$\kappa=\frac{1}{1+\left(\frac{k_8}{k_4}+\frac{k_3}{k_9}\right)+\left(\frac{k_7k_8}{k_4k_5}+\frac{k_2k_3}{k_9k_{10}}\right)\frac{1}{M}}. \tag{25}$$

κ is, of course, completely symmetrical in A and B, and represents the transmission coefficient for either $A\rightarrow B$, or its reverse, $B\rightarrow A$.

The transmission coefficient as derived above is for unit energy range. The observed transmission coefficient, when the energy distribution is thermal, is an average of the expression κ, above, weighted by the term $K\ddagger$, the equilibrium constant of the activated molecule.

VII. CONCLUSION

Many other unimolecular reactions have been studied that illustrate even more diverse phenomena. These aspects of the problem are discussed in *The Theory of Rate Processes*.[10]

It is seen that the rate of any one of these reactions can be written in two ways: (a) strictly in terms of molecular constants, or (b) by equilibrium theory with a transmission coefficient that depends upon molecular constants and reduces to unity for a broad range of experiment. The advantage of the latter is that it is founded upon the broad and powerful concepts of statistical mechanics, such that when summing over all possible quantum paths of reaction we merely use well-established partition functions. Otherwise we would need to invent a complete new set of mathematical tools for this summation process, and the result in the end would be of no more value. With the derivation of Eq. (12), and with the use of Eq. (6), (all of these are based upon equilibrium considerations), all rates, including the transmission coefficient, can be derived strictly from equilibrium theory. The big problem still remain of course, is the construction of satisfactory potential energy surface, and the quantum mechanical calculation of transmission coefficients.

THE JOURNAL OF CHEMICAL PHYSICS VOLUME 22, NUMBER 3 MARCH, 1954

The Infrared Spectra of Monochlorogermane and Monochlorogermane-d_3*

R. C. Lord and C. M. Steese†
Spectroscopy Laboratory and Department of Chemistry, Massachusetts Institute of Technology, Cambridge 39, Massachusetts

(Received October 26, 1953)

Infrared absorption spectra of GeH_3Cl and GeD_3Cl have been observed and the fundamentals located at 2121.2, 847.7, 422.6 cm^{-1} (parallel) and 2129.4, 874.6, 604.1 cm^{-1} (perpendicular) in GeH_3Cl, and at 1522, 614, 421 cm^{-1} (parallel) and 1530, 630, 434 cm^{-1} (perpendicular) in GeD_3Cl. Analysis of the rotational structure of the perpendicular bands in GeH_3Cl leads to these values of the rotational constants: A'', 2.603 cm^{-1}; ζ_4, −0.059; ζ_5, −0.124; ζ_6, +0.209. Agreement with microwave A'' is satisfactory. Thermodynamic quantities are computed for GeH_3Cl and GeD_3Cl.

EXPERIMENTAL

Preparation of GeH_3Cl

THE vibrational spectra of various monohalides of carbon and silicon have been investigated in detail, along with the rotational fine structure in many instances. The spectra of the germanium analogs have not been studied, however, and for various reasons are of interest. In the present paper the rotation-vibration spectrum of GeH_3Cl as resolved by a prism instrument is reported, along with the vibrational spectrum of the deuterium analog GeD_3Cl.

The preparation was based on the original preparative method of Dennis and Judy[1] in which gaseous monogermane (GeH_4) and HCl react in the presence of aluminum chloride to form GeH_3Cl and hydrogen. The widest departure from the procedure of Dennis and Judy was the use of stopcocks instead of mercury float valves. Apiezon "*M*" grease was not suitable as a stopcock lubricant, since it is rather readily dissolved by

* This paper is based on a thesis submitted by C. M. Steese to the Graduate School of the Massachusetts Institute of Technology in partial fulfillment of the requirements for the degree M.S. in Chemistry. The work received financial support from the Office of Ordnance Research (Contract DA-19-020-ORD-896), which is gratefully acknowledged. Deuterium was obtained on allocation by the Stable Isotopes Division, U. S. Atomic Energy Commission.

† Present address: Department of Chemistry, California Institute of Technology, Pasadena, California.

[1] Dennis and Judy, J. Am. Chem. Soc. **51**, 2321 (1929).

the chlorinated products, but Dow-Corning Silicone high-vacuum grease proved satisfactory. However, after extended contact with the chlorinated germanes it tended to become tough and rubbery, and occasionally stopcocks would develop striations. It is quite possible that a fluorocarbon grease might prove to be the ideal stopcock lubricant under these conditions.

GeH_4 was obtained from Metal Hydrides, Inc.,‡ and was used without further purification after its infrared spectrum had been examined. The spectrum showed only the previously reported bands[2] of GeH_4 with the exception of one of moderate intensity at 1035 cm^{-1}. This new band is believed from its structure to belong to GeH_4 also. Mathieson anhydrous HCl and Baker's reagent grade anhydrous $AlCl_3$ were also used without further purification.

After the reaction had proceeded to a considerable extent,[3] the GeH_3Cl produced was separated from the lower-boiling unreacted GeH_4 and HCl, and from higher-boiling reaction products, by a series of bulb-to-bulb distillations. The efficiency of these distillations was

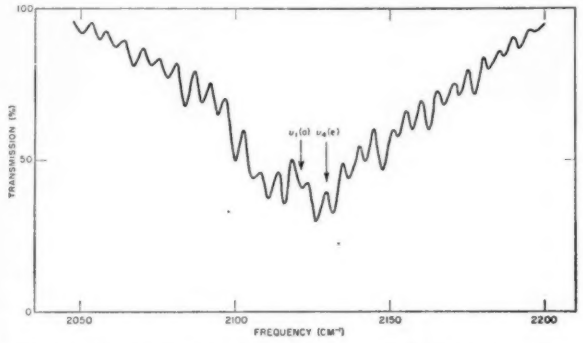

FIG. 1. Rotational structure of perpendicular band ν_4 and parallel band ν_1 in monochlorogermane.

monitored carefully by frequent determination of the infrared spectra of the fractionated products. The final fraction of purified GeH_3Cl, when condensed, was a colorless liquid which darkened slowly on standing. GeH_3Cl gas also gradually decomposed on standing at low pressure (10 cm) and room temperature, a yellowish film being deposited on the walls of the glass vessel. However, the liquid was apparently quite stable when stored at dry-ice temperature. The over-all yield of this preparation was quite poor, being around 5 percent of the starting GeH_4 uncorrected for recoverable, unchanged GeH_4.

GeD_3Cl was prepared from GeD_4 as a starting material in the same way. A better yield was obtained, probably because of the experience acquired with the GeH_3Cl. GeD_3Cl is also a colorless mobile liquid stable at dry-ice temperature for periods in excess of a week.

‡ We are indebted to Dr. M. D. Banus, of Metal Hydrides, Inc., Beverly, Massachusetts, for preparation of both GeH_4 and GeD_4.

[2] A. H. Nielsen and H. H. Nielsen, Phys. Rev. **48**, 861 (1935); Straley, Tindal, and Nielsen, Phys. Rev. **62**, 161 (1942).

[3] Details of the preparative procedure will be found in the M.S. thesis of C. M. Steese.

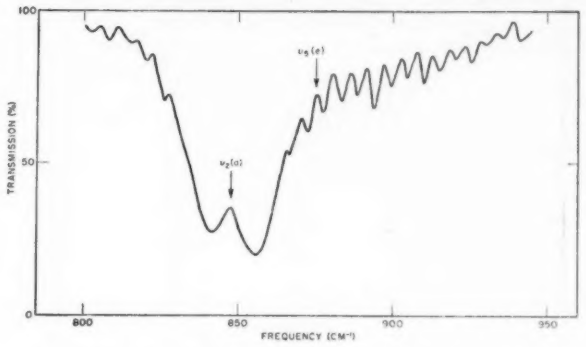

FIG. 2. Rotational structure of perpendicular band ν_5 and parallel band ν_2 in monochlorogermane.

Determination of the Infrared Spectra

The absorption spectra of GeH_3Cl and GeD_3Cl vapor were recorded with a Perkin-Elmer Model 12B spectrometer modified[4] to permit the removal of atmospheric water vapor and carbon dioxide. Spectra were taken with prisms of LiF, NaCl, KBr, and TlBr—TlI, each prism being used in its region of optimum dispersion. Achieved resolution was about 3 cm^{-1} throughout, and absolute frequency measurement (in cm^{-1} in vacuum) reliable to 1 cm^{-1}. The precision with which measurements could be repeated was better than this with the perpendicular bands of GeH_3Cl. When these bands

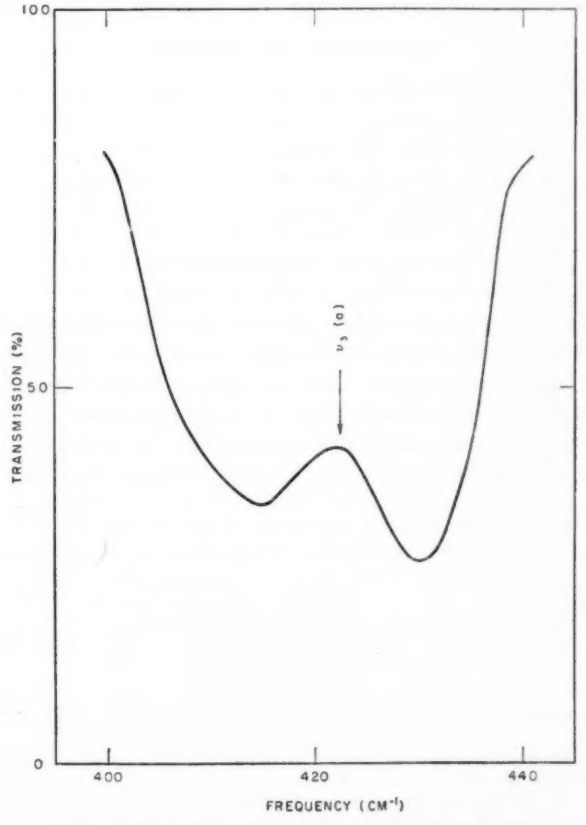

FIG. 3. Parallel band ν_3 in monochlorogermane.

[4] Lord, McDonald, and Miller, J. Opt. Soc. Am. **42**, 149 (1952).

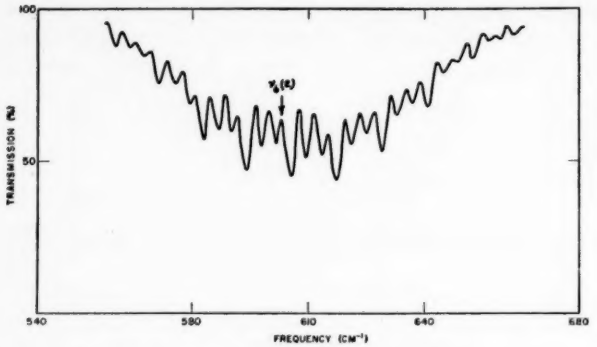

FIG. 4. Rotational structure of perpendicular band ν_6 in monochlorogermane.

were measured, spectra of carbon monoxide, ammonia, water vapor, and carbon dioxide (whichever was appropriate) were run immediately before and after the GeH_3Cl spectrum. With the help of the standard frequencies for these bands,[5–7] which are known to 0.1 cm^{-1} or better, the sub-bands of the perpendicular bands of GeH_3Cl could be measured with a precision approaching 0.2 cm^{-1}.

The absorption cell was 6 cm long with KBr windows and carried a side arm in which GeH_3Cl and GeD_3Cl could be condensed. Pressures used varied from 2 mm to 50 mm. The individual fundamental bands of GeH_3Cl are shown in Figs. 1–4 and the fundamental frequencies for GeH_3Cl and GeD_3Cl listed in Table I.

DISCUSSION OF SPECTRA

There is little question from the rotational structure of the infrared bands that GeH_3Cl is a symmetrical top of C_{3v} symmetry. The assignment of the three symmetrical and three degenerate fundamentals shown in Table I is likewise unambiguous, although the bands of vibrations 1 and 4 overlap, as do those of 2 and 5. Location of the center of the parallel band of vibration 4 was effected as follows. A smooth envelope was drawn through the peaks of the *weak* sub-bands at both edges of the perpendicular band where the parallel band has negligible absorption. The two parts of this envelope were then joined smoothly at the band center. The contour so obtained was assumed to be that of the *weak* sub-band peaks near the center of the band, and the difference between it and the observed weak sub-band peaks then was ascribed to the absorption of the parallel band. Several points on the parallel-band contour were thus obtained, and the envelope and center of the band estimated therefrom.

TABLE I. Fundamental frequencies of GeH_3Cl and GeD_3Cl.

Vib'l. species and band type	Vibr. no.	Type of vibration	Frequency in cm^{-1} GeH_3Cl	Frequency in cm^{-1} GeD_3Cl	Product rule
A_1 (parallel)	1	Ge−H stretching	2121.2	1522	$\tau_{obs}=1.94$
	2	GeH_3 bending	847.7	614	$\tau_{calc}=1.97$
	3	Ge−Cl stretching	422.6	421	
E (perpendicular)	4	Ge−H stretching	2129.4	1530	$\tau_{obs}=2.69$
	5	GeH_3 bending	874.6	630	$\tau_{calc}=2.71$
	6	GeH_3 rocking	604.1	434	

[5] K. N. Rao, J. Chem. Phys. **18**, 213 (1950).
[6] Oetjen, Kao and Randall, Rev. Sci. Instr. **13**, 515 (1942).
[7] Randall, Dennison, Ginsburg, and Weber, Phys. Rev. **52**, 160 (1937).

Parallel Bands

The spacing of the lines in parallel bands is governed by the rotational constant B, which is known from microwave studies[8] to have the value of 0.144 cm^{-1}. It is thus impossible to resolve individual lines of spacing $2B$ with our prism spectrometer. Moreover because of the very small ratio of B to the other rotational constant A, which ratio controls the intensity ratio of the Q branch to that of the P and R branches, the latter are each nearly ten times stronger than the Q branch. It therefore proved to be impossible even to resolve the Q branch, and a doublet structure was observed for the parallel bands in all cases. The $P-R$ spacing from the formula of Gerhard and Dennison[9] should be 16.1 cm^{-1} at room temperature, and the observed spacings vary from 14.4 to 15.7 cm^{-1}. This can be regarded as sufficient agreement, in view of the overlapping of two parallel bands by perpendicular ones and the effect of the numerous germanium-chlorine isotopic combinations on the shape of the third.

TABLE II. Frequencies in cm^{-1} (vac) of sub-bands in the 2129 cm^{-1} band of GeH_3Cl.

Assignment	Frequency in cm^{-1}	Rel. int.	$^RQ_K-{}^PQ_K$	$^RQ_K+{}^PQ_K$
$^RQ_{13}$	2196.5	w	135.4	4257.6
$^RQ_{12}$	2191.9	s	124.9	4258.9
$^RQ_{11}$	2186.8	w	114.2	4259.4
$^RQ_{10}$	2182.0	w	103.7	4260.3
$^RQ_9$	2177.4	s	93.7	4261.1
$^RQ_8$	2172.4	w	83.3	4261.5
$^RQ_7$	2167.6	w	73.2	4262.0
$^RQ_6$	2162.8	s	62.7	4262.9
$^RQ_5$	2157.5	w	51.9	4263.1
$^RQ_4$	2152.8	w	42.1	4263.5
$^RQ_3$	2147.9	s	32.0	4263.8
$^RQ_2$	2142.4	w	20.9	4263.9
$^RQ_1$	2136.9	w	10.6	4263.2
$^RQ_0$	2131.5	s		
$^PQ_1$	2126.3	w		
$^PQ_2$	2121.5	w		
$^PQ_3$	2115.9	s		
$^PQ_4$	2110.7	w		
$^PQ_5$	2105.6	w		
$^PQ_6$	2100.1	s		
$^PQ_7$	2094.4	w		
$^PQ_8$	2089.1	w		
$^PQ_9$	2083.7	s		
$^PQ_{10}$	2078.3	w		
$^PQ_{11}$	2072.6	w		
$^PQ_{12}$	2067.0	s		
$^PQ_{13}$	2061.1	w		
$^PQ_{14}$	2055.9	w		
$^PQ_{15}$	2050.0	s		

[8] Dailey, Mays, and Townes, Phys. Rev. **76**, 136 (1949); J. M. Mays and B. P. Dailey, J. Chem. Phys. **20**, 1695 (1952).
[9] S. L. Gerhard and D. M. Dennison, Phys. Rev. **43**, 197 (1933).

Perpendicular Bands

The large size of the rotational constant A enables an easy resolution of the sub-bands of the perpendicular bands in GeH_3Cl. In GeD_3Cl, however, where A has half its value in GeH_3Cl, such resolution was not achieved, although it was hoped in advance that resolution would be possible, at least for the band due to the Ge—D stretching vibration. The frequencies of the various sub-band peaks for the three perpendicular bands of GeH_3Cl are listed in Tables II–IV.

Location of band centers and assignments of the sub-band peaks are facilitated by the usual intensity alternation resulting from the nuclear spin of the protons. The band center lies between the ${}^RQ_0$ and ${}^PQ_1$ sub-bands, the former being the strongest Q branch near the center of gravity of the band and the latter the first weak Q branch on the low-frequency side of ${}^RQ_0$.

TABLE III. Frequencies in cm^{-1} (vac) of sub-bands in the 875 cm^{-1} band of GeH_3Cl.

Assignment	Frequency in cm^{-1}	Rel. int.	${}^RQ_K-{}^PQ_K$	${}^RQ_K+{}^PQ_K$
${}^RQ_{12}$	941.3	s	133.1	1749.5
${}^RQ_{11}$	935.8	w	120.8	1750.8
${}^RQ_{10}$	930.2	w	110.0	1750.4
${}^RQ_9$	925.6	s	99.3	1751.9
${}^RQ_8$	920.2	w		
${}^RQ_7$	915.0	w		
${}^RQ_6$	910.1	s		
${}^RQ_5$	904.7	w		
${}^RQ_4$	899.5	w		
${}^RQ_3$	894.2	s		
${}^RQ_2$	888.8	w	22.4	1755.2
${}^RQ_1$	883.2	w	10.6	1755.8
${}^RQ_0$	877.4	s		
${}^PQ_1$	872.6	w		
${}^PQ_2$	866.4	w		
	...			
${}^PQ_9$	826.3	s		
${}^PQ_{10}$	820.2	w		
${}^PQ_{11}$	815.0	w		
${}^PQ_{12}$	808.2	s		

Assignment of the sub-band peaks in the heavily overlapped band of vibration 5 is made by choosing appropriate K values for sub-bands of comparable intensity on each side of the band where interference is negligible. Interpolation can then be made to overlapped sub-bands.

The equation for the sub-band frequencies is given by[10]

$$\nu=\nu_0+[A_v'(1-2\zeta_i)-B_v']\pm 2[A_v'(1-\zeta_i)-B_v']K+[A_v'-B_v')-(A_v''-B_v'')]K^2. \quad (1)$$

For the purpose of obtaining the coefficient of the K term, $({}^RQ_K-{}^PQ_K)/2$ was plotted against K. The resultant straight line through the origin has a slope equal to this coefficient. Similarly the coefficient of K^2 was found from a plot of $({}^RQ_K+{}^PQ_K)/2$ against K^2, the slope giving the coefficient and the intercept the constant terms in Eq. (1). Least-squares treatment of the individual points leads to the following equations for the sub-band peaks of the three perpendicular bands:

$$\nu_4=2132.1\pm 5.19K-0.02K^2 \quad (2)$$

$$\nu_5=\ 877.6\pm 5.52K-0.02K^2 \quad (3)$$

$$\nu_6=\ 605.5\pm 3.84K+0.005K^2. \quad (4)$$

From Eqs. (1)–(4) and the expression for the ζ-sum of XYZ_3 molecules,[11] which has the value $B'/2A'$, it follows that

$$12A'-14B'=29.08 \quad (5)$$

if the variation in A' and B' implied by the subscript v be disregarded. Substitution of the microwave value[8] of B_0 (0.144 cm^{-1}) for B' then gives $A'=2.591$ cm^{-1}, which represents an average value of A' for the three perpendicular vibrations, i.e., $(A_4'+A_5'+A_6')/3$.

If it be assumed that $B'=B''$ for all perpendicular vibrations, the coefficients of the K^2 terms then yield a

TABLE IV. Frequencies in cm^{-1} (vac) of sub-bands in the 604 cm^{-1} band of GeH_3Cl.

Assignment	Frequency in cm^{-1}	Rel. int.	${}^RQ_K-{}^PQ_K$	${}^RQ_K+{}^PQ_K$
${}^RQ_{13}$	656.4	w		
${}^RQ_{12}$	652.2	s	92.2	1212.2
${}^RQ_{11}$	648.4	w	84.8	1212.0
${}^RQ_{10}$	644.6	w	77.3	1211.9
${}^RQ_9$	640.8	s	69.6	1212.0
${}^RQ_8$	636.7	w	61.3	1212.1
${}^RQ_7$	632.7	w	53.7	1211.7
${}^RQ_6$	628.8	s	46.0	1211.6
${}^RQ_5$	625.0	w	38.2	1211.8
${}^RQ_4$	620.8	w	30.8	1210.8
${}^RQ_3$	617.1	s	23.3	1210.9
${}^RQ_2$	613.5	w	15.9	1211.1
${}^RQ_1$	609.2	w	7.6	1210.8
${}^RQ_0$	605.4	s		
${}^PQ_1$	601.6	w		
${}^PQ_2$	597.6	w		
${}^PQ_3$	593.8	s		
${}^PQ_4$	590.0	w		
${}^PQ_5$	586.8	w		
${}^PQ_6$	582.8	s		
${}^PQ_7$	579.0	w		
${}^PQ_8$	575.4	w		
${}^PQ_9$	571.2	s		
${}^PQ_{10}$	567.3	w		
${}^PQ_{11}$	563.6	w		
${}^PQ_{12}$	560.0	s		

TABLE V. Rotational constants of GeH_3Cl.

A''	$=2.603\pm0.006$ cm^{-1}
B''	$=0.144$ cm^{-1} (microwave result)
A_4'	$=2.586\pm0.006$ cm^{-1}
A_5'	$=2.582\pm0.008$ cm^{-1}
A_6'	$=2.607\pm0.006$ cm^{-1}
ζ_4	$=-0.059\pm0.004$
ζ_5	$=-0.124\pm0.007$
ζ_6	$=+0.209\pm0.004$

[10] G. Herzberg, *Infrared and Raman Spectra* (D. Van Nostrand Company, Inc., New York, 1945), p. 429.

[11] See E. Teller, Hand- und Jahrbuch der chem. Physik **9**, II, 43 (1934). See Table I of R. C. Lord and R. E. Merrifield, J. Chem. Phys. **20**, 1348 (1952).

TABLE VI. Fundamental frequencies of CH_3Cl, SiH_3Cl, and GeH_3Cl.

Vibn. no.	CH_3Cl	SiH_3Cl	GeH_3Cl
1	2966.2	2196.0	2121.2
2	1354.9	1097.5	847.7
3	732.1	551.0	422.6
4	3041.8	2147.4	2129.4
5	1454.6	951.2	874.6
6	1015.0	666.2	604.1

TABLE VII. Thermodynamic functions for GeH_3Cl in calories/deg/mole.

$T°K$	$-(F^0-E_0^0)/T$	$(H-E_0^0)/T$	S^0	C_p
200	49.78	8.55	58.34	10.38
298.16	53.39	9.61	62.99	13.09
400	56.37	10.79	67.16	15.30
500	58.89	11.85	70.74	16.93
600	61.15	12.82	73.97	18.28
700	63.20	13.69	76.89	19.39
800	65.05	14.45	79.51	20.32
900	66.82	15.16	81.99	21.10
1000	68.48	15.81	84.28	21.75

set of equations from which the individual A' values can be found. These latter, when substituted back into Eq. (1), in turn yield ζ values for the three perpendicular vibrations. The results are listed in Table V.

The value of A'' of 2.603 cm^{-1} is consistent with the microwave results of Mays and Dailey,[8] who evaluate the Ge—H distance as 1.52±0.03A and the H—Ge—H bond angle as 110°54′±90′. These values correspond to $A''=2.667\pm0.07$, which agrees with the infrared value within the stated experimental error. It is perhaps worth noting that both values also agree within their limits of error with an A'' calculated from the sum of the covalent radii of germanium (1.22A) and hydrogen (0.32A) with an assumed tetrahedral H—Ge—H angle. The Ge—H distance in GeH_4 has been reported by Tindal, Straley, and Nielsen[2] from infrared rotation-vibration spectra to be 1.478A, but it has been pointed out[12] that there may be minor objection to their method of evaluation of the rotational constants.

[12] Reference 10, p. 456, footnote 50.

VIBRATIONAL FREQUENCIES FOR MONOCHLORIDES OF METHANE, SILANE, AND GERMANE

It is instructive to consider the frequencies of these three molecules shown in Table VI in relation to one another. The values for CH_3Cl are those of Barker and co-workers as quoted by Herzberg[10] and for SiH_3Cl are those of Monfils.[13] In view of the fact that the degenerate frequencies 4 and 5 are higher than the corresponding symmetrical ones 1 and 2 in both CH_3Cl and GeH_3Cl, it is surprising that the reverse is true for both pairs in SiH_3Cl. Also it is remarkable that the degenerate and corresponding symmetrical frequencies have such a wide separation in SiH_3Cl. Since the fundamental frequencies in each species do not lie near one another, such an irregular spacing in SiH_3Cl is hard to understand on grounds of mechanical interaction within either species. A possible explanation is that vibrations 2 and 4 have been mislocated. These would be expected to lie just above 900 and 2200 cm^{-1}, respectively.

TABLE VIII. Thermodynamic functions for GeD_3Cl in calories/deg/mole.

$T°K$	$-(F^0-E_0^0)/T$	$(H-E_0^0)/T$	S^0	C_p
200	50.85	9.14	59.99	12.20
298.16	54.78	10.67	65.45	15.30
400	58.13	12.17	70.30	17.59
500	60.98	13.42	74.40	19.25
600	63.54	14.51	78.05	20.52
700	65.84	15.41	81.24	21.52
800	67.95	16.24	84.19	22.28
900	69.92	16.96	86.87	22.88
1000	71.76	17.58	89.35	23.35

THERMODYNAMIC FUNCTIONS FOR GeH_3Cl AND GeD_3Cl

These functions, calculated by the usual methods on the basis of the harmonic-oscillator, rigid-rotator approximation, are given for the ideal-gas state at one atmosphere pressure in Tables VII and VIII.

[13] A. Monfils, Compt. rend. **236**, 795 (1953); J. Chem. Phys. **19**, 138 (1951).

l-Type Doubling in C_2H_2 and HCN*

T. A. WIGGINS, J. N. SHEARER, E. R. SHULL† AND D. H. RANK
Physics Department, The Pennsylvania State University, State College, Pennsylvania

(Received October 15, 1953)

A high-resolution infrared grating spectrometer has been used to investigate l-type doubling of energy levels of the linear molecules C_2H_2 and HCN. Resolving power of 145 000 was obtained at 4100 cm^{-1} which permitted the resolution of the Q branch of $\nu_1+\nu_5{}^1(\Sigma_g{}^+\rightarrow\Pi_u)$ of C_2H_2 to $J''=6$. The difference between the $B'-B''$ value determined from the Q branch and the same quantity obtained from the P and R branches of this band yields a value of $q=4.72\times10^{-3}$ cm^{-1}. The doublet structure in the difference band $01^10\rightarrow01^12(\pi\rightarrow\pi)$ of HCN has been resolved for $J''\geq6$ in the R branch and $J''\geq10$ in the P branch. This $\pi\rightarrow\pi$ band is treated as two bands with slightly different molecular constants. Evaluation of rotational constants shows that different α values are obtained for the + and − components of these π states. The difference in frequency between lines of equal J'' in the $000\rightarrow002$ and $01^10\rightarrow01^12$ bands is shown to be a quadratic function of J''. The value obtained for q' was 7.68×10^{-3} cm^{-1}.

INTRODUCTION

THE change in the B values caused by l-type doubling in linear molecules has been observed and described by Herzberg.[1]

Making use of high resolution and precise methods of measuring wavelength recently developed in this laboratory,[2] it has been possible to investigate l doubling in linear molecules in more detail. It will be shown that some of the assumptions usually made in the analysis of $\pi\rightarrow\pi$ bands are not justified and that more constants are required to give an adequate description of these bands.

The spectrometer has been described completely elsewhere.[2] It is sufficient to state that an eight-inch 15 000 lines/inch Bausch and Lomb plane transfer grating was used double-passed with ten-meter optics. The signal from the Eastman PbS detector was fed into a Baird phase-sensitive amplifier. Uniform scanning of the spectrum was accomplished making use of a sliding wedge prism arrangement. The precision of relative frequency measurement of the lines in the P and R branches of the 4100 cm^{-1} band of C_2H_2 and the "hot" band lines of HCN at 6500 cm^{-1} is ±0.005 cm^{-1}. The precision obtained in measurement of the lines of the Q branch of $\nu_1+\nu_5{}^1$ of C_2H_2 and lines of the 002 band of HCN was considerably higher.

Resolution of 145 000 was obtained in the case of the Q branch of the C_2H_2 band. Theoretical resolution with the slit widths used was 175 000. The absorption tube was 320 cm long. It was necessary to reduce the pressure in the case of the acetylene band to 1.3 mm of mercury to achieve maximum resolution. The resolution obtained with the HCN "hot" band was somewhat lower since it was necessary to use a pressure higher than desirable to develop the "hot" lines with sufficient intensity.

ACETYLENE

The perpendicular band $\nu_1+\nu_5{}^1(\Sigma_g{}^+\rightarrow\Pi_u)$ of acetylene at 4092 cm^{-1} has been measured to show the difference between the B' values obtained from the Q branch compared to that obtained from the P and R branches. This effect of doubling has been observed and explained by Herzberg.[1] He has shown that due to the selection rules the π^- levels of the upper vibrational state are involved in the Q-branch transitions while the π^+ levels are involved in the production of the P and R branches. With the resolution available it has been possible to resolve the Q branch so that a value for $B_-'-B''$ can be found, where B_-' denotes the constant for the π^- levels of the upper state. The Q branch of this perpendicular band is shown in Fig. 1. Intensity alternation is shown with the antisymmetric levels (odd values of J'') having the greater weight. Resolution to $J''=6$ is shown. It would require theoretical resolving power to resolve the $J''=5$ line.

If we neglect the effect of the D correction terms we can write the expression representing the frequencies of

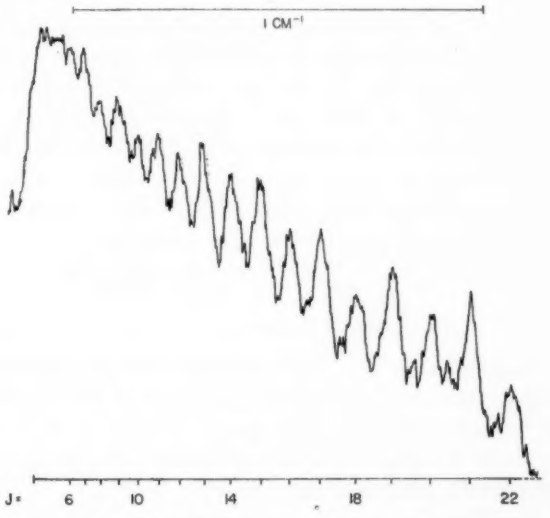

FIG. 1. The Q branch of C_2H_2 at 4092 cm^{-1}. The line $J''=6$ is resolved showing resolution of 145 000.

* This research was assisted by support from Contract N6onr-269 Task V of the U. S. Office of Naval Research.

† Present address: Linde Air Products Company, Tonawanda Laboratory, Tonawanda, New York.

[1] G. Herzberg, Revs. Modern Phys. 14, 219 (1942).

[2] Rank, Shull, Bennett, and Wiggins, J. Opt. Soc. Am. 43, 952 (1953).

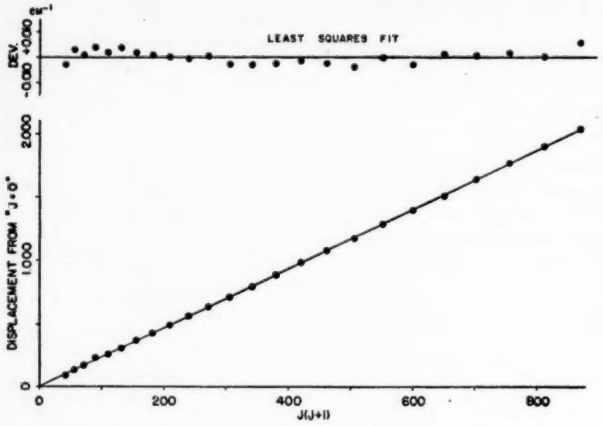

FIG. 2. Plot of frequencies in the Q branch of C_2H_2 *versus* $J(J+1)$. The upper plot shows the deviations between the measured frequencies and a least squares fit.

the Q branch as follows:

$$\nu=\nu_{0-}-B_-'+(B_-'-B'')J(J+1) \quad J>0. \qquad (1)$$

A plot of the measured frequencies in this branch *versus* $J(J+1)$ is shown in Fig. 2. Since the plot of this experimental data shows no trace of curvature it can be seen that the assumption regarding D is amply justified. The deviations from the least squares fit of the data are shown in the upper portion of Fig. 2. The average deviation was found to be ± 0.002 cm^{-1}.

If we make the assumption that $D'=D''=D$, the expression for the frequencies of the lines of the P and R branches of this band becomes

$$\nu=\nu_{0+}-(B_+'+D)+(B_+'+B''+2D)m +(B_+'-B''+2D)m^2-4Dm^3, \qquad (2)$$

where $m=J+1$ for the R branch and $-J$ for the P branch.

The frequencies of eight lines out to $J''=17$ in the P and R branches of this band were measured making use of the second-order 1.22μ Fabry-Perot white light fringes as wavelength standards. The measured lines were fitted to Eq. (2) by least squares. The average deviation was ± 0.003 cm^{-1}. We have obtained the following molecular constants for this band expressed in cm^{-1}:

$$B''=1.17658 \qquad \nu_{0+}=4092.34$$
$$B_+'=1.16952 \qquad \nu_{0-}=4092.37$$
$$B_-'=1.17424 \qquad q=4.72\times10^{-3}.$$
$$D=1.0\times10^{-6}$$

These constants can be compared with previous work on acetylene. Herzberg[3] quotes a value of $B''=1.17692$ cm^{-1}. Bell and Nielsen[4] obtained a value of $B_+'-B''=-0.0078$ compared with -0.00706 cm^{-1} obtained in the present investigation.

[3] G. Herzberg, *Infrared and Raman Spectra* (D. Van Nostrand Company, Inc., 1945), p. 396.
[4] E. E. Bell and H. H. Nielsen, J. Chem. Phys. **18**, 1382 (1950).

HYDROGEN CYANIDE

The difference band $01^10\rightarrow01^12(\pi\rightarrow\pi)$ associated with the 000→002 band of HCN has been observed under sufficient resolution to resolve the l doublets in the R branch for $J''\geq6$ and in the P branch for $J''\geq10$. The lines of the 000→002 band of HCN have been measured recently in this laboratory by Yost[5] with a precision comparable to that obtainable in the photographic infrared. The work of Yost showed that no rotational perturbations appeared in this band. B'' has recently been investigated with high precision.[6,7]

We have measured 20 lines in the 002 band by the Method of Exact Orders.[2] These lines are listed in Table I and are marked with an a. There is still

TABLE I. Frequencies in vacuum wave numbers in two bands of HCN.

m	$(000\overset{\nu_c}{\rightarrow}002)$	$(01^10\overset{\nu_h}{\rightarrow}01^12)$		$\Delta\nu_h$
		π^-	π^+	
−26	6429.277[a]			...
−24	37.208[a]	...	...	...
−23	41.116[a]	...	...	...
−21	48.807[a]	...	...	...
−20	52.593	6413.691	6413.910	−0.219
−19	56.338[a]	17.422	17.632	0.210
−18	60.046[a]	...	...	...
−17	63.712	24.791	24.982	0.191
−16	67.335[a]	28.409	28.594	0.185
−15	70.918	31.986	32.156	0.170
−14	74.459[a]	35.529	35.679	0.150
−13	77.958	39.031	39.183	0.152
−12	81.415[a]	42.489	42.615	0.126
−11	84.832	45.922	46.029	0.107
−10	88.207	49.294	49.399	0.105
− 8	94.832	6455.972		...
− 7	98.082	59.221		...
− 6	6501.290	62.414		...
− 5	04.457	65.586		...
− 4	07.582	68.716		...
− 1	16.704[a]	...		...
Q	19.661	80.771		...
2	25.447	86.640		...
3	28.277	89.472		...
4	31.064	92.269		...
7	39.170	6500.455	6500.366	+0.089
8	41.787	03.085	02.974	0.111
9	44.362	05.681	05.549	0.132
10	46.893	08.263	08.107	0.156
11	49.382[a]	...	...	...
12	51.828	13.254	13.050	0.204
13	54.229[a]	15.679	15.456	0.223
14	56.586	18.066	17.815	0.251
15	58.901[a]	20.413	20.137	0.276
17	63.400[a]	24.977	24.668	0.309
18	65.585[a]	27.193	26.846	0.347
19	67.726	29.359	28.997	0.362
20	69.824[a]	...	...	...
22	73.891[a]	35.631	35.195	0.436
23	75.859[a]	...	...	...
25	79.664[a]	...	...	...
27	83.301[a]	...	...	...

[a] Measured frequencies. The other frequencies in this band are computed.

[5] E. L. Yost, M. S. thesis, The Pennsylvania State College, June, 1953.
[6] Rank, Ruth, and Vander Sluis, J. Opt. Soc. Am. **42**, 693 (1952).
[7] A. E. Douglas and D. Sharma, J. Chem. Phys. **21**, 448 (1953).

probably a small systematic error in these measurements somewhat less than 0.010 cm^{-1} across the complete P branch. We shall assume the microwave B'' to be 1.47823 cm^{-1} and B' to be 1.45691 cm^{-1}, which at the present time are the most probable values of these constants. The remaining lines of the 002 band listed in Table I have been obtained by interpolation between measured lines. The frequencies of the lines of the 002 band thus determined were used as standards for measurement of the $\pi\rightarrow\pi$ band lines. The results of these measurements are compiled in Table I.

Determination of q

On the basis of the theory presented by Douglas and Sharma[7] the frequency separation of the l doublets in a $\pi\rightarrow\pi$ band is given by

$$\Delta\nu=q'(m^2+m-1)-q''(m^2-m-1), \qquad (3)$$

where $m=-J$ for the P branch and $J+1$ for the R branch, $q'=B_-'-B_+'$ and $q''=B_-''-B_+''$. Making use of the direct measurement of $q''=7.47\times10^{-3}$ cm^{-1} by Shulman and Townes[8] by microwave methods, the second term on the right side of Eq. (3) can be calculated for each doublet. In Fig. 3 we have plotted $\Delta\nu+q''(m^2-m-1)$ *vs* (m^2+m-1). The least squares treatment of this data yielded $q'=7.76\times10^{-3}$ cm^{-1}. It was found necessary in making the plots in Fig. 3 to consider the doublet separation to be negative in the P branch and positive in the R branch so that both plots would have the proper intercepts and equal slopes.

An alternate method of analysis of the l doublets is possible which should yield much more reliable values of $q'-q''$ than the above treatment. However, this second method does not give as precise an absolute value of the q's as is obtainable from the microwave measurements. We can express the separation of the l doublets to sufficient approximation by

$$\Delta\nu=(q'-q'')m^2+(q'+q'')m. \qquad (4)$$

A plot of the data using Eq. (4) is given in Fig. 4. The

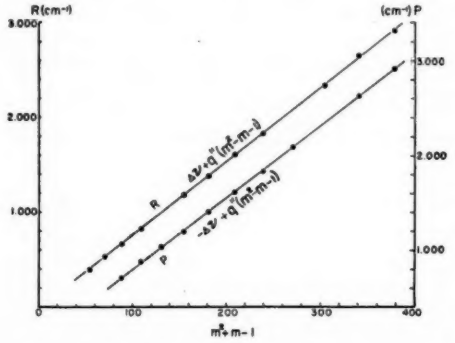

FIG. 3. Splittings in the P and R branches of the $\pi\rightarrow\pi$ band of HCN at 6481 cm^{-1}. The frequency difference between the doublets is added to the quantity $q''(m^2-m-1)$ and the sum plotted *versus* (m^2+m-1). The separation in the P branch is taken to be negative, and the R branch to be positive.

[8] R. G. Shulman and C. H. Townes, Phys. Rev. **77**, 421 (1950).

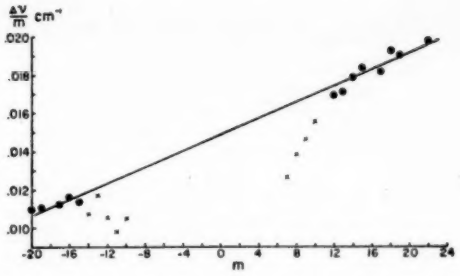

FIG. 4. Plot of the doublet separation $\Delta\nu/m$ *versus* m for the lines of the $01^10\rightarrow01^12$ band of HCN. The points indicated by X were not used in the determination of q.

absolute value of q is determined by the absolute value of the doublet separations which can be subject to systematic error when close line pairs are involved. We have put the data to least squares using only the completely resolved doublets, i.e., $\Delta\nu\geq0.17$ cm^{-1}. From this analysis we obtain $q''=7.59\times10^{-3}$ and $q'=7.80\times10^{-3}$. Even though the absolute value of q'' does not agree exactly with the microwave q'' we believe $q'-q''$ is much more accurate than the value obtained from the use of Eq. (3). From $q'-q''$ determined from Eq. (4) the most probable value of q' is 7.68×10^{-3} cm^{-1}.

The absence of intensity alternation in the doublets such as would occur in a symmetric molecule prevents a unique assignment of the lines of the doublets to a given energy level. However, on the basis of the required signs for the doublet separations noted above, it is concluded that the higher-frequency component of the R branch is associated with the same energy level as the lower-frequency component of the P branch and *vice versa*. To show this, an energy level diagram was constructed similar to the one shown by Herzberg[9] for a $\pi\rightarrow\pi$ band. The result is the same as shown by Herzberg[10] for $^1\pi\rightarrow{}^1\pi$ bands of diatomic molecules. This result differs from the diagram for linear molecules only in the order of the doublet components in the P branch. It is concluded that the π^+ (lower-energy) levels are associated with the higher-frequency doublet component in the P branch and the lower-frequency component in the R branch; the π^- (higher-energy) levels with the lower-frequency doublet component in the P branch and the higher-frequency component in the R branch.

Since as was noted above the energy levels are double in π states, we actually have two sets of rotational constants and effectively a $\pi\rightarrow\pi$ band is two bands which are almost identical. We shall call one of these bands π^+ and the other π^-. If we assume $D'=D''$ for these hot bands the frequencies of the band lines can be expressed by the following equation:

$$\nu_h=\nu_{0h}-(B_h'-B_h'')+(B_h'+B_h''+4D_h)m+(B_h'-B_h'')m^2-4D_hm^3. \qquad (5)$$

A fit of the band lines by means of least squares was

[9] See reference 3, p. 389.

[10] G. Herzberg, *Spectra of Diatomic Molecules* (D. Van Nostrand Company, Inc., New York, 1950), second edition, p. 267.

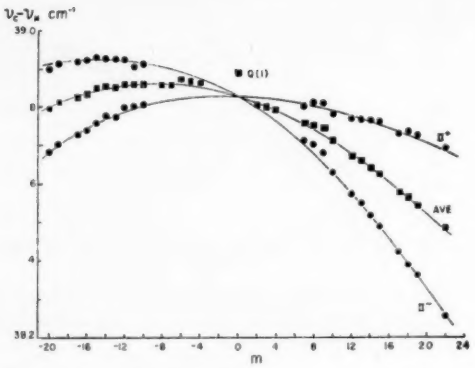

FIG. 5. The difference between frequencies in the 000→002 band and the $01^10\rightarrow01^12$ band of HCN are plotted *versus m*.

performed. The fit gave an average deviation of ±0.007 cm^{-1}.

Douglas and Sharma[7] have pointed out that it should be possible to determine α_2 from the difference in frequency of "hot" and "cold" band lines (average frequency of l doublets) of the same J. The attempt of these authors to evaluate α_2 in this manner from the 003 band and its accompanying "hot" band was unsuccessful and perplexing. We have made an attempt to perform the same type of analysis as Douglas and Sharma on the 002 band and its accompanying hot band with even more perplexing results. Since our relative frequency measurements were considerably more accurate than those made in the photographic infrared, our scatter of points was much smaller than that obtained by Douglas and Sharma. The plot of the difference between the frequencies of the "cold" lines and the average frequency of the appropriate doublets *versus m* yielded a smooth curve instead of the straight line predicted by first order-theory.

The difference between the frequencies for the same value of J in the "hot" and "cold" bands can be shown to be

$$\nu_c-\nu_h=\nu_{0c}-\nu_{0h}+B_h'-B_h''+(\alpha'+\alpha'')m+(\alpha'-\alpha'')m^2. \quad (6)$$

The quantities $\nu_c-\nu_h$ are plotted *versus m* in Fig. 5 for the + and − hot bands and also for the average of the + and − bands.

The molecular constants for the π^+ and π^- bands have been determined applying least squares methods to the data using Eq. (5) and Eq. (6). In addition, the conventional Δ_2F'' method was used for the π^+ and π^- bands and also for the average of the two bands. The results are summarized in Table II. The fifth figure beyond the decimal point has little significance and is carried as an inferior number. The agreement with the results obtained by Douglas and Sharma[7] for the 01^10 state average is excellent. It should be pointed out that our analysis shows unequivocally that the π^+ and π^- states yield α_2 values of a completely different order of magnitude. It also appears that the α_2 value for the 01^12 state is slightly larger than that for the 01^10 state.

TABLE II. Rotational constants of $01^10\rightarrow01^12$ bands in vacuum wave numbers determined by different methods.

Constant	Δ_2F''	Eq. (5)	Eq. (6)
		π^+ band	
B''	1.47870	1.47868	···
B'	···	1.45788	···
α''	−0.00057	−0.00097	+0.00025
α'	···	−0.00045	−0.00006
ν_0	···	6480.807	6480.809
		π^- band	
B''	1.48519	1.48503	···
B'	···	1.46444	···
α''	−0.00696	−0.00680	−0.00691
α'	···	−0.00753	−0.00746
ν_0	···	6480.810	6480.806
		Doublet average	
B''	1.48194	1.48185	···
B'	···	1.46116	···
α''	−0.00371	−0.00363	−0.00333
α'	···	−0.00425	−0.00376
D''	3.40×10^{-6}	···	···
$Q(1)$ calc	6480.767		
$Q(1)$ obs	6480.771		

We are indebted to Dr. A. E. Douglas of the National Research Council at Ottawa for pointing out a systematic error in our first measurements of this band and supplying us with his extensive Δ_2F'' values obtained from numerous "hot" bands in the photographic infrared. We are also grateful to Jean M. Bennett for performing a large part of the least squares calculations.

Generalization of the Radial Dilution Square Law in Ultracentrifugation*

RODES TRAUTMAN AND VERNE SCHUMAKER
University of California, Radiation Laboratory, Donner Laboratory, Berkeley, California
(Received April 22, 1953; revised September 29, 1953)

The classical square law of radial dilution, which relates the concentration of a single component to the boundary position in the ultracentrifuge cell, has been examined and found to be valid for a single component as well as for a multicomponent system even though the sedimentation rates are dependent on concentration.

The square law has been generalized to give corrected concentrations without the necessity of determining boundary positions explicitly. A system of warped coordinates has been introduced to simplify this application of the square law. A special template and its use is described which incorporates both the warped coordinates and the baseline and which enables very rapid reading of areas from routine ultracentrifugal runs.

A MACROSCOPIC moving boundary theory for ultracentrifugation paralleling either the weak or the strong electrolyte theory developed for electrophoresis[1–6] is complicated by the inhomogeneous field and sector shape of the centrifuge cell. Moreover, it is necessary to consider the dependence of sedimentation coefficient ("s rate") on concentration, since this effect yields area anomalies,[7] and also gives a time dependence to areas[8] in addition to that indicated by the radial dilution square law.[9a] This paper presents an extension of the classical square law of radial dilution to single component and multicomponent systems in which there exists a dependence of sedimentation rate on concentration. This analysis is for the velocity ultracentrifuge for solutions in which diffusion, artificial sharpening and blurring effects, and convection can be present in the boundary regions, if these effects are sufficiently small in comparison to sedimentation so that the phase just preceding the bottom of the cell in sedimentation (and the meniscus in flotation) remains a plateau solution during centrifugation. By a plateau solution is meant a phase of limited radial extent in which the concentration is independent of the radius, but may be time dependent. A necessary condition for a plateau solution is that the schlieren pattern return to the baseline; thus implicitly the assumption is made that no component has completely traversed the length of the cell.

SINGLE-COMPONENT SYSTEM

A boundary region in a cell can be defined as a region in which the concentration depends on the distance from the center of rotation x. Let the material be hypothetically rearranged to give an equivalent infinitely sharp boundary between the two concentrations at the extremes of the boundary region. The boundary position $\bar{x}$, a function of the time, is defined as the location of this step in concentration[1,3] and, for the sector cell, is the square root of the second moment of the concentration gradient curve[10,11] (see Fig. 1 and Eq. 12).

For the sector cell, the law of conservation of mass can be applied on a differential basis to give an equation of continuity[9b] which is valid at any radius x and time t. In the plateau region, c is independent of x; therefore, the partial derivatives can be replaced by total derivatives and the equation of continuity becomes

$$dc/dt = -2\omega^2 sc. \tag{1}$$

Refer to Fig. 1 and choose a lamina of very small width at position x which lies in the plateau region to the right of x_2. Let x' be the distance of this lamina from the center of rotation at any time t. Let the lamina move through the cell with the s rate of the enclosed molecules which is, by definition

$$s \equiv (dx'/dt)/\omega^2 x'. \tag{2}$$

Now the quantity Q of material behind this lamina is a constant. Therefore, both the equivalent infinitely sharp boundary at a distance $\bar{x}$ and the lamina at x' move down the cell subject to the following condition (expressed per unit half-angle per unit thickness of cell):

$$(x'^2 - \bar{x}^2)c = Q \qquad \frac{dQ}{dt} = 0. \tag{3}$$

Differentiating with respect to time gives

$$\left(2x'\frac{dx'}{dt} - 2\bar{x}\frac{d\bar{x}}{dt}\right)c + (x'^2 - \bar{x}^2)\frac{dc}{dt} = 0. \tag{4}$$

* This work was supported (in part) by the U. S. Atomic Energy Commission and by a grant from the Life Insurance Medical Research Fund.

[1] L. G. Longsworth, J. Am. Chem. Soc. **65**, 1755 (1943).
[2] H. Svensson, Arkiv Kemi, Mineral. Geol. **A22**, No. 10, 8 (1946).
[3] V. P. Dole, J. Am. Chem. Soc. **67**, 1119 (1945).
[4] H. Svensson, Acta Chem. Scand. **2**, 841 (1948).
[5] R. A. Alberty, J. Am. Chem. Soc. **72**, 2361 (1950).
[6] R. A. Alberty and H. H. Marvin, J. Phys. and Colloid Chem. **54**, 47 (1950).
[7] J. P. Johnston and A. G. Ogston, Trans. Faraday Soc., **42**, 789 (1946).
[8] W. F. Harrington and H. K. Schachman, J. Am. Chem. Soc. **75**, 3533 (1953).
[9] T. Svedberg and K. O. Pedersen, *The Ultracentrifuge* (Clarendon Press, Oxford, 1940); *a*, p. 7; *b*, p. 21.
[10] R. Goldberg, J. Phys. Chem. **57**, 194 (1953).
[11] R. Trautman, "Theoretical considerations on cell shape, convection, and an area anomaly pertinent to developing a moving boundary theory for ultracentrifugation," University of California Radiation Laboratory Progress Report No. UCRL 1869, contract No. W-7405-eng 48 (July 8, 1952).

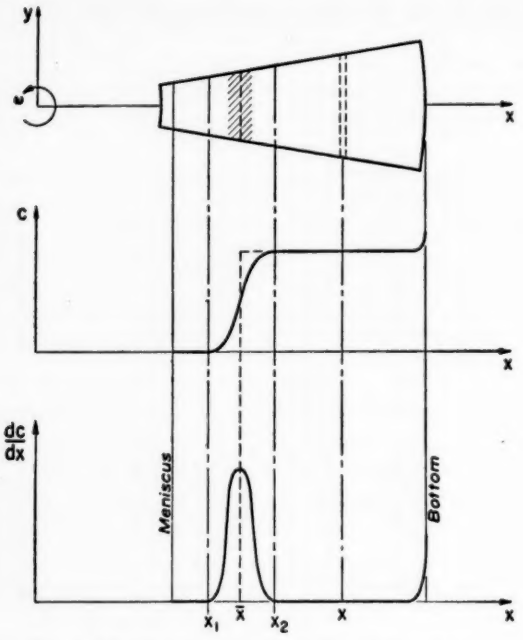

FIG. 1. Distribution of mass during sedimentation in the sector cell.

From the equation of continuity, dc/dt can be eliminated,

$$\left(2x'\frac{dx'}{dt}-2\bar{x}\frac{d\bar{x}}{dt}c\right)-(x'^2-\bar{x}^2)2\omega^2sc=0. \tag{5}$$

Substitute Eq. (2) into Eq. (5) and rearrange,

$$(d\bar{x}/dt)/\omega^2\bar{x}=s. \tag{6}$$

Therefore, the s rate of the equivalent boundary position of a single component is the same as the s rate of the molecules in the plateau region. As long as a plateau region exists, this result is independent of the actual shape of the boundary.

In order to determine the relationship between the plateau concentration c and boundary position $\bar{x}$, Eq. (1) can be divided by Eq. (6),

$$\frac{d\ln c}{dt}=-2\frac{d\ln\bar{x}}{dt}. \tag{7}$$

Integrating from c^0 and x_0 at $t=0$ to c and $\bar{x}$ at time t, gives

$$c^0/c\doteq(\bar{x}/x_0)^2. \tag{8}$$

Equation (8) shows that the square law is valid for a single component even if the dependence of s on c causes a marked change in the sedimentation coefficient during the course of the run.[12]

[12] This conclusion is different than that presented without derivation by Kinell. [P.-O. Kinell, J. Chem. Phys. 44, 53 (1947); P.-O. Kinell and B. G. Ranby, *Advances in Colloid Science* (Interscience Publishers, Inc., New York, 1950); Vol. III, p. 181]. The authors of this paper believe an ambiguous interpretation of the symbol dx must have been used to obtain his result.

EXTENSION TO MULTICOMPONENT SYSTEM OF NONINTERACTING COMPONENTS

The effect of radial dilution upon the observed area of a multicomponent system will now be considered. Throughout the following derivation, it is assumed that no component has completely traversed the length of the cell, and that a plateau region exists between the boundary position of the fastest component and the bottom of the cell. This will be denoted the γ plateau. Any disturbance in the boundary region, such as convection,[8] will not affect the validity of this treatment, as long as all disturbances, if any, extend from wall to wall of the cell and as long as no convection of any form occurs in the γ plateau region. Equation (8) may be written for each of the m components in the cell; however, the individual $\bar{x}$'s may not be observed on the pattern because of the superposition of the boundaries. For the ith component,

$$c_i^0=\left(\frac{\bar{x}_i}{x_0}\right)^2c_i^\gamma, \tag{9}$$

where the superscript γ refers to the γ plateau region. Multiplying by the specific refractive increment α_i,

$$c_i^0\alpha_i=\left(\frac{\bar{x}_i}{x_0}\right)^2c_i^\gamma\alpha_i. \tag{10}$$

The left-hand side of Eq. (10) is the initial concentration expressed in refractive index units. Summing Eq. (10) for all of the m components in the cell,

$$\sum_{i=1}^{m}c_i^0\alpha_i=\sum_{i=1}^{m}\left(\frac{\bar{x}_i}{x_0}\right)^2c_i^\gamma\alpha_i. \tag{11}$$

Regardless of the shape of the concentration gradient curve between x_0 and the plateau, for each component the quantity $(\bar{x}_i/x_0)^2$ obeys the following relationship as shown by Goldberg:[10]

$$\left(\frac{\bar{x}_i}{x_0}\right)^2=\frac{\int_{x_0}^{x_p}\left(\frac{x}{x_0}\right)^2\frac{\partial\alpha_ic_i}{\partial x}dx}{\alpha_ic_i^\gamma}, \tag{12}$$

where x_p is any point in the γ plateau region. Substitute Eq. (12) in Eq. (11)

$$\sum_{i=1}^{m}c_i^0\alpha_i=\sum_{i=1}^{m}\int_{x_0}^{x_p}\left(\frac{x}{x_0}\right)^2\frac{\partial\alpha_ic_i}{\partial x}dx$$

$$=\int_{x_0}^{x_p}\left(\frac{x}{x_0}\right)^2\frac{\partial\sum_{i=1}^{m}\alpha_ic_i}{\partial x}dx. \tag{13}$$

Dividing by $\sum_{i=1}^{m} \alpha_i c_i^{\gamma}$

$$\frac{\sum_{i=1}^{m} \alpha_i c_i^{0}}{\sum_{i=1}^{m} \alpha_i c_i^{\gamma}} = \frac{\int_{x_0}^{x_p} \left(\frac{x}{x_0}\right)^2 \frac{\partial \sum_{i=1}^{m} \alpha_i c_i}{\partial x} dx}{\sum_{i=1}^{m} \alpha_i c_i^{\gamma}}. \tag{14}$$

The right-hand side of Eq. (14) is, by definition, $(\bar{x}^{\text{obs}}/x_0)$, where $(\bar{x}^{\text{obs}})^2$ is the second moment of the observed concentration gradient curve. Therefore, the generalized square law of radial dilution may be written in two forms:

$$\frac{\sum_{i=1}^{m} \alpha_i c_i^{0}}{\sum_{i=1}^{m} \alpha_i c_i^{\gamma}} = \left(\frac{\bar{x}^{\text{obs}}}{x_0}\right)^2, \tag{15}$$

or

$$\Delta n^0 = \int_{x_0}^{x_p} \left(\frac{x}{x_0}\right)^2 \frac{\partial n}{\partial x} dx, \tag{16}$$

where n is the total observed index of refraction at any point x and

$$\Delta n^0 = \sum_{i=1}^{m} \alpha_i c_i^{0}.$$

By application of Eq. (15), the total observed area on the schlieren pattern can be corrected for the effects of radial dilution if the boundary position $\bar{x}^{\text{obs}}$ is determined for the complete pattern.

If several peaks are observed on the schlieren pattern, Eq. (16) can be written

$$\Delta n^0 = \frac{\int_1 \left(\frac{x}{x_0}\right)^2 \frac{\partial n}{\partial x} dx}{\Delta n_1} \Delta n_1 + \frac{\int_2 \left(\frac{x}{x_0}\right)^2 \frac{\partial n}{\partial x} dx}{\Delta n_2} \Delta n_2 + \cdots, \tag{17}$$

where the integral from x_0 to x_p has been broken into a consecutive series of integrals each one extending through a peak, and Δn_i is the observed (time dependent) area of the ith peak. The subscripts 1, 2, ... denote the various peaks. Equation (17) gives immediately

$$\Delta n^0 = \left(\frac{\bar{x}_1}{x_0}\right)^2 \Delta n_1 + \left(\frac{\bar{x}_2}{x_0}\right)^2 \Delta n_2 + \cdots. \tag{18}$$

Therefore, the sum of the square-law corrected areas equals the sum of the initial concentrations.

WARPED COORDINATES

Equations (15) and (18) are difficult to apply, because they involve determination of the second moment of the concentration gradient curve. This difficulty may be eliminated by the application of the warped coordinate technique of measuring areas. Equation (16) can be written as the limit of a sum from x_0 to x_p, but for practical purposes the limiting process can be stopped when the Δx_i are small enough to give the accuracy desired

$$\Delta n^0 \approx \sum_{j=1}^{q} \left(\frac{x_j}{x_0}\right)^2 y_j \Delta x_j, \tag{19}$$

where $y_j = \partial n/\partial x$ is an ordinate on the schlieren pattern and q is the number of parts into which the interval between x_0 and x_p is divided. Since, in the limit, the intervals into which the pattern is divided do not need to be of uniform size, they may be chosen so that $(x_j/x_0)^2 \Delta x_j$ is a constant. Then

$$\text{constant} = (x_j/x_0)^2 \Delta x_j = \Delta z. \tag{20}$$

Choose the ordinate y_j at the center of each Δz interval. Then (20) becomes

$$\Delta n^0 = \Delta z \sum_{j=1}^{q} y_j. \tag{21}$$

Thus, the schlieren area corrected for radial dilution can be determined as a simple summation of ordinates. The position of these ordinates can be marked off at the center of each Δz interval. The required relationship between x and z can be found by taking the limit and integrating Eq. (20),

$$\int_0^z dz = \int_{x_0}^{x} \left(\frac{x}{x_0}\right)^2 dx,$$

which gives

$$z = \frac{x_0}{3}\left[\left(\frac{x}{x_0}\right)^3 - 1\right],$$

and, inversely,

$$x = x_0\left(1 + \frac{3z}{x_0}\right)^{\frac{1}{3}}.$$

Thus, the midpoint of the first interval is

$$x_1 = x_0\left[1 + \frac{3(\frac{1}{2}\Delta z)}{x_0}\right]^{\frac{1}{3}}.$$

In constructing the template, Fig. 2, advantage has been taken of the fact that the baseline (the pattern that would have been obtained if no lipoprotein molecules were present) is the same, at a given time after start of

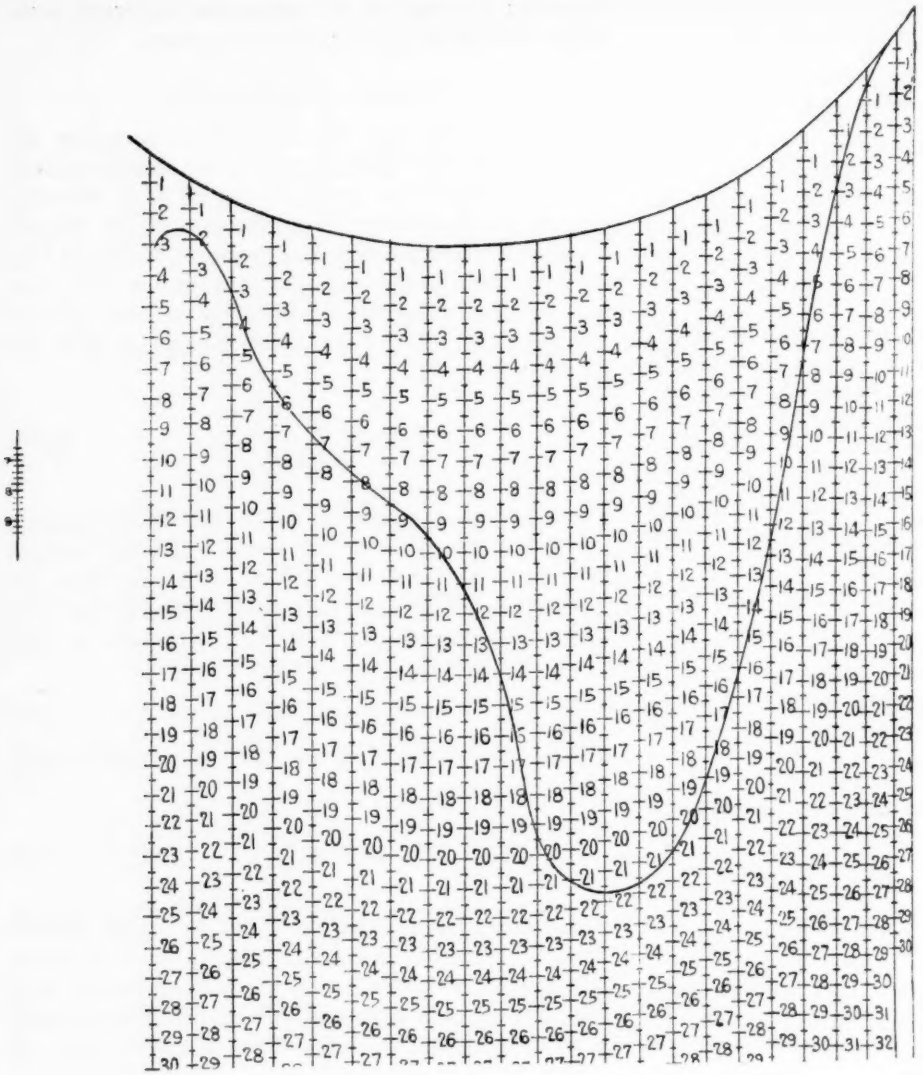

FIG 2. Template of warped coordinates. The bottom of the cell is the vertical line at the extreme right. The salt redistribution baseline is the upper curve and is the zero for the ordinate scale measured downwards. The scale at the extreme left is used in positioning the template. The observed schlieren pattern of the floating lipoprotein sample is traced using a $5x$ enlarger. Square-law corrected areas are obtained by summing the readings taken off the vertical lines which are located at the center of the Δz intervals.

MU-5846

centrifugation, for the several cells used. Therefore, it can be incorporated in the template, and the ordinate scale is marked off on the vertical lines in equal units below the baseline. These vertical lines lie at the center of the Δz interval.[13]

The task of determining the area of the pattern has now been reduced to the simple job of summing the ordinates. This is easily done with an adding machine that will print both the subtotals and the number punched in. The adding machine tape gives the integral curve corrected for radial dilution, and also the slope of this curve (the ordinate) at each point. It is important to remember that since the vertical lines lie at the center of the Δz interval, the sum obtained represents all the area up to a point midway to the next vertical line.

[13] It is possible to use a standard set of warped coordinates for all ultracentrifugal patterns. The formulation is

$$\Delta n^0 = \left(\frac{x_r}{x_0}\right)^2 \Delta z \sum_{j=1}^{q} y_j,$$

where x_0 is the observed meniscus position for sedimentation or the bottom of the cell for flotation, and x_r is the value chosen in constructing the warped coordinates.

ACKNOWLEDGMENT

The authors wish to acknowledge the extensive discussions with Dr. William F. Harrington and Dr. Howard K. Schachman of the Virus Laboratory, University of California, concerning their work on the Johnston-Ogston area anomaly, and for making available their data and derivations prior to publication. Also the authors are indebted to Dr. Robert A. Alberty for carefully reading and criticizing the manuscript.

The Determination of Concentrations in the Ultracentrifugation of Two-Component Systems*

R. TRAUTMAN, V. N. SCHUMAKER, W. F. HARRINGTON AND H. K. SCHACHMAN
The Donner Laboratory, Radiation Laboratory and the Virus Laboratory, University of California, Berkeley

(Received August 25, 1953)

An analysis of mass distribution in the ultracentrifugation of mixtures of two sedimentable components has been made. This treatment predicts the magnitude of the slow component concentration in the region between the slow and fast boundaries as well as the change in this concentration during the run. The theory has been applied to a series of mixtures and is in agreement with the experimental data. The existence of convection during the ultracentrifugation of mixtures is briefly discussed as well as the application of the theory to a determination of concentrations in unknown systems.

INTRODUCTION

RECENT work by Harrington and Schachman[1] on the ultracentrifugal analysis of known mixtures of a two-component system demonstrates that the sector cell and inhomogeneous field complicate the conservation of mass analysis first proposed by Johnston and Ogston.[2] It was observed in their work that the area of the schlieren peak of the slow component decreased with distance moved much more than accounted for by the square law; this decrease could be related to changes in the sedimentation coefficients due to radial dilution. This paper presents a theoretical extension of the Johnston-Ogston analysis and applies the theory to the determination of the initial concentrations in two-component mixtures.

THEORY

The concentration relationships in a two component mixture are shown in Fig. 1, following the hypothesis of Johnston and Ogston and using the boundary and phase notation of moving boundary electrophoresis theory.[3,4] Trautman and Schumaker[5] have indicated that the square law of radial dilution is valid for the sum of all the components in the cell even if there is a dependence of sedimentation coefficient on concentration, provided there is no convection present in the solution containing all of these components. Thus in the two-component mixture it is assumed that there is no convection ahead of the fast boundary (i.e., in the γ solution). Therefore the square law of radial dilution may be written

$$c_F^0+c_S^0=\left(\frac{\bar{x}^{\text{obs}}}{x_0}\right)^2 c_S^{\text{obs}}+\left(\frac{\bar{x}_F^{\text{obs}}}{x_0}\right)^2 c_F^{\text{obs}}. \qquad (1)$$

The symbol $\bar{x}$ indicates the equivalent boundary position which would result if the material were rearranged to give infinitely sharp boundaries.[6] The superscript "obs" denotes quantities which may be observed on the schlieren pattern. By inspection (Fig. 1), the following relations may be written:

$$\begin{aligned} c_S^{\text{obs}}&=c_S^{\beta}, \\ c_F^{\text{obs}}&=c_F^{\gamma}+c_S^{\gamma}-c_S^{\beta}. \end{aligned} \qquad (2)$$

Substituting Eq. (2) into Eq. (1) and rearranging,

$$c_F^0-c_F^{\gamma}\left(\frac{\bar{x}_F^{\text{obs}}}{x_0}\right)^2 =\left(\frac{\bar{x}_F^{\text{obs}}}{x_0}\right)^2(c_S^{\gamma}-c_S^{\text{obs}})+\left(\frac{\bar{x}_S^{\text{obs}}}{x_0}\right)^2-c_S^0. \qquad (3)$$

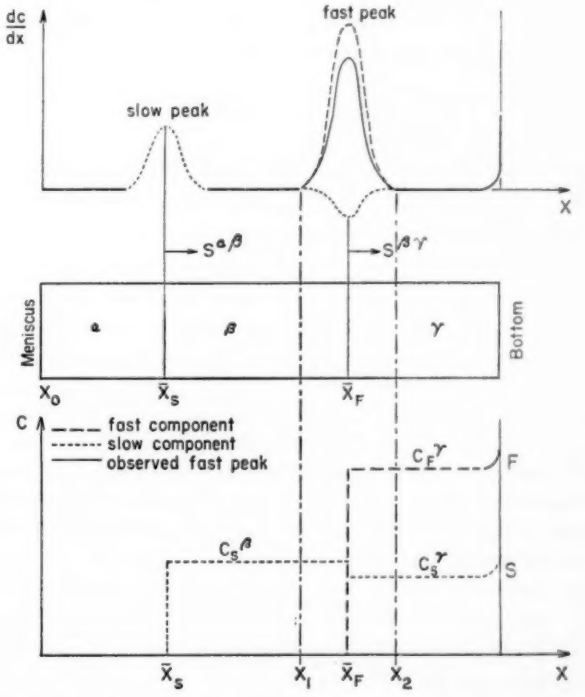

FIG. 1. Boundary and phase notation for a two-component system in the ultracentrifuge.

* This work was supported (in part) by the U. S. Atomic Energy Commission and by contract between the University of California and the U. S. Office of Naval Research.

[1] W. F. Harrington and H. K. Schachman, J. Am. Chem. Soc. **75**, 3533 (1953).

[2] J. P. Johnston and A. G. Ogston, Trans. Faraday Soc. **42**, 789 (1946).

[3] L. G. Longsworth, J. Am. Chem. Soc. **67**, 1109 (1945).

[4] V. P. Dole, J. Am. Chem. Soc. **67**, 1119 (1945).

[5] R. Trautman and V. N. Schumaker, J. Chem. Phys. (in press).

[6] R. Goldberg, J. Phys. Chem. **57**, 194 (1953).

The fast component in the γ phase obeys the square law: $c_F^0 = (\bar{x}_F^\gamma/x_0)^2 c_F^\gamma$ where $\bar{x}_F^\gamma$ is the equivalent boundary position which would be obtained if just the fast component were rearranged. Therefore, if $\bar{x}_F^{obs} = \bar{x}_F^\gamma$, the left-hand side of Eq. (3) vanishes. Rearranging the remaining terms,

$$\frac{(\bar{x}_S^{obs}/x_0)^2 c_S^{obs}}{c_S^0} = \frac{(\bar{x}_F^{obs}/x_0)^2 c_S/\gamma c_S^0 - 1}{(\bar{x}_F^{obs}/\bar{x}_S^{obs})^2 - 1} \equiv r. \quad (4)$$

For simplicity of notation, the right-hand side of Eq. (4) has been denoted by "r." The quantity $(r-1)$, which is the increase in the square law corrected area, will subsequently be termed the "buildup" of the slow component. Then, substituting Eq. (4) into Eq. (1),

$$\frac{(\bar{x}_F^{obs}/x_0)^2 c_F^{obs}}{c_F^0} = 1 - \frac{c_S^0}{c_F^0}(r-1). \quad (4a)$$

Notice that it was not necessary to assume that the sedimentation coefficients were constant during the run and hence Eqs. (4) and (4a) are valid even if the dependence of s on c is significant. The equations do, however, involve two basic assumptions: (1) There is no convective transport in the γ solution, and (2) the boundary position of the fast component $\bar{x}_F^\gamma$ coincides with the observed boundary position $\bar{x}_F^{obs}$.[7] The usefulness of Eq. (4) is limited, since both c_S^γ and c_S^0 are unknown quantities. However, as is shown below, the ratio c_S^γ/c_S^0 which appears on the right-hand side of Eq. (4) may be related to the observed quantity $\bar{x}_F^{obs}$ and to the s rates of the fast and the slow components. Let σ be a quantity such that

$$c_S^\gamma/c_S^0 = (x_0/\bar{x}_F^{obs})^{2\sigma}. \quad (5)$$

Solving this equation for σ, and making use of the equation of continuity and the definition of sedimentation coefficient,

$$\sigma = \frac{\ln c_S^\gamma/c_S^0}{2 \ln x_0/\bar{x}_F^{obs}} = \frac{\int_0^t s_S^\gamma dt}{\int_0^t s_F^\gamma dt}. \quad (6)$$

To evaluate σ, it is necessary to assume that some function relating s to c holds during the course of the run. It has been suggested by Harrington and Schachman[1] that

$$s_S^\gamma = s_S^0 f_1(c_F^\gamma, c_S^\gamma), \quad s_F^\gamma = s_F^0 f_2(c_F^\gamma, c_S^\gamma), \quad (6a)$$

where

$$f_1(c_F^\gamma, c_S^\gamma) = f_2(c_F^\gamma, c_S^\gamma).$$

[7] The percent error in the calculation of c_S^0 using Eq. (4) is nearly equal to the percent error in $\bar{x}_F^{obs} - \bar{x}_S^{obs}$.

If this formulation is correct, the σ may be evaluated,

$$\frac{\int_0^t s_S^\gamma dt}{\int_0^t s_F^\gamma dt} = \frac{s_S^0}{s_F^0} = \sigma. \quad (7)$$

In reality, however, $f_1(c_S^\gamma, c_F^\gamma)$ is probably not identical to $f_2(c_F^\gamma, c_S^\gamma)$. Still, it is quite reasonable to suppose that the ratio of the functions is nearly equal to unity and essentially constant during any one run. In this case Eq. (7) is more closely approximated by:

$$\sigma \approx \frac{s_S^0}{s_F^0} \frac{f_1(c_S^0, c_F^0)}{f_2(c_S^0, c_F^0)}. \quad (8)$$

After determining c_S^0 and c_F^0 from the pattern using Eqs. (7) and (9), a better value of σ can be calculated if the functions f_1 and f_2 are known. The approximation $\sigma = s_S^0/s_F^0$ is probably sufficiently accurate to allow a useful determination of c_S^0, as will be shown experimentally in the next section of this paper.

Equation (4) may now be written:

$$r = \frac{(\bar{x}_F^{obs}/x_0)^{2(1-\sigma)} - 1}{(\bar{x}_F^{obs}/\bar{x}_S^{obs})^2 - 1}, \quad (9)$$

$$c_S^0 = (\bar{x}_S^{obs}/x_0)^2 c_S^{obs}/r. \quad (10)$$

Equations (9) and (4a) have been plotted in Fig. 2 for the special case in which $\sigma = s_S^0/s_F^0 = 0.700$. The dependence of the sedimentation coefficient of the slow component on its own concentration was assumed to be negligible ($k_S = 0$). Thus, $\bar{x}_S^{obs}$ was given by the relationship: $\bar{x}_S^{obs} = x_0 \exp(\omega^2 s_S^0 t)$. The position of the fast peak $\bar{x}_F^{obs}$ was calculated by integrating the equations†

$$s_F^\gamma = s_F^0/(1 + k_F c_F^\gamma) = (d\bar{x}_F^{obs}/dt)/\omega^2 \bar{x}_F^{obs},$$

$$c_F^\gamma = (x_0/\bar{x}_F^{obs})^2 c_F^0.$$

This yields

$$\ln \frac{\bar{x}_F^{obs}}{x_0} - \frac{k_F c_F^0}{2}\left[\left(\frac{x_0}{\bar{x}_F^{obs}}\right)^2 - 1\right] = \omega^2 s_F^0 t, \quad (11)$$

which is the functional relationship between x and t for a single component with s *versus* c dependence at constant temperature. It should be noticed (Fig. 2) that the percentage change in the buildup of the slow peak is different from the percentage change in the build down of the fast peak. Thus a 10 percent drop in the square-law corrected slow area during the run could have a

† If $s_F^\gamma = s_F^0(1 - k_F c_F^\gamma)$, then the corresponding relationship is

$$\frac{(\bar{x}_F^{obs})^2 - k_F c_F^0 x_0^2}{x_0^2 - k_F c_F^0 x_0^2} = \exp(2\omega^2 s_F^0 t).$$

concomitant 300 percent increase in the fast square-law corrected area.

Equation (9) can be rewritten in a more familiar form by making a fairly good approximation

$$a^x \approx 1 + x \ln a,$$

which is valid when $x \ln a$ is small. Thus (9) becomes

$$\frac{(\bar{x}_S^{obs}/x_0)^2 c_S^{obs}}{c_S^0} = \frac{1-\sigma}{1-\dfrac{\ln \bar{x}_S^{obs}/x_0}{\ln \bar{x}_F^{obs}/x_0}} = \frac{\int_0^t s_F^\gamma dt - \int_0^t s_S^\gamma dt}{\int_0^t s_F^\gamma dt - \int_0^t s_S^\beta dt}, \quad (12)$$

where it has been assumed that $\ln \bar{x}_S^{obs}/x_0 = \omega^2 \int_0^t s_S^\beta dt$. Here the quantity s_S^β is the s rate of the slow component which would be observed in a plateau region of concentration c_S^β. This equation bears a formal similarity to that obtained by Johnston and Ogston. From Eq. (12) it is to be expected that observed areas will have a time dependence over that of the square law of radial dilution alone.

MATERIALS AND METHODS

The validity of this analysis has been tested by applying it to data obtained by Harrington and Schachman[1] consisting of a series of five runs on mixtures of bushy stunt virus (BSV) and tobacco mosaic virus (TMV). In these mixtures the concentration of the slow component (BSV) was held constant (3 mg/cc or a Δn of $50 \cdot 10^{-5}$ index of refraction units) and the concentration of the fast component (TMV) was varied from 2 mg/cc to 10 mg/cc. The resulting buildups were from 50 to 300 percent. The runs were made at 15 220 rpm in a Spinco Model E analytical ultracentrifuge, using a bar as a schlieren diaphragm. In order to obtain the required data to test the theory, not only area measurements were needed but also the equivalent boundary positions. These were not the maximum ordinates, but the square root of the second moments about the center of rotation,[5,6] and were calculated by dividing the projected (4.5×) area into vertical strips and weighting each strip properly.

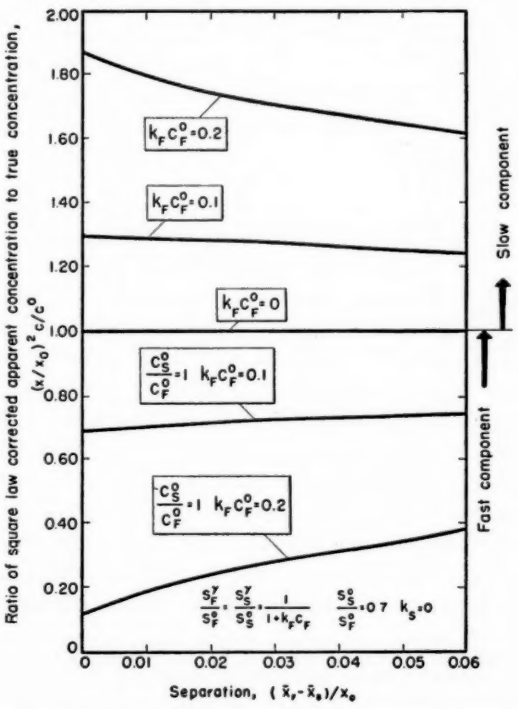

FIG. 2. Theoretical plot of area changes over and above radial dilution during ultracentrifugation as a function of boundary separation (two component system).

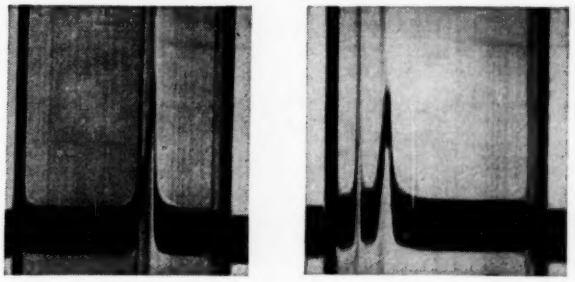

FIG. 3. Convection in the ultracentrifugation of a TMV-BSV mixture. Mixture of 3 mg/cc BSV+6 mg/cc TMV. Pictures taken at 16 and 36 min after reaching speed. Bar angle, 50°. Solvent was 0.01M phosphate, *p*H 7. Speed, 15 220 rpm. Sedimentation is to the left.

The difference between the maximum ordinate and the second moment (which is closely approximated by the center of gravity) is accentuated in skew boundaries. Figure 3 shows a schlieren pattern from a 3:6 mixture in which the slow peak is visibly skew. The reason for the appearance of skew boundaries in the mixture runs will be discussed later. Note, however, that in the 3:6 mixture the fast boundary is extremely sharp. Measurements of the boundary positions on the sharp, fast boundaries were made from the projected image using a transparent scale, and also, directly on the plate, using a microcomparator.[8] Areas were determined: (1) by averaging five separate planimeter measurements using both the outside and inside areas from 7.5× tracings, and (2) from summation of the strips used in calculating $\bar{x}_S^{obs}$ on the 4.5× projector. Areas agreed between the methods within a standard deviation of 2 percent, which was the standard deviation of either method alone.

In order to evaluate σ, the infinite dilution sedimentation coefficients had to be precisely determined. To determine these coefficients, an s *vs* c plot was made and extrapolated to infinite dilution. To get the required precision, each point on the s *vs* c plot must be corrected

[8] H. K. Schachman and W. F. Harrington, J. Polymer Sci. (to be published).

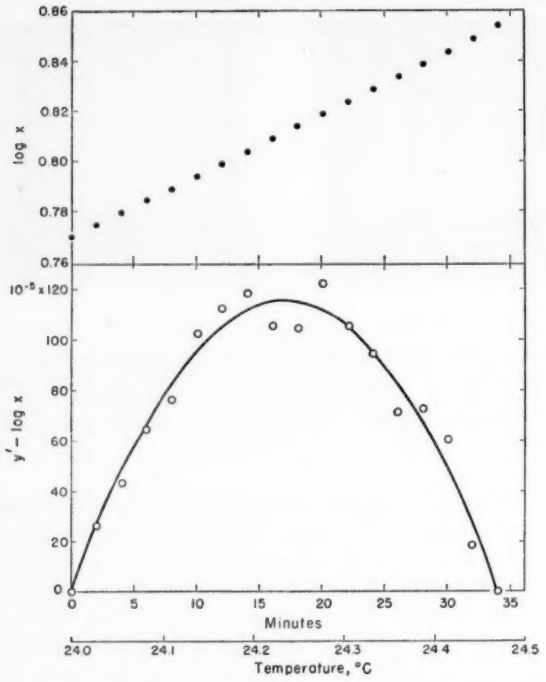

FIG. 4. Log$x$ *vs* t and expansion of log$x$ *vs* t plot for 1 percent TMV. Temperature scale below.

for two effects: (1) the influence of temperature changes during the run, and (2) the influence of radial dilution on s *vs* c dependence. The temperature correction may be handled by several methods.[9,10] In order to correct for the radial dilution effect, Kegeles[11] has suggested that a least-squares line be drawn through the log$x$ *vs* t data and plotted for the *average* concentration between the first and the last frames.

Another method, which takes into account both radial dilution and temperature corrections, has been used to obtain our data. Generally only three of the five places of the logarithm can be plotted in log$x$ (cm) *vs* time (min) graphs. The remaining two places contain the slight change in shape which is to be determined. In order to plot these, the equation for the straight line between the first and last points is determined and the difference between the observed log and the straight line at that same time (t) is calculated. The difference is plotted as a function of t. Such a plot for a 10 mg/cc TMV solution is shown in Fig. 4. Thus initial s rates can be determined by subtracting the initial slope on the expanded plot from the slope of the straight line chosen. This initial s rate is that of the material at the initial concentration c^0 and the initial temperature of the run. If the temperature change during the run is assumed to be linear, then a linear temperature scale may also be included on the expanded log$x$ *vs* t plot (see Fig. 4). Therefore, the slope of the expanded plot at any time t_1, subtracted from the slope of the straight line, gives the s rate of the material at the concentration $c_{t_1}=c^0(x_0/\bar{x}_{t_1})^2$, and at the corresponding temperature.

RESULTS AND DISCUSSION

The data obtained from the mixture runs is summarized in Table I; the values of σ are calculated from Eq. (9) using the known value of $c_S{}^0$. From s *vs* c plots made on the same samples of TMV and BSV, the ratio of infinite dilution s rates, $s_S{}^0/s_F{}^0$, is 0.70, which is in agreement with the values calculated. Alternately, using the independently determined value of $s_S{}^0/s_F{}^0=0.70$, $c_S{}^0$ was calculated for each frame of each run, and, as seen from Table I, this value is 49 ± 2, which is in excellent agreement with the expected value of 50 ± 1 obtained from a run of 3 mg/cc BSV alone.

It is interesting to note that the value of σ comes out as a constant not only for each run, but also from run to run. Since $c_F{}^0$ was varied from 2 mg/cc to 10 mg/cc this means that within experimental error the value of the function f_1 in Eq. (6a) is identical to f_2. Therefore, the relative decrease in the sedimentation rate of BSV appears to be identical to that of TMV in the γ phase. It would be of value to determine if $\sigma=s_S{}^0/s_F{}^0$ for other systems.

If theoretical curves are drawn from Eq. (9) (Fig. 2), it is evident that the buildup $(r-1)$ is a decreasing function of time. This progressive decrease in buildup is due to the effect of the radial dilution of the fast component upon the sedimentation coefficient of the slow in the γ phase. Therefore, immediately behind the fast boundary the quantity of slow component being uncovered is not sufficient to maintain a plateau in the β phase. Consequently, there is a tendency toward density inversion in the region between the boundaries. Thus, one of the aspects of sector centrifugation of mixtures predicted by this theory is the existence of convection in the region between the slow and the fast boundaries. If the theory is correct, convection is always present in mixture runs during sedimentation. The magnitude of this convection increases with increasing s *vs* c dependence of the fast components.

The manifestations of this convection can be observed on the schlieren pattern. (1) In Fig. 3 the slow peak is skew in frame 5 but is visibly more symmetrical at a later time in frame 10.[12] Slow component alone is symmetrical for the entire run. (2) An apparently isolated peak not obeying the square law implies that some process other than sedimentation is present. In the frames where the peaks are separated, base line region is seen, yet the slow area drops off more than accounted for by the square law. In spite of this convection between

[9] R. Cecil and A. G. Ogston, Biochem. J. **43**, 592 (1948).
[10] Max A. Lauffer, J. Am. Chem. Soc. **66**, 1195 (1944).
[11] G. Kegeles and F. J. Gutter, J. Am. Chem. Soc. **73**, 3770 (1951).

[12] It can be shown from the theory that the rate of convective mass transport is proportional to the rate of change of the buildup. In addition it should be noted that the ratio of convected mass to total mass in the β phase is decreasing. Therefore, the effect of convection on the shape of the boundary is greater at the beginning of the run.

TABLE I.

3:2 Mixture					3:8 Mixture				
Frame	$\left(\frac{\bar{x}s}{x_0}\right)^2_{cs^{obs}}$	$(r-1)100$	cs^0	σ	Frame	$\left(\frac{\bar{x}s}{x_0}\right)^2_{cs^{obs}}$	$(r-1)100$	cs^0	σ
5	62.0	24%	47.6	0.713	6	157.4	215%	48.6	0.708
6	60.6	21%	46.5	0.721	7	145.4	191%	54.1	0.680
7	61.5	23%	48.3	0.710	8	147.9	196%	50.1	0.700
8	60.1	20%	46.4	0.721	9	137.6	175%	48.7	0.704
9	58.9	18%	45.4	0.724	10	131.4	163%	48.5	0.709
10	58.9	18%	45.5	0.726	11	126.0	152%	47.6	0.714
3:4 Mixture									
Frame	$\left(\frac{\bar{x}s}{x_0}\right)^2_{cs^{obs}}$	$(r-1)100$	cs^0	σ					
4	87.9	76%	49.0	0.706					
5	87.1	74%	49.2	0.705					
6	84.7	69%	47.5	0.715					
7	82.1	64%	50.2	0.699					
3:6 Mixture					3:10 Mixture				
Frame	$\left(\frac{\bar{x}s}{x_0}\right)^2_{cs^{obs}}$	$(r-1)100$	cs^0	σ	Frame	$\left(\frac{\bar{x}s}{x_0}\right)^2_{cs^{obs}}$	$(r-1)100$	cs^0	σ
5	114.8	130%	53.1	0.682	8	201.0	302%	51.3	0.692
6	108.6	117%	50.9	0.695	9	199.8	300%	54.4	0.676
7	107.8	116%	52.7	0.684	10	191.9	284%	51.4	0.692
8	102.1	104%	49.7	0.702	11	174.5	249%	49.5	0.703
9	98.9	98%	48.8	0.704	12	174.4	249%	51.1	0.694
10	94.2	89%	46.4	0.721	13	182.4	266%	50.2	0.698

the fast and slow peaks, the s rate of the slow peak calculated from $\log\bar{x}_S$ *vs* t plots was not significantly different from the value of $s_S{}^\beta$ determined from the s *vs* c plot of BSV.

There is another type of convection which can presumably take place, but which was not observed to be significant in these runs. If the buildup in the β phase is such that the concentration there is greater than the total concentration in the γ phase, then it is to be expected that the β phase will tend to convect into the γ phase by a hydrostatic leveling process. In the 3:10 mixture, such an effect is to be expected from the theory, but the buildup drops off so quickly with distance that it falls below the density inversion level before an appreciable amount of the slow component is displaced.

In a concentration analysis of noninteracting systems, ideally the individual component of the mixture should be isolated in order to establish the infinite dilution sedimentation constants through a series of runs at varying concentrations. In such a study the expanded $\log x$ *vs* t plot can be utilized to obtain accurate sedimentation coefficient data at known concentrations. In many cases, however, it may not be feasible to isolate and study the mixture components independently. Nevertheless it is still possible to obtain reasonably accurate values for infinite dilution sedimentation constants by plotting the fast component against total concentration and the slow component against its *apparent* concentration as determined from area measurement. The ratio of infinite dilution sedimentation constants σ then allows a determination of true concentration for each component in any subsequent mixture run.

The theory may possibly apply in the study of equilibrium systems in which the equilibrium position is dependent on total protein concentration and the rate of equilibration is slow compared to the time of a centrifuge run. Systems containing antigen-antibody complexes such as those studied by Singer and Campbell[13] exhibit such behavior. Again the infinite dilution sedimentation constants can be evaluated from a dilution series and as long as both components are present at the lower concentrations, a reasonable determination of σ can be made. This method should be valuable in determining equilibrium constants for these systems.

[13] S. J. Singer and Dan H. Campbell, J. Am. Chem. Soc. **74**, 1794 (1952).

Proton Magnetic Resonance Spectrum of Ammonia and the Interactions Involved in Hydrogen Bond Association

RICHARD A. OGG, JR.
Department of Chemistry, Stanford University, Stanford, California
(Received December 15, 1953)

High-resolution proton magnetic resonance spectra are presented for the liquid and vapor states of ammonia. The vapor spectrum displays the expected spin-spin interaction multiplet structure. This is likewise found in the liquid state, provided the ammonia is rigorously anhydrous. A trace of water results in the appearance of a single resonance—an effect attributed to chemical exchange of protons. A marked shift of resonance between the liquid and vapor states is found, interpreted as decreased shielding in the liquid state. This effect, not observed for the non-polar substance propane, is discussed in connection with so-called "hydrogen bonding."

PROTON magnetic resonance spectra in ammonia have been studied with the 30-megacycle high-resolution spectrometer of the research and development laboratories of Varian Associates. The isotopically ordinary ammonia was a synthetic product of high purity, stored in a cylinder containing metallic sodium (to remove traces of water). Additional drying was achieved in the vacuum system by condensation in a trap containing metallic sodium. Samples from this solution were distilled into a small two-legged Faraday tube constructed of 5 mm o.d. Pyrex glass tubing. This was then sealed off while cooled in liquid nitrogen. Insertion of the appropriate leg of the sample tube into the spectrometer probe allowed study of proton resonance in ammonia vapor and liquid, respectively. The spectrum of the saturated vapor at room temperature (partial pressure about ten atmospheres) is presented in Fig. 1. Despite the rather low signal to noise ratio, the spectrum shows very clearly the expected triplet structure, due to spin-spin interaction with the N^{14} nucleus. The proton spectrum of the corresponding liquid sample is presented in Fig. 2B, and is seen to be a sharp singlet.

Another Faraday sample tube was prepared as above, with the additional precaution of including a sample of redistilled metallic sodium within the tube itself. By careful distillation of the ammonia from one leg to another a colorless (sodium free) sample was finally obtained. The spectrum of this liquid is presented in Fig. 2A, and is seen to have a triplet structure substantially identical with that of the vapor. The marked difference between the spectra in Figs. 2A and 2B is obviously due solely to a trace of water in the liquid sample of 2B, despite the precautions taken to assure anhydrous conditions. (This trace probably resulted from moisture adsorbed on the glass.) The ultimate rigorous drying in the Faraday tube containing sodium sufficed to reduce the water content below the critical level (see below).

A sample of ammonia containing approximately 15 percent of the N^{15} isotope was prepared in the vacuum system by interaction of isotopically enriched ammonium salt (from Eastman Kodak Company) and con-

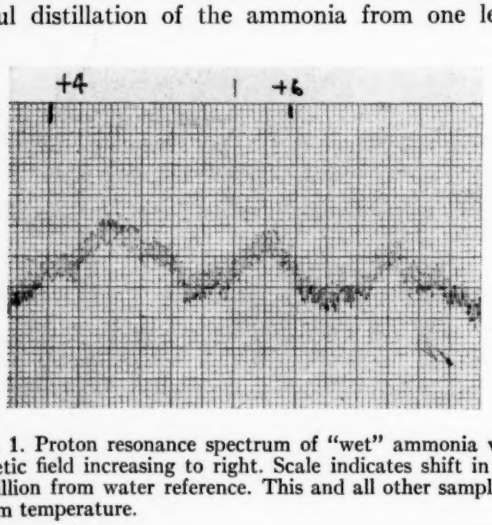

FIG. 1. Proton resonance spectrum of "wet" ammonia vapor. Magnetic field increasing to right. Scale indicates shift in parts per million from water reference. This and all other samples are at room temperature.

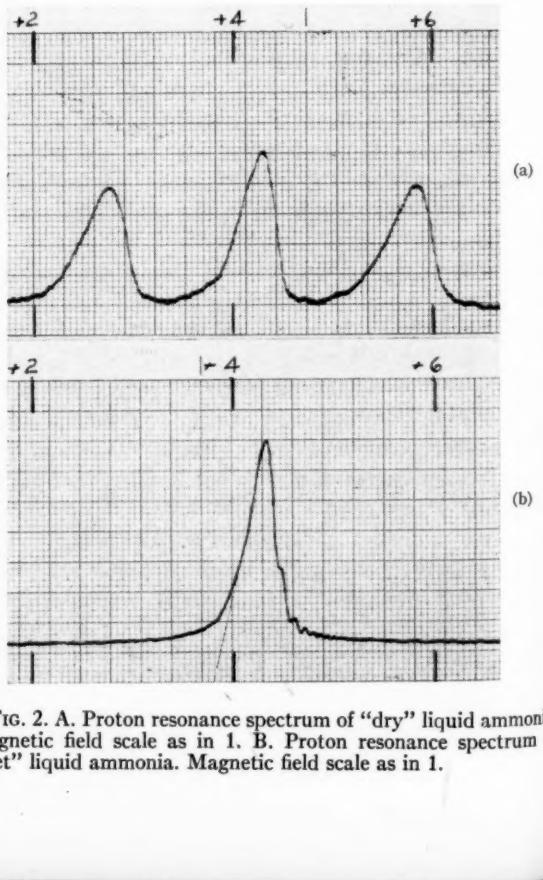

FIG. 2. A. Proton resonance spectrum of "dry" liquid ammonia. Magnetic field scale as in 1. B. Proton resonance spectrum of "wet" liquid ammonia. Magnetic field scale as in 1.

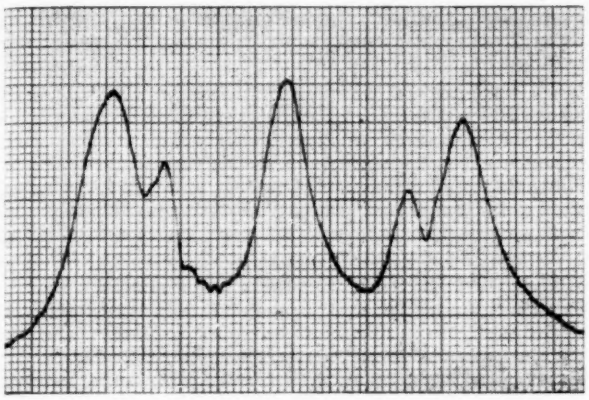

FIG. 3. Proton resonance spectrum of "dry" liquid ammonia enriched in N^{15} isotope.

centrated aqueous sodium hydroxide. After drying with metallic sodium this was distilled into a Faraday tube containing sodium, and handled as above. The spectrum of this sample is presented in Figs. 3 and 4. The additional satellite peaks are clearly the spin-spin doublet expected from the nuclear spin quantum number $\frac{1}{2}$ for the N^{15} nucleus. The ratio of multiplet separations agrees quantitatively with the relation of the known gyromagnetic ratios of N^{14} and N^{15} nuclei.

The effect of a trace of water (estimated not to exceed one part in ten million) in causing disappearance of the proton resonance spin-spin structure in liquid ammonia is attributed to the reaction

$$H_2O+NH_3 \rightleftarrows OH^-+NH_4^+,$$

resulting in rapid exchange of protons between ammonia molecules. From the data for an aqueous medium it may be inferred that the above reaction is endothermic by only a few kilocalories per mol. With an activation energy of this magnitude a sufficiently great rate constant is expected. This ionic reaction is not possible in gas phase, and it is significant that the "wet" vapor yields a multiplet spectrum.

Ammonia is typical of the liquids showing "hydrogen bond" association. The retention of multiplet structure for the proton resonance in the really pure substance indicates clearly that this "hydrogen bonding" is a purely electrostatic dipole-dipole interaction, with no electron exchange between neighboring molecules. However, it is to be noted that there is a marked shift of the absolute position of the proton resonance between the vapor and the liquid. The scale at the top of Figs. 1 and 2 indicates the position of the proton resonance in reference to that in pure liquid water, one unit displacement corresponding to one part per million (30 cycles). This also gives the absolute magnitude of multiplet separations. It is seen that the vapor resonance occurs at *higher* magnetic fields. With the geometry employed the correction for bulk magnetic susceptibility is

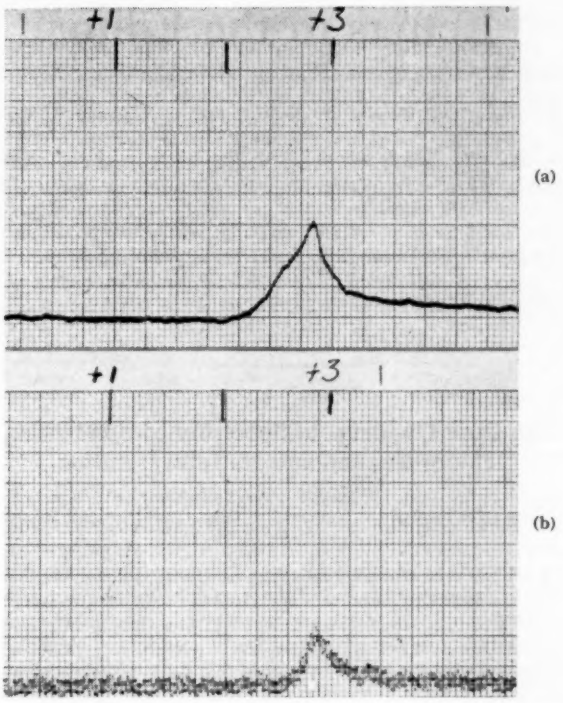

FIG. 4. A. Proton resonance spectrum of liquid propane. Magnetic field scale as in 1. B. Proton resonance spectrum of gaseous propane. Magnetic field scale as in 1.

negligible but it is to be noted that any residual correction would be such as to place the resonance in the liquid at *higher* fields than that in the vapor (that is the observed separation is a lower limit). It was judged desirable to make a similar liquid-vapor comparison with a typical nonpolar substance. That chosen was propane, whose physical properties are very similar to those of ammonia. A similar Faraday tube was constructed containing liquid and gaseous propane. For this substance no detectable difference in absolute position of the proton resonance between vapor and liquid was observed.

The normal interpretation of the liquid-vapor difference for proton resonance in ammonia would lead to the conclusion that protons in the liquid are *less* shielded diamagnetically than those in the molecules of the vapor. In short, the strong electrostatic dipole-dipole attraction between neighboring molecules in the liquid polarizes the molecules in such a sense as actually to *decrease* the electron density effective in shielding the protons. This effect must be explained by any satisfactory theory of "hydrogen bonding." Where no appreciable dipole interaction occurs, as in propane, evidently the distortion of neighboring molecules in a liquid leads to negligible change in proton shielding.

The author wishes to acknowledge the assistance of Dr. James Shoolery, of Varian Associates, in the performance of the nuclear magnetic resonance studies.

Letters to the Editor

THIS section will accept reports of new work, provided these are terse and contain few figures, and especially few half-tone cuts. The Editorial Board will not hold itself responsible for opinions expressed by the correspondents. Contributions to this section should not exceed 600 words in length and must reach the office of the Editor not later than the 15th of the second month preceding that of the issue in which the Letter is to appear. No proof will be sent to the authors. A publication charge of $10.00 per Letter is made which, when honored, will entitle the Institution to 100 free reprints.

The Pure Quadrupole Spectrum of Solid Hexachlorobenzene and Its Interpretation

JULES DUCHESNE AND ANDRÉ MONFILS*
Institut d'Astrophysique, University of Liège, Cointe-Sclessin, Belgium
Received December 14, 1953)

RECENTLY the pure quadrupole transitions for the mono- and dichlorobenzenes were studied at different temperatures.[1] The purpose of this note is to extend these previous data to hexachlorobenzene and to suggest a general interpretation of the behavior of the spectra through this series of compounds. In our experiments a frequency-modulated regenerative oscillator was used and the absorption lines were viewed on an oscilloscope. The resonant frequencies observed for Cl^{35}, as a function of temperature, are given in Fig. 1 and are in good agreement with an

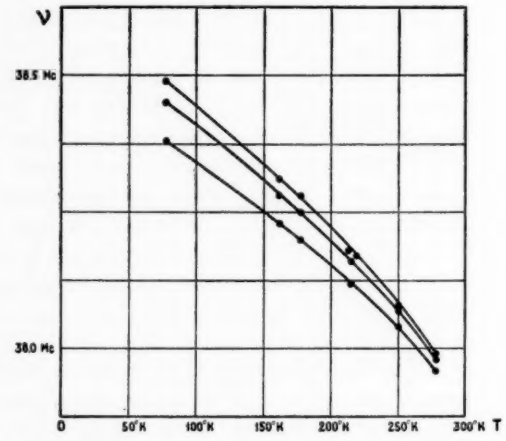

FIG. 1. Resonance frequency of Cl^{35} as a function of temperature in C_6Cl_6.

earlier measurement made at liquid-nitrogen temperature.[2] It is shown on Fig. 1 that, within the range of measurements considered, the three component frequencies of the lines decrease with increasing temperature, as was already observed in other cases.[1,3] However, each component shifts to a different extent, so that decreasing spacings are obtained on going from 77 to 278°K.

We now turn to the nuclear quadrupole coupling constants derived from the resonance frequencies found at 173°K for hexachlorobenzene and already known for other chlorobenzenes.[1] A temperature as high as this was selected in order that the data should be as complete as possible, and average couplings have been used when multiple lines were present. We have represented these couplings in Fig. 2 in terms of the number of Cl atoms substituted in the benzene ring. It is seen that they increase in magnitude from C_6H_5Cl to p-$C_6H_4Cl_2$, though they remain approximately constant in isomeric molecules (m-$C_6H_4Cl_2$, p-$C_6H_4Cl_2$), provided these are not substituted in adjacent positions. On the other hand, the CCl bonds in chlorobenzenes[4] have a small amount of double-bond character ($C=Cl^+$), which is known to be almost constant for isomers and decreases slowly when the number of chlorines increases.[5] On account of this π-bonding effect, eqQ ought to be smaller than would be the case if only the pure σ bond were considered, and it follows that this factor alone explains the general behavior of the couplings. Now, by linear extrapolation through the first two experimental points, the eqQ value for C_6Cl_6 becomes 73.00 Mc, instead of the actual value of 76.52 Mc. The theoretical result would have been the true one if the regular changes in the proportion of the double-bonded structures had been entirely responsible for the phenomena. The abrupt anomalies which only appear when adjacent chlorines are present and amount to 1.6 Mc for $O-C_6H_4Cl_2$ and to 3.5 Mc for C_6Cl_6 presumably rest on the fact that in these particular molecules the CCl bonds do not remain planar but are bent out of the benzene ring.[6] As a consequence, a further decrease of the resonating double-bonded structures is to be expected, and if it is assumed that their proportion varies approximately as $\cos\Phi$ (Φ being the angle between the π orbitals), a change of about 5 percent must result from a CCl bending of 18° found in $O-C_6H_4Cl_2$.[6] The increase observed in eqQ is therefore explained on this basis and could not depend upon a change in the

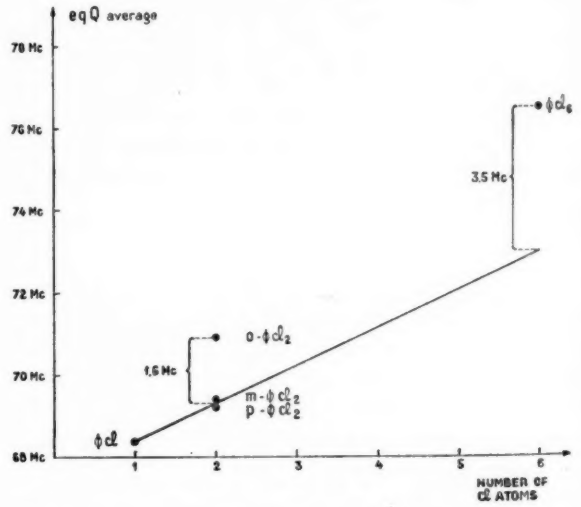

FIG. 2. Cl^{35} quadrupole couplings in the chlorobenzenes at 173°K.

ionic character of the CCl bonds which would give a reverse effect. The fact that the eqQ value predicted for 1·3·5 trichlorobenzene (70.2 Mc) is smaller than that observed for $O-C_6H_4Cl_2$ (70.9 Mc) indicates that the addition of a chlorine is less effective in reducing resonance than an 18° CCl bending. As the change in eqQ is larger for C_6Cl_6 (3.5 Mc) than for $O-C_6H_4Cl_2$ (1.6 Mc), it is almost certain that the CCl bending is more important in the former compound than in the latter one, and it may be estimated at about 25°. This result differs noticeably from that obtained by Bastiansen and Hassel[6] who found only 12°.

The suggested theory now allows the prediction of eqQ values for any chlorine derivatives of benzene.

* Aspirant du Fonds National Belge de la Recherche Scientifique.
[1] C. Dean and R. V. Pound, J. Chem. Phys. **20**, 195 (1952).
[2] Weatherly, Davidson, and Williams, J. Chem. Phys **21**, 761 (1953).
[3] R. Livingston, J. Phys. Chem. **57**, 496 (1953).
[4] L. Pauling, *The Nature of the Chemical Bond* (Cornell University Press, Ithaca, New York, 1939).
[5] J. A. A. Ketelaar, Rec. trav. chim. Pays-Bas **58**, 266 (1939); J. Sherman and J. A. A. Ketelaar, Physica **6**, 572 (1939).
[6] O. Bastiansen and O. Hassel, Acta Chem. Scand. **1**, 489 (1947).

On the Relation between the Chemical Reactivity and Energy Levels of the Chemical Reagent

S. NAGAKURA AND J. TANAKA
Institute of Science and Technology, University of Tokyo, Meguro-ku, Tokyo, Japan
(Received December 23, 1953)

IN a previous paper,[1] it was shown that the electron migration of the monosubstituted benzene molecule can be explained by taking into consideration the interaction between the highest occupied and the lowest vacant orbital of both the benzene ring and the substituent. In this letter, the cationoid substitution reaction of aromatic compounds will be treated from the same point of view.

The highest occupied level of benzene (H_B) and the lowest vacant levels of some cationoid reagents (V_S) such as nitro and halogen cations[2] can be obtained as shown in Fig. 1. The lowest vacant levels of the iodine molecule and the silver cation are also given in the figure for the purpose of comparison. These two substances are taken as the typical examples which can form the molecular complex with benzene but cannot react with it.[3] By a study of this figure, it is seen that there is a very distinct difference in the location of the lowest vacant orbital between cationoid reagents and the silver cation or the iodine molecule. Namely, in the case of molecular complex formation, the highest occupied level of benzene (H_B) lies lower than the lowest vacant orbital of the partner, whereas in the system benzene-cationoid reagent, the level H_B lies higher than the lowest vacant level of the reagent. As is well known, it may be expected that in these two cases the π electron of benzene migrates to some extent toward the partner by the interaction of the level H_B with the level V_S and the extent of the electron transfer becomes greater the lower the V_S.[1] So the above-mentioned fact seems to show that in the interaction between the cationoid reagent and reactants the extraordinarily large electron transfer might occur compared with the case of the molecular complex formation.

This may be important in considering the mechanism of the cationoid substitution because it may be inferred from this fact that in the course of the substitution reaction almost one π electron should remove from benzene or other reactants toward the reagent. As the Greek result of this large electron transfer, the reactant may probably become similar to its odd cation in the electronic structure and the reagent cation to the neutral radical. Then, immediately, the reagent will attach to a carbon atom in the reactant. In that case, which carbon the reagent attaches to will be determined by the free valency values calculated with the cation of the reactant because it is generally known that the radical substitution reaction will occur at the point of the large free valency values.[4] In practice, the free valencies calculated with cations of some monosubstituted benzenes and naphthalene by the use of the simple LCAO method can explain the orientation effect obtained experimentally with their cationoid substitutions as shown in Table I.

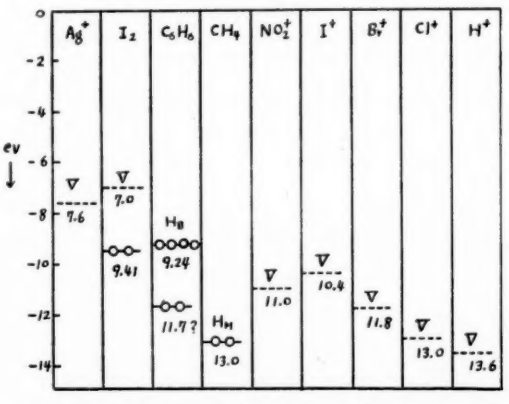

FIG. 1. Energy level diagrams for some reagents and reactants. The method of estimation of these energy levels is described in the previous paper. Vacant levels are shown by dotted lines. The vacant levels of silver, iodine, bromine, chlorine, and hydrogen cations are taken as the first ionization potentials of these atoms. The vacant level for the nitronium ion is taken as the ionization potential of nitrogen dioxide. Ionization potential data necessary for determinations of these energy levels are obtained from the following references: benzene, W. C. Price and R. W. Wood, J. Chem. Phys. 3, 439 (1935); methane, R. E. Hornig, J. Chem. Phys. 16, 105 (1948); iodine, J. D. Morrison and A. J. C. Nicholson, J. Chem. Phys. 20, 1221 (1952); nitrogen dioxide, E. C. G. Stueckelberg and H. D. Smyth, Phys. Rev. 36, 478 (1930).

TABLE I. Calculated free valency values for the cation of some aromatic compounds.

Compound	Free valency values			Orientation	
	o	*m*	*p*	Theoretical	Observed
Toluene	0.502	0.454	0.697	$p>o>m$	$p>o>m$
Phenol	0.497	0.431	0.622	$p>o>m$	$p>o>m$
	α		β		
Naphthalene	0.566		0.437	$\alpha>\beta$	$\alpha>\beta$

According to this mechanism, nonoccurrence of the general cationoid substitution on unsubstituted paraffins such as methane[5] in contrast to its ease in benzene can easily be explained because the highest occupied level of methane (H_M) lies lower than the lowest vacant level of most cationoid reagents as shown in Fig. 1, and therefore the occurrence of the large electron transfer may be difficult in this case. Furthermore, from this point of view it may be expected that the hydrogen cation, whose lowest vacant orbital lies evidently lower than the level H_B may react with benzene (see Fig. 1.) This expectation is fulfilled by the fact that the hydrogen atom of benzene can be exchanged with deuterium by the cationoid substitution reaction.[6] The above-mentioned mechanism seems to be interesting in connection with the one electron transfer theory on the organic reaction suggested by Weiss.[7]

[1] To be published in J. Chem. Phys.
[2] M. J. S. Dewar, *The Electronic Theory of Organic Chemistry* (Oxford University Press, London, 1949), p. 16.
[3] H. A. Bensei and J. H. Hildebrand, J. Am. Chem. Soc. **71**, 2703 (1949); L. J. Andrews and R. M. Keefer, J. Am. Chem. Soc. **71**, 3644 (1949), **72**, 3113 (1950); R. S. Mulliken, J. Am. Chem. Soc. **72**, 600 (1950), **74**, 811 (1952), J. Phys. Chem. **56**, 801 (1952).
[4] D. H. Hey and G. H. Williams, Disc. Faraday Soc. **14**, 216 (1953).
[5] See reference 2, p. 163.
[6] Ingold, Raisin, and Wilson, J. Chem. Soc. 1637 (1936).
[7] J. Weiss, Trans. Faraday Soc. **42**, 116 (1946).

Microwave Spectrum of Cyclopentanone

GUNNAR ERLANDSSON
Department of Physics, University of Stockholm, Stockholm, Sweden
(Received December 22, 1953)

THE microwave spectrum of cyclopentanone has been investigated in the region 18.5–25.6 kMc/sec. 22 lines have been identified as pure rotational transitions with $\Delta J=1$ or $\Delta J=0$. These lines are listed in Tables I and II. Most frequency measurements are accurate to ± 5 Mc/sec. The analysis is based on the theory of the rigid asymmetric rotator. Frequency calculations have been carried out by means of the continued fraction method of King, Hainer, and Cross.[1] The following values have been used for the rotational constants:

$$A=6.6189\ \text{kMc/sec},\quad B=3.3508\ \text{kMc/sec},\quad C=2.4099\ \text{kMc/sec},$$

and the asymmetry parameter $\kappa=-0.5529$. The corresponding moments of inertia are

$$I_A=76.361\ \text{AA}^2,\quad I_B=150.837\ \text{AA}^2,\quad I_C=209.73\ \text{AA}^2.$$

The difference $I_A+I_B-I_C=17.47\ \text{AA}^2$ is too large to be caused by the hydrogen atoms alone. The results thus confirm the assumption of a nonplanar carbon ring.[2] Bond distances cannot be calculated accurately from the present results. A $C-C$ distance of 1.52A seems, however, to be reasonable.

TABLE I.

Transition	$\bar{\nu}_{calc}$	$\bar{\nu}_{obs}$
$2_{1.1}-3_{1.2}$	18 572	18 573
$3_{0.3}-4_{0.4}$	21 564	21 565
$3_{1.2}-4_{1.4}$	20 864	20 863
$3_{1.2}-4_{1.3}$	24 505	24 503
$3_{2.2}-4_{2.3}$	22 905	22 911
$3_{2.1}-4_{2.2}$	24 382	24 381
$3_{2.1}-4_{2.2}$	23 340	23 335
$3_{2.0}-4_{2.1}$	23 462	23 462

TABLE II.

Transition	$\bar{\nu}_{calc}$	$\bar{\nu}_{obs}$
$14_{4.11}-14_{4.10}$	23 548	23 551
$19_{6.14}-19_{6.13}$	20 891	20 893
$22_{7.16}-22_{7.15}$	22 194	22 206
$25_{8.18}-25_{8.17}$	23 251	23 256
$28_{9.20}-28_{9.19}$	24 086	24 089
$31_{10.22}-31_{10.21}$	24 720	24 723
$34_{11.24}-34_{11.23}$	25 169	25 172
$37_{12.26}-37_{12.25}$	25 452	25 460
$40_{13.28}-40_{13.27}$	25 584	25 594
$43_{14.30}-43_{14.29}$	25 580	25 589
$46_{15.32}-46_{15.31}$	25 455	25 464
$49_{16.34}-49_{16.33}$	25 217	25 234
$52_{17.36}-52_{17.35}$	24 883	24 899
$55_{18.38}-55_{18.37}$	24 466	24 484

Each one of the lines in Table I is accompanied by a few weaker satellite lines on the high-frequency side, the strongest one being about $\frac{1}{3}$ of the main line. These may be due to some low-lying vibrational states. The corresponding Q-branch lines are not so easily associated with the ground-state lines since their spacings are larger.

[1] King, Hainer, and Cross, J. Chem. Phys. **11**, 27 (1943).
[2] Aston, Fink, and Schumann, J. Am. Chem. Soc. **65**, 341 (1943).

Force Constants of Hydrides

SHASHANKA SHEKHAR MITRA
Department of Physics, Allahabad University, Allahabad, India
(Received January 11, 1954)

IT has been found that the square root of the force constants of the hydrides of the elements occupying the same period of the periodic table are additive with the group numbers.

The force constant (k_e) is given by

$$4\pi^2\mu_A{}^2C^2\omega_e{}^2=5.8883\times10^{-2}\mu_A\omega_e{}^2 \text{ d/cm},$$

where the symbols have their usual meanings. The experimental data fit well in the formula

$$(k_e)^{\frac{1}{2}}=A+Bn, \tag{1}$$

where A and B are constants and n is the number of electrons in the outermost shell of the atom of the element considered. Equation (1) is shown graphically in Fig. 1. The values of A and B are 271.6 and 101.4, respectively, for the II period, and 205.7 and 73.0, respectively, for the III period. Table I gives the observed and calculated values of $(k_e)^{\frac{1}{2}}$ for the second and third period elements. The additivity could not be examined for the other periods due to insufficiency of experimental data.

TABLE I.

Periods n	II period Hydrides	$(k_e)^{\frac{1}{2}}10^{-1}$ obs	$(k_e)^{\frac{1}{2}}10^{-1}$ calc	III period Hydrides	$(k_e)^{\frac{1}{2}}10^{-1}$ obs	$(k_e)^{\frac{1}{2}}10^{-1}$ calc
1	LiH	32.00	37.30	NaH	27.96	27.87
2	BeH	47.56	47.44	MgH	35.71	35.17
3	BH	57.11	57.58	AlH	40.25	42.47
4	CH	66.98	67.72	SiH	49.78	49.77
5	NH	77.68	77.86	PH	57.07	57.07
6	OH	88.26	88.00	SH	...	64.37
7	FH	98.25	98.14	ClH	71.81	71.67

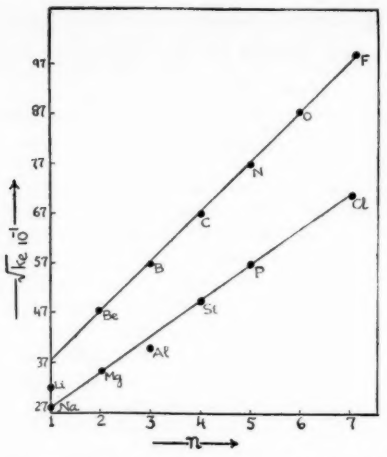

FIG. 1. The square root of the force constants (dynes/cm) of the hydrides of the II and III period elements have been plotted against the group numbers.

The force constant of SH is not known experimentally, and it has been predicted to be 4.154×10^5 d/cm by the formula (1).

It has also been observed that a simple relationship exists between the force constants of the hydrides of the second and third period elements. When the square root of the force constant of the III period hydrides are plotted against that of the II period molecules a straight line passing through the origin is obtained and is shown in Fig. 2. This implies that the ratio of the

TABLE II.

III period hydrides	$(k_e)^{\frac{1}{2}}10^{-1}$ obs	II period hydrides	$(k_e)^{\frac{1}{2}}10^{-1}$ obs	$R^{\frac{1}{2}}$	$R^{\frac{1}{2}}$ (mean)
NaH	27.96	LiH	32.00	0.8738	
MgH	35.71	BeH	47.56	0.7509	
AlH	40.25	BH	57.11	0.7047	
SiH	49.78	CH	66.98	0.7433	0.7329
PH	57.07	NH	77.68	0.7347	
SH	64.69*	OH	88.26	...	
ClH	71.81	FH	98.25	0.7310	

force constants of the hydrides of the III and II period elements is a constant for all the groups, i.e.,

$$\frac{k_e(\text{III period})}{k_e(\text{II period})}=R, \tag{2}$$

R being a constant. Table II shows the constancy of $R^{\frac{1}{2}}$. $(k_e)^{\frac{1}{2}}$ of SH has been predicted (marked with asterisk) from the mean value

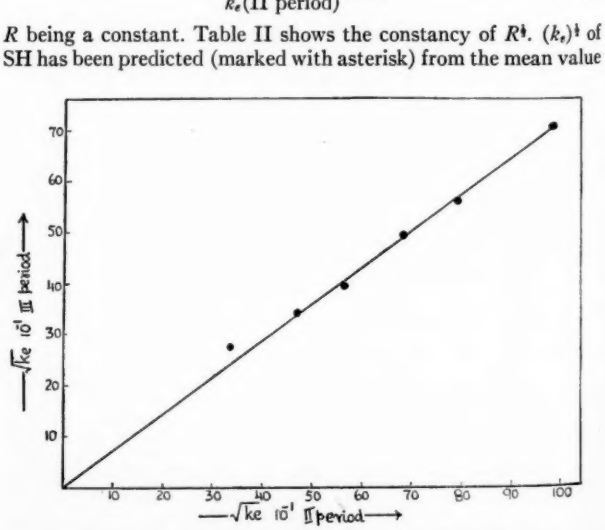

FIG. 2. The square root of the force constants (dynes/cm) of the hydrides of the III period elements have been plotted against those of the II period hydrides.

of $R^{\frac{1}{2}}$ excluding the I group. This procedure gives a value 4.184 $\times 10^5$ d/cm for the force constant of the molecule and is in very close agreement with the value predicted by Eq. (1). The data have been taken from standard sources.[1]

The author wishes to acknowledge his grateful thanks to Dr. K. Majumdar for his guidance in the work and to Dr. D. Sharma for his interest.

[1] (a) Herzberg, *Molecular Spectra and Molecular Structure* (1951), Vol. I; (b) Rosen, *Donnés Spectroscopiques concernant les Molécules diatomiques* (1951).

Microwave Spectrum of Pyridine

BØRGE BAK, LISE HANSEN, AND JOHN RASTRUP-ANDERSON
Chemical Laboratory, University of Copenhagen, Copenhagen, Denmark
(Received December 18, 1953)

IN a recent communication,[1] two of the authors discussed the microwave spectrum of pyridine observed by us in the 18 700–25 800 MHz interval. By comparing the microwave spectrum as predicted from electron-diffraction measurements on pyridine[2] with observed absorption lines it was found that the asymmetry parameter κ would have to be 1.00, 0.85, or 0.70. Since Stark displacement measurements on a line at 20 211 MHz (interpreted as a $6_{-2}\rightarrow 6_0$ transition) seemed to indicate that $\kappa=0.70$, a preliminary analysis of the microwave spectrum was attempted on this basis. Experiments now performed with an improved "Stark" cell immediately revealed, however, that the "J" of the line at 20 211 MHz certainly exceeds 6(~9–11). The interpretation given above, therefore, has to be abandoned, and our attention was hereafter focused on the possibility $\kappa=0.85$. In the meantime, McCulloh and Pollnow[3] have interpreted the pyridine spectrum observed by them in the 22 140–27 300 MHz region. They found $\kappa=0.84777$, $A=6039.13$, $B=5804.72$, and $C=2959.25$ MHz. A was found to refer to the $N-H(4)$ axis. By using these rotational constants we have found good agreement with our observed frequencies as shown for a few examples in Table I. A recalculation of the rotational constants may be carried through by observing that

$$\frac{1.5(1_{10}\rightarrow 2_{11})-(2_{12}\rightarrow 3_{13})}{(6_{42}\rightarrow 7_{25})-(6_{52}\rightarrow 7_{35})}=\frac{2(\kappa^2+15)^{0.5}+3.5\kappa-4.5}{E_{-3}^{7}(\kappa)-E_{-2}^{6}(\kappa)-E_{-2}^{7}(\kappa)+E_{-3}^{6}(\kappa)}=\frac{9851.7}{918.0}=10.7317$$

if experimental values are used. By trial and error it is found that $\kappa=0.84704$, $(A-C)/2=1540.8$ MHz, and $(A+C)/2=4499.8$ MHz. These constants indicate that the transitions $6_{42}\rightarrow 7_{25}$, $6_{52}\rightarrow 7_{35}$, and $3_{30}\rightarrow 4_{13}$ should be found at 21 394.2, 20 476.2, and 20 599.6 MHz, respectively. The agreement with observed frequencies is a trifle better than in Table I. We do not want to suggest, however, that the rotational constants so calculated ($A=6040.6$, $B=5804.9$, $C=2959.0$ MHz) are "better" than those derived by McCulloh and Pollnow, but a comparison between the two sets of rotational constants is instructive as to the error in the constants.

TABLE I. Observed and calculated pyridine microwave lines using the rotational constants found by McCulloh and Pollnow.

Transition	Observed frequency	Calculated frequency
$1_{10}\rightarrow 2_{11}$	20 373.8	20 373.41
$2_{12}\rightarrow 3_{13}$	20 709.0	20 709.74
$2_{02}\rightarrow 3_{03}$	20 722.5	20 723.10
$3_{30}\rightarrow 4_{13}$	20 594.0	20 603.8
$6_{52}\rightarrow 7_{35}$	20 481.5	20 489.5[a]
$6_{42}\rightarrow 7_{25}$	21 399.5	21 398.7[a]
$5_{24}\rightarrow 5_{23}$	20 691.0	20 688.68[a]
$6_{24}\rightarrow 6_{23}$	20 648.5	20 645.01[a]
$8_{54}\rightarrow 8_{53}$	20 430.0	20 428.8[b]
$8_{44}\rightarrow 8_{63}$	20 666.8	20 665.5[b]
$9_{64}\rightarrow 9_{63}$	20 211.25	20 211.7[b]
$9_{54}\rightarrow 9_{73}$	20 678.5	20 677.4[b]
$11_{84}\rightarrow 11_{83}$	19 405.4	19 405.3[a]
$12_{94}\rightarrow 12_{93}$	18 760.9	18 760.7[a]

[a] Uncorrected for centrifugal distortion effect.
[b] Calculated and corrected for centrifugal distortion effect by Pollnow.

Among the experimental results in Table I, the observation of the $1_{10}\rightarrow 2_{11}$ transition is especially valuable since its frequency is simply $3B+C$. By careful Stark measurements on this line its identity was unambigously established. These experiments also served to verify the selection rules used by McCulloh and Pollnow since the Stark displacements as calculated by means of the tables by Golden and Wilson[4] and the dipole moment (2.36d) of pyridine[5] (using A+C=9000 MHz) are significantly different in the two cases as shown in Table II.

TABLE II. Comparison between observed and calculated displacements of the two Stark components ($M=0$, $M=1$) of the line at 20 373.8 MHz.

Electric field intensity volts/cm	Calculated μ_a lines		Observed	Calculated μ_b lines	
250		− 6.69	− 6.5		−5.80
262.5		− 7.37	− 7.2		−6.39
275		− 8.10	− 8.1		−7.03
287.5		− 8.85	− 8.8		−7.66
300		− 9.63	− 9.6		−8.37
312.5		−10.46	−10.5		−9.06
325.0		−11.31	−11.2		−9.81
675	7.06	···	8.0	9.62	
775	9.31	···	10.0	12.69	
875	11.87	···	13.2	16.19	
	$M=0$	$M=1$		$M=0$	$M=1$

Two independent checks have, therefore, served to show that the pyridine dipole moment, lying in the $N-H(4)$ axis, coincides with the axis of *least* moment of inertia. We want to stress this point because the A value (6039 MHz) corresponding to this may be said to be somewhat high. The rotational Raman spectrum of benzene[6] shows that here $A=5682$ MHz. Microwave absorption measurements on fluorobenzene[7] gave $A=5664$ MHz. While the benzene carbon-hydrogen nuclear skeleton appears to be very nearly conserved in fluorobenzene the possibility that this might be the case for the 5 carbon atoms and the 5 hydrogen atoms of pyridine now seems to be excluded. The pyridine molecule is definitely more "slim" than benzene. Studies of deuterated species of pyridine are in progress in order to establish its interesting structure.

[1] B. Bak and J. Rastrup-Andersen, J. Chem. Phys. **21**, 1305 (1953).
[2] V. Schomaker and L. Pauling, J. Am. Chem. Soc. **61**, 1769 (1939).
[3] K. E. McCulloh and G. F. Pollnow, J. Chem. Phys. **21**, 2082 (1953).
[4] S. Golden and E. B. Wilson, Jr., J. Chem. Phys. **16**, 669 (1948).
[5] M. A. Rau and B. N. Narayanaswamy, Z. physik. Chem. **B26**, 23 (1934).
[6] B. Stoicheff, J. Chem. Phys. **21**, 1410 (1953).
[7] G. Erlandsson, Arkiv Fysik (1953).

Gamma-Ray Polymerization of Acrylamide in the Solid State*

ROBERT B. MESROBIAN AND PAUL ANDER, *Polymer Research Institute, Polytechnic Institute of Brooklyn, Brooklyn, New York*
AND
DAVID S. BALLANTINE AND G. J. DIENES, *Brookhaven National Laboratory, Upton, Long Island, New York*
(Received January 18, 1954)

THE polymerization of vinyl monomers can be initiated by heat, ultraviolet radiation, and various catalysts. More recently, ionizing radiation has been shown to effectively initiate vinyl polymerization.[1] However, polymerization in the solid state by ionizing radiation is not reported in the literature, although several papers have been published that describe briefly the thermal polymerization of divinyldiphenyl,[2a] Leuchs' anhydride,[2b] and in greater detail the peroxide catalyzed polymerization of acetaldehyde.[2c] The purpose of this note is to describe some experiments which demonstrate that crystalline acrylamide undergoes polymerization upon irradiation with γ rays from an intense

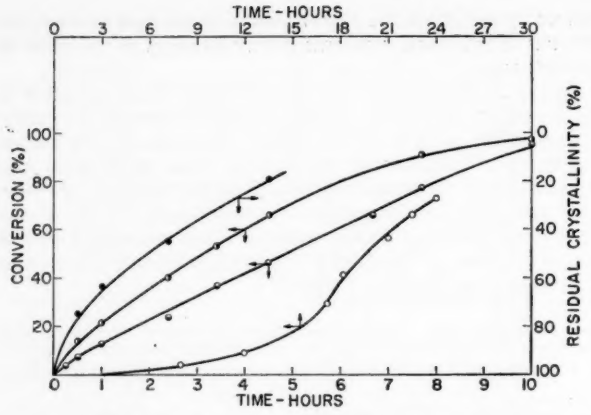

FIG. 1. Solid-state polymerization of acrylamide initiated by gamma radiation (Co^{60}, 220 000 rep/hour) at several temperatures. ● Residual crystallinity in material exposed at 35°C. ◑ Percent conversion at 55°C. ◒ Percent conversion at 35°C. ○ Percent conversion at 5°C.

Co^{60} source. Below its melting point the monomer shows little or no tendency to polymerize thermally.

Three-gram samples of sublimed acrylamide, mp 84°C (American Cyanamide Company), were sealed in vacuum in Pyrex ampules and irradiated. The polymer was isolated by using methanol as a precipitant. Viscosity, osmotic pressure, and turbidity measurements were performed on water solutions of the polymer.

Rate curves obtained at several temperatures are shown in Fig. 1. Thermocouples attached to the samples showed that the temperature was maintained constant to ±1°C during these experiments and no sintering of the samples was ever observed. Residual crystallinity of the bulk sample, as determined by the integrated intensity of several x-ray reflections, is also shown for comparison. Some of the characteristics of the polymer are given in Table I.

The percent conversion *vs* time curves at 35 and 55°C indicate that the order of the reaction lies between zero- and one-half-order dependence on monomer concentration at the radiation intensity employed. However, sufficient data are not available to enable one to suggest a polymerization mechanism. It is evident from the run at 5°C that a long induction prevails before the onset of polymerization. At still lower temperatures the induction period becomes very long. However, radicals are certainly produced since on warming a previously irradiated sample to room temperature violent polymerization occurs. Radicals are obviously frozen in, an effect which has also been noted with other crystals.[3]

Since the polymer is amorphous, it is not surprising that the residual crystallinity of the exposed material decreases with irradiation (Fig. 1). The fact that appreciable crystallinity remains even at high conversions of monomer demonstrates that the crystalline domain of unreacted monomer in the vicinity of polymer chains is only slightly affected by the latter.

The molecular weight characteristics of polymer formed at various conversions are listed in Table I. It is suggested that the progressive increase in intrinsic viscosity with conversion is due to branching. Indeed, at conversions above about 50 percent the formation of gel occurs. In the one low-conversion sample studied, the ratio of weight to number average molecular weight is 2.2 which, within experimental error, coincides with the value of 2.0 for the most probable distribution predicted for polymerization reactions having a definite termination step.[4]

TABLE I.

Conversion %	Polymerization temp (°C)	Intrinsic viscosity at 25°C 100 $cm^3 \cdot g^{-1}$	Number average molecular weight[a]	Weight average molecular weight[b]
12.7	35	1.27	19 800	43 000
13.8	55	1.68	48 000	···
21.4	55	1.88	···	···
40.3	55	2.02	···	···

[a] From osmotic pressure measurements at four concentrations using Igepal CO-630 (Antara Chemicals, Inc.) as wetting agent.
[b] From light scattering measurements at four concentrations.

* Work partially done under contract with the U. S. Atomic Energy Commission.

[1] For a recent review see F. S. Dainton and E. Collinson, Ann. Rev. Phys. Chem. **2**, 99 (1951).
[2] (a) Valyi, Janssen, and Mark, J. Phys. Chem. **49**, 462 (1945); (b) Miller, Fankuchen, and Mark, J. Appl. Phys. **20**, 531 (1949); (c) Letort, Duval, and Rollin, Compt. rend. **224**, 50 (1947).
[3] J. V. Schmitz and E. J. Lawton, Science **113**, 718 (1951).
[4] P. J. Flory, *Principles of Polymer Chemistry* (Cornell University Press, Ithaca, New York, 1953), Chapter VIII.

On Thermal Diffusion in the Liquid Phase

J. JEENER AND G. THOMAES*
Faculty of Science, University of Brussels, Belgium
(Received December 29, 1953)

PREVIOUSLY, systematic investigations of thermal diffusion (Soret effect) in organic solutions have been performed in this laboratory under the direction of L. de Brouckère and I. Prigogine.[1–5] The methods used were based on either direct optical study of thermal diffusion or on thermogravitation. The first method is of course the most accurate; the second procedure is used when one is interested in more qualitative results or when the enrichment is too small to be observed by the direct method.

In the stationary state of thermal diffusion we have the relation

$$\frac{1}{x_A x_B}\frac{\partial x_B}{\partial z}=\frac{D'}{D}\frac{\partial T}{\partial z}, \tag{1}$$

where D' is the coefficient of thermal diffusion, D the ordinary diffusion coefficient, x_A, x_B the mole fractions of A and B ($x_A+x_B=1$). A simple kinetic model based on the usual theory of transport processes in condensed media[6] has been developed by I. Prigogine for the Soret ratio D'/D[1,5]. Formula (1) applies to a stationary state; for this reason, the energy of activation of formation of a "hole" which seems to play an important role in ordinary diffusion and viscosity does not enter in the ratio D'/D because one can assume that the two inverse processes occur through the "same" hole. The formula which can be derived for molecules of about the same size is

$$\frac{D'}{D}=\frac{q_A-q_B}{kT^2}, \tag{2}$$

where q_A and q_B are the energies required to remove the molecules A and B from their equilibrium positions. The Soret ratio D'/D is thus directly related to intermolecular forces. Assuming that the energies q_A and q_B are a fraction $1/X$ of the total binding energy in the liquid and assuming that only dispersion forces exist, this formula becomes

$$\frac{D'}{D}=\frac{2}{X}\frac{1}{RT^2}[(E_A^v)^{\frac{1}{2}}-(E_B^v)^{\frac{1}{2}}(x_A(E_A^v)^{\frac{1}{2}}+x_B(E_B^v)^{\frac{1}{2}})], \tag{3}$$

where E_γ^v is the energy of vaporization of the pure compound γ. This formula predicts that the compound with higher energy of vaporization (or more generally the higher "density of cohesion"[1]) becomes concentrated towards the cold wall. This theoretical prevision has been checked with a number of organic solutions studied in our laboratory.

We thought it might be interesting to study solutions of molecules as simple as possible in order to avoid effects related to asymetrical shapes or orientation of the molecules. For this reason we have measured the Soret coefficient D'/D for the binary mixtures of the following compounds: $CCl_4-CCl_3CH_3-CCl_2(CH_3)_2-C(CH_3)_4$, whose thermodynamic properties have already been investigated.[7]

TABLE I.

A[a]	B	x_B	mean T(°C)	$10^4 \cdot D'/D$
1 CCl_4	CCl_3CH_3	0.50	−2.8	0 ±1
		0.46	12.0	3.5 ±0.7
			24.2	3.5 ±1
2 CCl_4	$CCl_2(CH_3)_2$	0.53	−2.8	2.4 ±0.6
3 CCl_4	$C(CH_3)_4$	0.50	−2.8	29 ±1.5
		0.28	−2.8	26 ±1.5
4 CCl_3CH_3	$CCl_2(CH_3)_2$	0.39	−2.8	0.5 ±1
			12.0	3 ±0.7
			25.0	18 ±1
5 CCl_3CH_3	$C(CH_3)_4$	0.30	−2.8	17.5 ±1
6 $CCl_2(CH_3)_2$	$C(CH_3)_4$	0.47	−2.8	17 ±2

[a] A becomes more concentrated in the cold part of the thermal diffusion cell.

The experiments were carried out with the apparatus described by G. Thomaes,[3] in which a system without convection is subjected to a vertical temperature gradient, the concentration gradient being measured continuously by an optical system. In order to test this method, we also measured the diffusion coefficient of the system $CCl_4-C(CH_3)_4$ as a function of concentration by the diver method of B. Gerlach.[8] Both methods gave values of D of the same order of magnitude in the case of equimolecular solutions ($D_{\text{therm}}=2.10^{-5}$, $D_{\text{diver}}=1$, 3.10^{-5}) while dilute solutions of $C(CH_3)_4$ in CCl_4 studied in the thermal diffusion apparatus gave values of D much larger than expected. This might be explained by a slow convection of the liquid (see Table I).

As in all the former papers of this laboratory, the theory gives the correct sign of D'/D. Besides it is in good quantitative agreement with the experimental results for the system $CCl_4-C(CH_3)_4$ ($X=5$), but it cannot actually explain the rapid increase of D'/D with temperature in the case of systems 1 and 4.

We are much indebted to Professor de Brouckère and Professor Prigogine for constant advice and interest, and to the Institut Interuniversitaire des Sciences Nucléaires for financial aid.

* Chercheur agréé de l'Institut Interuniversitaire des Sciences Nucléaires.

[1] Prigogine, de Brouckère, and Amand, Physica **16**, 577 (1950).
[2] Prigogine de Brouckère, and H. Amand, Physica **16**, 851 (1950).
[3] G. Thomaes, Physica **17**, 885 (1951).
[4] R. Buess, Bull. Soc. chim. Belg. **61**, 463 (1952).
[5] I. Prigogine, L. de Brouckère, and R. Buess, Physica **18**, 915 (1952).
[6] Glasstone, Laidler, and Eyring, The Theory of Rate Processes (McGraw-Hill Book Company, Inc., New York, 1941).
[7] V. Mathot and A. Desmyter, J. Chem. Phys. **21**, 782 (1953).
[8] B. Gerlach, Ann. Physik **5**, **10**, 437 (1931).

Infrared Dichroism in the 13.8μ Band of n-$C_{36}H_{74}$ Single Crystals and Polyethylene.

SAMUEL KRIMM
Department of Physics, University of Michigan, Ann Arbor, Michigan
(Received January 11, 1954)

STUDIES on the 13.8μ band in the infrared spectrum of n-paraffins and of polyethylene have established that this band is due to the CH_2 rocking vibration in the plane perpendicular to the chain axis,[1,2] and that the splitting into two components, at about 720 cm^{-1} and 730 cm^{-1}, is probably a result of interaction between rocking modes on neighboring chains in the crystal.[3,4] In melted paraffins and in the amorphous regions of polyethylene this vibration occurs only at 720 cm^{-1}, and, therefore, polarization measurements on cold-drawn polyethylene (in which both components exhibit perpendicular polarization) always show a higher dichroic ratio for the 730 cm^{-1} band than for that at 720 cm^{-1}. Theoretical considerations[4] indicate that the two components arise from in-phase and out-of-phase rocking motions of CH_2 groups on neighboring chains. As a consequence, it is to be expected that each of the components will be polarized along a difference crystallographic axis. In order to check this, polarized spectra of single crystals of a n-paraffin $C_{36}H_{74}$ were obtained; the results agree with this theoretical prediction.

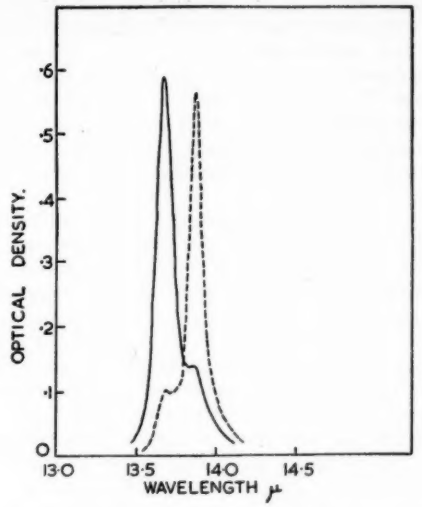

FIG. 1. Spectrum in 13.8μ region of n-$C_{36}H_{74}$ single crystals, using polarized radiation: —— electric vector parallel to a axis, – – – – electric vector parallel to b axis.

Crystals of $C_{36}H_{74}$ were grown from a di-isopropyl ether solution, being obtained as thin parallelopipeds. X-ray diffraction photographs showed that the c axis of the crystal was approximately perpendicular to the plane of the platelet and also established the orientation of the a axis and b axis. A b-axis length of 5.56A indicates that the crystal is a modification, different from the normal form,[5] in which the long chain axes are tilted at a small angle to the basal plane. The sample used consisted of a number of such single crystals oriented identically (as nearly as possible) on a rock salt plate. Using a silver chloride polarizer, spectra were obtained with the electric vector parallel to the a axis and to the b axis of the crystal.

The polarized spectrum in the 13.8μ region of the single crystals of $C_{36}H_{74}$ is shown in Fig. 1. It is seen that each component is almost completely polarized along one crystallographic axis, the 720-cm^{-1} band along the b axis and the 730-cm^{-1} band along the a axis. The doublet at 1460 cm^{-1} shows the same characteristics: the low-frequency component is polarized along the b axis and the high-frequency component along the a axis.

The perpendicular polarization of both components in cold-drawn polyethylene is a consequence of the fact that the alignment of the c axis along the stretching direction is accompanied by a random orientation of the a and b axes perpendicular to this direction. It has been found possible, however, by heat relaxation of a stretched sample, to disorient the crystallites in such a way that the a axis turns into the stretching direction.[6] On the basis

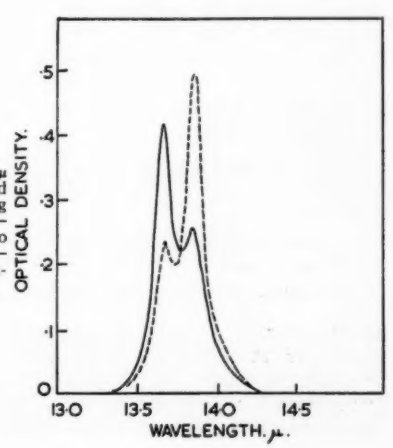

FIG. 2. Spectrum in 13.8μ region of machine-extruded polyethylene film, using polarized radiation: —— electric vector parallel to machine direction, – – – – electric vector perpendicular to machine direction.

of the above results on paraffin crystals, one would expect the 730-cm^{-1} component to show parallel polarization; the spectrum of such a heat-relaxed sample showed this to be true. The same type of preferred orientation is also found in some machine-extruded films. The spectrum of such a polyethylene film is shown in Fig. 2; the parallel polarization of the 730-cm^{-1} band is evident. The expected orientation of the crystallites, *viz.* with the *a* axis lying along the machine direction, was confirmed by x-ray photographs.

Knowing that in polyethylene the absorption at 730 cm^{-1} is associated with *a* axes of crystals whereas that at 720 cm^{-1} is attributable to *b* axes as well as to amorphous material, it is possible, assuming reasonable simplified crystallite distributions, to calculate readily the dichroic ratio of only the amorphous band at 720 cm^{-1}. Such a calculation has indicated that the amorphous regions in cold-drawn and in machine-extruded specimens are indeed oriented, a result in agreement with previous x-ray studies.[7] The author wishes to express his appreciation to Dr. F. P. Reding of Carbide and Carbon Chemicals Company for making available the $C_{36}H_{74}$, and to Dr. P. H. Lindenmeyer of Visking Corporation for furnishing the machine-oriented polyethylene.

[1] N. Sheppard and G. B. B. M. Sutherland, Nature **159**, 739 (1947).
[2] G. B. B. M. Sutherland and A. Vallance Jones, Nature **160**, 567 (1947).
[3] R. S. Stein and G. B. B. M. Sutherland, J. Chem. Phys. **21**, 370 (1953).
[4] R. S. Stein (to be published).
[5] A. Muller, Proc. Roy. Soc. (London) **A120**, 437 (1928).
[6] A. Brown, J. Appl. Phys. **20**, 552 (1949).
[7] S. Krimm and A. V. Tobolsky, J. Polymer Sci. **7**, 57 (1951).

Dielectric Behavior of Methyl Bromide in 3-cm Region

KRISHNAJI AND PREM SWARUP
Department of Physics, University of Allahabad, Allahabad, India
(Received January 4, 1954)

THE dielectric behavior of the symmetric top methyl bromide molecules has been studied in gaseous state in the 3-cm microwave region at moderate pressures. The dielectric properties of a polar medium in which storage and dissipation of microwave energy are involved can be represented by complex dielectric constant $\epsilon=\epsilon'-j\epsilon''$, where $(\epsilon'-1)$ represents the electric susceptibility of the gas and ϵ'' is the dielectric loss factor which is related to the microwave absorption coefficient by the linear relation:

$$\alpha(\text{per cm})=2\pi\bar{\nu}\epsilon'',$$

where $\bar{\nu}$ is the frequency (cm^{-1}) at which the absorption is measured.

The absorption of methyl bromide in the centimeter *r* region is due to a number of rotational lines[1,2] clustered about 0.63 cm^{-1} and due to the inversion of the molecule in its ground vibrational state. The inversion frequency in this case is virtually zero but the absorption line is spread out to microwave region owing to the collision broadening effect. The absorption in the three-centimeter region is solely due to inversion, the contribution[3] of the resonant lines at 0.63 cm^{-1} being negligible.

The theoretical value of the absorption coefficient is calculated by the quantum-mechanical expression of VanVleck and Weisskopf[4] for absorption:

$$\left.\begin{aligned}\frac{\alpha}{\bar{\nu}^2}&=\frac{4\pi^2\Sigma N_{JK}|\mu_{JK}|^2}{3kT}\left[\frac{\langle\Delta\nu\rangle_{Av}}{\Delta\bar{\nu}^2+(\bar{\nu}-\bar{\nu}_0)^2}+\frac{\langle\Delta\nu\rangle_{Av}}{\Delta\bar{\nu}^2+(\bar{\nu}+\bar{\nu}_0)^2}\right]\\&=\pi\cdot I\cdot p\left[\frac{\langle\Delta\nu\rangle_{Av}}{\Delta\bar{\nu}^2+(\bar{\nu}-\bar{\nu}_0)^2}+\frac{\Delta\bar{\nu}}{\Delta\bar{\nu}^2+(\bar{\nu}+\bar{\nu}_0)^2}\right]\end{aligned}\right\}\quad(1)$$

$$=2\cdot\pi\cdot I\cdot p[\langle\Delta\nu\rangle_{Av}/\Delta\bar{\nu}^2+\bar{\nu}^2]\text{ for }\bar{\nu}_0=0,\quad(2)$$

where α (per cm) is the absorption coefficient; I is the intensity factor (per cm mercury); p is the pressure (cm Hg); $\langle\Delta\nu\rangle_{Av}$ is the line-width parameter (cm^{-1}); $\bar{\nu}_0$(cm^{-1}) is the resonance frequency. In the case when resonant frequency $\bar{\nu}_0$ is zero, this expression (1) reduces to the well-known Debye expression (2). Table I gives

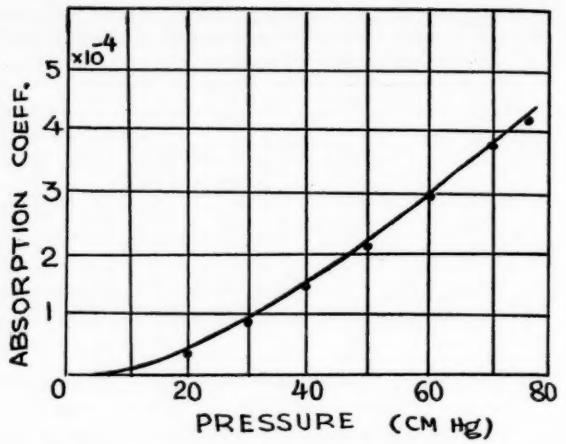

FIG. 1. Pressure variation of absorption coefficient of methyl bromide (—— experimental, ··· theoretical).

the values of the parameters used for calculations. The values of these two parameters at atmospheric pressure are the same as given by Walter and Hershberger[3] and Bleaney and Loubser,[1] respectively.

The experimental techniques adopted in the measurements of absorption and susceptibility have already been reported.[5-8] The experimental values of the absorption coefficient in unbounded medium taken at room temperature and 3.3-cm wavelength have been plotted against pressure in Fig. 1 which also displays the theoretical points by small circles. There is a close agreement between the two sets of values. From the experimental curve of absorption *vs* pressure, we find that the curve follows p^2 law up to 35-cm pressure. It is, therefore, possible to represent accurately the data of the absorption coefficient tabulated in Table II for

TABLE I.

Parameters	Pressure in cm Hg 20	30	40	50	60	Atmos
$2\cdot\pi\cdot I\cdot p\times10^4$	10	15	20	25	30	38
$(\Delta\nu)_{Av}$ (cm^{-1})	0.032	0.05	0.06	0.08	0.096	0.122

pressures up to 35 cm Hg by an equation:

$$\frac{\alpha}{\bar{\nu}^2}=(\text{const})p^2,$$

in which the constant comes out to be 1.22×10^{-6} cm per (cm Hg)^2. From the absorption values we have calculated the values of the

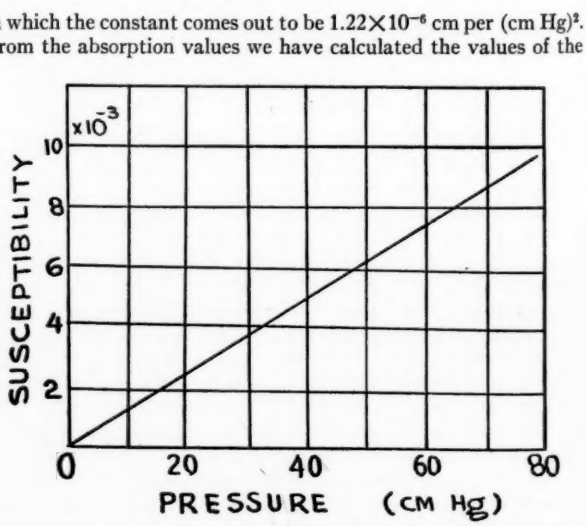

FIG. 2. Pressure variation of electric susceptibility of methyl bromide.

TABLE II.

	Pressure cm Hg						
	20	30	40	50	60	70	76
$\alpha\times10^4$ cm^{-1}	0.5	1.0	1.6	2.3	3.0	3.8	4.3
$\epsilon''\times10^4$	0.26	0.53	0.85	1.2	1.6	2.0	2.3
$(\epsilon'-1)\times10^3$	2.4	3.4	5	6.2	7.4	8.8	9.5

dielectric loss factors at various pressures, which are tabulated in Table II.

The experimental values of the electric susceptibility $(\epsilon'-1)$ have been plotted in Fig. 2 against pressure which gives a straight line similar to that expected and observed by authors in the case of ammonia[7] and ethyl chloride.[8] The values are also tabulated in Table II.

Our results of the absorption coefficient and $(\epsilon'-1)$ at atmospheric pressure are in agreement with the values of Walter and Hershberger, 4.2×10^{-4} cm^{-1} and 9.5×10^{-3}, respectively. Bleaney and Loubser had taken the data at two-atmos pressure. The value of the line-width parameter as 0.122 cm^{-1} at one-atmos pressure gives a close agreement between the theoretical and measured absorptions; the collision diameter calculated from this value comes out to be 9 angstroms, much higher than the Kinetic theory value of about 5.8 angstroms as also shown by Bleaney and Loubser.[1]

The complex dielectric constant of gaseous methyl bromide at 3.3-cm wavelength, atmospheric pressure, and room temperature comes out to be:

$$\epsilon=1.0095-j(0.00023).$$

[1] B. Bleaney and J. H. N. Loubser, Proc. Phys. Soc. (London) **63**, 483 (1950).
[2] Gordy, Smith, and Trambarulo, *Microwave Spectroscopy* (John Wiley and Sons, Inc., New York, 1953).
[3] J. E. Walter and W. D. Hershberger, J. Appl. Phys. **17**, 814 (1946).
[4] J. H. VanVleck and V. F. Weisskopf, Revs. Modern Phys. **17**, 227 (1945).
[5] Krishnaji and Prem Swarup, J. Sci. Ind. Research (India) **12B**, 1 (1953).
[6] Krishnaji and Prem Swarup, J. Appl. Phys. (in press).
[7] Krishnaji and Prem Swarup, Z. Physik **136**, 374 (1953).
[8] Prem Swarup, J. Sci. Ind. Research (India) (communicated).

The λ4050 Group of Cometary Spectra in the Acetylene-Oxygen Flame

NORMAN H. KIESS AND ARNOLD M. BASS
National Bureau of Standards, Washington, D. C.
(Received September 8, 1953)

THE group of emission bands which has been observed in spectra of comets and late class *N*-stars, in the region of λ4050, has been produced recently in the laboratory in a number of sources.[1] Durie[2] has observed the λ4050 emission in the flame reaction of fluorine with organic compounds, but to the best of our knowledge these bands have not been observed before in flames burning in oxygen. We have recently observed a band emission in the λ4050 region in the radiation from the luminous zone of a fuel-rich acetylene-oxygen flame. This luminous zone appears at a fuel-to-oxygen ratio of about 2.6 times stoichiometric, and remains in the flame well beyond the ratio of 4 times stoichiometric. The low dispersion spectrum in this region shows a group of bands similar to that observed by Durie[2] and by Herzberg.[3] Figure 1 is a reproduction of the spectrum as photographed with a Hilger *E*-2 spectrograph with glass optics. The source for this exposure was an acetylene-oxygen flame, of fuel-to-oxygen ratio three times stoichiometric, burning on a welding torch with a port diameter of 1 mm. The exposure time was 1 minute on a spectrum analysis No. 1 plate. The bands of the λ4050 group are clearly discernible as they extend unchanged over the whole slit, while the other features of the spectrum (which are mostly CH) show a marked decrease in intensity in going from the inner cone to the outer cone. Through the cooperation of the Spectroscopy Section of this Bureau, these bands were photographed in the second order of a 21-foot grating spectrograph with dispersion of 0.88A/mm. The spectrum at this high resolution resembles that described by Douglas[4] as obtained in a discharge between carbon electrodes. Our spectrum is much richer in lines, as would be expected by considering the much higher temperature of our source. Figure 2 is a reproduction of a densitometer tracing of the spectral region between 4050 and 4075A. This tracing was taken from a spectrum analysis No. 1 plate exposed for 4½ hours by using as a source a three times stoichiometric acetylene-oxygen flame burning on a rectangular slot burner of dimensions 50 mm by 0.076 mm. The region of the flame selected for this trace lies above the reaction zone.

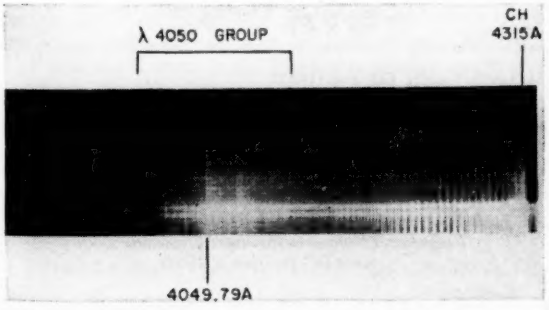

FIG. 1. Emission spectrum of acetylene-oxygen flame as photographed with Hilger E-2 glass prism spectrograph.

Douglas has suggested that these bands may be explained as arising from a $\Sigma-\Pi$ transition of a linear C_3 molecule, and he has presented an analysis of the rotational structure of the band which forms a head at 4050A. For most of the lines of this band

TABLE I. Extended analysis of the λ4050 band of C_3.

	Wave number cm^{-1}		
J	*P*(*J*)	*Q*(*J*)	*R*(*J*)
48	24598.61		24678.44
49		24637.45	
50	94.20		77.09
51		34.59	
52	89.58		75.96
53		31.58	
54	84.90		74.63
55		28.51	
56	80.03		73.20
57		25.45	
58	75.46		71.61
59		22.28	
60	70.74		70.17
61		19.06	
62	65.84		68.37
63		15.62	
64	60.87		66.52
65		12.38	
66	55.82		64.38
67		08.81	
68	50.75		62.18
69		05.27	
70	45.49		
71		01.71	
72	40.29		
73		598.08	
74	34.83		
75		94.38	
77		90.65	
79		86.76	
81		82.87	
83		78.88	
85		74.83	
87		70.74	
89		66.54	
91		62.32	
93		58.13	
95		53.74	
97		49.38	
99		44.85	
101		40.29	
103		35.72	
105		31.11	
107		26.22	
109		21.60	
111		16.60	

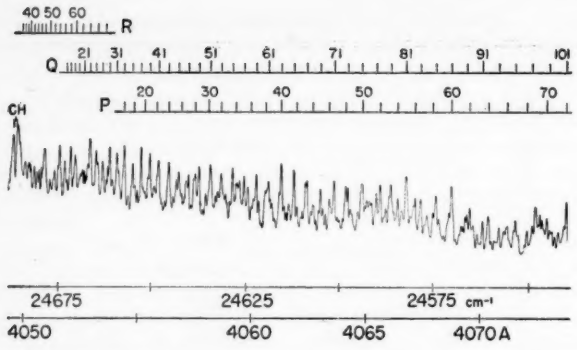

FIG. 2. Densitometer trace of the λ4050 band in emission from acetylene-oxygen flame. Original plate photographed with 21-foot grating spectrograph, dispersion 0.88A/mm.

our measurements agree with those of Douglas to better than 1 cm^{-1} in the spectral range in which the data overlap. Because of the higher excitation temperature which we used, we have been able to extend the analysis suggested by Douglas to higher rotational quantum numbers. The extended analysis is presented in Table I. The lines for J less than 48 are omitted since the wavelengths which we measured are essentially the same as those reported by Douglas. For the type of transition postulated by Douglas, our measurements lead to the following constants:

$$B'=0.413\ cm^{-1} \qquad B''=0.430\ cm^{-1}$$

$$D'=0.45\times10^{-6}\ cm^{-1} \qquad D''=0.90\times10^{-6}\ cm^{-1}$$

$$\nu_0=24675.75\ cm^{-1}.$$

These values for B'', B', and D'' are in very close agreement with those of Douglas. For D' Douglas reports a value of 0.26×10^{-6} cm^{-1} which is considerably smaller than that which we found.

[1] For a recent complete review of this problem see B. Rosen and P. Swings, Ann. d'Astrophys. **16**, 82 (1953).
[2] R. A. Durie, Proc. Roy. Soc. (London) **A211**, 110 (1952).
[3] G. Herzberg, Astrophys. J. **96**, 314 (1942).
[4] A. E. Douglas, Astrophys. J. **114**, 466 (1951).

Regularity of the *F*-Center Maxima in Fused Silica and α Quartz

ALVIN J. COHEN
Multiple Fellowship on Glass Science, Mellon Institute, Pittsburgh, Pennsylvania
(Received January 4, 1954)

IN a careful study of color centers in fused silica, Yokota[1] observed an absorption band at 548–550 mμ (2.3 ev, see Table I) upon x-irradiation of samples prepared under reducing conditions. His work has shown that this absorption band has many of the properties of F centers with the exception that no wavelength shift is observed on cooling to liquid oxygen temperature. He attributed the band to electrons trapped in oxygen vacancies. Yokota[2] has also observed an absorption maximum at 2.68 ev (462 mμ) upon x-irradiation of crystalline α quartz and interpreted this band as an F band corresponding to the 2.3-ev one in fused silica. Niira[3] has proposed a plausible theory to account for the above shift in frequency. Bappu's[4] work on natural α quartz of purple color, generally known as amethyst, shows the existence of an absorption band at 550 mμ at 28°C. The 550-mμ band in amethyst is temperature sensitive, is quickly removed at 400–450°C, and is readily converted to an "F' band" by flooding with blue light.[4] Consequently, it would seem that Bappu is correct in calling the amethyst band an F band, and it is in fact the band which corresponds almost exactly to the F band in fused quartz. A comparison of the wavelengths of the F bands of these two materials is given in Table I. Yokota's and Niira's assignment of the F-center peak in α quartz is considered incorrect, and no conclusions can be drawn as yet about the influence of crystalline or amorphous environment on F centers in quartz.

TABLE I.

T°C	Material	Band max in mμ	Reference
−190	amethyst quartz	527	4
−183	fused quartz	548–550[a], 539[b]	1
+ 28	amethyst quartz	550	4
+ 23	fused quartz	548–550[a], 539[b]	1
+198	amethyst quartz	560	4

[a] Value taken from graph, p. 318, reference 1.
[b] Same band as (a) but is from value of 2.3 ev given in text, p. 318, reference 1.

The F-center band of α quartz corresponding closely with the F-center band of fused silica has been seen thus far only in the amethyst-colored material and not in the smoky variety. Yokota's 2.68-ev band has not been found by other investigators, either in other samples of natural smoky quartz or smoky quartz colored by x-radiation. Mohler[5] finds in this region of the smoky quartz spectrum absorption peaks at 400, 500, and 606 mμ; Smakula[6] observes a peak between 400 and 435 mμ depending on crystal orientation; the author finds peaks at 425 and 625 mμ in natural smoky quartz from the Dinkey Lakes region of California oriented either parallel or perpendicualr to the optic axis. These two peaks may be bleached rapidly at 400°C and regenerated by x-radiation. Wafers of naturally colorless Brazilian α quartz cut parallel to the optic axis developed the same two absorption peaks after 3×10^{6} r of gamma irradiation. Marshall[7] finds absorption peaks in natural smoky quartz from Jessieville, Arkansas, that substantially agree in wavelength with the results found in this laboratory.

The occurrence of smoky quartz lacking a "550-mμ" band and amethyst with such a band may be explained by one or more of the following mechanisms: (1) if the α quartz turns smoky on x-irradiation, or by proximity to natural radioactivity *in situ;* it (a) has been formed under oxidizing conditions so that anion vacancies do not exist; (b) contains chemical impurities that preclude the existence of anion vacancies; (c) does have anion vacancies, but these do not form F centers. (2) If the α quartz turns purple under the same conditions that other α quartz turns smoky, it (a) has been formed under reducing conditions so that anion vacancies exist; (b) contains chemical impurities such that anion vacancies exist in order to preserve electroneutrality; (c) has anion vacancies more favorable for electron trapping than in (1). Work on this problem is now in progress in this laboratory.

Leela[8] has measured the static paramagnetism of amethyst and attributed the observed paramagnetism entirely to iron impurity. If, however, the 550-mμ band of amethyst is indeed due to F centers (which are always paramagnetic), Leela's interpretation of the results should be re-examined.

[1] R. Yokota, J. Phys. Soc. Japan **7**, 316 (1952).
[2] R. Yokota, J. Phys. Soc. Japan **7**, 222 (1952).
[3] K. Niira, Busseiron Kenkyu **50**, 17 (1952); Chem. Abstracts **46**, 7421*c* (1952).
[4] M. K. V. Bappu, Indian J. Phys. **26**, 1 (1952); Chem. Abstracts **46**, 7427*a* (1952).
[5] N. M. Mohler, Am. Mineralogist **21**, 258 (1936).
[6] A. Smakula, J. Opt. Soc. Am. **40**, 266*a* (1950).
[7] Royal Marshall, California Institute of Technology (private communication).
[8] M. Leela, Nature **172**, 464 (1953).

Cl in SO_2Cl Pure Quadrupole Spectra*

P. J. BRAY AND D. ESTEVA
Rensselaer Polytechnic Institute, Troy, New York
(Received January 4, 1953)

A NUMBER of new quadrupole resonances of chlorine in sulfonyl chlorides and some other compounds have been found using a frequency modulated self-quenching superregenera-

TABLE I. Cl^{35} quadrupole resonance frequencies.

	Compound	Frequency at liquid nitrogen temperature (megacycles per second)	Approximate signal-to-noise ratio
1	2,5-dichlorobenzenesulfonyl chloride[a] $Cl_2C_6H_3SO_2Cl$	37.3200 ±0.0020 36.3913 ±0.0020 34.4484 ±0.0020	8 5–6 6–8
2	2,5-dichlorobenzenesulfonic acid[a] $Cl_2C_6H_3SO_3H\cdot 2H_2O$	36.4500 36.1600 35.6222	3 7 2–3
3	2,5-dichlorobenzenesulfonic acid sodium salt $Cl_2C_6H_3SO_3Na$	36.5040 35.2117	9–10 6
4	2,5-dimethylbenzenesulfonyl chloride $(CH_3)_2C_6H_2SO_2Cl$	32.7579 [d] 32.5269 ±0.0020 32.3178 32.2698	15[e] 2–[e] 6[e] 8[e]
5	benzenesulfonyl chloride $C_6H_5SO_2Cl$	32.8920 32.5380 32.4700 ±0.0020	15[e] 15[e] 10[e]
6	*p*-chlorobenzenesulfonic acid sodium salt *p*-$ClC_6H_4SO_3Na$	35.1366	3–4
7	ethanesulfonyl chloride $C_2H_5SO_2Cl$	32.5190	2
8	*l*-butanesulfonyl chloride $CH_3(CH_2)_3SO_2Cl$	32.7592	3–4
9	2-thiophenesulfonyl chloride[a] SCH:CHCH:CSO₂Cl	33.1507	22[e]
10	*o*-chlorobenzoic acid[a,b] *o*-ClC_6H_4COOH	36.3049	7–8
11	pentachlorophenol[a] C_6Cl_5OH	38.5794 38.1915 37.3750 37.1292 ±0.0020	6 7–8 4 2–
12	α-bromo-*p*-chloroacetophenone[a,f] $ClC_6H_4COOH_2Br$	34.8224	12

[a] Sample melted in vial into polycrystalline solid.
[b] This resonance may suffer from saturation or randomness in the crystalline composition. It appears as a series of humps rather than sharp lines.
[c] This is the maximum signal-to-noise ratio observed.
[d] These two resonances so far have always appeared together.
[e] Broader and more diffuse than usual, but very large.
[f] Piezoelectric in feather crystal form from DPI. This disappears completely when the sample is melted down.

tive oscillator. The audio amplification section used previously[1,2] has been replaced by a Tektronix Type 122 low-level preamplifier.

The sulfonyl chloride resonances reported in Table I should be compared with previous Cl in SO_2Cl resonances.[1,3] A conservative estimate of ±1 kcps should be assigned to these present measurements except where noted. The lowest resonance in 2,5-dichlorobenzenesulfonyl chloride may tentatively be assigned to Cl in SO_2Cl on the basis of the general frequency range of Cl in SO_2Cl resonances as reported here and elsewhere.[1,3] The frequencies obtained for 2,5-dichlorobenzenesulfonic acid and its sodium salt tend to confirm this assignment.

Both 2,5-dimethylbenzenesulfonyl chloride and benzenesulfonyl chloride[4] apparently have at least three different crystalline phases into which they may freeze. The resonance in 2,5-dimethylbenzenesulfonyl chloride appears to progress stepwise over a period of days from the lowest to the highest frequency in a sample initially frozen at liquid nitrogen temperature and kept frozen under refrigeration at 0–10°C.

The resonances in compounds 1, 2, 3, 6, 10, 11, and 12 should be compared with the chlorobenzene derivatives data of Meal.[5] Correlation of the Cl in SO_2Cl frequencies (and others reported here and in reference 1) with the substituent parameter sigma of Hammett will be presented in a later paper.

The *o*-chlorobenzoic acid resonance completes the *meta* and *para* values of Meal[5] and shows that the −COOH substitution progressively strengthens the field gradient at the chlorine nucleus in the order *para*, *meta*, *ortho*. The resonance is brought out of the noise with an increased extent of frequency modulation. It is still unusual in shape at room temperature in all samples studied to date (see *b* under Table I).

It is surprising that four resonances arise in pentachlorophenol. Work is continuing on this compound and on the phase changes in benzenesulfonyl chloride and 2,5-dimethylbenzenesulfonyl chloride. It is possible that further investigation will disclose so far unnoticed phase changes in other frozen liquids. Temperature dependence and Zeeman splitting studies are also in progress.

Possibly of interest is the fact that at least one of the plastic caps employed on the sample-containing vials[6] exhibits a very strong resonance in the 23 mcps region at liquid nitrogen temperature. This resonance has the exact shape of a quadrupole resonance (which differs markedly from an external signal) but is unaffected by magnetic fields even of 1200 gauss or by electric fields of 300 volts/cm or so. It has not been found at room temperature. Rough treatment and mutilation of the cap are ineffectual in changing the size or frequency of the resonance. Annealing has not yet been tried.

* Research supported by a grant in aid from the Rensselaer Polytechnic Institute Research Grants Committee.
[1] P. J. Bray and P. J. Ring, J. Chem. Phys. **21**, Dec. 1953.
[2] C. Dean, thesis, Harvard University, 1952.
[3] D. W. McCall and H. S. Gutowsky, J. Chem. Phys. **21**, 1300 (1953).
[4] Resonance first reported by McCall and Gutowsky (reference 3).
[5] H. C. Meal, J. Am. Chem. Soc. **74**, 6121 (1952).
[6] New York Laboratory Supply Company No. 15691 1 Dram Black Molded Screw Cap.

Self-Consistent Orbitals for Radicals

J. A. POPLE AND R. K. NESBET
Department of Theoretical Chemistry, Cambridge, England
(Received November 25, 1953)

ROOTHAAN[1] has described an iterative method of determining LCAO molecular orbitals for closed shell ground states. This can be generalized. to apply to the ground state of radicals or to any excited state which can be represented by a single determinant wave function. For such a state we may associate M electrons with orthonormal orbitals $\phi_1^\alpha\cdots\phi_M^\alpha$ and α-spin functions and the remaining N electrons with orbitals $\phi_1^\beta\cdots\phi_N^\beta$ and β-spin functions. There is no *a priori* reason, however, why any of the orbitals in one set should be identical with any in the other. The total determinantal wave function is, then,

$$\Phi=[(M+N)!]^{-\frac{1}{2}}\Sigma_P(-1)^P P\{\phi_1^\alpha(1)\alpha(1)\cdots \times\phi_M^\alpha(M)\alpha(M)\phi_1^\beta(M+1)\beta(M+1)\cdots \times\phi_N^\beta(M+N)\beta(M+N)\}. \quad (1)$$

The corresponding electronic energy is easily found by the standard reduction procedure and is

$$E=\sum_i^{\alpha+\beta} H_i+\tfrac{1}{2}\sum_i^{\alpha+\beta}\sum_j^{\alpha+\beta} J_{ij}-\tfrac{1}{2}\left(\sum_i^{\alpha}\sum_j^{\alpha}+\sum_i^{\beta}\sum_j^{\beta}\right)K_{ij}. \quad (2)$$

Here Σ^α, Σ^β, and $\Sigma^{\alpha+\beta}$ indicate summation over $\alpha-$, $\beta-$, and all orbitals, respectively. H_i, J_{ij}, and K_{ij} are defined by

$$H_i=\int\bar{\phi}_i H\phi_i dv$$
$$J_{ij}=\int\int\bar{\phi}_i(1)\bar{\phi}_j(2)(1/r_{12})\phi_i(1)\phi_j(2)dv_1dv_2 \quad (3)$$
$$K_{ij}=\int\int\bar{\phi}_i(1)\bar{\phi}_j(2)(1/r_{12})\phi_j(1)\phi_i(2)dv_1dv_2,$$

H being the Hamiltonian for a single electron in the field of the nuclei alone.

If we now write the molecular orbitals ϕ_i in LCAO form

$$\phi_i=\Sigma_r\chi_r C_{ri}, \quad (4)$$

where χ_r are any general set of specified single electron functions, then self-consistent values of C_{ri} are determined by the condition that the first variation of (2) should vanish, subject to the orthonormality conditions. Following the method and notation of reference 1, it is easily shown that the coefficients must satisfy

equations which can be written in matrix form

$$\mathbf{F}^\alpha \mathbf{c}_i^\alpha = \epsilon_i^\alpha \mathbf{S}\mathbf{c}_i^\alpha; \quad \mathbf{F}^\beta \mathbf{c}_i^\beta = \epsilon_i^\beta \mathbf{S}\mathbf{c}_i^\beta, \tag{5}$$

where $\mathbf{c}_i^\alpha$, $\mathbf{c}_i^\beta$ are column vectors specifying the coefficients of the orbitals ϕ_i^α and ϕ_i^β, respectively. The matrices $\mathbf{F}^\alpha$ and $\mathbf{F}^\beta$ are

$$\mathbf{F}^\alpha = \mathbf{H} + \mathbf{J} - \mathbf{K}^\alpha; \quad \mathbf{F}^\beta = \mathbf{H} + \mathbf{J} - \mathbf{K}^\beta, \tag{6}$$

and the (rs)th elements of S, H, J, K^α are

$$(\mathbf{S})_{rs} = \int \bar{\chi}_r \chi_s dv; \quad (\mathbf{H})_{rs} = \int \bar{\chi}_r H \chi_s dv$$

$$(\mathbf{J})_{rs} = \sum_{tu} (p_{tu}^\alpha + p_{tu}^\beta) \int\int \bar{\chi}_r(1) \bar{\chi}_t(2) (1/r_{12}) \chi_s(1) \chi_u(2) dv_1 dv_2$$

$$(\mathbf{K}^\alpha)_{rs} = \sum_t p_{tu}^\alpha \int\int \bar{\chi}_r(1) \bar{\chi}_t(2) (1/r_{12}) \chi_u(1) \chi_s(2) dv_1 dv_2 \tag{7}$$

$$p_{tu}^\alpha = \sum_i^\alpha \bar{C}_{ti} C_{ui}; \quad p_{tu}^\beta = \sum_i^\beta \bar{C}_{ti} C_{ui}.$$

An iterative calculation of the coefficients can be based on the following steps:

(a) assume a set of coefficients $\mathbf{c}_i^\alpha$, $\mathbf{c}_i^\beta$ satisfying the necessary orthonormality conditions.

(b) Use these to calculate the matrices $\mathbf{J}$, $\mathbf{K}^\alpha$, $\mathbf{K}^\beta$, and, hence, $\mathbf{F}^\alpha$ and $\mathbf{F}^\beta$.

(c) Determine a new set of coefficients from Eqs. (5).

(d) Repeat the process until self-consistency is obtained.

Equations (5) are a direct generalization of those obtained by Roothaan[1] and reduce to them in the special case when the number of α electrons is equal to the number of β electrons ($M = N$).

They can be applied to the determination of orbitals in a single radical or radical ion along lines that have already been used for closed shell ground states.[2-5]

One of us (R.K.N.) is a Predoctoral Fellow of the National Science Foundation.

[1] C. C. J. Roothaan, Revs. Modern Phys. **23**, 69 (1951).
[2] J. F. Mulligan, J. Chem. Phys. **19**, 347 (1951).
[3] F. O. Ellison and H. Shull, J. Chem. Phys. **21**, 1420 (1953).
[4] R. C. Sahni, Trans. Faraday Soc. **49**, 1246 (1953).
[5] R. G. Parr and R. S. Mulliken, J. Chem. Phys. **18**, 1338 (1950).

Nuclear Quadrupole Resonances in Some Chlorine Compounds*

QUITMAN WILLIAMS AND T. L. WEATHERLY
School of Physics, Georgia Institute of Technology, Atlanta, Georgia
(Received December 28, 1953)

PURE quadrupole resonance has been observed in three chlorine compounds. The Cl^{35} resonance frequencies are listed in Table I. Measurements were made at liquid-nitrogen temperature using a frequency modulated regenerative detector. Frequencies were determined with a Signal Corps BC 221 frequency meter.

The resonance frequency for 1-chloro-2,4-dinitrobenzene is higher than the value 34.622 Mc reported by Livingston[1] for monochlorobenzene. This increase in the Cl^{35} resonance frequency produced when NO_2 groups replace hydrogen atoms in monochlorobenzene is also evident in the measurements of Dean and Pound.[2]

TABLE I. Cl^{35} quadrupole resonance frequencies at −196°C.

Compound	Frequency (Mc)
1-Chloro-2,4-dinitrobenzene	37.796
4-Chloro-3,5-xylenol	34.348 34.415
Ethyltrichlorosilane	18.756 18.842 18.865

Two resonances were found for 4-chloro-3,5-xylenol at frequencies slightly lower than those for parachlorophenol[2] at this temperature. Thus the substitution of CH_3 groups for hydrogen at carbon atoms 3 and 5 decreases the resonance frequency. The existence of two resonance frequencies for 4-chloro-3,5-xylenol presumably results from two nonequivalent chlorine positions in the crystal lattice.

The three absorption lines found for ethyltrichlorosilane occur at relatively low frequencies, indicating a decrease in resonance frequency with increased electronegativity difference. These frequencies are slightly lower than those reported by Livingston[3] for $SiCl_4$. This frequency decrease is probably the result of increased ionic character of the remaining C—Cl bonds when one chlorine atom is replaced by a C_2H_5 group.

* Sponsored by the Office of Ordnance Research, U. S. Army.
[1] R. Livingston, Phys. Rev. **82**, 289 (1951).
[2] C. Dean and R. V. Pound, J. Chem. Phys. **20**, 195 (1952).
[3] R. Livingston, J. Phys. Chem. **57**, 496 (1953).

Temperature-Dependent Color Changes in Some Merocyanines

YEHUDA HIRSHBERG AND ERNST FISCHER
The Daniel Sieff Research Institute, The Weizmann Institute of Science Rehovoth, Israel
(Received December 28, 1953)

IN the course of investigations of thermochromism and photochromism in spiropyrans,[1,2] the absorption spectra of several merocyanines were measured at reduced temperatures. In all cases pronounced changes in color were observed when solutions of these compounds were cooled from room temperature to various lower temperatures, down to about 110°K.

Spectrophotometric measurements showed these color changes to be due to the fact that with decreasing temperature one absorption band, at longer wavelength, grows less intense while a second band, at shorter wavelength, grows more intense. A typical case is shown in Fig. 1, where the absorption spectrum is

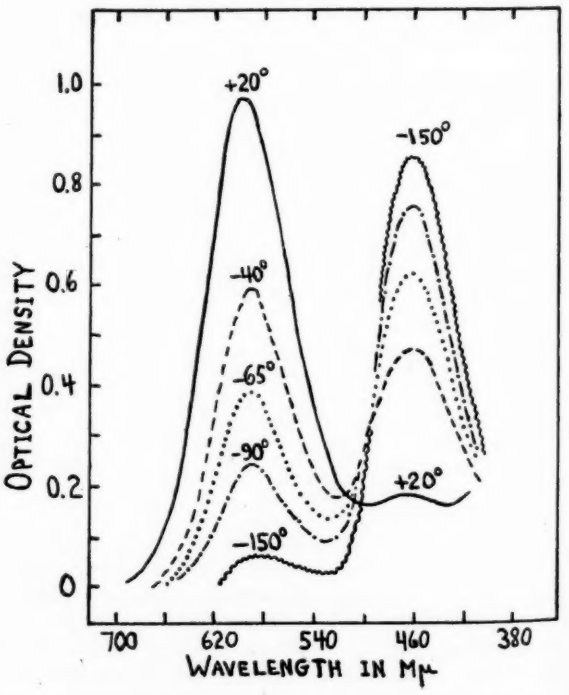

FIG. 1. Absorption spectrum, at several temperatures, of (*I*) in a mixture of ethanol and methanol. (Conc. 2 mg/liter).

recorded for an alcoholic solution of compound (*I*) at several temperatures. Similar results were obtained with (*II*), (*III*), (*IV*), and several related compounds.[3] From the change with

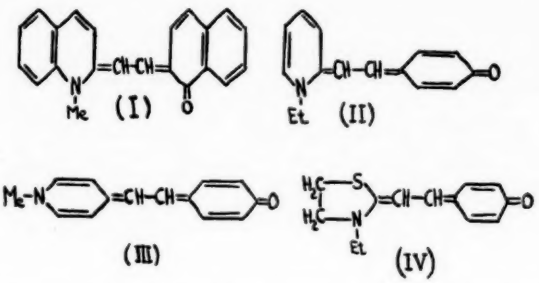

temperature of the thermal equilibrium between the two modifications characterized by the two absorption bands, the energy difference between these modifications was estimated at 2–3 kcal/mole.

The apparatus used in these experiments has been described elsewhere.[2]

Further investigations are now under way on these phenomena and their relation to photochromism.

[1] E. Fischer and Y. Hirshberg, J. Chem. Soc. 4522, 1952.
[2] Y. Hirshberg and E. Fischer, J. Chem. Soc. (to be published).
[3] The authors are indebted to Dr. Anna Weizmann for a sample of (I), and to Dr. E. B. Knott for samples of all the other compounds measured.

Maxima in the Potential Energy-Distance Functions of Diatomic Molecules

R. F. Barrow
Physical Chemistry Laboratory, Oxford University, Oxford, England
(Received December 28, 1953)

ONE conclusion of a recent theoretical study of the oxygen molecule by Meckler[1] is that there may be quite pronounced maxima in the potential energy-distance curves for the ground state $X^3\Sigma_g^-$ and for the state $b^1\Sigma_g^+$ of the oxygen molecule. The possibility of such maxima occurring at least in excited states was indicated some years ago by Mulliken's work[2] on AgI, and there is evidence from observations of predissociation that the lowest[1] Π states in BH and AlH behave similarly (see, for example, Herzberg[3]).

The present thermochemical and spectroscopic information about the AlF molecule can only be reconciled if it is assumed that there is a maximum in the state $A^1\Pi$ at about 21 kcal above the dissociation limit.[4] This conclusion prompted an examination of the data for AlCl and for the silver halides. The results (kcal mole^{-1}) are summarized in Table I. The information is not uniformly reliable, and particularly some of the latent heats of sublimation may be in considerable error, but there is a clear suggestion that maxima of height up to about 20 kcal may be more common at least in excited states than has been generally supposed.

TABLE I.

Molecule	State	$D_{spect.}$	$D_{thermochem.}$	Height of potential maximum
AlCl	$A^1\Pi$	121.7	117.3	4.4
AgCl	$B(^3\Pi_{0^+})$	94.9	78.3	16.6
AgBr	$B(^3\Pi_{0^+})$	83.9	73.4	10.5
AgI	$B(^3\Pi_{0^+})$	69.4	60.5	8.9

This question has important bearings upon the spectroscopic determination of dissociation energies of certain important molecules like NO and CO: indeed this has been realized for some time (see, for example, Herzberg[3] and Gaydon[5]). However, the indications now are that potential maxima are no longer to be regarded as rather special anomalies; and, as a result, the acceptance of a spectroscopic dissociation energy based on the observation of a *single* limit is to be treated with perhaps more scepticism than it has received hitherto. The present position stresses the need for more theoretical and experimental information about the interaction of atoms at moderately large values of the internuclear distance.

[1] A. Meckler, J. Chem. Phys. **21**, 1750 (1953).
[2] R. S. Mulliken, Phys. Rev. **50**, 310 (1937).
[3] G. Herzberg, *Molecular Spectra and Molecular Structure* (D. Van Nostrand Company, Inc., New York, 1950), Vol. I.
[4] H. C. Rowlinson and R. F. Barrow, Proc. Phys. Soc. (London) **A66**, 437 (1953).
[5] A. G. Gaydon, *Dissociation Energies* (Chapman and Hall, London, 1953).

Erratum: Theory of Absorption Spectra of Carotenoids

[J. Chem. Phys. **20**, 1661 (1952); **21**, 381 (1953)]

Gentaro Araki
Faculty of Engineering, Kyoto University, Yosida, Kyoto, Japan

THE interpretation of the sectional area A of the pipe in which π electrons are enclosed was not appropriate as given in these letters. In the correct interpretation $4A$ should be replaced for A in the previous letter. Then Eq. (2) becomes $\delta=(L/\pi)^3/\{A(N-2)\}$, and consequently we have $A=181.1$ atomic units after some new adjustment for fitting experiment.

Errata: Mechanism of the Hg($^3P_1$) Photosensitized Decomposition of Ethylene

[J. Chem. Phys. **21**, 2075–2076 (1953)]

A. G. Mitchell and D. J. LeRoy
Department of Chemistry, University of Toronto, Toronto, Canada

EQUATIONS (1a), (1b), (2), (3), (4), (5a), and (5b) should read, respectively, (a), (b), (1), (2), (3), (*i*), and (*ii*).

On the Ionicity of Gaseous Thallous Chloride

Aubrey P. Altshuller
1911 Clover Street, Cleveland, Ohio
(Received December 28, 1953)

AN attempt was made recently to calculate the dipole moments of gaseous thallous halides[1] by means of the electrostatic treatment used successfully for alkali metal halides by Rittner.[2] The calculated dipole moment of thallous chloride of about 3.8 *d* was 0.7 *d* less than the observed moment of 4.44 *d*. This difference was explained as probably due to the uncertainty in the polarizability of Tl^+. While this uncertainty may be partially responsible for the difference, it is also true that the assumption made that the gaseous thallous halides are completely ionic in character is probably incorrect. Although TlCl is undoubtedly a highly polar molecule, recent interpretations[3,4] of nuclear quadrupole coupling constants indicate that there may be a 15–20 percent contribution from *s-p* hybridization to the Tl–Cl bond. (This partially covalent character of TlCl in the gaseous state contrasts with the apparently negligible contribution from homopolar binding to the lattice energies of solid thallous halides.[5,6]

If this interpretation[3,4] of the microwave data is correct, there will be a contribution to the total moment of TlCl from the atomic dipoles arising at the Tl and Cl atoms as a result of charge asymmetries caused by hybridization of the bonding orbits.[7,8] An atomic moment arising from the nonbonding hybridized orbitals will also be present which will tend to oppose the net atomic moment due to the hybridization of the bonding orbitals. Furthermore, a homopolar dipole will also be present due to the difference in the sizes

of the Tl and Cl atoms. The Tl^+ in the gaseous molecule may be calculated to have a radius of 0.9A (average of 0.95, 0.94, and 0.85A) from the ionic radius of 1.59A given by Rittner[2] for Cl^- in gaseous alkali halides and the internuclear distances of TlCl, TlBr, TlI.[1] If these radii are used then $Tl^+ < Cl^-$ and the homopolar dipole will be directed with its negative end towards the Tl atom and will thus oppose the ionic moment. (The partially covalent character of the bond should reduce the difference in these radii somewhat and consequently reduce the magnitude of the homopolar moment.) Since $\mu_{\text{ionic}} + \mu_{\text{homopolar}} < \mu_{\text{ionic}} < \mu_{\text{obs}}$, it would seem that the resultant of the atomic moments arising from hybridization of the bonding and nonbonding orbitals must act in the same direction as the ionic moment so that $\mu_{\text{ionic}} + \mu_{\text{homopolar}} + \mu_{\text{atomic}} = \mu_{\text{obs}}$.

The brief discussion given above would appear to indicate that the exact calculation of the dipole moment of a molecule of large but not 100 percent ionic character with some orbital hybridization is quite likely to be difficult and that the simple electrostatic treatment can only be expected at best to give a fair approximation to the observed moment.

[1] A. P. Altshuller, J. Chem. Phys. **21**, 2074 (1953).
[2] E. Rittner, J. Chem. Phys. **19**, 1030 (1951).
[3] Gordy, Smith, and Trambarulo, *Microwave Spectroscopy* (John Wiley and Sons, Inc., New York, 1953), Chapter 7.
[4] B. P. Dailey, J. Phys. Chem. **57**, 490 (1953).
[5] J. E. Mayer, J. Chem. Phys. **1**, 327 (1933).
[6] This difference is in accord with the increasing ionic character observed in going from the gaseous to the solid states for other halides (reference 4).
[7] R. S. Mulliken, J. chim. phys. **46**, 497 (1949).
[8] C. A. Coulson, Proc. Phys. Soc. (London) **207A**, 63 (1951).